NASA Conference Publication 3342

# NASA Microgravity Materials Science Conference

*Compiled by*
*F. Szofran, D. McCauley, and C. Walker*

Proceedings of a conference held
at Huntsville, Alabama
June 10–11, 1996

October 1996

NASA Conference Publication 3342

# NASA Microgravity Materials Science Conference

*F. Szofran, Compiler*
*Marshall Space Flight Center • MSFC, Alabama*

*D. McCauley, Compiler*
*University of Alabama in Huntsville • Huntsville, Alabama*

*C. Walker, Compiler*
*Universities Space Research Association • Huntsville, Alabama*

National Aeronautics and Space Administration
Marshall Space Flight Center • MSFC, Alabama 35812

Proceedings of a conference held
at Huntsville, Alabama
June 10–11, 1996

October 1996

# Foreword

The Microgravity Materials Science Conference was held June 10 - 11, 1996 at the Von Braun Civic Center in Huntsville, Alabama. It was organized by the Microgravity Materials Science Discipline Working Group, sponsored by the Microgravity Science and Applications Divisionp at NASA Headquarters, and hosted by the NASA Marshall Space Flight Center and the Alliance for Microgravity Materials Science and Applications (AMMSA). It was the second NASA conference of this type in the microgravity materials science discipline. The microgravity science program sponsored approximately eighty investigations and sixty-nine principal investigators in FY96, all of whom made oral or poster presentations at this conference. The conference's purpose was to inform the materials science community of research opportunities in reduced gravity in preparation for a NASA Research Announcement (NRA) scheduled for release in late 1996 by the Microgravity Science and Applications Division at NASA Headquarters. The conference was aimed at materials science researchers from academia, industry, and government. A tour of the MSFC microgravity research facilities was held on June 12, 1996. This volume is comprised of the research reports submitted by the Principal Investigators after the conference and presentations made by various NASA microgravity science managers.

# Table of Contents

Dr. Michael J. Wargo, NASA Headquarters ..... 1
*The 1996 Microgravity Materials Science NASA Research Announcement (NRA)*

Mr. Robert C. Rhome, NASA Headquarters ..... 7
*Microgravity Science and Applications Program*

Prof. John H. Perepezko, University of Wisconsin ..... 13
*Topics of Interest in Microgravity Materials Science*

Mr. Joel K. Kearns, NASA Marshall Space Flight Center ..... 45
*Microgravity Materials Science: Ground and Flight Research Resources and Procedures*

Dr. Robert S. Snyder, NASA Marshall Space Flight Center ..... 53
*Microgravity Materials Science: Ground-Based and Flight Research Resources and Procedures*

Prof. Alexander A. Chernov, Universities Space Research Association ..... 57
*Growth of Faceted Crystals - Stability, Flows, Defects (invited paper)*

Agenda and Presentation Program ..... 61

World Wide Web ..... 69

**Principal Investigator Research Reports**

Dr. Reza Abbaschian, University of Florida ..... 71
*In-Situ Monitoring of Crystal Growth Using MEPHISTO*

Dr. Spiro D. Alexandratos, University of Tennessee at Knoxville ..... 77
*Synthesis and Characterization of Single Macromolecules: Mechanistic Studies of Crystallization and Aggregation*

Dr. M. Cengiz Altan, University of Oklahoma ..... 83
*Microgravity Impregnation of Fiber Preforms*

Dr. Timothy J. Anderson, University of Florida ..... 89
*An Electrochemical Method to Visualize Flow and Measure Diffusivity in Liquid Metals*

Dr. J. Barry Andrews, University of Alabama at Birmingham ..... 95
*Coupled Growth in Hypermonotectics*

Dr. J. Barry Andrews, University of Alabama at Birmingham ..... 101
*The Effect of Convection on Morphological Stability During Coupled Growth in Immiscible Systems*

Dr. Alan J. Ardell, University of California at Los Angeles ..... 107
*Ostwald Ripening of Liquid and Solid "Droplets" in Liquid Metal Matrices*

## Table of Contents (cont'd)

Dr. Klaus J. Bachmann, North Carolina State University ..... 113
*Fundamental Aspects of Vapor Deposition and Etching Under Diffusion Controlled Transport Conditions*

Dr. Mark A. Barteau, University of Delaware ..... 119
*Molecularly Tailored Surfaces via Self-Assembly Processes: Synthesis, Characterization and Modeling*

Dr. Robert J. Bayuzick, Vanderbilt University ..... 125
*Effects on Nucleation by Containerless Processing*

Dr. Robert J. Bayuzick, Vanderbilt University ..... 131
*Investigation of the Relationship Between Undercooling and Solidification Velocity*

Dr. Christoph Beckermann, University of Iowa ..... 137
*Equiaxed Dendritic Solidification Experiment (EDSE)*

Dr. Lynn A. Boatner, Oak Ridge National Laboratory ..... 143
*Surface Morphological Properties of Stationary Melt Pools in Single Crystals of Stainless Steel*

Dr. John F. Brady, California Institute of Technology ..... 145
*Dispersion Microstructure and Rheology in Ceramics Processing*

Dr. Kenneth Brezinsky, Princeton University ..... 149
*Combustion Synthesis of Materials in Microgravity*

Dr. Robert A. Brown, Massachusetts Institute of Technology ..... 153
*Application of Parallel Computing for Two- and Three-Dimensional Modeling of Bulk Crystal Growth and Microstructure Formation*

Dr. Ared Cezairliyan, National Institute of Standards and Technology ..... 155
*Thermophysical Properties of High Temperature Liquid Metals and Alloys*

Dr. Soyoung Stephen Cha, University of Illinois at Chicago ..... 161
*Three-Dimensional Velocity Field Characterization in a Bridgman Apparatus: Technique Development and Effect Analysis*

Dr. Ivan O. Clark, NASA Langley Research Center ..... 167
*Microgravity Chemical Vapor Deposition*

Dr. Peter A. Curreri, NASA Marshall Space Flight Center ..... 173
*Fundamental Studies of Solidification in Microgravity Using Real-Time X-Ray Microscopy*

Dr. Jonathan A. Dantzig, University of Illinois at Urbana-Champaign ..... 179
*Adaptive-Grid Methods for Phase Field Models of Microstructure Development*

Dr. Jeffrey J. Derby, University of Minnesota ..... 185
*Atomistic Simulations of Cadmium Telluride: Toward Understanding the Benefits of Microgravity Crystal Growth*

## Table of Contents (cont'd)

Dr. Michael Dudley, State University of New York at Stony Brook..... 187
*Combined Synchrotron White Beam X-ray Topography and High Resolution Triple Axis X-ray Diffraction Characterization and Analysis of Crystals Grown in Microgravity and Ground-Based Environments*

Dr. Prabir K. Dutta, Ohio State University..... 193
*Reverse Micelle Based Growth of Zincophosphate Sodalite: Examination of Crystal Growth*

Dr. M. Samy El-Shall, Virginia Commonwealth University..... 199
*Studies on Nucleation, Polymerization, and Nanoparticle Composites in Supersaturated Vapors Under Microgravity*

Dr. Alexandre I. Fedoseyev, University of Alabama at Huntsville..... 205
*Investigation of Vibrational Control of the Bridgman Crystal Growth Technique*

Dr. Merton C. Flemings, Massachusetts Institute of Technology..... 211
*Alloy Undercooling Experiments in a Microgravity Environment*

Dr. Merton C. Flemings, Massachusetts Institute of Technology..... 217
*The Measurement of the Viscosity and Surface Tension of Undercooled Melts Under Microgravity Conditions and Supporting MHD Calculations*

Dr. Archibald L. Fripp, NASA Langley Research Center..... 223
*Compound Semiconductor Growth in Low-g Environment*

Dr. Archibald L. Fripp, NASA Langley Research Center..... 229
*Melt Stabilization of PbSnTe in a Magnetic Field*

Dr. Randall M. German, Pennsylvania State University ..... 235
*The Gravitational Role in Liquid Phase Sintering*

Dr. Donald C. Gillies, NASA Marshall Space Flight Center..... 241
*Solidification of II-VI Compounds in a Rotating Magnetic Field*

Dr. Martin E. Glicksman, Rensselaer Polytechnic Institute..... 243
*Isothermal Dendritic Growth Experiment*

Dr. Arun M. Gokhale, Georgia Institute of Technology..... 249
*Effect of Gravity on the Evolution of Spatial Arrangement of Features in Microstructure: A Quantitative Approach*

Dr. Richard N. Grugel, Universities Space Research Association..... 255
*Evaluation of Microstructural Development in Bulk, Undercooled Alloys*

Dr. Richard N. Grugel, Universities Space Research Association..... 261
*Novel Directional Solidification Processing of Hypermonotectic Alloys*

Dr. Richard N. Grugel, Universities Space Research Association..... 267
*Utilizing Controlled Vibrations in a Microgravity Environment to Understand and Promote Microstructural Homogeneity During Floating-Zone Crystal Growth*

## Table of Contents (cont'd)

Dr. William H. Hofmeister, Vanderbilt University ..... 273
*Microgravity Processing of Oxide Superconductors*

Dr. Douglas E. Holmes, Electronic Materials Engineering ..... 279
*Dimensional Stability of Supermatrix Semiconductors*

Dr. Kenneth A. Jackson, University of Arizona ..... 281
*Non-Equilibrium Phase Transformations*

Dr. William L. Johnson, California Institute of Technology ..... 287
*Physical Properties and Processing of Undercooled Metallic Glass Forming Liquids*

Dr. William L. Johnson, California Institute of Technology ..... 289
*Thermo-Physical Properties of Metallic Glasses and Undercooled Alloys – AC Modulation Calorimetry on the TEMPUS Facility*

Dr. Monica L. Kaforey, Case Western Reserve University ..... 293
*Dislocation Formation During Growth of Semiconductor Crystals*

Dr. Alain S. Karma, Northeastern University ..... 299
*Role of Dynamic Nucleation at Moving Boundaries in Phase and Microstructure Selection*

Dr. Mohammad Kassemi, Ohio AeroSpace Institute/NASA LeRC ..... 305
*Identification of Gravity-Related Effects on Crystal Growth From Melts With an Immiscibility Gap*

Dr. Joseph L. Katz, Johns Hopkins University ..... 311
*Measurement of Liquid-to-Solid Nucleation Rates in Undercooled Metallic Melts*

Dr. Kenneth F. Kelton, Washington University at St. Louis ..... 317
*Phase Formation and Stability: Composition and Sample-Size Effects*

Dr. Anantha Krishnan, CFD Research Corporation ..... 323
*Influence of Natural Convection and Thermal Radiation on Multi-Component Transport and Chemistry in MOCVD Reactors*

Dr. Shankar Krishnan, Containerless Research, Inc. ..... 329
*Containerless Optical Property Measurements on High Temperature Liquids*

Dr. David J. Larson, State University of New York at Stony Brook ..... 335
*Orbital Processing of Eutectics*

Dr. David J. Larson, State University of New York at Stony Brook ..... 337
*Orbital Processing of High Quality Zn-Alloyed CdTe Compound Semiconductors*

Dr. Sandor L. Lehoczky, NASA Marshall Space Flight Center ..... 339
*Crystal Growth of Selected II-VI Semiconducting Alloys by Directional Solidification*

## Table of Contents (cont'd)

Dr. Sandor L. Lehoczky, NASA Marshall Space Flight Center ..... 345
*Growth of Solid Solution Single Crystals*

Dr. Ben Q. Li, Louisiana State University ..... 351
*Study of Magnetic Damping Effect on Convection and Solidification Under G-Jitter Conditions*

Dr. Thomas A. Lograsso, Iowa State University..... 357
*Microstructural Development During Directional Solidification of Peritectic Alloys*

Dr. David H. Matthiesen, Case Western Reserve University ..... 363
*Diffusion Processes in Molten Semiconductors*

Dr. David H. Matthiesen, Case Western Reserve University ..... 369
*The Study of Dopant Segregation Behavior During the Growth of GaAs in Microgravity*

Dr. Tony Maxworthy, University of Southern California..... 373
*Numerical and Laboratory Experiments on the Interactive Dynamics of Hele-Shaw Flows and Directional Solidification*

Dr. Aleksandar G. Ostrogorsky, Rensselaer Polytechnic Institute ..... 379
*Space- and Ground-Based Crystal Growth Using A Magnetically Coupled Baffle*

Dr. Mark S. Paley, Universities Space Research Association ..... 385
*Gravitational Effects on the Morphology and Kinetics of Photo-Deposition of Polydiacetylene Thin Films From Monomer Solutions*

Dr. Witold Palosz, Universities Space Research Association..... 391
*Investigation of Convective Effects in Crystal Growth by Physical Vapor Transport*

Dr. John H. Perepezko, University of Wisconsin at Madison..... 397
*Analysis of Containerless Processing and Solidification Microstructures*

Dr. David R. Poirier, University of Arizona ..... 403
*Comparison of Structure and Segregation in Alloys Directionally Solidified in Terrestrial and Microgravity Environments*

Prof. Dennis Readey, Colorado School of Mines ..... 409
*The Effects of Gravity, Reaction Environment, and Composition on the Combustion Synthesis of the $TiB_2$-$TaB_2$ System*

Prof. Dennis W. Readey, Colorado School of Mines..... 415
*The Effects of Microgravity on Vapor Phase Sintering*

Dr. Liya L. Regel, Clarkson University ..... 421
*Detached Solidification: Steady State Results*

## Table of Contents (cont'd)

Dr. Won-Kyu X. Rhim, Jet Propulsion Laboratory ..... 427
*Thermophysical Property Measurements of Molten Semiconductors*

Dr. Won-Kyu X. Rhim, Jet Propulsion Laboratory ..... 433
*Undercooling Limits and Thermophysical Properties in Glass-Forming Alloys*

Dr. Michael B. Robinson, NASA Marshall Space Flight Center ..... 439
*A Study of the Undercooling Behavior of Immiscible Metal Alloys in the Absence of Crucible-Induced Nucleation*

Dr. Franz E. Rosenberger, University of Alabama at Huntsville ..... 445
*Self-Diffusion in Liquid Elements*

Dr. Charles S. Rosenblatt, Case Western Reserve University ..... 451
*Determination of the Surface Energy of Smectic Liquid Crystals From the Shape Anisotropy of Freely Suspended Droplets*

Dr. Albert Sacco, Worcester Polytechnic Institute ..... 457
*Modeling of Macroscopic/Microscopic Transport Phenomena in Zeolite Crystal Solutions Under Microgravity Conditions*

Dr. Jogender Singh, Pennsylvania State University ..... 463
*Gravitational Effect on the Development of Laser Weld-Pool and Solidification Microstructure*

Dr. N. B. Singh, Northrop-Grumman Corporation ..... 467
*Flight Experiment to Study Double-Diffusive Instabilities in Silver Doped Lead Bromide Crystals*

Dr. R. J. Slobodrian, Universite Laval ..... 475
*Fractal Aggregates in Microgravity*

Dr. Frans A. Spaepen, Harvard University ..... 481
*Kinetics of Nucleation and Growth From Undercooled Melts*

Dr. Doru M. Stefanescu, University of Alabama at Tuscaloosa ..... 487
*The Pushing/Engulfment Transition for Zirconia Particles in Aluminum and Zinc Matrices*

Dr. Ching-Hua Su, NASA Marshall Space Flight Center ..... 493
*Crystal Growth of ZnSe and Related Ternary Compound Semiconductors by Vapor Transport*

Dr. Frank R. Szofran, NASA Marshall Space Flight Center ..... 499
*Magnetic Damping of Solid Solution Semiconductor Alloys*

Dr. Daniel R. Talham, University of Florida ..... 505
*The Features of Self-Assembling Organic Bilayers Important to the Formation of Anisotropic Inorganic Materials in Microgravity Conditions*

## Table of Contents (cont'd)

Dr. Eugene H. Trinh, Jet Propulsion Laboratory ..... 511
*Dynamic Nucleation of Deeply Undercooled Melts and Measurement of the Surface Tension and Viscosity*

Dr. Rohit K. Trivedi, Iowa State University ..... 517
*Interface Pattern Selection Criterion for Cellular Structures in Directional Solidification*

Dr. James D. Trolinger, MetroLaser, Inc. ..... 523
*Investigation of the Effects of Microgravity on Transport Properties in a Virtual Space Flight Chamber*

Dr. Gretar Tryggvason, University of Michigan ..... 529
*Fundamentals of Mold Free Casting: Experimental and Computational Studies*

Dr. Peter W. Voorhees, Northwestern University ..... 535
*Coarsening in Solid-Liquid Mixtures*

Dr. John S. Walker, University of Illinois at Urbana ..... 541
*Models of Magnetic Damping for Semiconductor Crystal Growth in Microgravity*

Dr. Richard Weber, Containerless Research, Inc. ..... 547
*Process-Property-Structure Relationships in Complex Oxide Melts*

Dr. John S. Wettlaufer, University of Washington ..... 553
*Thin Film Mediated Phase Change Phenomena: Crystallization, Evaporation and Wetting*

Dr. Heribert Wiedemeier, Rensselaer Polytechnic Institute ..... 557
*Defect Generation in CVT Grown $Hg_{1-x}Cd_xTe$ Epitaxial Layers Under Normal and Reduced Gravity Conditions*

Dr. Heribert Wiedemeier, Rensselaer Polytechnic Institute ..... 561
*Vapor Transport Crystal Growth of Mercury Cadmium Telluride in Microgravity – USML-2*

Dr. William R. Wilcox, Clarkson University ..... 567
*Use of Microgravity to Control the Microstructure of Eutectics*

NASA Headquarters
Office of Life and Microgravity Sciences and Applications
Microgravity Science and Applications Division

# The 1996 Microgravity Materials Science

# NASA Research Announcement (NRA)

**Michael J. Wargo, Sc.D.**
michael@microgravity.msad.hq.nasa.gov
Program Scientist for Materials Science
June, 1996

# Microgravity Materials Science Research

- Goal: Use microgravity to seek and understand quantitative cause and effect relationships between the processing, properties and structure of materials.
  - Electronic and Photonic Materials
  - Metals and Alloys
  - Glasses and Ceramics
  - Polymers
- Current Research Areas:
  - Crystal Growth
  - Materials Solidification
  - Thermophysical Property Measurements

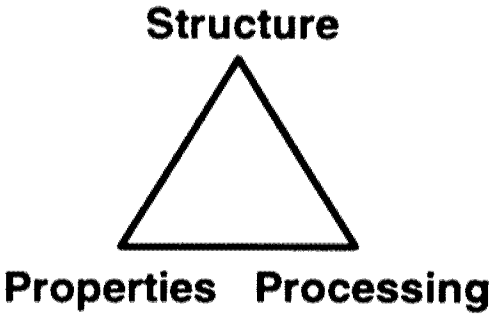


- Potential benefits:
  - Better understanding and control of materials properties for applications varying from high performance opto-electronic devices to corrosion resistant metals
  - Better understanding and prediction of microstructure controlled properties of cast metals and alloys
  - Improved utility of mathematical models for predicting materials properties during terrestrial processing

# Microgravity Materials Science

- **NASA Research Announcement (NRA)**
  - **Ground based research**
    - Provides the intellectual underpinnings of the flight program
    - Experimental and theoretical
    - Well articulated microgravity relevance
      - Demonstration of the role of gravity; benefits to be accrued from conducting research in microgravity
      - Support for the microgravity materials science program
    - Funding for up to 4 years
    - Average $100k/year
  - **Flight experiments**
    - High scientific and technical merit
    - Well articulated need for a long duration, high quality microgravity environment
    - Experimental and theoretical maturity to support a Science Concept Review within approximately two years
    - Average $175k/year

- **Advice from the Reviewers**
  - Reviewers appreciate clear and concise writing.
    - Proof read text and use clearly marked figures with appropriate captions.
  - Reviewers will not "read between the lines."
    - While they may be familiar with your previous work, they will not assume that you are aware of important issues unless you indicate them explicitly.
    - What materials are to be investigated (experimentally or theoretically)
  - Appendices and supplementary material should be added judiciously.
    - Reviewers appreciate inclusion of publication reprints that report previous results that are key to the success of the proposed work. However, these should be kept to an absolute minimum.

- **Proposals**
  - Schedule
    - NRA Release: Fall, 1996
    - Proposals Due: Spring, 1997
    - Reviews: Spring/Summer, 1997
    - Selections: Summer/Fall, 1997
  - Review Process
    - Panels: proposals grouped by common theme
    - Proposals initially read and evaluated by at least 3 reviewers
      - Lead Primary Reviewer
      - Second Primary Reviewer
      - Reader
    - Scoring is by panel consensus: It is the score of the panel, not individuals.
    - Significant emphasis on scoring consistency

- **Advice from the Reviewers (continued)**
  - Reviewers expect proposals written within the designated guidelines that provide the information required for evaluation.
    - In some cases microgravity relevance is vague or non-existent
    - Length (20 pages)
    - Supporting material (appendices/supplementary material)
    - Budget
  - Collaboration: Multiple Proposals vs Long, High Budget Proposals
    - Reviewers typically preferred separate proposals where clear indication was given to collaboration with other proposers.
    - Reviewers opined that large, expensive proposals were difficult to evaluate.
      - If they were within the length guideline, there was not enough detail concerning each part.
      - If they were outside the length guideline, reviewers saw this as unfair to other proposals that stayed within guideline.

**Mr. Robert C. Rhome, P.E.**
**Division Director, Microgravity Science and Applications Division**
**NASA Headquarters**

*Presentation charts from Monday's morning session*

Office of Life and Microgravity Sciences and Applications

# Microgravity Science and Applications FY 1996 Research Program

## Microgravity Science Principal Investigators

| Science Discipline | Ground-Based Principal Investigators | | Flight Definition Investigators | | Flight Principal Investigators | FY 96 Total | FY 95 Total | FY 94 Total |
|---|---|---|---|---|---|---|---|---|
| | Ongoing | New* | Ongoing | New* | | | | |
| Biotechnology | 51 | --- | 2 | --- | 5 | 58 | 60 | 24 |
| Combustion Science | 27 | 14 | 6 | 1 | 7 | 55 | 43 | 43 |
| Fluids & Transport Phenomena | 36 | 33 | 8 | 7 | 9 | 93 | 78 | 81 |
| Materials Science | 23 | 24 | 8 | 4 | 12 | 71 | 76 | 72 |
| Low Temperature μg Physics | 11 | 9 | 2 | --- | 3 | 25 | 19 | 23 |
| Sub-Total | 148 | 79 | 26 | 12 | | | | |
| Total | 225 | | 38 | | 36 | 298 | 276 | 243 |

Note: "New*" represents PIs who were not funded in FY 95 and who were selected for FY 96 funding from peer-reviewed proposals submitted in response to a NASA Research Announcement in that discispline.



RCR MSAD 05/01/96

Office of Life and Microgravity Sciences and Applications

# Microgravity Science and Applications FY 1996 Research Program

## Microgravity Science Principal Investigators

| Science Discipline | Ground-Based Principal Investigators | | Flight Definition Investigators | | Flight Principal Investigators | FY 96 Total | FY 95 Total | FY 94 Total |
|---|---|---|---|---|---|---|---|---|
| | Ongoing | New* | Ongoing | New* | | | | |
| Biotechnology | 51 | — | 2 | — | 5 | 58 | 60 | 24 |
| Combustion Science | 27 | 14 | 6 | 1 | 7 | 55 | 43 | 43 |
| Fluids & Transport Phenomena | 36 | 33 | 8 | 7 | 9 | 93 | 78 | 81 |
| Materials Science | 23 | 24 | 8 | 4 | 12 | 71 | 76 | 72 |
| Low Temperature μg Physics | 11 | 9 | 2 | — | 3 | 25 | 19 | 23 |
| Sub-Total | 148 | 79 | 26 | 12 | | | | |
| Total | 225 | | 38 | | 36 | 298 | 276 | 243 |

Note: "New*" represents PIs who were not funded in FY 95 and who were selected for FY 96 funding from peer-reviewed proposals submitted in response to a NASA Research Announcement in that discispline.

RCR MSAD 05/01/96

Office of Life and Microgravity Sciences and Applications

# Development of the Microgravity Science Research Community

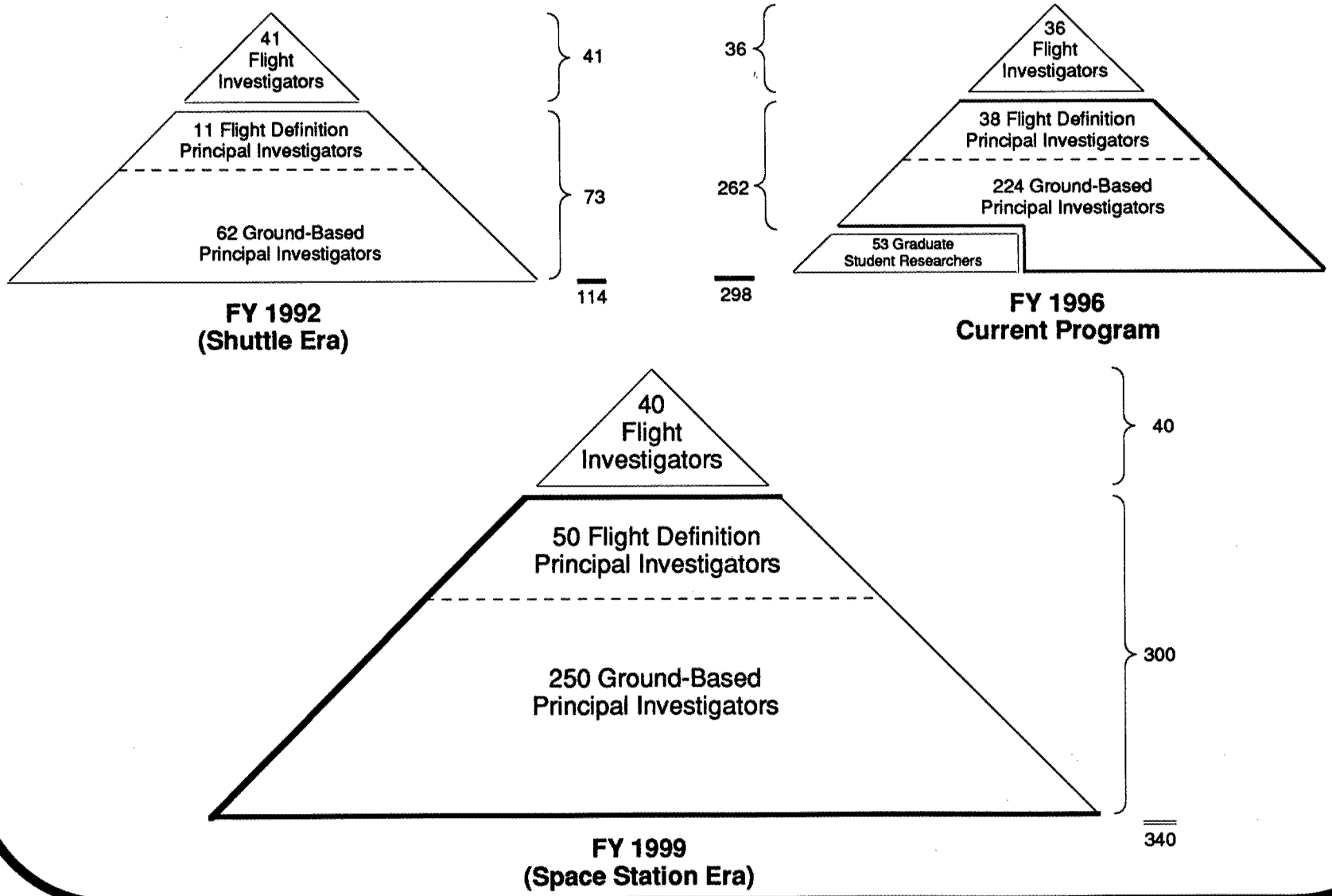


RCR/UG 06/08/95

Office of Life and Microgravity Sciences and Applications

# Development of the Microgravity Science Research Community

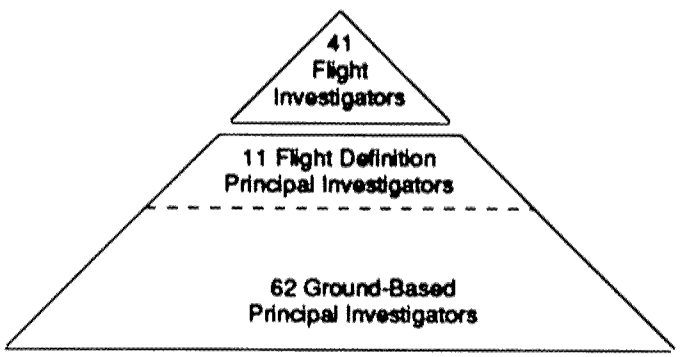


41

73

114

**FY 1992**
**(Shuttle Era)**

36

262

298

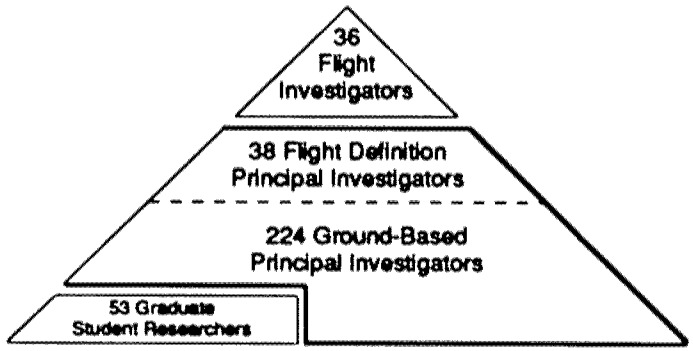


**FY 1996**
**Current Program**

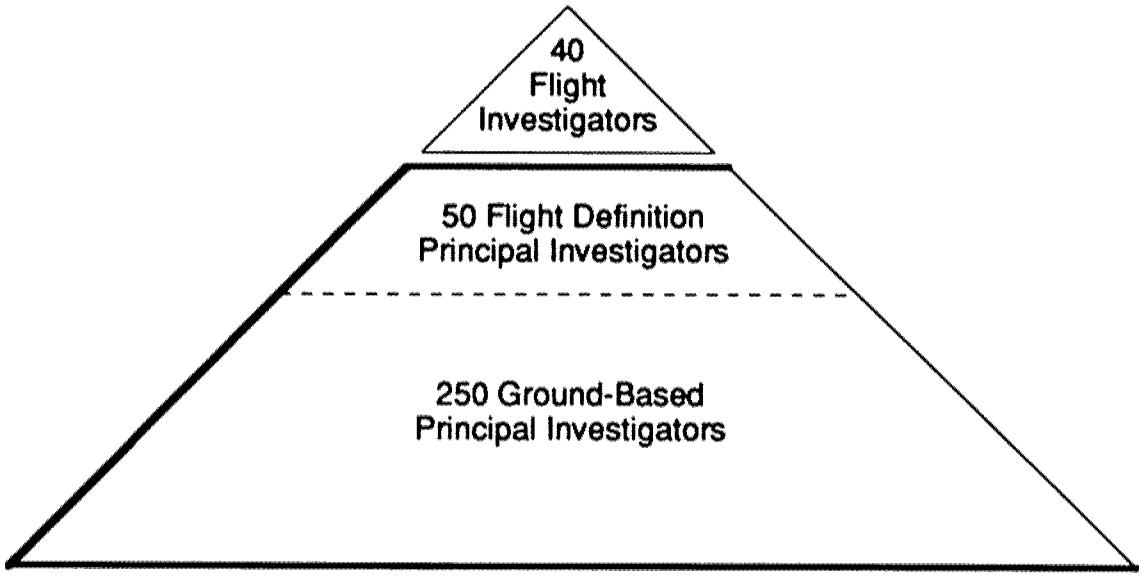


40

300

340

**FY 1999**
**(Space Station Era)**

RCR/UG 06/08/95

# MICROGRAVITY MATERIALS SCIENCE CONFERENCE

Von Braun Civic Center
Huntsville, AL
June 10-11, 1996

Topics of Interest in
Microgravity Materials Science

J. H. Perepezko
University of Wisconsin-Madison

June 10, 1996

MSAD Materials Science Discipline Working Group:

- Professor John H. Perepezko (chair), University of Wisconsin
- Dr. Frank R. Szofran (vice-chair), NASA-Marshall
- Professor Timothy Anderson, University of Florida
- Professor Jonathan Dantzig, University of Illinois
- Dr. Richard H. Hopkins, Northrop Grumman Science and Technology Center
- Professor Dennis W. Readey, Colorado School of Mines
- Professor Rohit Trivedi, Iowa State University
- Professor Peter W. Voorhees, Northwestern University
- Dr. Michael J. Wargo, NASA Headquarters

# MATERIALS SCIENCE DISCIPLINE

Goals

- Develop the basic understanding of relationships between microstructure and properties of materials during microgravity processing.

- Apply process modeling and advanced processing concepts to achieve designed microstructures.



Objectives

- Utilize the microgravity environment to advance the understanding of materials processing, including phase transformations during solidification and deposition, transport phenomena and structure-property relationships.

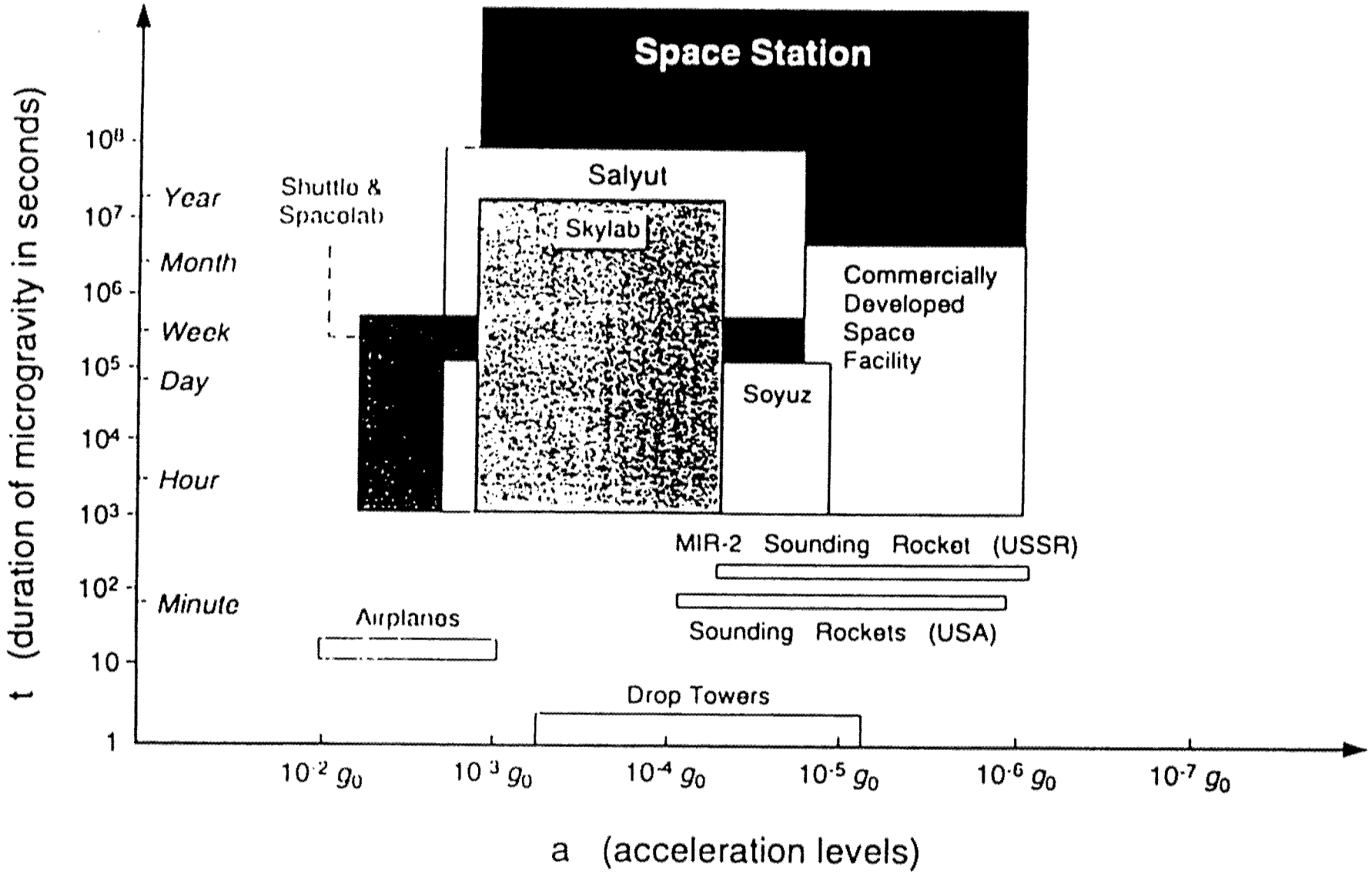


**FIGURE 1** Characteristic duration and acceleration levels. SOURCE: Microgravity Science and Applications Division, NASA.

| Microgravity Environment | Materials Response |
|---|---|
| • Buoyancy Driven Convection Flows Minimized | Precise Temperature and Composition Control for High Quality Crystals |
| • Body Force Effects Minimized | Uniform Spacing and Alignment in Multiphase Materials |
| • Containerless Melt Processing | Eliminate Contamination and Nucleation Due to Containment |
| • Interfacial Phenomena | Wetting and Surface Energy Driven Flows |

Benchmark Materials

## Priorities

### Technological Applications

> Containerless Processing
> Directional Solidification/Crystal Growth
> Casting

### Science Knowledge Base

1. Solidification Kinetics and Undercooling
2. Microstructural Morphology/Prediction
3. Process Analysis and Modeling
4. Interfacial Phenomena

### Critical Support Base

- Ground based experience
- Thermophysical property data

# Research Areas

- Solidification Kinetics and Undercooling

  - Nucleation
  - Undercooling
  - Metastable Phase Development
  - Competitive Growth
  - Microstructural Transitions
  - Glass Formation

- Microstructural Morphology/Prediction

  - Plane Front Solidification

    > Single Crystals
    > Aligned Composites
    > Phase Spacing

- Interface Instability

  > Cells
  > Dendrites
  > Segregation

- Microstructural Scale

  > Coarsening/Coalescence
  > Scaling Laws

- Process Analysis and Modeling

  > Macrosegregation
  > Heat and Mass Transport Analysis
  > Structure Prediction

- Interfacial Phenomena

  > Surface Energy Driven Flows
  (Temperature or Composition Gradients)
  > Particle Incorporation
  > Wetting Behavior
  > Bubble Formation - Porosity Control
  > Joining Applications

## A LESSON

There is abundant and compelling evidence that any space experiment must be planned, executed, and analyzed carefully following the knowledge base developed from terrestrial studies. When this approach has been pursued, real progress and significant advancement of microgravity science have been achieved.

## General Issue

Reliable Processing and Analysis Models Based on a Sound Ground Based Experience and Established Thermophysical Properties are Essential. ALL Microgravity Materials Science Studies Should be Designed, Executed and Interpreted on This Basis.

# Solidification Processes

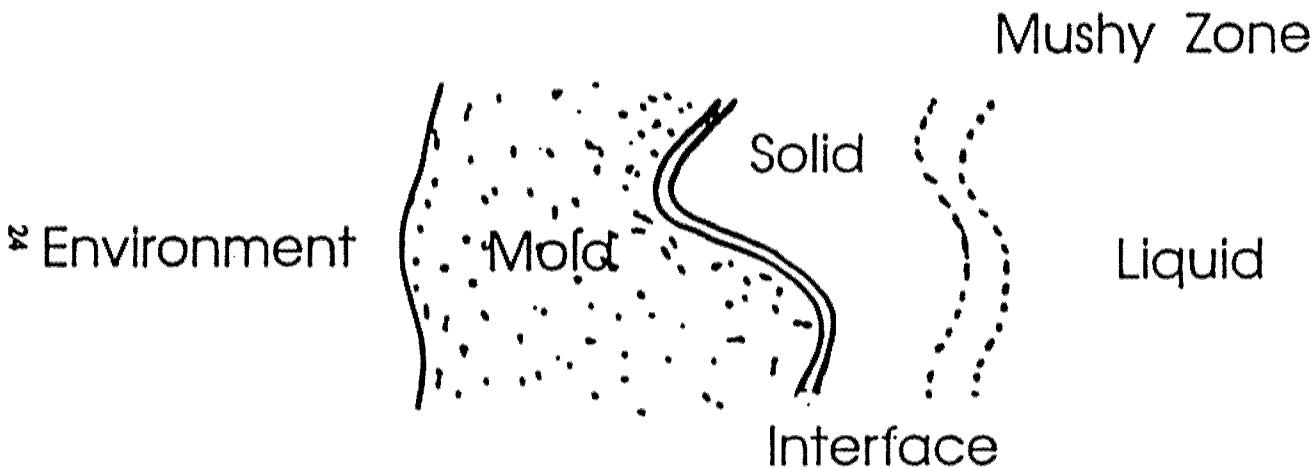


Heat Transfer Coefficients
- Interface, environment

Heat evolution
- Mushy zone model

Material properties

# Process Analysis and Modeling

- Assess role of individual variables
- Control and Vary Independently Process Parameters
- Reduce Complex Processes to Fundamental Units
- Explore Regimes Unavailable to Experiment
- Design Experiments to Emphasize Phenomena of Interest
- Interpret Results
- Improve Yield from Microgravity Experiments

# Thermophysical Properties

- Emissivity, Electrical Conductivity, Optical Properties
- Calorimetry
  - Specific heats
  - Heats of mixing, formation, transformations, ...
- Transport Coefficients
  - thermal conductivity
  - viscosity
  - diffusion constants
- Density Data
- Thermodynamic Modulii
  - thermal expansion coefficients
  - compressibility, etc.
- Vapor Pressures and Activity Coefficients
- Surface Tension/Interfacial Energies

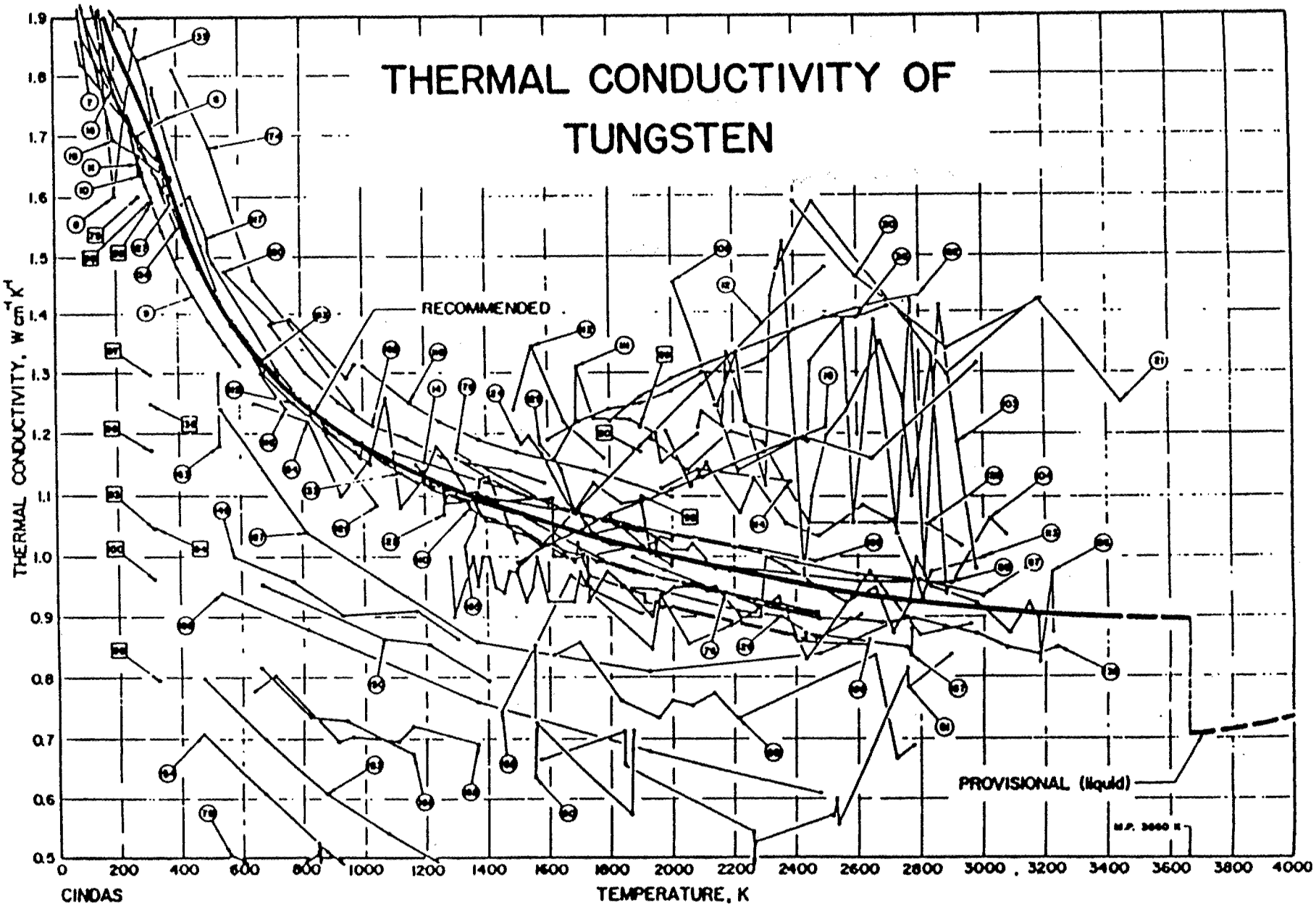
THERMAL CONDUCTIVITY OF TUNGSTEN
RECOMMENDED
PROVISIONAL (liquid)
M.P. 3660 K
THERMAL CONDUCTIVITY, W cm⁻¹ K⁻¹
TEMPERATURE, K
CINDAS
1.9
1.8
1.7
1.6
1.5
1.4
1.3
1.2
1.1
1.0
0.9
0.8
0.7
0.6
0.5
0
200
400
600
800
1000
1200
1400
1600
1800
2000
2200
2400
2600
2800
3000
3200
3400
3600
3800
4000

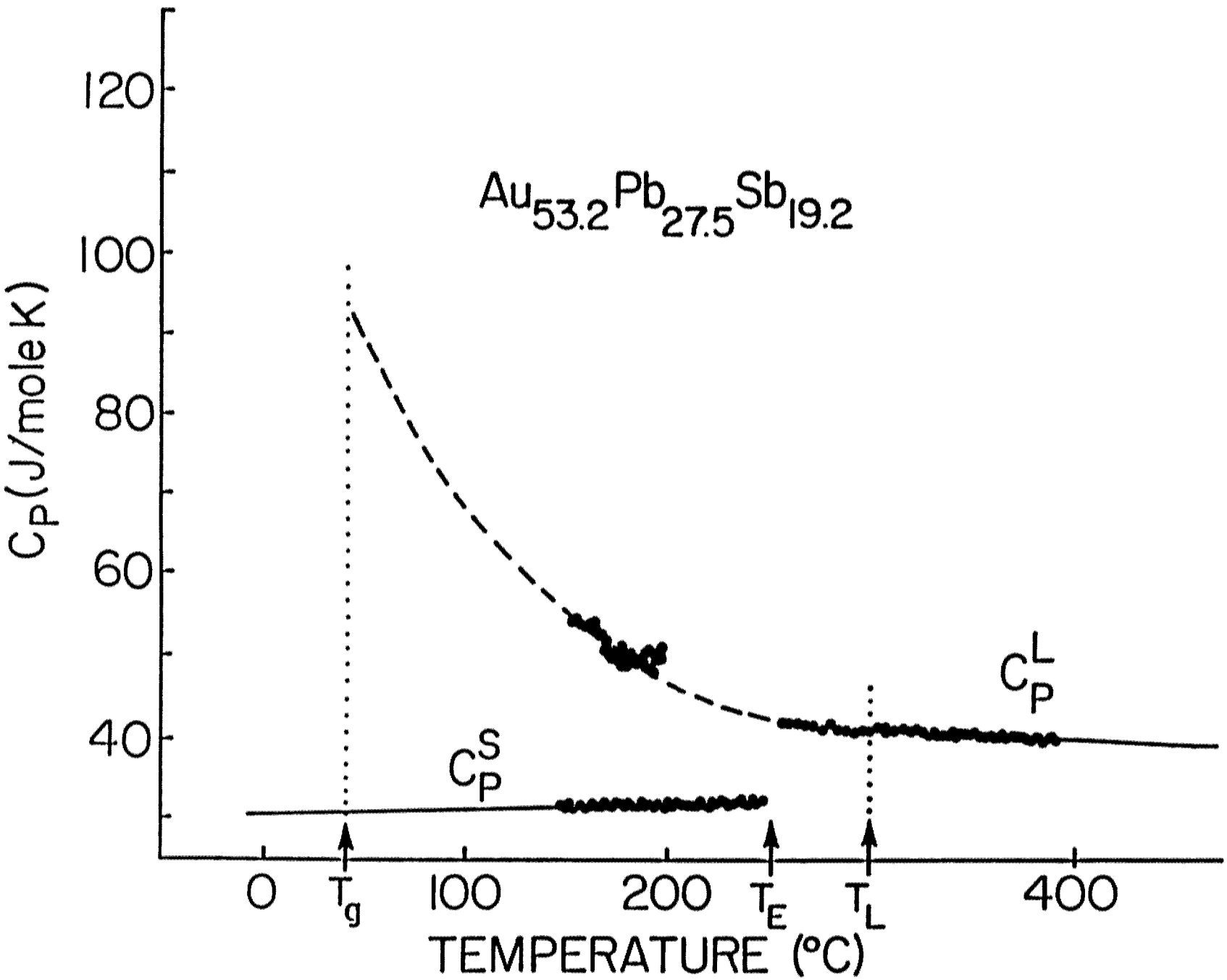
$Au_{53.2}Pb_{27.5}Sb_{19.2}$
$C_P$ (J/mole K)
120
100
80
60
40
$C_P^S$
$C_P^L$
0
$T_g$
100
200
$T_E$
$T_L$
400
TEMPERATURE (°C)

# Experimental Results

$$D = AT^2$$

| | Experiments | T [°C] | A [$10^{-11}\frac{cm^2}{sK^2}$] | Mission |
|---|---|---|---|---|
| Sn(Sn112) | 5 | 270-775 | 7.53 | FSLP |
| Sn(Sn124) | 5 | 270-775 | 7.33 | FSLP |
| $In_{80}Sn_{20}(Sn124)$ | 4 | 260-900 | 8.97 | D1 |
| $In_{80}Sn_{20}(In113)$ | 4 | 260-900 | 8.03 | D1 |
| $In_{85}Sn_{15}/In_{75}Sn_{25}$ | 4 | 260-900 | 7.58 | D1 |
| In(In113) | 2 | 250-750 | 8.32 | D2 |
| Pb(Pb204) | 6 | 350-1055 | 5.06 | D2 |
| Sb(Sb123) | 2 | 700-800 | 6.32 | D2 |
| Sn(In) | 6 | 350-1055 | 8.00* | D2 |
| In(Sn) | 2 | 250-750 | 9.50 | D2 |

*: $D = AT^2 + B$ with $B = 1.1 \cdot 10^{-5}\frac{cm^2}{s}$.

# Different Theories:

Arrhenius: $$D = D_0 \exp\left(-\frac{Q}{kT}\right)$$

Vortex(Frohberg): $$D = \frac{r^2 \nu_0}{2z^2 Q^2}(kT)^2$$

Hard Spheres(Enskog): $$D = \frac{3}{8}\sigma(T)\frac{\pi}{6\xi g(\sigma)}\sqrt{\frac{kT}{\pi M}}$$

Eyring(Hicter): $$D = B \cdot T + D_0 \exp\left(\frac{-Q}{kT}\right)$$

# Selfdiffusion Lead
# Pb204 in Pb

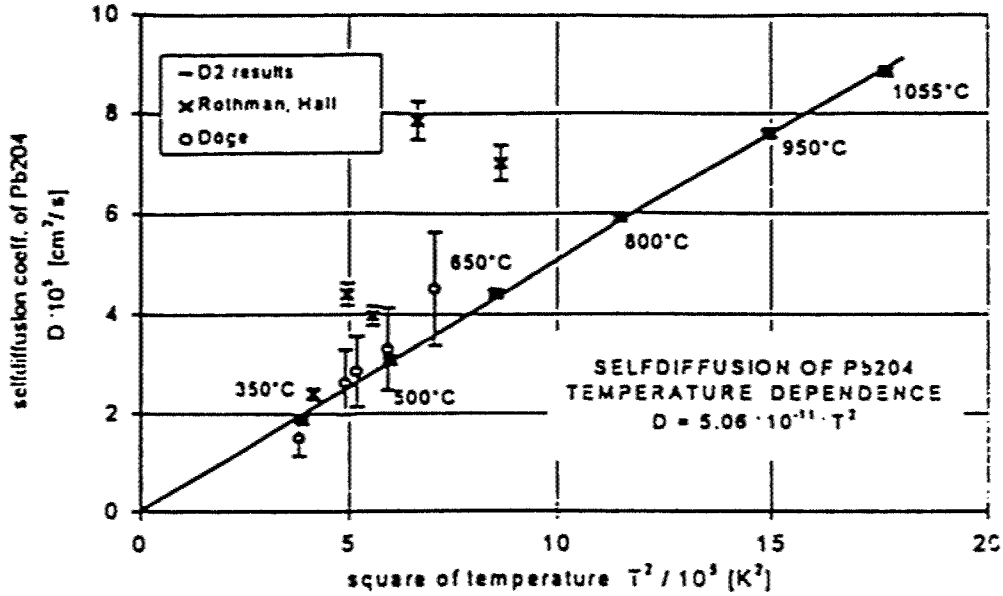


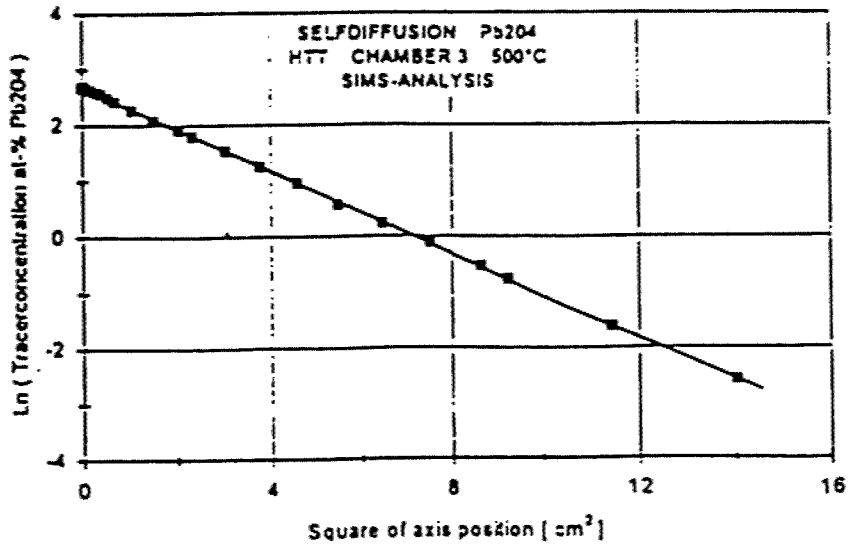

# BENCHMARK EXPERIMENTS

Benchmark Experiments are designed to achieve a measurement accuracy not possible in a one gravity environment. This would imply testing of theories to new levels of resolution that will serve as a standard for years. This area encompasses research on transient and equilibrium phenomena, as well as other thermophysical measurements of interest to Materials Science.

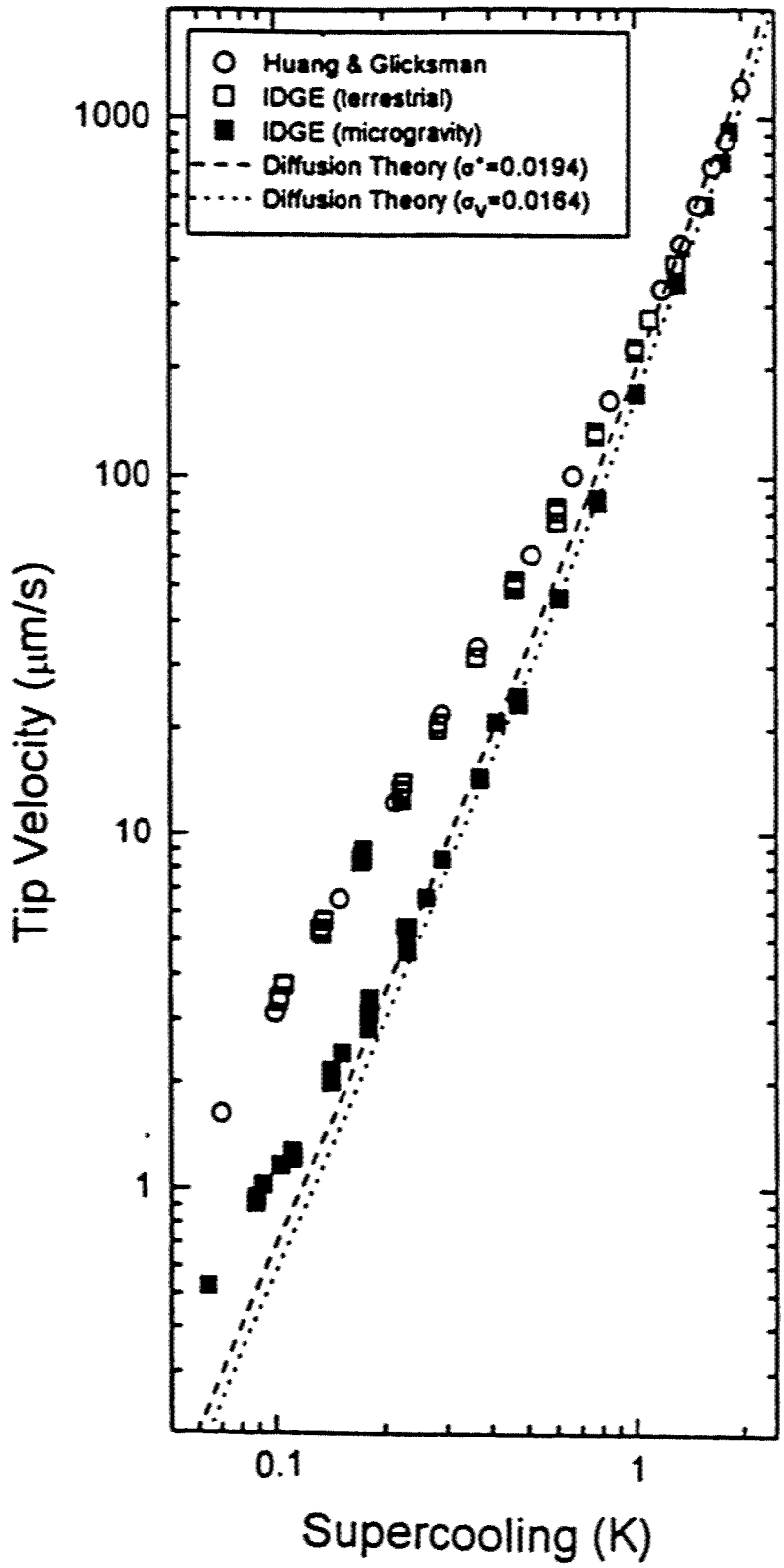


**Fig. 3.** Plot of dendrite tip velocity as a function of supercooling for both terrestrial, and microgravity data sets.

# A-1. DENDRITE COARSENING

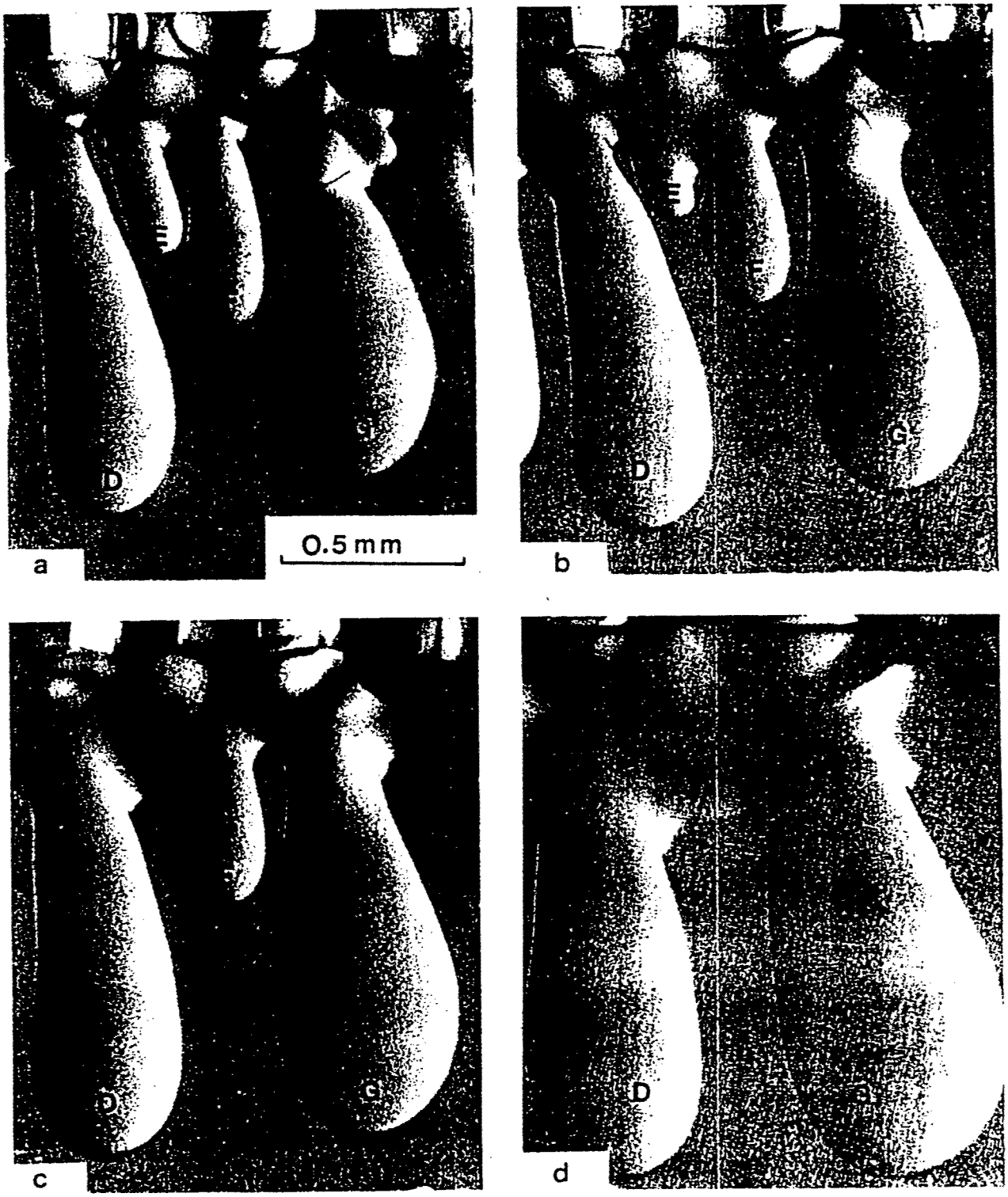


CD-85-16832

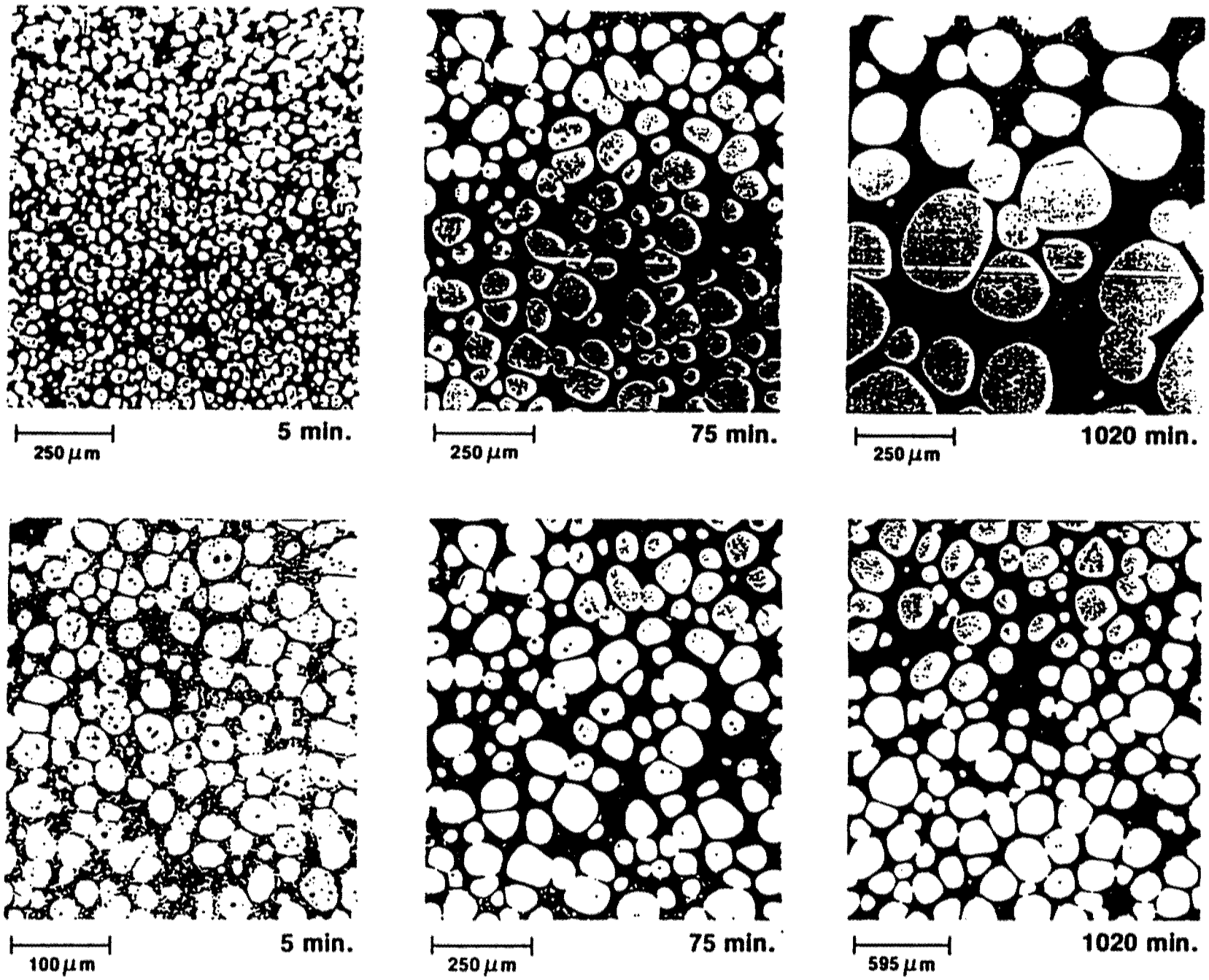
250 μm
5 min.
250 μm
75 min.
250 μm
1020 min.
100 μm
5 min.
250 μm
75 min.
595 μm
1020 min.

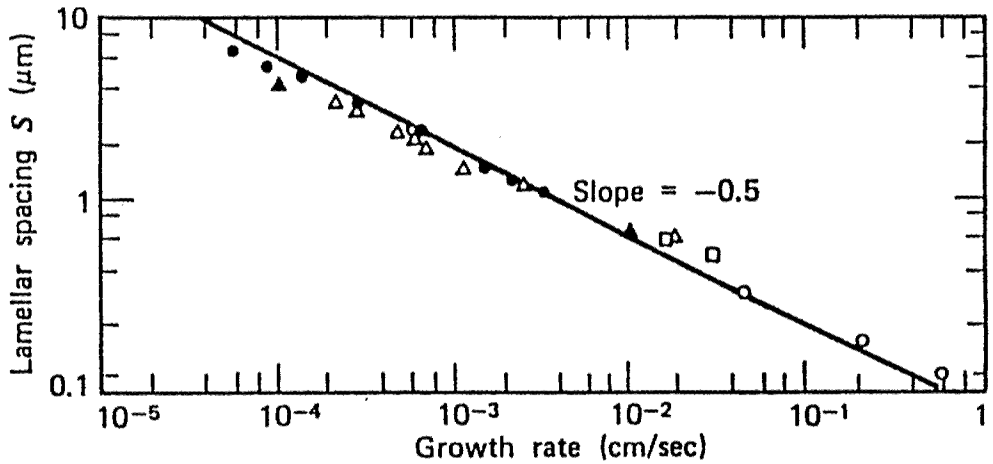


***Figure* 9.38** Summary of experimental data on lamellar spacing versus rate of solidification in Pb–Sn alloys [From H. E. Cline and J. D. Livingston, Trans. Met. Soc. AIME **245**, 1990 (1969).]

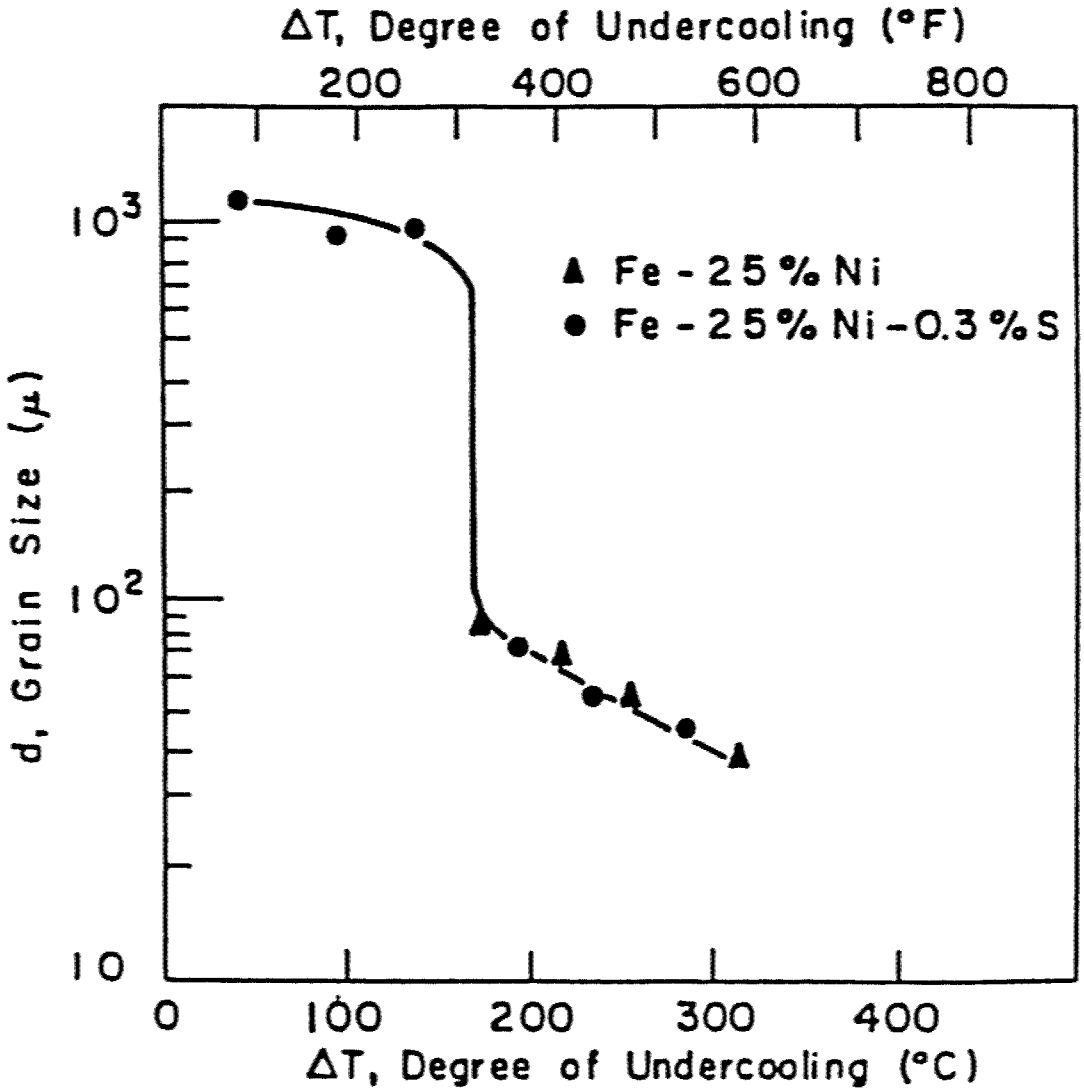
ΔT, Degree of Undercooling (°F)
200
400
600
800
$10^3$
$10^2$
10
d, Grain Size (μ)
▲ Fe - 25% Ni
● Fe - 25% Ni - 0.3% S
0
100
200
300
400
ΔT, Degree of Undercooling (°C)

# Research Areas in Electronic Materials

- Convection and segregation effects during physical vapor transport growth (examples, HgCl, ZnSe, SiC).

- Segregation, convection, and double diffusive transport during directional freezing of optical and semiconductor crystals (e.g. $PbBr_2$, bismuth germanium oxide, dinitrobenzene, GaAs).

- Marangoni and thermally-driven convective fluid flow behavior during solution growth (e.g. TGS, KDP).

- Solidification of semiconductor alloys with wide miscibility ranges (e.g. Si-Ge).

- Containerless processing of high purity semiconductor and superconductor crystals (e.g. yttrium barrier copper oxide).

- Solidification of uniform binary organic materials with large nonlinear optic coefficients (e.g. m- Nitroaniline-Cl-Nitroaniline).

- Marangoni effects during liquid encapsulated Bridgman growth (e.g. GaAs).

- Magnetic damping effects during directional crystal growth.

- Reduction of stress generation and twinning during directional freezing (e.g. CdTe).

- Defect Generation - Knowledge is largely empirical. Influenced by melt flow.

  > Growth Rate and Flow Contributions
  > Concentration and Distribution
  > Explanation for Reduction in μg

**Defect Structures for USML-1/$Cd_{96}Zn_{04}Te$/Primary**

1-g (200x) μ-g (200x)

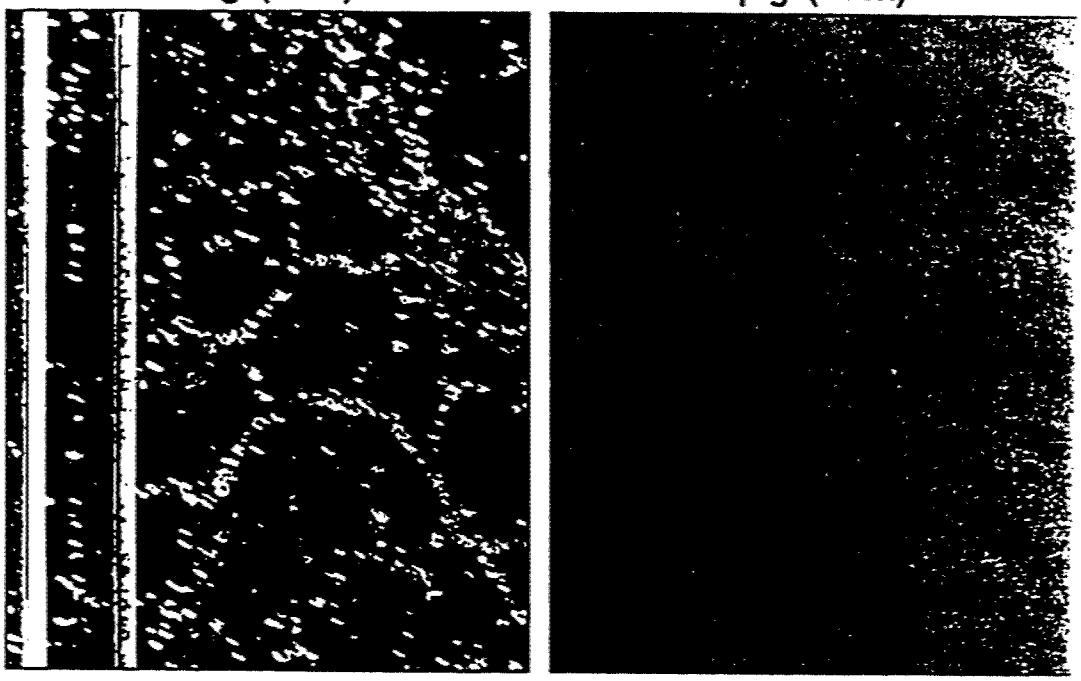

**Defect Structures for USML-1/$Cd_{96}Zn_{04}Te$/Secondary**

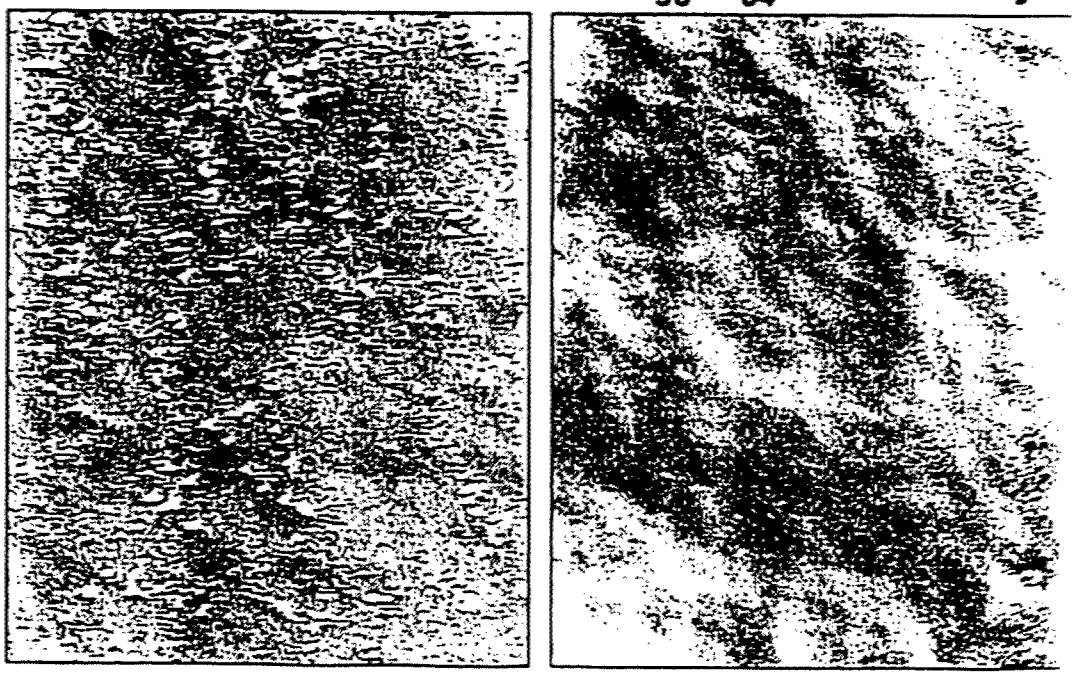

Dr. David Larson.

# Research Areas in Glasses and Ceramics

Containerless Processing
Epitaxial and Single Crystal Growth
Glass Formation
Nucleation
Surface and Interfacial Phenomena
Glass Processing (Fining)
Composite Formation
Fiber/Whisker Fabrication
Foam Production
Bulk Transport Phenomena
Crystal Growth
Phase Separation
Bubble Dynamics
Glass Processing (Melting and Homogenization)
Ceramic Powder Processing/Sintering
Joining
Gas Phase Processing/CVD
Thermophysical Properties
Chemical Reaction and Kinetics
Colloid Processing
Combustion Synthesis
FGM
Granular Material Flow
Non-Contact Shaping

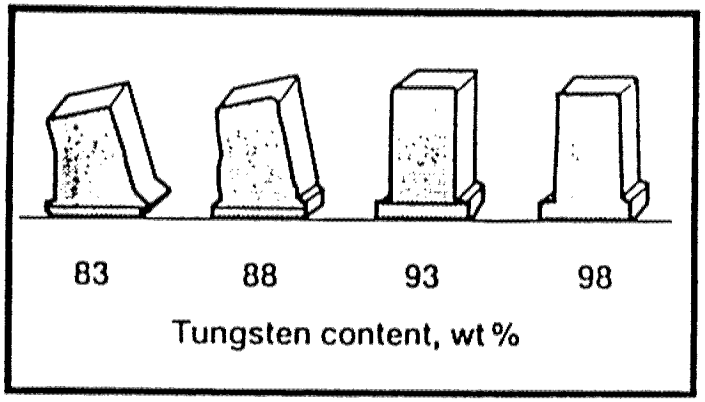


*Figure 2.—Slumping of samples with low W content sintered in gravity at 1477 °C for 30 min. Ratio of Ni to Fe, 7:3.*

Prof. R.M. German
Penn State

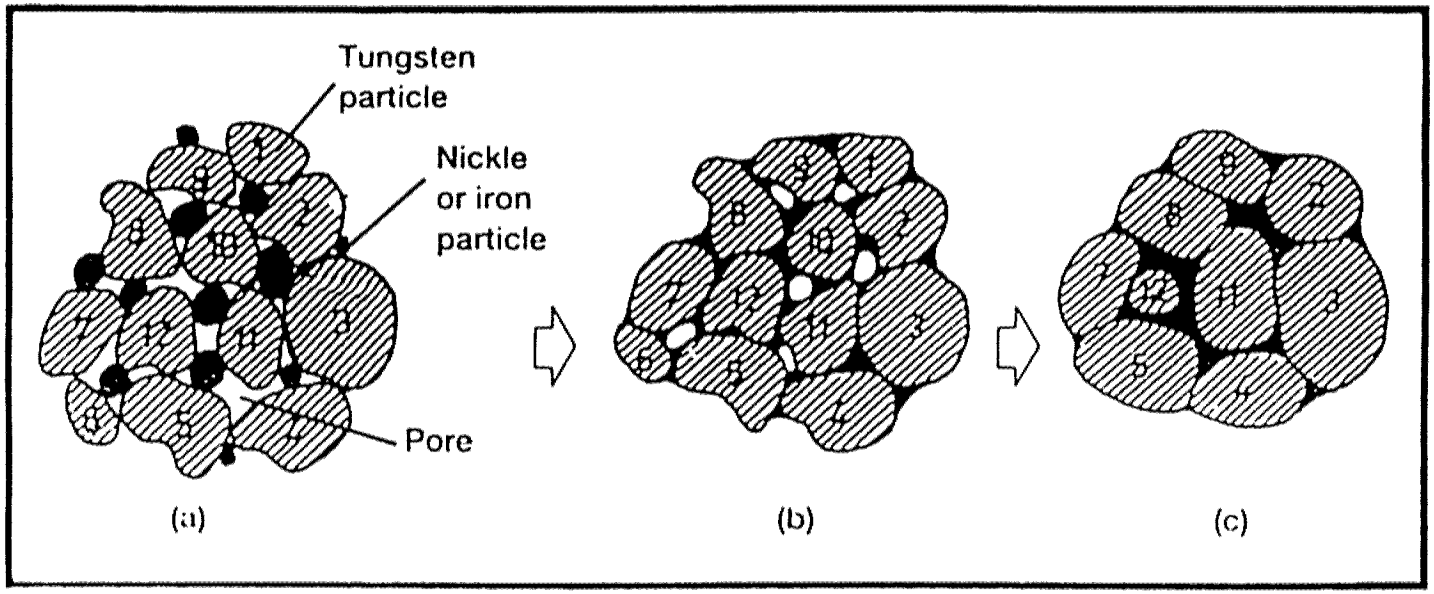


*Figure 4.—Classic stages of liquid-phase sintering involving powders that form a liquid on heating. (a) Presintered. (b) Sintered for 1 min (liquid formation and spreading). (c) Sintered for 15 min (complete densification).*

# Research Areas in Polymers and Macromolecules

Areas of interest:

- Non-linear optical materials
- Solvent selection
- Monomer synthesis
- Processing
  - vapor deposition
  - photopolymerization
  - sol-gel
  - solution growth

Fundamental phenomena:

- Polymerization mechanisms
- Nucleation phenomena
- Growth kinetics
- Effects of convection
- Morphological studies
- Defect Concentration (esp. NLO)
- Stratification (particles and aggregates) and anisotropy

SEM micrographs of 1μm thick films of copper phthalocyanine deposited during STS-20 flight and ground control - Courtesy of 3M Corporation

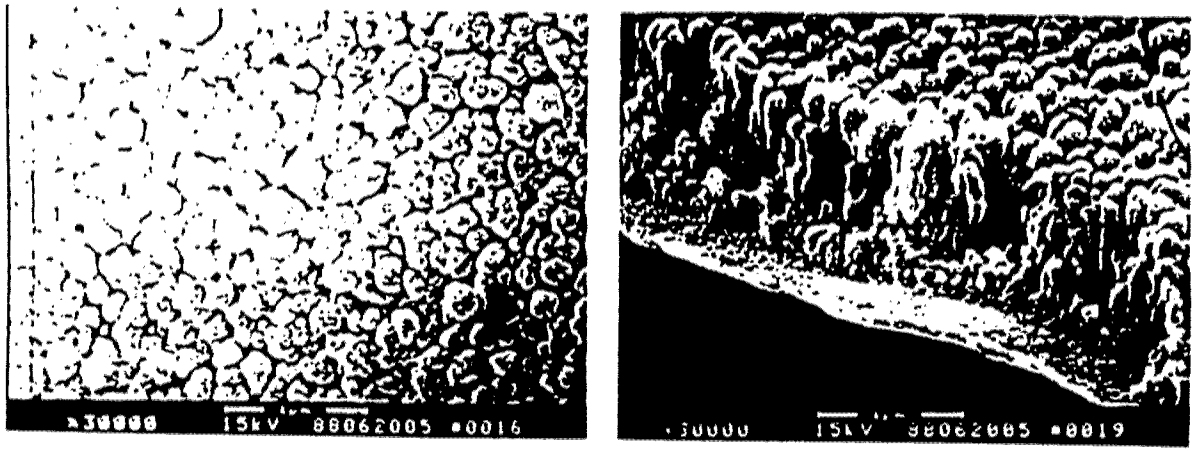


micro-g

30,000X

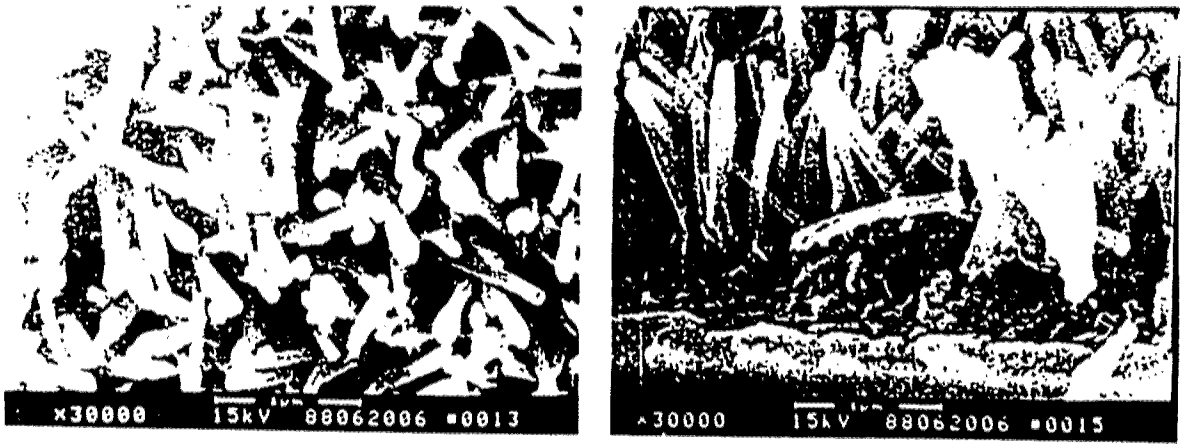


unit-g

0

45 Deg. View

# RESEARCH OPPORTUNITIES

- Electrodeposition
- Joining
- Novel Materials
- Extraterrestrial Materials (HEDS)

# Microgravity Materials Science: Ground and Flight Research Resources and Procedures

Robert Snyder

Joel Kearns

June 10, 1996

# Resources

- Science, Engineering and Management Staff - 30 years of Experience
- Ground Research Facilities/Support
- Definition of Objectives/Requirements
- Flight Experiment Technology
- Scientific Flight Apparatus
  - Existing
  - To New Specifications

# Resources

- International Cooperation
- MEPHISTO (CNES)
- TEMPUS (DARA)
- AGHF (ESA)
- LIF (NASDA)
- MIM (CSA)

# Resources: Ground Based

- Drop Towers and Tubes (MSFC/LeRC)
- DC-9 Parabolic Aircraft (LeRC/DFRC)
  - Aircraft Apparatus
- Specialized Apparatus/Instrumentation

# Resources: Near-Term Flight

- LMS Mission (1996)
  - PEP/CGH using AGHF
- MSL-1 Mission (1997)
  - LPS/DPIMS using LIF
- USMP-4 Mission (1997)
  - AADSF/IDGE/MEPHISTO
- Glovebox Investigations (Shuttle & Mir)
- Small Apparatus for Shuttle Middeck

# Resources: Space Station

- EXPRESS Rack for Small Apparatus - 1999
- Microgravity Sciences Glovebox - 1999
- Space Station Furnace Facility - 2000
- High Gradient Furnace with Quench - 2000
- Low Gradient Furnace (ESA) - 2001
- MSP-1 Mission (2001)
- Additional Apparatus to Follow

# Procedures: Flight

- Science Concept Review
  - Science Objectives/Requirements
  - Experiment/Apparatus Concept
  - Evaluation by Peers
- Requirements Definition Review
  - Experiment/Project Plan
  - Evaluation by Peers

# MICROGRAVITY MATERIALS SCIENCE: GROUND-BASED AND FLIGHT RESEARCH RESOURCES AND PROCEDURES

Robert S. Snyder
Chief, Microgravity Science and Applications Division
NASA Marshall Space Flight Center

This paper will mainly concentrate on the ground-based and flight programs and the procedures necessary to accomplish them. As most of you already know, one joins the microgravity science program by writing a proposal in response to one of our bi-annual NASA Research Announcements (NRA's). In addition to the rigorous peer review that your proposal receives for the science you propose, your proposed need for a microgravity environment is carefully evaluated. The maturity of your science and your reasons for doing the experiment in space divide the proposals into those recommended for ground-based research and those recommended for flight definition.

This division of the research program became necessary after the early days of microgravity science when all good proposals were put into the flight program. As we have developed an understanding of the microgravity environment with its advantages and limitations, our opportunities to fly have not increased as fast as the number of excellent proposals we receive. We have also appreciated that the ground-based program provides a way to develop a good idea wherein the precise role of gravity can be defined and analyzed before incurring the pressures of a flight experiment.

The microgravity environment is different than your laboratory in more ways than just the gravity level. As a result, NASA has developed specific ways of helping you to get your experiment into orbit. These processes have evolved into a fairly complex system that is very strange to the neophyte scientist who is used to directing his or her own experiments in the laboratory down the hall. Although the Space Shuttle was originally planned to be a familiar environment for scientists with easy access to the racks using commercial instrumentation, the reality is significantly different.

Since access to the Space Shuttle and its resources are more limited than first anticipated, NASA has developed procedures to assure that only the best experiments will go into space. Grouping experiments together so they can share a single facility and its resources is one way of maximizing access to the limited resources available on orbit. The facility

must balance all of the many scientists' needs and compromise is necessary in many areas. However, each scientist has certain basic requirements that must be met for his or her experiment's success.

These statements and explanations of what is needed in terms of experiment operation and performance to satisfy the objectives becomes an agreement between the Principal Investigator and NASA. It sets forth a clear understanding of the science objectives for space. The Science Requirements Document supersedes the original proposal and becomes the major document used by project managers and engineers to define the experiment. Changing or augmenting the Science Requirements Document is difficult once the facility and its supporting documentation for the mission takes shape. Enumerating the various reviews of safety, hardware verification, and testing is unnecessary, but these reviews do assure that the hardware will function as defined. Although the NASA system is cumbersome, it does work. If the Science Requirements Document is clearly understood by the scientists and engineers, and the facility is designed and tested to satisfy these requirements, reliable experimental results will be produced. In many cases, these results will be unanticipated but this will rarely be due to the hardware.

Assuming that the science research and hardware develop according to schedule and costs, the next challenge is how the science is to be done in the facility once it's in space. The simple answer is that you write procedures for somebody else to do your experiment. However, the way you would do your experiment must be put into a format that the engineers planning the resources and facility operations will understand and interpret correctly. Preparing these procedures can be as important as developing the facility itself. Finally, when the time comes for your experiment to fly in space, you must proceed through a cadre of mission operations personnel who have translated your science requirements and procedures into NASA's own functional objectives, experiment timelines, and training manuals.

Although this process is not what was visualized when the Principal Investigator was first accepted into the flight definition program, there is help available. NASA has tasked civil service scientists in materials science, most with Ph.D.'s, to work with you in getting your experiment into space. When a flight definition experiment Principal Investigator is named, a NASA Project Scientist is assigned to answer questions and interface with other

NASA personnel. The Project Scientist will spend a significant amount of his or her time helping to get the experiment into orbit.

The system is complex, but the results from space have been exciting. As the microgravity science program evolves and all parties become more comfortable with this strange way of doing science, we can look forward to new discoveries and new challenges. It is important to remember that acceptance into the flight program brings the scientist into contact with many new people and their part of the experiment. Use your NASA Project Scientist to understand how these other team members can help you.

# GROWTH OF FACETED CRYSTALS: STABILITY, FLOWS, DEFECTS

A.A. Chernov
Universities Space Research Association
4950 Corporate Drive, Suite 100
Huntsville, AL 35806
Tel: 205-895-0582 or 205-544-9196
Fax: 205-895-9222 or 205-544-8762

Recent precise microgravity experiments [1] and related calculations [2] give us more confidence that the physics of instability of a growing rough interface is adequately reflected quantitatively by the picture developed since the mid-century. Still it remains much room to elaborate behavior of dissipative structures in poly- and even in one-component systems with rough interface.

Growth of a rough interface is determined by the isotropic interfacial kinetic coefficient and interfacial stiffness. Interface kinetics is also so fast that transport phenomena determine growth rate at the radii of the interface curvature exceeding ca. $10\mu m$ or even less. If, however, the growing interface is singular the interface kinetics is strongly (and singularly) anisotropic and slow enough to control even growth rate of the mm-size crystals not saying on their polygonal shape. Growth rate is determined not only by molecular incorporation at steps (i.e. not on the whole surface) but also by step generations by dislocations and 2D nucleation [3]. These circumstances make the growth kinetics of faceted crystals much more complex and provide more space for coupling of transport and non-linear interfacial phenomena.

This overview [4-9] talk was focused on stability of an infinite vicinal interface growing by propagation of equidistantly separated elementary steps. The problem is: will such step train pertain regular equidistant arrangement or will it transform by itself into bunches of steps alternated by low step density regions?

Our earlier experiments with $NH_4H_2PO_4$ (ADP) crystals discovered that if mother aqueous solution flows in the same direction as the steps the flow induces strong destabilization [4]. Mutually opposite step and solution flows are stabilizing. This destabilization and stabilization are

caused by solution flow drag of the inhomogeneous diffusion field within the boundary layer just above the growing perturbed surface with inhomogeneously distributed steps. This diffusion field inhomogeniety is strong because the incorporation rate at the interface is proportional to the step density so that the logarithmic derivative of the interface kinetic coefficient $\simeq 1/\bar{p}$, $\bar{p}$ being the vicinal slope of the unperturbed interface. Typically, $\bar{p} \simeq 10^{-2} - 10^{-3}$. For comparison, if the interface is rough, this derivative is $\simeq \bar{p}$ and effect disappears at $\bar{p} << 1$. In general terms, the described kinetic and flow induced stabilization/destabilization effect is associated with symmetry breaking by both the interface kinetics and the liquid flow.

Further development of the described instability results in steepening of the step bunches traveling along the growing surface and appearance, sometimes, macrosteps with their risers possessing simple crystallographic orientations. The step bunches possessing high density of elementary steps trap point defects in amounts different from the one by widely separated elementary steps. Therefore, the bunches produce in the crystal bands of material which properties are different from the ones of material made by single steps. Such bands have been revealed and studied on Czochralsky Si, LPE GaAs [10], and LPE GaP (T. Tambo, K. Pak and T. Nishinaga, see [3] p. 194). Steep risers may also loose their stability producing inclusions of mother liquor. Such inclusions arranged in chains normal to the step bunch riser and parallel to the growing face have been observed by Yu. G. Kuznetsov on $NH_4H_2PO_4$ crystals growing from aqueous solutions in our laboratory.

We may therefore conclude that morphological instability of a growing vicinal face results in essential internal inhomogeniety of the single crystal which are not induced by external variations of growth conditions associated with liquid flow.

Linear perturbation analysis was employed in which originally flat interface declined from singular orientation by the small angle with tangent $\simeq \bar{p}$ was perturbed into a periodic wave with the wave number $k_x$ [4-8]. This perturbation causes modulation of step density and, thus, of the diffusion field above this interface even if one ignores the wavy shape of the interface. The latter, however, induced additional perturbations in the liquid flow. Recent analysis [9] shows that the

hydrodynamic perturbations may be noticeable for long waves, of the order of several centimeters for other typical parameters, and may be ignored for shorter wavelengths. Therefore, modulations of step density superimposed on the unperturbed tangential liquid flow is the most important stabilizing or destabilizing factor.

It was found that, for the stabilizing mutually antiparallel step and solution flows there exist a critical shear flow above which the interface should be stable with respect to perturbations of any wavelength, i.e. absolutely stable. For $\bar{p} = 10^{-2}$ and step kinetic coefficient $\beta_{st} = 0.1\, {}^{cm}/_{s}$, diffusivity $D = 10^{-5}\, {}^{cm^2}/_{s}$, this shear flow is $0.63\ s^{-1}$. This complete stabilization comes from the fact that anistropic kinetics suppress the long wave perturbations while surface stiffness suppresses the short wave ones.

Let us assume now that the solution or melt are stagnant with respect to the crystal lattice, as it may be achieved at zero gravity. Then, the growth step motion is equivalent to the counterflow of solution which should cause stabilization. Such self-stabilization effect was predicted in our calculations both for solutions [6], melt [7] and alloy [8] growth. In this case, the higher the growth rate at a given average unperturbed step density, the more stable is the interface. Again, surface energy stabilizes interface with respect to the short wavelength perturbation (large wave numbers $k_x$) with relatively weak dependence on the growth rate $V\left(k_x \sim \sqrt{V}\right)$. The anisotropy of interface kinetics, on the contrary, stabilizes the interface with respect to the long wave perturbations (small $k_x$) and thus expands stability area in the plane ($k_x$, $V$), roughly to a half-plane corresponding to sufficiently large $V$ (see [6, 9] for graphs).

The solution flow stabilizes or destabilizes the interface if the flow rate at a distance $k_x^{-1}$ from the interface becomes comparable to the phase velocity $v_x$ of step bunches traveling along the growing interface. At low vicinal slopes, $\bar{p}$ (more precisely, if $\beta_{st}\bar{p} / Dk_x << 1$), the phase velocity is not much different from the average step velocity. At conventional supersaturations of several percent, the step velocity is ca. $10^{-4}\, {}^{cm}/_{s}$ (for $NH_4H_2PO_4$), in aqueous solution at room

temperature. Therefore, at $\bar{p} \simeq 10^{-3}$ and $k_x \simeq 10^2 cm^{-1}$ the solution flow becomes important if the shear $S \simeq V_x k_x \simeq 10^{-2} S^{-1}$. (Shear $S$ is defined as the derivative of the tangential flow rate $\tilde{\tilde{u}}$ with respect to the coordinate, normal to the interface.) For comparison, natural convection producing flow rate $u \simeq 0.1 {}^{cm}/_{s}$ corresponds to the shear $S \simeq {}^{u}/_{\delta} \simeq 0.1 s^{-1}$ even for the thick hydrodynamic boundary layer $S \simeq 1cm$. Therefore, the described flow effects on stability might be important even in slightly moving solutions. Experiments in well defined and very slow flows are desirable.

## References


1. M.E. Glicksman, M.B. Koss, and E.A. Winsa, Phys. Rev. Lett. 73 (1994) 573.
2. R.F. Sekerka, S.R. Coriell, and G.B. McFadden, J.Cryst. Gr. 154 (1995) 370, also J. Cryst. Gr. to appear in 1996.
3. A.A. Chernov, Modern Crystallography III. Crystal Growth. Springer Series in Solid State, vol. 36 (Springer, Berlin, 1984).
4. A.A. Chernov, Yu. G. Kuznetsov, I.L. Smolsky, and V.N. Rozhansky, Sov. Phys - Crist. 31 (1986) 705.
5. A.A. Chernov, J. Cryst. Gr., 118 (1992) 333.
6. A.A. Chernov, S.R. Coriell, and B.T. Murray, J. Cryst. Gr. 132 (1993) 405.
7. A.A. Chernov, S.R. Coriell, and B.T. Murray, J. Cryst. Gr. 149 (1995) 120.
8. S.R. Coriell, B.T. Murray, and A.A. Chernov, J. Cryst. Gr. 141 (1994) 219.
9. S.R. Coriell, B.T. Murray, A.A. Chernov, and G.B. McFadden, J. Cryst. Gr. (1996, submitted).
10. E. Bauser in: Handbook of Crystal Growth. vol 3b, Ed D.T.J. Hurle (North Holland, Amsterdam, 1994), p. 879.

# Agenda

Monday (June 10, 1996)

| | | |
|---|---|---|
| 8:00 a.m. | Continental Breakfast and Conference Registration | |
| 8:30 a.m. | Introductions | Dr. Michael J. Wargo, NASA HQ |
| 8:35 a.m. | Welcome from the Director, Marshall Space Flight Center | Dr. J. Wayne Littles, NASA MSFC |
| 8:40 a.m. | Microgravity Science and Applications Program | Mr. Robert C. Rhome, NASA HQ |
| 9:00 a.m. | The Role of Microgravity Science in the Human Exploration and Development of Space | Dr. Bradley M. Carpenter, NASA HQ |
| 9:20 a.m. | Topics of Interest in Microgravity Materials Science | Prof. John H. Perepezko, Univ. of Wisconsin |
| 9:40 a.m. | Microgravity Materials Science: Ground-Based and Flight Research Resources and Procedures | Mr. Joel K. Kearns, NASA MSFC<br>Dr. Robert S. Snyder, NASA MSFC |
| 10:20 a.m. | Break | |
| 10:40 a.m. | Remarks to PI's and Comments to Prospective Proposers | Dr. Michael J. Wargo, NASA HQ |
| 11:00 a.m. | Question and Answer Session | |
| 11:20 a.m. | INVITED PAPER: "Growth of Faceted Crystals - Stability, Flows, Defects" | Prof. Alexander A. Chernov, USRA |
| 12:00 p.m. | Lunch (boxed lunches) | |
| 1:00 p.m. | Parallel Session I | |
| 2:30 p.m. | Break | |
| 2:45 p.m. | Parallel Session II | |
| 4:15 p.m. | Break | |
| 4:30 p.m. | Parallel Session III | |
| 6:30 p.m. | Adjourn | |
| 7:00 p.m. | Social at the U.S. Space and Rocket Center | |

# Agenda (cond't)

Tuesday (June 11, 1996)

| | | |
|---|---|---|
| 8:00 | a.m. | Continental Breakfast |
| 8:00 | a.m. | Parallel Session IV |
| 10:00 | a.m. | Break |
| 10:15 | a.m. | Parallel Session V |
| 12:15 | p.m. | Lunch (boxed lunches) and Poster Session |
| 2:30 | p.m. | Parallel Session VI |
| 4:30 | p.m. | Adjourn |

Wednesday (June 12, 1996)

| | | |
|---|---|---|
| 9:00 | a.m. | Optional tour of the microgravity facilites at the NASA Marshall Space Flight Center (until noon) |

# Presentation Program

## Monday (June 10, 1996)

**Parallel Sessions I** (1:00 p.m. - 2:30 p.m.)

**Basic Aspects I**
Chair: Dr. Peter W. Voorhees
North Hall II

Dr. J. Barry Andrews
*The Effect of Convection on Morphological Stability During Coupled Growth in Immiscibles*

Dr. Tony Maxworthy
*Numerical and Laboratory Experiments on the Interactive Dynamics of Hele-Shaw Flows and Directional Solidification*

Dr. Robert A. Brown
*Applications of Parallel Computing for Two- and Three-Dimensional Modeling of Bulk Crystal Growth and Microstructure Formation*

**Metals and Alloys I**
Chair: Dr. John H. Perepezko
Salon I

Dr. Timothy J. Anderson
*An Electrochemical Method to Visualize Flow and Measure Diffusivity in Liquid Metals*

Dr. Arun M. Gokhale
*Effect of Gravity on the Evolution of Spatial Arrangement of Features in Microstructure: A Quantitative Approach*

Dr. Lynn A. Boatner
*Surface Morphological Properties of Stationary Melt Pools in Single Crystals of Stainless Steel*

**Electronic Materials I**
Chair: Dr. Richard H. Hopkins
Orchestra Rehearsal Room

Dr. Frank R. Szofran
*Magnetic Damping of Solid Solution Semiconductor Alloys*

Dr. Archibald L. Fripp
*Melt Stabilization of PbSnTe in a Magnetic Field*

**Parallel Sessions II** (2:45 p.m. - 4:15 p.m.)

**Metals and Alloys II**
Chair: Dr. Rohit Trivedi
North Hall II

Dr. William L. Johnson
*Physical Properties and Processing of Undercooled Metallic Glass Forming Liquids*

Dr. Ared Cezairliyan
*Thermophysical Properties of High Temperature Liquid Metals and Alloys*

**Metals and Alloys III**
Chair: Prof. Timothy Anderson
Salon I

Dr. Frans Spaepen
*Kinetics of Nucleation and Growth From Undercooled Melts*

Dr. John H. Perepezko
*Analysis of Containerless Processing and Solidification Microstructures*

SPECIAL PRESENTATION:
Dr. R.J. Slobodrian
*Fractal Aggregates in Microgravity*

**Ceramics and Glasses**
Chair: Prof. Dennis W. Readey
Orchestra Rehearsal Room

Dr. Kenneth F. Kelton
*Phase Formation and Stability: Composition and Sample-Size Effects*

Dr. Richard Weber
*Process-Property-Structure Relationships in Complex Oxide Melts*

# Presentation Program (cond't)

**Parallel Sessions III** (4:30 p.m. - 6:30 p.m.)

**Basic Aspects II**
Chair: Prof. Jonathan Dantzig
North Hall II

Dr. Christoph Beckermann
*Equiaxed Dendritic Solidification Experiment (EDSE)*

Dr. Rohit Trivedi
*Interface Pattern Selection Criterion for Cellular Structures in Directional Solidification*

Dr. David J. Larson, Jr.
*Orbital Processing of Eutectics*

**Metals and Alloys IV**
Chair: Dr. Peter W. Voorhees
Salon I

Dr. David R. Poirier
*Comparison of Structure and Segregation in Alloys Directionally Solidified in Terrestrial and Microgravity Environments*

Dr. Alan J. Ardell
*Ostwald Ripening of Liquid and Solid "Droplets" in Liquid Metal Matrices*

Dr. David H. Matthiesen
*The Study of Dopant Segregation Behavior During the Growth of GaAs in Microgravity*

**Electronic Materials II**
Chair: Dr. Frank R. Szofran
Orchestra Rehearsal Room

Dr. Ching-Hua Su
*Crystal Growth of ZnSe and Related Ternary Compound Semiconductors by Vapor Transport*

Dr. Michael Dudley
*Combined Synchrotron White Beam X-ray Topography and High Resolution Triple Axis X-ray Diffraction Characterization and Analysis of Crystals Grown in Microgravity and Ground-Based Environments*

Dr. Sandor L. Lehoczky
*Growth of Solid Solution Single Crystals*

## Tuesday (June 11, 1996)

**Parallel Sessions IV** (8:00 a.m. - 10:00 a.m.)

**Metals and Alloys V**
Chair: Prof. Dennis W. Readey
North Hall II

Dr. Robert J. Bayuzick
*Investigation of the Relationship Between Undercooling and Solidification Velocity*

Dr. Klaus J. Bachmann
*Fundamental Aspects of Vapor Deposition and Etching Under Diffusion Controlled Transport Conditions*

Dr. Reza Abbaschian
*In Situ Monitoring of Crystal Growth Using MEPHISTO*

Salon I

**Electronic Materials III**
Chair: Dr. Richard H. Hopkins
Orchestra Rehearsal Room

Dr. Heribert Wiedemeier
*Vapor Transport Crystal Growth of Mercury Cadmium Telluride in Microgravity - USML-2*

Dr. Archibald L. Fripp
*Compound Semiconductor Growth in a Low-g Environment*

Dr. David J. Larson, Jr.
*Orbital Processing of High-Quality Zn-Alloyed CdTe Compound Semiconductors*

# Presentation Program (cont'd)

**Parallel Sessions V** (10:15 a.m. - 12:15 p.m.)

**Metals and Alloys VI**
Chair: Prof. Jonathan Dantzig
North Hall II

Dr. Robert J. Bayuzick
*Effects on Nucleation by Containerless Processing*

Dr. Merton C. Flemings
*Alloy Undercooling Experiments in a Microgravity Environment*

Dr. Peter W. Voorhees
*Coarsening in Solid-Liquid Mixtures*

**Metals and Alloys VII**
Chair: Prof. John H. Perepezko
Salon I

Dr. Randall M. German
*The Gavitational Role in Liquid Phase Sintering*

Dr. Martin E. Glicksman
*Isothermal Dendritic Growth Experiment*

Dr. William L. Johnson
*Thermo-Physical Properties of Metallic Glasses and Undercooled Alloys - AC Modulation Calorimetry on the TEMPUS Facility*

**Electronic Materials IV**
Chair: Prof. Timothy Anderson
Orchestra Rehearsal Room

Dr. David H. Matthiesen
*Diffusion Processes in Molten Semiconductors*

Dr. Aleksandar G. Ostrogorsky
*Space- and Ground-Based Crystal Growth Using a Magnetically Coupled Baffle*

Dr. Sandor L. Lehoczky
*Crystal Growth of II-VI Semiconducting Alloys by Directional Solidification*

**Posters** (see below) (12:15 p.m. - 2:30 p.m.)

**Parallel Sessions VI** (2:30 p.m. - 4:30 p.m.)

**Metals and Alloys VIII**
Chair: Dr. Richard H. Hopkins
North Hall II

Dr. Franz Rosenberger
*Self-Diffusion in Liquid Elements*

Dr. J. Barry Andrews
*Coupled Growth in Hypermonotectics*

**Metals and Alloys IX**
Chair: Dr. Rohit Trivedi
Salon I

Dr. Doru M. Stefanescu
*Particle Engulfment and Pushing by Solidifying Interfaces (PEP-si)*

Dr. Merton Flemings
(Dr. Julian Szekely)
*The Measurement of the Viscosity and Surface Tension of Undercooled Melts Under Microgravity Conditions and Supporting MHD Calculations*

Dr. William H. Hofmeister
*Microgravity Processing of Oxide Superconductors*

**Electronic Materials V**
Chair: Dr. Frank R. Szofran
Orchestra Rehearsal Room

Dr. Kenneth A. Jackson
*Non-Equilibrium Phase Transformations*

Dr. N. B. Singh
*Flight Experiment to Study Double-Diffusive Instabilities in Silver-Doped Lead Bromide Crystals*

Dr. P.K. Dutta
*Reverse Micelle Based Synthesis of Microporous Materials in Microgravity*

# Presentation Program (cont'd)

**Posters** (12:15 p.m. - 2:30 p.m.)

Dr. Spiro D. Alexandratos
*Synthesis and Characterization of Single Macromolecules: Mechanistic Studies of Crystallization and Aggregation*

Dr. M. Cengiz Altan
*Microgravity Impregnation of Fiber Preforms*

Dr. Mark A. Barteau
*Molecularly Tailored Surfaces via Self-Assembly Processes: Synthesis, Characterization and Modeling*

Dr. John F. Brady
*Dispersion Microstructure and Rheology in Ceramics Processing*

Dr. Kenneth Brezinsky
*Combustion Synthesis of Materials in Microgravity*

Dr. Soyoung Stephen Cha
*Three-Dimensional Velocity Field Characterization in a Bridgman Apparatus: Technique Development and Effect Analysis*

Dr. Ivan O. Clark
*Microgravity Chemical Vapor Deposition*

Dr. Peter A. Curreri
*Fundamental Studies of Solidification in Microgravity Using Real-Time X-Ray Microscopy*

Dr. Jonathan A. Dantzig
*Adaptive-Grid Methods for Phase Field Models of Microstructure Development*

Dr. Jeffrey J. Derby
*Atomistic Simulations of Cadmium Telluride: Toward Understanding the Benefits of Microgravity Crystal Growth*

Dr. M. Samy El-Shall
*Studies on Nucleation, Polymerization and Nanoparticle Composites in Supersaturated Vapors Under Microgravity*

Dr. Alexandre Fedoseyev
*Investigation of Vibrational Control of the Bridgman Crystal Growth Technique*

Dr. Donald C. Gillies
*Solidification of II-VI Compounds in a Rotating Magnetic Field*

Dr. Richard N. Grugel
*Evaluation of Microstructural Development in Bulk, Undercooled Alloys*

Dr. Richard N. Grugel
*Novel Directional Solidification Processing of Hypermonotectic Alloys*

Dr. Richard N. Grugel
*Utilizing Controlled Vibrations in a Microgravity Environment to Understand and Promote Microstructural Homogeneity During Floating-Zone Crystal Growth*

# Presentation Program (cont'd)

**Posters** (cont'd)

Dr. Douglas E. Holmes
*Dimensional Stability of Supermatrix Semiconductors*

Dr. Monica L. Kaforey
*Dislocation Formation During Growth of Semiconductor Crystals*

Dr. Alain Karma
*The Role of Dynamic Nucleation at Moving Boundaries in Phase and Microstructure Selection*

Dr. Mohammad Kassemi
*Determination of Gravity-Related Effects on Crystal Growth From Melts With an Immiscibility Gap*

Dr. Joseph L. Katz
*Measurement of Liquid-to-Solid Nucleation Rates in Undercooled Metallic Melts*

Dr. Anantha Krishnan
*Influence of Natural Convection and Thermal Radiation on Multi-Component Transport and Chemistry in MOCVD Reactors*

Dr. Shankar Krishnan
*Containerless Optical Property Measurements on High Temperature Liquids*

Dr. Ben Q. Li
*Study of Magnetic Damping Effect on Convection and Solidification Under G-Jitter Conditions*

Dr. Thomas A. Lograsso
*Microstructural Development During Directional Solidification of Peritectic Alloys*

Dr. Richard J. Matyi
*Quantitative Analysis of Crystal Defects by Triple Crystal X-Ray Diffraction*

Dr. Mark S. Paley
*Gravitational Effects on the Morphology and Kinetics of Photo-Deposition of Polydiacetylene Thin Films From Solution*

Dr. Witold Palosz
*Investigation of Convective Effects in Crystal Growth by Physical Vapor Transport*

Prof. Dennis Readey
*The Effects of Microgravity on Vapor Phase Sintering*

Dr. Liya L. Regel
*Detached Solidification: Steady State Results*

Dr. Won-Kyu Rhim
*Thermophysical Property Measurements of Molten Semiconductors in 1-g and Reduced-g Conditions*

Dr. Won-Kyu Rhim
*Undercooling Limits and Thermophysical Properties in Glass-Forming Alloys*

Dr. Michael B. Robinson
*Undercooling of Immiscible Alloys Without Container-Induced Wetting and Nucleation*

# Presentation Program (cont'd)

**Posters** (cont'd)

Dr. Charles Rosenblatt
*Determination of the Surface Energy of Smectic Liquid Crystals From the Shape Anisotropy of Freely Suspended Droplets*

Dr. Albert Sacco
*Modeling of Macroscopic/Microscopic Transport and Growth Phenomena in Zeolite Crystal Solutions Under Microgravity Conditions*

Dr. Jogender Singh
*Gravitational Effect on the Development of Laser Weld-Pool and Solidification Microstructure*

Dr. Daniel R. Talham
*The Features of Self-Assembling Organic Bilayers Important to the Formation of Anisotropic Inorganic Materials in Microgravity Conditions*

Dr. Eugene H. Trinh
*Dynamic Nucleation of Deeply Undercooled Melts and Measurement of the Surface Tension and Viscosity*

Dr. James D. Trolinger
*Investigation of the Effects of Microgravity on Transport Properties in a Virtual Space Flight Chamber*

Dr. Gretar Tryggvason
*Fundamentals of Mold Free Casting: Experimental and Computational Studies*

Dr. John S. Walker
*Models of Magnetic Damping for Semiconductor Crystal Growth in Microgravity*

Dr. J.S. Wettlaufer
*Thin Film Mediated Phase Change Phenomena: Crystallization, Evaporation and Wetting*

Dr. Heribert Wiedemeier
*Defect Generation in CVT Grown Hg1-xCdxTe Epitaxial Layers Under Normal and Reduced Gravity Conditions*

Dr. William R. Wilcox
*Use of Microgravity to Control the Microstructure of Eutectics*

# World Wide Web

This conference proceedings volume is available on the World Wide Web at the NASA Marshall Space Flight Center Technical Reports Web site (http://mtrs.msfc.nasa.gov/mtrs/). A World Wide Web site (http://otis.msfc.nasa.gov/notice1.html) was created for this conference and was used to keep those with access to the WWW apprised of changes in the Agenda and Presentation Program and provided information about available hotels, registration information, and the required formats for the two-page summaries and the research reports.

Each active Marshall Space Flight Center microgravity materials science PI was required to submit a two-page summary of their investigation; several non-renewed investigators also submitted summaries. These summaries were collected and bound into a volume which was distributed at the conference to all attendees, and this volume is available for distribution upon request. The summaries were posted to the conference's Web site.

Additionally, each investigator was required to submit a research report, which was bound into this NASA Conference Publication. One copy of this Conference Publication was mailed to each conference attendee and related NASA personnel, and additional copies will be available in the usual manner for NASA publications.

The Marshall Space Flight Center's Microgravity Science and Applications Division plans to utilize the information distributing capabilities of the Internet as fully as time and funding allows. Additional MSFC microgravity Web sites are likely to be created to meet specific sub-discipline needs. Persons interested in keeping track of NASA microgravity meetings and research progress should make it a habit to browse the many Web sites available to the public.

Other useful NASA and NASA microgravity-related sites include:

NASA Home Page - http://www.nasa.gov

NASA Headquarters' Office of Life and Microgravity Sciences and Applications - http://www.hq.nasa.gov/office/olmsa/olmsa.html

NASA Headquarters' Microgravity Science and Applications Division - http://microgravity.msad.hq.nasa.gov/

NASA MSFC's Space Science Laboratory - http://wwwssl.msfc.nasa.gov/

NASA MSFC's Microgravity Science and Applications Division - http://otis.msfc.nasa.gov/

NASA MSFC's Technical Reports - http://mtrs.msfc.nasa.gov/mtrs/)

NASA LeRC's Space Experiments Division - http://zeta.lerc.nasa.gov/sedhome.htm

Microgravity-Related Meetings (maintained by Fred Kohl, NASA LeRC) - http://zeta.lerc.nasa.gov/ugml/ugml.htm

Individual Shuttle Missions (Past and Future) - http://www.ksc.nasa.gov/shuttle/missions/missions.html

Advanced Concepts at NASA - http://www.hq.nasa.gov/office/acrp/oac.html

Today @ NASA (press releases, etc.) - http://www.hq.nasa.gov/office/pao/NewsRoom/today.html

**Research Report: NASA Grant No. NAG-3-1096**

## *In Situ* Monitoring of Crystal Growth using MEPHISTO

Reza Abbaschian
Department of Materials Science and Engineering
University of Florida, Gainesville, FL

S.R. Coriell
National Institute of Standards and Technology
Gaithersburg, MD

## I. Objectives

The primary research objectives of this investigation are to determine the morphological stability threshold of faceted interfaces in the absence of convection and to understand the role of interfacial kinetics on the morphological stability under diffusive conditions during unidirectional solidification of Bi alloyed with Sn.

## II. Microgravity Research

Under terrestrial (1-g) conditions, the role of interfacial kinetics can be masked in the presence of thermosolutal convection, particularly if hydrodynamic fluctuations are present. The diffusion-dominated microgravity environment experienced on orbit is therefore essential for studying interfacial kinetics effects during solidification.

## III. Background

Facet formation is a common feature during solidification of many technologically important materials, particularly elemental and compound semiconductors such as Si, Ge, GaAs and GaSb. In these materials, atomic attachment on atomically flat interfaces requires an additional driving force in the form of interfacial supercooling, also termed the kinetic undercooling. For the growth of atomically flat interfaces, the presence of solutal atoms or impurities are particularly important because they can poison the interfaces, resulting in a change in the local growth rate or, in extreme cases, a change of the habit plane of the growing crystal. Also of importance is the presence of defects such as screw dislocations and twinning which can markedly affect the growth anisotropy. In addition, theoretical calculations[1] indicate that the anisotropy in surface tension and interface kinetics is one of the underlying causes for the existence of preferred growth directions in cells and dendrites, and also extend the morphological stability threshold, thereby affecting the distribution of the solute in the grown crystal.

## IV. Experimental Procedure

The MEPHISTO facility is designed to simultaneously process three samples, each approximately 900 mm long and 6 mm in diameter. One of the samples is dedicated to the study of Seebeck signals, which allows *in situ* measurement of the solid/liquid interface temperature

during solidification. Another sample is used for Peltier marking, which involves passing brief electrical pulses to mark the shape and position of the interface for later metallographic examination. The third sample, which incorporated two thermocouples, is used for temperature measurement as well as for resistance measurements to track the position of the interface. The internal structure of the MEPHISTO facility is shown in Figure 1(a), while the arrangement of the experimental samples along with important dimensions, positions of the two solid/liquid interfaces, locations of thermocouples and the temperature profile are shown schematically in Figure 1(b). For the USMP-2 flight experiments, Bi alloyed with 0.1 at.% Sn rods were prepared in 5.8 mm diameter quartz crucibles. The rods were then removed from the crucible and inserted in 6 mm diameter quartz tubes for integration in the flight hardware. The gap between the rod and the tube, which is later filled by argon gas, is necessary for the thermal management of the hardware. During the experiments, the middle ~50 cm length of the samples was melted, thus creating two s/l interfaces. One of the furnaces was kept stationary and the other moved back and forth at rates from 1.85 μm/s to 40.01 μm/s in order to melt or solidify the desired region of the samples. In order to eliminate the gap between the sample and quartz tubes, spring-loaded compensators are used to push the unmelted ends together, effectively filling the tube with the liquid metal.

## V. Results

It was found that the interface was nearly flat, with a slight curvature (concave toward solid) near the solid/liquid/crucible triple junction. The development of a plane front microstructure is illustrated in Figure 2, which shows the transition from the faceted cellular/dendritic structure of the earth grown portion of the sample to a plane front morphology at the moving interface. As shown, only a few dominant orientations emerge from the initial (rapidly cast) microstructure. A schematic overview of the microstructural evolution of the resistance sample grown in space is shown in Figure 3. For solidification at velocities ranging from V1 = 1.85 to V3 = 6.71 μm/s, the growth occurs in a planar mode, with only two grains observable in the cross section. In contrast, distinct cellular morphology was seen at velocities V5 = 26.88 and V6 = 40.01 μm/s. The microstructural evolution at the intermediate V4 velocity (13.34 μm/s) appears to be cellular in one grain, and planar in the other. The transition to cellular mode was detected in one grain, but not in the other, after approximately 14 mm of directional solidification. The other grain continued to grow in a plane front mode until the end of the solidification cycle (30 mm). The Peltier and Seebeck samples generally had microstructures similar to those shown in Figure 3, except that no cellular growth was observed at V5 in these samples.

In general, anisotropic interfacial properties are expected to play a role in the morphological stability of planar interfaces, as well as the evolution of cellular and dendritic structures; this has been predicted theoretically[1,2] by extending the linear stability analysis[3] in the weakly nonlinear regime. These treatments indicate that such anisotropies tend to stabilize the growth of a planar interface. The flight experiments generally support these predictions. However, the most interesting aspect of the transition at the V5 (26.9 μm/s) velocity was the existence of a distinct bias toward preferential breakdown of some grains. The preferential breakdown is shown via a low magnification micrograph in Figure 4. It can be seen that the bottom grain continues to grow in the plane front mode for a significant distance while the upper one is growing in a cellular mode. The distance of separation between the morphological instability of the two grains at this velocity is approximately 1.2 cm.

Cellular transition at a higher growth velocity (V6: 40 μm/s) exhibited features which were similar to those at V5, except that the differential instability of the neighboring grains was not as pronounced. We believe that it is the anisotropy in interfacial kinetics, rather than in the surface energy or thermal conductivity, which is exerting a strong influence on the morphological stability. However, as the growth rate increases, the faceted interface(s) go through a kinetic roughening transition, behave as non-faceted, and reduce the stabilizing effect of interfacial kinetics.

The interfacial undercooling was measured using the Seebeck technique in which the differential thermo-emf is measured from two s/l interfaces[4], one stationary and the other moving. The stationary interface acts as a reference junction for the moving interface temperature (interfacial undercooling), which can be measured from a differential signal at the sample ends. For isotropic materials or single crystals, the differential voltage is directly proportional to the interfacial undercooling, while for polycrystals and particularly for anisotropic materials, additional terms are introduced from effects associated with thermo-emfs of grain boundaries in the gradient zone.

Figure 5 shows the Seebeck generation during a 2 mm solidification cycle at the beginning of the space experiment. Upon stopping the furnace translation, the signal increases through a transient, which is related primarily to the solutal decay (diffusional decay of the solute-rich boundary layer and concurrent decay of the chemical undercooling), with some early contributions from thermal and kinetics adjustments as the interface comes to rest. As such, the Seebeck voltage change upon stopping the furnace translation is due to contributions from chemical ($\Delta T_c$), kinetic ($\Delta T_k$), and capillarity (curvature related, $\Delta T_r$) sources. For plane front solidification, the capillarity contribution can be ignored, while the chemical contribution can be calculated provided the convecto-diffusive state of the liquid can be quantified.

The temperature depression due to compositional changes for the purely diffusive state can be calculated using the classical approach. The governing equation for the plane front solidification in initial transient (for the present velocity, a steady state would be achieved at a distance > 15 cm) is:

$$C_l^* = C_0 \left\{ \frac{1-k}{k} \left[ 1 - \exp\left( -k \frac{V}{D_l} x \right) \right] + 1 \right\} \qquad (1)$$

The chemical contribution is then given by:

$$\Delta T = m_l (C_l^* - C_o) \qquad (2)$$

where $C_l^*$ is the composition of the liquid at the interface, $C_0$ is initial alloy composition (0.1 at.%), k is the equilibrium partition coefficient (0.029), V is the growth velocity ($1.85 \times 10^{-4}$ cm/s), $D_l$ is the liquid diffusivity ($5.315 \times 10^{-5}$ $cm^2/s$ for Sn in Bi for an average temperature in the gradient zone of 435.5°C)[5], $x$ is the distance solidified and $m_l$ is the liquidus slope (-2.32 K/at.%).

Based on the above equations, the temperature depression due to compositional changes after 2 and 7 mm solidification is 0.155 and 0.533 K, respectively, from which we can deduce the magnitude of non-solutal contributions such as the kinetic undercooling. The resulting values corresponded to a kinetic undercooling of 0.055 and 0.07 K after 2 and 7 mm solidification, respectively

The kinetic undercooling in the case of dislocation-assisted growth is generally related to the growth velocity by:

$$V=a\Delta T_k^n \qquad (3)$$

where V is the growth velocity and a and n are constants. In order to compare with microgravity experiments, the kinetic law for pure Bi single crystals was previously determined based on 72 measurements at growth velocities ranging from $2 \times 10^{-4}$ to $9.5 \times 10^{-3}$ cm/s. The resulting values for a and n were 0.0274 cm/s(K)$^n$ and 1.65, respectively[6]. The above-determined interface kinetics supercoolings compare well with those calculated based on the kinetic undercooling for pure Bi single crystals (0.048 K), using eq. 3. However, it should be emphasized that the constants in eq. 3 were derived for pure Bi single crystals, which can be appreciably different for the rate equation for alloys[7].

## VI. Summary

The morphological stability of various crystallographic orientations is significantly affected by the anisotropy in interfacial properties of the faceted alloy in general, and the interface kinetics in particular. The post-flight microstructural analysis showed that the growth of one grain occurred in a plane front mode while the neighboring orientations exhibited a transition to a cellular mode. The most important aspect of such a staggered breakdown was the relatively large extent to which the plane front growth continued in one orientation.

The differential Seebeck signals allowed the monitoring of interfacial phenomena. While these signals are extremely sensitive to the interaction between thermal gradients and local microstructural detail, the magnitude of kinetic undercooling could nevertheless be calculated from the decay in the Seebeck signal at the end of solidification.

## VII. References


1. S.R. Coriell and R.F. Sekerka, J. Cryst. Growth, (34), p.157 (1976).
2. S.R. Coriell, J. Cryst. Growth, (141), p.219 (1994).
3. W.W. Mullins and R.F. Sekerka, J. Cryst. Growth, (35), p.444 (1964).
4. S.D. Peteves and G.J. Abbaschian, J. Cryst. Growth, (79), p.775 (1986).
5. K. Niwa *et al.*, J. of Metals, (9-1), 96 (1957).
6. R. Abbaschian *et al.*, AIAA 95-0608, Publ.:AIAA, Washington D.C. (1995).
7. R. Abbaschian and R. Mehrabian, J. Cryst Growth, (44), 453 (1978).

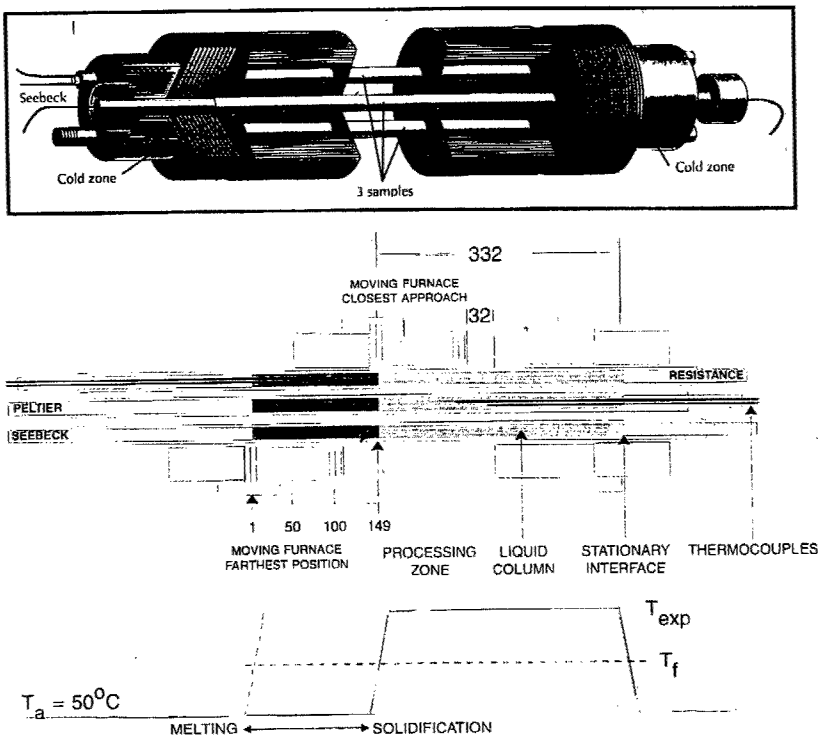


Figure 1: (a) Mephisto core assembly and (b) arrangement of the experimental samples and the temperature profile.

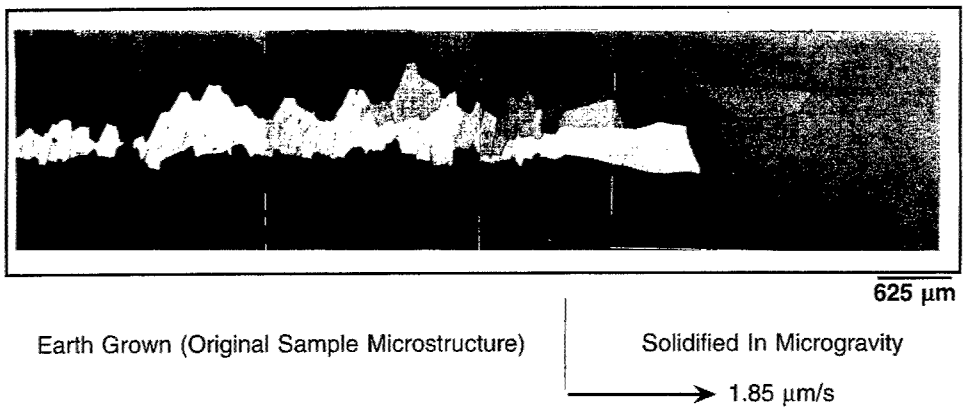


Figure 2: Microstructural appearance of the interface between the earth and microgravity processed portions of the Peltier sample.

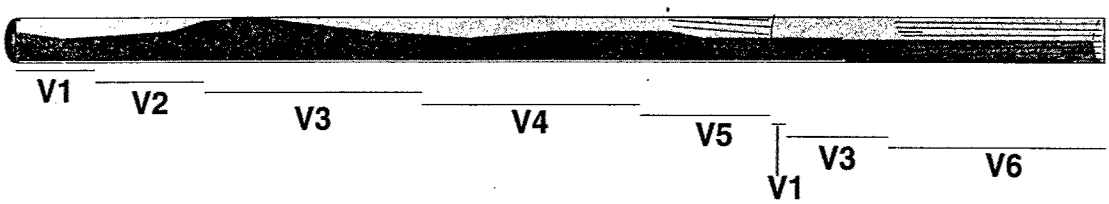


Figure 3: Summary of sample sections preserved during final solidification.

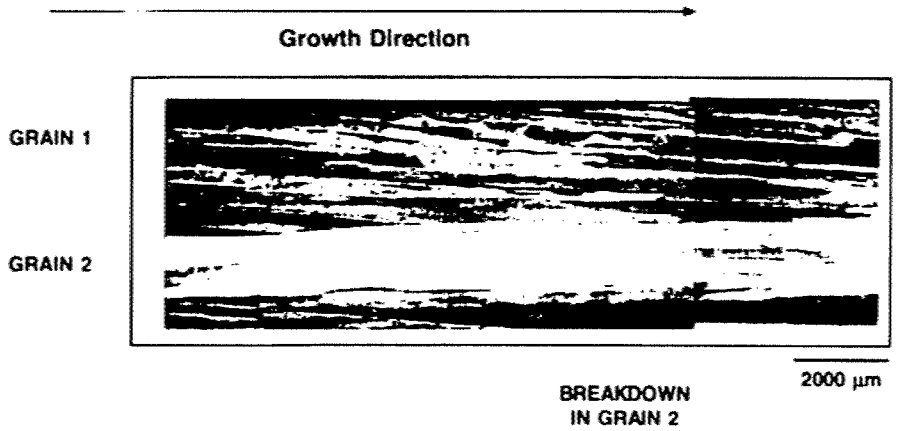


Figure 4: Microstructural appearance showing that the top grain is cellular while the bottom continues in a plane front mode for 12.2 mm before transitioning to cellular growth.

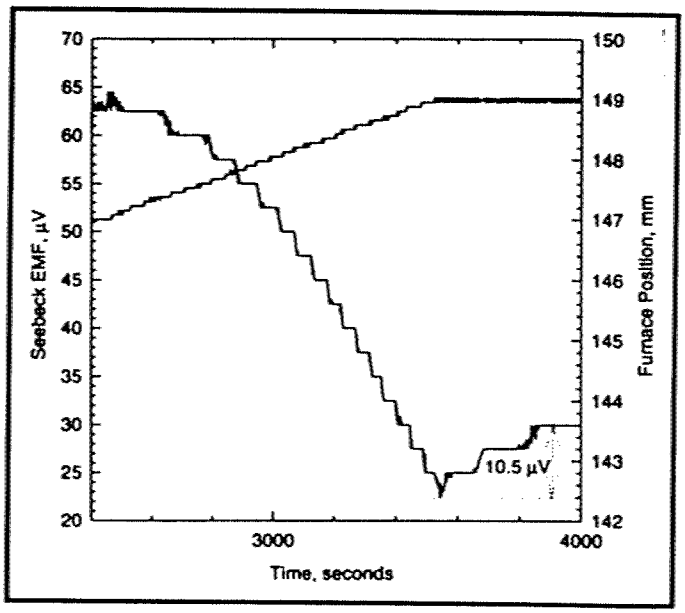


Figure 5: Seebeck signals that correspond to the 2 mm directional solidification in plane front growth with columnar grains.

# SYNTHESIS AND CHARACTERIZATION OF SINGLE MACROMOLECULES: MECHANISTIC STUDIES OF CRYSTALLIZATION AND AGGREGATION

[1] Reinhard Festag, [1] Spiro D. Alexandratos, [1] Kelsey D. Cook, [2] David C. Joy, [3] Paul J. Phillips, [1] Bernhard Wunderlich

[1] Department of Chemistry, [2] Dept. of Biochemistry & Cellular & Molecular Biology, [3] Dept. of Materials Science and Engineering, University of Tennessee, Knoxville, TN 37996-1600, Phone 423 974 3399, E-mail alexsd@utk.edu

## Introduction

The principal objective is to prepare single-molecule polymer particles and crystals in isolation from each other and from invasive solvent and/or cosolutes. Most knowledge about single polymer molecular properties is restricted to the behavior of isolated chains in very dilute solutions[1]. For isolated single- or few-molecule particles, one is able to control polymer-polymer interactions in order to compare the effects of interchain and intrachain entanglements on the chemical and physical properties of an amorphous polymer particle or a polymer crystal.

## Routes to single molecules

From an extensive literature search and preliminary experiments, we found five different methods suitable for separation and solidification of single macromolecules: (1) the Langmuir method[2], (2) electrospray[3], (3) freeze drying of glassy solutions[4], (4) rapid precipitation[5] and crystallization and (5) microemulsion polymerization[6]. For methods (1) to (4) it is always essential that the polymer solution used for the experiments is dilute enough to ensure the presence of single molecules without intermolecular entanglements. The methods are different approaches to transfer the isolated molecules into isolated solid particles. The fifth method achieves the single-molecule particle via hindering the polymerizing molecules from mixing in

the first place. The Langmuir and the electrospray method seemed to be most promising and versatile and are therefore discussed in detail in the following.

Isolation and characterization:

1. The Langmuir method

For the Langmuir method a dilute polymer solution is spread onto a liquid surface. Ideally the liquids are immiscible and the polymer is not soluble in the liquid of the subphase. The polymer solution forms a thin layer on top of the subphase and the polymer chains are isolated from each other because of their low concentration (see fig. 1). When the top solvent is evaporated, the polymer chains stay separated and single-molecule particles remain on the surface of the subphase.

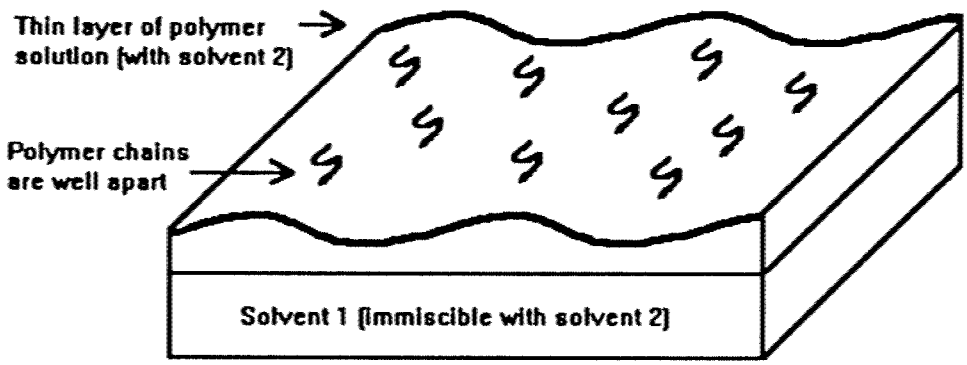


*Fig. 1: Principle of the Langmuir method*

Single-molecule particles were prepared with this method from a $1*10^{-4}$ wt% poly(ethylene oxide) (PEO, $M_n = 1.4*10^6$) solution in benzene, spread onto a water surface at 80 °C, because PEO is not soluble in hot water. After collecting and annealing at 45 °C for 10 h, regular shaped crystals result. The morphologies were analyzed with a transmission electron microscope[7]. Besides monoclinic structures, twinned crystals were found. Also observed were crystals with deviations from regular crystal faces, which are probably caused by insufficient molecular length to complete the crystal, a phenomenon directly related to the single molecule structure.

## 2. The electrospray method

The electrospray (ES) technique is applicable to a wide range of polymer/solvent combinations and is relatively simple and controllable. Polymer solution is sprayed through a metal needle and an electric field at the needle tip charges the surface of the emerging liquid, dispersing it by Coulomb forces into a fine spray of charged droplets. The small charged droplets evaporate while drifting to the counter electrode. Due to the relative involatility of charge carriers, the charge density increases during evaporation. The droplets disintegrate on reaching the Rayleigh stability limit[8], at which the Coulomb forces overcome the surface tension that holds the droplet together. Individual droplets do not split evenly, but emit a tail of much smaller offspring droplets[9]. After repeated fissions those small offsprings lead ultimately to gas phase single-molecule ions.

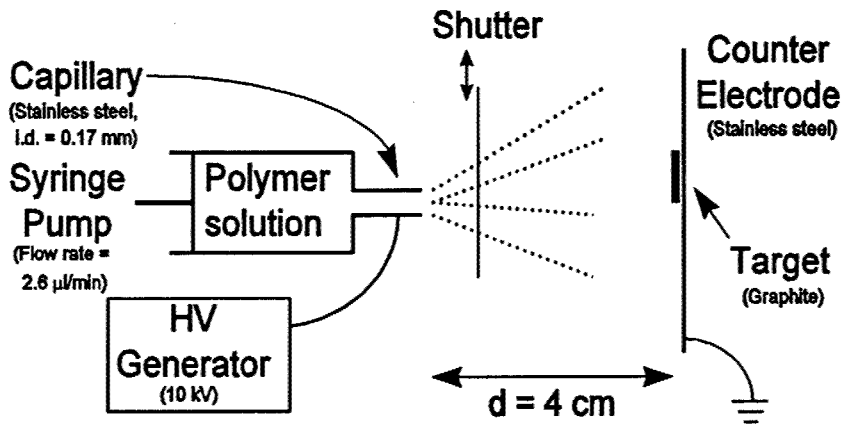


*Fig. 2: Sketch of the electrospray setup*

Experiments were performed with an amorphous polymer (polystyrene, PS) with $M_w$ of 330,000 and low polydispersity ($M_w/M_n$ = 1.26). To keep the polymer chains separated, dilute solutions ($3*10^{-6}$ to $1*10^{-4}$ wt%), well below the critical overlap concentration[1] were used. Chloroform was used as solvent. Its high ionization potential should facilitate the charging of the polymer in preference to the solvent. Electrosprayed samples of PS were obtained with the setup shown in fig. 2. Sample targets were investigated with a scanning electron microscope (see fig. 3).

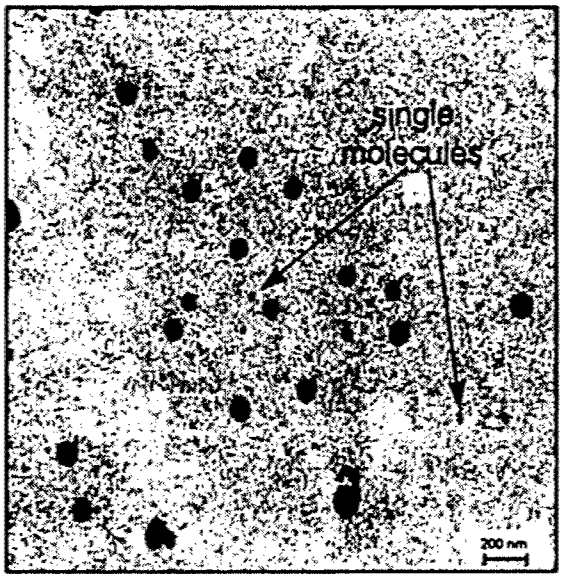


*Fig. 3: SEM micrograph of electrosprayed PS ($M_w$=330,000), concentration $1*10^{-4}$ wt% in chloroform, sprayed for 5 minutes, original magnification 50,000*

Figure 3 shows round particles well separated from each other. Clearly two different kinds of particles can be distinguished: Those with a diameter between 80 and 120 nm, and much smaller ones with a diameter of about 20 nm. An analysis of 20 electron micrographs of different regions of a target shows a similar bimodal size distribution in each region. Since the polymer is nearly monodisperse, different particle sizes must originate from different numbers of polymer chains in the particle. Based on particle size, polymer density and molecular weight, it was found that the smallest particles are indeed single molecule particles[10]. A large particle with an average diameter of 95 nm consists of around 400 polymer molecules. Since a nascent droplet with a typical radius in the micrometer range[11] would contain several hundred polymer molecules, the larger particles evidently originate from simple evaporation of initial droplets without undergoing a large number of fission processes. Either such droplets are not initially charged or the process of droplet subdivision with charge separation is impeded.

A possible explanation is as follows. Starting with a nascent droplet, the first fission process generates several small offspring droplets and a relatively large residual droplet. The small off-springs contain only zero to three polymer molecules and account for most of the small particles

observed. In the residual droplet the concentration increases very rapidly with the number of generations due to solvent evaporation. After only a few fission processes entanglements of the polymer chains begin to occur, impeding further fissioning. The number of fission processes is therefore limited by the overlap concentration of the polymer.

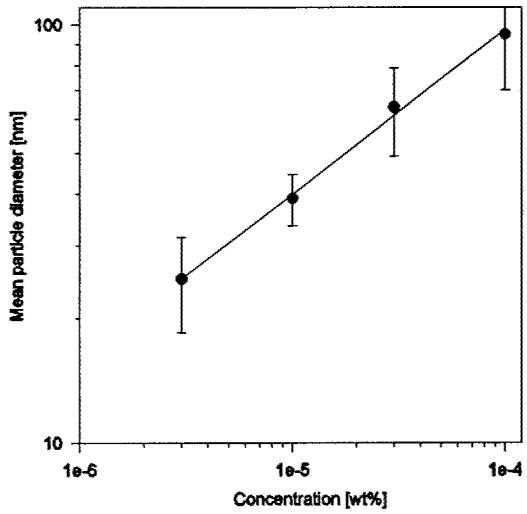


*Fig. 4: Mean particle diameter of the large cluster versus concentration for electrosprayed poly styrene ($M_w$=330,000)*

To verify this hypothesis electrospray was performed using different concentrations of polystyrene in the initial solvent. Bimodal size distributions resulted in each case. The minimum size of small particles was unaffected, corroborating that those particles are single molecule particles. The size of the bigger particles decreased with concentration. A log-log plot of the particle diameter versus the concentration reveals a straight line (see fig. 4). The experimentally found exponent of 2.6 instead of 3 reflects an additional influence on the particle size from the increased number of fission processes possible at droplets with lower initial concentrations.

## Conclusion and outlook

This work has showed, that the Langmuir method as well as the electrospray method are suitable

for the isolation of single molecules. The electrospray has in addition the unique advantage that one can tailor the number of chains in a particle. Via variation of the initial concentration we were able to produce particles with different sizes and accordingly around 5, 10 and several 100 molecules in it. Therefore the electrospray is ideally suited to address questions related to the behavior of defined single-, few- and multi-chain polymer particles, although quantities are limited. For the crystalline polymer PEO, we were able to study the particle shape as a function of the annealing time. The main goal of future research is to extend the range of molecular variables and single-molecule systems available for study. The annealing and crystallization conditions could be easily controlled with an electrospray apparatus under microgravity conditions. The produced particles could be trapped rather than collected at a target. Those trapped particles are free floating under microgravity conditions and have no interactions between each other. Therefore the crystallization kinetics of particles of different chain numbers can be studied without any influence of coalescence or surface effects.

References


1 H. Morawetz, *Macromolecules in Solution (Second Ed.)*, John Wiley, New York, 1975.

2 M.C. Petty, *Langmuir-Blodgett films*, Cambridge University Press., Cambridge, 1996.

3 A.G. Bailey, *Electrostatic Spraying of Liquids*, John Wiley, New York, 1988.

4 I. Barnikol, W.K. Barnikol, A. Beck, M. Campagnari-Terbojević, N. Jovanović, G.V. Schulz, Makromol. Chem. **137**, 111-121, 1970.

5 R.F. Boyer, R.D. Heidenreich, J. Appl. Phys. **16**, 621-639, 1945.

6 M. Antonietti, R. Basten, S. Lohmann, Macromol. Chem. Phys. **196**, 441-466, 1995.

7 H. Bu, S. Shi, E. Chen, H. Hu, Z. Zhang, B. Wunderlich, J. Macromol. Sci., Pure Appl. Chem., accepted 1996.

8 Lord Rayleigh, Philos. Mag. **14**, 184-186, 1882.

9 D.C. Taflin, T.L. Ward, E.J. Davis, Langmuir **5**, 376-384, 1989.

10 R. Festag, B. Wunderlich, D.C. Joy, S.D. Alexandratos, K.D. Cook, SPIE Proc. **2809**, accepted 1996.

11 P. Kebarle, L. Tang, Anal. Chem. **65**, 972A-986A, 1993.

# MICROGRAVITY IMPREGNATION OF FIBER PREFORMS

M. C. Altan, F.-C. Lai, & R. A. Kline, School of Aerospace and Mechanical Engineering
B. P. Grady & E. A. O'Rear, School of Chemical Engineering and Materials Science
University of Oklahoma, Norman, OK, 73019, U.S.A.
(405)325-5011; altan@mailhost.ecn.uoknor.edu

## INTRODUCTION

It is well-known that the spreading of liquids and the wetting of solid surfaces in a microgravity environment exhibit a number of interesting phenomena. Many of these phenomena are also technologically important in fabricating high-performance parts in space such as the structural components needed to build the space station or similar large space platforms. The ability to manufacture geometrically complex, lightweight and high-performance composite parts in space primarily depends on controlling flow processes such as filling a mold cavity, spreading or coating of a solid surface, and impregnation of a porous fiber preform. For example, most high-performance molding operations involve impregnation of a fibrous preform where the balance between viscous and surface forces as well as nonisothermal effects significantly affect the fluid behavior. Hence, favorable processing conditions for obtaining superior products may exist in a microgravity environment.

## PROPOSED STUDY

The proposed study involves the experimental and theoretical investigation of impregnation of a porous medium placed in a thin gapwidth, diverging planar cavity. In particular, the radially diverging flow and spreading of a Newtonian and a viscoelastic thermosetting resin through: i) ceramic porous media, and ii) glass fiber preforms will be studied. These materials are used most often to fabricate high-performance molded parts and are particularly suitable for lightweight space structures. In addition, the possibility of utilizing a surface modification process invented at the University of Oklahoma to facilitate wetting of the ceramic porous media and fibrous preforms with an organic resin will be investigated. The real-time diagnostics for the bulk flow behavior

and the spatial formation of macro- and microvoids will be accomplished by optical means as well as piezoelectric transducers. In the case of impregnation by an organic thermosetting resin, the effect of microgravity on the fiber/resin interface and adhesion quality will be analyzed at micron and submicron levels with an Atomic Force Microscopy (AFM) and a Small Angle X-ray Scattering system (SAXS) after the resin is fully cured. Microgravity experiments will also be conducted to determine important molding parameters on earth.

In this investigation the following microgravity related phenomena will be analyzed:

- The dynamics of the bulk fluid motion and the dynamic shape of the free surface under microgravity.
- The effect of gravity on the interrelation between the external pressure, free surface velocity, bulk volume fraction of the preform, and average pore size.
- The effect of microgravity on the development of micro- and macrovoids within the porous media. The spatial distribution of void density and size with respect to flow direction.
- The effects of external as well as exothermal heating on the microgravity flow patterns, pressure built-up, void formation, and impregnation stability.
- The effects of surface modification and surfactants on the microgravity impregnation of porous media. The role of surfactants in formation and possible reduction of void size and overall void content.

## STATEMENT OF WORK

This research project involves a four-year experimental and theoretical study of dynamic impregnation process of both isotropic and anisotropic porous media under normal and microgravity conditions. The research effort, in general, can be classified into following primary areas.

### Impregnation Experiments

The main experimental setup will be a disk-shaped, thin gapwidth mold cavity where the fluid is introduced at the cavity center. This cavity will be assembled using a top and a bottom plate (i.e.,

mold walls) separated by a thin spacer plate. The experimental setup, known as a center-gated disk, will generate a time-dependent, two-dimensional, axisymmetric diverging flow. Since the mold cavity thickness is rather small compared to its overall planar size, significant shear gradients exist through the thickness in addition to the deceleration components on the flow plane. This flow geometry and a similar experimental setup has been used to investigate dynamic contact line behavior [1]. With this setup, filling experiments can be performed at 5-50 psi inlet pressure using corn syrup and silicone oil (viscosity at 2,000 cp) with total filling time ranging from 3 to 30 s.

In the initial stages of this study, isothermal filling experiments will be conducted using silicone oil with viscosities ranging from 5 to 2,000 cp. If the radius and thickness of a mold cavity are in the range of 4" - 6" and 1/8" - 3/8", respectively, it is estimated that the mold can be completely filled within 2 to 20 s with a flow rate ranging from 1 to 45 $cm^3/s$. In this flow rate range, gear, diaphragm or peristaltic pumps can be used to inject silicone oil with viscosity up to 2,000 cp and inlet pressures up to 100 psi. Within the range of these experimental parameters, impregnation characteristics of: 1) alumina ($Al_2O_3$) based isotropic ceramic foam material (manufactured by Hi-Tech Ceramics, Inc.) and 2) glass preforms with plain, unidirectional, and 4 Harness Satin weave patterns (manufactured by Textile Technologies Industries and Atkins & Pearce) will be analyzed, as they are readily available, relatively inexpensive, and commonly used in the composites industry. The surface modified versions of these materials will also be tested. The porosity of the ceramic foam and the volume fraction of glass preform within the mold is another important experimental variable to be studied. It is anticipated that impregnation of at least two different porosity levels for the ceramic and three different volume fractions (e.g., 30-60%) for the glass preform will be investigated. Speed of the fluid front, spatial pressure drop, and macroscale void content will be evaluated based on real-time diagnostics using piezoelectric transducers. For isothermal experiments, the top mold wall will be made of clear acrylic so that the wetting of top wall and impregnation can be observed and video taped for further analysis. Both 1-g and ground-based microgravity experiments for the isothermal case are anticipated to be completed within the first two years. The experimental data will help us to quantify the effects of fluid viscosity, inlet pressure, porosity, and capillary phenomena under different filling conditions. In addition, fundamental formulation of the dynamic filling of anisotropic porous media in

microgravity is expected to be accomplished. Thus, numerical models can be developed to incorporate important physical phenomena uncovered by the microgravity experiments.

Subsequent experimentation will study impregnation using a non-Newtonian, thermosetting resin. Best candidates for such experiments are low viscosity epoxy resins which are specially developed for resin transfer molding. Among these, Derakane (DOW Plastics), Tactix (DOW plastics), and Hysol (Dexter) offer the best processing windows. Our choice at this point is Derakane epoxy vinyl ester resins with viscosity less than 400 cp at 25°C. Upon heating, the viscosity is expected to drop to 100 cp or less at 40-60°C. The total cure time can be adjusted from less than one minute to several hours by selecting the proper mix of catalysis, promoters, accelerators, and retarders [2,3]. To control the reaction kinetics, the temperature profile of the mold needs to be regulated. Embedded surface heating elements will be used to heat the mold to a specific temperature. The upper limit for the mold temperature is approximately 65°C. This temperature setting is sufficient for the fast cure of Derakane resins. During non-isothermal filling and curing experiments, the radial temperature variation on the mold will be continuously monitored to quantify the microgravity and capillary effects on the filling rate, temperature distribution and overshoot due to exothermic reactions. Another important aspect of non-isothermal impregnation with a thermosetting resin is the use of specially treated silica based preforms to achieve much better wetting characteristics and minimum void content.

Surface Modification and Formation of Microvoids

The wetting properties of the glass preform will be modified in two stages. In the first phase, the effect of surface active agents or surfactants on microvoid formation will be examined. The real-time ultrasonic measurements will be an important tool in evaluating the effectiveness of different surfactants in eliminating microvoids. Appropriate surfactants should facilitate wetting of the highly polar silica surface with an organic resin. Surfactants have been used previously in epoxy resins, such as in the formulation of aqueous emulsions. However, they were optimized for stabilization of the colloidal phase, not for wetting. The use of surfactants in these systems is not trivial and simple addition of an arbitrary surfactant will probably not be successful. To be effective in wetting, the surfactant must be present at the advancing front. In situations of

equilibrium wetting, large lyophobes favor wetting as they tend to drive the surfactant out of solution to the front and do the best job. However, in a large surface area matrix, the surfactant molecules are rapidly depleted from solution. As such, mass transfer resistance of surfactant diffusion to the three-phase contact region may dominate and compromise any beneficial effect. We propose to overcome this problem by pretreatment of the preform with surfactant. With a low point of zero charge, silica can be easily coated with a cationic surfactant like cetyl trimethly ammonium bromide (CTAB). Figure 1 shows data from our labs for the absorption of CTAB onto a large surface area, porous silica powder. At very low coverages (below the region covered in these earlier experiments), surfactant molecules adsorb as individual species in the so-called Henry's Law region. At higher concentrations, there is a marked increase in slope with greater rates of adsorption for a given increase in concentration of the bulk. This signifies the onset of cooperative adsorption and the formation of surface aggregates. Adsorption continues to increase until the surface is saturated or the critical micelle concentration is reached and aggregate formation begins in the supernatant. The exact structure of the aggregates on the surface at different points of the adsorption isotherm has been firmly established. At high coverage in the plateau region, it is generally conceded that aggregates are bilayer in nature. Intermediate points, however, may be hydrophobic monolayers called hemimicellas or patchwise bilayers. Consequently, the character of surfactant effects on wetting by the resin could depend strongly on the particular region of the adsorption isotherm utilized. We know from our own experience that both cationic and nonionic surfactants adsorb nicely onto silicas [4]. We will evaluate preforms modified with representative surfactants such as cetyl trimethylammonium bromide and octylphenol polyethoxylate. If effective, this would represent an easy method for prior treatment of the preform to reduce the formation of microvoids.

Material Characterization and Microscopic Testing

Complimenting the real-time acoustic studies, small angle x-ray scattering (SAXS) and atomic force microscopy (AFM) will be used to fully characterize voids both locally and globally with size ranging from one nanometer to, say, ten microns. Acoustic analysis gives both local and global information about larger voids; for smaller voids global information will be determined via

SAXS while local information will be determined via AFM. The University of Oklahoma SAXS system uses pinhole optics, hence the overall properties of the voids, such as number density and size distribution, as well as any void anisotropy can be examined. Scattering patterns will be measured in the fiber directions and the two transverse directions to quantify the anisotropic morphology. Samples will be microtomed and the microtomed surface will be examined with a Digital Instruments AFM located at the University of Oklahoma. This method will allow us to examine distributions of voids in a plane for different parts of the mold simply by microtoming different parts of the sample. AFM measurements will also be used to help interpret data from SAXS measurements, since SAXS provides an indirect measure of void morphology while AFM directly images the voids.

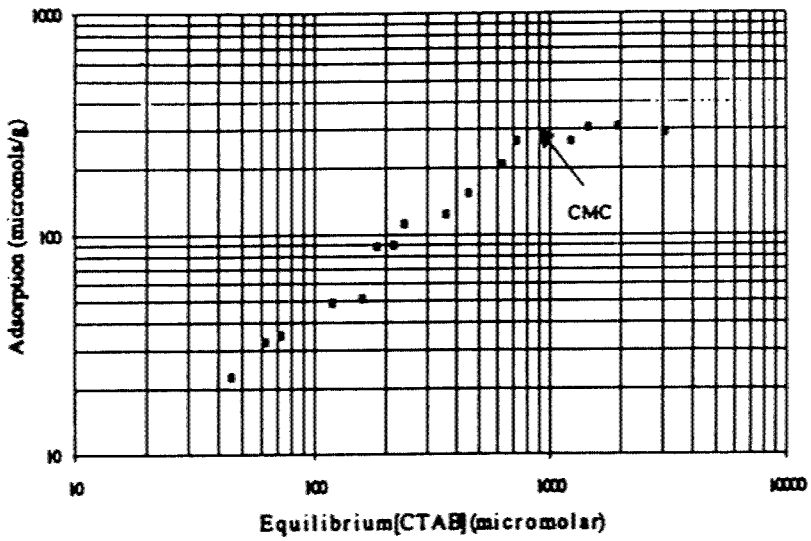


Fig. 1 Adsorption Isotherm for CTAB on HI-SIL 233.


REFERENCES

1. Elliot, G. E. P. and Riddiford, A. C., "Dynamic Contact Angles, I. The Effect of Impressed Motion" J. Colloid Interface Sci., 23: 389-398, 1967.
2. Fabricating Tips: Derakane Epoxy Vinyl Ester Resins, Revised Edition, DOW Plastics, 1994.
3. Derakane Epoxy Vinyl Ester Resins: Chemical Resistance and Engineering Guide, DOW Plastics, 1993.
4. O'Haver, J. H., Harwell, J. H., O'Rear, E. A., Snodgrass, L. J., and Waddell, W. H., "In Situ Formation of Polystyrene in Adsorbed Surfactant Bilayers on Precipitated Silica," Langmuir 10: 2588-2593, 1994.

## An electrochemical method to visualize flow and measure diffusivity in liquid metals

T. J. Anderson and R. Narayanan
University of Florida, Gainesville, Fl 32611

**Objectives:** The main objective of this program is to develop and demonstrate a novel electrochemical sensor for determining the fluid dynamic state in low Prandtl number, opaque liquid metals at high temperature. The basic idea is to use solid state electrochemical cells constructed at the container boundaries to control and detect the concentration of a tracer species. In this project, yttria stabilized zirconia (YSZ) is used as a solid oxygen-ion-conducting electrolyte and separates a `working' liquid metal electrode from a `reference' electrode. Atomic oxygen, dissolved in the liquid metal at the ppm concentration level, is detected by electrochemical cells operating in the galvanic mode. The same cell configuration is also used to establish localized concentration boundary conditions through coulometric titration of oxygen. Information about the dynamic state of the liquid metal is then obtained by perturbing the oxygen distribution in the liquid and observing the dynamic response of the measured EMF of the detection cells.

The magnitude of convective velocities encountered in the microgravity processing of liquid metals (e.g., bulk crystal growth of semiconductors) can be comparable to diffusive velocities. Thus accurate values of the oxygen diffusivity are necessary to separate the diffusive component of the oxygen flux from the convective component. Unfortunately, gravity driven convection in the melt prevents accurate measurement of the mass diffusivity of oxygen in liquid metal systems on earth. A second objective of this project is to perform the necessary ground based investigations that will lead to the flight definition of a series of microgravity experiments to measure the temperature dependent diffusivity of oxygen in liquid metals. In addition to providing accurate values of the oxygen diffusivity for the flow visualization studies, these results should provide the research community with a benchmark for the development of improved ground based cell configurations. Another science objective of this study is to establish the constitutive behavior of " Fickian" diffusion of oxygen in liquid metals. Available ground- based data is insufficiently accurate to discern if the temperature dependence of the diffusivity is of the classical Arrhenius type. The results of a recent German microgravity experiment, however, suggest a non- Arrhenius functional form.

**Need for Microgravity:** The outcome of this research program will be a tool to experimentally determine the convective state in a contained liquid metal system. As such this tool should be useful to those performing microgravity research on a variety of processes including bulk crystal growth of compound semiconductors and the casting of metals.

Although a variety of methods have been used to study the fluid dynamics of high temperature, opaque liquid metal systems, many of these techniques are of low sensitivity, intrusive, or not easily adaptable to flight based experimentation. In contrast, this tool is non-intrusive (the oxygen levels are typical of those present in liquid metal processing) and capable of detecting velocities as low as $10^{-4}$ cm/sec.

This technique is also highly adaptable to flight experimentation given power, weight,safety and signal level requirements. This method to visualize flow provides a fresh approach to a difficult problem that has the potential not only to enhance our understanding of the fluid dynamics of low Prandtl number fluids, but also provide a critical experimental link between computational fluid dynamics and processed material properties.

Both experimental and modelling results indicate that convection driven by solutal or thermal gradients is present in ground based diffusivity experiments. These results include an order of magnitude increase in the measured diffusivity of oxygen in liquid tin when the solutal gradient is reversed in transient or steady state titration experiments and observations of changes in the measured diffusivity when varying the alignment of the cell axis with respect to the gravity vector or varying the aspect ratio of the cell. This should lead to flight measurements of the oxygen diffusivity in liquid metals to provide a benchmark for this popular electrochemical technique and give insight into the functional form of the diffusivity in liquid metals.

**Summary of results:** The feasibility of this approach has been demonstrated by this team in initial studies in which an alumina tube was fitted with 17 micro-electrochemical cells and 9 thermocouples. See Figure 1. A series of experiments was performed at various values of the Rayleigh number in which the oxygen concentration was abruptly changed at the bottom liquid metal/solid electrolyte interface and monitored at the other cells located along the tube circumference. The results of these experiments clearly indicated convective dominated transport as expected at 1 g.

This feasibility study was performed in a cylindrical geometry and the transitions to different dynamical states predicted for this geometry were observed. Specifically, the measurements provided evidence for convection driven by small transverse gradients below the critical Rayleigh number. Experimental evidence was also obtained on the formation of unicellular flow patterns or axisymmetric flow cells depending on the aspect ratio, formation of vertically stacked flow cells, and the transition to oscillatory flow. These typical flow patterns are schematically depicted in Figure 2. The experiments were conducted by introducing oxygen at the bottom sensor and observing the response at the other sensors which were placed along the ampoule wall at various heights and azimuthal positions. Evidence of axisymmetric flow in an experiment conducted in an aspect ratio ( height/radius) of 1.2 is given in Figure 3a. Here it was seen that the response from 4 azimuthally displaced sensors for a given height was nearly identical, the slight offset at long times arising from possible furnace asymmetry. An experiment conducted in a taller cell with an aspect ratio of 3. gave a unicellular pattern. On account of a unicellular pattern the response from the 0° sensor could be expected to be consistently greater than the response from the 180° sensor. An increase in the Rayleigh number indicates an increase in flow velocities and one would expect that the difference in the response from these two sensors would decrease. This is all seen in Figure 3b. An experiment performed in an aspect ratio of 5.3 gave evidence of vertically stacked flow. The experimental arrangement was also tested in a pulsing mode. Here the idea was to resonate with natural frequencies in the convective state, to amplify the signal and thus improve the sensitivity of the technique. The flow velocity estimated from theoretical scaling arguments compared favorably with values calculated from experimental

measurements. A key development in advancing the technique was the incorporation of micro electrolyte rods in a non conducting container.

Considerable progress has been made in the experimental determination of the oxygen atomic diffusivity. Measurements have been made in liquid tin as a function of temperature. As a result there is evidence that solutal convection can corrupt the measurement of oxygen diffusivity in liquid metals. Experiments conducted with different cross sections were performed to determine the geometrical effect on the extent of convection. Figure 4 shows the results of a typical set of experimental runs made in a square base and circular base geometry. As seen the measured diffusivities were lower in a square base geometry indicating a lower level of convection in a square base cell compared to a circular base cell. This was expected from predictions from fluid mechanical models.

Future plans call for an examination of binary melts, molecular dynamic simulations of the diffusivity and assessment of the flow visualization sensor for different liquid systems and geometries. This ground based work will put us in a firm position to perform future microgravity experiments to answer such questions as: What is the correct functional dependence of diffusivity on temperature? What is a benchmark value as the diffusivity to judge and design improved ground experiments? What are the limitations and ranges of validity of the novel flow visualization sensor?

**Acknowledgment:** The experiments were performed by Dr. C. Mallika and Mr. S.K. Prasad. This work was funded by NASA through grants NCC8-51 and NCC8-20

**Figure 1.** ELECTROCHEMICAL CELL DESIGN USED IN PRESENT FLOW VISUALIZATION STUDIES

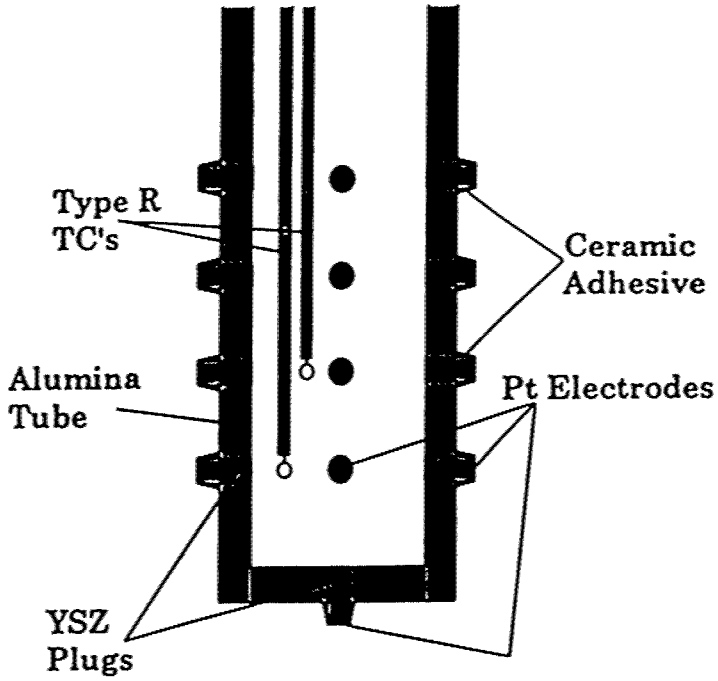


TC: Thermocouple
YSZ: Yttria-Stabilized Zirconia Solid Oxide Electrolyte

**Figure 2.** Schematic of Flow Profiles

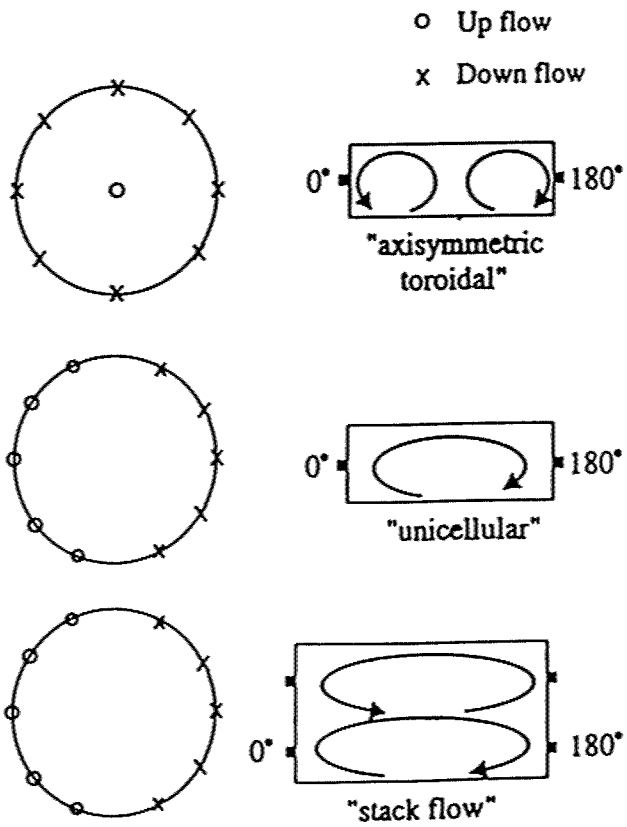

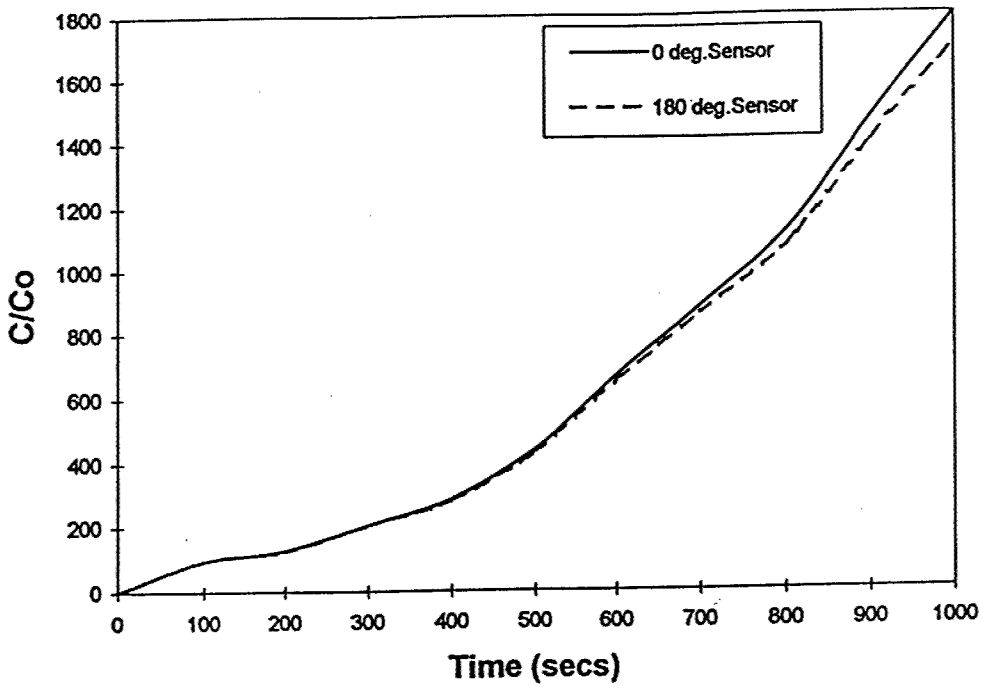


**Figure 3a.** Concentration profiles showing axisymmetric flow pattern. ( Aspect Ratio = 1.2, Ra = 2425, Melt : Pb)

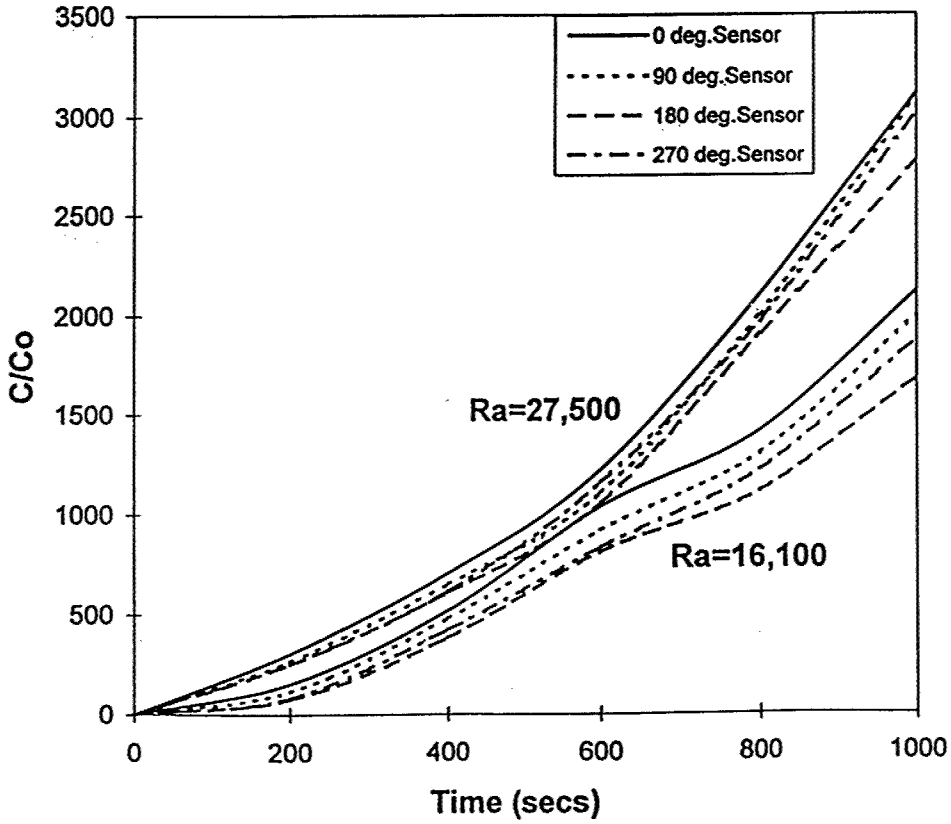


**Figure 3b.** Concentration profiles recorded at different Rayleigh numbers for a fixed aspect ratio. (Aspect Ratio = 3.0, H = 1 cm)

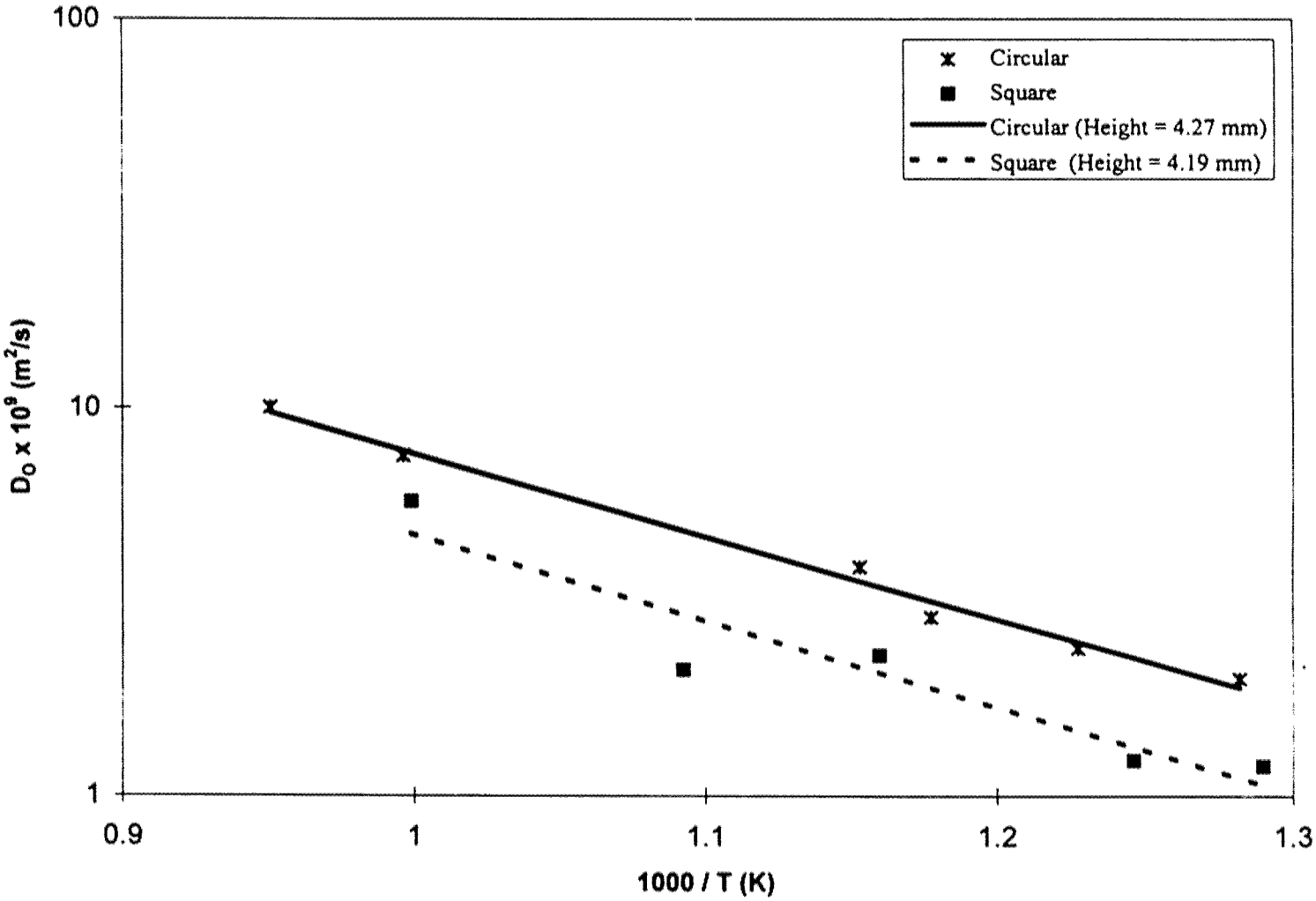


**Figure 4.** Comparison of the measured diffusivity values for a circular and square base geometry.

# COUPLED GROWTH IN HYPERMONOTECTICS

Barry Andrews
Materials and Mechanical Engineering
University of Alabama at Birmingham
Birmingham, AL 35294-4461
Phone: (205) 934-8452
e-mail: banfrews@eng.uab.edu

Sam Coriell
Metallurgy Division
National Institute of Standards and Technology
Gaithersburg, MD 20899
Phone: (301) 975-6169
e-mail: coriell@coral.nist.gov

## Introduction

The overall objective of this project is to increase knowledge of the physics controlling solidification in immiscible alloy systems. The investigation involves both experimental and theoretical aspects and includes the development and testing of a model for monotectic solidification. The model consists of two parts. The first portion involves a stability analysis to determine the conditions necessary for coupled growth. The second portion involves a detailed analysis of the events taking place at the solidification front. Testing of the model will require directional solidification of a range of alloy compositions at several solidification rates. Due to a tendency towards sedimentation in these immiscible systems and the possibility of convective instability, experimentation must be carried out under low-gravity conditions.

The monotectic reaction ($L_1 \rightarrow \alpha + L_2$) which occurs in many immiscible systems should make it possible to produce aligned fibrous composite structures through directional solidification. It should even be possible to produce these desired structures in the miscibility gap region (hypermonotectic alloys) if the proper processing conditions are utilized. Steady state growth conditions and interface stability will simply require use of the proper thermal gradient to growth rate ratio during processing (1 - 7). However, almost every hypermonotectic alloy known produces a solute boundary layer that results in convective instability. The flows generated and the resulting composition variations along the sample strongly affect the ability to maintain a

stable, macroscopically planar solidification front (5). The Coupled Growth in Hypermonotectics (CGH) experiment is designed to investigate the ability to establish stable growth conditions in these intriguing alloy systems. Details of the experiment including the specialized requirements for processing immiscible alloys are covered in the following sections.

Furnace Assembly

In the CGH experiment it is desirable to use a relatively high thermal gradient (approximately 100°C/cm) in order to obtain reasonable growth rates (approximately 1 μm/s). The furnace facility made available for this experiment was the Advanced Gradient Heating Facility (AGHF). The AGHF uses a tungsten- rhenium wound heater core and molybdenum diffuser block which provides a hot zone capable of reaching temperatures of 1400°C for short time periods. In the cold zone of the AGHF heat is extracted by an assembly containing a low melting point liquid metal which is held in direct contact with the cartridge. This furnace configuration has the capability of providing high thermal gradients but the capabilities are somewhat hampered by the necessity to use a protective cartridge assembly around the ampoule containing the sample. In addition, the samples utilized in this study are highly conductive (Al-In alloys) which further impedes the ability to reach high gradients. The end result is that thermal gradients of approximately 85°C/cm can be maintained using a sample temperature of 1100°C in the hot zone.

Ampoule Design

In order to properly carry out the desired experimentation several factors must be addressed concerning ampoule design. One of the most important factors for processing immiscible alloys is selection of the proper ampoule material in order to control wetting behavior of the alloy. In addition, it is necessary to design the ampoule assembly so that it is possible to avoid the formation of free surfaces due to thermal contraction of the melt and solidification shrinkage during processing. Alloy production and sample loading procedures must also be utilized which will minimize the formation of any voids during processing due to dissolved and/or entrapped

gases. Also, it is desirable to design an ampoule assembly that can help control thermal end effects so that a relatively uniform solidification rate is maintained during processing.

For immiscible alloys, segregation may occur when the lower volume fraction immiscible liquid phase perfectly wets the ampoule walls. In preparation for this experiment it was necessary to test a range of ampoule materials to determine if the wetting characteristics were compatible with the aluminum-indium alloys to be processed. Materials which were perfectly wet by the indium-rich immiscible liquid were unsatisfactory. Obviously, in order for an ampoule material to be acceptable it must also be chemically compatible with the molten sample for extended time periods. Long duration exposure tests were also carried out on the alloy/ampoule combinations at temperatures of 1200°C in order to identify any reactions. When both contact angle and chemical compatibility factors are considered, the only acceptable materials tested in this study were aluminum nitride and hot-pressed silicon nitride.

The sample material utilized in this investigation, an aluminum-indium alloy, goes through a rather significant expansion and contraction during heating and directional solidification. This expansion results in more than 2 cm of displacement at the end of the sample and must be accommodated. In the ampoule design for the CGH experiment, sample expansion and contraction was accommodated using a piston and spring assembly. The piston acted on the melt to prevent free surface formation and as such must had to be located at the hot end of the ampoule. For the AGHF design, the spring must also be placed in the hot zone of the furnace and can see temperatures approaching 1300°C. In the current ampoule assembly special carbon coil springs are being used that were designed and produced specifically for this application. The finite length of the samples results in variations in the heat transfer conditions during directional solidification that lead to a non-uniform solidification rate. In previous tests the solidification rate at the ends of the sample have been found to be as much as three times those at the central portion of the sample. In the current experiment, the thermal end effects have been reduced by artificially extending the thermal length of the main sample by adding dummy samples at the hot and cold end. These dummy samples are separated from the main sample by aluminum nitride pistons. The lengths of the hot and cold dummy samples can be adjusted in order to minimize variations in the solidification front velocity. The addition of the dummy

samples changed the maximum deviation from the nominal solidification rate from a factor of approximately 2.5 to a factor of approximately 1.3.

The ampoule assembly first considered for this experiment utilized a dummy sample on the cold end which extended almost to the end of the ampoule. Initial modeling of the anticipated temperature profile indicated that heat loss due to conduction down the dummy sample to the furnace cold zone would make it impossible to reach the desired temperatures for homogenization. This difficulty was solved by replacing a portion of the dummy cold sample with an alumina piece which served as an insulator. By breaking the high conductivity path it was possible to reach temperatures in excess 1200°C in the main sample region of the ampoule.

A sketch of the ampoule assembly developed for and currently being utilized in this experiment is shown in Figure 1. The assembly consists of a high temperature graphite spring, a graphite compression limiter, aluminum-nitride pistons, main and dummy samples, an $Al_2O_3$ rod and a silver chloride seal.

Results of Ground Based Tests

Extensive ground based testing has been carried out in order to evaluate the performance of the ampoule assembly discussed above. Experiments have been carried out using both the engineering model of the AGHF, which is essentially identical to the flight furnace, and a prototype of NASA's High Gradient Furnace with Quench (HGFQ) which may be used aboard space station. Some of the first tests demonstrated the ruggedness of the AlN ampoules when an over conservative thermal protection circuit caused furnace shut down after the sample had been at 1200°C for several hours. Safety interlocks built into the software prevented furnace reactivation until the sample had completely solidified and cooled to several hundred degrees Celsius. However, it was possible to remelt the sample and go through the normal processing steps without any deleterious impact on the ampoule. For most ampoule materials, when metallic samples are solidified and remelted, cracking results in total loss of the ampoule assembly.

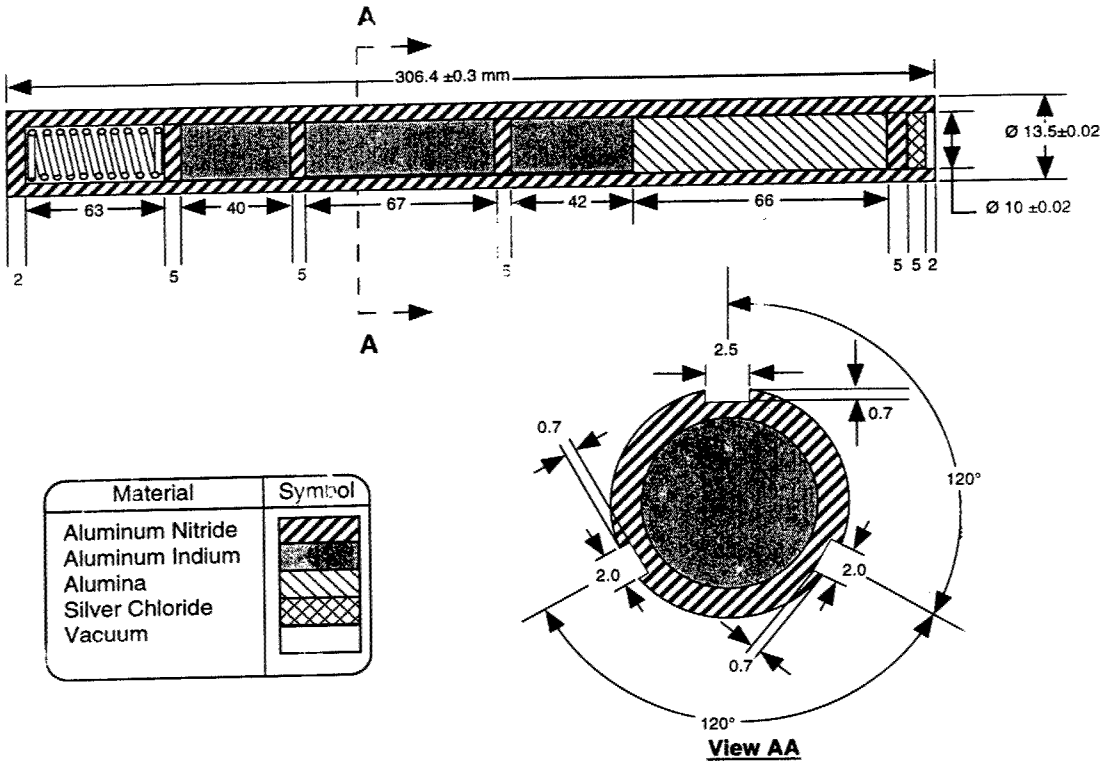


Figure 1: Schematic of the Ampoule Assembly

Difficulty was encountered in some of the early tests when the aluminum-indium alloy leaked past the piston into the carbon spring area at the hot end of the ampoule. Since aluminum will react with carbon at these temperatures to form aluminum carbide, the spring can be destroyed due to this leakage. The ampoule assemblies that were being utilized in these early runs had a significant variability in the piston to bore gaps. Measurements were taken from assemblies that did not leak and indicated that, at least for the initial spring pressures utilized (approximately 0.1 atm pressure on the melt), leakage did not occur for a piston to bore gap of 40 μm. In the final design, higher spring pressures were utilized which resulted in pressures of approximately 0.3 atm on the melt. A piston to bore gap of between 14 and 20 μm was utilized for these ampoule assemblies.

Thermal gradients and solidification rates were determined in these tests from thermocouples attached in grooves along the outside of the ampoules. The results from these tests revealed thermal gradients of approximately 85°C/cm in the AGHF engineering model furnace. Gradients of up to 140°C/cm were obtained in the prototype of the HGFQ. Solidification rate variations, as

determined from the thermocouples, were somewhat surprising. Results indicated lower solidification rates at the beginning and end of solidification of the main sample with a slight maximum in between. This variation, which is opposite that predicted, may be caused by the lower thermal conductivity AlN pistons at each end of the main sample. While this solidification rate variation was not expected it may prove beneficial by helping to maintain interfacial stability during the initial and final transients which occur during directional solidification.

The LMS mission is scheduled to launch on June 20, 1996. Three Al-In samples will be processed during this mission using the ampoule assembly described above. Results of these experiments will be reported during the Fall of 1996.

## REFERENCES


1. Andrews, J. B. et al, "The Effect of Processing Conditions on Solidified Microstructures in Immiscible Systems," Materials Science Forum, 77, 269-281, 1991.

2. Andrews, J. B. et al, "Directional Solidification in Immiscible Systems: The Influence of Gravity," Advances in Space Research, Vol. 11, No. 7, (7)291-(7)295, 1991.

3. Andrews, J. B. et al, "Solidification in Immiscible Systems," Proceedings for the IKI/AIAA Microgravity Science Symposium, Moscow, USSR, May, 238-246, 1991.

4. Andrews, J. B. et al, "The Influence of Gravity Level During Directional Solidification of Immiscible Alloys," Journal of Crystal Growth, 119, 152-159, 1992.

5 Hayes, L. J., and Andrews, J. B., "The Influence of Convection on Composition and Morphology of Directionally Solidified Hypermonotectic Alloys," Proceedings for the 7th International Symposium on Experimental Methods for Microgravity Materials Science, Las Vegas, Nevada, February, 1995.

6. Dwyer, Z. B., "Factors Affecting Stable Planar Growth During Directional Solidification of Hypermonotectic Al-In Alloys," Ph.D. Dissertation, 1994.

7 Merrick, R. A., "Direct Observation of Microstructural Developments During Directional Solidification of Immiscible Transparent Metal Analogue Materials," Master's Thesis, University of Alabama at Birmingham, 1992.

# THE EFFECT OF CONVECTION ON MORPHOLOGICAL STABILITY DURING COUPLED GROWTH IN IMMISCIBLE SYSTEMS

Barry Andrews
Materials and Mechanical Engineering
University of Alabama at Birmingham
Birmingham, AL 35294-4461
Phone: (205) 934-8452
E-mail: bandrews@eng.uab.edu

Sam Coriell
MetallurgyDivision
National Institute of Standards and Technology
Gaithersburg, MD 20899
Phone: (301) 975-6169
E-mail: coriell@coriell@coral.nist.gov

## Introduction

This study is designed to investigate the influence of convection on morphological stability of the solid-liquid interface during directional solidification in immiscible systems. Recent findings[1,2] indicate that gravity level has a dramatic influence on the structure obtained during directional solidification in these systems. Evidence from ground based experimentation by the investigators indicates this variation in microstructure may be due to fluid flow which occurs on both a microscopic scale at the solid-liquid interface and on a macroscopic scale during the solidification process[1-3]. The overall fluid flow generated appears to be capable of disrupting the coupled growth process necessary for the development of desired fibrous microstructures.[1-4]

This study will combine observations made utilizing transparent metal-analog systems with a detailed analysis of fluid flow on a microscopic and macroscopic scale. The first step will involve a theoretical analysis to determine the anticipated fluid flow at the solidification front. The analysis will then move into a combined experimentation/theoretical stage where experimentation will be carried out to either verify or disclose weaknesses in the theoretical

portion of the analysis. The findings will make a significant contribution to a better understanding of the role of fluid flow on steady state solidification and coupled growth in immiscible alloys.

## Background

It should be theoretically possible to process a hypermonotectic alloy under conditions that would result in coupled growth between the $L_2$ and $S_1$ phases.[1-5] Solidification under these conditions would result in an aligned fibrous microstructure consisting of fibers of the $L_2$ in a higher volume fraction than that found for the monotectic composition. The composition variations and temperature gradients during solidification of a hypermonotectic sample could be maintained such that the liquid temperature never fell into the region of liquid immiscibility. As a result, the primary phase, which is $L_2$ in this case, would not form in advance of the solidification front and the sedimentation problems usually associated with processing hypermonotectic alloys could be avoided.[1-4]

Unfortunately, alloys processed under conditions which should easily result in morphological stability and a macroscopically-planar solidification front usually do not produce the desired microstructure.[1-4] A simple analysis reveals that steady-state directional solidification in a hypermonotectic alloy would result in a composition profile which causes the liquid density to increase with distance from the solidification front. This variation could lead to convective instability.

Recent results indicate a strong dependency of the microstructure on gravity level, and thus convection, during processing. Low-gravity conditions (0.01g) obtained using NASA's KC-135 zero-g aircraft resulted in the formation of an aligned fibrous microstructure, while a less desirable, dispersed microstructure was produced during the high-g (1.8g) portions of flight. These results support the hypothesis that the breakdown of coupled growth is due, at least partially, to buoyancy driven flows.

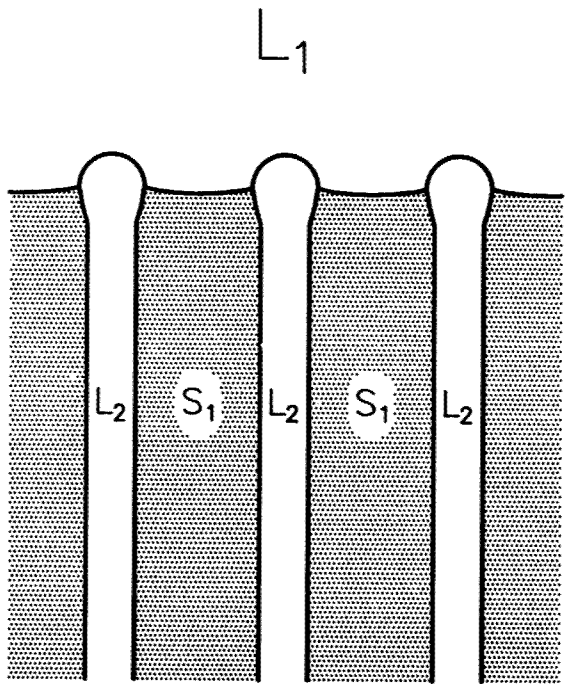


Figure 1. Schematic of the solidification front observed during coupled $S_1$-$L_2$ growth in hypermonotectic samples.

Development of the Model

We propose to model first the temperature and solute distribution in the liquid at the solidification front. This will be done both on a microscopic and macroscopic scale. The sketch in Figure 1 shows a typical structure at the solidification front. This structure will be utilized as a starting condition. Obviously, the thermal and solutal fields will lead to density variations in the liquid which will tend to drive convection. The model will take into account the microscopic density variations in the liquid between the fibers at the solidification front and the macroscopic density variation brought about due to the general depletion of solute in advance of the solidification front for a hypermonotectic alloy.

For growth of a bulk sample of hypermonotectic composition, two distinct length scales appear, namely, the interrod spacing, which is of the order of micrometers, and the sample size, which is of the order of centimeters. We will initially consider these as separate problems, and only attempt to study their interaction after a thorough understanding of each is developed. For

growth at the monotectic composition, the central problem is understanding the microscale phenomena, while for growth at hypermonotectic composition, there is the possibility of bulk convection which may disrupt the coupled growth of composite structures.

At the microscale level, the coupled growth of a monotectic has many similarities with the coupled growth of eutectics. Recently, the theory of coupled eutectic growth, which is based on the Jackson and Hunt theory,[6] has been extended by numerical computations[7] and the underlying assumptions have been elucidated.[8-10] initially, we will extend the Jackson-Hunt eutectic theory to monotectic growth. While the basic geometry of eutectic and monotectic growth are similar, in eutectic growth it is an excellent approximation to neglect diffusion in the two solid phases. For monotectic growth, one of the phases formed is now a liquid and diffusion is clearly important in this phase. In addition, in monotectic growth there is a fluid-fluid interface which can give rise to fluid flow driven by gradients of surface tension.

On the macroscopic level, except for growth at the monotectic composition, the solute concentration changes from approximately the monotectic composition at the interface to the bulk composition far from the interface. To treat the macroscopic flow problem, we propose to average over the microscopic features. Basically, this will provide boundary conditions at the interface, which will differ from the single phase problem, but will allow us to treat the bulk flow using the methods previously developed.[11] Such calculations would determine the processing conditions, namely, temperature gradients, growth velocity, and bulk composition, necessary to avoid the onset of thermosolutal convection. For hypermonotectic compositions sufficiently far from the monotectic, the system will be convectively unstable. We propose to use a finite element code to model the fluid flow in the unstable regime. Such calculations would provide flow velocities and determine macrosegregation during monotectic growth. The development of this model will lead to a better understanding of the relative significance of the factors effecting solidification in immiscible systems.

## Experimental Verification

Following the development of the theoretical model, experimentation will be carried out for verification. A transparent metal-model system will be utilized in order to facilitate flow visualization. Initial experimentation will be carried out with very small cell spacings (approximately 10μm. The small spacing between cell walls will result in a very large damping effect on fluid flow. After results are obtained for this small cell spacing, the cell thickness will be increased slightly in order to decrease damping and the experimentation repeated. Close attention will be paid to any changes in fluid flow resulting from the reduced damping. The thickness of the cells will be systematically increased and the effect of reduced damping quantified. The resulting increase in fluid flow is expected to eventually lead to the disruption of the coupled growth process at the solidification front.

Eperiments will be carried out using a temperature-gradient-stage microscope and will be archived using time-lapse video tape recording. This approach will facilitate determination of the flow velocities for comparison with velocities predicted from the model. The succinonitrile-glycerol $(CH_2CN)_2$-$(C_3H_5(OH)_3)$ system will be utilized for this study.

## Summary

This study will investigate the influence of fluid flows on processes at the solidification front and the structures obtained during directional solidification of immiscible alloys. The first portion of the investigation will involve the development of a model describing fluid flow during the solidification of immiscible materials. This portion of the project will be followed by experimentation designed to test the ability of the theoretical model to predict fluid flow in samples processed under one-g conditions and the effect of this fluid flow on sample morphology. Fluid flow will be regulated through the use of thin sample cells that will help damp fluid motion. The findings from this study will result in a dramatic improvement in the level of understanding of immiscible alloys and the influence of fluid flow on the coupled growth process.

## References


1. J.B. Andrews, Z.B. Dwyer, R.A. Merrick, A.C. Sandlin, and S. R. Coriell, "Solidification in Immiscible Systems," Proceedings for the AIAA/IKI Microgravity Science Symposium, Moscow, USSR, May, 1991, 238-246.

2. J.B. Andrews, A.C. Sandlin, and R.A. Merrick, "Directional Solidification in Immiscible Systems: The Influence of Gravity," Advances in Space Research, Vol. 11, No. 7, (7)291-(7)295, 1991.

3. J.B. Andrews, R.A. Merrick, Z.B. Dwyer, A.C. Sandlin, M.B. Robinson, "The Effect of Processing Conditions on Solidified Microstructures in Immiscible Systems," Materials Science Forum, 77, pp. 269-282 (1991).

4. J.B. Andrews, A.L. Schmale, A.C. Sandlin, "The Influence of Gravity Level During Directional Solidification of Immiscible Alloys," Journal of Crystal Growth, 119, pp 152-159 (1992).

5. M.C. Flemings, Solidification Processing, eds. B.J. Clark and M. Gardner, (McGraw-Hill, Inc.), (1974).

6. K.A. Jackson and J.D. Hunt, "Lamellar and Rod Eutectic Growth," Transactions of the Metallurgical Society of AIME, 236 (1966) 1129-1142.

7. D.A. Kessler and H. Levine, J. Crystal Growth 94 (1989) 871.

8. K. Brattkus, B. Caroli, C. Caroli, and B. Roulet, J. Phys. France 51 (1990) 1847.

9. P. Magnin, R. Trivedi, "Eutectic Growth: A Modification of the Jackson and Hunt Theory", Acta Metall. Mater. Vol. 39, No. 4, pp. 453-467, 1991.

10. B. Drevet, D. Camel, J.J. Favier, "Solute Boundary Layer and Convection in Solidification of Eutectic Alloy", Proceedings VIIth European Symposium on Materials and Fluid Sciences in Microgravity, Oxford, UK, 10-15 September, 1989, ESA SP-295 (January, 1990) pp. 101-108.

11. S.R. Coriell and G.B. McFadden, "Instability During Directional Solidification: Gravitational Effects," Progress in Low-Gravity Fluid Dynamics and Transport Phenomena, J.N. Kostes and R.L. Sani, Editors, (AIAA), (1990).

# OSTWALD RIPENING OF LIQUID AND SOLID "DROPLETS" IN LIQUID METAL MATRICES

Alan J. Ardell
University of California, Los Angeles
Department of Materials Science and Engineering
School of Engineering and Applied Science
6531-G Boelter Hall
Box 951595
Los Angeles, CA 90095-1595
(310) 825-7011
(310) 206-7353 fax
aardell@ucla.edu

## INTRODUCTION

### Background

Ostwald ripening (coarsening) involves the growth of large particles at the expense of small ones in a polydisperse array. The driving force for coarsening is the reduction of interfacial area, hence energy, that accompanies growth as solute atoms are transported by diffusion from small to large particles. The first complete theories of diffusion-controlled coarsening were published in the seminal papers of Lifshitz and Slyozov [1] and Wagner [2] (LSW). In the LSW theory the precipitates are assumed to be spherical and sparsely dispersed throughout the matrix, their mean separation far exceeding their average size. One prediction of the LSW theory is that the average particle radius, $\langle r \rangle$, increases with aging time, $t$, according to the familiar kinetic law

$$\langle r \rangle^3 - \langle r_o \rangle^3 = kt, \tag{1}$$

where $\langle r_o \rangle$ is the value of $\langle r \rangle$ at the onset of coarsening ($t = 0$) and $k$ is a rate constant. Another important prediction of the LSW is the distribution of particle sizes. Most relevant to this project is the predicton that there must be a small decrease in the residual supersaturation, $X^\alpha - X_e^\alpha$, with aging time, where $X^\alpha$ is the average solute concentration in the $\alpha$-phase matrix at $t$. $X^\alpha - X_e^\alpha$ obeys the asymptotic relationship [1]

$$X^\alpha - X_e^\alpha \approx (\kappa t)^{-1/3}. \tag{2}$$

The rate constant $\kappa$ is related to the physical parameters of the system by the equation [3]

$$\kappa = \frac{D\Delta X_e}{9}\left(\frac{G_m^{\alpha''}}{\sigma V_m}\right)^2, \tag{3}$$

where D is the coefficient of solute diffusion in the continuous $\alpha$-phase, $\sigma$ is the free energy of the particle/matrix interface, $V_m$ is the partial molar volume of solute atoms in the dispersed (precipi-

tate) β phase, $\Delta X_e = X_e^\alpha - X_e^\beta$, where $X_e^\alpha$ and $X_e^\beta$ are the solute concentrations (in atom fraction) of the α and β phases in true thermodynamic equilibrium (particles of "infinite" size), $G_m^{\alpha''} = d^2G_m^\alpha/dX^2$ is the second derivative of the molar free energy of mixing, $G_m^\alpha$, of the α phase with respect to composition, evaluated at $X_e^\alpha$, R is the gas constant and T is the absolute temperature. The rate constants κ and $k$ are related as $k = \kappa/\ell^3$, where $\ell$ is the so-called capillary length [4]; $\ell = 2V_m/\Delta X_e G_m^{\alpha''}$.

It has long been recognized that the LSW theory should be modified in some way to account for the fact that in any system containing a finite volume fraction, $f$, of precipitates there must be diffusional interactions, or overlapping diffusion fields, that affect the rate at which an individual precipitate grows. Also, when $f$ is large physical encounters among the growing particles can become important. Considerable theoretical effort has been directed towards finding a quantitative solution to this problem. The differences among the theories and the extent to which they have succeeded in predicting the effect of $f$ on coarsening behavior have been reviewed [4-6]. All extant theories predict that finite $f$ accelerates the growth rates of individual particles because the diffusion distances decrease as $f$ increases. The temporal dependence of $\langle r \rangle$ is unaffected by $f$, but $k$ in equation (1) must be replaced by $k_f = kF(f)$, where $F(f)$ is some function of $f$ which depends on the particular theory [in the LSW limit $f = 0$ and $F(0) = 1$]. This, in turn, influences the particle size distributions, invariably broadening them. There is also an effect of $f$ on κ, such that κ becomes $\kappa_f = k_f/(\ell\langle u \rangle)^3$ [3], where $\langle u \rangle = \langle r \rangle/r^*$ and $r^*$ is the radius of a particle that is neither growing nor shrinking at time $t$ (in the LSW theory $\langle u \rangle = 1$, i. e. $r^* = \langle r \rangle$). When $f > 0$, $\langle u \rangle < 1$; the extreme value of $\langle u \rangle$ in the limit $f = 1$ is $\langle u \rangle = 8/9$ [7].

Ostwald ripening has been intensively investigated in solid alloys in which the dispersed phase is coherent with the continuous matrix phase. Coherency introduces the issues of the influence of elastic energy on the morphology of individual particles and spatial correlations among groups of precipitates. The research activity in this aspect of coarsening behavior is currently quite intensive, and much of the progress to date has been summarized in a recent review article by Voorhees [4]. The motivation for investigating coarsening in liquid systems is that the underlying assumptions of the LSW theory are ideally fulfilled when the continuous phase is a liquid. In a liquid matrix the particles of the dispersed phase, be they liquid or solid, are usually spherical in shape, and both the continuous and dispersed phases are free of the internal stresses that complicate Ostwald ripening of coherent precipitates in solid systems.

Experimental investigations of Ostwald ripening in liquids are difficult to execute because they are plagued by the differences in mass density between the dispersed and continuous phases, which produce gravity-driven sedimentation forces in terrestrial laboratories. In principle, sedimentation

can be circumvented in experiments conducted in a microgravity environment. Under these circumstances the only other difficulty that arises is the possible existence of a temperature gradient, which can influence the ripening process by Marangoni convection. The various phenomena that can affect Ostwald ripening in liquids are described in a comprehensive review article by Ratke [8].

Coarsening in Liquids

Experimental work on coarsening in liquids has been done in terrestrial laboratories, and many of these experiments have dealt with the coarsening of solid particles in a liquid matrix in the context of liquid-phase sintering; the liquid matrix here is actually the minority phase. In the only microgravity experiments done to date, Kneissl and Fischmeister [9] investigated alloys containing from 2 to 5 wt. % Pb, over which the volume fraction of Pb varies from 0.0032 to 0.020. The alloys were cooled as rapidly as possible from the temperature of ripening (450 °C), in the hope of preserving the dispersions in the state to which they had evolved. The microstructures were then examined afterwards using metallographic methods, which severely limited the amount of data obtained. Kneissl and Fischmeister were able to examine only one microstructure from each alloy because it was possible to use only one aging time. Their entire analysis of the kinetics and particle size distributions was obtained from examination of the microstructures before and after the space flight. For this reason the data of Kneissl and Fischmeister have been re-analyzed and re-interpreted [10,11], the effect of $f$ being attributed to Marangoni motion during cooling.

## EXPERIMENTAL APPROACH OF THE RESEARCH PROGRAM

Experiments on coarsening in liquids under microgravity conditions can yield a much greater quantity of reliable data if the investigation does not rely exclusively on post-mortem metallographic examination. The novel objective of this research is to investigate coarsening by continuously monitoring the electrical resistivity, $\rho$, of the liquid as a function of $t$. The scientific basis for this approach is the dependence of $\rho$ on $X^{\alpha}$, which varies with $t$ according to equation (2). In principle, $\rho$ is affected by both the precipitate and matrix phases in any two-phase alloy. However, Rossiter [12] has shown that for a dilute dispersion of spherical particles in the limit of small $f$, the resistivity of the two-phase alloy is described by

$$\rho \cong \rho_m\left(1+\frac{3f}{2}\right). \tag{4}$$

where $\rho_m$ is the resistivity of the continuous (matrix) phase. When $\rho$ depends linearly on $X^{\alpha}$, which is often the case for dilute solutions, we can write

$$\rho_m - \rho_A = KX^{\alpha}, \tag{5}$$

where $\rho_A$ is the resistivity of the pure solvent (A) and K is a calibration constant. Therefore, when $f$ is very small $\rho = \rho_m$, which then depends uniquely on $X^\alpha$.

There are two factors that can influence the accuracy of the data. One is a potential limitation imposed by the physics of the coarsening process itself and the other is a limitation associated with temperature control. Using values of the other parameters relevant to the coarsening of liquid Pb in Zn at 450 °C published by Kneissl et al. [13], namely $D = 3 \times 10^{-10}$ m$^2$/s, $V_m = 18 \times 10^{-6}$ m$^3$/mol, $X_c^\alpha = 0.0046$, $X_c^\beta = 0.93$ and $\sigma = 0.114$ J/m$^2$, and taking $\langle u \rangle = 1$, it can be shown that $\kappa = 1.34 \times 10^{13}$ s$^{-1}$. This value of $\kappa$ is *9 to 12 orders of magnitude larger than those typical of solid systems.* Such a large value of $\kappa$ implies that between 10 and 1000 s, the concentration of Pb in solution can be expected to decrease by $\approx 1.53 \times 10^{-5}$, i.e. by only about 15.3 appm at 450 °C. The changes in solute concentration accompanying coarsening in liquids will generally be the order of *tens of parts per million*! Using data on the variation of $\rho$ with solute concentration in liquid Zn-Pb alloys [14], the resistivity can be expected to change by 0.027 n$\Omega$·m between 10 and 1000 s at 450 °C. Changes this small are readily measurable using modern instrumentation, and variations much smaller than this can be detected without difficulty.

In reality, however, the temperature coefficient of the resistivity of liquid metals is so large that without a unique experimental arrangement, the expected temperature fluctuations during normal temperature control would completely eliminate any chance of measuring the changes in $\rho$ estimated above. It can be shown that this effect is *nearly 2000 times larger than the change in resistivity we expect from the change in solute concentration during coarsening*. To overcome this problem we intend to use a containerless method of measuring electrical resistivity called *differential resistometry*, which involves measurements of the change in inductance of mutual inductance coils; several comparable methods are in use today [15-19]. In this technique the specimen containing the two-phase mixture of, say, Pb droplets dispersed in a Zn-rich liquid matrix, is configured as part of a bridge circuit in which one of the other legs is a dummy specimen maintained at exactly the same temperature. The dummy specimen is ideally a saturated liquid solution of Pb in Znat the experimental coarsening temperature, so that its composition is constant as a function of aging time. The output of the bridge circuit will therefore depend only on the *difference* in concentration between the actual and dummy specimens, and will be unaffected by temperature fluctuations since both the actual and dummy specimens are always at exactly the same temperature. There is no need to measure absolute values of $\rho$ because only the change of $\rho$ with aging time is important. The frequency of the bridge circuit must be chosen so that the resistance of the bulk liquid is measured, rather than the surface resistance, but it is not difficult to show that the skin depth exceeds a typical specimen diameter (e.g. 2 mm) at readily accessible frequencies (~10 kHz).

There are numerous potentially interesting alloy systems with liquid monotectics that can serve as potential candidates for the proposed research, but in view of previous efforts the best candidates are the Zn-Pb and Pb-Cu alloy systems. In Zn-Pb alloys the dispersed phase consists of liquid Pb droplets, while in Pb-Cu alloys the "droplets" are solid Cu particles. Ratke et al. [10,11] and Uffelmann et al. [20] have concluded, based on limited data, that the coarsening behavior in these two systems deviates from the predictions of the LSW theory and later modifications thereof. Whether or not the deviant behavior is real, and not due to experimental difficulties, there is at least some information on these alloys that will be of value for guiding new experiments. The behavior of other alloy systems will also be explored; Zn-Bi alloys and Pb-rich Pb-Zn alloys, in which coarsening of liquid droplets or solid particles in a liquid matrix can be investigated, depending on composition and temperature, are prime candidates. In all the alloy systems the principal objective will be to investigate the role of volume fraction at much smaller volume fractions than those in other liquid alloys investigated to date. The coarsening of liquid Pb droplets in the Zn-rich Zn-Pb alloys studied by Kneissl and Fischmeister ($0.003 < f < 0.020$) clearly satisfies the requirement that $f$ be small.

Proof of concept will be tested in two different ways: 1. The first attempt will be to investigate the output of the bridge circuit as a function of time when both of the active legs contain pure liquid Zn. In this case the output of the circuit should be either zero, if perfectly balanced, or constant, if there is a slight imbalance. In either case the output should not vary with fluctuations in temperature of the furnace as it is being controlled. The circuit will be tested in this way for temperatures up to about 600 °C. The experiments will involve trial-and-error winding of Cu coils, using Cu sheathed in high-temperature insulation, wound on quartz or ceramic forms. Different solutes will then be added to the Zn in one of the legs of the bridge circuit and the change in resistivity noted. The results will be compared with published data on the concentration dependence of resistivity, and other liquid alloys will be tested to establish the accuracy of the technique. 2. The second test of the proposed method will be to perform an actual aging experiment on a well-studied solid system, in this case Cu-rich Cu-Co alloys. Coarsening in this system has been investigated by several groups [6], but never by *in-situ* experiments such as those proposed. If the changes in $\rho$ during coarsening of coherent f.c.c. Co precipitates, the volume fractions of which are quite small in these alloys (0.005 to 0.03 is common), can be detected, the prospects for succeeding with the proposed liquid alloys will be excellent. The reason for this optimism is that the dependence of resistivity on concentration in Cu-Co alloys is only about four times larger than in Zn-Pb alloys (though the temperature dependence of $\rho$ for solids is generally much smaller than for liquids). Therefore if the experiments provide meaningful data on coarsening in Cu-Co alloys, the expectation is that they should succeed in liquid systems as well.

## REFERENCES


1. I. M. Lifshitz and V. V. Slyozov, *J. Phys. Chem. Solids* **19** (1961) 35.
2. C. Wagner, *Z. Elektrochem.* **65** (1961) 581.
3. A. J. Ardell, *Interface Science* **3** (1995) 119.
4. P. W. Voorhees, *Annu. Rev. Mater. Sci.* **22** (1992) 197.
5. P. W. Voorhees, *J. Stat. Phys.* **38** (1985) 231.
6. A. J. Ardell, in *Phase Transformations '87*, ed. by G. W. Lorimer, Institute of Metals, London (1988), p. 485.
7. A. J. Ardell, *Acta Met.* **20** (1972) 61.
8. L. Ratke, in *Prog. in Astronautics and Aeronautics*, ed. by J. N. Koster and R. L. Sani, AIAA, Washington, DC, **130** (1990), p. 661.
9. A. Kneissl and H. Fischmeister, in *Proc. 5th European Symposium on Materials Sciences Under Microgravity, Results of Spacelab-1*, European Space Agency Rept. SP-222 (1984), p. 63.
10. L. Ratke, H. Fischmeister and A. Kneissl, in *Proc. 6th European Symposium on Materials Sciences under Microgravity Conditions*, European Space Agency Rept. SP-256 (1987), p. 161.
11. L. Ratke, H. Fischmeister and A. Kneissl, in *Proc. 7th European Symposium on Materials and Fluid Sciences in Microgravity*, European Space Agency Rept. SP-295 (1987), p. 135.
12. P. L. Rossiter, *The Electrical Risistivity of Metals and Alloys*, Cambridge University Press, Cambridge, England (1987), p. 169.
13. A. Kneissl, P. Pfefferkorn and H. Fischmeister, in *Proc. 4th European Symposium on Material Sciences Under Microgravity*, European Space Agency Rept. SP-191 (1984), p. 55.
14. V. Y. Asonovich, I. T. Sryvalin and V. A. Kozlov, *Russian Metallurgy* **4** (1969) 137.
15. D. W. Nyberg and R. E. Burgess, *Can. J. Phys.* **40** (1962) 1174.
16. R. C. Callarotti, *J. Appl. Phys.* **43** (1972) 3949.
17. A. J. Hamdani, *J. Appl. Phys.* **44** (1973) 3486.
18. W. Wejgaard and V. S. Tomar, *J. Phys. E: Sci. Instr.* **7** (1974) 395.
19. W. Bauhofer, *J. Phys. E: Sci. Instr.* **10** (1977) 1212.
20. D. Uffelmann, W. Bender. L. Ratke and B. Feuerbacher, *Acta Metall. Mater.* **43** (1995) 173.

# FUNDAMENTAL ASPECTS OF VAPOR DEPOSITION AND ETCHING UNDER DIFFUSION CONTROLLED TRANSPORT CONDITIONS

Klaus J. Bachmann
Departments of Materials Science and Engineering and Chemical Engineering
North Carolina State University, Raleigh, NC 27695-7919,
Tel. (919) 515-2538, e-mail: bachmann@mte.ncsu.edu

## Objectives and Preceding Research

Through the development of atomic probe and surface spectroscopic techniques considerable advances have been made recently regarding the understanding of interactions of solid surface with small molecules at up to monolayer coverage. However, large gaps still exist in the understanding of heteroepitaxial overgrowth of a substrate under steady-state conditions of chemical vapor deposition (CVD) and vapor etching (CVE) particularly in regimes of high fluxes of reactants and products. High reactant flux is important in the context of (i) stoichiometry control for compounds exhibiting high decomposition pressure at the process temperature and (ii) high throughput, which, along with maintaining low thermal budget, is an important aspect of single wafer semiconductor processing. Since the kinetic limitations to growth and the need for relief of process induced strain favor rapid processing at elevated temperature over low temperature processing, we focus in this paper onto conditions of rapid thermal organometallic chemical vapor deposition and vapor etching at superatmospheric pressure.

We build in this study on preceding research based on low pressure chemical vapor deposition, especially pulsed chemical beam epitaxy (PCBE) and a novel method of real-time process monitoring, p-polarized reflectance spectroscopy (PRS)[1]. Although the anticipated work at superatmospheric pressure presents challenging problems that do not exists under the conditions of PCBE significant information can be gained from the low pressure work to guide research at higher vapor density, which is briefly reviewed here. In PCBE pulsed ballistic beams of the source vapors, e.g., t-butylphosphine(TBP) and triethylgallium (TEG) for GaP growth, are directed onto a substrate wafer, e.g., a Si (100) wafer that is heated from the backside inside an evacuated chamber. Figure 1 shows the implementation of PRS. A HeNe laser, chopper and Glan-Thompson polarizer mounted outside the deposition chamber provides for a chopped highly p-polarized beam of light that impinges onto the substrate at its pseudo-Brewster angle. At this angle of incidence,

the reflectance for p-polarized light is of the order of $10^{-5}$ thus establishing high sensitivity to changes in the bulk dielectric function of the substrate and to the deposition of a heteroepitaxial film on its surface. The reflected beam is phase sensitively detected by a silicon photodiode in conjunction with a lock-in analyzer. Also, the scattered light is into a solid angle of $5^{o}$ off the plane of incidence is detected by a photomultiplier in conjunction with a second lock-in analyzer. Since the reactant and product molecules that participate in the surface reactions associated with deposition or etching are polarizable, their individual contributions $P_i$ to the polarization sum up to the $P_{srl}$ of a surface reaction layer (srl), thus establishing a well defined dielectric function of the srl according to $\varepsilon_{srl} = [1+4\pi P_{srl}]$. Therefore the complex reflectivity is described by the Fresnel equations for a four-layer stack: ambient - srl - thin film - substrate which is shown in Fig. 1. Figure 2 shows a typical PRS signal for steady state growth of GaP on Si(100). The initial rise before commencing growth is due to the temperature-dependent change of the dielectric function upon heating. The extra intensity in the reflected and in the scattered light signals at the onset of nucleation and overgrowth is related to the fact that a corrugated film, in this case composed of islands of GaP and ambient, has an effective dielectric function that is smaller than that for the contiguous film. Thus only upon complete overgrowth of the Si surface by a contiguous GaP film

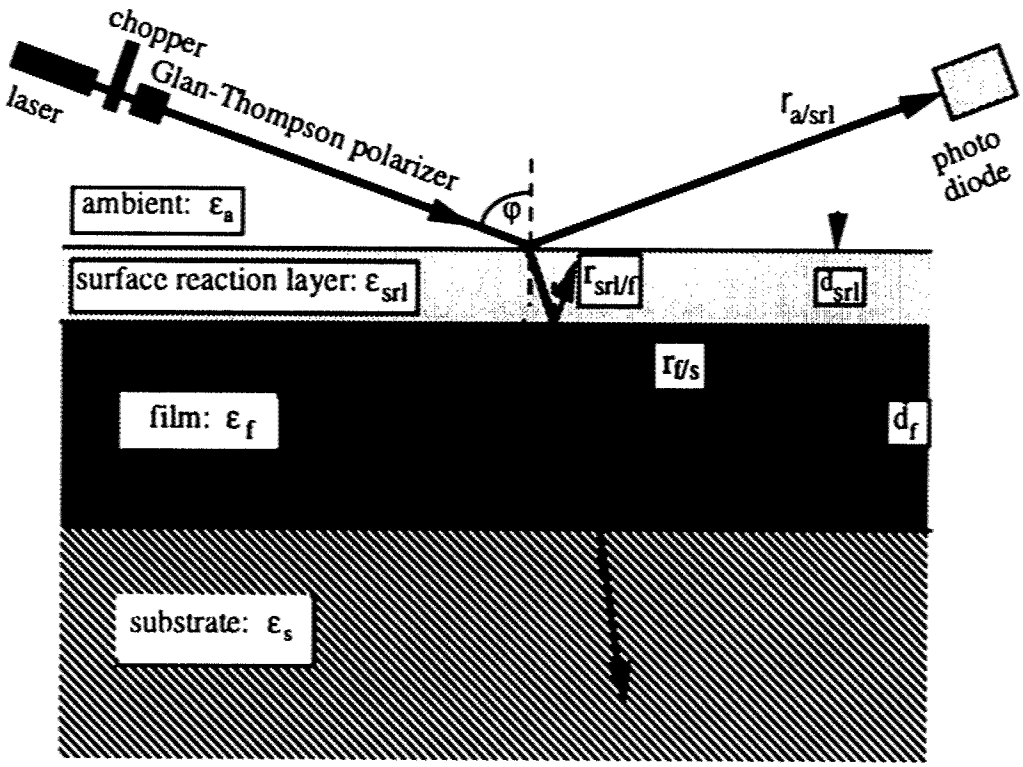


Figure 1. Schematic representation of the implementation of p-polarized reflectance for a four-layer stack ambient - surface reaction layer - film - substrate

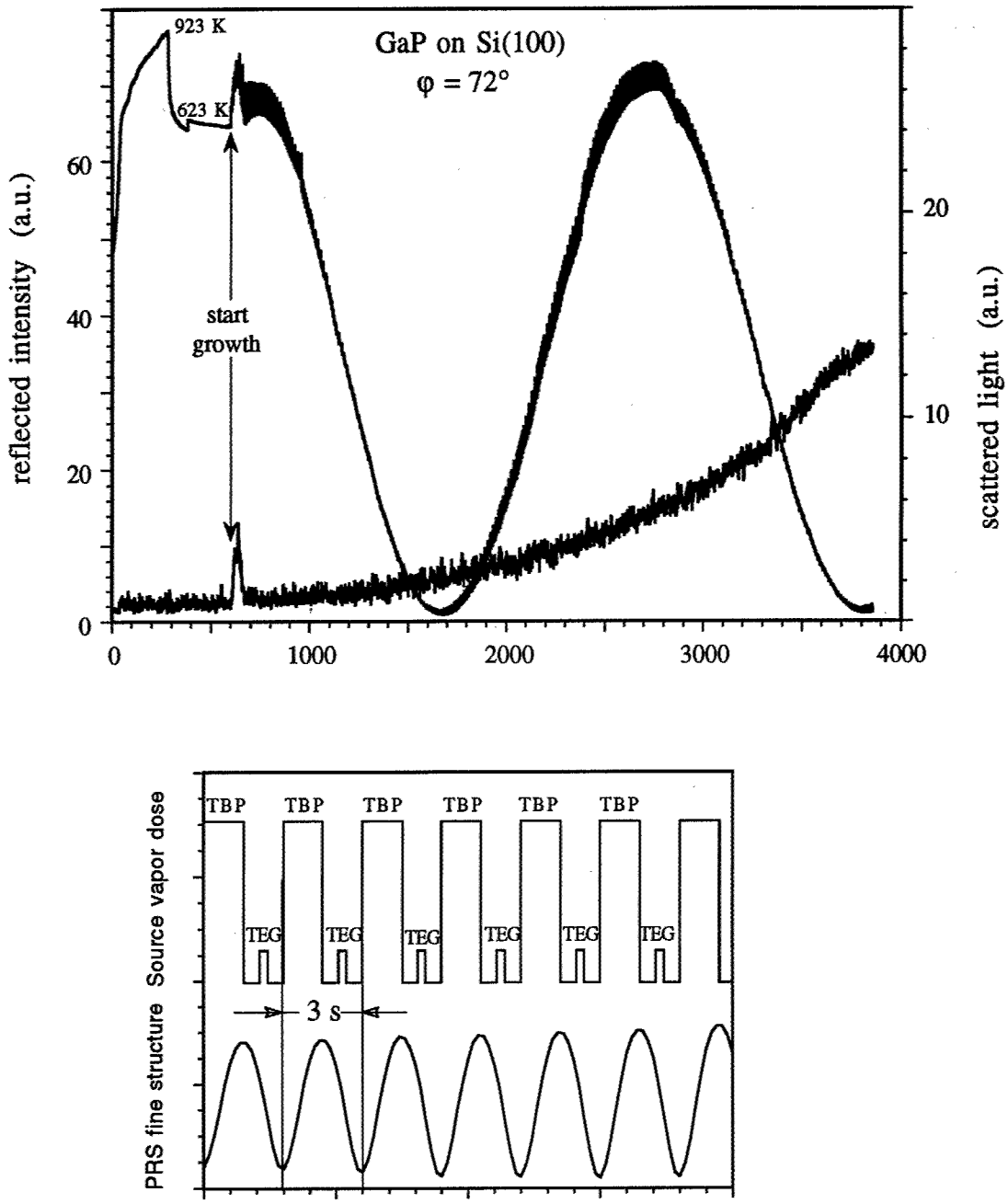


Figure 2. Top: Single wavelength PR intensity and scattered light intensity vs. time for growth of GaP on Si(100); bottom: Correlation of PRS signal and source vapor pulse cycles.

the reflected signal joins into the predicted oscillations due to interference of the partial waves reflected at the substrate/film and film/srl interfaces. Superimposed to these slow oscillations that provide real-time information on the growth rate of the film is a periodic fine structure - not

resolved in Fig. 2 (top). The periodicity of this fine structure shown on a magnified scale in Fig. 2 (bottom) matches the periodicity of the TBP/TEG source vapor pulse cycle. By counting the number of source vapor pulses per interference fringe we can determine the average growth rate per cycle. While for a given height and width of the TBP and TEG pulses changes in the length of the pause after the TBP pulse does not affect the growth rate per cycle, a pronounced increase in the growth rate per cycle is observed with increasing length of the pause after the TEG pulse[2]. Thus the pyrolysis of TBP into surface species that support growth is fast and the conversion of TEG into surface species that support growth is slow, that is, the kinetics of shedding the alkyl ligands of the TEG molecule is a rate limiting step. Another observation that may become important for the anticipated research is that, in steady-state at high source vapor fluxes, several monolayers of GaP may be deposited per cycle. This implies that the reflectance in steady state at high source vapor flux the srl contains more than a monolayer of fragments of TEG and possibly TBP to sustain the growth. In this case, homogeneous chemical reactions can proceed in the srl both in parallel and sequentially to surface reactions[3]. Further details can be extracted from the time dependent rise and decay times in the PR fine structure and extensions of the single wavelength monitoring to spectroscopic measurements. Also, substantial supplementing information can be obtained by combining PRS with timed mass spectrometric sampling and on-line scanning tunneling microscopy, which for reasons of space cannot be discussed here in detail. The application of remote real-time process monitoring and control has the advantage that the essential information to be gained is collected while the experiment is in progress, so that - based on the real-time information - process modifications can be implemented by the team of ground-based observers, if not in real-time within the execution of a particular run, then at least between successive experiments that are expected to be of substantially shorter duration than bulk crystal growth experiments. Thus the evaluation of experiments becomes decoupled from the scheduling of sample recovery to a large extent.

## Deposition and Etching at High Vapor Density

The research program on deposition and etching at high vapor densities initiated here is motivated by the potential advantages provided by high nutrient density in the context of throughput and control of compound stoichiometry. The objectives of our research program on CVD and CVE processes at elevated pressure are:

(i) The design, construction and testing of a prototype of the first confinement shell of a vapor processing experimental module (VPEM) comprised of a load-lock/wafer storage, etching and deposition chambers;

(ii) investigations of heteroepitaxy and etching of $Ga_xIn_{1-x}P$ heterostructures as model system;

(iii) software development for process simulation and remote control of data acquisition and process execution.

The overall goal of the program is to establish a comprehensive science base for space experiments and to evaluate engineering options for the construction of the VPEM, including an assessment of cost and critical points in the deployment and maintenance of this module, in particular safety and waste management issues. Under ground-based conditions, uncontrolled natural convection can be avoided by forced channel flow for $Gr<Re^2$, where Gr and Re are the Grashof and Reynolds numbers, respectively. This sets a minimum linear flow velocity $v_f >> \sqrt{\beta_t \Delta T |\mathbf{g}| l_c}$, where $\beta_t$, $\Delta T$, $l_c$ and **g** are the volume expansion coefficient, the temperature differential along the characteristic dimension of the reactor $l_c$ and **g** is the gravity vector. For the anticipated operating temperature and the reactor geometry shown in Fig. 4, linear flow velocities in excess of 1m/s are required for nitrogen as carrier gas at 10 bar pressure, corresponding to Reynolds numbers $Re>>2x10^3$. Thus experimentation at 1**g** must be analyzed in terms transport and homogeneous gas phase reactions

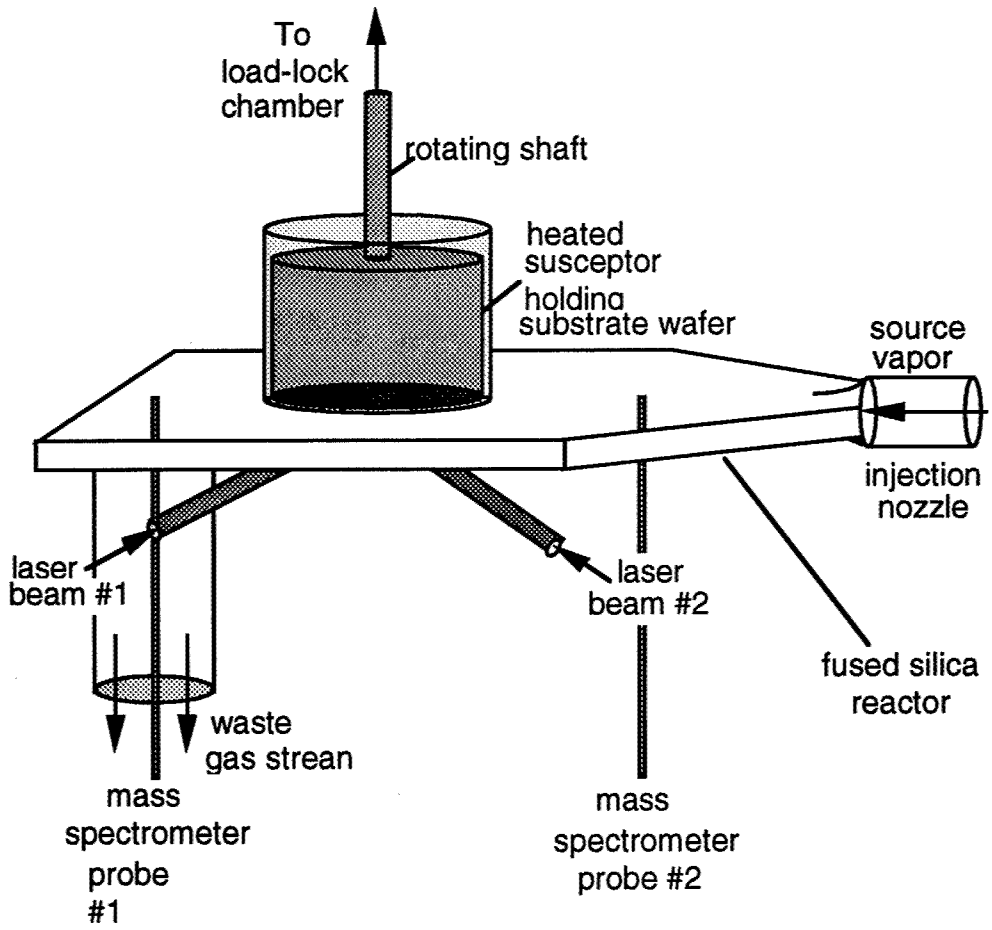


Figure 3. Schematic representation of fused silica reactor kept at isobaric conditions in first steel confinement shell

coupled to three-dimensional time-dependent flow and surface reactions leading to deposition or etching. Also, real-time optical process monitoring must anticipate and deal with noise related to scattering that is associated with temporal and spatial variations in vapor density. These are difficult tasks, requiring advances in applied mathematics both with regard to the modeling of fluid dynamics coupled to complex chemical reactions and control theory that are outside the scope of the program discussed here. Fortunately Gr scales with |g|, so that, at microgravity, much smaller flow velocities can be used and larger temperature gradients can be sustained in the channel under conditions of laminar flow. Thus work in a microgravity environment permits variations in process conditions not accessible on the ground and is desirable for calibration and validation of the predictions of simulations of surface kinetics and well behaved flow. Under conditions of laminar flow, transport is dominated by diffusion across a boundary layer of width $\delta \approx (l_c x/Re)^{1/2} = (\nu_a x/\rho v_f)^{1/2}$, where $\nu_a$ and $\rho$ are the absolute viscosity and vapor density, respectively, and distance x is measured from the leading edge of the substrate wafer in the gas stream. At x=0, the rate of impingement of source molecules is given by $Z_a = p_i/(2\pi m_i k_B T)^{1/2}$, where $p_i$, $m_i$, $k_B$ and T are the partial pressure and mass of the vapor species i, the Boltzmann constant and temperature. At x>0, the diffusive flux $J_{di} = D_i(\partial\rho_i/\partial z)_{z=o} = D_i\Delta\rho_i/\delta \leq (\rho v_f/\nu_a x)^{1/2} D_i \rho_i$. Since $\rho_i$ is proportional to $p_i$ while diffusivity $D_i = 2k_B{}^{3/2}T^{3/2}/3\pi^{1/2}m_i{}^{1/2}\sigma_i p_i$, $J_d$ increases with increasing vapor density, but primarily due to the effects of the total pressure on $\delta$. Since $\rho$, $\rho_i \propto T^{-1}$ and $D_i \propto T^{3/2}$, process temperature effects are expected to be weak. In summary, experimentation at microgravity provides unique opportunities for the study of diffusive transport coupled to homogeneous vapor phase reactions and heterogeneous surface reactions in vapor deposition and etching at high source vapor flux with real-time monitoring and control of the progression of series of experiments by ground-based teams of investigators. The return on the investments made is expected to be knowledge making an impact on the advancement of materials science and engineering.

## References


[1] N. Dietz and K.J. Bachmann, *Real-Time Monitoring of Epitaxial Processes by Parallel-Polarized Reflectance Spectroscopy*, Mater. Res. Bull. **20**, 49, (1995)

[2] K.J. Bachmann, U. Rossow and N. Dietz, *Real-time monitoring of heteroepitaxial growth processes on the silicon (001) surface by p-polarized reflectance spectroscopy*, Mater. Sci. & Eng. **B35**, 472 (1995)

[3] K.J. Bachmann, U. Rossow, N. Sukidi, H. Castleberry and N. Dietz, *Heteroepitaxy of GaP on Si(100)*, J. Vac. Sci. Technol. **B**, in print

# MOLECULARLY TAILORED SURFACES VIA SELF-ASSEMBLY PROCESSES: SYNTHESIS, CHARACTERIZATION AND MODELING

M. A. Barteau, N. J. Wagner & A. M. Lenhoff
Department of Chemical Engineering
University of Delaware
Newark, DE 19716
Phone: (302) 831-8905
Fax: (302) 831-2085
e-mail: barteau@che.udel.edu

## Objectives and Significance

The objectives of the proposed research are to develop experimental and theoretical techniques to design, fabricate, and characterize materials with specialized interfacial properties and to assess the role of gravitational forces in the fabrication of these materials. The desired interfacial properties, to be derived from nanometer-scale and larger functional units self-assembled into ordered arrays at the interfaces of bulk materials, include electronic, biological, and catalytic functions. We have already demonstrated the formation of ordered arrays of individual catalytic molecules including enzymes and polyoxometalates (POMs); we have also demonstrated the ability of individual molecules in these arrays to produce localized electronic behavior, including resonant tunneling. The capability to synthesize materials with well-defined interfacial structures and nano-scale functions may also be extended to assemble multi-layered structures.

The technological thrusts from this work can fill an important gap in the design and synthesis of materials with sophisticated functional properties. Characterization of most real bulk materials with valuable interfacial characteristics, such as catalysts and adsorbents, shows them to retain an appreciable degree of heterogeneity; novel design and synthesis approaches have succeeded in reducing such heterogeneity, but such incremental methods are unlikely to accomplish the task unambiguously. At the other extreme, ideal systems such as single crystals (metals, metal oxides, and organometallic clusters for catalysis; high $T_c$ superconductors) are often difficult to incorporate into true bulk materials, and in those cases they have few direct applications. Similarly, although a broad spectrum of modern techniques has become available to produce small units with complex functionality (proteins via recombinant DNA technology; fullerenes; surfactant assemblies such as micelles and vesicles), the incorporation of these units into technologically useful materials remains an obstacle. Overcoming this obstacle is the goal of this research; the route we will follow is based on our success in preparing and characterizing self-assembled monolayers of proteins and inorganic polyoxometalates on graphite. Self-assembly of these nanometer-size units allows the incorporation of much greater functional complexity than, for instance, the more widely studied

self-assembly of alkanethiols on metals. Nevertheless, our experience shows it to proceed spontaneously and reproducibly; furthermore, although our emphasis to date has not been on functional characterization, we have already observed interesting electronic properties in ordered monolayers of polyanions.

In this research, we will build on our prior work by studying the self-assembly on solid surfaces of inorganic, organic, and biological units. These include the ones we have used to date—POMs as precursors to electronic and catalytic materials, proteins as precursors to biological materials such as affinity sorbents, biosensors, and other devices incorporating aspects of molecular recognition—as well as new ones, including colloidal latices and liquid crystalline polymers, that have applications in corrosion-resistant coatings, tribology and membranes. The characteristic sizes of the adsorbates to be probed in this work span more than three orders of magnitude, from the nanometer to the micron scale, comparison and modeling of which will shed important light upon the underlying mechanisms of adsorption-induced self organization, and particularly the role of gravitational forces.

This research will comprise two specific components:

1. Preparation and characterization of ordered arrays. Most of the arrays we have studied to date were prepared on highly oriented pyrolytic graphite (HOPG) and their structure characterized by scanning tunneling microscopy (STM). We will expand the range of surfaces used and examine the effects of surface and solution properties on array formation, including *in situ* observation. STM will remain a major component of our structural characterization work, but we will also apply other experimental techniques, e.g., atomic force microscopy (AFM), especially for insulating substrates, sorbates through which tunneling is difficult, and situations where these alternative techniques can yield information beyond that available by STM. Electronic properties can, as we have previously demonstrated, be characterized by tunneling spectroscopy, while catalytic and biological properties will also be probed as appropriate.

2. Theoretical studies of array formation. Theoretical tools such as statistical mechanics, as well as molecular simulations, are increasingly being applied to explain and predict molecular ordering. However, relatively little of this work has involved the study of structure formation at surfaces, particularly for functional units of the colloidal size to be used in our studies. We plan to develop and implement statistical mechanical and simulation techniques aimed at predicting the structure of the interfacial layer. A hybrid Grand Canonical Monte Carlo—Brownian Dynamics simulation tool is proposed to study the dynamics of the adsorbed layers, to interpret the experimental results, and to help in the theoretical modeling.

Microgravity relevance

The microgravity component of this study of the formation and structure of 2-D arrays represents a significant but logical extension of our work aimed at a quantitative understanding of the underlying mechanisms, where intermolecular or interparticulate (colloidal) forces represent the dominant driving force. There are two specific areas in which microgravity can be important. The first is in understanding the fundamental forces involved, and their roles in the formation of ordered arrays. The various colloidal forces scale differently with particle characteristics, notably size, so that as these characteristics are changed, the relative contributions of the forces change. At the lower (nanometer) end of the colloidal size range, gravity is unimportant, so terrestrial gravity should not, in principle, affect ordering. At the upper (micrometer) end of the size range, however, gravity may become important, so an understanding of ordering over the full size range requires that the effects of gravity must be fully accounted for or eliminated in this limit.

The second area of microgravity importance is in fabrication, where the elimination of the deleterious influence of phenomena other than the colloidal forces makes microgravity an attractive environment for studying the phenomena involved. In particular, the minimization of natural convection and gravity-driven contact with container walls in a microgravity environment would permit materials syntheses controlled primarily by the colloidal forces that govern self-assembly.

Research Plans–Experimental

We have previously studied array formation and properties for various functional units, including polyoxometalates, proteins, sugars, polystyrene latices, and liquid crystal polymers. We plan a systematic investigation of the effects on array formation of the particle type, surface characteristics and solution composition. Ideally one would wish to specify conditions for formation of ordered arrays of known structure. The principal control variables are particle nature and concentration, counterion identity, concentration, solvent, and surface. The structural variables to be characterized are array spacing, array symmetry, 2-D *vs.* 3-D adsorption or deposition, and orientation.

The classes of particles to be studied differ in both shape and properties, allowing us to examine the generality of the propensity for ordering and to demonstrate the variety of potential material properties that can be produced using self-assembly principles. Specifically, we will study POMs, proteins, dendrimers, silica particles, polystyrene latices and rod-like polymers, which differ in a range of characteristics. The dendrimers and silica and polystyrene particles are close to the ideal spherical charged particles on which the theoretical developments will primarily be based. The POMs and proteins we will use are, while not spherical, at least roughly globular; POMs with the

Keggin structure have greater symmetry, while proteins display much more heterogeneity and anisotropy of shape and function. Although their interactions are predominantly electrostatic and van der Waals in origin, the surface properties of the Keggin ions can, in addition, be modified by the addition of prosthetic groups. The rod-like polymers (*e.g.*, poly-β-L-glutamate in m-cresol), on the other hand, are quite different in shape; they also have different surface functionalities, so that the mechanisms of interaction driving self-assembly may be different.

Array formation will be studied on covalent semiconductors such as silicon, polar conductive solids (*e.g.*, partially reduced oxides), and insulators such as mica and quartz, to examine the effects of surface polarity on adsorption and array formation. Since the surface can be examined in an electrochemical cell, the potential of the adsorbing surface can be varied as well in the case of conducting and semiconducting materials. Thus surface characteristics will be varied in both their chemical and electrical properties.

The goal of these experiments will be to determine which of the variables noted above have the greatest influence on the formation of ordered 2-D arrays. In order to accomplish this, a key requirement will be the capability to vary individual parameter values systematically. For this purpose the dendrimers, latex particles and silica particles are likely to offer appreciable size ranges, while the latex particles will offer different surface charge densities. Unfortunately the latex and silica particles are difficult to obtain at the nanometer end of the size range with small degrees of polydispersity, so we will be more dependent on POMs and proteins here. In this case we can vary particle composition systematically, however. For the Keggin ions, for example, systematic variation of composition of $[Si^{m+}W_{12-n}V_nO_{40}]^{m-n-8}$ for n = 0 to 3 can be used. In addition, the effects of exchanging $H^+$ for $N_4^+$ both before and after deposition will be examined to gain insights into the influence of counterions. For proteins, we have available to us a set of single-site mutants of T4 lysozyme to serve the same function.

For colloidal particles at the nanometer end of the size range, Brownian transport is dominant and the effects of gravity would be expected to be small. However, for larger particles it is important to determine at what point gravitational forces become significant, and hence a benefit would be expected from performing experiments in microgravity. For this purpose we will synthesize silica particles in the range of 20 nm to 1 micron in size by the Stöber process. Such particles can be made nearly monodisperse (a few percent polydispersity) and very spherical. Mixing of particles of different sizes is also possible, as is the intentional introduction of size polydispersity. Acid-washed silica is negatively charged, and hence such particles can serve as analogs to the smaller particles of which we will study self-assembly in aqueous media, with electrostatic interactions dominant. In addition, the silica particles can be coated with a wide variety of silane coupling

agents to achieve near-hard sphere behavior. Alternatively, attractive potentials or repulsive electrostatic potentials can be introduced, and tuned by the appropriate choice of solvent. Using such particles, we will perform paired adsorption experiments with the adsorption surface held horizontal in one case and vertical in the other. Significant differences in the structures of the resulting adsorbate layers can then be attributed to gravitational effects.

Quantitative determination of array parameters and ordering will be carried out by direct imaging, by Fast Fourier Transform (FFT) analysis of the images, and by preparation of radial distribution functions for less well ordered layers; the latter two are especially useful for direct comparison with results of our theoretical work. In addition, fundamental questions regarding the depth profile and uniformity of the adsorbed layer may be answered through neutron reflectivity measurements of adsorbed particles on surfaces corresponding to those for which STM and AFM measurements are available.

Research Plan–Theoretical

The main goals of the theoretical program are to determine the relationship between fundamental physico-chemical properties of the nano-particles and the final state and properties of the adsorbed layer. Given robust methods that can fit the experimental observations, fundamental parameter variation studies can be performed to guide the experimental program. The ability to specify molecular level properties and predict the structure and function of the adsorbed layer with some confidence would greatly reduce the experimental work required to understand the system fully. The insight gained can help simplify the experimental program by providing guidance on the sensitivity to molecular properties and make predictions for future experiments on untried systems.

The tools we will use to attain these goals are based on statistical mechanical methods, as well as simulations. Beyond them, we also require methods to infer interaction potentials from bulk measurements. These aspects are discussed below.

Brownian dynamics and Monte Carlo simulations provide a direct method to solve the proposed statistical mechanical models for the ordering of nano-scale particles near surfaces, and for interpretation and optimization of the experimental investigations. Further, the simulations extend the theoretical results beyond the model systems amenable to analytical treatment, to systems more closely capturing the complexity of proteins, polyions, and polymers. Our current efforts in high performance computing on massively parallel computers will be modified to study idealized nano-particles in solution in contact with idealized surfaces.

Monte Carlo simulations will be performed to predict equilibrium structures and ordering in both surface layers and in the fully three-dimensional problem. This technique is computationally efficient, can be applied to large ensembles with multiple adsorbing species, and can be extended to calculate chemical potentials for direct comparison with the integral equation theories. The equilibrated systems computed here are to be compared directly with the experimental measurements and provide good initial conditions for studying the dynamical properties of the equilibrated, adsorbed layers by Brownian dynamics.

The simulation results are to be directly compared against the results of the statistical mechanical models to test their validity, and to determine the minimum level of description necessary in the analytical formulation. By fitting the potential of interaction between model particles from bulk solution properties of the actual experimental systems, and determination of the surface properties by standard characterization techniques, the simulations can then be directly compared against the experimental STM/AFM images and results. The goal of this work is to determine if the bulk solution properties and surface characterization are sufficient information to determine the systems' behavior during adsorption. Further, the diffusion and transport of ions and proteins in the surface layer and between the surface and solution can then be studied, properties that are difficult to impossible to determine experimentally.

Summary

These 2-D arrays of discrete biological and catalytic functions represent a new class of materials which provide numerous opportunities both for the development of new catalysts and separation devices, and as model systems for the resolution of long-standing questions in these fields. The combination of experimental and theoretical investigations of these systems will provide an unprecedented opportunity to examine the generality of these self-assembly phenomena, and to develop new synthesis strategies for these novel materials, both in earth-bound and microgravity environments.

# EFFECTS ON NUCLEATION BY CONTAINERLESS PROCESSING

Robert J. Bayuzick, William H. Hofmeister, and Craig W. Morton
Vanderbilt University
P.O. Box 1593 Station B, Nashville, TN 37235

M. B. Robinson
George C. Marshall Space Flight Center
Huntsville, AL 35812

## Introduction

The factors that influence the nucleation behavior of a material are important for both scientific and practical reasons. Nucleation from the melt is of course the origin of most solids; therefore, an understanding of the phenomena is essential. In practical terms, an understanding of nucleation and the accompanying impacts of undercoolability and rapid solidification in obtaining unique phases and/or microstructures have the potential for significant advances in materials processing.

In this project, a comprehensive investigation on nucleation of the solid from an undercooled liquid is being conducted using pure metals. The critical factors that affect a liquid's ability to undercool to a significant extent before the onset of nucleation are being sought and quantified using classical nucleation theory as a framework for the undercooling results. Since classical nucleation theory is a theory of thermodynamic fluctuations, particular attention is being placed on the effect of flow in the melt on undercooling. Three ground based containerless processing techniques have already been applied to the effort to obtain sets of undercooling data. These are free fall in the 105 m drop tube at the George C. Marshall Space Flight Center, electromagnetic levitation at Vanderbilt University, and electrostatic levitation at the Jet Propulsion Laboratory. TEMPUS, an electromagnetic heating and positioning unit for conducting containerless experiments, will be used on the Spacelab mission known as Microgravity Sciences Laboratory - I (MSL-1). Experiments on nucleation behavior in laminar and turbulent flow regimes in undercooled melts will be carried out. Statistical comparisons of the results using comparisons of the means and variances of the distributions will be used to determine if the probabilities of nucleation as a function of undercooling are the same in both flow regimes. Therefore, the statistical comparisons of the results will allow greater insight into nucleation phenomena.

## Relevance to Microgravity Research

Conclusive experiments to discern the lack of effects of liquid flow on nucleation behavior in undercooled melts (or alternatively, the existence of effects of flow on nucleation behavior) demand well characterized flows within the melts and control of such flows. The experiments also demand accurate measurement of the nucleation temperatures. Ground based techniques cannot presently meet the requirements. On the other hand, operations in a microgravity environment can meet the requirements and, therefore, enable such experiments. The freedom from strong levitation forces and

their side effects allows power inputs and temperature profiles to be fine tuned. This in turns provides the ability to control flows while maintaining identical cooling rates into the undercooled regime. It also promotes sample positioning stability so that accurate temperature measurements can be accomplished. In addition to providing process control, low earth orbit experiments allow for the direct measurement of the heat capacity and viscosity of undercooled liquids to be carried out along with nucleation experiments. The measurements of these thermophysical properties would then result in measures of bulk free energy change upon solidification and the diffusion coefficient, thereby removing major ambiguities in comparing experimental results to predictions of classical nucleation theory.

## Background: Classical Nucleation

Through the theoretical development of nucleation phenomena, Classical Nucleation Theory represents a simple but useful starting point in investigations. The classical nucleation rate equation has the form of a thermally activated rate reaction and can be given as:

$$J_v = K_v \exp\left[-\frac{\Delta G'}{kT}\right] \qquad 1$$

where $J_v$ is the volume nucleation rate, $K_v$ is referred to as the preexponential factor, T is the temperature, k is Boltzmann's constant, and $\Delta G'$ is the activation energy for nucleation. From the work of Fisher and Turnbull[1] and the assumption of a spherical embryo, further simplification results in one of the approximations for homogeneous nucleation:

$$J_v \approx 10^{33} \exp\left[-\frac{16\pi\sigma_{lu}^3}{3\Delta G_v^2\, kT}\right] \qquad 2$$

where $\sigma_{lu}$ is the interfacial free energy between parent and daughter phases and $\Delta G_v$ is the volume free energy difference between parent and daughter phases.

In most nucleation experiments, heterogeneous nucleation is assured by either intrinsic or extrinsic impurities. Heterogeneous sites will reduce the solid-liquid interfacial free energy barrier by some amount proportional to the "wetability" of the impurity. The preexponential will also decrease in heterogeneous nucleation by a factor proportional to the available heterogeneous site.

## Statistical Analysis of Nucleation Data

In the work of Skripov[2], the Poisson distribution is applied to the statistical analysis of nucleation. Since the formation of solid embryos and nuclei in pure metals is thought to be a process governed by the random fluctuations of density within the liquid , the use of Poisson statistics based on chance occurrences is a satisfying approach to the quantification of the nucleation process. According to the Poisson distribution, the probability of the occurrence of m accidental events in a time interval $\tau$ is given by

$$\omega(m,\tau) = \frac{(\lambda\tau)^m \exp(-\lambda\tau)}{m!} \qquad 3$$

where $\lambda$ is a constant probability density and corresponds to the mean rate of occurrence of events pertaining to a given set of experimental conditions.
For the statistical treatment of nucleation under non-isothermal conditions, equation 3 can ultimately be transformed to give the probability density function as

$$\omega(T) = \frac{J_v V}{\dot{T}} \exp\left[ -\int_{T_0}^{T} \frac{J_v V}{T} dT \right] \qquad 4$$

where V is the volume solidified by a single nucleation event, $\dot{T}$ is the cooling rate and $T_O$ is the equilibrium freezing point. The statistical analysis of a set of undercooling data can be performed under the assumption that each undercooling represents one independent stochastic event.

Determination of Activation Energy and Preexponential with Statistical Analysis

With a large number of experiments, it is possible to generate a histogram of undercoolings. Histograms are discrete probability distributions which can be normalized accordingly to generate a discrete probability density. Equation 4 can be used to generate a theoretical density curve, which can be compared to the data. In order to find the best fit of the probability density curve to the data, a non-linear fitting routine (the Levenberg-Marquart method in this case) is used. The variables of the fit are $K_v$ and the exponential factor. These two variables are inextricably linked, and, in general, the uncertainty of the fit of $K_v$ and the exponential factor is larger than the covariance of the two variables, i.e. the fit of $J_v$.

Ground Based Nucleation Experiments

In general, nucleation experiments involve the measurement of the undercooling achieved before nucleation in a continuous cooling experiment. A single sample is melted, raised to a particular temperature and cooled until nucleation occurs. The process is repeated numerous times and a set of undercoolings obtained. This can be accomplished on single samples with electromagnetic or electrostatic levitation processing techniques. Both techniques are containerless and allow repeated experiments to be performed on a single sample without touching the sample. Processing in electromagnetic levitation requires gas flows for cooling. In electrostatic levitation the specimen can be maintained in a vacuum environment. Drop tubes are also used with vacuum environments. However, multiple samples are required for experiments.

Results for zirconium indicate fundamental differences in the nucleation behavior in the different ground based processing techniques using samples of the same purity. The distributions of undercoolings are all non-Gaussian with similar mean undercoolings; however, the distributions are wider for the electromagnetic levitator and the drop tube than for the electrostatic levitator. For

samples of differing purity levels processed by the same technique, the distributions retain the same shape but shift their centers to higher undercoolings (lower nucleation temperatures) as the material purity is increased. Analysis of variance tests indicate that the distributions are different at the 95% confidence level. The values for the preexponential factors and activation energies ranged from $10^8$ to $10^{13}$ and 13 kT to 24 kT, respectively.

## The IML-2 Spacelab Flight

Experiments were attempted in TEMPUS on a previous Spacelab Mission. Unfortunately, the positional stability of samples was such that the samples impacted with the sample cage during processing. During the first unsuccessful experiment, it was possible to calibrate the model of sample response to TEMPUS parameters. With this model, the desired time temperature profile and one undercooling (265 K) was achieved during the subsequent experiment before the second sample impacted with the cage. Post-flight analysis of the IML-2 samples showed that the low undercooling was due to cross contamination from other flight samples and the sample holders. During transport, launch and landing, abrasion resulted in particulate material generation. During flight, these particulates floated inside the TEMPUS facility chamber and contaminated all of the samples examined.

## MSL-1 Flight Experiment

Along with several improvements made to the TEMPUS hardware, a revised protocol was developed for the MSL-1 mission. Two null hypothesis tests will be used to accept or reject equivalence of nucleation mechanisms in zirconium in the laminar and turbulent regimes. The first test will involve the equality of means. If the hypothesis of equality of means is rejected at the 99% confidence level, the nucleation mechanisms in the two regimes will be said to be different. If the hypothesis of the equality of means is accepted at the 99% confidence level, then a second test, involving the dispersion of nucleation temperatures, will be applied. If the hypothesis of equality of the dispersion of nucleation events is rejected at the 95% confidence level, the nucleation mechanisms will now be said to be different. On the other hand, if the null hypothesis of equality of variance is accepted at the 95% confidence level, the nucleation mechanisms will be said to be the same. Because of the uncertainty in determination of sample variance, a test of variance is less sensitive than a test of means, consequently a lower confidence level is accepted for the test of variance.

## Nucleation Temperature Determination

For statistical analysis of nucleation data, a precise determination of the relative undercooling is needed. Thus, in these experiments, absolute temperature accuracy is secondary to relative precision. In each experiment, the melting temperature is measured and the undercooling measurement is related to this fixed temperature. The uncertainty of relative measurements is lower than the uncertainty of the absolute measurement. The temperature measurement uncertainty for low earth experiments in TEMPUS is 1.4 K as compared to 5 K for the ground based techniques.

## Monte Carlo Simulations

In order to evaluate the uncertainty associated with the determination of $K_v$ and the exponential factor from a sampling of undercoolings from the population of nucleation events, Monte Carlo simulations were used. Selection of $K_v$ and a most probable nucleation temperature uniquely defines the exponential factor and the parent distribution of undercoolings. $K_v$ and the exponential factor are then used to numerically calculate a nucleation rate ($J_v$). The nucleation rate is numerically integrated and used to construct a cumulative distribution such that:

$$F(T) = 1 - \exp\left[ -\frac{V}{\dot{T}} \int_{T_0}^{T} J_v(T)\,dT \right] \qquad 5$$

This cumulative distribution is a continuous function from zero to one. In the Monte Carlo technique, a random number from zero to one is generated for each undercooling in the sample. The undercooling is then chosen as the undercooling at which the value of F(T) is equal to the random number. Temperature error is added to the sample by adding a Gaussian distribution of random noise (with a standard deviation equal to the temperature measurement uncertainty) to the undercooling value. The sample is then binned into a histogram and normalized accordingly. The above non linear curve fitting routine is then used to determine the values of the exponential factor and the preexponential term.

Due to the strong temperature dependence of the nucleation equations, the width (or variance) of the probability distribution function is small. Thus, as temperature measurement uncertainty approaches the variance of the parent distribution, the uncertainty in the fitted values increases. As a demonstration, the Fisher-Turnbull expression was used to generate a parent distribution. Two preexponential factors were used, $10^{15}$ and $10^{33}$ at a common mode undercooling $T = 0.85\ T_O$. This is indicative of experience with achievable undercoolings in zirconium samples. The results are shown in Figure 1. Each data point represents the mean $K_v$ value from 100 Monte Carlo simulations of a data sample of 100 undercoolings from the parent distribution. The error bars represent the one sigma deviation of the set of $K_v$ fits. From a sampling standpoint, these calculations represent sets where n=100 only. At $K_v = 10^{15}$ the parent distribution is sufficiently wide such that the fitted values recover the "true" value within 2 orders of magnitude when temperature measurement uncertainty is less than 1.5 K. At $K_v = 10^{33}$, temperature uncertainty drastically affects the ability of the fit to recover the preexponential of the parent distribution.

## Preparation for MSL-1 Experiments

In preparation for the MSL-1 experiments, several testing steps are currently being performed. These tests have been designed to verify the proper operation of the TEMPUS facility, to quantify differences between the flight unit and the ground based equipment, and to provide data for the adjustment of modeling parameters such as positioning force and coupling efficiency. During the flight, the first few experiments will be pulsed heating experiments. The thermal profiles resulting from these pulses will be used to verify the accuracy of the high temperature coupling behavior. Upon verification of the thermal modeling and the minimum safe positioning voltages, flow condition testing will be performed

to ensure that two distinct flow regimes are achieved and to provide quantitative information on the character of the flow regimes.

## Nucleation Experiments on MSL-1

The experiments will characterize the flow regimes and power coupling behavior such that the thermal profiles of the two flow conditions are identical. Approximately 100 nucleation experiments on each of two zirconium samples will be performed. The protocol for nucleation experiments on sample one will begin with ten nucleation experiments in the laminar regime followed by ten experiments in the turbulent regime. All experiments, and combinations thereof, will be checked for independence of undercooling and cycle number. If no linear correlation is found, then 79 additional nucleation experiments will be performed in random order. The last experiment on sample one will be run in the laminar regime. A similar protocol will be run for sample two, except the first block will be run in the turbulent regime, the second block in the laminar regime, then random order will be used until the last cycle, when the sample will be solidified in the turbulent regime. This protocol will yield two sets of data for each sample, a total of four sets.

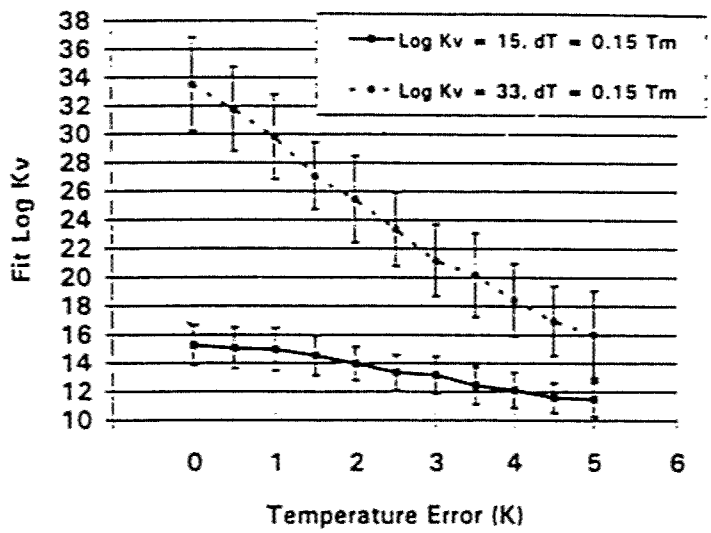


Figure 1: The effects of temperature measurement error on the calculated value for log $K_v$.

## References


1. Turnbull, D. and Fisher, J. C.; "Rate of Nucleation in Condensed Systems", The Journal of Chemical Physics, 17, 1 (1949) 71-73.
2. Skripov, V. P.; "Homogeneous Nucleation in Melts and Amorphous Films", in Current Topics in Materials Science; Crystal Growth and Materials, Vol. 2, eds. E. Kaldis and H. j. Scheel (North Holland Publishing Co.) 1977, p. 328.
3. Turnbull, D.; "Formation of Crystal Nuclei in Liquid Metals", Journal of Applied Physics, 21 (1950) 1022.

# INVESTIGATION OF THE RELATIONSHIP BETWEEN UNDERCOOLING AND SOLIDIFICATION VELOCITY

Robert J. Bayuzick, William H. Hofmeister, and B. Timothy Bassler
Vanderbilt University
P.O. Box 1593 Station B, Nashville, TN 37235
bayuzick@vuse.vanderbilt.edu, hof@vuse.vanderbilt.edu, basslebt@vuse.vanderbilt.edu

## 1) Project Objective and Hypothesis

The study of solidification velocity is important for two reasons. First, the manner in which the degree of undercooling and solidification velocity affect the microstructure of the solid is fundamental. Second, there is disagreement between theoretical predictions of the relationship between degree of undercooling of the liquid and solidification velocity and experimental results.

Thus, the objective of this work is to accurately and systematically quantify the solidification velocity as a function of undercooling for pure metals and alloys. The key theoretical parameters of interface temperature, thermal gradient, and solutal gradient will be extracted through modeling. The results will be examined in order to gain an understanding of the mechanisms controlling interface movement. They will be compared to solidification theory and possible improvements on existing theories will be sought. The primary hypothesis to be examined is that present theories on solidification velocity do not predict the behavior at high undercoolings.

In order to closely monitor the progression of the thermal field developed by recalescence in containerlessly processed metals and alloys, a novel technique using a ten by ten array of photodiodes in conjunction with a high speed data acquisition system has been developed. Of primary interest is the velocity of the solid/liquid interface at undercoolings greater than 10 % of the equilibrium freezing point ($T_M$), because present theories and reported experimental results diverge above this level. Solidification velocity measurements will be made on pure nickel, pure titanium, nickel based alloys, and titanium based alloys.

The measurement of the solidification velocity as a function of undercooling, with an emphasis on high undercoolings (>10% $T_M$), requires containerless processing techniques to limit heterogeneous nucleation sites and to directly observe the interfacial movement. Electromagnetic levitation and electrostatic levitation are the ground based methods of containerless processing that are best suited for experiments in which the solidification velocity is determined by imaging techniques.

2) Experimental Method

From examination of prior experimental results for the solidification velocity as a function of undercooling it is clear that, in all of the systems, there is a discontinuity in the growth rate with increasing undercooling. It is this phenomena and the mechanisms causing it that will be the primary focus of this research. Presently accepted theory (e.g. Boettinger, Coriell, and Trivedi Theory) and the desire to examine single phase solidification provide the basis for the selection of the specific metals and alloys to be examined in this work.

Based on the slope of the liquidus line, the partition coefficient, the interdiffusion coefficient and solid solubility, alloys were chosen for this experimental effort. Two pure metals were chosen as benchmarks upon which the study of various alloys would be based. All of the alloys with these pure elements were examined and candidates were selected based on the following criterion. The phase diagram had to be well defined in the low solute regime, there had to be enough solid solubility to solidify a range of solute concentrations to a single phase, and the alloys had to be experimentally practical. In addition, the slope of the liquidus line had to be large enough to make the solutal undercooling have a significant contribution to the total undercooling. Finally, from the remaining candidate substitutional alloys, three alloys of each "benchmark" metal were chosen: one with a "small" partition coefficient, one with a "medium" partition coefficient and one with a "large" partition coefficient. An interstitial alloy was also chosen in order to examine a case with a much greater diffusion coefficient. By using this selection process the effect of various amounts of solute, varying partition coefficients, and varying interdiffusion coefficients on the solidification velocity as a function of undercooling will be quantitatively determined.

To the nickel, in order of increasing partition coefficient, tin, silicon, and titanium will be added to examine substitutional alloying effects. The interstitial alloy that has been chosen for study is the nickel-carbon system. To the titanium, again in order of increasing partition coefficient, nickel, platinum, and aluminum will be added to examine substitutional alloying effects. The interstitial alloy that has been chosen for study is the titanium-oxygen system. Table 1 shows the elements and alloys listed along with their solubility limits and their partition coefficient range.

Table 1 - Elements and Alloys Chosen for Investigation

| **Material** | **Maximum Solubility (wt%)** | **Partition Coefficient** |
|---|---|---|
| Nickel | ----- | ----- |
| Nickel-Tin | 19.3 | 0.4-0.6 |
| Nickel-Silicon | 8.2 | 0.5-0.7 |
| Nickel-Titanium | 11.6 | 0.9-1.0 |
| Nickel-Carbon | 0.6 | 0.1-0.4 |
| Titanium | ----- | ----- |
| Titanium-Nickel | 12 | 0.2-0.4 |
| Titanium-Platinum | 31 | 0.7-0.8 |
| Titanium-Aluminum | 33.8 | 0.8-1+ |
| Titanium-Oxygen | 3.0 | 1.7 |

For each alloy, data sets of the solidification velocity as a function of undercooling will be collected over a range of compositions. Through modeling corresponding to the specific experimental conditions, the bulk undercoolings will be related to interfacial undercoolings, thermal gradients and solutal gradients. These data sets will be compared to present theories relating solidification velocity to undercooling. The areas of deviation between theoretical predictions and experimental data will be examined. This will be done with a concentration on the mechanisms, both microscopic and macroscopic, driving solidification over the entire range of undercoolings achieved.

3) Experimental Results

The solidification velocity of electromagnetically levitated metals has already been measured using ultra high speed imaging. A ten by ten square array of photodiodes in conjunction with a data

acquisition system was employed to observe the progression of the solid/liquid interface during solidification. The output of each photodiode in the array was sampled simultaneously at rates ranging from 2 ms per frame (500 frames per second) to 1 μs per frame (1,000,000 frames per second). The movement of the solidification front was followed by monitoring the progression of the thermal field developed by recalescence. As the solidification front proceeded across the surface of the sample, an image of the lower hemisphere of a levitated and undercooled drop was projected onto the array of photodiodes. Then as the interface moved across the surface of a sample, its bright/dim nature caused an increase in output in each photodiode that it crossed. This allowed the position of the interface to be monitored with the photodiode array as it progressed across the drop's surface. From the data, which was collected as a succession of frames in time, the velocity of the interface was determined. This was done by measuring the distance that the interface moved between frames and dividing by the time between frames.

The surface temperature of the drop was measured during solidification, simultaneously with ultra high speed imaging, by a narrow band pass pyrometer. The output from the pyrometer was recorded at 1 kilohertz using standard data acquisition techniques. The pyrometer was exposed to the same view of the levitated sample as the imaging system via a beam splitter in order to precisely measure the surface temperature of the samples during each experiment.

The solidification velocity of electromagnetically levitated pure nickel, pure titanium, nickel-carbon alloys, titanium-aluminum based alloys, and nickel-aluminum based alloys were measured as a function of undercooling. For pure nickel, the solidification velocity was measured at undercoolings ranging from ~4% $T_M$ ($T_M$ is the equilibrium melting temperature) to ~15% $T_M$. The results indicate that the solidification velocity increases with increasing undercooling up to ~10% $T_M$ in the manner described by the equation $V=0.044\Delta T^{2.7}$. The solidification velocity then remains constant at ~30 m $sec^{-1}$ with increasing undercooling. For pure titanium the solidification velocity was measured from ~8% $T_M$ to ~14% $T_M$. The results indicate that the solidification velocity begins at 10.3 m $sec^{-1}$ at 8% $T_M$ and increases in the manner described by the equation $V=0.057\Delta T^{2.5}$ up to 44 m $sec^{-1}$ at an undercooling of 14.4% $T_M$. The solidification velocity of three different nickel-carbon alloys was also measured. The alloys consisted of 0.6 a/o carbon,

1.7 a/o carbon, and 2.8 a/o carbon, each alloy being within the solid solubility limit of the system. The undercooling range tested was similar to that of pure nickel. The results indicate that the solidification velocity of the 0.6 a/o carbon alloy as a function of undercooling is similar to that of pure nickel. The solidification velocity of the 1.7 a/o carbon alloy increased more slowly than pure nickel, remained relatively low up to ~12% $T_M$, at which point the velocity increased to ~30 m sec-1, and then remained constant with increasing undercooling. For the 2.8 a/o carbon alloy the solidification velocity increased even more slowly than the 1.7 a/o carbon alloy up to ~13% $T_M$ and then increased to ~30 m $sec^{-1}$.

A titanium-aluminum alloy tested was a gamma alloy consisting of 60 a/o aluminum and was tested over undercoolings ranging from ~2% $T_M$ to ~20% $T_M$. The solidification velocity versus undercooling results for this alloy showed three regions. They were: 1) for undercoolings <9%$T_M$, the velocity increased slowly with increasing undercooling, 2) for undercoolings between 9% $T_M$ and 18% $T_M$, the velocity increased rapidly with increasing undercooling, and 3) for undercoolings >18% $T_M$, the velocity was constant (~10 m $sec^{-1}$) with increasing undercooling. The effect of solute on the solidification velocity of this alloy was tested by adding erbium to the metal. In general, the effect of the erbium was to slow the solidification velocity and lower the velocity plateau (~4m $sec^{-1}$) reached by the material at large undercoolings. For comparison the solidification of equiatomic nickel-aluminum was also measured. To date, only two experiments have been run. The results were that, at an undercooling of 11% $T_M$, the solidification velocity was 1.9 m $sec^{-1}$ and, at an undercooling of 13.1% $T_M$, the solidification velocity was 2.5 m $sec^{-1}$. Both velocities are significantly slower than those in TiAl for comparable undercooling (about 3.8 m $sec^{-1}$ and about 4.5 m $sec^{-1}$, respectively.)

4) Microgravity Relevance

In order to do the research described herein, it is absolutely necessary to use containerless processing techniques. Deep undercooling must be achieved without the triggering of multiple nucleation sites. The presence of a container is likely to inhibit deep undercooling and is likely to induce multiple nucleation when solidification does occur. In addition, as has already been

argued, indirect measurements of solidification cannot discern the presence of multiple nucleation events. However, direct imaging techniques are essential for determination of the true nature of any given solidification process and, therefore, accurate measurements of solidification velocity. Such techniques require containerless processing to freely observe solidification of undercooled melts.

The treatments and theories of solidification velocities are based on quiescent conditions. As long as solidification velocities are an order of magnitude greater than the streamline velocities in the melt, results for quiescent and animated melts will be similar. For pure metals highly undercooled in the electromagnetic levitator, this is the case and, therefore, electromagnetic levitation is a perfectly capable technique. However, for pure metals at lower undercoolings and for many alloys and intermetallic compounds over a very wide range of undercoolings including the higher undercoolings, solidification velocities become of the same order as the streamline velocities in the electromagnetic levitator. In such cases, results are likely to differ significantly from quiescent conditions. Electrostatic levitation induces a charge distribution on the surface of the levitated drop and body forces induce modest flow fields in the melt. The latter is likely to be important only at very low undercoolings in pure metals and low undercoolings in alloys. The role of the charge field perturbing the results has no been treated but effects that impact the solidification velocity could be possible. Drop tube experiments are not practical because the constant observation required by the proposed imaging experiments is not possible. Low earth orbit experiments could eliminate the effects that are induced in the samples by ground based containerless processing techniques, thus confirming or contrasting the ground based experimental results.

# EQUIAXED DENDRITIC SOLIDIFICATION EXPERIMENT (EDSE)

C. Beckermann, Associate Professor
Department of Mechanical Engineering
The University of Iowa
Iowa City, IA 52242-1527
U.S.A.
Tel: (319) 335-5681
Fax: (319) 335-5669
email: becker@icaen.uiowa.edu

Co-Investigators: H.C. de Groh, NASA Lewis;
I. Steinbach, ACCESS;
B.T. Murray, NIST.

## OBJECTIVES

The objective of the research is to determine the microstructural evolution of and thermal interactions between several equiaxed crystals growing dendritically in an undercooled melt of a pure substance. By extending the free dendrite tip growth experiments of Glicksman and coworkers (Isothermal Dendritic Growth Experiment, IDGE) to the case of multiple equiaxed crystals growing towards each other, a more complete understanding of equiaxed dendritic solidification will be achieved. In particular, microgravity benchmark data will be obtained on the growth and interaction of equiaxed dendrites in the pure diffusion limit and compared to corresponding ground-based experimental data to ascertain the influence of convection. Together with numerical simulations of the experiments, using an inverse approach, this will enable the testing of existing theories of equiaxed dendritic solidification and the development of refined or new models. The proposed research is needed to establish a more firm scientific basis for the coupling of microstructural evolution models to macroscale numerical simulations of casting processes in order to optimize structure and control segregation.

## BACKGROUND AND PRESENT STATUS

Equiaxed dendritic crystals can occur in both pure materials and alloys and are present in most castings. Equiaxed dendrites of a transparent model substance are shown in Fig. 1a. A large, fine-grained equiaxed zone is often promoted, through use of grain refiners, mold vibration, or electromagnetic stirring, to reduce macrosegregation and improve mechanical properties. An example of an equiaxed solidification structure, and the effect of inoculation, is shown in Fig. 1b for a nickel-base superalloy turbine blade. There have been numerous attempts at analytically modeling and/or experimentally observing the characteristics of equiaxed dendritic solidification. A brief overview of the most recent developments is provided in the following.

(i) *free, steady-state growth of an isolated, branchless dendrite tip into an infinite, undercooled liquid.*

Theories have been developed to ascertain the influence of undercooling on the dendrite tip velocity and radius. In recent microgravity experiments, Glicksman and coworkers (IDGE, USMP-2) were able to verify a model based on the Ivantsov solution for diffusion around the tip and marginal stability theory. The effects of convection on dendrite tip growth have been observed in the past, but available theories are of a limited nature and have not been experimentally verified completely.

(ii) *approximate models of the growth of an equiaxed dendritic crystal in a unit cell.*

Several diffusion-based analyses have been proposed [1-6]. Without resolving individual dendrite arms, a conceptual, spherical envelope is drawn around the crystal, and the one-dimensional diffusion equation is solved in the undercooled liquid between the envelope and the boundary of

(a) equiaxed dendrites of a transparent model alloy ($NH_4Cl$-$H_2O$) (unpublished)

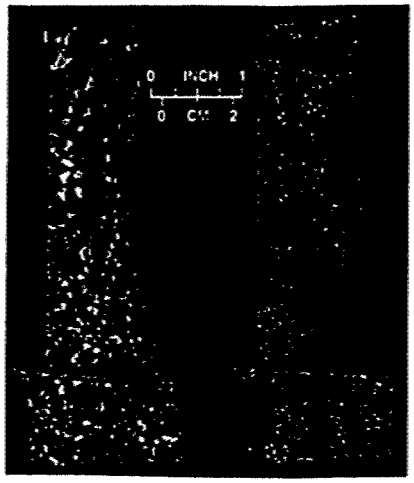


(b) equiaxed grain structure of a nickel-based superalloy turbine blade (left and right panels without and with grain refiner, respectively) (from ICCA consortium)

**Fig. 1 Illustration of equiaxed solidification.**

the unit cell; see Fig. 2. The knowledge of the diffusion flux at the envelope surface can then be used to calculate the evolution of the internal solid volume fraction inside the envelope. The growth of the envelope is described by the available theory for the free growth of an isolated dendrite tip (see above). For the limiting case of steady growth of a pure substance into an infinite liquid, it can be shown that the internal solid fraction of the grain is equal to the dimensionless thermal undercooling. The main advantage of the unit cell models is that they can readily be incorporated into macroscopic solidification simulation codes to represent the microstructure in a casting. These models have only been validated on a bulk level, through comparisons with measured cooling curves and grain structures. Such comparisons can be ambiguous, mainly because of an inadequate knowledge of nucleation and the presence of convection.

Unit-cell or volume averaged models are of an approximate nature, and some of the important but presently unresolved issues are: (i) the separate consideration of diffusion in the dendrite tip region (to calculate the tip/envelope velocity with the help of the Ivantsov solution) and in the extradendritic space "ahead" of the envelope (to back out the internal solid volume fraction) may not be valid since there is only a single diffusion field in the liquid around the equiaxed dendrite; in particular, the internal solid fraction evolution models have never been scrutinized experimentally; (ii) use of a steady-state growth model (based on the "far-field" undercooling) for the dendrite tip/envelope neglects initial and final transients; a steady-state growth period may, in fact, not exist; the interaction of the diffusion fields of neighboring dendrites, responsible for the final transient, has never been studied; (iii) present models do not account for the non-spherical shape of the crystal envelopes, the crystallographic orientation of the grains, and the three-dimensional nature of the diffusion fields; (iv) present models of equiaxed solidification (not just growth of a free, isolated dendrite tip) that include convection are immature, especially for a multi-crystal system. The proposed experiments and simulations will address these shortcomings by providing data on the transient evolution of the envelope shape and velocity, and the solid morphology and fraction inside the envelope, in a multi-crystal system, for the testing and refinement of unit-cell models.

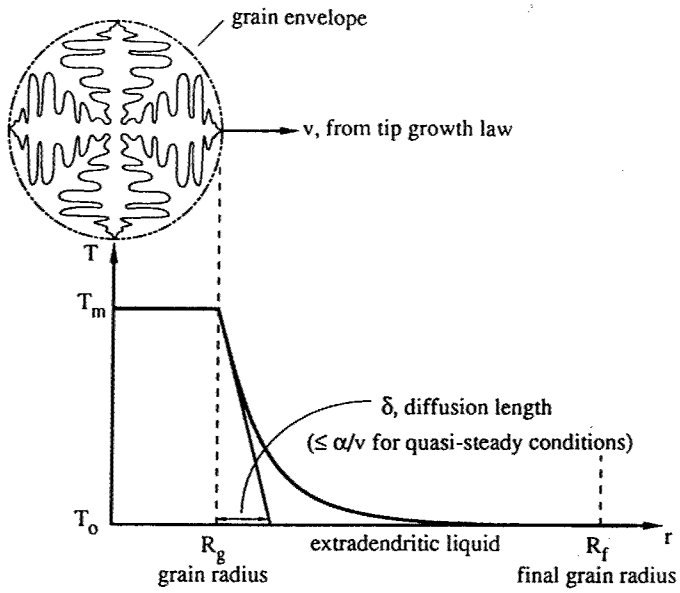


**Fig. 2 Schematic illustration of the unit-cell approach for equiaxed solidification of a pure substance.**

(iii) *direct, microscopic simulations of the growth of equiaxed dendrites.*

Recent computations using phase-field models have shown promise to compute dendrite morphologies for purely diffusional transport. The phase field variable identifies the phase at a point, without having to explicitly track the interface. Several numerical results have recently been presented for free dendritic growth from an undercooled melt of a pure substance [7, 8]. These computations are limited to two-dimensions and growth at relatively high dimensionless undercoolings. One of the present co-investigators (B.T. Murray) has performed preliminary phase-field model calculations (unpublished research) to study the interaction of equiaxed dendrites of pure nickel grown towards each other. One example of the calculations is shown in Fig. 3, where two dendrites with four-fold symmetry have their main horizontal branches growing along the same axis. While the high undercoolings used for the simulations are achievable for metals, they cannot be achieved for the transparent organic systems which allow visual quantification of the dendritic growth process. At lower undercoolings (i.e., smaller growth velocities), the extent of the diffusion layer is much larger (relative to the crystal size) and thus requires a much larger computational domain than presently achievable. The ongoing development of adaptive numerical techniques will relax this restriction on high undercoolings in the near future. The proposed microgravity experiment will provide the benchmark data needed for the planned extensions of the phase-field model.

*(iv) mesoscopic simulations.*

A new model has recently been proposed by one of the present co-investigators (I. Steinbach) that attempts to bridge the gap between the unit-cell models and the direct, microscopic simulations. This model is based on a modified phase-field approach, where the phase-field variable identifies the grain envelope, instead of the solid and liquid phases. The results of sample calculations are presented in Fig. 4 (unpublished research). Due to the reduced computing requirements compared to the direct, microscopic simulations, it is possible to simulate the growth of multiple grains (Fig. 4) as well as growth in three dimensions (Fig. 4bc), both of which are important for simulating the proposed microgravity experiment. Realistic undercoolings can be implemented without difficulty. The model also allows for random orientations of the grains. The main shortcoming of this

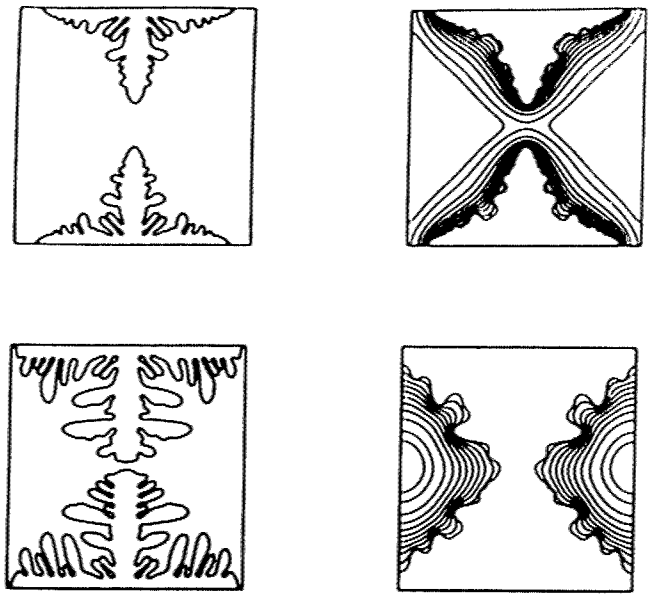

**Fig. 3 Microscopic phase-field simulation of the on-axis growth of two equiaxed dendrites towards each other (left panels: phase-field contours, right panels: isotherms) (unpublished research, B.T. Murray).**

mesoscopic model is that the local velocity of the envelope surface must be specified through a separate relationship. Unlike the unit-cell models, however, the non-spherical shape of the envelope is resolved and the three-dimensional, transient diffusion field around the envelopes is calculated directly. Thus, using envelope orientation, shape and velocity data measured in the planned experiments, it will be possible to close the model and determine unmeasured parameters.

*(v) effects of convection.*

Previous ground-based research due to the principal investigator concentrated on the effects of convection on equiaxed dendritic solidification. The drag coefficients of plastic model dendrites and $NH_4Cl$ crystals were measured in special Stokes flow settling facilities [9]. A correlation was developed that allows for the calculation of the drag on a single equiaxed dendrite, based on the concept of a porous envelope. This correlation was extended to the case of multiple equiaxed crystals, covering the full range of crystal densities and solid fractions [10]. Additional data and verification is needed for multiple equiaxed grains in the presence of a significant extradendritic liquid fraction, and the proposed ground-based experiments will lead to an increased understanding of the complicated flow patterns in an assemblage of equiaxed crystals. Solute transport from growing equiaxed dendrites is being measured in separate experiments, where a crystal is dropped in a melt column with a precisely controlled undercooling. By comparing the growth rates in the proposed microgravity and ground-based experiments, additional data on the effects of convection on the growth rates can be obtained.

## RESEARCH PLANS

We plan to perform well-controlled equiaxed dendritic solidification experiments on the scale of several crystals to provide benchmark data for testing and refinement of equiaxed microstructure evolution models, both with and without convection. The program is a combination of space experiments (diffusion limit), ground-based experiments (with convection), and supporting analysis and simulation. The experiments will use a modified version of the Millikelvin

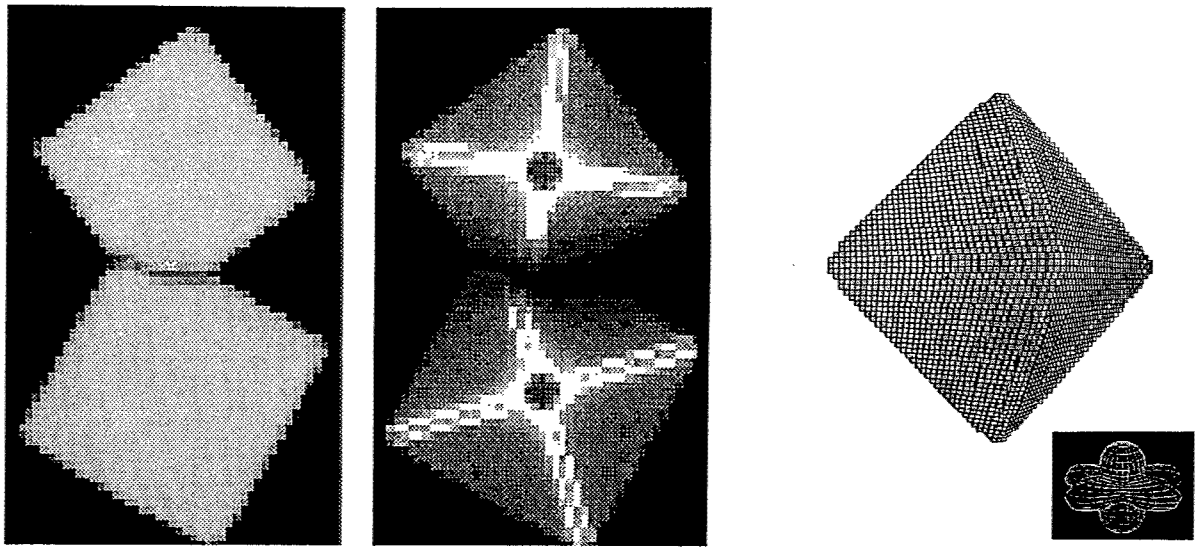

(a) growth of two crystals having different orientations towards each other (left panels: grain fraction, right panels: internal solid fraction

(b) three-dimensional simulation (grain fraction)

**Fig. 4 Examples of mesoscopic simulations (unpublished research, I. Steinbach).**

Thermostat (MITH) and involve the growth of up to four equiaxed crystals of the transparent, pure model material SCN simultaneously towards each other. Of interest are the evolution of the dendrite morphology, dendrite envelope, internal solid fraction in a multi-crystal setting, and the nature and interactions of the thermal fields around neighboring crystals. The influence of convection will be ascertained by comparing the results of microgravity and ground-based experiments. Critical to the success of the research will be the planned micro- and meso-scale simulations of the experiments, enabling (i) the extraction of additional information about the relation between the experimental data and the physical conditions and (ii) the development of refined or new models for both the diffusion and the convection case. The specific goals and tasks can be summarized as follows:

(i) perform microgravity experiments using SCN and a modified version of the Millikelvin Thermostat (MITH), where up to four equiaxed crystals are grown towards each other; measure the orientation and shape of the crystals, the temporal variation of the velocities of the primary and secondary dendrite tips, dendrite arm spacing and thicknesses, and melt temperatures at selected locations as a function of the initial undercooling;

(ii) perform corresponding ground-based experiments and measurements; visualize and measure the flow field in the growth chamber; explore the possibilities of varying the crystal spacings and measuring the volume change due to phase change (to back out the fraction solidified); compare to microgravity data and quantify the influence of convection;

(iii) perform mesoscopic simulations of selected experiments in the limit of diffusional heat transport, using the measured crystal orientations and dendrite tip velocities, as well as initial and boundary conditions, as input; perform inverse analyses to back out the thermal undercoolings responsible for the observed tip velocities as well as to calculate the solid fraction evolution behind the tips; if possible, compare the latter to the experiments; explore

the possibility of performing mesoscopic numerical simulations including thermal convection in order to better model the ground-based experiments;

(iv) deduce a refined unit-cell (or volume-averaged) model of equiaxed dendritic solidification from the mesoscopic simulations for the diffusion case and, ultimately, extend it to include convection;

(v) perform microscopic phase-field simulations to further the understanding of the underlying physical mechanisms associated with the growth of isolated and multiple dendrites.

## REFERENCES


1. M. Rappaz and Ph. Thevoz, *Acta Metall.*, Vol. 35, pp. 1487-1497, 1987.

2. M. Rappaz and Ph. Thevoz, *Acta Metall.*, Vol. 35, pp. 2929-2933, 1987.

3. D.M. Stefanescu, G. Upadhya and D. Bandyopahyoy, *Metall. Trans. A*, Vol. 21A, pp. 997-1005, 1990.

4. L. Nastac and D.M. Stefanescu, *Metall. Trans. A*, Vol. 24A, pp. 2107-2118, 1993.

5. C.Y. Wang and C. Beckermann, *Metall. Trans. A*, Vol. 24A, pp. 2787-2802, 1993b.

6. C.Y. Wang and C. Beckermann, *Mater. Sci. and Eng. A*, Vol. A171, pp. 199-211, 1993c.

7. A.A. Wheeler, B.T. Murray and R.J. Schaefer, *Physica*, Vol. D66, p. 243, 1993.

8. B.T. Murray, W.J. Boettinger, G.B. McFadden and A.A. Wheeler, in *Heat Transfer in Melting, Solidification, and Crystal Growth*, eds. I.S. Habib and S. Thynell, ASME HTD-234, New York, p. 67, 1993.

9. R. Zakhem, P.D. Weidman and H.C. de Groh III, *Metall. Trans. A*, Vol. 23A, pp. 2169-2181, 1992.

10. C.Y. Wang, S. Ahuja, C. Beckermann and H.C. de Groh III, *Metall. Mater. Trans. B*, Vol. 26B, pp. 111-119, 1995.

# SURFACE MORPHOLOGICAL PROPERTIES OF STATIONARY MELT POOLS IN SINGLE CRYSTALS OF STAINLESS STEEL

**L. A. Boatner, D. Corrigan, S. A. David, and Michel Rappaz**
**Oak Ridge National Laboratory**

**and**

**G. Workman and G. Smith**
**Materials Processing Laboratory**
**The University of Alabama, Huntsville**

The formation of surface ripples during welding or by stationary arc or laser melting and the overall gross surface morphological features of melt pools represent problems that have existed for a number of years but which are not fully understood at the present time. Several mechanisms have been invoked to explain the formation of small surface ripples, most of these being related in some way to the effects of capillarity. Surface ripples are sometimes associated with an effect called "solute banding." In this case, the whole melt pool does not appear to move with a constant velocity, and bands can be seen in transverse or longitudinal micrograph sections of the melt pool. In other cases, ripples appear only at the top surface without any in-depth correlation with the overall properties of the original melt.

Kotecki et al [1] studied the formation of ripples in GTA (Gas Tungsten Arc) spot welds. They observed concentric ripples after solidification which they attributed to oscillations of the liquid surface. If the arc plasma is fluctuating, the melt pool oscillated with the same frequency (forced oscillation). If the arc was generated from batteries, oscillations were only observed when the power was interrupted (natural oscillations of the molten pool). These authors made a one-to-one correspondence between the number of ripples observed in the solidified weld and the number of pool oscillations measured during solidification. However, their analytical model of natural oscillations in terms of a vibrating drum membrane was over simplistic. More recently, Postacioglu et al [2] have made a detailed calculation of natural and forced oscillations of a melt pool with particular attention to keyhole formation.

In a now classic paper, Anthony and Cline [3] took a totally different approach to explaining ripple formation during continuous laser melting. They considered the simple situation of a one-dimensional Marangoni flow induced by a surface tension gradient and calculated the pressure difference along the surface. They then converted this pressure gradient into a metallostatic head difference but ignored the capillarity contribution (i.e., the Laplace force).

Nakane [4] has made a detailed experimental investigation of ripples formed during GTA welds, under DC and AC conditions. In DC GTA welds made at a low welding speed, he observed macro ripples which were also associated with solute-band formation. These ripples seem to be due to fluctuations of the arc, and if the velocity is low, they can also be observed on the underneath surface when full penetration welds are made (i.e., massive movement of the pool occurs.) At higher speeds, the macro ripples partially disappear and micro ripples appear. These were due to variations of the rectified arc current (300 Hz).

In the present study, stationary melt pools were formed in austenitic single crystals in order to study the formation of the solidification microstructure. ripple formation, and the overall surface morphology of the solidified melt. . Although the melt-pool shape is stationary in this case, the dendritic microstructure can be analyzed using an approach similar to that derived for welds made at constant velocity [5]. The small ripples that form under these conditions can be analyzed using the formalism of standing capillary waves. This formalism will summarized, and the results will be presented and discussed. New problems associated with the overall shape of the solidified melt pool have also been identified, and these will be treated as well.


1. D. J. Kotecki, D. L. Cheever and D. G. Howden, Welding Research Supplement (1972) 386-91
2. N. Postacioglu, P. Kapadia and J. Dowden, J. Phys. D, Appl. Phys. **22** (1989) 1050-61.
3. T. R. Anthony and H. E. Cline, J. Appl. Phys. **48** (1977) 3888-94.
4. K. Nakane, *Ripple Formation on the Surfaces of GTA Welding Beads*, Memoirs School Sc. Eng., Waseda Univ. **44** (1980) 1-39.
5. M. Rappaz, S. C. David, J. Vitek and L. A. Boatner, Met. Trans. **A, 21A** (1990) 1767.

# DISPERSION MICROSTRUCTURE AND RHEOLOGY IN CERAMICS PROCESSING

J. F. Brady
Division of Chemistry and Chemical Engineering
210-41
California Institute of Technology
Pasadena, CA 91125
USA
Phone: 818-395-4183
Fax: 818-568-8743
email: jfbrady@caltech.edu

## Abstract

Improved ceramic materials may be obtained by using a mixture, either by size or composition, of fine particles. Critical to the success of such a mixture is the control of the dispersion microstructure during processing. Microstructure formation and rheology of concentrated bidisperse suspensions will be investigated by a combination of Stokesian Dynamics simulation and analytical modeling. Unbounded shear flows and slip-casting will be simulated, and the influence of particle size ratio, volume concentration, shear rate and thermal energy on microstructure formation determined. Analytical models will be developed to predict structure formation and flow behavior during ceramics processing. Owing to size or compositional differences, particle mixtures are subject to gravitational phase separation or demixing, and processing in microgravity may provide an attractive environment for producing advanced ceramics.

## Introduction

Ceramics provide a potentially very useful class of materials owing to their physical properties; they are light, hard, resistant to abrasion, chemically inert, stable at high temperatures, and excellent thermal and electrical insulators [1]. Further, by casting from a liquid suspension and subsequently sintering, many complex parts and shapes can be fabricated [2]. Although the resultant properties of ceramics can be outstanding, they often suffer from extreme brittleness. This brittleness is caused by the propagation of cracks, which is in turn due to microstructural defects. These defects may be caused by a number of different factors, such as particle agglomeration, migration or segregation prior to sintering, or due to inhomogeneous volume change upon sintering. If a ceramic's microstructure can be controlled and rendered homogeneous prior to (and after) sintering optimal material properties may be realized in an economic way.

Typically, high-performance ceramics are produced using monodisperse submicron-sized particulate suspensions from which the ceramics are cast. By controlling the size and processing a dense uniform microstructure may be formed prior to sintering. This route has met with limited success even though the maximum volume fraction of ceramic particulates that can be achieved prior to sintering is 0.74. The limited success may stem from the fact that a perfect crystal of mono-sized particles has slip planes that yield easily, and from the fact that there is still a large amount of void space that must be eliminated upon sintering.

An alternate approach is to use a mixture of particle sizes [3,4]. It is well know that solids fractions of 90% can be obtained with a bidisperse suspension of spherical particles. And even greater loadings are possible with tridisperse systems. Crystalline slip planes can be eliminated with a mixture of particle sizes. In addition to achieving high solids fractions, and therefore reducing potential sintering inhomogeneities, a mixture of two different types of particles can also impart desirable properties in a 'composite' ceramic. For example, zirconia in alumina has been used to arrest crack propagation owing to the transformation toughening of zirconia under stress [5].

## Research Objectives

For bi- or poly-disperse suspensions to be successful, the microstructure must be controlled during processing. It has been observed experimentally that for the same total volume fraction, a mixture of two particle sizes leads to a reduction in the suspension viscosity, with obvious advantages for ease of processing [6-14] (see figure 1). Although there are several heuristic models to explain this viscosity reduction phenomena, there is no fundamental explanation and very little theoretical work has been done. Furthermore, the viscosity reduction is only one factor. Of much greater importance is the microstructure formed during processing, for this determines the ultimate success or failure of the ceramic. As an example of the importance flow has on microstructure, figure 2 shows the flow-induced ordering that can occur in monodisperse Brownian suspensions [15,16]. To date there have been no studies of microstructure formation during flow of bidisperse suspensions.

A thorough understanding of the factors that control dispersion microstructure during processing is needed so that rational design of ceramic materials is possible. Will a well mixed dispersion remain randomly mixed, or will size segregation occur under flow? Can a highly ordered microstructure free of defects be formed during processing? Can the maximum solids fraction be obtained leading to optimal ceramic properties? A number of critical questions need to be answered in order to move composite ceramics forward. The objective of this research is to address these questions by a combined numerical and analytical study of structure formation and rheology of bidisperse suspensions under flow. Stokesian Dynamics simulation of concentrated bidisperse suspensions of unbounded shear flows and slip-casting will be conducted, and the influence of particle size ratio, volume concentration, shear rate and thermal energy on microstructure formation determined. Analytical models [17-19] will be developed to predict structure formation and flow behavior during ceramics processing.

## References

1. National Research Council 1989 *Materials Science and Engineering for the 1990s*, National Academy Press.
2. Somiya, S. 1989 *Advanced Technical Ceramics*, Academic Press.
3. Reed, J.S. 1988 in *Ceramic Transactions, Ceramic Powder Science II*, The American Ceramic Society, p.601.
4. Brook, R.J., Tuan, W.H. and Xue, L.A. 1988 in *Ceramic Transactions, Ceramic Powder Science II*, The American Ceramic Society, p.811.
5. Hannink, R.H.J. and Swain, M.V. 1994 *Ann. Rev. Mater. Sci.* **24**, 359.
6. Ferris, K.J. 1968 *Trans. Soc. Rheol.* **12**, 281.
7. Chong, J.S., Christiansen, E.B. and Baer, A.D. 1971 *J. Appl. Polym. Sci.* **15**, 2007.
8. Rodriguez, B.E., Kaler, E.W. and Wolfe, M.S. 1992 *Langmuir* **8**, 3282.
9. Hoffman, R. 1992 *J. Rheol.* **36**, 947.

10. Shapiro, A.P. and Probstein, R.F. 1992 *Phys. Rev. Lett.* **68**, 1422.
11. Chang, C. and Powell, R.L. 1993 *J. Fluid Mech.* **253**, 1.
12. Chang, C. and Powell, R.L. 1994 *J. Rheol.* **38**, 85.
13. Woutersen, A.T.J.M. and de Kruif, C.G. 1993 *J. Rheol.* **37**, 681.
14. Wagner, N. J. and Woutersen, A.T.J.M. 1994 *J. Fluid Mech.* **278**, 267.
15. Phung, T. 1993 *Ph.D. Thesis*, California Institute of Technology.
16. Phung, T.N., Brady, J.F. and Bossis, G. 1996 *J. Fluid Mech.* **313**, 181.
17. Brady, J.F. 1993 *J. Chem. Phys.* **99**, 567.
18. Brady, J.F. 1994 *J. Fluid Mech.* **272**, 109.
19. Brady, J.F. and Vicic, M. 1995 *J. Rheol.* **39**, 545.

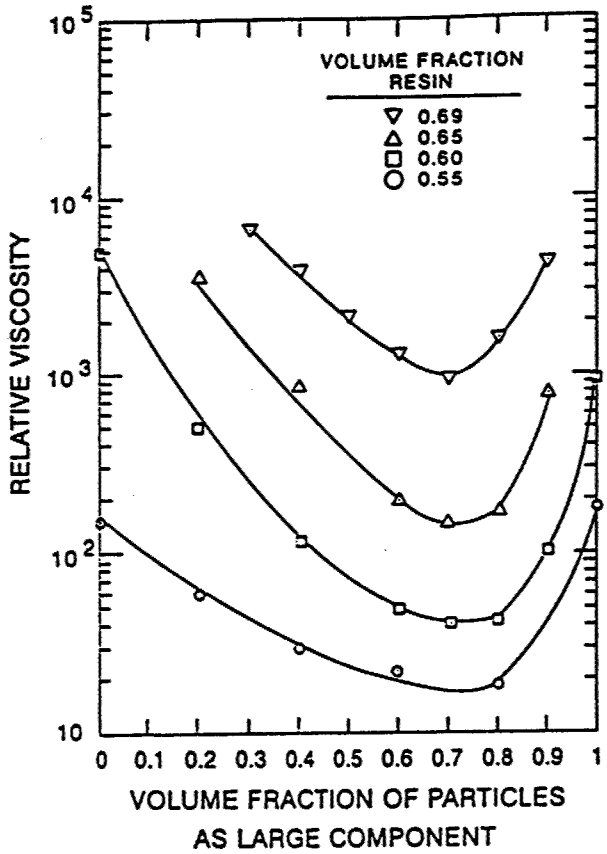


Figure 1. Relative viscosity of a bidersperse suspension at high shear rates. Note the pronounced minimum in the viscosity at a certain fraction of large particles (Hoffman 1992).

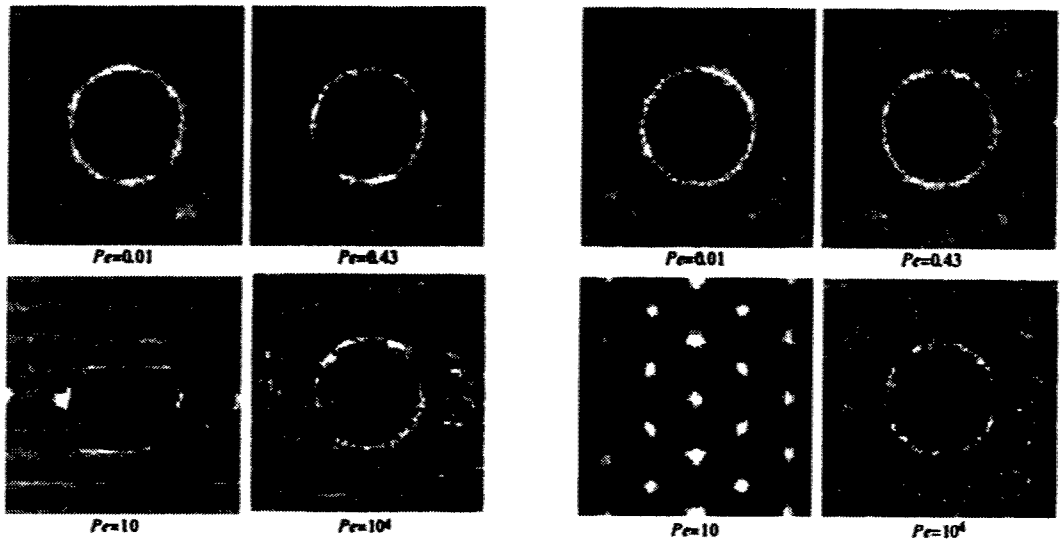


Figure 2. Projections of the pair-distribution function for monodisperse Brownian hard spheres at a volume fraction of 0.45 deteremined by Stokesian Dynamics simulation. The left shows the projection in the velocity--velocity-gradient plane and the right shows the projection in the vorticity–velocity-gradient plane. Note the formation of a shear-induced 'string' phase for intermediate Peclet numbers (Phung 1993).

# COMBUSTION SYNTHESIS OF MATERIALS IN MICROGRAVITY

NAG8-1261

Dr. Kenneth Brezinsky, Senior Research Scientist, Principal Investigator, Princeton University, Mechanical & Aerospace Engineering Department, Princeton, N.J. Tele: (609) 258-5225; e-mail: kenb@cougarxp.princeton.edu

Prof. Irvin Glassman, Co-Investigator, Princeton University, Mechanical & Aerospace Engineering Department, Princeton, N.J. Tele: (609) 258-5199; e-mail: iglassman@princeton.edu

Prof. C.K. Law, Co-Investigator, Princeton University, Mechanical & Aerospace Engineering Department, Princeton, N.J. Tele: (609) 258-5271; e-mail: cklaw@phoenix.princeton. edu.

Homogeneous suspensions of metal particles in supercritical nitrogen that can only be formed in a microgravity environment are proposed as the subject of this new study. Microgravity is a crucial part of the experimental program because of three unique effects of this type of environment on the proposed experiments. The first and key effect is that particle settling can be inhibited so that a true homogeneous suspension critical to a novel synthesis approach can be obtained. Specifically, a nitride synthesis approach has been proposed in which the nitride product would be generated from a flame propagating through a controlled density suspension of titanium particles in nitrogen at temperatures and pressures just past the critical point (supercritical nitrogen). This approach offers advantages both as a process technique and as a means of scientific study, namely: 1) The suspension provides a more porous medium than a solid powder compact or a loose bed for transport of nitrogen to reacting particles; 2) The high (approximately 40 atmospheres) but not extremely high pressure provides an adequate and more convenient supply of nitrogen, without bubble formation, for the complete reaction of individual titanium particles; 3) The density and therefore concentration of nitrogen for the limit of kinetically controlled product formation is controllable because of the almost infinite isothermal compressibility near the critical point; 4) The particles can be sufficiently separated by varying and maintaining at microgravity the particle density of the suspension so that, in principle, agglomeration is not a problem; 5) The burning intensity can be controlled by varying and maintaining at microgravity the particle suspension density; 6) The final titanium nitride product will be in the form of powders whose shapes and sizes are in principle controllable through the selection of the initial titanium particles and, at microgravity, unaltered by settling. Such shape and size specific powders are expected to be of great commercial value.

The second effect is that a microgravity environment eliminates the hydrostatic pressure that exists on Earth in a column of fluid simply due to its weight. This hydrostatic pressure varies with position in a vertical column of fluid. For properties of supercritical fluids which are extremely sensitive to pressure, as is the density near the critical point, variations will exist, on Earth, along the column length. To avoid these variations and maintain a homogeneous supercritical nitrogen environment, a microgravity based experimental program is paramount.

A third advantage of microgravity conditions is to provide a "containerless" environment. The quartz and stainless steel materials that will contain the titanium powder have been shown to contribute to the contamination and reduced yield of the nitride product. In microgravity, suspensions can be created and maintained so that wall effects are minimized.

Initial experiments will be aimed at the design and development of a means of formation of a uniform suspension of powder particles in supercritical nitrogen. Subsequent experiments in a microgravity environment will focus on obtaining spatially resolved temperature and particle characteristics across the flame. The microgravity environment envisioned for the initial research is that available on the DC-9 aircraft.

The experiments proposed in the new research program are based on results and interpretations that were developed in a previously funded NASA program, NAG3-1418, on the supercritical combustion synthesis of titanium nitride. The essential results and conclusion of the previous work are now described.

To increase the interstitial mass loading of nitrogen for enhanced product yield in the SHS synthesis of metallic nitrides, the synthesis was conducted in cryogenic nitrogen at supercritical states just above the critical point. This state regime has the unique characteristic that the density increases significantly with pressure. The viability of this concept has been experimentally substantiated for loosely-packed titanium powders. Results showed that the bubbling that characterized the synthesis process in liquid nitrogen was avoided and liquid-like initial densities were maintained. Yields of titanium conversion to titanium nitride of almost 75% were achieved. This level of conversion is comparable to the highest of previously reported values obtained for titanium in gaseous nitrogen at ultra high pressures. Analysis of the experimental supercritical and literature data on high-pressure gas synthesis shows that the yield does not correlate well with pressure in accordance with the previous concept that filtrational transport is the controlling mechanism, especially for the after-burn condition. The data, however, were satisfactorily correlated against fluid density. Mass diffusion is the apparent relevant process for after-burn in

low nitrogen density environments, and nitrogen loading in the interstices of the powdered titanium controls the yield at high initial nitrogen densities.

Three significant contributions evolved from the study. First, the utility of supercritical nitrogen as a means of increasing the product yield in the SHS of metallic nitrides was demonstrated. Specifically, by working in slightly supercritical states, the fluid density and hence the interstitial mass loading can be significantly increased without the need of ultra high pressures as for the synthesis in gaseous nitrogen. Secondly, this approach has been applied to the synthesis of titanium nitride and has resulted in yields up to 75%, which even slightly exceed the highest value previously obtained by using high-pressure gaseous nitrogen. Thirdly, it has been demonstrated that previous and present data on high-pressure TiN SHS can be correlated in terms of the fluid density, instead of the system pressure, which implies that mass diffusion instead of filtration is the controlling process for after-burn in low density environments and that nitrogen loading in the interstices of the powdered titanium controls the yield at high initial nitrogen densities.

Publications resulting from the NASA work.

"Self-Propagating High-Temperature Synthesis of Titanium Nitride In Supercritical Nitrogen", John A. Brehm, M.S.E. Thesis, Princeton University, June 1995.

"High Temperature Combustion Synthesis Using Supercritical Nitrogen", K. Brezinsky, J.A. Brehm, C.K. Law and I. Glassman, Extended Abstract #70, 1995 Technical Meeting of the Eastern States Section of the Combustion Institute.

"Supercritical Combustion Synthesis of Titanium Nitride", K. Brezinsky, J.A. Brehm, C.K. Law and I. Glassman, reviewed paper accepted for presentation and publication, 26th International Symposium on Combustion, August 1996.

# APPLICATION OF PARALLEL COMPUTING FOR TWO- AND THREE-DIMENSIONAL MODELING OF BULK CRYSTAL GROWTH AND MICROSTRUCTURE FORMATION

Robert A. Brown
Department of Chemical Engineering
Massachusetts Institute of Technology
Cambridge, MA 02139
Phone: 617-253-5726
E-mail: rab@mit.edu

## Objectives

The quality of metal, oxide, and semiconductor crystals grown from the melt depends fundamentally on heat, mass and species transport in the melt and crystal, and on the interactions of these fields with the formation of microstructure, microdefects, dislocations and voids in the grown crystal. Modeling of these individual processes and understanding their complex interactions is fundamentally important to the successful growth of crystals in a microgravity environment and to the interpretation of experiments from ground-based and microgravity research. The research program described here focuses on the development of simulation tools for analysis of detailed, integrated models of melt crystal growth systems. To be quantitative for modeling microgravity experiments, such models must be three-dimensional and, many times, time dependent, and must include convection in the melt, heat transfer by conduction, radiation and convection in all phases, and species transport in the melt phase. Most importantly, the models must couple together these transport processes to yield an integrated picture of transport throughout the system.

The first goals of this research are to develop robust algorithms for the solution of integrated models of melt crystal growth to allow the analysis of such systems. An important feature of this proposal is the application of scaleable parallel computing to these applications, where *scaleable parallel computers* can be either clusters of workstations connected by a low-performance network, such as an ethernet, or aggregates of such workstations that are self-contain in one unit and connected by a high-performance fiber optic link. Such machines are becoming commonly available in universities, government laboratories, and industry. The focus of our effort will be the development of an integrated simulation of vertical Bridgman (VB) crystal growth and a simulation of cellular microstructure formation for large collections of cells during binary alloy solidification.

## Numerical Algorithms

Many of the numerical algorithms are built around the finite-element/Newton methods that we have developed with good success for the solution of material processing models that represent complex physicochemical hydrodynamics and transport. The numerical algorithms combine accurate finite element and finite difference discretizations of the field equations and boundary conditions, quasiorthogonal mapping methods for coupling the action of free- and moving-boundaries, local mesh refinement for capturing features of these solution fields, and Newton's method for solution of the nonlinear algebraic equations that arise in the solution of steady-state problems or in implicit integration methods for transient problems. Efficient implementation on parallel computers requires algorithms for the solution of the large (up to millions), sparse, asymmetric and indefinite linear algebraic equation systems that arise at each Newton iteration.

Two approaches are being investigated for this problem: direct LU factorization using concurrent factorization and storage (CFS) and preconditioned iterative methods using Krylov iteration methods and incomplete LU (ILU) factorization and domain decomposition, Schwarz preconditioners; we call these algorithms Schwarz/Krylov methods. The CFS method has the

advantage of the great robustness of a direct method, but suffers from the large memory requirement and high complexity (operation count) of a direct factorization algorithm. The iterative methods have low complexity, but can have convergence and efficiency difficulties, unless an adequate preconditioner is found for the iteration. Both approaches are being compared with each other, and with classical frontal factorization methods, for the equations arising from finite element discretization of a two-dimensional natural convection problem, which exhibits all the difficulties inherent in matrices generated by modeling of physicochemical processes.

The CFS algorithm uses domain decomposition to divide the computational effort for the LU factorization among the processors of a MIMD parallel computer. The factorization proceeds by forming the Schur compliment on the partition established by the processors; this reduced matrix is distributed among the processors and factored in parallel. Pivoting during the LU factorization is allowable within the rows and columns of the matrix on a single processor. The CFS algorithm has been demonstrated to be more efficient than classical frontal matrix methods on a single processor and gives good performance on a moderate sized parallel computer. Parallel efficiencies of between 65 and 75 percent are achieved.

Schwarz/Krylov iterative methods for use with Newton's method have been developed using block preconditioners for the entire Jacobian matrix based on approximate Schur complement decompositions. The approximate Schur complement is computed using either an additive or multiplicative Schwarz, domain decomposition method coupled with an ILU solution for the matrix on each subdomain. Computational tests for the natural convection problem demonstrate the robustness and efficiency of this approach, especially for fine finite element discretizations. Moreover, the Schwarz/Krylov methods are shown to be more efficient that the CFS method with increasing problem size and are expected to have higher parallel efficiencies.

The Schwarz/Krylov methods are being incorporated into a state-of-the art simulator for the Vertical Bridgman crystal growth process that can be used to simulation earthbound and space experiments. Calculations for the VB system will focus on Bismuth germanate and on the silicon-germanium alloy. The simulations will be expanded to consider three-dimensional convection, where model problems will be used to compute flow transitions in systems important for microgravity processing and to study the effect of g-jitter on three-dimensional flows in vertical Bridgman crystal growth of semiconductors.

## Dynamics of Two-Dimensional Cellular Solidification

Experiments, theory and previously limited numerical simulations point to the conclusion that the cellular solidification interface which forms during solidification of a binary alloy is a spatiotemporally chaotic state, with the concept of the cellular wavelength only defined in a statistically-averaged sense. We have developed a fixed mesh, embedded interface simulation for simulating large collections of solidification cells in an effort to probe this effect and to collect computational statistics on this phenomena.

The fixed mesh/embedded interface method uses finite difference discretization and implicit time stepping of the conservation equations for solute and heat transfer on a regular grid with an embedded interface separating melt and solid. The interface position affects these fields through the concentration and temperature fields in the grid cells surrounding the interface. The normal velocity of the interface is computed from the solute conservation equation and used to explicitly advance in time the interface shape through a kinematic description of the surface in terms of arc-length and inclination angle. Initial simulations are reported for the succinonitrile-acetone organic alloy system, which is used in many thin-film solidification experiments. These results show the onset of cellular dynamics and the beginning of chaotic interactions. A parallel version of the simulation will be used to simulate large collections of cells and collect statistical data.

# THERMOPHYSICAL PROPERTIES OF HIGH TEMPERATURE LIQUID METALS AND ALLOYS

Ared Cezairliyan (Principal Investigator)
Metallurgy Division
National Institute of Standards and Technology (NIST)
Gaithersburg, MD 20899
Telephone: 301-975-5931

and

Shankar Krishnan (Co-Investigator)
Containerless Research Incorporated (CRI)
906 University Place
Evanston, IL 60201-3149
Telephone: 847-467-2678

## Objective

The objective of this research is to extend, for the first time, the laser polarimetry technique for measuring normal spectral emissivity to the microsecond time regime. This will enable accurate determination of the true temperature of liquid specimens at high temperatures in rapid pulse heating experiments. In addition to the measurement of other experimental quantities, the proposed project will yield data on selected thermophysical properties with unsurpassed accuracy that can be used in support of microgravity related research. The properties to be measured include enthalpy, specific heat capacity, heat of fusion, and electrical resistivity above the melting temperatures of selected refractory metals and alloys.

## Relevance to Microgravity

Thermophysical property values for liquid metals and alloys are needed in modeling solidification and crystal growth, in containerless processing, and for casting and welding design. A number of these processing techniques are currently being practiced in the reduced gravity environment. Our research supports these efforts by providing thermophysical measurements methodology and accurate thermophysical properties data on selected key materials.

## Background

Research on materials at high temperatures, including measurements of thermophysical properties, necessitates non-contact methods (optical pyrometry) for the measurement of specimen temperature. Determination of "true" temperature is an extremely important parameter in experiments that involve accurate thermophysical measurements at high temperatures. Yet, because of the difficulties associated with the measurements of high temperatures, large uncertainties exist in thermophysical properties data reported in the literature. Ideal measurements require a blackbody configuration for the specimen that is either impractical or impossible to achieve in high temperature experiments, particularly for liquid specimens. An alternate approach is to determine the true temperature from measurements of surface radiance temperature and a knowledge of the normal spectral emissivity of the specimen surface. Pyrometric techniques are sufficiently advanced to provide the means for accurate measurements of surface radiance temperature, however, determination of normal spectral emissivity for the specific surface presents a serious difficulty.

Available data on emissivity for many materials at high temperatures are in considerable disagreement, even for pure metallic elements. In many cases, the disagreement among the literature data is believed to be largely due to differences in surface roughness and/or to problems such as specimen evaporation, surface contamination, chemical reactions, etc. This suggests that for accurate temperature determinations, it is essential to measure normal spectral emissivity simultaneously with the surface radiance temperature of the specimen.

During the last decade, accurate direct measurements of normal spectral emissivity have been made possible as the result of research conducted at Rice University and Containerless Research Incorporated (CRI) [1,2]. These investigations have led to the development and application of a laser polarimetry technique for the measurement of normal spectral emissivity of electromagnetically-levitated high-temperature liquids. The working principle of the laser polarimetric technique is that, when quasi-monochromatic light of linear polarization is incident on a specularly-reflecting surface at an oblique angle, the reflected light is generally elliptically polarized. By accurately measuring the polarization state of the reflected light, normal spectral emissivity can be determined.

During the past three decades, the development of subsecond pulse-heating techniques at the National Institute of Standards and Technology (NIST) [3,4] has enabled the measurement of

selected thermophysical properties of a number of electrically-conducting solids at high temperatures (primarily in the range 1500 K up to and including their melting temperature). The measured properties include not only normal spectral emissivity but also heat capacity, electrical resistivity, thermal expansion, hemispherical total emissivity, temperature and energy of solid-solid phase transformations, and melting temperature [5]. The basic technique involves rapid resistive self-heating of the specimen from room temperature to the maximum temperature of interest in less than 1 s by passing an electrical current pulse through it, and simultaneously measuring the pertinent experimental quantities with millisecond resolution.

Three years ago, NIST and CRI began a NASA-sponsored joint effort to integrate the laser polarimeter and the millisecond pulse-heating system to conduct research with the objective of validating and establishing accuracy of the laser polarimetry method and obtaining accurate emissivity data on selected metals.

## Accomplishments

A high-speed laser polarimeter was developed and integrated into the millisecond-resolution pulse heating system at NIST (Figs. 1 and 2). Operation of the combined system was tested. Accurate measurements of normal spectral emissivity were performed on two refractory metals, molybdenum (Fig. 3) and tungsten, by two independent techniques, namely spectral radiometry and laser polarimetry in millisecond-resolution pulse-heating experiments [6]. The measurements were in the wavelength range 600 to 650 nm and covered the temperature range 2000 to 2800 K for both metals. The agreement between the normal spectral emissivity values obtained by the two techniques was within 1% over the entire temperature range, demonstrating reliability of the direct measurements of normal spectral emissivity with the new laser polarimetry technique. Also, measurements of enthalpy and electrical resistivity were performed on two different specimens (tubular and solid cylindrical) of a nickel-base alloy in the temperature range 1300 to 1500 K. Radiometric measurements on the tubular specimen and polarimetric measurements on the cylindrical specimen yielded property results within 2%, further indicating the reliability of the laser-polarimetric technique. In addition, applicability of the laser polarimetry technique to non-contact detection of phase transformations in metals and alloys at high temperatures was demonstrated by performing a preliminary series of experiments on nickel (magnetic transformation), iron (structural transformation), zirconium (solid-liquid transformation - melting point), and 53Nb-47Ti alloy (solid-liquid transformation - solidus point)(Fig. 4).

## Future Research Plans

At present, the high-speed laser polarimetry method is successfully used at NIST in millisecond-resolution pulse-heating experiments on solid materials up to their melting points. Melting point of the specimen is the upper temperature limit for the measurements with the millisecond system. In order to extend the measurements to liquid materials, experiments have to be conducted about 1000 times faster. For this purpose, an ultra-fast laser polarimeter will be developed for use in conjunction with the microsecond-resolution pulse-heating system available at NIST. Operation of the ultra-fast laser polarimeter will enable measurements of normal spectral emissivity (near 650 nm), thus true temperature, of liquid materials. The specimen will be heated from room temperature to any desired high temperature (up to 5000 K) in 100 to 300 μs and the measurement system will operate at 2 MHz rate. This system, the first one of its kind, will be used to accurately measure selected thermophysical properties (enthalpy, specific heat capacity, heat of fusion, and electrical resistivity) of selected high-melting-point electrically-conducting liquid materials at temperatures above 1500 K. The materials to be studied include refractory metals, such as niobium, molybdenum, tungsten, and industrially important nickel- and titanium-base alloys, such as Inconel 718, 90Ti-6Al-4V, in the range from their melting point to about 1000 K above their melting point). Additionally, studies will be made to establish the nature of thermodynamic equilibrium in these fast experiments vis-a-vis steady-state techniques, like levitation melting.

## References


[1] S. Krishnan, *J. Opt. Soc. Am.* **A9**, 1615 (1992).

[2] S. Krishnan, P. C. Nordine, J. K. R. Weber, R. H. Hauge, and J. L. Margrave, in *Temperature, Its Measurement and Control in Science and Industry*, Vol. 6, Part II, J. F. Schooley, Ed. (Amer. Inst. of Phys., New York, 1992), p. 943.

[3] A Cezairliyan, M. S. Morse, H. A. Berman, and C. W. Beckett, *J. Res. Natl. Bur. Stand. (US)*, **74A**, 65 (1970).

[4] A. Cezairliyan, *J. Res. Natl. Bur. Stand. (US)*, **75C**, 7 (1971).

[5] A. Cezairliyan, *Int. J. Thermophys.*, **5**, 177 (1984).

[6] A. Cezairliyan, S. Krishnan, and J. L. McClure, *Int. J. Thermophys.*, **17** (1996), in press.

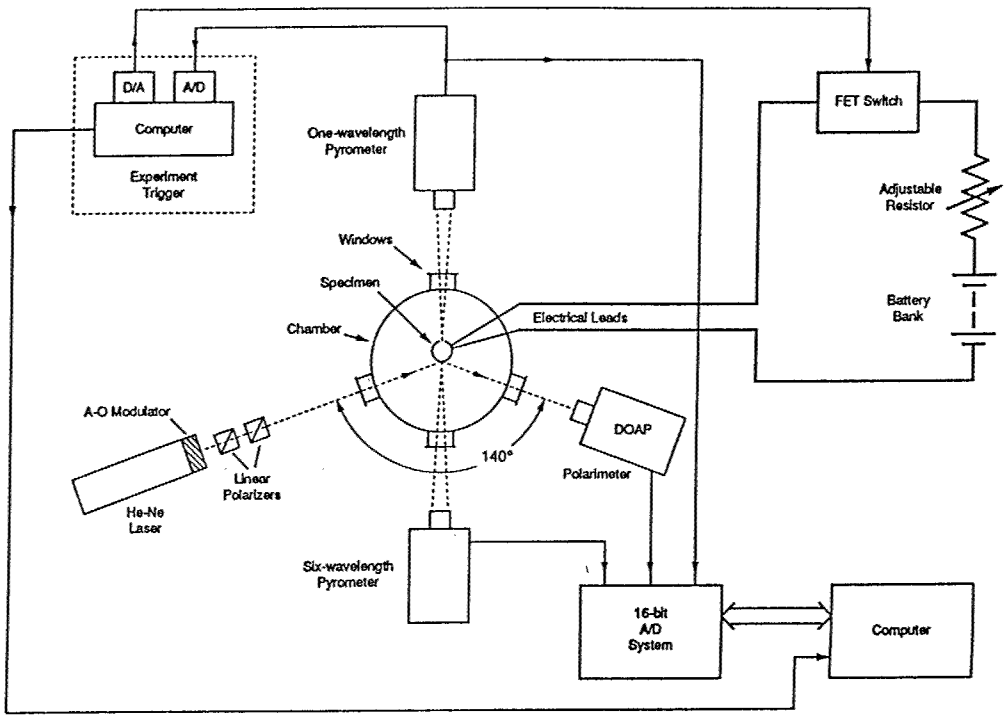


**Figure 1**. Functional diagram of the overall experimental arrangement including the pulse-heating system and the radiometric and polarimetric instrumentation.

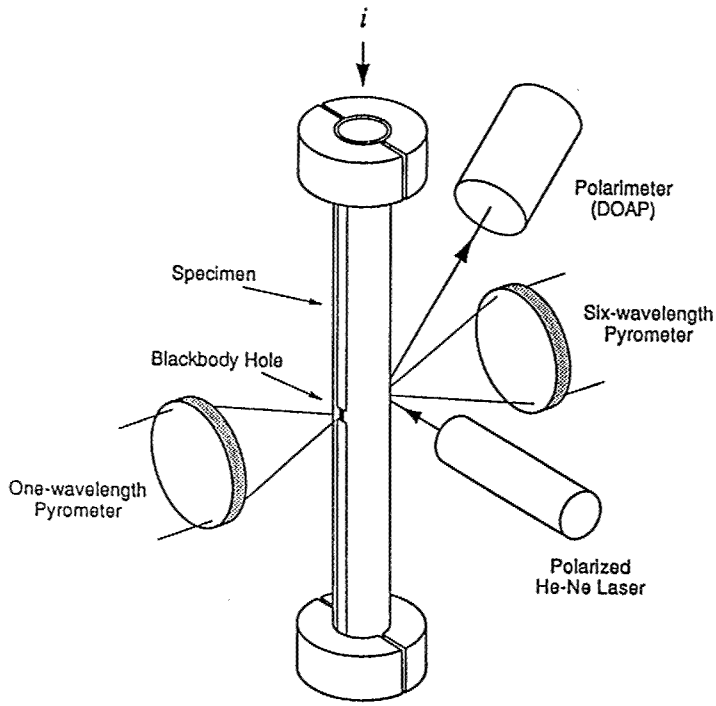


**Figure 2**. Schematic diagram of the specimen and the configuration of the pyrometers and the polarimeter. Dimensions are not to scale.

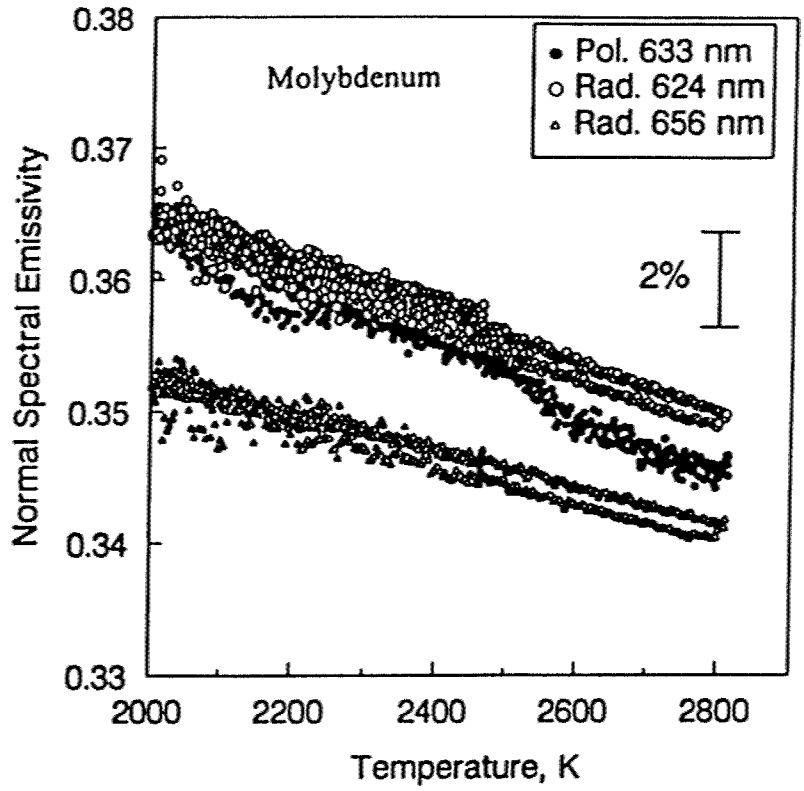


**Figure 3.** Normal spectral emissivity of molybdenum determined from radiometric (at 624 and 656 nm) and polarimetric (at 633 nm) measurements.

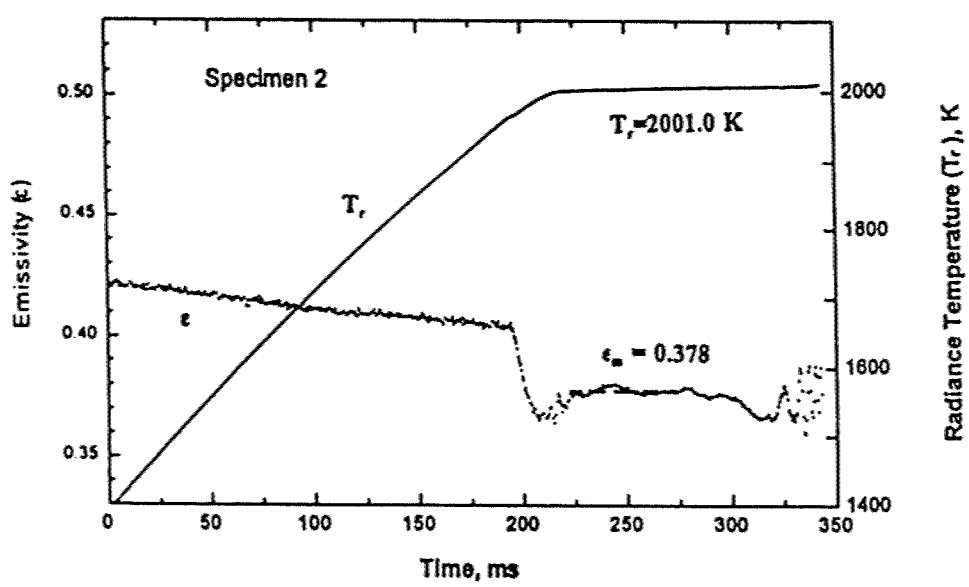


**Figure 4.** Radiance temperature and normal spectral emissivity of the alloy 53Nb-47Ti before and at the beginning of melting.

# THREE-DIMENSIONAL VELOCITY FIELD CHARACTERIZATION IN A BRIDGMAN APPARATUS: TECHNIQUE DEVELOPMENT AND EFFECT ANALYSIS

Soyoung Stephen Cha
Department of Mechanical Engineering
University of Illinois at Chicago
2039 ERF, 842 West Taylor Street
Chicago, Illinois 60607-7022
Phone: (312) 996-9612
E-Mail: SSCha@uic.edu

## Introduction

The structural perfection of crystal growth strongly depends on the influence of thermally-induced flows in the melt [1-3]. In both ground-based and space-based processing, these velocity fields need to be measured to identify their effects on the physical properties of processed materials. In spite of efforts to minimize fluid flow problems, their influence cannot be completely eliminated. Consequently, measurement of three-dimensional (3-D) three-component (3-C) velocity fields is very essential for optimizing apparatus design and process parameters. The experimental velocity characterization is also vital to validation and improvement of numerical process modeling.

Here, the proposed research is to characterize the 3-D 3-C velocity fields and other important solidification parameters in a Bridgman crystal growth configuration. In this effort, two unique experimental techniques for measuring 3-D 3-C fields will be developed. The developed techniques are then employed to observe the flow fields. In addition to the velocity measurements, other pertinent information will also be extracted from the experiments and then these will be compared with those from numerical modeling. The Bridgman configuration is one

of the most basic arrangements and its investigation is of great technological importance. The ultimate goal of this proposal is to expand the application to space-based experiments in the future through technique perfection and hardware miniaturization, not only for crystal growth but also for other allied areas. Measurements of 3-D 3-C velocity is a profound task in understanding fundamentals of all microgravity-related physics involving fluids [4].

## Research Description, Objectives, and Plan

One objective is to simultaneously develop two distinct experimental techniques for 3-D 3-C detection, that is, stereo-imaging velocimetry (SIV) [5,6] and holographic diffraction image velocimetry (HDIV) [7-10], closer to a state appropriate for microgravity experiments. The simultaneous development of the SIV and HDIV is desirable because of their complementary nature. It is believed that these complementary techniques together can eventually cover a broad range of space experiment requirements including complex or transient phenomena. The SIV based on CCD sensing as shown in Fig. 1 is advantageous in system simplicity for building compact hardware and in software efficiency for continual near-real-time velocity monitoring. However, it exhibits weaknesses insofar as it requires relatively low-population large-particle seeding, being based on frame-by-frame tracking of individual particles for velocity extraction, and limited detection resolution, utilizing solid-state imaging arrays. These cause limitations in data-point sampling rate, spatial resolution, and dynamic range. The HDIV approach as demonstrated in Fig. 2 does not have these limitations. It is effective at a high particle population due to its utilization of statistical correlation of diffraction image section patterns for velocity extraction. It also possesses excellent detection resolution due to its use of high quality holographic film for image recording. These characteristics contribute to a high data-point sampling rate, good spatial resolution, and wide dynamic range; however, the velocity extraction is rather involved and allows only post-experiment data processing. Above all, the holographic approach can be a very effective system regarding the detection of 3-D 3-C velocity from a single observation direction without specific particle focusing. It is not constrained by illumination direction. It can thus offer greater experimental freedom, including measurement within hard-to-reach regions.

Another objective is to conduct crystal growth experiments with a transparent Bridgman apparatus and a transparent liquid. The velocity fields in directional solidification and melting processes will be extracted with both the SIV and HDIV in addition to other processing information. In order to achieve our aims of evaluating the applicability of the developed techniques and obtaining the process information through experiments, the Bridgman crystal growth will be accomplished by establishing isothermal hot and cold zones with a minute tilt. This slight deviation from the hydrodynamic equilibrium between the zones can induce 3-D flow perturbation. The flow thus generated will be seeded with tracer particles and captured by the experimental techniques. Other important measurements to be made in addition to the flow field can be temperature by thermocouple thermometry, interface shape by photography, etc.

The third objective is to compare all the results from experiments as well as from computational modeling. In computer simulation of experiments, the experimental boundary conditions and other physical properties will be fed into the existing numerical codes. Two basic forms of detrimental segregation can result from the convection in the solute field in front of the interface: that is, end-to-end macrosegregation by a strong level of convection and radial segregation by a low level of mixing near the interface. Assessment of velocity effects on these phenomena will also be explored. The proposed cross-measurement and cross-evaluation of the velocity fields and other processing parameters is important for enhancing confidence in each experimental method and gaining information that is not possible by the other one. More importantly, the evaluation can allow further refinement of the experimental and numerical techniques for future applications.

The first year will be devoted to the prototype algorithm development for near-real-time velocity measurement by the SIV. During this period, the development of the prototype algorithms for velocity extraction of the HDIV is also pursued. In a parallel effort, a simple experiment will be conducted. Due to the time limitation, the experiment is restricted only to evaluating the initially developed systems and the new velocity-extraction algorithms.

## References


1. W. E. Langlois, "Buoyancy-Driven Flows in Crystal Growth Melts," Annual Review of Fluid Mechanics, Vol. 17, pp. 191-215, 1985.

2. M. E. Glicksman, S. R. Coriell, and G. B. McFadden, "Interaction of Flows with the Crystal-Melt Interface," Annual Review of Fluid Mechanics, Vol. 18, pp. 307-335, 1986.

3. D. H. Kim, P. M. Adornato, and R.A. Brown, "Effect of Vertical Magnetic Field on Convection and Segregation in Vertical Bridgman Crystal Growth," Journal of Crystal Growth, Vol. 89, pp. 339-356, 1988.

4. N. Ramachandran, D. O. Frazier, S. L. Lehoczky, and C. R. Baugher, "Joint Launch + One Year Science Review of MSML-1 and USMP-1 with the Microgravity Measurement Group," NASA Conference Publication 3272, 1994.

5. B.B. Miller, M.B. Meyer, and M.D. Bethea, "Stereo Imaging Velocimetry," International Symposium on Space Optics, Garmisch-Partenkirchen, FRG, Sponsored by EOS and SPIE, April 18-22, 1994.

6. M.B. Meyer and M.D. Bethea, "A Full Field 3-D Velocimeter for NASA's Microgravity Science Program," AIAA Paper 92-0784, 1992.

7. S.S. Cha, K.J. Huang, and J.S. Slepicka, "Double-Reference-Beam Off-Axis Holographic Particle Image Velocimetry," ASME Fluid Engineering Conference on Holographic Particle Image Velocimetry, Vol. 148, pp. 23-26, 1993.

8. K. Huang, J.S. Slepicka, and S.S. Cha, "Cross-Correlation of Three-Dimensional Images for Fluid Velocity Measurements," in SPIE Proceedings of Optical Diagnostics in Fluid and Thermal flow, Vol. 2005, pp. 655-666, 1993.

9. S.S. Cha, K.J. Huang, and J.S. Slepicka, "Holographic Technique for Three-Dimensional Three-Component Particle Fields," Optics Letters, Vol. 19, pp. 1577-1579, 1994.

10. S.S. Cha, "Holographic Diffraction Image Velocimetry for Three-Dimensional Three-Component Particle Fields or Solid Objects," Patent File Serial No. 08/261775, 1994.

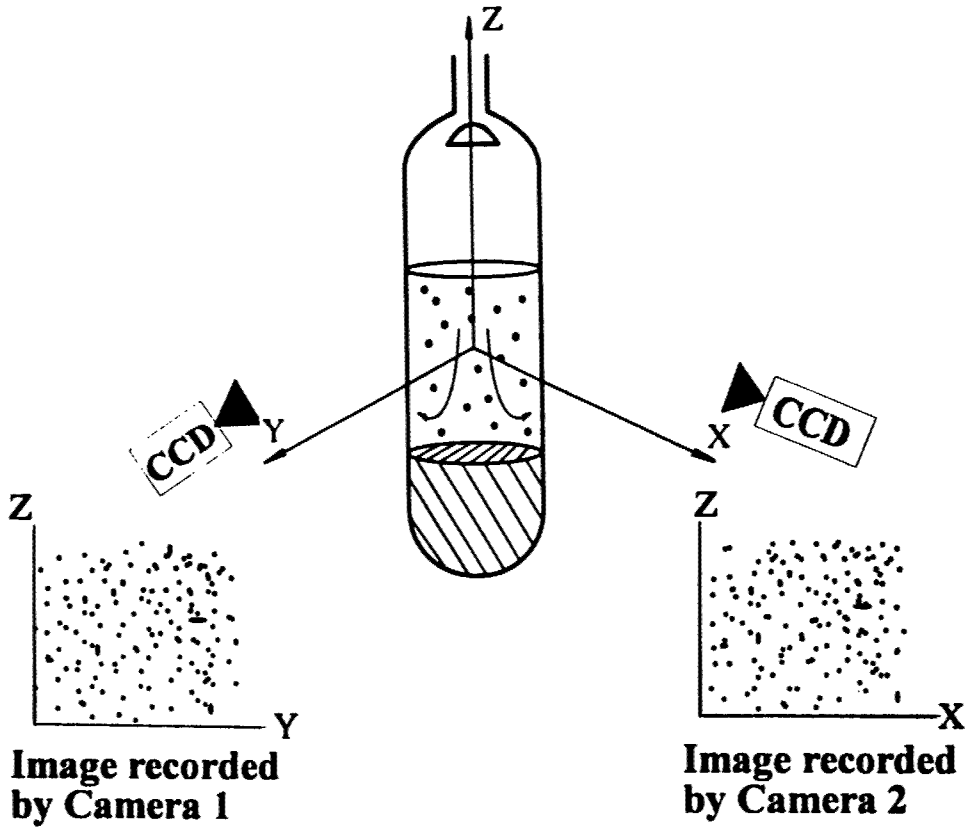


Figure 1. SIV setup

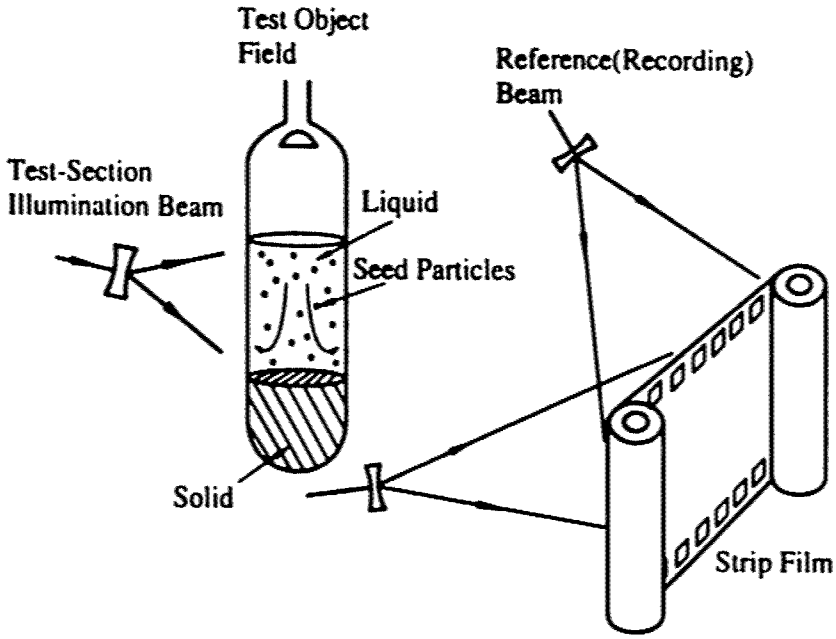


(a) Hologram recording of the HDIV system

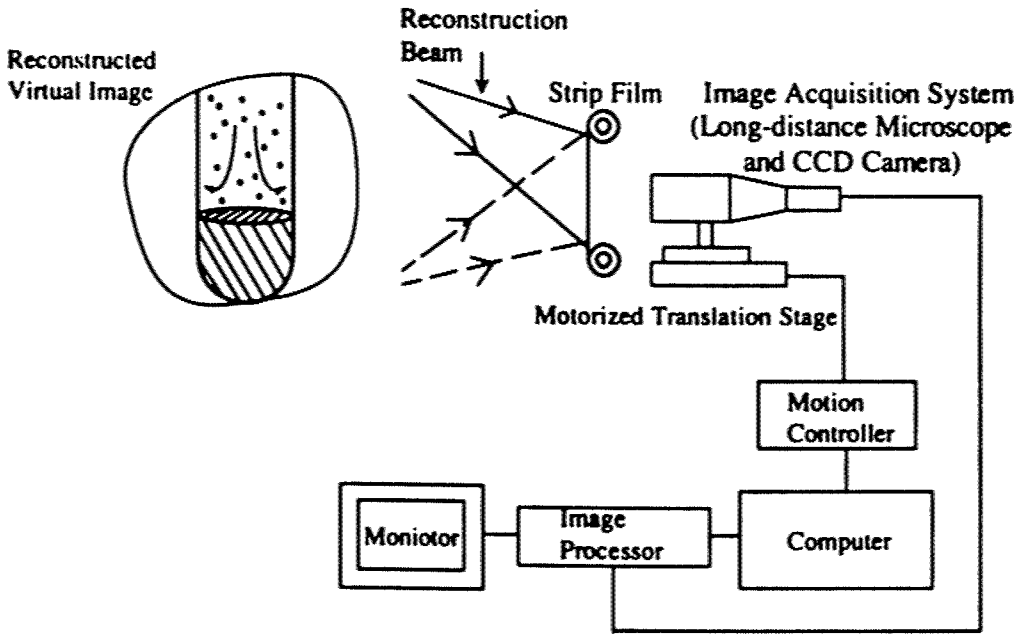


(b) Reconstruction/analysis of the HDIV system

Figure 2. HDIV setup

# MICROGRAVITY CHEMICAL VAPOR DEPOSITION

Principle Investigator: Ivan O. Clark, NASA Langley Research Center, Hampton, VA
Co-Investigators: William A. Jesser, Univ. of VA, Materials Sci & Eng., Charlottesville, VA;
Paul V. Hyer and Edward J. Johnson, Lockheed Martin, Hampton, VA

## OBJECTIVES

Commercial chemical vapor deposition (CVD) processes use reactors developed through decades of empirical trial and error. Better understanding of the complex physical and chemical processes underlying CVD and validation of emerging computational fluid dynamic codes are both needed so that future reactors can be designed and processing conditions optimized much more efficiently and effectively. This research seeks to develop this improved understanding of the CVD processes through experimental and numerical studies using gravitational effects as an investigative tool. An important part of the research effort is to determine key features of meaningful reduced-gravity experiments such as maximum acceptable acceleration levels, minimum experiment time, and critical experimental geometries and instrumentation.

## BACKGROUND

CVD is an important industrial process with applications in such diverse fields as semiconductors, optics, wear- and corrosion-resistance, and coating of fibers for composites. The nature and quality of the layers formed are dependent on mass and energy transport as well as homogeneous and heterogeneous chemical reactions and nucleation. In unigravity, scientific studies of the CVD process are hindered by the difficulty of separating the heat and mass transport due to externally forced convection from that due to the internal processes of buoyant thermal convection, buoyant solutal convection, and thermal (Soret) and solutal diffusion. The strong buoyant convection is a dominant effect in the heat and mass transport of CVD. In many cases, the velocity components due to buoyancy exceed those due to external forced convection [1]. Complications also arise from the forced convection due to volume changes caused by both chemical reactions and thermal effects. By conducting experiments in reduced gravity, this strong buoyant convection will be greatly reduced and other important heat and mass transport effects such as coupled thermal-solutal diffusion and deviations from the ideal-gas behavior will be resolvable. Better

understanding of these effects is essential in order to achieve desired improvements in perfection, uniformity, and size of grown layers and in order to provide an engineering design basis for CVD systems.

## APPROACH

Ground-based experiments and numerical investigations have provided both basic scientific information on the heat and mass transfer effects central to the CVD process and information necessary for defining specific, follow-on reduced-gravity investigations. A horizontal CVD reactor has been used for indium phosphide (InP) deposition by metalorganic chemical vapor deposition (MOCVD) from trimethylindium ($In(CH_3)_3$) and phosphine ($PH_3$) in hydrogen carrier gas. A replica of the growth reactor flow channel (Figure 1) has been used for flow and thermal field measurements. In the numerical efforts, finite volume techniques have been used to model flow and deposition for MOCVD of InP and CVD of silicon. Additional numerical efforts have focused on thermophoretic corrections for laser velocimetry data and on optimizing experiment geometries and operating parameters for flight experiments.

## SIGNIFICANT RESULTS

This research has produced results which have enhanced the current understanding of CVD while indicating areas in which further work is needed. The deposition rate of InP thin films has been measured and modeled across the width of the reactor and in regions upstream and downstream from the susceptor for a variety of flow and pressure conditions [2-4]. The deposition pattern of InP demonstrates the importance of modeling and measuring deposition upstream of the leading edge of the susceptor (Figure 2). The growth pattern in this region indicates at least two reaction paths for the deposition of InP on the substrate. These two reaction paths were modeled by assuming that the upstream peak was formed by a relatively low-temperature heterogeneous reaction while a relatively high-temperature, gas-phase reaction was necessary as an intermediate step in the formation of the second deposition maximum. The selection of the reaction scheme was described in detail by Black [3]. As an additional test of the numerical code, the deposition of silicon from silane ($SiH_4$) was also modeled.

The research has produced results relevant to the design of microgravity experiments. Work performed by this group and others [5] shows that, while highly symmetric flows might be expected from a vertical axisymmetric reactor, very slight deviations from an axial gravity vector can result in highly non-axisymmetric flows. By contrast, flow in a horizontal rectangular duct is relatively stable with respect to small directional changes in the gravitational vector within the vertical symmetry plane. The modeling effort has clearly demonstrated that using gas mixtures to simulate reduced gravity fails due to thermal diffusion effects. Initial indications are that steady experimental gravitational levels of less than $10^{-3}$g should be sufficient for meaningful reduced-gravity experiments. Flow measurement experiments and numerical modeling have shown the importance of careful inlet design for obtaining fully-developed flow without the occurrence of flow-separation or recirculation in the inlet nozzle. With a 10-degree entry cone, hydrogen ($H_2$) exhibits jet type flow as far as the susceptor while nitrogen ($N_2$) flows develop more rapidly. A blunt entry adaptor with radial inlet shows promise for more rapidly establishing fully developed flow.

This research effort has demonstrated the importance of full knowledge of the thermal boundary conditions for accurately modeling CVD. For this reason, infrared (IR) imaging has been used to provide temperature measurements of three walls of the MOCVD reactor flow channel in hydrogen and nitrogen flows. Figure 3 shows the replica flow channel from above configured with a pair of gold-surface mirrors for the simultaneous acquisition of thermal images of the top and side walls. Figure 4 shows the thermal images. The impact on the upper wall thermal field of the separated jet is clearly visible for the $H_2$ flow. This interpretation is confirmed by the LV measured flow field shown in Figure 5 where the $H_2$ jet is clearly visible in a vertical transverse plane approximately 6 cm upstream of the leading edge of the susceptor. These measurements have shown that the transport gas and flow field strongly influence the reactor wall temperatures. This result strongly suggests that IR imaging techniques can provide a valuable production line tool for CVD fabrication plants. By examining the external wall temperature of the reactor during thermal ramp-up, the affects of minor variations in assembly can be rapidly detected and corrected with resulting increase of production yield.

## REFERENCES


1 E.J. Johnson, P.V. Hyer, P.W. Culotta, and I.O. Clark: "Laser Velocimetry Measurements in Non-isothermal CVD Systems," Laser Anemometry: Advances and Applications, Vol. 2, 1991, eds., A. Dibbs and B. Ghorashi, ASME, pp. 483-489.

2 L.R. Black, I.O. Clark, J. Kui, and W.A. Jesser: "3-D Numerical Modeling of InP MOCVD with Comparison to Growth Experiments, Proceedings of Fluent Inc. 1992 Users' Group Meeting, October 13-15, 1992, Burlington, VT, p.377-384.

3 L.R. Black: Three-Dimensional Numerical Modeling of InP MOCVD with Experimental Verification, Ph.D. Dissertation, University of Virginia, Charlottesville, VA, 1993.

4 L.R. Black, E.J. Johnson, P..V. Hyer, P.W. Culotta, and I.O. Clark: "An Improved 3-D Numerical Model of InP MOCVD with Comparison to Growth and Laser Velocimetry Experiments," Proceedings of Fluent Inc. 1993 Users' Group Meeting, October 5-7, 1993, Burlington, VT, p. 93-102.

5 P. Bontoux, B. Roux, G.H. Schiroky, B.L. Markham, and F. Rosenberger: "Convection in the vertical midplane of a horizontal cylinder. Comparison of two-dimensional approximations with three-dimensional results," Int. J. Heat Mass Transfer, vol.29, no.2 (1986) p.227-240.


Figure 1. Horizontal chemical vapor deposition reactor: (a) photographic side view of replica reactor flow channel used for laser velocimetry showing the stainless steel entry cone, the fused-silica reactor, and the steel exhaust chamber; and (b) schematic of flow channel in the region of the susceptor. Thermal energy for chemical reaction is provided by rf-heating the graphite susceptor. Net flow is from left to right.

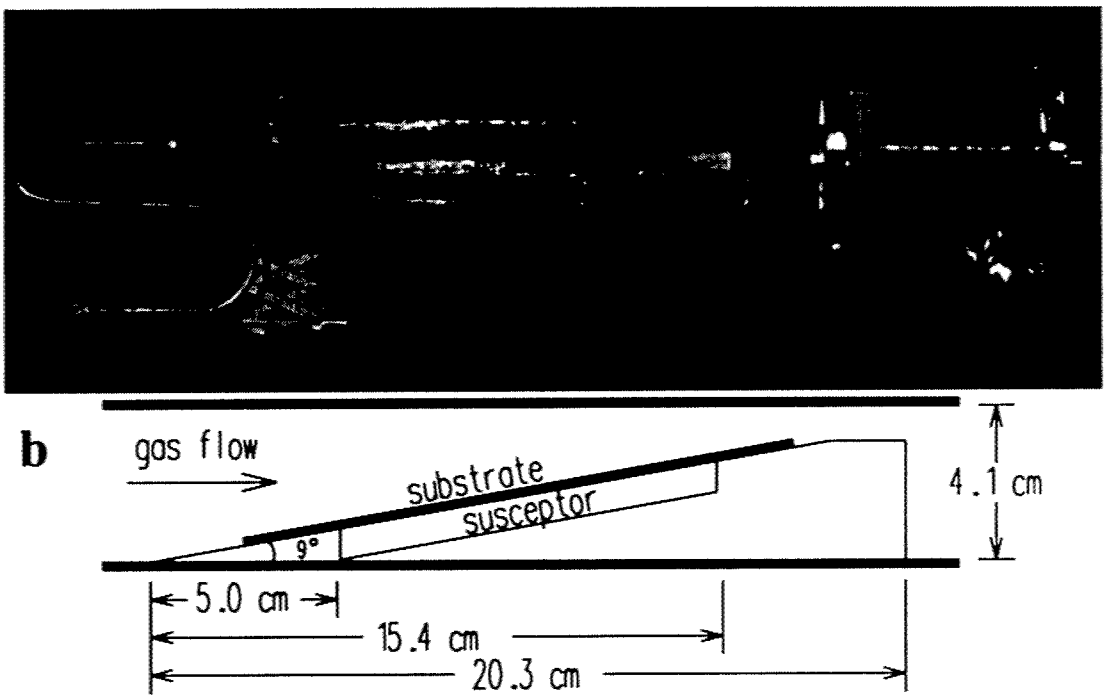

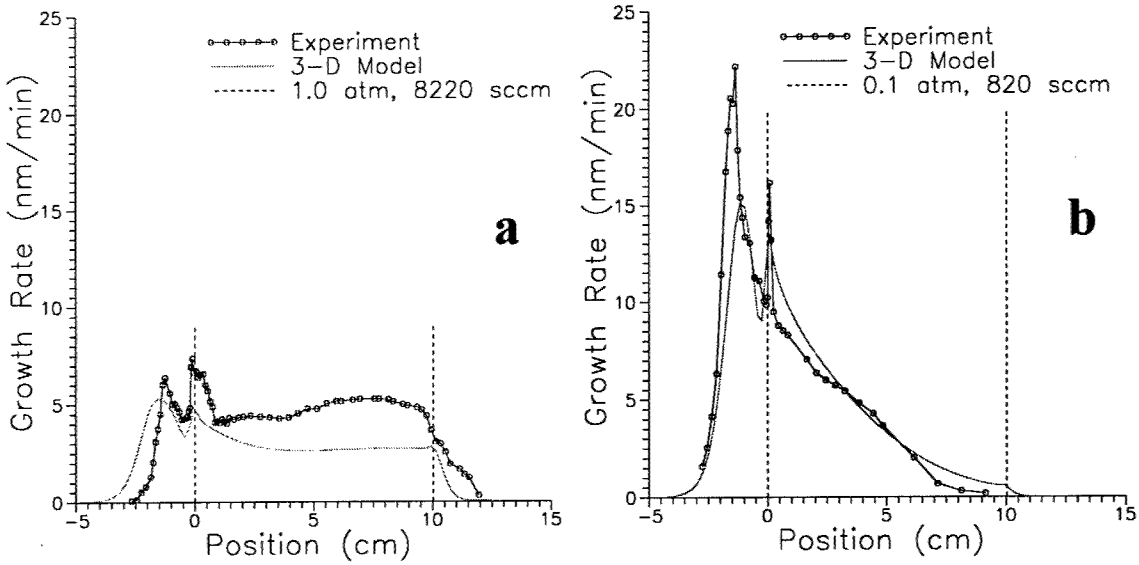


Figure 2. Comparison, along the centerline of the reactor, of the InP growth rate predicted by the 3-D numerical model with that determined by experiment. For both cases, the average axial velocity is 3.6 cm/sec and the carrier gas is hydrogen. The vertical lines show the leading and trailing edges of the susceptor with the origin at the leading edge. (a) deposition at 1.0 atm with total mass flow rate of 8220 sccm. (b) deposition at 0.1 atm with total mass flow rate of 820 sccm.

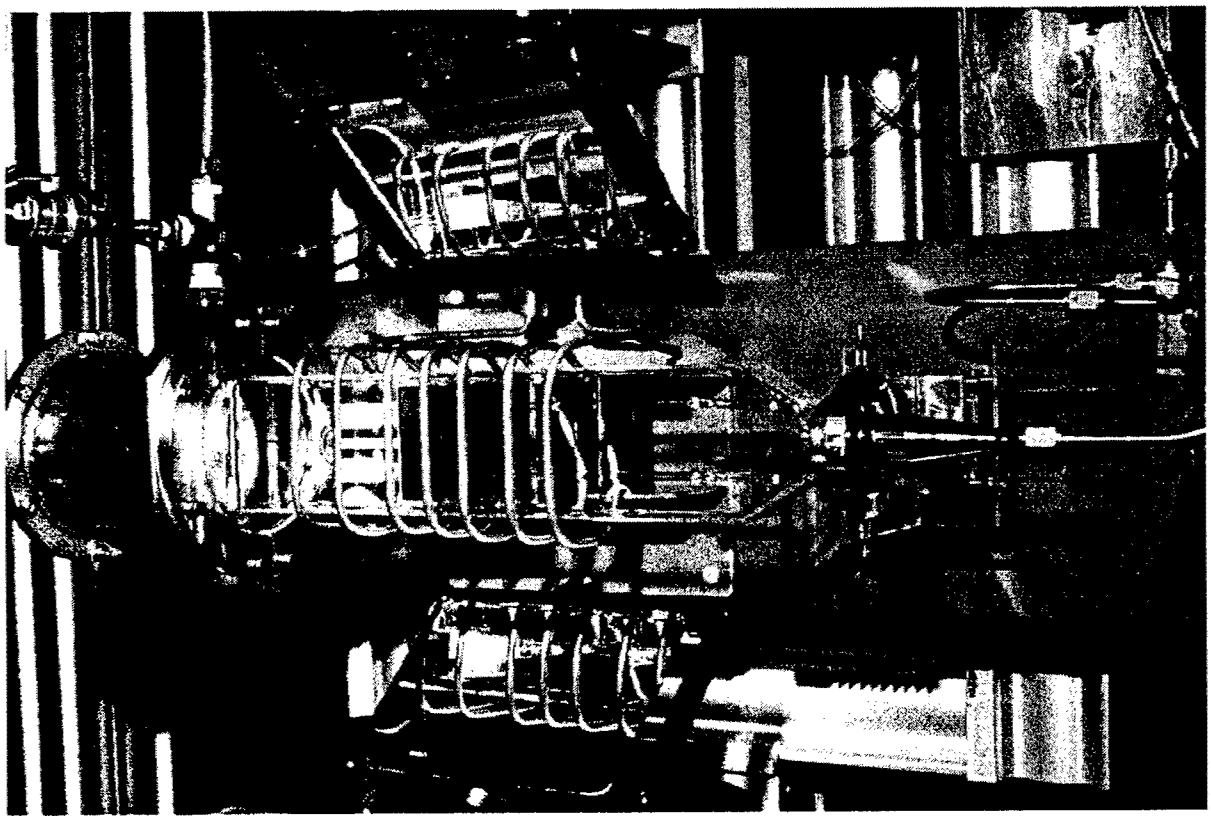

Figure 3. Visual photographic top view of replica horizontal reactor flow channel showing the stainless steel entry cone, the fused-silica reactor, and the steel exhaust chamber as in Figure 1a. The coil around the susceptor region of the reactor is the rf heating coil. Gold-surfaced mirrors have been added at approximately 45 degrees off-vertical to allow the simultaneous infrared photography of the reactor top and side walls. Net flow is from right to left of image. Orientation shown is rotated 90 degrees from Figure 4.

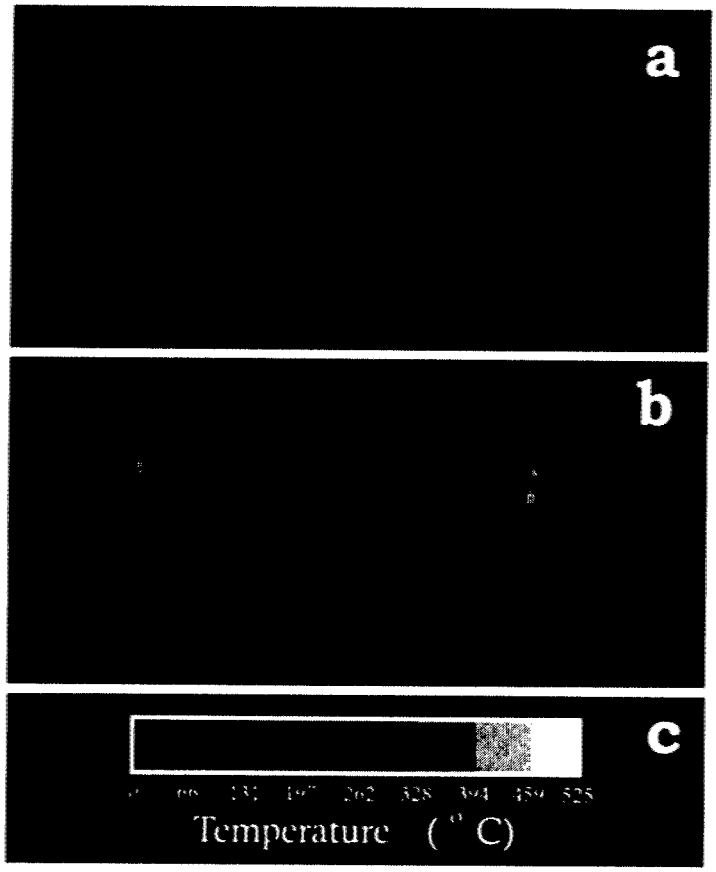


Figure 4. Infrared images of heated CVD reactor for 8000 sccm flow of: (a) nitrogen and (b) hydrogen. (c) is a common temperature scale. Horizontal lines across the images are caused by heating coils. Gas flow is from bottom to top in each image.

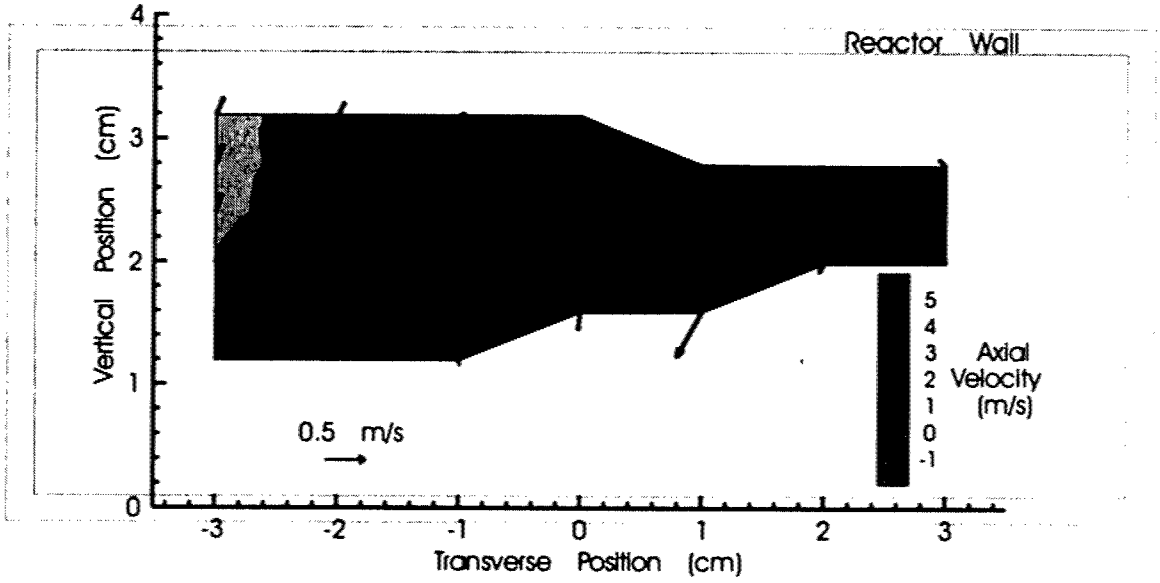


Figure 5. Contours in a vertical plane of the axial velocity component of the hydrogen transport gas. Positive axial velocities are in the direction of net velocity. Arrows represent in-plane velocity components.

# Title: "Fundamental Studies of Solidification in Microgravity using Real-Time X-Ray Microscopy"

Investigators: Peter A. Curreri, P.I.
William F. Kaukler, Co-P.I.
Subhayu Sen, Co-I
Biliyar N. Bhat, Co-I

Metal alloy and semiconductor crystal solidification experiments in microgravity to date have not been designed to provide detailed unambiguous information of the solute distribution in the liquid and the interfacial and phase morphologies, even though these experiments relied on a predicted diffusion limited solute profile along a planar solid-liquid interface to provide the experimental benefit from microgravity. If the experiment design gives direct, continuous, and unambiguous measurement of the fundamental independent variables, (including solute profile, interfacial morphology, phase nucleation and growth in the liquid, and phase incorporation into the solid) the microgravity results will be more consistent and provide a higher resolution test of theories.

## *Objectives of the Investigation:*

The objective of this research is obtain fundamental measurements of the dynamics of solidification in metallic or semiconducting materials with microstructural resolution. These data will be used to test the classical type boundary layer theories as applied to microgravity solidification. The data will also be applied to test coupled growth theories application to the normal and microgravity solidification of eutectics and monotectic alloys. Our method will be to utilize X-ray Transmission Microscopy (XTM) to provide direct measure of the solute profile in the liquid, phase coalescence and growth in the liquid, and the detailed interface morphology (e.g. dendrites and cells) during solidification of metal alloys and semiconductors in normal and eventually microgravity.

## *Relationship of the Investigation to Microgravity Research:*

Precise control over solidification processes is acquired by improvements in the theory. Experimentation to refine the mathematical models require precise knowledge of all pertinent parameters that define the model and to do so during the dynamic processes of heat and mass transport during solidification.

Low-gravity dampening of convective transport as a means to simplify experimental conditions has been pursued with some enthusiasm by the solidification science and technical community. However, the cost of microgravity experiments is very high. Progress in some of the most critical areas of solidification and crystal growth systems utilizing microgravity, has been limited due to a lack of precise knowledge of the fundamental solidification variables. This

necessitates, now more than ever, that space experiments be designed with the highest scientific yield.

Unambiguous testing of current alloy solidification models requires precise knowledge of the shape and extent of the solute boundary layer, real local growth rate, solid-liquid interfacial morphology, as well as formation of the different phases. Experiments that rely on post solidification microstructural and compositional analysis provide only an indirect assessment of these critical variables. A common interfacial marking technique, Peltier Pulsing, disturbs the solidification processes. Interface quenching gives data only at the time of interruption of the solidification process.

As part of the MSAD Advanced Technology Development program we have applied a state of the art sub-micron source, capable of 10 to 100 keV acceleration energies, to image by, XTM, the solidification of metallic or semiconductor alloys in real time with present resolutions of up to 30 μm, Fig. 1.

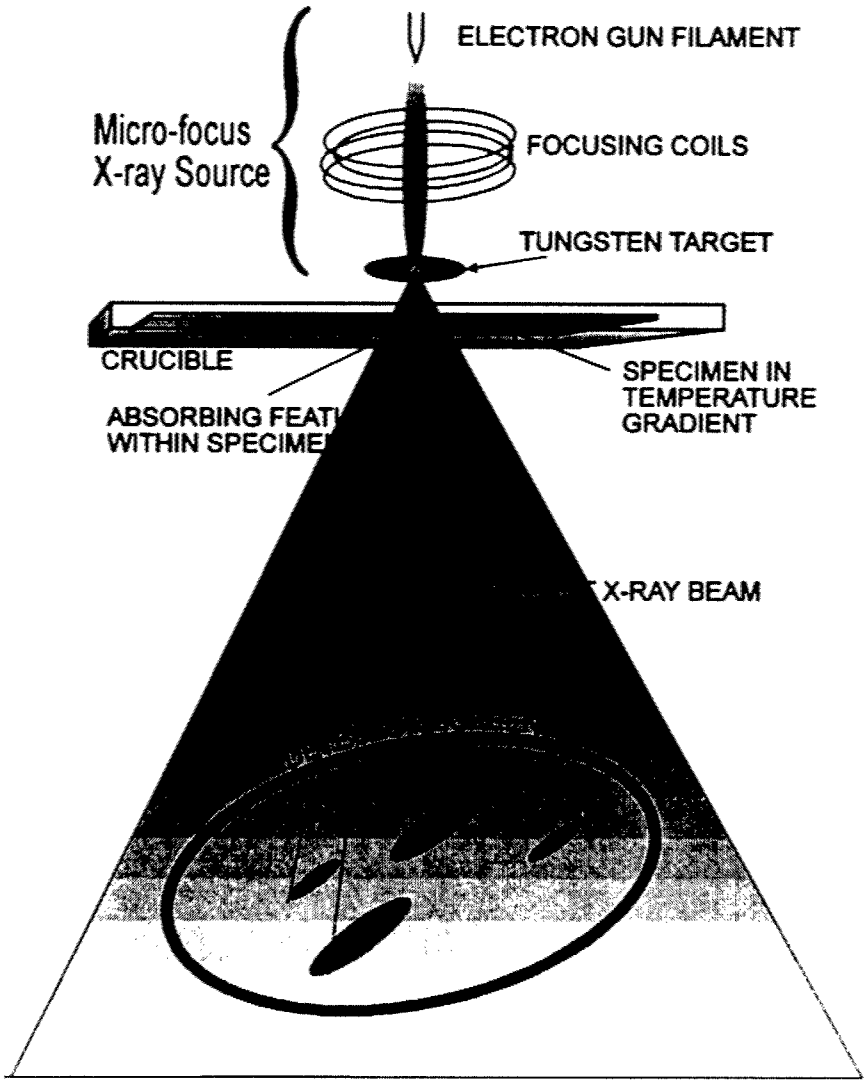


Figure 1. X-ray Transmission Microscope for solidification studies schematic diagram showing image projection from micro-focus source.

### *Capabilities of XTM Real-time Solidification Studies*

We have successfully imaged in real-time: interfacial morphologies, Fig. 2, nucleation, coalescence, incorporation of phases into the growing interface, and the solute boundary layer in the liquid at the solid-liquid interface, Fig. 3. We have also measured true local growth rates and can evaluate segregation structures in the solid. Unlike techniques that rely on lattice diffraction which cannot be used to image the solute profile or concentration, x-ray transmission (or shadow) microscopy relies on the differential adsorption of the x-ray beam to provide contrast and thus has potential to image concentration gradients in the solid and liquid.

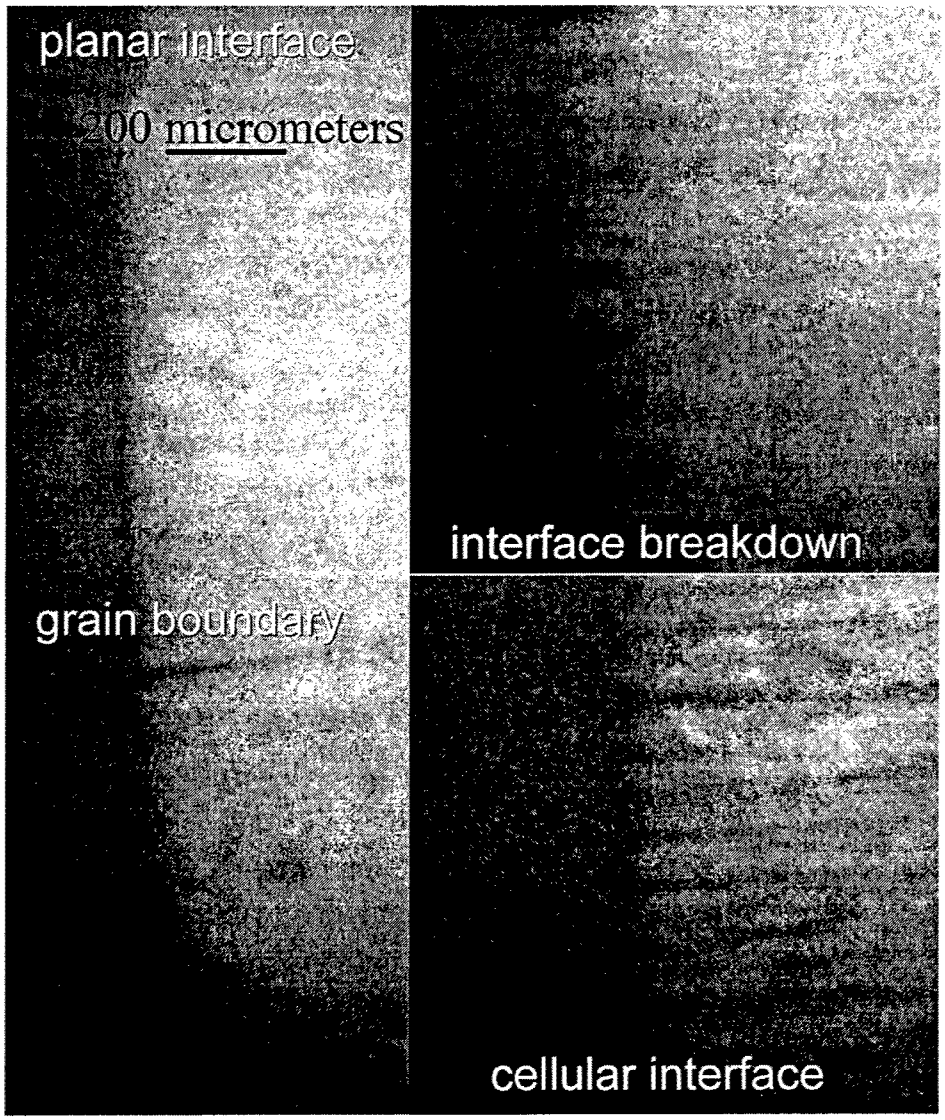


Figure 2. Al 2% Ag interfaces. Each are 2 second exposures at 55 kV acceleration and 200 μA current. Left figure shows planar interface growing at 1 μm/sec; grain boundaries intersect the interface isotherm. Upper right image captured the initial stages of cellular breakdown after the rate was increased to 2 μm/sec from 1.5 μm/sec. The lower right part shows the steady state cellular growth at 2 μm/sec.

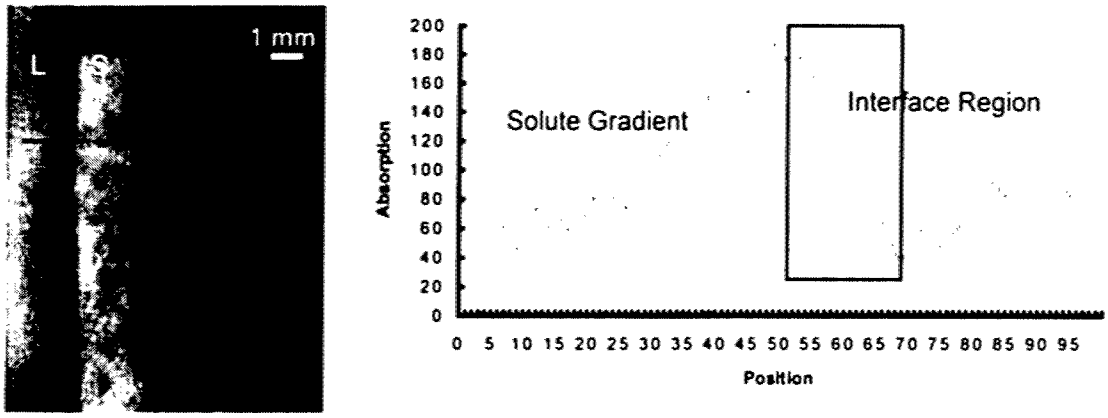


Figure 3. A) Al-18 In solid/liquid interface growing at 12.4 μm/sec in a 45 °C/cm temperature gradient showing solute rejection to the liquid after the step increase of translation rate. B) Optical intensity (absorption) profile along the line in A) crossing the solute layer and interface. Solute gradient is clearly seen on the left part of the graph. Increasing In content represents increased absorption. The diffuse interface region is in the marked area. Note the solute layer is not uniform along the length of the interface.

The ability to image these features in real time will enable more fundamental and detailed understanding of solidification dynamics in microgravity than had previously been possible, thus, allowing the full benefits of microgravity experiments be applied towards rigorous testing of critical solidification models.

A microfocus X-ray capability in Spacelab or Space Station would provide the opportunity for better fundamental data for a number of current discipline areas in microgravity materials science. Some examples are particle pushing in composites, semiconductor crystal growth and diffusion experiments. Our XTM experiments verified the feasibility of observing pushing/engulfment by the solidification interface of spherical 30-70 μm zirconia particles in 5 mm aluminum matrix in near real time. Important effects observable in real-time include solid-liquid interfacial curvature due to thermal conductivity difference between the melt and particles or voids, Fig. 4. Semiconductor crystal growth experiments under X-ray radiography have provided the first direct measurement of the extent and structure of the solute boundary layer. Growth conditions can be manipulated to maintain a planar interface during crystal growth by monitoring the process by XTM.

The XTM is also a valuable tool for post solidification metallography. The 3-dimensional distribution of solute and solidification features within the specimen volume can be viewed without sectioning or other treatment when the solute has sufficiently higher atomic mass than the solvent, Fig. 5. Thus the XTM could provide the first practical method for on orbit microstructural (metallographic) analysis by the astronauts or by telescience.

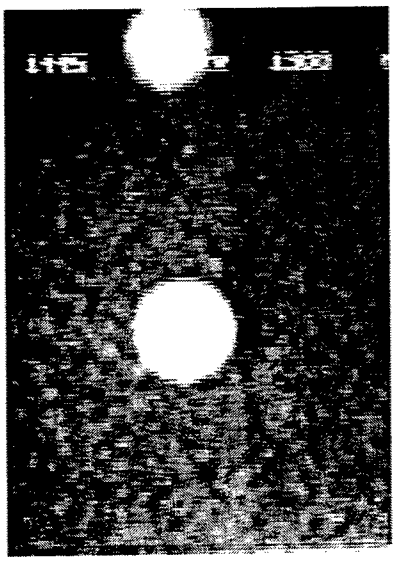

Fig. 4. A 250 μm and a 300 μm void in Al at a solid-liquid interface showing the local curvature caused by the low thermal conductivity of the voids. The interface is growing from right to left at 2 μm/sec in a 45 °C/cm temperature gradient.

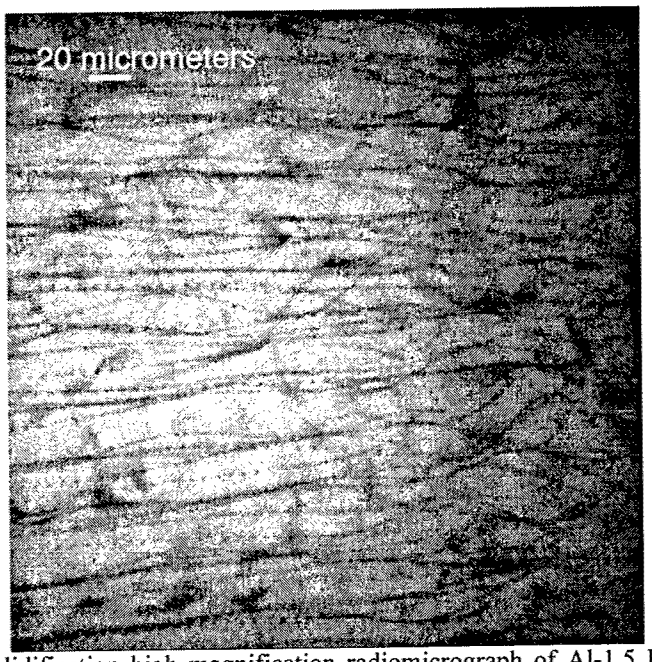


Figure 5. Post-solidification high magnification radiomicrograph of Al-1.5 Pb monotectic alloy showing fine fibers of Pb. This specimen was unidirectionally grown at 1 μm/sec in a temperature gradient of 45 °C/cm. The fibers can be seen to grow somewhat aligned on the left and meandering or twisting on the right due to some unknown phenomenon

We have examined flight ampoules with XTM to observe particle and thermocouple placement, crucible flaws and cracks in collaboration with the Particle Pushing and Engulfment flight experiment (Dr. Stefanescu, UA, P.I.). The value of an in flight XTM to guard against experiment failure and safety assurance is obvious.

### *Presentations and Publications*

Curreri, P.A., and W. Kaukler, "Real-Time X-Ray Transmission Microscopy of Solidifying Al-In Alloys," Metallurgical Transactions 27A 1996.

Curreri, P.A., and W. Kaukler, "Real-Time X-Ray Transmission Microscopy of Solidifying Al-In Alloys," presented at The Metallurgical and Materials Society Annual Meeting, Las Vegas, NV, Feb. 12-16, 1995) published in Proceedings of 7th International Symposium on Experimental Methods for Microgravity Materials Science, pg. 93-101, Robert Schiffman, Ed., The Minerals, Metals and Materials Society, 1995.

Curreri, P.A., and W. Kaukler, "X-Ray Transmission Microscopy Study of the Dynamics of Solid/Liquid Interfacial Breakdown During Metal Alloy Solidification," Presented at 8th International Symposium on Experimental Methods for Microgravity Materials Science, Feb 4-8, 1996, Anaheim, CA, 125 TMS Annual Meeting, to be published in proceedings.

Kaukler, W.K., and P.A. Curreri, "X-Ray Transmission Microscopy of Al-Pb Monotectic Alloys During Directional Solidification," ibid.

Kaukler, W. K. and P. A. Curreri, "Advancement of X-ray Microscopy Technology and it's Application to Metal Solidification Studies," to be presented at the 1996 SPIE Technical Conference in Space Processing of Materials, Aug. 4, 1996 and to be published as paper # 5 in Proceedings Vol. 2809.

Sen, S., W. Kaukler, P. Curreri, and D. M. Stefanescu, "Dynamics of Solid/Liquid Interface Shape Evolution Near an Insoluble Particle," in Preparation

# ADAPTIVE-GRID METHODS FOR PHASE FIELD MODELS OF MICROSTRUCTURE DEVELOPMENT

Jonathan A. Dantzig
Department of Mechanical and Industrial Engineering
University of Illinois at Urbana-Champaign
Phone: (217) 333-4107 E-mail: dantzig@uiuc.edu

Nigel Goldenfeld
Department of Physics
University of Illinois at Urbana-Champaign
Phone: (217) 333-8027 E-mail: nigel@uiuc.edu

## Introduction

Metallic microstructure is of great technological importance to American industry. For many years, materials scientists have studied and correlated the relationships between microstructures and mechanical properties. In particular, the size of microstructural features, such as grain diameter, interlamellar spacing in eutectics, *etc.*, have been correlated with mechanical properties.

Much work has also been done to relate processing conditions to the development of microstructural features. Some of this work dates back to the 1960's, where correlations were made between primary and secondary dendrite arm spacing and solidification parameters such as cooling rate and prevailing temperature gradients.[1,2] More recently, materials researchers have considered separately the phenomena which go into these correlations, including the roles of nucleation, growth, pattern selection, and crystalline anisotropy.

A first step to understanding the behavior of realistic microstructures is the problem of the growth of a single dendrite. Ivanstov[3] first produced a solution of the field equations for needle crystal growth into an undercooled melt. His solution has the curious property that only the product of the tip velocity and tip curvature is known, *i.e.*, thick dendrites growing slowly and thin dendrites growing rapidly are equally viable. This is contrary to experiment, however, where it is observed that a given set of processing conditions consistently produces dendrites of a particular size. This problem has been extensively studied both theoretically and experimentally in recent years. (See the review by Kessler, *et al.*[4]). Glicksman[5] has examined this problem in a series of elegant experiments, first on earth, and more recently in microgravity where isolated dendrites of transparent materials are grown into a liquid with known undercooling. Direct observation of the growth has provided detailed data for correlations of microstructural length scales with solidification processing conditions. These experiments provide a firm foundation for comparison with theory.

The complexity of the geometry in these structures has made theoretical predictions difficult, however. Several calculations of evolving dendrite shapes have been attempted. The goal of these calculations is to test the theory by comparing computed dendrite shapes and scaling laws with experimental observations. All of these calculations are done numerically, due to the geometric complexity. In some cases the interface shape is followed by front tracking, where the computational grid is locally deformed to the computed shape of the interface, and interfacial boundary conditions are applied explicitly. These methods have generally failed to produce realistic-looking dendrite

shapes because they require a mapping of the mesh to the deformed shape, and the evolving shapes are simply too complicated for this to work.

A very promising approach, called the "phase field model," was proposed by Langer,[6] and then implemented by Kobayashi,[7] Wheeler, *et al.*[8] and others.[9] In this model, the phase boundary is modeled as a diffuse interface whose limits are defined by values of the phase field parameter, $\phi \in [0, 1]$, where $\phi = 0$ represents the solid, $\phi = 1$ represents the liquid, and intermediate values correspond to the interface. Evolution equations, based on irreversible thermodynamics for the phase field can be developed,[10] and these evolution equations are coupled to the thermal (and solute) fields. These models are capable of producing very realistic looking dendrite shapes and are therefore quite promising. There are significant problems in the calculations, which we address in this proposal.

In order for the phase field calculations to be meaningful, the characteristic dimension of the computational grid must be significantly smaller than the interface thickness. However, one anticipates that the interface will traverse most of the domain during the calculation. Virtually all of the work in this area published to date employs a uniform mesh whose characteristic dimension is thus dictated by the thickness of the interface. For example, the work by Boettinger, *et al.*,[9] shows calculations of the evolution of dendrites in a dilute alloy. These calculations were performed on a grid of approximately 400,000 nodes, and the calculations consumed 72,000 CPU seconds on a CRAY Y-MP. Clearly, the computational requirements for these calculations precludes the systematic evaluation of parameter space needed to compare with experiments.

In the section which follows, we describe our ground-based research program to extend the phase field calculations into the more interesting part of parameter space. We believe that these calculations will give us great latitude to examine various theories of dendrite growth and understanding of pattern selection during solidification.

## Adaptive Meshing Techniques

We intend to examine pattern selection during phase transformations using adaptive meshing techniques. In these methods, we selectively refine a computational domain in the regions where higher precision is required, and leave the portions of the domain where relatively little variation occurs to be resolved on a coarser scale. These methods are ideally suited to this problem, where the large variations in the field variables are essentially confined to a very narrow region near the moving interface.

There are two key ideas in the application of adaptive mesh refinement. The first of these is a systematic means to determine where the mesh needs refinement through use of an estimator, and the second is the supporting data structure. We adopt for this work the error estimator developed by Zienkewicz and Zhu,[11] (Z&Z) and the quadtree data structure of Shephard.[12]

This error estimator has been used successfully to locate a solid-liquid interface and regions of high temperature gradients.[13] The estimator is based on predicting a smooth gradient field, and comparing it to the actual gradient field in the finite element solution. We adopt the Z&Z error estimator to identify regions in the mesh which require refinement, as well as regions where unrefinement may be performed.

An error estimator such as this one is particularly useful for locating a moving solidification interface, because there will always be a flux discontinuity arising from the Stefan condition,[14]

$$\mathbf{q}^{\text{solid}} - \mathbf{q}^{\text{liquid}} = \rho L_f \mathbf{v} \cdot \mathbf{n} \tag{1}$$

where $\mathbf{q}^{\text{solid}}$ and $\mathbf{q}^{\text{liquid}}$ represent the respective heat fluxes in the two phases at the interface, $\rho$ is the density, $L_f$ is the latent heat of fusion, $\mathbf{v}$ is the interface velocity and $\mathbf{n}$ is the normal vector to the interface.

The magnitude of the error estimator in each element is used as a measure of the element's candidacy for local refinement or The algorithms are referred to as *adaptive* because the mesh density is refined locally, based on the need for resolution. An element is marked for refinement when either (1) the error estimator in the element exceeds a specified tolerance, or (2) after refinement a neighbor element will have a difference in level of refinement exceeding one. These marked elements are then divided.

As an example, we consider the solidification of a dilute binary alloy in a square domain, with uniform initial temperature and concentration. In this problem, we wish to resolve both the interface motion and concentration boundary layer which develops ahead of the solidifying interface. This problem is modeled after an analysis by Crowley and Ockendon[15] who considered the one-dimensional solidification of such an alloy in a semi-infinite slab. Rubinstein[14] presented a similarity solution for this problem, where the interface temperature, $T_f$, and the interface compositions, $C_S^*$ and $C_L^*$, are all constant.

At time zero, the temperature of one corner is reduced below the solidus while the remainder of the boundary is insulated, and we follow the evolution of the temperature and concentration fields as the material solidifies. Although there is no analytical solution available for this case, we have assumed that the same interface conditions apply as in Rubinstein's solution, *i.e.*, that the interface temperature and concentrations are constant and as given in the similarity solution.

A sampling of the solution and meshes for the concentration problem is shown in Figure 1. It is interesting to note that all of the initial elements have been refined at least once in the concentration problem. We have confined our analysis to the initial stages of solidification, where the approximation to the similarity solution should be reasonable. These results clearly demonstrate the viability of this technique for tracking moving solidification interfaces.

## Cell Dynamic System Methods

Probably the most common way to explore phase transition kinetics is to solve directly the time-dependent Ginzburg-Landau (TDGL) equation. To solve the TDGL involves discretizing the PDE on a space-time lattice:

$$\Psi(\mathbf{x}, t) \rightarrow \Psi(\mathbf{n}\Delta x, i\Delta t) \equiv \Psi_{\mathbf{n}}^{i} \tag{2}$$

and using a time-stepping algorithm such as the explicit Euler scheme

$$\Psi_{\mathbf{n}}^{i+1} = \Psi_{\mathbf{n}}^{i} + \Delta t \left[ -\frac{\delta F}{\delta \Psi^*} \right]_{\mathbf{n}}^{i} \tag{3}$$

where $F$ is the free energy functional, $\Psi$ is the order parameter, $\mathbf{n}$ are a set of integers labeling the lattice sites, and $i$ labels the time step.

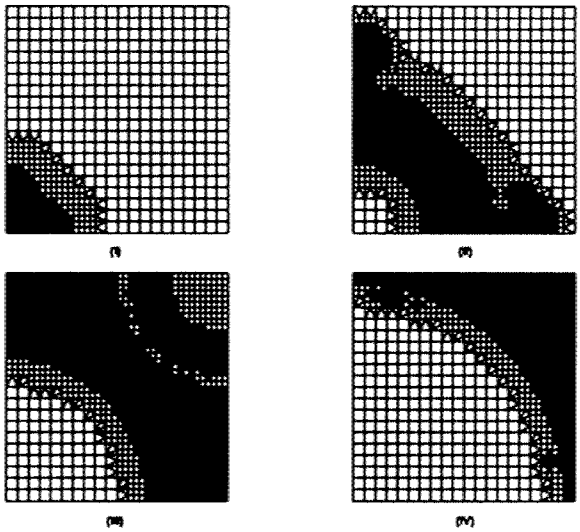

Figure 1: Sequence of meshes and interface locations for the 2-D concentration solution for solidification of a binary alloy from a corner. Note the unrefinement in the solid region, where the gradient is very small.

Of course, the continuum limit must eventually be taken: $\Delta x$, $\Delta t \to 0$, subject to possible stability criteria giving an upper bound to $\Delta t/\Delta x^2$. The disadvantage of this method is primarily that of speed and memory: to explore asymptotically large times, with a time step tending to zero requires many iterations of Eq. 3.

The cell dynamic system (CDS) method exploits universality in order to overcome this problem. The basic idea is to model the phenomenon directly by a set of coupled maps, defined on a coarse-grained space-time lattice, with spatial cells of dimension of order $2\pi\Lambda^{-1}$, where $\Lambda$ is the wave number to be resolved in the calculation.

As an illustrative example of the application of the CDS scheme to model ordering processes in materials science, consider Figure 2, which shows a complicated many-dendrite aggregate grown using a prototype CDS model for crystallization of a pure substance. The grey scale around the body of the crystal indicates the intensity of the heat field. The dynamic properties, morphologies and scaling laws of solidification were investigated using this simple model by Liu and Goldenfeld.[16] Other interesting applications of CDS models in materials science include studies of directional solidification[17] and eutectic growth.[18]

## Research Plan

Our goal is to use the adaptive meshing techniques described earlier to study phase transformations. The objective of this work is to study the evolution of microstructural patterns and scales in order to compare various theories to experimental observations. We plan to examine order-disorder transformations and dendritic growth. The former phenomenon will be studied using the CDS methods, while the latter will be approached using the phase field methods.

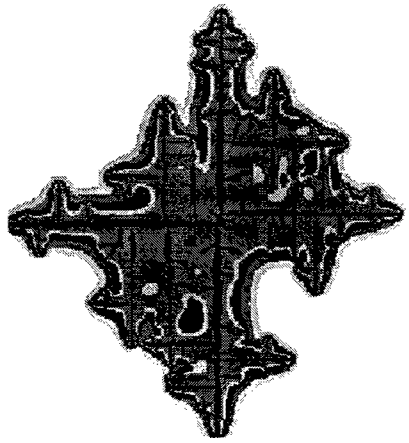

Figure 2: CDS simulation of crystal growth of a pure substance. The central part of the figure is the growing crystal, whereas the surrounding greyscale represents the temperature field.

As part of the research, we will devise a version of the existing finite-element adaptive grid code suitable for the CDS method. This will be done in two stages, first looking at the simpler case of the non-conserved order parameter equation (TDGL) discussed in the text above, and secondly implementing the mass conservation law with the Cahn-Hilliard equation. We will be particularly concerned with testing for mesh sensitivity and mesh anisotropy effects. To this end, we will calculate scattering form factors, characteristic length scaling and compare with existing numerical results. This exercise is crucial to the verification of the new methods we have proposed.

After developing and testing the codes, we will consider long-range forces, such as strain and hydrodynamic effects, which are known to be important in these structures. As stated before, our ultimate goal is to provide realistic predictions for real materials.

The application of the adaptive mesh refinement scheme for the study of dendritic growth will be carried out in several steps. First, we will recast the phase field equations in finite element form, in order that we may use the error estimator that we have developed. We will consider the resolution of the nonlinear equations using a Newton-Raphson algorithm to improve convergence. It is critical to the success of this work that the algorithms be tested and compared with analytical solutions and published data wherever possible. To that end, we will follow the course of Wheeler, *et al.*,[8] and consider several sample problems which are essentially one-dimensional. These include the growth of a sphere, as considered by Glicksman and Schaefer[19] and a plane. Moving up in complexity, we will investigate the growth of small sinusoidal disturbances on a plane and check that the stability spectrum is accurately reproduced. Finally, we will check our algorithm on non-trivial structures by looking at the problem of melting, rather than solidification. In this case, a planar interface is stable, and we shall attempt to follow the backwards and stable evolution of an Ivantsov parabola into a plane. These tests will give us confidence that the adaptive grid method is computationally efficient and does not introduce any artifactal instabilities into the problem.

During the course of this work, we will attempt to develop a transient form of the error estimator described in the previous section. We believe this is very important in order to reduce the computational cost and ensure accuracy. The present scheme, whereby the calculations are repeated for

each time slot, is not acceptable for the long term. Methods where we project the solution into the future, and base refinement on this projection are likely to be fruitful for these problems, where we have equations to describe the interface motion. We will then move on to consider two-dimensional problems, starting with a pure material growing into an undercooled melt. We will then proceed to consider the growth of alloys, that is adding the concentration field ahead of the solidifying interface.

## References


[1] R. E. Spear and G. R. Gardner. *Trans. AFS*, 71:209, 1963.

[2] M. C. Flemings, D. R. Poirier, R. V. Barone, and H. D. Brody. *J. Iron Steel Inst.*, 208:371, 1970.

[3] G. P. Ivantsov. *Dokladie Akadamie Nauk SSSR*, 58:567, 1948.

[4] D.A. Kessler, J. Koplik, and H. Levine. Pattern selection in fingered growth phenomena. *Advances in Physics*, 37:255, 1988.

[5] M. E. Glicksman, R. J. Schaefer, and J. D. Ayers. *Metallurgical Transactions*, 7A:1747, 1976.

[6] J.S. Langer. *Directions in Condensed Matter Physics*. World Scientific, 1986.

[7] S. Kobayishi. *J. Crystal Growth*, 88:87, 1988.

[8] A. A. Wheeler, B. T. Murray, and R. J. Schaefer. Computation of denrites using a phase field model. *Physica D*, pages 243-262, 1993.

[9] J. A. Warren and W. J. Boettinger. Prediction of dendritic growth and microsegregation patterns in a binary alloy using the phase-field method. *Acta Metallurgica*, in press.

[10] S.-L. Wang, R. F. Sekerka, A. A. Wheeler, B. T. Murray, S. R. Coriell, R. J. Braun, and G. B. McFadden. Thermodynamically consistent phase-field models for solidification. *Physica D*, pages 189–200, 1993.

[11] O.C. Zienkiewicz and J.Z. Zhu. Adaptivity and mesh generation. *Int. J. Numer. Meth. Eng.*, 32:783–810, 1991.

[12] M.S. Shephard, P.L. Baehmann, and K.R. Grice. The versatility of automatic mesh generators based on tree structures and advanced geometric constructs. *Comm. App. Num. Meth.*, 4:379–392, 1988.

[13] R. L. Lewis, H. C. Huang, A. S. Usmani, and J. T. Cross. Finite element analysis of heat transfer and flow problems using adaptive remeshing including application to solidification problems. *Int. J. Numer. Meth. Eng.*, 32:767–781, 1991.

[14] L. I. Rubinstein. *The Stefan Problem, Chapter I*. Translations of Mathematical Monographs. American Mathematical Society, 1971.

[15] A. B. Crowley and J. R. Ockendon. On the numerical solution of an alloy solidification problem. *Int. J. Heat Mass Transfer*, 22:941–947, 1979.

[16] F. Liu and N. Goldenfeld. *Phys. Rev. A*, 42:895, 1990.

[17] M. Grant B. Grossman, K. Elder and M. Kosterlitz. *Phys. Rev. Lett.*, 71:3323, 1993.

[18] J.M. Kosterlitz K.R. Elder, F. Drolet and M. Grant. *Phys. Rev. Lett.*, 72:677, 1994.

[19] R. J. Schaefer and M. E. Glicksman. *J. Crystal Growth*, 5:44, 1969.

# ATOMISTIC SIMULATIONS OF CADMIUM TELLURIDE: TOWARD UNDERSTANDING THE BENEFITS OF MICROGRAVITY CRYSTAL GROWTH

J.J. Derby and J.R. Chelikowsky
Department of Chemical Engineering and Materials Science
151 Amundson Hall
421 Washington Avenue, S.E.
University of Minnesota
Minneapolis, MN 55455-0132
Tel.: (612) 625-1313
Fax: (612) 626-7246
E-Mail: derby@maroon.tc.umn.edu, jrc@msi.umn.edu

## Introduction and objectives

Progress in crystal growth on earth or in space will depend on a more fundamental understanding of the important coupling between atomistic-scale processes which control the properties of grown crystalline material and the macroscopic transport conditions imposed by the growth system. Our long-term goal is to understand the mechanisms which influence crystal quality through the hierarchy of length and time scales relevant to these atomistic-scale and macro-scale processes. The immediate goal of the research summarized here is to employ atomistic simulation to understand better the melt growth of cadmium telluride (CdTe) and its alloy cadmium zinc telluride (CdZnTe). These materials are employed in a variety of technologically important electronic and electro-optical devices; however, the growth of high-quality, large-area single crystal substrate has proven to be extremely difficult under terrestrial conditions. We seek to obtain a more fundamental understanding of the properties of cadmium telluride so that the physical mechanisms responsible for growth can be elucidated. A secondary objective of our work is the prediction of high-temperature thermophysical properties of liquid and solid CdTe.

## Relationship to microgravity research

Recent growth experiments of $Cd_{0.96}Zn_{0.04}Te$ in a microgravity environment aboard USML-1 resulted in material which was far superior in structural perfection compared to earth-grown material under similar conditions. These dramatic results were attributed to the elimination of hydrostatic pressure from the melt column overlaying the crystal due to microgravity conditions, thereby reducing the hoop stresses that occur in a crystal as it grows and cools. In addition, it was speculated that the near absence of hydrostatic pressure allowed for the melt to solidify with minimal wall contact, thereby eliminating deleterious wall interactions. We will utilize atomistic simulation to understand the dynamics of the liquid/solid interface and of the solid material under the stress conditions corresponding to micro-gravity and terrestrial conditions. The work to be performed in this project will support current microgravity research on the melt growth of CdTe compounds and will provide for a quantitative, unambiguous method to understand the subtle effects of microgravity in these systems.

The primary thrust of this work will be to clarify the role of microgravity in interpreting the USML-1 results described above; however, this work promises to support future microgravity research in other substantial ways. Atomistic simulations will provide predictions of the high-temperature thermophysical properties of CdTe and its alloys. Accurate high-temperature properties are needed for reliable materials processing models, but such data are extremely difficult to obtain from experimental measurements (many of which have been undertaken in microgravity

environments). The prediction of these properties using atomistic simulation clearly complements ongoing and future microgravity process modeling and experimental property measurement efforts. Another likely benefit from this work is that a more complete understanding of the structure of molten CdTe and alloys will aid the development of seeding procedures for melt growth. For earth-based processes, reliable seeding techniques have not yet been developed for these materials, yet such procedures have been identified as one of the most needed process improvement to increase yields. Undoubtedly, as further microgravity experiments on the melt growth of CdZnTe are performed, seeded growth experiments will be desired and the knowledge obtained from atomistic simulations will be invaluable.

## Methodology

For the studies described here, we will employ new *ab initio* pseudopotential codes for molecular dynamical simulations using quantum forces developed by Chelikowsky and co-workers. This technique has several advantages over traditional plane wave approaches. This scheme eliminates the fictitious electronic coordinates and finds a self-consistent solution at each time step in the molecular dynamics simulation. By constraining the evolution of the system to the Born-Oppenheimer surface, we may lengthen the time-step involved. Often the molecular dynamics time step can be increased by an order of magnitude or more. This compensates for the time increase from obtaining a self-consistent solution at each step. If one couples this with a Langevin molecular dynamics procedure, then the time step may be increased further as this type of dynamics does not require energy conservation at each step. Another advantage is that this procedure allows one to consider simulations in which the cell volume and shape change in a physical way with temperature and pressure. Since the system is constrained to reside on the Born-Oppenheimer surface, the interatomic forces are "true" forces. Also, insulating systems can be handled as well as metallic, or charged systems. We have successfully applied these techniques to liquid silicon and germanium, and current work is being carried out on liquid gallium arsenide and gallium phosphide. We foresee no problems in extending this work to CdTe.

## Specific plans

Initial studies will focus on complexes within the liquid state and their effect on physical properties, melt undercooling, and nucleation phenomena. The propensity for the formation of tellurium complexes in the melt will be a major focus, since this behavior would also be expected to be important in explaining tellurium inclusions in the solid. The generation and propagation of defects in solid CdTe will also be studied and related to the USML-1 growth experiments. In addition, the validity of the cadmium vacancy condensation scenario to produce tellurium precipitates in the solid upon cooling will be assessed. The diffusion of various species, such as Cd interstitials and Zn, through the CdTe lattice will be studied.

Of particular interest is the study of solidification of CdTe. The generation of crystalline defects at the liquid/solid interface and from interactions between the interface and container walls are understood only on empirically. Emphasis will be placed on clarifying these phenomena during the solidification of CdTe. The mechanisms promoting tellurium inclusion capture and twinning will be pursued. Finally, the thermophysical properties of molten and solid CdTe will be predicted for conditions appropriate to melt growth. Especially important are predictions of high-temperature thermal conductivities, melt viscosity, diffusion coefficients, thermodynamic moduli, vapor pressures, and temperature-dependent melt surface tension.

# COMBINED SYNCHROTRON WHITE BEAM X-RAY TOPOGRAPHY AND HIGH RESOLUTION TRIPLE AXIS X-RAY DIFFRACTION CHARACTERIZATION AND ANALYSIS OF CRYSTALS GROWN IN MICROGRAVITY AND GROUND-BASED ENVIRONMENTS

M. Dudley (P.I.),
Dept. of Materials Science & Engineering,
SUNY at Stony Brook, Stony Brook NY 11794-2275
(516)-632-8500; FAX (516)-632-8052; e-mail: mdudley@ccmail.sunysb.edu

R.J. Matyi (Co-I.),
Dept. of Materials Science & Engineering,
University of Wisconsin-Madison, 1500 Engineering Drive, Madison WI 53706
(608)-263-1716; FAX (608)-262-8353; e-mail: matyi@engr.wisc.edu

## Research Objectives and relevance to Microgravity

Among the most important issues in any bulk crystal growth process is the reduction of the density of grown-in structural defects and the understanding of the relation between crystal growth and defect generation. The quantitative analysis of defects in semiconductor single crystals is typically complicated by the difficulty in separating the effects from various structural defects. Typically, semiconductor crystals contain a variety of defects; the effects of these structural defects are usually convolved together, making it difficult to quantitatively assess the concentrations of a specific defect type in a particular sample or to unambiguously relate a given defect to the crystal growth conditions.

The objective of the research proposed here is to carry out detailed studies of defect and general distortion distributions in crystals grown in both microgravity and ground based environments

(e.g. using modified Bridgman or Vapor Transport techniques) using a combination of synchrotron white beam X-ray topography (SWBXT)[1] and high resolution triple crystal X-ray diffractometry (HRTXD).[2] This unique combination of techniques is expected to reveal detailed differences between crystals grown in these two different environments and to enable meaningful assessment to be made of the influence of a microgravity environment on various aspects of the quality of crystals grown therein. SWBXT and HRTXD are complementary analytical techniques which are most sensitive and useful at contrasting ends of the "scale" of defect densities in crystals. By applying both techniques to the same crystals, it will be possible to provide detailed and quantitative assessments of the defect structure from regions that range from highly perfect (where SWBXT is expected to be the superior characterization tool) to highly imperfect (where HRTXD should be the superior method). This unified and continuous view of the defect structure should lead to valuable insights into the effect of growth conditions on the defect generation process. The proposed research program will draw upon the extensive experience that has been gained at the State University of New York - Stony Brook and University of Wisconsin - Madison in the analysis of defects in semiconductors using advanced methods of X-ray diffraction. Prof. Michael Dudley of SUNY - Stony Brook has worked closely with the crystal growth community at NASA's Marshall Space Flight Center (MSFC) in applying methods of SWBXT to numerous semiconductor crystals grown both on earth and in microgravity. His counterpart, Prof. Richard Matyi of UW - Madison, has been actively engaged in demonstrating the capabilities of HRTXD to a variety of semiconductor materials. By combining these complementary techniques it should be possible to obtain a deeper understanding of the process of defect generation than would be possible with either technique alone, or perhaps by any structural probe.

The significance of the research described here is that it will directly determine the influence of a microgravity environment on the detailed defect and distortion distribution in crystals produced in flight experiments, and will enable direct comparison to be drawn with crystals produced in ground based experiments. Confirmation will be obtained that effects resulting from the limited flight times available for microgravity crystal growth experiments do not exert control over the microstructure of the crystals grown, potentially detracting from the intended assessment of the influence of the magnitude of the gravity vector on these processes. Determination of the

influence of cooling rate on the defect microstructure of crystals is crucial for selection of experimental conditions under which the effects of the gravity vector on crystal growth quality can be usefully investigated. Once such selection has been optimized, differences in microstructure observed in microgravity grown crystals may be safely attributed to the influence of the gravity vector and not to artifacts related to compressed growth schedules.

## Significant Results to Date and Future Plans

To date, three materials have been studied independently using SWBXT and HRTXD, as funded programs commenced under NRA-93-OSSA-12: CdZnTe, ZnTe and ZnSe. Preliminary comparison of results obtained by these two techniques reveals good agreement.

For example in the case of CdZnTe, SWBXT revealed that the defect structure was very much dependent on the local cooling rate, with the best quality regions being obtained at the slowest cooling rates.[3] The best quality regions were revealed to have dislocation densities less than $10^3$ $cm^{-2}$, with no subgrain structure observable, and with a few Te precipitates observed. An example of a topograph recorded from a CdZnTe crystal, grown by Dr. D.J. Larson, Jr., aboard USML1, is shown in figure 1(a). Figure 1(b) illustrates the diffracted intensity about the 333 reciprocal lattice point from a similar CdZnTe wafer to the one shown in Figure 1(a). The Figure represents a "map" of the distribution of the diffracted intensity in reciprocal space. The data in the Figure is plotted as contours of equal intensity; the minimum contour corresponds to a diffracted intensity of $10^{-0.25}$ counts/second, with the remaining contours being plotted in increments of $10^{0.25}$ counts/sec (*i.e.* four contours per decade). Fig. 1(b) shows a well-defined crystal truncation rod, or surface streak, which extends perpendicular to the surface. This feature, which arises from the fact that the crystal surface truncates the bulk lattice, contains the dynamically diffracted intensity from the bulk crystal. The presence of a well-defined surface streak is indicative of two qualities of the diffracting crystal: (1) the bulk crystal has sufficient structural perfection in order to diffract dynamically, and (2) the crystal surface is of high enough quality to produce the surface streak at all. It should be noted, however, that the surface streak in this sample is less intense than is

typically seen in samples of highly perfect Ge or GaAs; this degradation is likely to be due to the grown-in dislocation density in this sample. This interpretation is supported by the diffuse intensity located off the surface streak in the vicinity of the 333 reciprocal lattice point. The roughly symmetric distribution of diffuse intensity about the 333 point is indicative of a relatively isotropic distribution of dislocations in the diffracting volume.

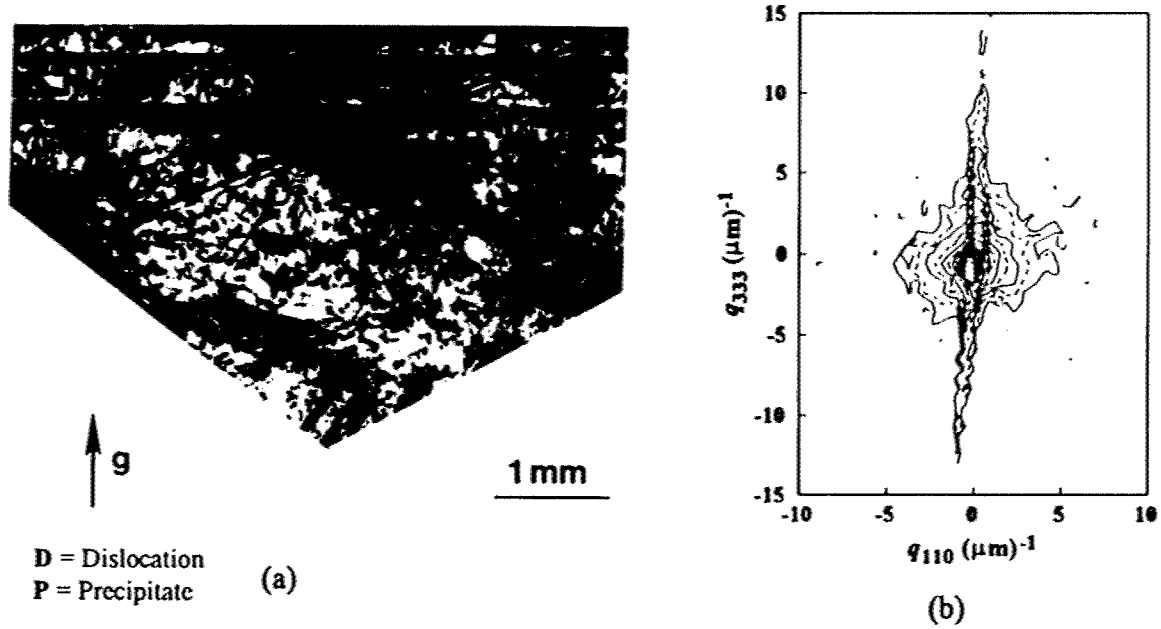


Figure 1.(a) SWBXT image recorded from microgravity grown CdZnTe; (b) triple crystal diffraction scan about the 333 reciprocal lattice point of an adjacent slice in the same boule.

Similarly, in ZnTe SWBXT reveals a well defined cellular structure of dislocations with subgrain diameters in the range of 300μm and relative tilts of the order of 5-10 seconds of arc.[4] An example of a topograph recorded from a ground based ZnTe sample, grown by Drs. C.-H. Su and D.C. Gillies at MSFC, revealing such a microstructure is shown in figure 2 (a). Figure 2(b) shows a 111 reciprocal space map of the same sample, which reveals multiple surface streaks; behavior which is characteristic of a sample with large mosaic blocks that are relatively perfect (low in dislocation density) but with a high degree of misorientation with respect to each other. HRTXD results are thus in agreement with SWBXT results.

In ZnSe, a much more even distribution of dislocations was revealed by SWBXT, with no cellular structure being discernible. An example of a topograph recorded from a ground based ZnSe

crystal, grown by Dr. C.-H. Su, revealing this microstructure is shown in figure 3 (a). Fig. 3(b) is a 220 reciprocal space map from a similar ZnSe sample. The absence of any surface streak and both the intensity and the angular extent of the diffuse intensity indicates a highly defective surface region in this sample. This interpretation agrees with SWBXT observations as illustrated in figure 3(a), again supporting our belief in the complementary nature of the two characterization techniques. It should be noted that HRTXD carried out on a ZnSe sample with a cleaved (rather than a polished) (110) surface showed a well-defined surface streak and a large amount of diffuse scatter that was distributed perpendicular to the [110] surface normal direction indicative of a high dislocation density. However, the uniformity of the diffuse intensity suggested that the dislocations are randomly distributed throughout the crystal and not concentrated into subgrain boundaries. This seems to indicate that polishing damage can obscure the true as-grown microstructure in ZnSe.

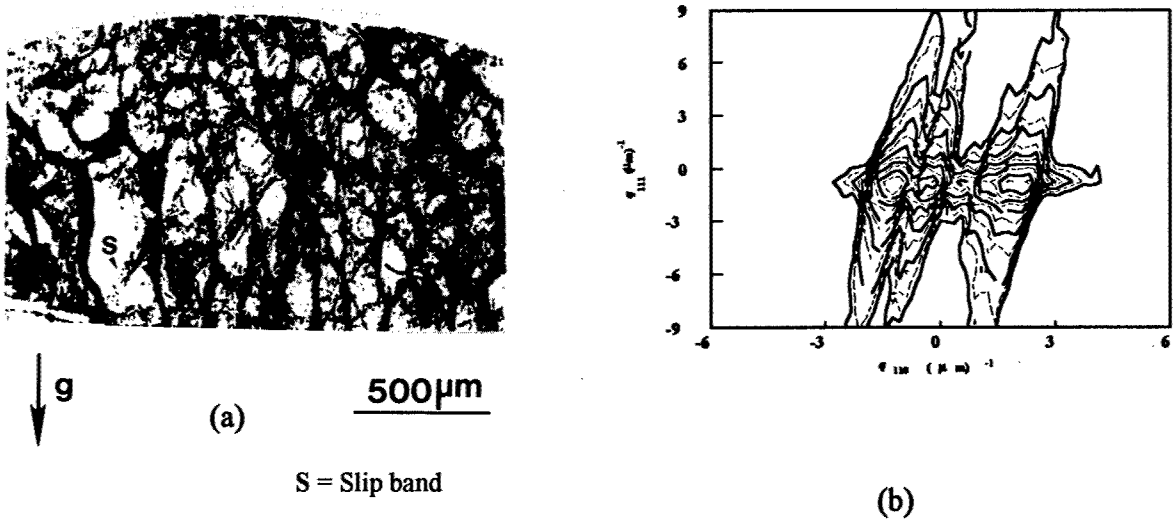


Figure 2. (a) SWBXT image recorded from ground-based ZnTe; (b) triple crystal diffraction scan about the 111 reciprocal lattice point of a similar sample. See text for details.

In future work, a complete description will be sought of the type and distribution of all defects present in the crystals to be examined. Crystals will initially be examined in boule form using both SWBXT and HRTXD in reflection geometry in order to reveal the overall distribution of defects and distortion around the cylindrical surface of the crystal. This will help determine the optimal wafering geometry to be adopted for the next stage of the research. Once the boules have been suitably wafered, SWBXT and HRTXD will be used, in sequence, to examine the defect and

distortion distributions in each of the wafers. Information so gathered will then be compiled to reconstruct to complete three dimensional defect and distortion distributions in the as-grown boule. This reconstructed information can then be used to compare with the predictions of growth models. A preliminary attempt at the latter has already been published.[5]

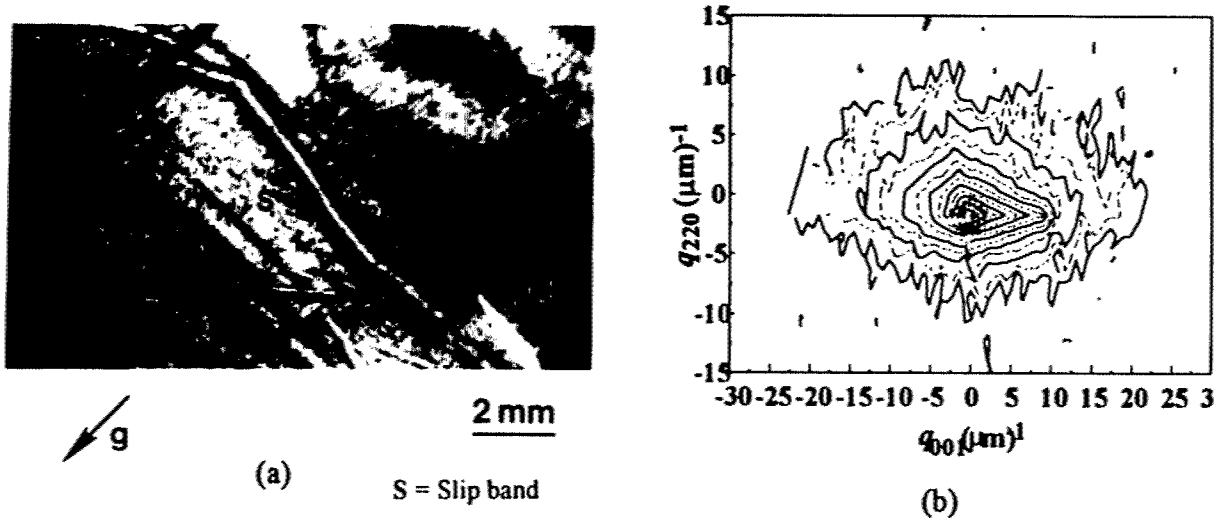


Figure 3 (a) SWBXT image recorded from ground-based ZnSe; (b) Triple crystal diffraction scan about the 220 reciprocal lattice point of a similar crystal.


1. M. Dudley, in "Applications of Synchrotron Radiation Techniques to Materials Science", D.L. Perry, R. Stockbauer, N. Shinn, K. D'Amico, and L. Terminello (Eds.) **Mat. Res.Soc. Symp. Proc., 307**, 213-224, (1993).
2. P.F. Fewster, **J. Appl. Cryst., 24**, 178 (1991); P.F. Fewster, **Appl. Surf. Sci., 50**, 9 (1991).
3. H. Chung, B. Raghothamachar, J. Wu, M. Dudley, D.J. Larson, Jr., and D.C. Gillies in "Defect and Impurity Engineered Semiconductors and Devices", A. Ashok, J. Chevallier, I. Akasaki, N.M. Johnson, and B.L. Sopori (Eds.), **Mat. Res. Soc. Symp. Proc., 378**, 41, (1995).
4. W. Zhou, M. Dudley, C.H. Su, M.P. Volz, D. Gillies, F.R. Szofran, and S.L. Lehoczky, in "Infrared Detectors - Materials, Processing, and Devices", A. Applebaum and L.R. Dawson (Eds.), **Mat. Res. Soc. Symp. Proc., 299**, 203, (1994); W. Zhou, M. Dudley, C.H. Su, M.P. Volz, D. Gillies, F.R. Szofran, and S.L. Lehoczky, **Mater. Sci. & Engin., B27**, 143, 1994.
5 D.J. Larson, R.P. Silberstein, D. DiMarzio, F.C. Carlson, D. Gillies, G. Long, M. Dudley, and J. Wu, **Semicond. Sci. Technol. 8**, 911, 1993.

# REVERSE MICELLE BASED GROWTH OF ZINCOPHOSPHATE SODALITE : EXAMINATION OF CRYSTAL GROWTH

K. S. N. Reddy, L. M. Salvati, Prabir K. Dutta*,
Department of Chemistry
120 West 18th Avenue
The Ohio State University
Columbus, OH 43210
Phone: 614-292-4532
email: Dutta.1@osu.edu

Phillip B. Abel, Kwang I. Suh, Rafat R. Ansari
NASA Lewis Research Center
21000 Brookpark Road
Cleveland, OH 44135.

**Abstract**

Formation of zincophosphates from zinc and phosphate containing reverse micelles (water droplets in hexane) has been examined. The frameworks formed resemble that made by conventional hydrothermal synthesis. Dynamics of crystal growth are however quite different, and form the main focus of this study. In particular, the formation of zincophosphate with the sodalite framework was examined in detail. The intramicellar pH was found to have a strong influence on crystal growth. Crystals with a cubic morphology were formed directly from the micelles, without an apparent intermediate amorphous phase over a period of four days by a layer-by-layer growth at the intramicellar pH of 7.6. At a pH of 6.8, an amorphous precipitate rapidly sediments in hours. Sodalite was eventually formed from this settled phase via surface diffusion and reconstruction within four days. These diverse pathways were possible due to changes in intramicellar supersaturation conditions by minor changes in pH.

## Introduction

Microporous materials include a large group of solids of varying chemical composition as well as porosity. The framework structure is made up of interconnecting T-O-T' bonds, where T and T' can be Si, Al, P, Ga, Fe, Co, Zn, B and a host of other elements.[1] Materials with Si-O-Al bonding in the framework are called zeolites and find extensive use.[2] Study of the nucleation, crystal growth as well as development of new synthesis conditions is an active area of research.[3] Crystal growth of these materials is a complicated chemical process. To the best of our knowledge, the influence of supersaturation on growth of microporous frameworks has not been systematically examined. We report here the discovery that by using reverse micelles as reactants for the growth of zincophosphate sodalite framework, control can be exercised over the supersaturation levels, and distinct crystal growth pathways are observed.

Certain surfactant molecules, dissolved in organic solvents, are capable of solubilizing water in the polar core and these entities are called reverse micelles or microemulsions. We have shown in an earlier communication that zinc and phosphate ions introduced via reverse micelles will interact with each other and lead to the nucleation and subsequent growth of zincophosphate sodalite crystals.[4] In this study, we explore this system in more detail. The particle size development, their crystallinity and morphology during crystal growth process has been studied.

## Experimental Section

The surfactant sodium bis (2-ethyl hexyl) sulfosuccinate (AOT) (Aldrich, > 98%) was used to make the reverse micelles. Three solutions were prepared: 0.065 M AOT in n-hexane, 0.2 M $Zn(NO_3)_2$ aqueous solution, and 0.5 M $H_3PO_4$, 0.24 M NaOH and 0.93 M of TMAOH as another aqueous solution. The zinc and phosphate micelle solutions were prepared by mixing 8 ml of the aqueous solutions with 200 ml of the n-hexane solution in two separate containers. After shaking the mixtures for a minute, the solutions were equilibrated for 48 hours, centrifuged and the remaining aqueous phases were removed from the hexane. The micellar solutions were allowed to age for up to three weeks. The zinc and phosphate containing micellar solutions, aged for different times were mixed in various volume proportions as outlined in the text. The reactions were carried out at

25°C. Elemental analysis was done by inductively coupled plasma spectroscopy and combustion methods. Micelle size and particle growth were monitored by quasi elastic light scattering. $^{31}P$ NMR spectra of the phosphate micelle solutions were recorded at room temperature. X-ray powder patterns were determined with diffractometer using nickel-filtered Cu K$\alpha$ ($\lambda$=1.5405 Å) radiation. Particle size and morphology were determined by scanning electron microscopy (SEM) and transmission electron microscopy. Non contact AFM measurements were also made on several samples.

Results

(a) Formation of Sodalite: Sodalite is a member of the microporous family of frameworks and has been extensively studied in the aluminosilicate as well as all silica systems.[5] Solutions of phosphate and zinc micelle aged for 8 days were used as starting materials for sodalite synthesis. Three compositions made by adjusting the relative ratios of the zinc and the phosphate micelle solutions between 0.8 and 1.2 were examined in more detail (identified as compositions A, B and C). $^{31}P$ NMR of compositions A, B and C show that they have intramicellar pH values of 7.6, 7.2 and 6.8, respectively.

(b) Particle Growth Characteristics: Laser light scattering obtained on all three compositions upon mixing the zinc and phosphate micelles indicated that the initial micelle size is of the order of 15-50 nm. For compositions B and C, there is a period of time in which the particle size remains below 100 nm, followed by a rapid increase. However, the period of time before the growth spurt is very different, about 16 hours for Composition B and less than 2 hours for Composition C, consistent with our visual observations. In the case of composition A, the growth seems more complicated. There is no growth spurt, rather a gradual increase, which reaches a maximum around 36 hours.

(c) Diffraction patterns of the recovered Particles: For composition A, the solution remains clear and evidence of reaction is provided by solids appearing at the bottom of the reaction vessel for the first time after 2 days. The diffraction patterns obtained from this sample show that it is sodalite. This shows that the settled particles are already crystalline, implying that crystal growth is occurring while suspended. For composition B, as soon as the solution became cloudy, it was centrifuged. This typically took about 12-16

hours. The diffraction pattern of this solid is characteristic of the sodalite framework. For composition C, examination of the particles formed immediately after the appearance of turbidity are mostly amorphous by diffraction. The settled amorphous solid was monitored by diffraction and transforms to sodalite over a 4-day period.

(d) Microscopy of the Recovered Particles : Electron microscopy was used to examine the morphology of the solids formed with each composition. Scanning electron micrograph of the crystals obtained after settling (4 days) for composition A show that the sizes of these crystals are between 500-600 nm. The morphologies are cubic crystals, or pyramids (half-cubes). At all observable stages of growth, the morphology of the sodalite crystals remain similar, with size and yield increasing in time. The surfaces of (100) faces of a cubic sodalite crystal were examined by non-contact atomic force microscopy (AFM). There appear to be flat terraces followed by steps, roughly aligned with the crystal side, as shown in Figure 1. The step heights were about 10Å in height, corresponding to a sodalite cage.

The SEM pictures of the particles obtained for composition B before settling show sizes less than 600 nm and eventually aggregate to form the 2-3 $\mu$m settled crystals.

For Composition C , first formed are discrete particles of approximately 5 $\mu$m. These particles settle, agglomerate and form a contiguous solid with time. Sodalite crystals grow out of this settled solid phase.

## DISCUSSION

Results above show that it is possible to grow zincophosphate frameworks from reactants initially contained in reverse micelles. We propose that the intramicellar pH is influencing the concentration of nucleating species responsible for formation of zincophosphate sodalite. Thus, in all three compositions (A-C), homogeneous nucleation is beginning in the micelle, and since the supersaturation of the nucleating species is varying, there is a wide range of nucleation rates. Even though the structure of the nucleating species is not identified, the necessity of hydrolysis of the Zn-O-P bond in their formation is recognized. In composition A, where the supersaturation is the lowest, crystal growth proceeds slowly, controlled by surface attachment kinetics. We consider the surface morphology indicated by AFM to be evidence for a layer-by-layer growth,

and is consistent with the cubic morphology observed by SEM. It is known that at low supersaturation, crystals of compact shapes are formed, since the minimum overall energy of the crystal surface is reached under very slow growth, equilibrium-like conditions.[6]

The growth process in Pathway B can be analyzed as an aggregation process. The early morphology of these crystals appears cubic in nature, suggesting that the initial growth process may be similar to that of composition A. The viable nuclei formed grow by incorporating other nuclei. The mobility of the nuclei by diffusion and convection contribute to the aggregation process. Such diffusion controlled micellar collisions have been proposed for growth of silica and carbonate particles. The size that nuclei will have to reach before aggregation begins is of interest. Since Pathway B results in direct formation of crystals from nuclei, particle size analysis during this crystal growth process provides this opportunity and indicates a size of 75 nm before rapid growth ensues.

The differences in crystal growth rates between compositions A and B are being assigned to the differences in micellar pH, which leads to two effects. First, it alters the concentration of solution species. Lazic has recently reported a reduction of the induction period in hydroxyapatite formation from amorphous calcium phosphate as a function of pH.[7] The second effect of pH on crystal growth arises from the surface charge on the particle.

In pathway C, the intra-micellar conditions result in higher supersaturation. This leads to rapid nucleation, and since the induction time for crystal formation is longer, amorphous particles are formed. The morphology of the particles formed initially in composition C supports the high supersaturation hypothesis. If the rate of particle growth is very high, then the heat of precipitation cannot be transferred efficiently into solution. This leads to convection and the particle is surrounded by depleted regions. The particle extends its surface highly anisotropically.

## Conclusions

This study shows that it is possible to make complicated structures, such as zincophosphate sodalite from reactants contained in reverse micelles. Overall, the reaction chemistry followed the conventional aqueous hydrothermal chemistry. The

internal pH's of the micelles could be controlled with aging. The important discovery, as contrasted to the aqueous system, is that it was possible to control the crystal growth kinetics by using reverse micelles.

**References**


1. Szostak, R. Handbook of Molecular Sieves, Van Nostrand, 1992.
2. Zeolites and Related Microporous Materials: State of the Art 1994, Eds. Weitkamp, J.; Karge, H.G.; Pfeifer, H.; Holderich, W., Elsevier, Amsterdam, 1994.
3. Davis, M.E.; Lobo R.F. Chem. Mater. **1992** *4*, 756.
4. Dutta, P.K.; Reddy, K.S.N.; Salvati, L.; Jakupca, M. Nature, **1995**, *374*, 44.
5. Bibby, D.M.; Dale, M.P. Nature, **1985**, *317*, 157.
6. Loades, S.D.; Carr, S.W.; Gay, D.H.; Rohl, A.L. J. Chem. Soc. Chem. Commun. **1994**, 1369.
7. Lazic', S. J. Cryst. Growth **1995**, *147*, 147.


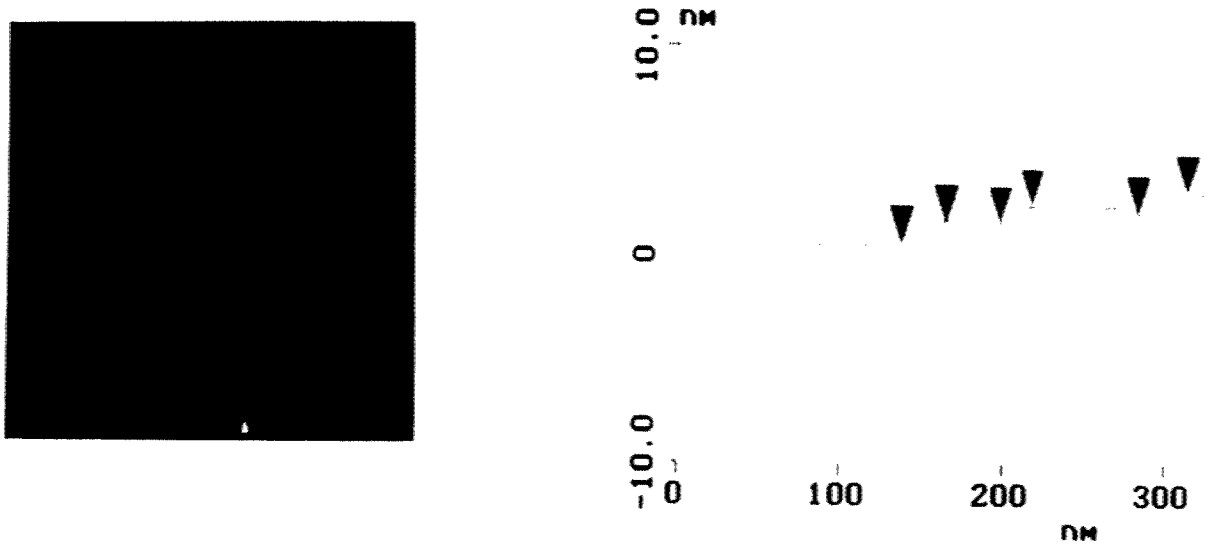


Figure 1. AFM trace of a sodalite crystal obtained via composition A along with the step heights.

# STUDIES ON NUCLEATION, POLYMERIZATION AND NANOPARTICLE COMPOSITES IN SUPERSATURATED VAPORS UNDER MICROGRAVITY

M. Samy El-Shall
Department of Chemistry
Virginia Commonwealth University
Richmond, VA 23284-2006
Phone: (804) 828-3518; Fax: (804) 828-8599
E-Mail: SELSHALL@GEMS.VCU.EDU

The general objective of the ground-based experiments is to advance the scientific understanding of nucleation and materials synthesis from the vapor phase which are strongly influenced by gravity and convection effects. These experiments will provide insights into the fundamental aspects of nucleation and related materials processes and will eventually lead to cloud chamber experiments on nucleation, gas phase polymerization and nanoparticle synthesis in a high quality, long duration, microgravity environment. The overall four-year research plan includes:

## 1. Vapor Phase Nucleation Studies

Nucleation is one of the most ubiquitous and important phenomenon in science and technology. It plays a role (sometimes central) in materials science and metallurgy, crystal growth and chemical processing, aerosol formation, cavitation, crack propagation, wind tunnels, atmospheric science and cosmochemistry. The major objective of the nucleation studies is to gain an understanding of the factors that control the formation of a new phase through a nucleation process. Measuring the homogeneous nucleation rates for different classes of substances in the vapor phase and comparing experimental data with predictions from different nucleation theories will accelerate the development of a quantitative nucleation theory. In addition, these measurements are important in determining the nucleating ability of different vapors and the conditions of their participation in the formation of ultrafine aerosols.

We plan to study the homogeneous nucleation of different classes of substances (simple fluids, polar, non-polar) using the diffusion cloud chamber technique.[1,2] Future experiments will be designed to compare the homogeneous nucleation rates obtained for the same fluid under identical temperature, pressure and supersaturation conditions but different gravity fields.

We will also develop a new technique for the study of nucleation on well-defined ions. Since different ionic species are characterized by different mobilities, it is almost impossible to obtain accurate quantitative data on ion nucleation without unambiguously identifying the nucleating ions. The new method is based on Resonant-Two-Photon Ionization (R2PI), in which well-defined molecular ions act as nucleation centers for the condensation of supersaturated vapors. The details of the ion nucleation experiments have been recently described.[3] These experiments allow, for the first time, to selectively and unambiguously generate specific ions of interest and study their nucleating behaviors during the process of condensation of supersaturated vapors.

## 2. Polymerization Studies

The study of gas phase polymerization is an important intellectual and technological frontier which promises unique results not only for a fundamental understanding of polymerization reactions, but also for the development of new materials with unique properties. In the past it has been almost impossible to study gas phase chain polymerization because the involatile product molecules condensed out of the gas phase. We have recently explored the application of new methods to study gas phase polymerization and we plan to further develop the following two approaches:

### A. Gas Phase Initiation of Bulk Polymerization

Recent research in our laboratory has lead to the discovery of a novel technique for cationic polymerization using metal ions generated in the gas phase by laser vaporization techniques.[4,5] The ions are pulled toward the monomer liquid by applying appropriate electric fields across the reaction chamber. Using this method, high molecular weight polymers ($10^6$ units, polyisobutylene) have been synthesized. The polymeric materials also contain micron - and submicron - sized metal particles. Example of a scanning electron micrograph (SEM) is shown in Figure 1-a. The surface morphology of the polymer film obtained is dependent on experimental conditions such as laser power, temperature, pressure and electric field strength. This is a significant result since the incorporation of ultrafine metal particles and clusters into the polymer matrices would greatly extend the scope of these polymeric materials in, for example, electrical, magnetic and optical applications.

Under certain experimental conditions (application of an electric field within the monomer liquid) we were able to deposit polymer wires or stripes as shown in Figure 1-b. The wires are 0.4 $\mu$m wide and spaced 2 $\mu$m apart. The control of these microstructures is hampered by the gravity effects which introduce convection and nonhomogeneous conditions. We propose to carry out these experiments in space, and we expect to be able to control the microstructures

and the size distribution of the metal particles in the polymer films. These new directions which are explored for the first time, could lead to the production of new polymeric films with unique material properties.

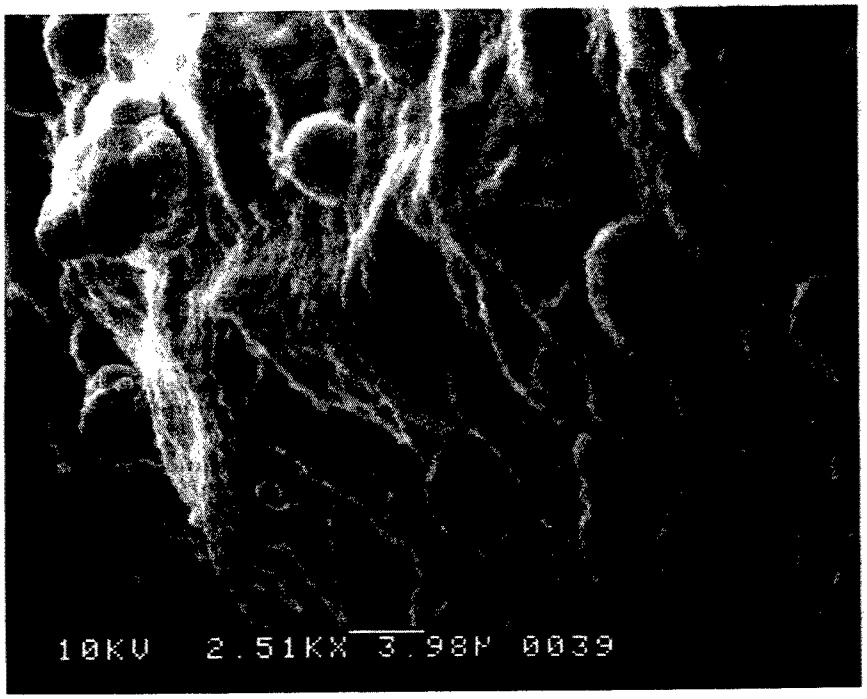


Figure 1-a : SEM micograph of polyisobutylene film containing ultrafine Zn particles.[5]

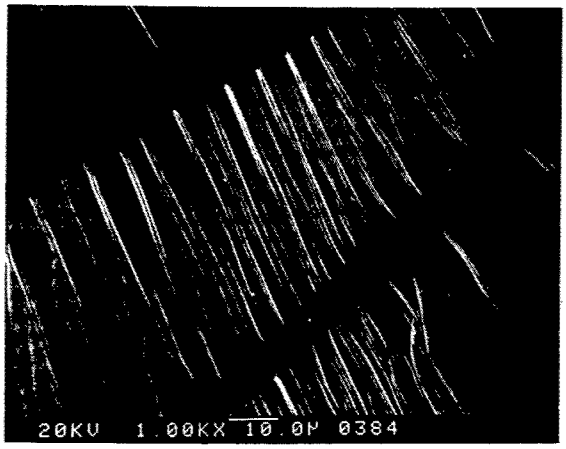


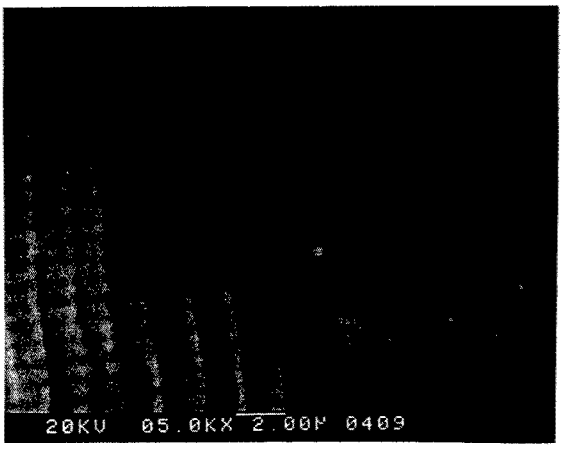


Figure 1-b : SEM micographs of polyisobutylene fibers and stripes obtained by applying a secondary electric field within the liquid monomer during the laser vaporization process.[5]

B. Gas Phase Polymerization in Supersaturated Vapors

We plan to study gas phase cationic polymerization by preparing supersaturated monomer vapors (e.g. styrene, phenylacetylene, isobutylene, etc.) in diffusion cloud chambers and initiating their polymerization by multiphoton ionization of the monomers or by generating metal cations within the supersaturated vapors. The experiments are natural extensions of our previous work on free radical polymerization in cloud chambers.[6-8] The difference is that it is now possible to generate well defined ions in supersaturated vapors by using the R2PI technique as already demonstrated by our work on ion nucleation[3]. The propagation rate constants for free ions are greater than those for free radicals or ion pairs. The initiating ions trigger the propagation of cationic polymer chains in the gas phase. When a single polymer of critical size can nucleate a drop of liquid monomer, the appearance of that drop signals the arrival of the polymer of that size. One can sense the arrival of polymer molecules and measure the rate of reaction in this way. Under microgravity conditions it would be possible to keep the growing polymers in the supersaturated vapor where they continue to propagate to larger sizes and thus kinetic information on the growing large polymers can be obtained. This is also a method to produce very narrow size distributions of polymers since few chains are growing in the vapor phase thus chain transfer and termination reactions can be minimized.

3. Nanoparticle Composites

Nanoscale particles possess several unique properties such as large surface areas, unusual adsorptive properties, surface defects and fast diffusivities. The control and characterization of these properties can ultimately lead to identifying many potential uses, particularly in the fields of catalysis and novel materials. Recently, we have developed a new method for generating nanoscale metal oxide particulates down to 10 nm size by laser vaporization of solids into inert or oxygen containing atmospheres and deposition onto cold surfaces in a diffusion cloud chamber.[9-12] A sketch of the experimental set-up is shown in Figure 2. Particulate sizes similar to interstellar grains, typically of 10 - 100 nm are obtained readily, and larger particles are possible. Convection plays an important role in determining the particle's size. The composition is controlled by the choice of the solid target and the gas mixture.[10]

Adjusting these parameters can yield compositions, sizes and topologies over a virtually unlimited range. Mixed particulates are generated by using several metal targets, and the composition is varied by adjusting the number of laser shots on each target. As examples, $CuO/ZnO$ and $TiO_2/Al_2O_3/ZnO$ were prepared.[12] The preparation of carbides was also demonstrated by adding $CH_4$, and nitrides by adding $N_2$ or $NH_3$ to the vapor.[9,12] Silicate and aluminum oxide particulates are of special stellar relevance, first because of their abundance,

and second, because their refractory nature makes them the first to condense out in protostellar nebulae. The $Al_2O_3$ and $SiO_2$ particles examined by SEM exhibit weblike structures as shown in Figure 3.

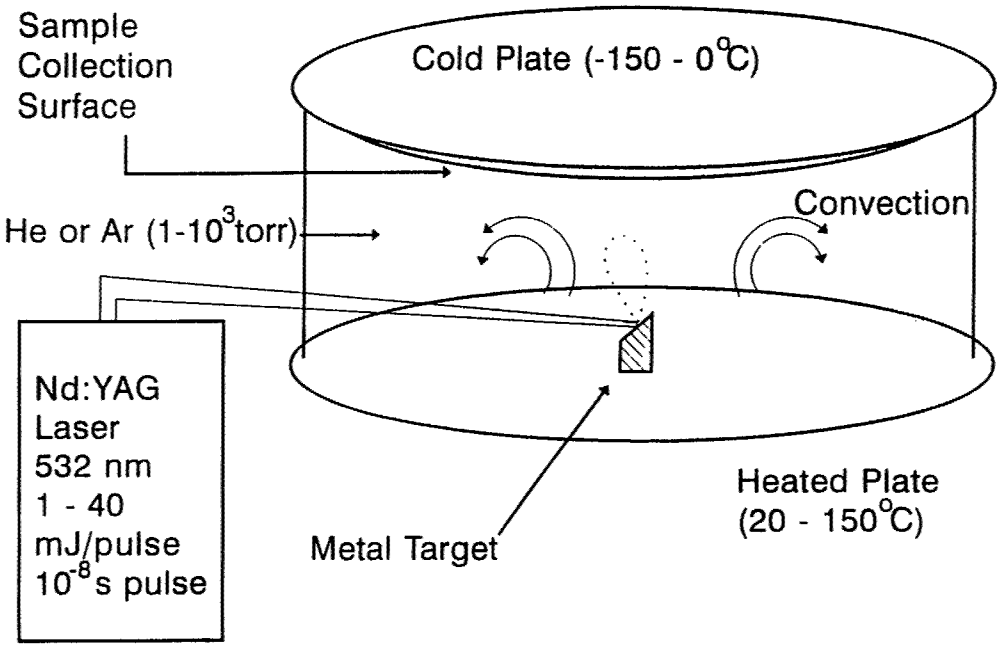


Figure 2 : Experimental set-up for the synthesis of nanoparticles using laser vaporization in a convective atmosphere.[12]

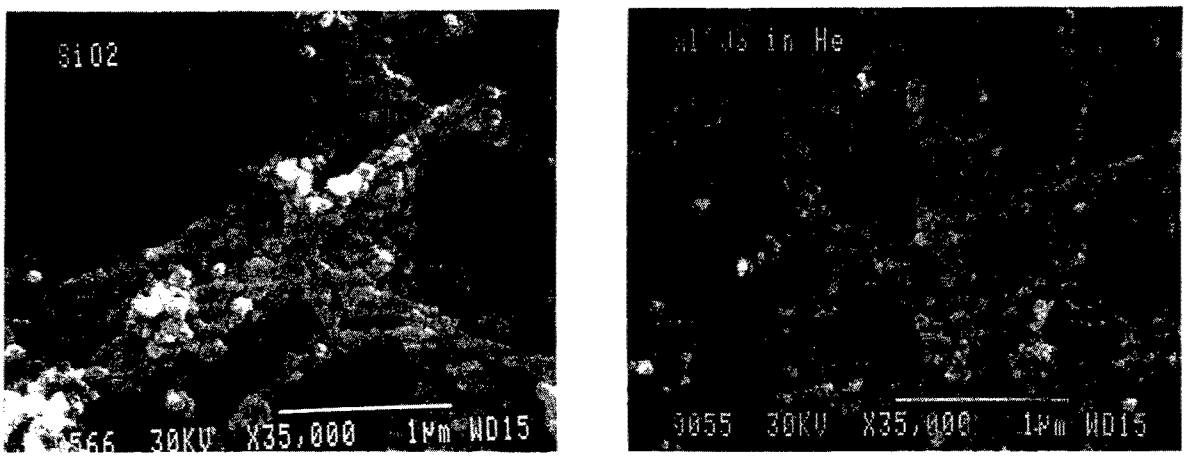


Figure 3 : SEM micographs of $SiO_2$ and $Al_2O_3$ nanoparticles.

In future work, we plan to generate the composite particulates under microgravity conditions since particle size-induced segregation effects will be dramatically reduced relative to ambient conditions. It should also be possible to grow clusters of certain sizes and make layered structures by artificially applying a gravitational force of specific duration. For example, it will be possible to form layered structures of $Si/SiO_2/Al/Al_2O_3$ clusters. The use of laser vaporization will make it possible to vaporize several different metals either simultaneously or sequentially and by controlling gravitational forces, it will be possible to deposit multilayers of engineered compositions and particle size distributions.

## References


1. M. S. El-Shall, J. Chem. Phys. 90, 6533 (1989).
2. D. Wright, R. Caldwell, C. Moxley and M. S. El-Shall, J. Chem. Phys., 98, 3356 (1993).
3. D. Kane, G. M. Daly and M. S. El-Shall, J. Phys. Chem., 99, 7867 (1995).
4. W. Vann and M. S. El-Shall, J. Am. Chem. Soc., 115, 4385 (1993).
5. W. Slack and M. S. El-Shall, Macromolecules, 28, 8456 (1995).
6. M. S. El-Shall, A. Bahta, H. M. Rabeony and H. Reiss, J. Chem. Phys. 87, 1329 (1987).
7. M. S. El-Shall and H. Reiss, J. Phys. Chem. 92, 1021 (1988).
8. M. S. El-Shall, H. M. Rabeony and H. Reiss, J. Chem. Phys., 91, 7925 (1989).
9. M. S. El-Shall, W. Slack, W. Vann, D. Kane and D. Hanley, J. Phys. Chem. 98, 3067 (1994).
10. M. S. El-Shall, W. Slack, D. Hanley and D. Kane, in "Molecularly Designed Ultrafine / Nanostructured Materials", Editors: K. E. Gonsalves, G. Chow, T. D. Xiao and R. C. Cammarata, Vol. 351, Materials Research Society Symposium Proceedings Series, 369-374 (1994).
11. M. S. El-Shall, S. Li, T. Turkki, D. Graiver, U. C. Pernisz and M. I. Baraton, J. Phys. Chem. 99, 17805 (1995).
12. 10. M. S. El-Shall, S. Li, D. Graiver and U. Pernisz in "Nanotechnology: Molecularly Designed Materials", Editors: G. Chow and K. E. Gonsalves, ACS Symposium series 622, Chapter 5, (1996).

# INVESTIGATION OF VIBRATIONAL CONTROL OF THE BRIDGMAN CRYSTAL GROWTH TECHNIQUE

Alexandre Fedoseyev and J. Iwan D. Alexander

Center for Microgravity and Materials Research, University of Alabama in Huntsville, Alabama, 35899, USA, Phone (205)895-6889, E-mail: alex@cmmr.uah.edu

## 1. Research project objectives

The primary objectives are to

- conduct a parametric theoretical and numerical investigation of vibro-convective buoyancy-driven flow in differentially heated cylindrical containers
- investigate buoyant vibro-convective transport regimes in Bridgman-type systems with a focus on the use of vibration to suppress, or control, convection in order to achieve *transport* control during crystal growth.
- assess the feasibility of vibro-convective control as a means of offsetting "g-jitter" effects under microgravity conditions
- exchange information with the experimental group at the General Physics Institute (GPI) of the Russian Academy of Science who are undertaking a complementary experimental program.

## 2. Significance and justification for microgravity research

The character of natural buoyant convection in rigidly contained inhomogeneous fluids can be drastically altered by vibration of the container boundaries or through the introduction of vibration sources into the interior of the fluid. In many terrestrial crystal growth situations, convective transport of heat and constituent components is dominated by buoyancy driven convection arising from compositional and thermal gradients. Thus, it can be concluded that vibro-convective flow can potentially be used to influence and even control transport in some crystal growth situations.

Control of convective transport continues to be an important aspect of crystal growth research. For example, control of convection through static and rotating magnetic fields is being actively pursued by several groups. In some cases, experimenters seeking to avoid buoyancy effects through use of microgravity environments have expressed interest in the use of magnetic fields even under low gravity conditions. However. there are many instances, whether due to materials properties or other practical considerations, use of magnetic fields to induce stirring or suppress flow may not be an option. In such cases, vibrational control could become an attractive alternative.

Recent numerical modeling work at the Institute de Mécaniques des Fluides de Marseille has confirmed that vibration can also be used to suppress buoyancy-driven flows. Furthermore, it was indicated that such suppression would be very effective at reduced gravity levels of $10^{-4}$ g or less. This raises the possibility that, under microgravity conditions, specific controlled vibration can be used to mask undesirable "g-jitter" induced convective effects. Such g-jitter convection can be caused by quasi-steady residual acceleration [1] (due to gravity gradient

and atmospheric drag effects [3]) as well as transient and oscillatory acceleration disturbances [4,5]. While active vibration isolation can be a partial solution, it will not solve the problems that might arise due to the quasi-steady and very low-frequency acceleration components related to the gravity gradient and other orbital factors. Thus as an alternative to vibration isolation, one might envisage using vibration to either suppress flow or to provide flow regimes tailored to particular crystal growth experiments. These flows would not be accessible under terrestrial conditions due to strong natural convection effects. Thus, the microgravity relevance of our proposed work is established.

## 3. Brief review of relevant research

It has been recognized for some time that oscillatory or pulsatile flow can significantly alter the transfer of mass, heat and momentum in fluid systems [6-17]. For example, analyses of heat transfer in (laminar) oscillating flows have shown that at high frequencies the effective diffusivity, $\kappa_{eff}$, behaves like $\kappa_{eff} \propto \Delta x^2(\omega\nu)^{1/2}/L$ and, at low frequencies, $\kappa_{eff} \propto \Delta x^2\omega^{3/2}\nu^{1/2}/L$, where $\nu$ is the kinematic viscosity, $\Delta x$ is the cross stream average of a fluid element over half the period of the oscillation and L is a characteristic geometric distance (e.g., between the plates). It was also shown that heat transfer was most enhanced when the characteristic heat transfer time was equal to half the oscillation period [10].

Buoyant vibro-convective motion can occur when oscillatory displacement of a container causes the acceleration of a container wall relative to the fluid inside. The vibration may be viewed as a time-dependent modulation of steady gravity. In a closed container filled with a homogeneous fluid, the fluid will eventually move as a rigid body with the container. If, however, the density of the fluid is not homogeneous, fluid motion may ensue. This will depend on the orientation of the vibration directions with respect to the local density gradients and, in some cases, a critical threshold must also be exceeded. For density gradients caused by temperature, such motion is called thermo-vibrational. A great deal of work related to the theory of thermo-vibrational convection has been carried out by Russian research groups. The main focus on has been on thermo-vibrational convection starting with the work of Zenkovskaya and Simonenko [18] who first obtained the equations of thermo-vibrational convection in a high frequency limit. Since then there have been many theoretical [19-23] and some experimental (e.g., [24]) studies of the stability of thermo-vibrational flows. One of the main conclusions that can be drawn from these works is that for vibrations with specially chosen axes, the natural buoyancy driven convection which would prevail in the absence of vibration can be suppressed at certain frequencies and amplitudes [23]. This has recently been analyzed in more detail [25] using the full equations of motion and Gershuni's time-averaged equations. The possibility of using vibration as a means of controlling and suppressing convection was confirmed. A comprehensive introduction to vibrational convection and other time-dependent modulation can be found in reference [24]

The problem of vibrational convection arising due to other buoyancy sources, such as compositional density gradients, has also been approached. The onset of purely solutal and thermosolutal convection has been examined for horizontally stratified layers subject to vertical vibration [26,27].

There are several examples of experimental work concerning the influence of vibration on crystal growth from melts and solutions [28-37]. These works involved a wide range in intensities and frequencies (including ultrasound). Experimental attempts to understand how low frequency vibrational stirring might be used to effect rapid mixing in melts and solutions have been made by Liu et al. [34]. The influence of low frequency vibration on interface location and shape during Bridgman growth of cadmium telluride was examined by Lu et al. [35]. Other effects of low frequency vibrational convection on crystal growth include the increase in local perfection of binary compound semiconductors [37], changes in interface shape [30], and the facetting of germanium crystals [38]. The elimination of striations in indium antimonide may also be due to the formation of a stationary melt flow due the torsional vibration [39].

Experimental results also clearly show that in certain cases vibrational convection can provide enhanced nutrient fluxes during the solution growth of Rochelle salt and potassium dihydrogen phosphate (KDP) [40,41]. Zharikov [42] identified a characteristic low frequency (< 100 Hz) vibrational flow regime in the liquid near a growing crystal. The form, dimensionality and intensity of the flow were studied and the effects of vibration on heat and mass transfer were analyzed for the case of Czochralski and Bridgman growth of sodium nitrate ($NaNO_3$). He showed that the vibration could drastically alter the character of flow and concluded that vibration could exert a strong influence on transport and impurity incorporation and locally influence growth kinetics.

Uspenskii and Favier [43] considered the interaction between high frequency and natural convection in Bridgman-type crystal growth. They used the average thermo-vibrational flow equations to theoretically examined the problem of suppressing natural convection using high frequency (~ $10^4$ Hz) low amplitude vibration and compared the efficiency of vibrational damping to that of magnetic field damping. Using the physical properties representative of GaSb, GaAS, etc., they found that under terrestrial conditions, (for high electro-conductivities) the magnetic field is more effective than vibration in damping flow in the horizontal Bridgman configuration. In contrast, for vertical Bridgman, lateral vibration was most effective. The horizontal velocity decreased by a factor of 10 and the vertical velocity by about 20. In comparison a 1 Tessla vertical magnetic field only resulted in a factor of 6 decrease in maximum velocity. They speculated that it might be possible to combine magnetic fields with vibration to reach optimal damping conditions.

## 4. Proposed research

The proposed research will involve a numerical investigation of vibro-convective transport regimes with application to the control of convection and transport during growth of crystal by the Bridgman technique. The work is motivated by recent developments in the understanding of low frequency thermo-vibrational convection and by current and planned experimental work at the GPI. Although, in principle, the theoretical research described below can be carried out independently of a particular experimental program, information exchange will enable both groups to place their work on a firm practical foundation.

The basic problems to be analyzed will be the suppression or control of buoyancy-driven convection in melts during plane-front directional solidification. The work will involve the analysis of vibrational interaction with natural convection and its effects on the temporal evolution of melt temperature and composition during growth. The philosophy behind our

approach is to use numerical modeling in two ways: synergistically with experimental developments and as a predictive tool. The synergism with experiment will allow careful interpretation of both experimental and modeling results for what can be a highly non-linear physical situation. By exploring regimes and system properties currently inaccessible to experiment, the model can also be used as a predictive tool. The work will involve an extensive investigation of the vibrational flow regimes with and without the presence of natural buoyancy-driven convection and will be initially guided by previous results. As we progress toward our goal of defining the applicability of vibrational control of convection we will compare the ability of vibration to suppress flow with that of a magnetic field and also explore the consequences of using simultaneous vibration and magnetic field control.

## 5. References


[1] J.I.D. Alexander, Low gravity experiment sensitivity to residual acceleration: A review, Microgravity Science and Technology, III (1990) 52.

[2] J.I.D. Alexander and C.A. Lundquist, Motions in fluids caused by microgravitational acceleration and their modification by relative rotation, AIAA Journal, 26 (1988) 34.

[3] H. Hamacher, R. Jilg and U. Mehrbold, Analysis of microgravity measurements performed during D-1, Proc. 6th European Symposium on Materials Sciences in Microgravity Conditions, Bordeaux, France (ESA SP-256 1987).

[4] M.J.B. Rogers and J.I.D. Alexander, Analysis of spacelab-3 acceleration data, AIAA J. Spacecraft and Rockets, 28 (1992) 52.

[5] J.I.D. Alexander, J. Ouazzani, S. Amiroudine and F. Rosenberger, Analysis of the low gravity tolerance of Bridgman-Stockbarger crystal growth II. Transient and periodic acceleration, J. Crystal Growth, 113 (1990) 21.

[6] G.I. Taylor, Proc. Roy. Soc. London A 219 (1953) 186.

[7] R. Aris, Proc. Roy. Soc. London A 259 (1960) 370.

[8] W.N. Gill and R. Shankarsubramanian, Proc. Roy. Soc. London A 316 (1970) 370.

[9] E. Brocher, J. Fluid Mech. , 133 (1983) 245.

[10] U.H. Kurzweg, J. Fluid Mech., 156 (1983) 291.

[11] U.H. Kurzweg, J. Heat Transfer, 107 (1985) 459.

[12] M. Kaivany, Int. J. Heat Mass Trans., 29 (1985) 2002.

[13] C. H. Joshi, R.D. Kamm, J.M. Drazen, and A.S. Slutsky, J. Fluid Mech., 114 (1983) 245.

[14] R. Smith,J. Fluid Mech., 114 (1982) 379.

[15] E.J. Watson, 113 (1983) 233.

[16] D. Farell and W. E. Larsen, Water Resources Res., 9 (1973) 173.

[17] Y. Kamotani, A. Prasad and S. Ostrach, AIAA Journal 19 (1981) 511.

[18] S. M. Zen'kovskaya and I. B. Simonenko, On the effect of high-frequency vibrations on the convection onset. Izv. Akad. Nauk SSSR, Mekh. Zhidk. Gaza **5** (1966) 51 (in Russian)

[19] G. Z. Gershuni and E. M. Zhukhovitsky, On free thermal convection in vibrational field in weightlessness. Dokl. Akad. Nauk SSSR **249** (1979) 580. (in Russian).

[20] G. Z. Gershuni and E. M. Zhukhovitsky, On convective instability of fluid in vibrational field in weightlessness. Izv. Akad. Nauk SSSR, Mekh. Zhidk. Gaza **4** (1981) 12. (in Russian).

[21] G. Z. Gershuni, E. M. Zhukhovitsky and Yu. S. Yurkov, On vibrational thermal convection in weightlessness conditions. Hydromechanics and Heat - Mass Transfer in Weightlessness., Nauka, Moscow (1982) (in Russian).

[22] G. Z. Gershuni, E. M. Zhukhovitski and A. Nepomniashi, Stability of convective flows, (Nauka, Moscow, 1966) p. 109.

[23] G. Z. Gershuni and E. M. Zhukhovitski, Convective stability of incompressible Fluids, (Keter, Jersualem, 1976) Chapter 8.

[24] V. G. Kozlov and S. B. Shatunov, Experimental study of the onset of vibrational convection in a horizontal flat fluid layer with internal heat release. Numerical and Experimental Modelling of Hydromechanic Phenomena in Weightlessness., Sverdlovsk (1988) 79 (in Russian).

[25] A. Lizee, Contribution à la convection vibrationelle; contrôle actif de la convecyion naturelle, Thesis, Univesitie of Aix-Maseille II (1995) (In French).

[26] B.T. Murray, S.R. Coriell and G.B. McFadden, The effect of gravity modulation on thermosolutal convection during directional solidification, J. Crystal Growth, 110 (1990) 713.

[27] B. V. Saunders, B.T. Murray, G.B. McFadden, S.R. Coriell and A.A. Wheeler, The effect of gravity modulation on thermosolutal convection in an infinite layer of fluid, Phys. Fluids A 4 (1992) 1176-1189.
[28] A.P. Kaputsin, Influence of ultrasound on crystallization kinetics, (Acad. Sci, USSR. Moscow, 1962) (in Russian).
[29] V. Ship and V. Vanichek in: Rots Kristallov, Vol. III (Acad. Sci, USSR. Moscow, 1961).
[30] B. Langenecker and W.H. Fransen, Phil. Mag. 7 (1962) 2079.
[31] A.F. Witt and H.C. Gatos, J. Electrochem. Soc. 114 (1967) 413.
[32] A.A. Wheeler, J. Crystal Growth 56 (1982) 67.
[33] S.M. Manucharyan and H.G. Nalbandyan, Crystal Res. Technol. 17 (1982) 295.
[34] W.S. Liu, M.F. Wolf, D. Elwell and R.S. Feigelson, Low frequency vibrational stirring: a new method for rapidly mixing solutions and melts, J. Crystal Growth, 82 (1987) 589.
[35] Y.-C. Lu, J.-J. Shiau, R.S. Feigelson and R.K. route, Effect of vibrational stirring on the quality of Bridgman grown CdTe, J. Crystal Growth, 102 (1990) 807.
[36] E.V. Zharikhov, L.V. Prihod'ko and N. Storozhev, Crystal Res. Tech.nol. 24(1989) 761.
[37] G.V. Nikitina, V.N. Romanenko and V.M. Tuchkevitch, in : Crystalization and phase transitions, (Acad. Sci, BSSR. Minsk, 1962) (in Russian).
[38] A.P. Izergin, Yu.S. Pavlenko and S.A. Strotlev, Izv. Vysshikh Uchebnykh Zavedenii, Ser. Fiz. 1 (1959) 107 (in Russian).
[39] Y. Hawakawa, M. Nagura and M. Kunagawa, Semicond. Sci. Tech. 3 (1988) 372.
[40] V.V. Klubovitch, I.F. Kashevitch, V.V. Mikhevitch and N.K. Tolotchko, Kritallografiya 29 (9184) 822.
[41] V.V. Klubovitch, S.E. Mozzharov, N.N. Sobolenko, N.K. Tolotchko and V.V. Azarov, in: Digest of Tech. Papers, 7th All-Union Conf. on Crystal Growth, 2 (VINITI, MOscow, 1988) 114 (in Russian).
[42] E.V. Zharikov, L.V. Prihod'ko and N. Storozhev, J. Crystal Growth 99 (1990) 910-914.
[43] V.V. Uspenskii and J.J. favier, High frequency vibration and natural convection in Bridgman-scheme crystal growth, Int. J. Heat Mass Transfer, 37 (1994) 691-698.

# ALLOY UNDERCOOLING EXPERIMENTS IN A MICROGRAVITY ENVIRONMENT

Professor M. C. Flemings and D. M. Matson
Department of Materials Science and Engineering
Massachusetts Institute of Technology
77 Massachusetts Avenue Room 8-407
Cambridge, MA 02139
Phone : (617)253-3233
e-mail : flemings@mit.edu, matson@mit.edu

## Introduction and Objectives :

The central focus of this program is the study of the effect of microgravity on metastable solidification. Research is on how microgravity influences undercooling in metastable solidification and what effect microgravity has on phase selection and on subsequent microstructural evolution. The technical approach selected involves planning for the upcoming Material Science Laboratory (MSL-1) shuttle-based experiment and conducting related ground-based solidification research in collaboration with the NASA Marshall Space Flight Center.

In the ground-based research, we have been employing advanced sensing methods to observe the solidification behavior of the alloys to be studied in space (Fe-Cr-Ni) and of the simpler Fe-Ni and pure Ni systems. Thermal and video imaging is done for dendrite velocities up to 45 meters per second. We are able to observe the progress of the growth front, and its change in morphology at high undercoolings. We can see the metastable-to-stable phase transitions when they occur, and measure relative velocities of the stable and metastable phases as they grow simultaneously into the undercooled melt.

These studies are providing baseline data for interpretation of flight experiments, and also providing new and significant insight into the fundamentals of solidification of undercooled melts. A listing of the publications which have resulted from the current work is included at the end of this report.

Microgravity :

Undercooling in containerless processing has shown promise in producing metastable phases and materials which exhibit improved chemical homogeneity and ultra-fine grain sizes. One aim of this research is to achieve greater undercoolings in microgravity than are possible on earth. Higher undercoolings should result in new metastable phases, finer structures, and perhaps novel properties.

We are also seeking to understand the role of convection in the metastable-to-stable phase transition that has been observed in multi-component alloys, notably in the Fe-Ni and Fe-Cr-Ni alloy systems. The delay time observed in this transformation appears to be dependent on solid movement and coalescence, probably the result of convective flow. Ground-based experiments require maintaining a balance between the levitation force and gravity, while space experiments need far less energy to position the sample. With a reduction in melt convection, we look forward to determining the effect of microgravity on the incubation time. Microgravity is thus and integral requirement for the successful attainment of the goals of this program.

Ground-based experimentation

Samples of pure Ni, binary Fe-Ni, and ternary Fe-Ni-Cr alloys are electrodynamically levitated, induction heated and then subsequently cooled to produce undercoolings up to about 25% of the absolute equilibrium liquid freezing temperature. A schematic of the experimental facility is shown on the left side of Figure 1. External triggering is used in some experiments to fix the

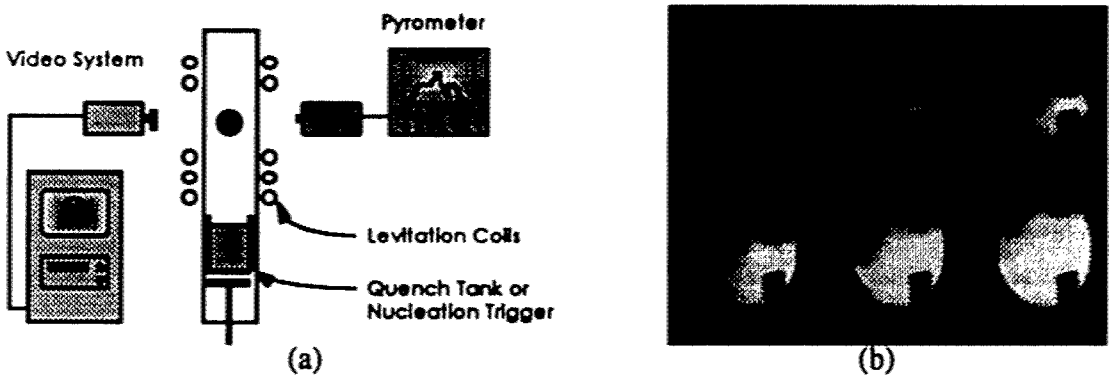


Figure 1 : MIT high speed digital video facility for containerless undercooling studies

(a) Schematic of ground-based equipment
(b) Video record of 150° undercooling with 74 μsec between frames

undercooling and nucleus location. The rapid thermal rise accompanying recalescence has been successfully imaged at sufficiently high spatial resolution (64 x 64 pixels) and temporal resolution (40,500 frames per second) to observe interface shape and motion. Dendrite velocities within the melt were calculated from the surface velocities observed by employing a simple geometric model of growth. A mosaic of high speed digital video images obtained from levitated pure nickel nucleation triggering experiments are shown on the right side of Figure 1 where the growing solid appears lighter than the surrounding undercooled liquid. Growth velocities for both glass-encased and containerless samples of nickel are plotted as a function of undercooling in the first part of Figure 2 and compared to current growth theory.

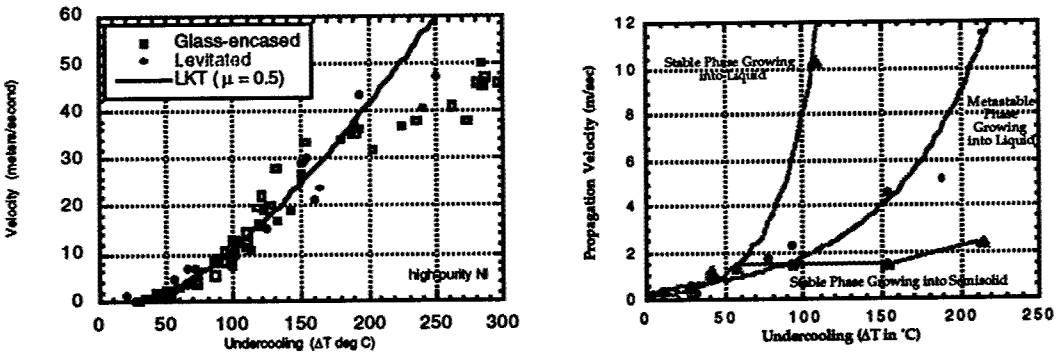


(a) (b)

Figure 2 : Propagation velocity as a function of undercooling

(a) Pure nickel samples using both glass-encased and containerless techniques
(b) Fe-15wt%Cr-15wt%Ni steel flight alloy samples with velocity tracking of simultaneous growth of metastable and stable phases into the undercooled melt and growth of the stable phase into the semisolid formed after primary recalescence

Observations from the video recordings were that, (1) an apparent change in morphology of the growth front from angular to spherical occurred in the range of 150-200 K, and (2) when apparent "multiple" nucleation events are observed, the "new" crystal is crystallographically related to the parent dendrite indicating sub-surface connection. Comparable experiments were conducted on the binary Fe-Ni system over a wide composition range. A similar change in interface morphology is observed in the alloy at comparable undercoolings. Some key questions which remain unanswered are why the growth velocity deviates from theory at higher undercoolings and why the apparent growth morphology changes.

Thermal, video, and subsequent metallography show that in most of the binary and ternary alloys studied, over most undercoolings, the BCC phase is the preferred phase to grow (in absence of external chilling). This is the case even though the FCC phase is thermodynamically preferred. The second part of Figure 2 shows the propagation velocity of the metastable and stable phases for one of the flight alloy systems. Ground-based imaging has also, for the first time, resulted in measurement of the growth of the stable phase into the semi-solid mixture following primary recalescence, as seen in Figure 2.

After a "primary recalescence" and subsequent "incubation time" the metastable phase transforms to the stable phase, usually in a "secondary recalescence". Figure 3 shows this delay as a function of undercooling for several alloys. The left side of the Figure shows the pyrometer traces used to evaluate the incubation time, while the right side shows a plot of this delay time for two hypoeutectic alloys. The delay time between these two recalescence events appears to result because physical movement of the metastable phase is necessary to create favorable sites for heterogeneous nucleation of the stable phase. Melt convection, from gravity and /or applied levitation power in ground-based experiments, is thought to influence this behavior.

In other experiments we find that by external chilling of undercooled samples, the FCC (stable) phase grows preferentially to the metastable phase. We are currently trying to understand this surprising result through experimental modeling studies.

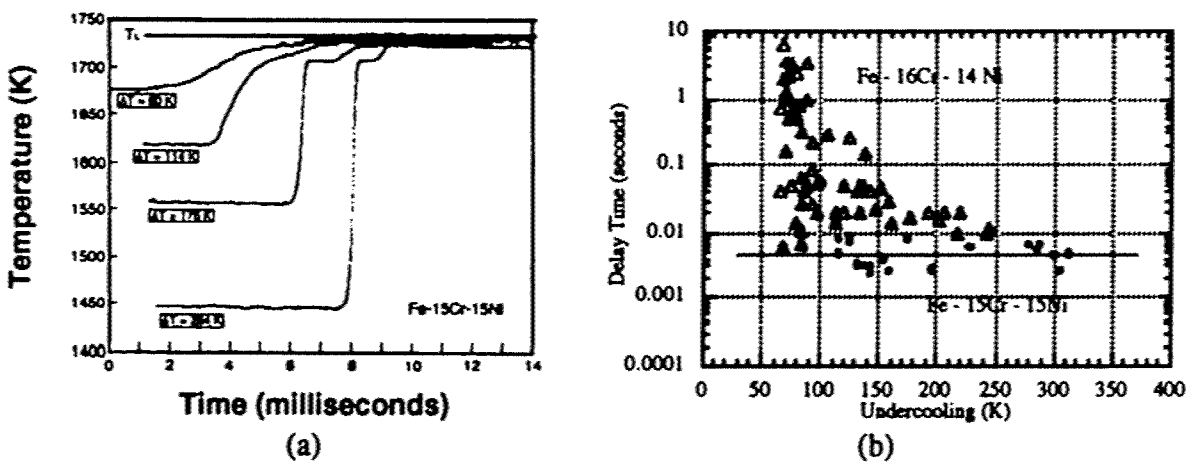


Figure 3 : Incubation time between recalescence events

(a) pyrometer traces for various undercoolings of Fe - 15wt%Cr - 15wt%Ni
(b) delay time as a function of initial undercooling for flight alloys

## Preparations for Flight

We have selected Fe-Cr-Ni steel alloys for flight undercooling experiments. The optimal processing conditions have been identified through ground-based modeling and experimentation to address the two key issues of undercooling in microgravity and the effects of melt convection on subsequent microstructural evolution. Two alloy compositions have been selected for study along the 70 weight percent iron isopleth in the ternary alloy phase diagram; one sample of the commercially important Fe-18.5wt%Cr-11.5wt%Ni alloy and two samples with a composition of Fe-15wt%Cr-15wt%Ni will be flown.

On all alloy compositions the first set of experiments involves attempting to obtain moderate undercoolings and measuring the delay between recalescence events; surface tension and viscosity measurements will also be conducted in collaboration with colleagues of Dr. Julian Szekely of MIT. The second set of tests will employ nucleation stimulation using a physical trigger over a wide range of undercoolings to obtain solidification velocity measurements as a function of undercooling and phase. Two coating configurations will be flown to attempt to select the primary phase which will nucleate. Finally, deep undercooling tests will be run under spontaneous nucleation conditions in an attempt to obtain novel solidification microstructures in microgravity in collaboration with Dr. Wolfgang Löser and Dr. Dieter Herlach. Phase transformation delay analyses will also be conducted as part of this phase of testing.

In-flight data requirements have been successfully developed and submitted with the experiment protocol for the upcoming MSL-1 mission on Columbia utilizing the TEMPUS containerless processing facility. Analysis of both ground-based and microgravity processed samples will continue as part of the post-flight activity in support of the objectives of this program.

## Publications :


[1] M.C. Flemings and T. Koseki, "Solidification of Stainless Steels in Strip Casting," Proceedings of The Ethem T. Turkdogan Symposium Fundamentals and Analysis of New and Emerging Steelmaking Technologies, Iron and Steel Society, 1994, pp. 207-215.

[2] T. Koseki and M.C. Flemings, "Rapid Dendrite Growth During Chill Casting", Proceedings, 2nd Pacific Rim International Conference on Modeling of Casting and Solidification, Sendai, Japan, 1995.

[3] T. Koseki and M.C. Flemings, "Effect of External Heat Extraction on Dendritic Growth into Undercooled Melts", ISIJ International Vol. 35, 1995, pp. 611-618.

[4] T. Koseki and M.C. Flemings, "Solidification of Undercooled Fe-Cr-Ni Alloys: Part I. Thermal Behavior," Metallurgical Transactions, Vol. 26A, 1995, pp. 2991-2999.

[5] T. Koseki and M.C. Flemings, "Solidification of Undercooled Fe-Cr-Ni Alloys: Part II. Microstructural Evolution ", accepted Metallurgical Transactions 1996.

[6] D.M. Matson, A. Shokuhfar, J.W. Lum, and M.C. Flemings, "Imaging the Double-recalescence Behavior of Undercooled Fe-Cr-Ni Alloys using a High-speed Video Technique", Proceedings Int. Symp. on Adv. Mat., 117th JIM Conference, Honolulu, Hawaii, 11-13 December 1995.

[7] J.W. Lum, D.M. Matson, and M.C. Flemings, "High Speed Imaging and Analysis of the Solidification of Undercooled Nickel Melts", accepted Metallurgical Transactions, 1996.

[8] J.W. Lum, "High-speed Imaging and Analysis of the Solidification of Undercooled Alloy Melts", Massachusetts Institute of Technology M.S. Thesis, June 1996.

# THE MEASUREMENT OF THE VISCOSITY AND SURFACE TENSION OF UNDERCOOLED MELTS UNDER MICROGRAVITY CONDITIONS AND SUPPORTING MHD CALCULATIONS

Merton C. Flemings, Gerardo Trapaga, and Robert Hyers
Department of Materials Science and Engineering
Massachusetts Institute of Technology
(617) 253-3233 and (617) 253-3236
flemings@mit.edu, trapaga@navier.mit.edu, rwhyers@mit.edu

## Introduction

The scientific and technical objective of our experiment on the MSL-1 Space Shuttle mission is to utilize the electromagnetic levitation system, TEMPUS, for the experimental determination of the surface tension and viscosity of metallic melts, in both the superheated and the undercooled state, using the unique attributes of microgravity.

The accurate determination of the thermophysical properties of liquid materials is important for a number of reasons, including process modeling, nucleation studies, and, in general, the study of the physics of the liquid state. However, measurement of surface tension and viscosity is very difficult for reactive and undercooled high melting-point materials. A containerless method is required to measure these properties of undercooled liquid metals, since any heterogeneous contact will initiate solidification of these metastable melts. Also, some controversy exists over whether the temperature dependence of the viscosity obeys an Arrhenius-type ( $\mu = \mu_o e^{-\left(\frac{E}{kT}\right)}$ ) or a power law relationship ( $\mu = \mu_o T^{-n}$ ). The ability to extend the measurement of viscosity into the undercooled regime may help to resolve this debate.

The transition to turbulent flow is a critical issue for the measurement of viscosity. It is expected that our ongoing work will help in defining the range of experimental parameters that will allow operation in a non-turbulent or transitional flow regime.

## Background

In an electromagnetic levitation device, a high frequency alternating current is passed through suitably wound coils to generate an electromagnetic field. When a specimen is placed between the coils, eddy currents are induced. These currents heat the sample by Joule heating and interact with the magnetic field to produce a distributed force in the sample (Lorentz force).

A current pulse through the heating coils can be used to deform a levitated sample. The deformed sample would then relax to its original spherical shape ($R_o$) through a series of oscillations. For small deformations, the frequency of oscillations $\omega_n$ of mode $n \geq 2$ is related to the surface tension ($\gamma$) and density ($\rho$) according to the Rayleigh formula: [1]

$$\omega_n = \sqrt{\frac{n(n-1)(n+2)\gamma}{\rho R_o^3}}$$

while the decay modulus of the oscillations ($\tau_n$) is related to the viscosity ($\mu$) according to an expression developed by Lamb:[2]

$$\tau_n = \frac{\rho R_o^2}{(n-1)(2n+1)\mu}$$

The Rayleigh equation has been used extensively for measuring the surface tension of a variety of melts, although some problems were encountered because the molten droplets were not spherical due to the effect of gravity.

An equation has been proposed by Cummings and Blackburn: [3]

$$\omega_R^2 = \frac{1}{5}\left(\omega_{n=2,m=0}^2 + 2\omega_{n=2,m=\pm1}^2 + 2\omega_{n=2,m=\pm2}^2\right) - 2\omega_T^2$$

to correct for gravitational and magnetic effects on surface tension measurements, but the validity of this correction had not been tested until the previous IML-2 mission. Here, $\omega_R$ is the effective Rayleigh frequency, and $\omega_T$ is the frequency of the sample's translational motion.

Samples for the experiments in MSL-1 were selected to cover a wide range of melting temperatures, densities and viscosities. An important part of our objective for this flight is to map out the range of operating conditions and materials properties to which this technique is applicable. The experiments will be performed on 7- and 8-mm diameter samples. The sample materials will include Au and AuCu samples for comparison to results obtained during IML-2 and PdSi which is known for its high viscosity at the melting point. In addition and as part of collaboration with other PI's, we will perform these measurements on Zr, Fe-Cr-Ni alloys, and zirconium-based glass forming alloys.

## Necessity of Microgravity

Ground based experiments introduce an inherent error in the measurement of surface tension. Also, the perfect symmetry of the samples, possible only in microgravity conditions, eliminates the splitting of oscillation modes that is observed in ground-based experiments. Based on purely theoretical grounds, one of the accomplishments of the IML-2 flight was to provide the first experimental results suggesting the validity of the correction factor developed by Cummings and Blackburn, as mentioned above. Surface tension measurements were obtained for gold, gold-copper and zirconium-nickel samples.

The reason for performing measurements of viscosity under microgravity conditions is quite different. Under earthbound conditions, the levitation forces needed are quite high and the associated rotational component of that force (the curl of JxB) gives rise to transitional or turbulent flows, making the measurement of viscosity impossible for normal metals. However, in microgravity, this internal flow velocity may be greatly reduced because much smaller positioning forces (i.e., about 1000 times smaller than under earthbound conditions) are needed to contain the sample. These reduced forces allow a laminar flow condition which will not interfere with the droplet oscillations.

## MHD calculations

The ground-based work for MSL-1 involves extensive calculations to determine to the electromagnetic force fields, the levitation (positioning) forces, the internal circulation in the droplet and the force required to deform the sample. The actual techniques for doing these calculations will be quite similar to those used for the preparation of the IML-2 experiments, which have been fully documented in a number of reports and publications.

More specifically, these calculations involve solving Maxwell's equations to compute the electromagnetic parameters of the system, using software that has been developed by our group at MIT. Using the electromagnetic body force field obtained from the solution of Maxwell's equations, we solve the fluid flow equations (mass and momentum conservation) to obtain the velocity fields in the sample. Finally, we combine the expressions for velocity fields within the specimen with the electromagnetic force field equations in order to describe the deformation of the specimen.

## Turbulence

It should be stressed that to measure the viscosity of a liquid, the internal flow velocity must be kept below a certain value to ensure laminar flow conditions or to prevent a transition to turbulence.

We know that in the laminar regime, the velocity is proportional to the square of the applied coil current, while in the turbulent regime, the velocity is approximately proportional to the coil current.

The accurate prediction of the transition from laminar to transitional (mildly turbulent or chaotic) flow is a new undertaking for this system; however, previous work on analogous systems can indicate the approximate range over which a transition will occur. For example, the secondary flow pattern of flow between two concentric spheres, with the inner rotating and the outer held fixed (see Fig. 1a), shows many of the features of the flow found in TEMPUS (Fig. 1b).

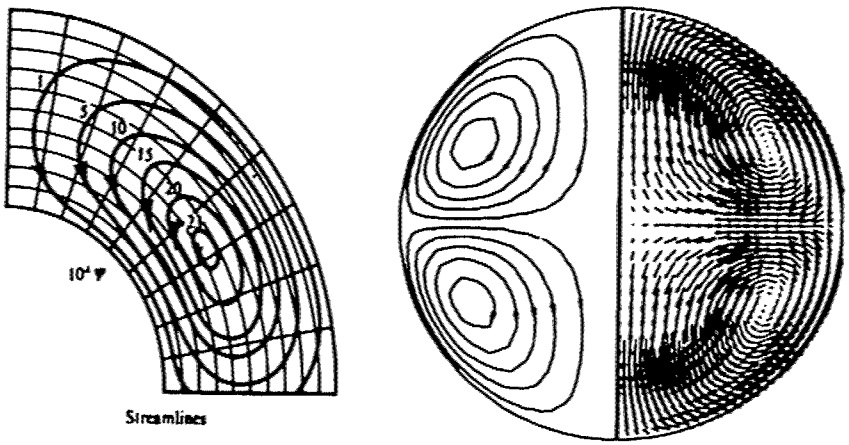


Figure 1: Comparison of pattern of secondary flow between two spheres for Reynolds number = 100 (left) [4, p. 204] with that in TEMPUS [5].

The transition to turbulence for this system was measured by Munson and Menguturk and analyzed by Joseph, et al. [4], with the first indication of enhanced viscosity, i.e. transitional behavior, occurring at a Reynolds number of about 290 (See Fig. 2). By analogy with related systems, one may state that such a transition would be likely to occur in TEMPUS when the Reynolds number, Re, defined as:

$$Re = \frac{uD}{\nu}$$

where u is the fluid velocity, D is the diameter of the circulating loop, and ν is the kinematic viscosity, would exceed about 300.

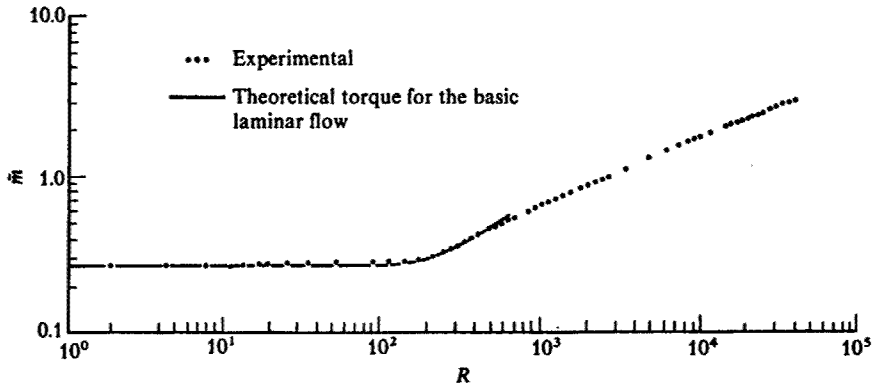


Figure 2: Torque vs. Reynolds Number for concentric spheres.
R is the Reynolds number. [4, p. 212]

In our experiment with a gold sample in the IML-2 mission, the positioning coil control voltage was 5V, and from the damping constant, we obtained a viscosity that was about 13 times the proper atomic value, which would indicate mildly turbulent or transitional behavior.

## Results to Date and Future Plans

Our efforts have consisted largely of a comprehensive program of mathematical modeling designed to give a detailed understanding of what can be expected from the flight experiments. To date, the main goal of the modeling work has been to develop the methodology and to perform calculations predicting the behavior of levitation-melted/electromagnetically-positioned metallic droplets under both earthbound and microgravity conditions. We have developed substantially improved computational techniques which will enable us to predict sample behavior with much greater confidence, allowing the more rational planning of the experiments.

In addition, our research program has involved collaboration with other members of the TEMPUS team in support and preparation for the mission. These activities include participating in the re-design of the IML-2 TEMPUS coil configuration to allow more stable positioning of samples, the May 1995 KC-135 campaign to test and select a coil system from among various candidate designs, and the January 1996 KC-135 campaign to test refinements for the coil system and demonstrate suitability for the MSL-1 mission.

A critical aspect of our current research involves the characterization of the different possible fluid flow regimes that the sample may experience during processing in TEMPUS. The details of the transition from laminar to turbulent flow are not well understood for this type of flow system. However, laminar flow conditions are essential to the accurate measurement of viscosity values. Our principal task in the coming months is to determine with high degree of precision the critical Reynolds number for such a transition.

We are currently using our modeling tools to perform the calculations necessary to design experiments using exotic materials (e.g., glass forming alloys or deep eutectics) for which this transition can be measured with a ground-based levitation technique. Subsequently, we will use our modeling techniques to extrapolate these results to flight sample materials and conditions. These ground-based results will allow us to bracket the transition from laminar flow during our flight experiments, and hence will also allow us to determine the limits of the oscillating droplet technique for measuring viscosity. These results will also provide a better control of the internal fluid flow in the sample. The control of these flows is important for the experiments on statistical nucleation and solidification front velocity.

Finally, we will concentrate on refinement of the data analysis techniques to improve precision and develop appropriate capabilities for real time data analysis during the mission.

## References


[1] J.W.S. Rayleigh, "On the Capillary Phenomena of Jets", Proceedings of the Royal Society of London, 29(1879), 71-97.

[2] H. Lamb, "On the oscillations of a Viscous Liquid Globe", Proceedings of the London Math. Society, 13(1) (1881), 51-66.

[3] D.L. Cummings and D.A. Blackburn, "Oscillations of magnetically levitated aspherical droplets", Journal of Fluid Mechanics, 224 (1991) 395-416.

[4] Joseph, Daniel D., Stability of Fluid Motions I, Springer-Verlag, New York: 1976. p. 204.

[5] Zong, J., B. Li, and J. Szekely, *Acta Astronautica*, vol. 26 no 6, 1992. p. 444.

# COMPOUND SEMICONDUCTOR GROWTH IN A LOW-G ENVIRONMENT

Archibald L. Fripp, PI, (804) 864-1503, a.l.fripp@larc.nasa.gov; William J. Debnam; William Rosch, (NRC), NASA Langley Research Center, Hampton, VA 23681; and
Dr. Ranga Narayanan, University of Florida, Gainesville, FL 32611

## Introduction

The primary objective of this series of experiments is to detect the effects the low gravity environment on convective mixing during crystal growth. The properties of an array of devices made from material such as PbSnTe are dependent on the ratio of the elemental components. Compositional uniformity in the resultant crystal is only obtained if the liquid is quiescent during growth.

PbSnTe is amenable to study because it is easily compounded, it has a relatively low vapor pressure, and it is miscible with the same crystal structure for all compositions. There is also existing, though limited, literature on its growth and properties. The nominal starting composition for this work is 20% SnTe and 80% PbTe that produces a bandgap to match the long wavelength atmospheric window.

PbSnTe is also interesting from a purely scientific point of view. It is potentially both solutally and thermally unstable due to the temperature and density gradients present during growth. Density gradients through thermal expansion are imposed in directional solidification because temperature gradients are required to extract heat. Solutal gradients occur in directional solidification of alloys due to segregation at the interface. The gradients vary with both experiment design and inherent materials properties.

In a simplified one dimensional analysis with the growth axis parallel to the gravity vector only one of the two instabilities works at a time. During growth, the temperature in the liquid increases ahead of the interface. Therefore the density due to thermal expansion is decreasing in that direction. However, the phase diagram shows that the lighter SnTe is preferentially rejected at the interface. This causes the liquid density to increase with distance away from the interface.

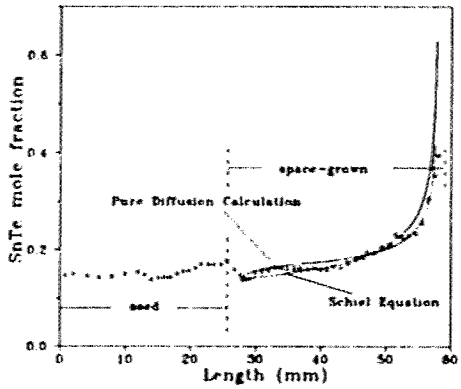


Figure 1. Comparison of Kinoshita's experimental result with the Schiel equation and a pure diffusion calculation.

Coriell et al.[1] have shown that the two opposing density gradients cannot be readily balanced to stabilize the flow. Moreover, both experiments[2,3,4,5] and numerical analyses[5,6] have demonstrated that radial thermal gradients will start fluid motion long before the onset of convection predicted by a one dimensional model. Hence, there will always be convection in the liquid.

The new effort on USMP-4 will grow another set of three crystals, again in the segmented ampoule. It will use the orientation that produced the most favorable growth on USMP-3. The variable, this time, will be ampoule translation rate. The growth rate, which is related to the translation rate, is a key growth parameter under control of the experimenter. Higher growth rates produce steeper solutal gradients but less penetration of this vital diffusion zone into the convecting fluid flow. Thus, the growth rate presents a dichotomy of effects; a high growth rate produces a steeper concentration gradient while a low growth rate allows the diffusion tail to extend into the thermal convection cells.

Lead tin telluride was also grown on Space Lab "J" by Kinoshita and Yamada[7]. Due to the inability to accurately predict the extent of melt back in their experiment, their seed was over 40% of the total length of the crystal. This subsequently reduced the growth length to a point where it is difficult to determine the effect of convection by looking at the resulting compositional profile. Figure 1 shows Kinoshita's data with our calculations for the two extremes of mixing in the liquid and illustrates the difficulty in seeing the difference between diffusion controlled and convection controlled crystal growth for this particular case.

## Experimental

The USMP-3 AADSF experiment used a single segmented ampoule to grow three separate PbSnTe crystals in series. The ampoule, represented in figure 2, allows each of the three crystals to grow with different conditions without affecting the outcome of the others. For USMP-3, each

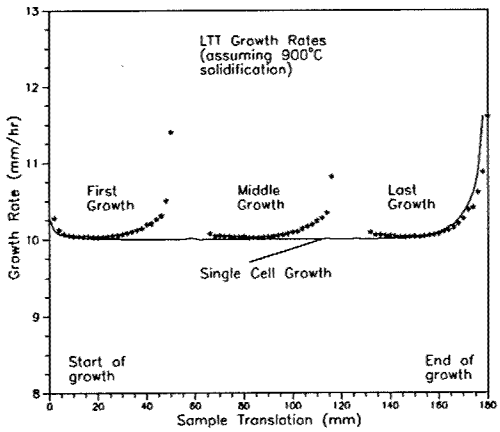


Figure 3. Growth rate comparison for an ampoule with a single long cell, and a segmented ampoule with three cells. The calculations used the properties of lead tin telluride, and assumed a 900 degree solidification temperature.

Figure 3 shows the calculated growth rates and interface shapes for PbSnTe crystals grown in both the one cell and three cell configurations. As a rough approximation of diffusion controlled growth, the growth rates and interface shapes were calculated assuming a constant composition and melt temperature of 900°C. The figure shows that the growth rate is very similar in each of the three cells for the same growth conditions. If the USMP-3 experiment were completed by stopping and starting growth of a single longer crystal, the growth conditions for each orientation would not be equivalent. The interface shapes, growth rates, and melt composition would all be different.

Ground based research efforts have been manifold and intensive yet all of the factors necessary for complete knowledge to design the flight experiment are still not crystal was grown identically except for the orientation of the ampoule with respect to the residual gravity vector. This cell design keeps the composition for the three different regions separated, such that each crystal will have identical starting compositions. Each cell is long enough to reach steady state before the liquid diffusion tail reaches the end of the ampoule.

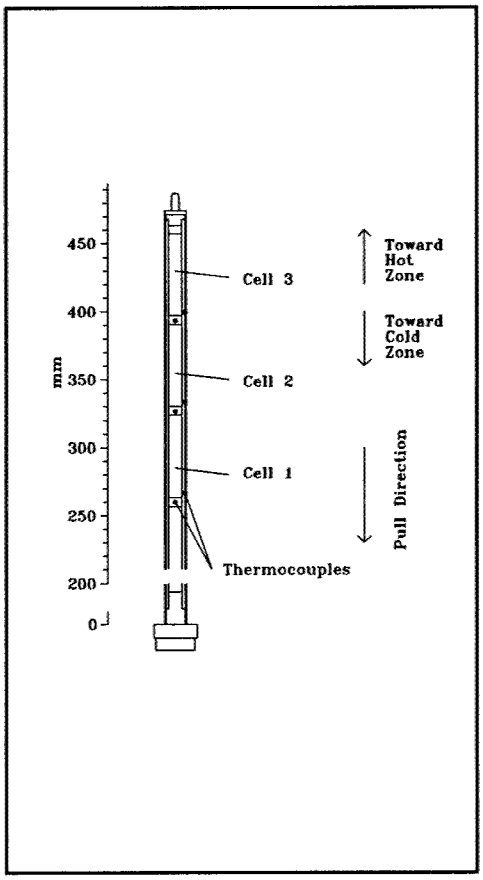


Figure 2. A typical segmented ampoule showing the three cells, and the location of the sample thermocouples. Growth is initiated by inserting the three cells into the hot zone and then slowly translating the sample into the cold zone.

known. The earliest efforts were in setting baseline crystal growth[8,9,10,11,12] parameters and measuring thermophysical properties[13,13,14]. Subsequent efforts were on furnace characterization,[15,16] development of melt-solid interface measurement techniques,[17,18,19] and measurements thereof.[20, 39,20] Other ground based efforts have been in measurements of both steady[22,23] and periodic[21,22] fluid flow.

Numerical modeling has been part of this effort from the beginning[23,24] and will continue to be so. To help extend from simple models to actual crystal growth systems, a heat transfer measurement device[25, 26] has been designed and used to measure ampoule/furnace interactions.

In the USMP-4 experiment the dichotomy of the effects of growth rate are investigated. High growth rates create steep concentration gradients, which exacerbates convection. With low growth rates, the lower concentration gradients extend the diffusion tail away from the quiescent boundary layer near the interface and into the thermal convection streamlines. Hence low growth rates will not only allow more time for mixing per unit length of crystal growth but also expose more of the diffusion tail to the thermally induced convection cells. The bounds of potential growth rates are determined by the crystal length to compositional steady state on the slow end and the need to maintain interfacial stability on the high end.

## Concluding remarks

We have a program to study of the effect of gravitational body force on the convective properties of alloy compound crystal growth as modified by both reduced gravity and the translation rate. Our material clearly illustrates these effects.

We are investigating the growth properties as functions of both gravity orientation and growth rate. We have both a strong experimental program and a strong supporting numerical analysis program.

This work and the work in an accompanying effort featuring magnetohydodynamic damping in the melt will complete the set of experiments on this exciting material.

## References


1. S.R. Coriell, M.R. Cordes, W.J. Boettinger and R.F. Sekerka; "Convective and Interfacial Instabilities During Unidirectional Solidification of a Binary Alloy"; J Crystal Growth, vol 49 (1980) p 13.

2. J.H. Hurst, "Electrochemical Visualization of Convection in Liquid Metals", PhD. Dissertation, The University of Florida, Chemical Engineering, (1990).

3. B. Sears, R. Narayanan, T.J. Anderson and A.L. Fripp, "Convection of Tin in a Bridgman System I. Flow Characterization by Effective Diffusivity Measurements"; J. Crystal Growth, vol 125 (1992) p 404.

4. B. Sears, A.L. Fripp, W.J. Debnam, G.A. Woodell, T.J. Anderson and R. Narayanan, "Convection of Tin in a Bridgman System II. An Electrochemical Method for Detecting Flow Regimes"; J. Crystal Growth, vol 125 (1992) p 415.

5. B. Sears, T.J. Anderson, R. Narayanan and A.L. Fripp, "The Detection of Solutal Convection During Electrochemical Measurement of the Oxygen Diffusivity in Liquid Tin"; Metallurgical Transactions B, vol 24B (1993) p 91.

6. F.M. Carlson, A.L. Fripp, and R.K. Crouch; "Thermal Convection During Bridgman Crystal Growth", J. Crystal Growth, 1984, vol 68, p. 747.

7. K. Kinoshita and T. Yamada; "PbSnTe Crystal Growth in Space," J Crystal Growth, vol 147 (1995) p 91.

8. Fripp, A.L.; Crouch, R.K.; Debnam, W.J.; and Clark, I.O.: Growth of PbSnTe: Earth Options and Space Opportunities. J. Electrochem. Soc. 127, 1980, p 17C.

9. Crouch, R.; Fripp, A.L..; Debnam, W.; and Clark, I.: The Role of Thermophysics in the Design, Optimization and Understanding of Semiconductor Crystal Growth in Space. Presented at the AIAA 14th Thermophysical Conference, Orlando, FL, June 1979.

10. Crouch, R.K.; Fripp, A.L.; Debnam, W.J.; Clark, I.O.; and Barber, P.: Experimental Investigation of the Effects of Gravity on Thermosolutal Convection and Compositional Homogeneity in Bridgman Grown, Compound Semiconductors, Acta Astronautica, 1985, vol. 12, p. 923.

11. Crouch, R.K.; Fripp, A.L.; Debnam, W.J.; Clark, I.O.; and Carlson, F.M.: Optimization Studies for the Growth of PbSnTe in Space, Advances in Ceramics, ed. Ed. B. Dunbar, vol. 5, 1983.

12. Fripp, A.L.; Crouch, R.K.: Compositional Control Required in Alloy Semiconductors Used in High Performance IR Detector Arrays. J. Infrared Phys. 19, 1979, p. 701.

13. R.K. Crouch, A.L. Fripp, W.J. Debnam: " Thermophysical Properties of Ge for Thermal Analysis of Growth from the Melt"; Materials Processing in the Reduced Gravity Environment of Space, Ed. G.E. Rindone, Elsevier Science Publishing Co., NY, 1982, p 657.

14. A.L. Fripp, R.K. Crouch, W.J. Debnam, I.O. Clark and J.B. Wagner: "Effects of Supercooling in the Initial Solidification of PbTe-SnTe Solid Solutions", J. Crystal Growth, 1985, vol.73, p 304.

15. T.I. Ejim, W.A. Jesser, and A.L. Fripp; "Solidification Behavior of Low and High Thermal Conductivity Materials in a Bridgman-Stockbarger Furnace", J. Crystal Growth, 1984, vol 69, p 509.

16. A.L. Fripp, W.J. Debnam, G.A. Woodell, and S. Sorokach; "Temperature Profiles in High Gradient Furnaces";[16161a] Proceedings of the Second Noncontact Temperature Measurement Workshop; January 17-19, 1989; Page 11; Pasadena, Ca. R.R. Hale, editor.

17. P. Barber, R.K. Crouch, A.L. Fripp, W.J. Debnam, R.F. Berry, and R. Simchick; "A Procedure to Visualize the Melt-Solid Interface in Bridgman Grown Crystals", J. Crystal Growth, 1986, vol. 74, p 228.

18. P.J. Barber, R.F. Berry, W.J. Debnam, A.L. Fripp, Y. Huang, K. Stacy and R.T. Simchick; "Modeling Melt-Solid Interfaces in Bridgman Growth"; J. Crystal Growth, vol. 97, pp.672-674 (1989).

19. P.G. Barber, A.L. Fripp, W.J. Debnam: "The Development of Procedures for the Direct Observation of the Location and Shape of the Melt-Solid Interface in the Bridgman Growth of Semiconductors"; J. Crystal Growth, vol. 104, p 315 (1990).

20. A.L. Fripp, W.J. Debnam, R.F. Berry, R.T. Simchick, S.K. Sorokach, D.J. Knuteson, and P.G. Barber; "Mapping of Interface Position and Shape by Non-Invasive Means During Bridgman Growth"; ACCG-8, July 15-20, 1990, Vail, Co.

21. D.J. Knuteson, A.L. Fripp, G. Woodell, W.J. Debnam, and R. Narayanan; "Oscillation Phase Relations in a Bridgman System"; ACCG-8, July 15-20, 1990, Vail, Co. and accepted for publication by J. Crystal Growth.

22. D.J. Knuteson, A.L. Fripp, W.J. Debnam and R. Narayanan;"Unsteady Convection in Tin in a Bridgman Configuration"; J. Crystal Growth, vol 110 )1991) p 348.

23. A. Nadarajah, and R. Narayanan; "Comparison between Morphological and Rayleigh- Marangoni Instabilities", in Dissipative Structures in Transport processes and Combustion edited by D.Meinkoehn and H. Haken, Springer Verlag series in Synergetics, 48, (1990), pp 215-228

24. F.M. Carlson, P-Y. Chin, A.L. Fripp, and R.K. Crouch; "Finite Element Analysis of the Effect of a Non-Planar Solid-Liquid Interface on the Lateral Solute Segregation During Unidirectional Solidification"; Materials Processing in the Reduced Gravity Environment of Space, eds., G. E. Rindone, Elsevier Science Publishing Co., NY, 1982, p. 629.

25. W. Rosch, W.A. Jesser, W. Debnam, A. Fripp, G. Woodell and T.K Pendergrass,"A Technique for Measuring the Heat Transfer Coefficient Inside a Bridgman Furnace", J. Crystal Growth; vol 128, pp 1187, 1993.

26. W. Rosch, A.L. Fripp, W.J. Debnam and T.K. Pendergrass, "Heat Transfer Measurements in the Bridgman Configuration"; J. Crystal Growth, vol 137 (1994) p 54.

# MELT STABILIZATION OF PbSnTe IN A MAGNETIC FIELD

Archibald L. Fripp, PI, (804) 864-1503, (a.l.fripp@larc.nasa.gov); William J. Debnam; William Rosch, (NRC), NASA Langley Research Center, Hampton, VA 2368, (804) 864-1503;
Arnon Chait, Lewis Research Center, Cleveland, OH 44135, (216)433-3558;
Minwu Yao, Ohio Aerospace Institute, Brook Park, OH 44142, (216)962-3094; and
Frank R. Szofran, Marshall Space Flight Center, Huntsville, AL 35812, (205) 544-7777

## OBJECTIVE

The objective of this research is to further elucidate gravity driven physical phenomena on the growth of the alloy compound semiconductor, PbSnTe. This work, coupled with the past microgravity experiment in the MEA and the existing flight program to grow PbSnTe in the AADSF, is the most comprehensive set of space processing experiments performed to date.

PbSnTe is a semiconductor material with a compositional dependent energy bandgap which is adjustable from 0 ev (≈40% SnTe) to 6.4ev (100% PbTe). It has a direct bandgap hence it can be used for both infrared lasers and detectors. The utilization of this and other materials in this general class is dependent on both the crystalline perfection of the material and the compositional homogeneity[1].

During crystal growth, temperature and concentration gradients often induce natural convection. It has been shown both experimentally and numerically that the flow mode, the solid/ liquid interface shape, and solute profiles in a solidifying liquid are greatly affected by natural convection. The variation of convective strength has a direct impact on solute distribution (segregation). The distortion of the interface, in turn, affects convection. Thus a complex interaction exists among convection, thermal solutal gradients and interface shape.

The PbSnTe melt has strong convective driving forces during the growth process. The thermal coefficient of expansion, $\beta_T$, and the solutal coefficient of expansion, $\beta_S$, have opposite signs with respect to distance in front of the interface. These expansion coefficients contribute to convection through the thermal and solutal Raleigh numbers.

It is well known that direct, quantitative analysis of convection solute segregation in molten metals and semiconductors is particularly difficult. These materials are generally opaque, which hinders non-intrusive measurements. Thus, most studies are limited to indirect measurement techniques. The role of numerical modeling then becomes crucial in analyzing the system. A better understanding of the complex phenomena in the solidification process can be achieved through synergistic theoretical and numerical analysis[2,3] in combination with various solidification experiments on earth and in space.

Numerical modeling helps predict the optimum growth conditions for both Earth and space based experiments. The combined behavior of the fluid, thermal, and solutal fields in the melt during space processing can be, in principle, modeled using a fully numerical 3D, time-dependent code. However, only representative portions of the experiment will be simulated due to the complexity of the double-diffusive convection of this experiment.

The application of magnetic fields in this proposal represents an additional challenge to the modeling efforts. The experience of others and by the proposers in simulations of magnetic field interactions with flows in conductive melts have shown that the present knowledge is sufficient for the estimation of the desired fields needed to achieve certain reduction in the flow intensity.

Approach:

This investigation uses a three prong approach. PbSnTe (20% SnTe) is grown on Earth in the superconductor magnetic furnace at MSFC and in Space in a magnetically damped furnace. The investigation also makes copious use of numerical modeling throughout both the Earth and Space experimental portions of the research.

The fundamentals of mhd[4,5] are a relatively simple marriage of Maxwell's equations and fluid dynamics. The movement, **V**, of an electrically conductive media in a stationary, to the lab frame, magnetic field, **B**, will produce an electric field, **E**= -**V**x**B**. The non uniformity of the flow will naturally produce a non uniform electric field hence an electric current, **J**, will flow and it will be subjected to a Lorentz force, **F**= **J**x**B**, from the same magnetic field that produced its driving force. This new force which is related

to the fluid motion acts as an additional viscosity term and is appropriately called magnetic viscosity. The relative effect of this magnetic viscosity is characterized by the Hartmann number.

Application of this simple theory is complicated by the complex boundary conditions and the non linear aspects of the magnetic field acting on both the current and the force term, consequentially both experimental efforts and numerical analysis are required to understand and utilize the phenomena.

Numerical simulations are an integral part of this study, but not in its traditional sense as an independent study encompassing some, but commonly not all, of the relevant experimental conditions. The direction of the modeling effort is toward the practical rather than theoretical aspects. A key purpose is to optimize the growth for the space experiment. Another major effort will be estimating of the required magnetic field strength in space.

Experiment

The Earth based experiments are relatively straight forward. Crystals are grown in a magnetic field. After growth they are evaluated for compositional uniformity and defect structure. The experimental parameters are ampoule dimensions, temperature gradient, and magnetic field strength and orientation. The solutal driving force can be varied by both changing the growth rate, the temperature gradient, ampoule size, and by changing the starting ratio of SnTe to PbTe. Numerical analysis helps select the experimental matrix.

Experimental results to date of 1 cm diameter crysals grown in a 80 C/cm thermal gradient with growth rate as a parameter are indistingusible from the totally mixed results obtained without magnetic fields, even with the 5T field. This result, for these conditions, was predicted by our numerical analysis.

The flight experiment will simulate that of the AADSF experiment but with the addition of the stabilizing magnetic field. Depending on further study, a specific Shuttle attitude may be requested for growth such that the crystal is grown with the ampoule axis aligned with the steady state gravity vector.

Numerical analysis

The primary objectives of the numerical analysis portion of this proposal are to provide a quantitative understanding of the complex transport phenomena during solidification of non-dilute binarys (such as PbSnTe), to furnish a numerical tool for furnace design and growth condition optimization, to provide estimates of the required magnetic field strength for low gravity growth, and to assess the role of magnetic damping for space and earth control of the double-diffusive convection. The modeling and solution procedure established previously will be largely retained and refined as the work continues.

In vertical Bridgman growth, the furnace is aligned parallel to the gravity vector. This arrangement results in a great simplification for numerical treatment. The flow and both the thermal and solutal fields are assumed to be axi-symmetric for low convection levels and axi-symmetric boundary conditions. At higher convection levels the flow may form one or more torus-like cells. At 1-g level, the magnitude of the convective flow may be very high, resulting in time-dependent or even turbulent flows which requires transient 3-D analysis.[6,7]

In the solidification process, the solute concentration at the interface is affected by the removal rate of excess solute rejected at the moving interface. Under ideal conditions (no convection), the rejected solute is transported by diffusion only. In reality, the transport of excess solute to and from the interface is greatly affected by additional factors such as the natural convection. In this study we consider buoyancy forces induced by both thermal and solutal expansions. For PbSnTe, it is important to note that the magnitude of $\beta_c\Delta T$ & $\beta_S\Delta C$ are globally of the same order and a positive change of $\Delta T$ & $\Delta C$ will reduce the density in the buoyancy term in the momentum equation. The segregation coefficient, $k<1$, and $\rho_{solute} < \rho_{solvent}$ imply that lighter solute is rejected at the interface. Consequently, the double-diffusive convection is solutally unstable in a classical vertical growth system.

Previous studies reported in the literature, e.g. the pioneering magnetic interaction studies by Kim, Adornato, and Brown[8] consider the thermal volumetric expansion only. However, for non-dilute alloys our results show that the effect of the solutal volumetric expansion is important and should not be neglected. Furthermore, the non-trivial interaction between the thermal and the solutal fields and their

coupled effects on the flow field in the melt through the buoyancy force term intricately depend on the magnitude and orientation of the gravity vector.

During shuttle flight in space, however, the magnitude and orientation of the gravity vector are generally unsteady functions of time. Consequently, the complete flow structure and segregation fields in the solidifying liquid during space growth are still theoretically unknown.

The application of a steady-state magnetic field offers a practical means of suppressing natural convection due to both the steady and unsteady changes in the residual acceleration. When an axial magnetic field is imposed, its effect on the convection in the melt is to interfere with the radial velocity component. As shown by asymptotic analysis,[8] the magnitude of the radial velocity decreases proportionally to the square of, the strength of the magnetic field. When the field is large enough, an almost uniaxial flow and hence the desired diffusion-dominant growth condition, may be obtained. Our numerical results suggest that magnetic damping on the convective flow in the melt is effective for micro-gravity crystal growth.

In our models we solve the coupled momentum, energy, and mass transport equations with the Boussinesq approximation applied to the temperature and concentration buoyancy terms. The influence of the magnetic field on the flow is expressed through the Lorentz force. The phase change on the solid-melt interface is determined from the phase diagram. The interface position is simultaneously solved using the front tracking approach. The furnace temperature profile is imposed through a radiative flux on the outer surface of the cartridge, details of which were determined from previous experimental data.

## Concluding remarks

This is a study of the effect of gravitional body force on the convective properties of alloy compound crystal growth as modified by both reduced gravity and by magnetohydrodynamic damping. This material will clearly demonstrate these effects.

We are investigating the growth properties as a function of both gravity and magnetic field. We have both a strong experimental program and a strong supporting numerical analysis program. This work

will complete the set of experiments. It will compare the effects of convection, as modified by a magnetic field, on the growth of this material both on Earth and in the Microgravity environment found in low Earth orbit.

## References


1. A.L. Fripp and R.K. Crouch; "Compositional Control Required in Alloy Semiconductors Used in High Performance IR Detector Arrays"; J. Infrared Phys., vol. 19, p 701 (1979).

2. M. Yao and H.C.de Groh III, "Three-Dimensional Finite Element Method Simulation of Bridgman Crystal Growth and Comparison with Experiments", Num. Heat Transf., Part A , vol. 24, pp.393-412 (1993).

3. M. Yao, R. Raman and H.C. de Groh III, "Numerical Modeling of Bridgman Growth in Space with MEPHISTO", Proceedings of Int. Conf. on Computational Eng. Science , 7/30-8/3, 1995, Mauna Lani, Big Island, Hawaii.

4. S. Chandrasekhar; Hydrodynamic and Hydromagnetic Stability; Dover ublications, New York, 1961.

5. J.D. Jackson; Classical Electrodynamics; John Wiley, New York; 1962.

6. D.J. Knuteson, A.L. Fripp, G.A. Woodell, W.J. Debnam and R. Narayanan, "Oscillation Phase Relations in a Bridgman System", J. Crystal Growth , vol. 109, p. 127 (1991).

7. D.J. Knuteson, A.L. Fripp, G.A. Woodell, W.J. Debnam and R. Narayanan, "Unsteady Convection in Tin in a Bridgman Configuration", J. Crystal Growth , vol. 110 p. 348 (1991).

8. D.H. Kim, P.M. Adornato and R.A. Brown; "Effect of Vertical Magnetic Field on Convection and Segregation in Vertical Bridgman Crystal Growth"; J. Crystal Growth, vol. 89, p 339 (1988).

# THE GRAVITATIONAL ROLE IN LIQUID PHASE SINTERING

Randall M. German and Ronald G. Iacocca
Engineering Science and Mechanics Department
The Pennsylvania State University
P/M Lab, 118 Research West
University Park, PA 16802-6809

telephone 814-863-8025 or 814-863-8208 and e-mail rmg4@psu.edu or rgi1@psu.edu

## Introduction

Liquid phase sintering (LPS) is a common process for the fabrication of high-performance, net-shape structures. Despite extensive industrial use, several processing difficulties trace to gravity. One easily recognized problem is solid-liquid separation. Like sand settling in water, differences in densities between the solid and liquid phases induce segregation. Consequently, only compositions with small quantities of liquid are fabricated on Earth. The tungsten heavy alloys (W-Ni-Fe or W-Ni-Cu compositions) are particularly sensitive to gravitational effects since the liquid-solid density difference is nearly 9 g/cm$^3$. After sintering on Earth, there is a significant gradient in grain coordination number, grain size, grain shape, and solid phase contiguity with the position in the compact. Grain coalescence occurs at gravity induced contacts, giving gradients from the stress in the microstructure due to gravity that affects the sintered grain size.

Gravity effects are evident at the macroscale as compact distortion. An excess of liquid causes shape loss, with the formation of an "elephant foot" geometry or even puddles of solid-liquid. The factors causing distortion in LPS are not understood. Previous work suggested that it was simply due to the solid-liquid ratio; however, experiments have produced compacts with more than 80 vol.% liquid that retain shape. Compositions that slump on Earth also distorted in microgravity,

but in the latter case they spheroidized. The model arising from these experiments considers three features - solid-liquid ratio, dihedral angle, and solid solubility change in the second phase when it turns liquid.

Our research uses microgravity to isolate gravitational effects on microstructure evolution during liquid phase sintering. The contrast and comparison of ground-based and microgravity samples, processed from the same powders, in the same furnace, using the same cycles provided the needed separation of variables. Modeling efforts conducted in parallel with the experiments provide a basis for assessing current understanding. The initial phase of the microgravity research focused on variations in sintering time and solid content using W-Ni-Fe compositions with a constant Ni:Fe ratio of 7:3, but varying W content from 78 to 98%. A critical parameter is the solid-liquid dihedral angle. Initially, the dihedral angle was adjusted by changing the sintering temperature using W-Ni-Fe alloys. However, we plan to gain more insight by changing the solid solubility in the liquid in the W-Ni-Cu system. This allows simultaneous control of dihedral angle, solubility, solid-liquid ratio, and sintering time.

## Science Objectives

Much research has occurred as part of this study and selected citations are given at the end of this document. Because of the large body of previously published work, this document can only hint at the range of findings. At the macroscopic level is concern for understanding distortion in liquid phase sintering. Various solid-liquid ratios were generated by changing the tungsten content from 78 to 98 wt.% with a constant 7:3 Ni:Fe ratio. Distortion was quantified using dimensional variation. Compacts that distort on Earth show spheroidization in microgravity. In microgravity, constraint by the specimen crucible limited reshaping during LPS, resulting in a "belly-band" on the diameter of the high liquid content samples. Thus, the fundamental distortion parameters are the same - conditions that destroy structural rigidity on Earth and lead to gravity induced distortion act in microgravity to allow surface tension forces to reshape the compact. Our research has quantified the slumping behavior versus LPS parameters and traced this to a few key microstructural parameters - solid content, dihedral

angle, and grain size. A viscous flow distortion model accurately predicts the component shape change during LPS. The relationship between connectivity and rigidity depends on bonding between the grains. A model from this research links the formation of a rigid skeleton to the dihedral angle. Experiments with W-Ni-Cu compositions will provide the critical tests to isolate the relations between solid content and dihedral angle leading to distortion.

As a second concern, gravity induces separation of solid and liquid if there are density differences during LPS. In W-Ni-Fe heavy alloys sintered on Earth, the compact bottom has a higher solid volume fraction, a higher contiguity, and a larger grain size. The gradient in solid phase structure is evident as a progressive increase in solid content and grain size with depth from the top surface. The higher solid content at the compact bottom accelerates grain growth. Disagreement exists on the limiting solid content in a freely settled solid region. Parallel experiments using model monosized particles show a cascade of particle density in the settled region that corresponds with observations on hard spheres. The premise from prior work that grains would remain dispersed in microgravity has proven false. Agglomeration occurs to form high solid content regions due to underlying solid-solid sintering, with grain contact caused by Brownian motion.

A major goal is to isolate gravity effects on microstructure coarsening during LPS. Based on experiments with dilute tungsten heavy alloys (50 wt.% W), microgravity samples, and ground-based samples, modifications to coarsening theories have been formulated to predict grain growth during LPS. The formulation accounts for the solid volume fraction effect, and includes gravity induced stress, coalescence, and liquid-solid segregation. The LPS study needs to vary the dihedral angle to change the grain contact area. This was proposed using sintering temperature variation. With a high dihedral angle, the increase in contiguity should reduce the solid-liquid interfacial area and slow diffusional growth. Alternatively, coalescence contributions should increase with a higher dihedral angle in the W-Ni-Cu system. Here solubility will be used to adjust dihedral angle over a wide range without requiring different sintering temperatures.

Beyond the envisioned macroscopic evolution and microscopic coarsening goals, new observations have arisen from the microgravity LPS experiments. These include a revisit to

the derivation of Young's equation based on new pore-liquid-solid equilibrium geometries. Another feature previously reported and observed in the microgravity samples is the emergence of a stable pore structure. This causes concern that basic models of densification in LPS might be incorrect and that previous suggestions of a buoyancy contribution are correct. Pore structure stability is a puzzling aspect of the microgravity. Accordingly, new ideas on densification, pore elimination, and solid settling in dilute solid content samples are embedded in the reflight experiments.

## Research Highlights

The research on the gravitational role during liquid phase sintering has resulted in a significant body of new findings:

- A universal grain size distribution for LPS materials has been isolated and described mathematically, and this distribution agrees with recent independent findings.
- The liquid volume fraction has been linked to the grain growth rate constant and solid-liquid density difference for LPS materials, giving the first LPS coarsening law.
- A model has been created for slumping and distortion during LPS. This model describes the role of gravity, component size, substrate friction, and surface tension on reshaping.
- Grain agglomeration has been predicted and observed in dilute solid content LPS systems and may be applicable to many situations.
- Based on pore stabilities in the microgravity samples, we have revisited the derivation of Young's equation and a missing gravity term.
- Coalescence has been documented in a zero dihedral angle LPS system to prove Ostwald ripening theories are incorrect in ignoring grain rotation as part of coalescence.
- Early evidence shows a nonrandom radial distribution in the grain size of LPS alloys.

- The settled region of Earth-based LPS samples has been analyzed for versus the solid-liquid density difference and included in a model for settled solid regions.
- A new generalized grain coordination number versus effective pressure model has emerged that is applicable to loosely packed particles.
- Pore structure observations in microgravity LPS samples show a high stability, suggesting a buoyancy contribution to pore elimination on Earth.

## Key Publications

C. M. Kipphut, A. Bose, S. Farooq and R. M. German, "Gravity and Configurational Energy Induced Microstructural Changes in Liquid Phase Sintering," *Metallurgical Transactions,* 1988, vol. 19A, pp. 1905-1913.

S. C. Yang and R. M. German, "Gravitational Limit of Particle Volume Fraction in Liquid Phase Sintering," *Metallurgical Transactions,* 1991, vol. 22A, pp. 786-791.

S. C. Yang and R. M. German, "Generic Grain Size Distribution for Liquid Phase Sintering," *Scripta Metallurgica et Materialia,* 1992, vol. 26, pp. 95-98.

R. M. German, A. Bose and S. S. Mani, "Sintering Time and Atmosphere Influences on the Microstructure and Mechanical Properties of Tungsten Heavy Alloys," *Metallurgical Transactions,* 1992, vol. 23A, pp. 211-219.

R. Raman and R. M. German, "A Mathematical Model for Gravity-Induced Distortion During Liquid Phase Sintering," *Metallurgical and Materials Transactions,* 1995, vol. 26A, pp. 653-659.

Y. Liu, D. F. Heaney and R. M. German, "Gravitational Effects on Solid Grain Packing in Liquid Phase Sintering," *Tungsten and Refractory Metals,* A. Bose and R. Dowding (eds.), Metal Powder Industries Federation, Princeton, NJ, 1995, pp. 121-128.

Liu, D. F. Heaney and R. M. German, "Gravity Induced Solid Grain Packing During Liquid

Phase Sintering," *Acta Metallurgica et Materialia,* 1995, vol. 43, pp. 1587-1592.

R. M. German, R. G. Iacocca, J. L. Johnson, Y. Liu and A. Upadhyaya, "Liquid-Phase Sintering Under Microgravity Conditions," *Journal of Metals,* 1995, vol. 47, no. 8, pp. 46-48.

Y. Liu, R. Iacocca, J. L. Johnson, R. M. German and S. Kohara, "Microstructural Anomalies in a W-Ni Alloy Liquid Phase Sintered under Microgravity Conditions," *Metallurgical and Materials Transactions,* 1995, vol. 26A, pp. 2485-2486.

D. F. Heaney, R. M. German and I. S. Ahn, "The Gravitational Effects on Low Solid-Volume Fraction Liquid-Phase Sintering," *Journal of Materials Science,* 1995, vol. 30, pp. 5808-5812.

R. M. German, "Grain Agglomeration in Solid-Liquid Mixtures Under Microgravity Conditions," *Metallurgical and Materials Transactions,* 1995, vol. 26B, pp. 649-651.

Y. Liu and R. M. German, "Contact Angle and Solid-Liquid-Vapor Equilibrium," *Acta Materialia,* in press

R. M. German and Y. Liu, "Grain Agglomeration in Liquid Phase Sintering," *Journal of Materials Synthesis and Processing*, 1996, vol. 4, pp. 23-34.

J. L. Johnson and R. M. German, "Solid-State Contributions to Densification During Liquid Phase Sintering," *Metallurgical and Materials Transactions,* 1996, vol. 4, pp. 23-34.

# SOLIDIFICATION OF II-VI COMPOUNDS IN A ROTATING MAGNETIC FIELD

D. C. Gillies, M. P. Volz & K. Mazuruk
ES75, Marshall Space Flight Center
Huntsville
AL, U.S.A.

K. W. Benz
Kristallographisches Institut
Universität Freiburg
Freiburg, Germany

S. Motakef
Cape Inc.
Wellesley
MA, U.S.A.

## Research Objective

The proposed research aims at bringing to maturity a new concept of crystal growth, namely the avoiding of solidification by mass transport through an established diffusion boundary layer by means of a rotating magnetic field (RMF). Microgravity solidification experiments have shown that even small residual accelerations are sufficient to destroy or prevent the formation of such a layer. The effect of a RMF on solidification is to superimpose a controlled stirring effect on the liquid column. By changing the strength and frequency of the field it is possible to affect the characteristics of the stirring and hence obtain controlled convection in the form of secondary flow which enhances mass transport in an axial direction. The technique enables one to achieve a great deal of control of the solidification process; the crystals obtained, especially those grown in low gravity flights have demonstrated exceptional properties. The principal geometries to be studied are zones in which there are constant dimensions and aspect ratios. During growth the thermal field and the composition field will remain essentially constant. Studies of flow in a cell specially emulating a traveling heater method (THM) zone or a float zone (FZ) geometry will be used to test the effect of field strength and frequency on the flow induced by the RMF. In particular the interaction of the field with buoyancy driven flow, and the transition from laminar to turbulent flow will be investigated, both by test cell measurements and by modeling.

Concurrent with the modeling and test cell studies, crystal growth of CdTe, Cd(Zn,Te) and Cd(Te,Se) by FZ and THM, HgCdTe and HgZnTe by THM, and model materials will take place. It is in the II-VI compounds where interface control is most difficult to achieve that RMF will be most valuable. The ground tests and modeling will be used to provide experimental parameters and define long duration low gravity flights.

## Microgravity Relevance

Both the THM and FZ techniques involve temperature profiles which are unstable in a gravitational field; the result is buoyancy driven convection. In 1-g, the RMF can significantly influence the nature of the flow, but the resultant patterns will be complex due to the competing natural convection. Although it is possible that significant benefits might result from using RMF in a 1-g environment and these will be investigated, the full and unmitigated potential can only be fully realized by conducting experiments using this technique in microgravity. A strong data base derived from microgravity grown crystals where the RMF effect can be more easily understood and more directly related to crystal quality will enable better optimization of the technique for future ground based processing. In addition, the float zone technique in low gravity is subject to the effects of surface tension driven convection; the RMF can be tuned to eliminate such a problem. Ground based data acquired from liquid cells operating with a RMF have demonstrated the stirring predicted by models, but the influence from buoyancy driven flow makes the unambiguous influence of the magnetic field difficult to interpret. The construction of a small RMF cell, tailored to fit in a microgravity glove box will be strongly advocated during the program.

## Hypothesis behind Work

In any directional solidification process, the interface and adjacent fluid environment play crucial roles, and affect the properties of the resulting solid. Under ideal conditions with no fluid flow, a quiescent region adjacent to the solid can be established, and mass transfer can take place through a diffusion layer. In practice such a regime is difficult to produce in any but a few systems. This is even true in a microgravity environment where one would expect the buoyancy forces to have only a small effect on the fluid. Even when such a layer can be produced it is vulnerable to changes in residual acceleration vector as caused by periodic variations in the drag component acting on the vehicle. Thus any diffusion layer tends to be extremely fragile, and can be easily contorted or destroyed by gravitational fluctuations as well as any mechanical or thermal changes.

There is also considerable difficulty involved in controlling interface shape. Due to thermal considerations the resulting interface is concave as seen from the melt in the complex alloys such as those listed. This is likely to lead to the nucleation of new crystals from the walls of the container rather than the annihilation of unwanted crystals. Diffusion controlled growth also necessitates the avoidance of constitutional supercooling. In turn this drives the need for high temperature gradients or very slow growth rates. It is anticipated that faster growth rates can be obtained for THM techniques than are normally achieved; this is one of the current drawbacks to the THM method. The proposed work addresses these problems by equalizing the thermal field and thus flattening the interface, and by transporting material through the zone by means of controlled convection.

There is an additional advantage to the RMF in float zone techniques. the RMF enables one to control the surface driven convection by imposing a controlled regime. The skin effect caused by frequency changes of the magnetic field affects the depth of penetration of the induced rotation and enables the establishment of better control of the surface of the zone. Such control makes it possible to grow material superior to that produced by a conventional microgravity float zone technique.

# ISOTHERMAL DENDRITIC GROWTH EXPERIMENT

M.E. Glicksman, M.B. Koss, J.C LaCombe, and L.T. Bushnell
Materials Science and Engineering Department
Rensselaer Polytechnic Institute
Troy, NY 12180-3590
USA
(518)276-6721, (518)276-2844, (518)276-8068, (518)276-6130
glickm@rpi.edu, kossm@rpi.edu, lacomj@rpi.edu, tennel@rpi.edu

D.C. Malarik and E.A. Winsa
Space Experiments Division
NASA Lewis Research Center
Cleveland, OH 44135
USA
(216)433-3203, (216)433-2861
msmala@limspop.lerc.nasa.gov, ewinsa@lims01.lerc.nasa.gov

## Introduction

The growth of dendrites is one of the commonly observed forms of solidification encountered when metals and alloys freeze under low thermal gradients, as occurs in most casting and welding processes. In engineering alloys, the details of the dendritic morphology directly relates to important material responses and properties. Of more generic interest, dendritic growth is also an archetypical problem in morphogenesis, where a complex pattern evolves from simple starting conditions. Thus, the physical understanding and mathematical description of how dendritic patterns emerge during the growth process are of interest to both scientists and engineers [1].

The Isothermal Dendritic Growth Experiment (IDGE) is a basic science experiment designed to measure, for a fundamental test of theory, the kinetics and morphology of dendritic growth without complications induced by gravity-driven convection. The IDGE, a collaboration between Rensselaer Polytechnic Institute, in Troy NY, and NASA's Lewis Research Center (LeRC), in Cleveland OH, was developed over a ten year period from a ground-based research program into a space flight experiment [2,3]. Important to the success of this flight experiment was provision of *in situ* near-real-time teleoperations during the spaceflight experiment [4].

## Background on Dendritic Growth Theory

A number of theories of dendritic crystal growth, based on various transport mechanisms, physical assumptions, and mathematical approximations, have been developed over the last fifty years. These theories attempt to predict a dendrite's tip velocity, $V$, and radius of curvature, $R$, as a function of the

supercooling, $\Delta T$ (see the review by one of the authors [1]). The growth of dendrites in pure melts is known to be controlled by the transport of latent heat from the moving crystal-melt interface as it advances into its supercooled melt. Ivantsov, in 1947, provided the first mathematical solution to the dendritic heat conduction problem [5], and modeled the steady-state dendrite as a paraboloidal body of revolution, growing at a constant velocity, $V$. The resultant thermal conduction field can be expressed exactly in paraboloidal coordinates moving with the dendritic tip. The temperature field solution is known as the Ivantsov, or "diffusion-limited" transport solution. This solution is, however, incomplete, insofar as it only specifies the dendritic tip growth Péclet number, $Pe=VR/2\alpha$, (here Pe is the growth Péclet number, and $\alpha$ is the thermal diffusivity of the molten phase) as a function of the initial supercooling, and not the unique dynamic operating state; $V$ and $R$. The Péclet number obtained from the Ivantsov solution for each supercooling yields instead an *infinite* range of $V$ and $R$ values that satisfy the diffusion-limited solution at that particular value of $\Delta T$.

In the early 70's, succinonitrile (SCN), a BCC organic plastic crystal, was developed as a model metal analog system for studying dendritic growth [6]. SCN solidifies like the cubic metals, i.e., with an atomically "rough" solid-liquid interface, yet retains advantages because SCN displays convenient properties for solidification experiments, such as a low melting temperature, optical transparency, and accurate characterization of its thermophysical properties. The use of SCN greatly facilitated dendritic growth studies over the past twenty years, where because of its use, dendritic tip velocities could be accurately measured and used as a critical test of theory [6,7].

Theoretical efforts have concentrated on trying to discover an additional equation or length scale, which when combined with the Ivantsov conduction solution, "selects" the observed operating states (see references within ref. [1]). Although the underlying physical mechanisms for these "theories of the second length scale" are quite different, their results are invariably expressed through a scaling constant, $\sigma^*=2\alpha d_o/(VR^2)$, where $d_o$ is the capillary length scale, a materials parameter defined from the equilibrium temperature of the crystal-melt interface, the solid-liquid interface energy, and the specific and latent heats. Although some theories predict the value of this scaling constant, in practice the scaling constant is used as an adjustable parameter to describe dendritic growth data in various materials.

Subsequent experiments with SCN showed that gravity-induced convection *dominates* dendritic growth in the lower supercooling range typical of metal alloy castings [8]. Convection, unfortunately confounds any straightforward analysis of dendritic solidification based on conductive heat transfer. There have been a few attempts to estimate the affect of natural or forced convection on dendritic growth [9], but these calculations are themselves based on yet unproven elements of dendritic growth theory, and, consequently, can not provide an independent test of the theory. In the higher supercooling range, where thermal convective influences diminish in comparison to thermal conduction, the morphological scale of dendrites becomes too small to be resolved optically at the high growth speeds encountered. The experimental situation prior to the microgravity experiment reported here, was that there appeared to be too narrow a range of supercoolings in any crystal-melt system studied terrestrially that remains both free of convection effects, and also permits an accurate determination of the dendrite tip radius of curvature.

## The Isothermal Dendritic Growth Experiment

The Isothermal Dendritic Growth Experiment (IDGE) a NASA sponsored series of Space Shuttle microgravity experiments, was designed to grow and photograph dendrites in the absence of convective heat transfer for a fundamental test of dendritic growth theories. The data and subsequent analysis on the dendritic tip growth speed and size from the first flight of the IDGE, in March of 1994 (USMP-2/STS-62), has demonstrated that although the theory can make predictions that are in reasonable agreement with the results of the experiment, there are several important areas of disagreement [10-13]. The details of the IDGE results and analysis can not be contained in the body of this short report. Rather, this report serves an annotated bibliography of research in dendritic growth and the IDGE.

## Results for IDGE on USMP-2

We measured the dendritic growth velocities and tip radii of curvature of succinonitrile in microgravity using the IDGE instrument flown on the USMP-2 platform in the payload bay of the space shuttle Columbia (STS-62). The on-orbit microgravity data, when compared to terrestrial dendritic growth data, demonstrate that: (1) convective effects under terrestrial conditions remain significant even up to values as high as $\Delta T = 1.7$ K supercooling. (2) In the supercooling range from 0.47 K to 1.7 K, the data remain virtually free of convective or non-Ivantsov conditions, and may be used reliably for examining diffusion-limited, infinite boundary dendritic growth theories. (3) A diffusion solution to the dendrite problem, combined with a unique (measured) scaling constant, $\sigma^*$, does not yield individual growth velocity and radius predictions consistent with the observed dendritic growth velocities and radii as a function of supercooling. (4) The failure of this conventional formulation is currently attributed to small departures from the Ivantsov thermal diffusion solution, which is formulated for *paraboloidal* dendrites. Ivantsov's theory describes the overall dependence of Péclet number on supercooling, but predicts a value higher (5% - 15%) than the data we observed in microgravity in the diffusion-limited regime. (5) The scaling parameter $\sigma^*$ does not appear to be a constant over a range of supercoolings. Finally, (6) the average $\sigma^*$ measurements from the terrestrial and microgravity data are in good agreement, despite a difference of over six orders of magnitude in the quasi-static acceleration environment of low-earth orbit and terrestrial conditions [10-13].

Before the IDGE, it was not possible to test separately the Ivantsov transport solution and the interface scaling hypothesis. To our knowledge, the IDGE provides the first solid evidence that Ivantsov's formulation for paraboloidal dendritic growth does not accurately describe dendritic growth in SCN. The approximate agreement achieved between the transport theory and the microgravity data indicates that dendritic growth is indeed most likely governed by the conduction of latent heat from the crystal-melt interface, but the detailed Ivantsov formulation to describe that conduction process is in need of some modification.

One of the key assumptions in the Ivantsov model that we are actively investigating is whether a dendrite can be modeled as a parabolic body of revolution. Early observations of dendrite morphologies lead researchers to approximate the tip shape with a paraboloid. The notion that dendrites are actually *not* paraboloids of revolution was first demonstrated by the data of Huang

and Glicksman [7], and more recently by other researchers [14-18] including LaCombe et al. [19]. By assuming the form of a 4th-order polynomial, rather than a 2nd-order parabola, it is possible to characterize more realistically the shape of dendrite tips. Such a fourth-order equation describing a dendritic profile is $Y=X^2/2 + Q(\phi)X^4$, where $X$ and $Y$ are dimensionless coordinates, normalized with the radius of curvature at the tip of the dendrite. $Q(\phi)$ will vary with the azimuthal direction, and is generally assumed to be proportional to $\cos(4\phi)$ [14-18]. However, the recent work of LaCombe et al. [19,20] has shown that the $\cos(4\phi)$ form does not adequately describe the axial asymmetry. This is seen most readily seen in Fig. 10 of [19] and Fig. 4 of [20] where the $\cos(4\phi)$ functional form is superimposed upon the experimentally observed data describing the actual shape. Furthermore, for terrestrial data, this shape is seen to be independent of supercooling, i.e., the three dimensional shape scales with the size of the dendrite.

At the lower supercoolings ($\Delta T < 0.4$ K), variations in the growth speed beyond that due to measurement uncertainties, and a significant deviation of the heat transfer from that predicted from diffusive transport theory with boundary conditions at infinity. Recently, two models, both based on Cantor and Vogel's confocal parabola modification to Ivantsov [21], described in the *Journal of Crystal Growth* have suggested mechanisms for the heat transfer of a dendrite growing into a supercooled melt. One model, by Sekerka et al. [22], describes how convection resulting from the residual micro-accelerations present on orbit could enhance the heat transfer. Another, by Pines et al. [23], describes the observed speed enhancement as a thermal boundary layer effect arising from the proximity of the growth chamber wall.

Both models, by the adjustment of one parameter, describe the trends in the IDGE microgravity data, and the Stagnant Film Model of Sekerka et al. also describes the terrestrial data. However, when examined in precise detail [24,25], we have shown that neither model is correct. The chief reason being that both models rely, and are thereby "handcuffed", by the Ivantsov solution, which we have already shown is incorrect. In addition, since both models are, in part, based on the same formulation, we could not discriminate between the two of them based on the IDGE data from USMP-2 alone.

Thus, in the higher supercooling range investigated, both the heat transfer and the crystal growth physics components of current dendritic growth theories are in need of modification. In the lower supercooling range, the data are inconsistent with several models of dendritic growth that attempt to modify the basic diffusion-limited theory with the boundaries at infinity to include convection or container effects.

## Results for IDGE on USMP-3

The scientific objectives of the second flight of the IDGE in February/March 1996 (USMP-3/STS-75) was to: characterize the three-dimensional shape of a dendrite tip; accumulate a dense data set on dendritic velocities and radii in the diffusion-limited infinite boundary regime; and to form dendritic velocity data sets to clarify current issues in the literature about whether convection or near-field boundary conditions affect the dendritic growth measurements in microgravity in the lower supercooling range. The telemetry data and preliminary analysis indicates both that we obtained the necessary film data for the proposed analysis, and that the

microgravity velocity data at the lowest supercoolings do not appear to be influenced by convection from the microgravity environment [25].

Finally, in the investigation of dendritic growth phenomena, the IDGE team members are the experimenters, manipulating parameters and conditions in near-real time, making measurements, and analyzing data, and changing the subsequent experimental parameters. However, with respect to the operations of the flight hardware from a terrestrial laboratory, the IDGE is part of a larger experiment in remote teleoperations, paving the way to the microgravity science operations on the future International Space Station (ISS). NASA headquarters and the Telescience Support Center (TSC) at LeRC, with the goal of developing the experience and expertise to set up remote, non-NASA locations from which to control ISS experiments, used our recent IDGE space shuttle experiment as a proof-of-concept of remote operations. During the flight of IDGE on STS-75 in February and March of 1996, team members monitored this experiment from at a remote laboratory set up at Rensselaer rather than at the Payload Operations and Control Center (POCC) at the Marshall Space Flight Center, in Huntsville, AL, where all such operations usually originate. During the last four days of the mission, we expanded the team at Rensselaer and uplinked commands to the experiment. During the entire 14 day mission we had graduate and undergraduate students, whom we had trained, present at the Rensselaer facility [26]. To prepare for the ISS era, we plan to do additional tests of remote telescience during IDGE third flight on USMP-4/STS-87.

## IDGE on USMP-4

The third flight, scheduled for launch in October 1997, will repeat the experimental protocols of the first two flights, but with a different sample material. This second test material, pivalic acid (PVA), is similar to SCN, but with a ten times higher surface energy anisotropy [27,28]. The surface energy anisotropy is an important parameter in the crystal growth physics of dendritic growth [1,28], and may be related to the three-dimensional anisotropy observed in the dendritic tip shape. In addition, we want to develop the data and analytical tools to characterize the non steady-state dynamic parameters, which lead to side branching and, we believe, will be another key in explaining the differences between the IDGE data and predictions from current steady-state dendritic growth models.

## Acknowledgments

We thank, for the continuing interest, and financial support, the NASA Life and Microgravity Sciences and Application Division, (Code U), Washington, DC, under Contract NAS3-25368, with liaison provided through the Space Experiments Division at NASA Lewis Research Center, Cleveland, OH.

## References


1. M.E. Glicksman and S.P. Marsh, "The Dendrite", in Handbook of Crystal Growth, ed. D.J.T. Hurle, (ElsevierScience Publishers B.V., Amsterdam, 1993), Vol **1b**, p.1077.
2. M.E. Glicksman, et al., Met. Trans. A, **19A**, 1945, (1988).
3. M.E. Glicksman, M.B. Koss, and E.A. Winsa, JOM, **47**(8), 49, (1995).
4. M.E. Glicksman, M.B. Koss, L.T. Bushnell, J.C. LaCombe, and E.A. Winsa, 6th International Symposium on Experimental Methods for Microgravity Science, ed. Robert J. Schiffman, (The TMS, 1995, p. 51).
5. Ivantsov, Dokl. Akad. Nauk SSSR **58**, 56 (1947)
6. M.E. Glicksman, R.J. Schaefer, and J.D. Ayers, Met. Trans. A, **7A**, 1747, (1976).
7. S.C. Huang and M.E. Glicksman, Acta Metall., **29**, 701, (1981).
8. M.E. Glicksman and S.C. Huang, Convective Transport and Instability Phenomena, ed. Zierep and Ortel, Karlsruhe, (1982), 557.
9. R. Ananth and W.N. Gill, J. Crystal Growth, **91**, 587, (1988), and **108**, 173, (1991).
10. M.E. Glicksman, M.B. Koss, and E.A. Winsa, Phys. Rev. Lett., **73**, 573, (1994).
11. M.E. Glicksman, M.B. Koss, L.T. Bushnell, J.C. LaCombe, and E.A. Winsa, ISIJ International, **35**, 604 (1995).
12. M.E. Glicksman, M.B. Koss, L.T. Bushnell, and J.C. LaCombe, Modeling of Casting, Welding, and Advanced solidification Processes VII, eds. M. Cross and J. Campbell (The Minerals, Metals, and Materials Society, Warrendale, PA, 1995).
13. M.B Koss., L.T. Bushnell, J.C. LaCombe, and M.E. Glicksman, Chem. Eng. Comm., (in press, 1996).
14. J. Maurer, B. Perrin, and P. Tabeling, Europhys. Lett. **14**, 575 (1991).
15. D. Kessler and H. Levine, Phys. Rev. A **36**, 4123 (1987).
16. D. Kessler and H. Levine, Acta Metall. **36**, 2693 (1988).
17. M. Ben Amar and E. Brener, Phys. Rev. Lett. **71**, 589 (1993).
18. E. Brener, Phys. Rev. Lett. **71**, 3653 (1993).
19. J.C. LaCombe, M.B. Koss, V.E. Fradkov, and M.E. Glicksman, Phys. Rev. E, **52** 2778 (1995).
20. J.C. LaCombe, M.B. Koss, M.E. Glicksman, L.T. Bushnell, and K.D. Hamly, Mat. Res. Soc. Symp. Proc., (in press, 1996).
21. B. Cantor and A. Vogel, J Crystal Growth, **41**, 109, (1977).
22. R.F.Sekerka, S.N. Coriell, G.B. McFadden, J. Crystal Growth, **154**, 370, (1995).
23. V. Pines, A.Chait, and M. Zlatkowski, J. Crystal Growth, (in press, 1996).
24. M.E. Glicksman, M.B. Koss, L.T. Bushnell, J.C. LaCombe, and E.A. Winsa, Reprint # AIAA 96-0251, (1996).
25. L.T. Bushnell, M.B. Koss, J.C. LaCombe, and M.E. Glicksman, J. Crystal Growth (in press, 1997).
26. M.B. Koss, J.C. LaCombe, M.E. Glicksman, L.T. Bushnell, D.C. Malarik, and E.A. Winsa, 8th International Symposium on Experimental Methods for Microgravity Science, ed. Robert J. Schiffman (The TMS, in press, 1996).
27. N.B. Singh and M.E. Glicksman, J. Crystal Growth, **98**, 573, (1989).
28. M. Muschol, D. Liu, and H.Z. Cummins, Phys. Rev. A, **46**(2), 1038, (1992).

# EFFECT OF GRAVITY ON THE EVOLUTION OF SPATIAL ARRANGEMENT OF FEATURES IN MICROSTRUCTURE: A QUANTITATIVE APPROACH

Arun M. Gokhale and Asim Tewari
School of Materials Science and Engineering
Georgia Institute of Technology
Atlanta, Georgia-30332-0245

## INTRODUCTION

The materials properties, processes, and performance often depend on the relative locations of the particles/features in microstructure, i.e., the spatial arrangement of the microstructural features. This is also an aspect of microstructure that may be significantly affected by gravity, particularly, if liquid phases are present during the evolution processes. Gravity may affect particle clustering, spatial correlations among particles sizes, short and long range particle-particle interactions, etc. The microstructural kinetics are in turn affected by the changes in these attributes. Therefore, one contribution of gravity to microstructural evolution is through its effect on the spatial arrangement of the microstructural features. Understanding of the role that gravity plays in this facet of microstructure development is expected to enhance our understanding of how the intrinsic materials processes govern the microstructural evolution.

At present there are no sufficiently well developed techniques for quantitative characterization and modelling of spatial arrangement of particles/features in microstructure. An important objective of this research program is to develop flexible practical procedures to quantify the spatial arrangement of microstructural features. Another important objective of the research is to apply the new methodology to quantify the evolution of spatial arrangement of tungsten grains during liquid phase sintering of a series tungsten heavy alloys (WHA). This part of the research is in collaboration with Professor R.M. German and his group at Pennsylvania State University. The ground based as well as microgravity environment (IML-2, July 1994) liquid phase sintering experiments were performed by Professor German and his colleagues at Penn. State. The research program at

Georgia Tech involves quantitative characterization and modelling of evolution spatial arrangement of tungsten grains in these liquid phase sintered specimens.

This paper reports important research results obtained in this research program during the last two years. The next section of the paper gives a brief background on important descriptor of the spatial distribution of particles, and that is followed by description of image analysis software and computer codes developed under this program to extract reliable quantitative data on important descriptors of the spatial arrangement. In the subsequent section, these techniques are applied to quantify the evolution of the spatial arrangement of tungsten grains during liquid phase sintering of some tungsten heavy alloys (WHA), and this is followed by the discussion of the results.

## CHARACTERIZATION OF SPATIAL ARRANGEMENT OF MICROSTRUCTURAL FEATURES

Theoretical Statistics literature contains a large number of contributions that deal with the statistics of spatial point patterns, and the quantitative descriptors that reflect various attributes of these patterns[1,2]. The radial distribution function is an important and well known descriptor of spatial arrangement of particle centers. The radial distribution function G(r) is equal to ratio of the average number of particle centers in a circular shell of radii r and (r+dr) around a typical particle and the corresponding number for completely randomly distributed point particles having the same average number density. For randomly distributed point particles G(r) is equal to one; a value significantly higher than one represents clustering, and a value lower than one signifies repulsion.

An unbiased and reliable estimation of the above spatial distribution functions is NOT possible through measurements on separate disconnected fields of view of microstructure observed under microscope due to the edge effect. Due to the edge effect, (i) distances between particles that are not in the same field of view can not be measured, and (ii) it is difficult to account for the particles that are partly in a given field of view; ignoring such particles can lead to a significant bias because larger particles are more likely to intersect the boundaries of a field of view. The problems due to the "edge effect" can be resolved by eliminating the edges! For this purpose, an image analysis software is developed to "cut and paste" perfectly matching larger number of contiguous microstructural fields in the memory of the digital image analyzer[3,4]. The creation of such an image

"montage" having large number of fields of view (say, 100 fields) eliminates the edge effect for all the practical purposes. Another computer code is developed to extract the size and the centroid coordinates of each particle in the montage; the Centroids of all the particles are referred to the same (0, 0) origin. The raw data from image analysis consist of a string of numbers for each particle, representing (X,Y) centroid coordinates, size, shape, perimeter, etc. A typical data set consists of such information on 1,000 to 5,000 particles. A separate computer code is required for estimation of each spatial distribution function. These calculations involve operations on reasonably large data sets, and require extensive number crunching.

## EXPERIMENTAL MEASUREMENTS ON LIQUID PHASE SINTERED SPECIMENS

The above characterization methodology was applied to quantitatively characterize the evolution of spatial arrangement of tungsten grains during liquid phase sintering (LPS) of two WHA alloys. The microgravity (IML-2) as well as normal gravity LPS experiments were conducted by Professor R.M. German and coworkers. The details of the LPS experiments are described elsewhere [5-8]. The measurements were performed on two W-Ni-Fe alloys containing 78 wt% and 93 wt% tungsten, liquid phase sintered at 1500°C for 1 and 120 minutes, in the earth's gravity or microgravity environment. All the specimens were pre-sintered. The radial distribution function of the tungsten grain sections was calculated from the data grain section centroids in a montage. Figure 1 shows the experimentally measured radial distribution function of tungsten grains in these specimens. Observe that the radial distribution function has evolved with the sintering time. Figure 2a shows the same radial distributions, now plotted on a normalized distance scale (r / R), where R is the corresponding average particle size. It is interesting to note that these normalized distributions almost superimpose on each other, i.e., the normalized radial distribution function appears to have reached a time invariant pseudo static form. *This implies that the overall spatial arrangement of the tungsten grain centers during LPS of WHA alloys in normal gravity reaches a pseudo-static form, when normalized by an appropriate microstructural scale factor.* Figure-2b shows the normalized radial distribution functions for the corresponding specimens liquid phase sintered in microgravity. It is interesting to note that for the microgravity liquid phase sintered specimens, the normalized radial distribution functions do not superimpose on each other. Figure-2c shows the normalized

radial distribution functions for 93wt% W microgravity specimens. In this case, the normalized distributions

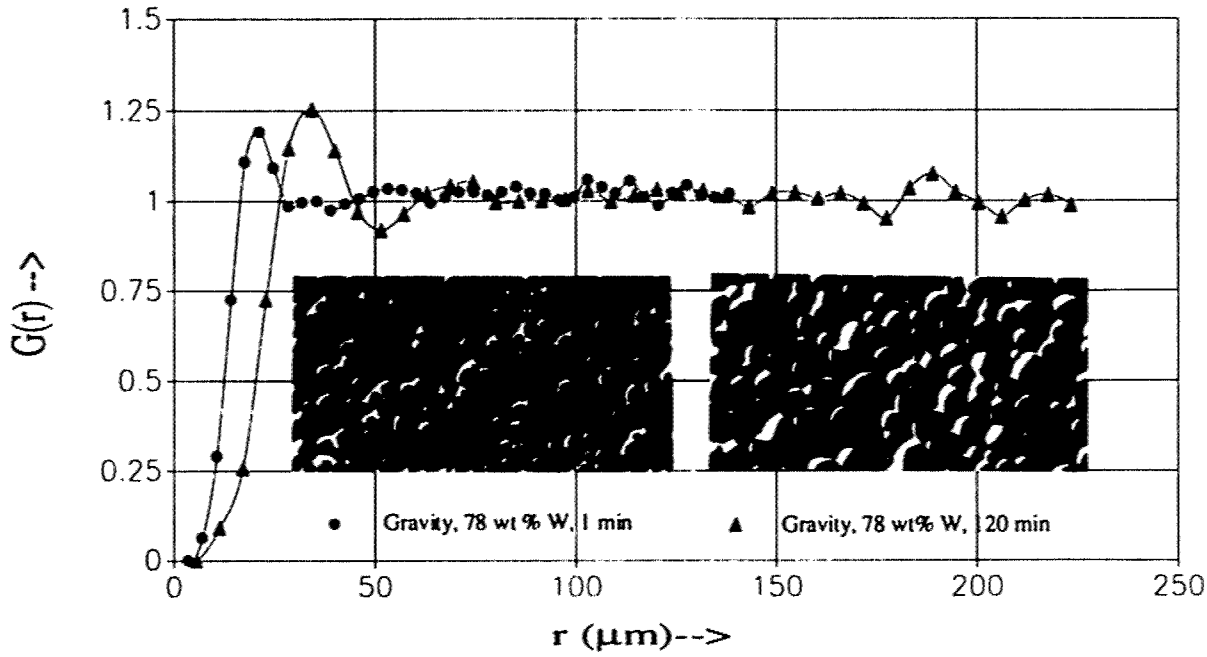


Figure 1: Evolution of radial distribution function in specimens liquid phase sintered in normal gravity (78 wt% W alloy)

superimpose at smaller distances (r < 2R), but the radial distribution for 120 min. specimen exhibits large oscillations at long distances, indicating the changes in the long range spatial arrangements with time that are not due to change in the microstructural length scales. Comparison of Figures 2a and 2b reveals that the gravity affects the evolution of the spatial arrangement of tungsten grains during the LPS. *In the microgravity, the changes in the radial distribution function are not just due to the changes in the microstructural length scales, whereas under earth's gravity the evolution of the spatial arrangement is mainly due to the evolution of the microstructural length scale.* Figure 3a compares the normalized radial distribution function of 78% W alloy liquid phase sintered in earth's gravity and microgravity for 1 minute. There are significant differences in the two radial distribution functions, although the alloy chemistry, sintering temperature, and time are identical. Both the distributions are normalized by the corresponding average grain size, and therefore these differences are not due to the differences in the microstructural length scales. Figure-3b compares the normalized radial distributions of tungsten grains in 93%W alloy liquid phase sintered for 120 minutes in microgravity and normal gravity. Observe that at large distances,

the radial distribution for normal gravity specimen has a constant value close to 1.0, whereas the radial distribution for microgravity specimen exhibits significant and almost periodic oscillations around the mean value of 1.0. These differences are <u>not</u> due to the noise in the data, because the same level of "noise" is expected in both the distributions. These observations demonstrate that the

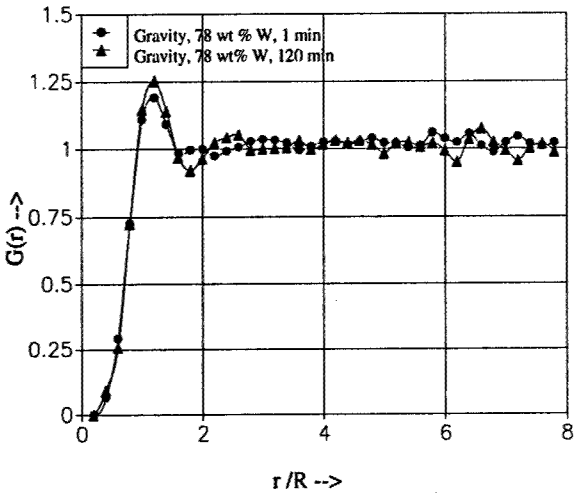


Figure 2a: Evolution of normalized radial distribution function in specimens liquid phase sintered in normal gravity (same as Figure 1, 78 wt% W alloy).

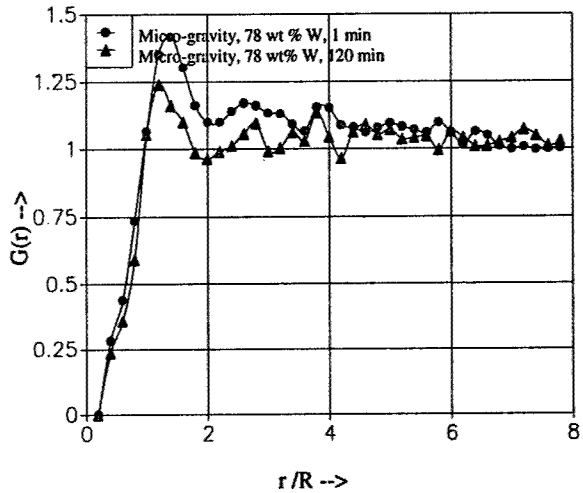


Figure 2b: Evolution of normalized radial distribution function in specimens liquid phase sintered in micro-gravity (78 wt% W alloy).

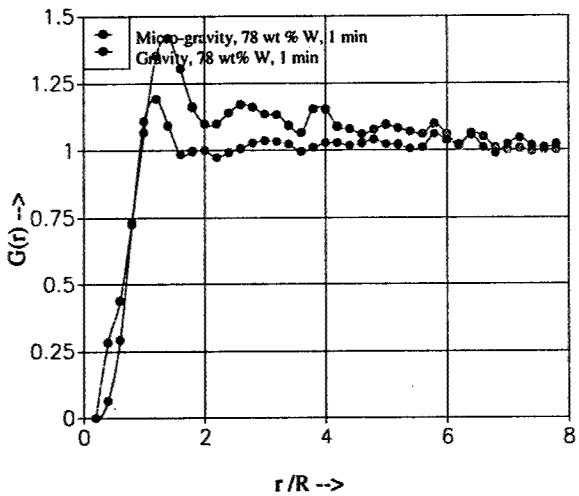


Figure 3a: Comparison of normalized radial distribution functions of 78 wt% W alloy sintered for 1 minute in normal gravity and micro-gravity.

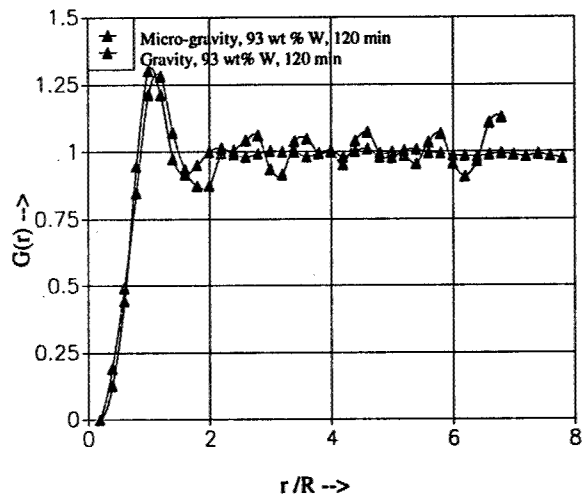


Figure 3b: Comparison of normalized radial distribution functions of 93 wt% W alloy sintered for 120 minute in normal gravity and micro-gravity.

gravity affects the spatial arrangement of tungsten grains, as well as the intrinsic process of the evolution of spatial arrangement of tungsten grains during LPS.

## CONCLUSIONS

A digital image analysis procedure is developed to quantify the spatial arrangement of microstructural features in a metallographic plane. This procedure is utilized to quantify the evolution of spatial arrangement of tungsten grains during LPS of two WHA alloys in microgravity and normal gravity. It is shown that the gravity affects the evolution of the spatial arrangement of tungsten grains during LPS. In the microgravity, the spatial arrangement of the tungsten grains does not follow a "scale factor" type evolution.

## REFERENCES


(1) B.D. Ripley: **Spatial Statistics**, John Wiley and Sons, London, U.K., 1981.

(2) B.D. Ripley: "Modelling Spatial Patterns", **J. Royal Stat. Soc.-B**, 1977, Vol. 39, PP. 172

(3) Pascal Louis and A.M. Gokhale: "Application of Image Analysis for Characterization of Spatial Arrangement of Features in Microstructure", **Metall. Mater. Trans.**, 1995, Vol. 26A, PP. 1449-1455.

(4) Pascal Louis and A.M. Gokhale: "Computer Simulation of Spatial Arrangement of Particles in Three-Dimensional Microstructures: Applications to Model Electrical Conductivity of a Polymer Matrix Composite", **Acta Met. et Mater.**, 1996, Vol. 44, PP. 1519-1528.

(5) R.G. Iacocca and R.M. German: "Experimental Design for Liquid Phase Sintering in Microgravity", in **Compaction, Sintering, and Secondary Operations**, Compiled by A. Lawley , **Advances in Powder Metallurgy and Particulate Materials**, 1993, Vol.2, PP. 181-194.

(6) R.M. German, R.G. Iococca, R.G. Johnson, J.L. Liu, and A. Upadhyaya: "Liquid Phase Sintering Under Microgravity Conditions", **Journal of Metals**, 1995 (Aug.), PP. 46-48.

(7) Y. Liu, R.G. Iococca, J.L. Johnson, R.M. German, S. Kohara: "Microstructural Anomalies in a W-Ni Alloy Liquid Phase Sintered Under Microgravity Conditions", **Metall. and Mater. Trans.**, 1995, Vol. 26A, PP. 2484-2486.

(8) R.G. Iococca, Y. Liu, and R.M. German: "Microstructural Examination of Tungsten Heavy Alloys Sintered in a Microgravity Environment", **Advances in Powder Metallurgy**, 1995, Vol.1, PP. 239-249.

# EVALUATION OF MICROSTRUCTURAL DEVELOPMENT IN BULK, UNDERCOOLED ALLOYS

Richard N. Grugel
Universities Space Research Association
c/o Marshall space Flight Center
MS - ES75, Huntsville, AL 35812

telephone: (205) 544-9165
fax: (205) 544-8762
e-mail: richard.grugel@msfc.nasa.gov

## Objective of this research

Solidification processing techniques such as melt spinning and spray atomization are utilized to achieve high cooling rates (>$10^4$ K/s) with the intent obtaining fine microstructures and/or novel, possibly metastable, phases. When the solidified product consists of powders, ribbons, or flakes having dimensions on the order of $10^{-2}$ to $10^{-4}$ cm the rapid heat removal necessary to achieve these goals is easily achieved. These powders must subsequently be consolidated which can compromise or destroy the desired microstructure. Furthermore, the end product consists of randomly oriented grains and lacks directional properties.

Alternatively, solidification can be induced in a "bulk" alloy melt which has been highly undercooled with respect to its equilibrium freezing point. Here it is envisioned that the undercooling will provide a driving force for rapid solidification and the above mentioned qualities. With nucleation induced a continuous microstructure is expected and the sample will constitute a volume sufficient to preclude the need for consolidation. To this end an experimental and modeling effort to examine and predict the thermal history and growth dynamics during solidification of undercooled Pb-Sn eutectic and hypereutectic (tin-rich) alloys has been undertaken. Here eutectic and dendritic, generally directional, growth proceeds from the sample top to the bottom with the constituents of the former section being considerably finer than that of the latter. These microstructural observations are in accordance with the model's predictions, i.e., the initially rapid dendritic growth velocity quickly decreases. Unfortunately, due to the alloy's opaque nature, such conclusions must be inferred after solidification is complete and the model can not be verified. To this end, a transparent, metal analogue, material was utilized so that the solidification dynamics could be directly observed and recorded for later evaluation.

Justification for microgravity research

The microgravity environment of space is envisioned as a novel processing arena for the solidification of metals and alloys. Contamination of high temperature and/or reactive materials is expected to be minimized as a container is not required to hold the melt; the samples are also not size limited. Undercooling of the liquid might be enhanced due to the quiescent environment which would minimize gravity driven convection. The intent of this work, however, is to conduct a thorough ground-based investigation which will evaluate microstructural development in bulk, undercooled alloys with the aim of ascertaining the advantage of processing in microgravity.

Significant results of the investigation

A model was developed to predict the growth velocity of primary Pb-Sn eutectic and Sn dendrites emanating from an induced nucleation site in "bulk," undercooled Pb-Sn alloys. The velocities were found to be initially rapid but quickly diminished, within the first 10% of solid to form, after which solidification continued at a relatively constant rate just under the equilibrium temperature. Examples of the calculations[1-3] for Lead - 61.9 wt pct Sn (eutectic) and Lead - 75 wt pct Sn alloys are shown, respectively, in Figures 1 and 2. Experiments were conducted[1-3] with undercooled alloys based on those compositions and representative micrographs are shown in Figures 3-6.

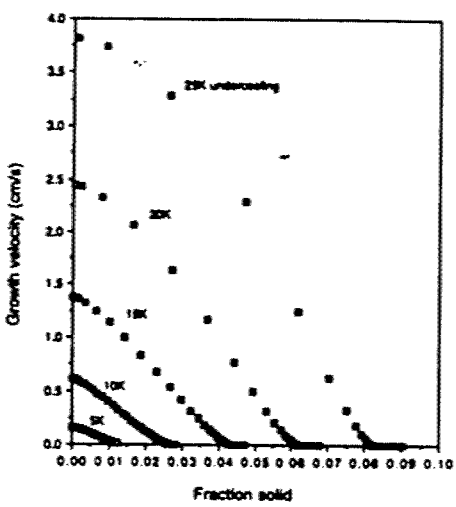


Figure 1

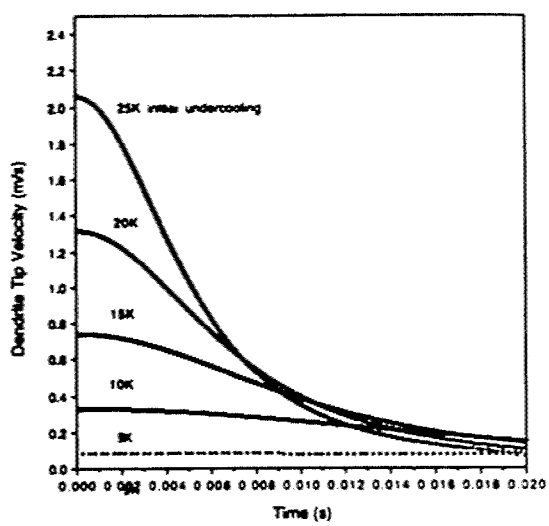


Figure 2

Figure 1: Calculated values of the eutectic velocity as a function of volume fraction solid for several initial undercoolings. Lead - 61.9 wt pct Sn. Sample size = 16mm long x 8mm diameter.

Figure 2: Calculated values of the dendrite velocity as a function of time after induced nucleation for several initial ΔT's. Lead - 75 wt pct Sn. Sample size = 16mm long x 8mm diameter.

Figure 3

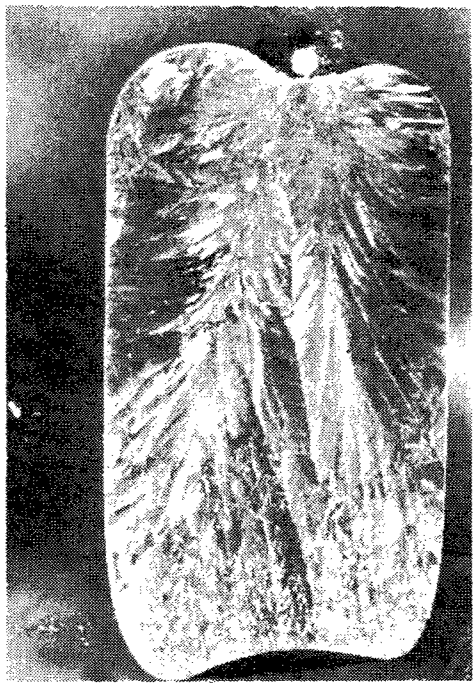

Figure 4

Figure 3: Initial $\Delta T = 5K$. Lead - 61.9 wt pct Sn. Sample size = 16mm long x 8mm diameter.

Figure 4: Initial $\Delta T = 15K$. Lead - 61.9 wt pct Sn. Sample size = 16mm long x 8mm diameter.

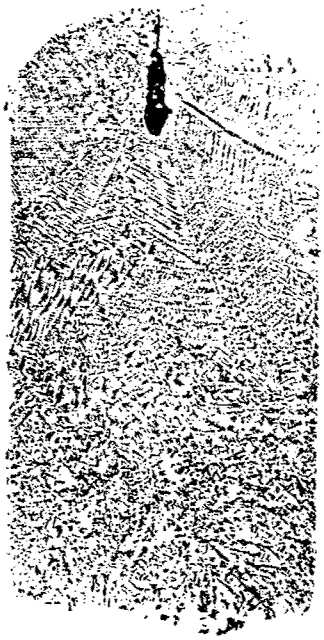

Figure 5

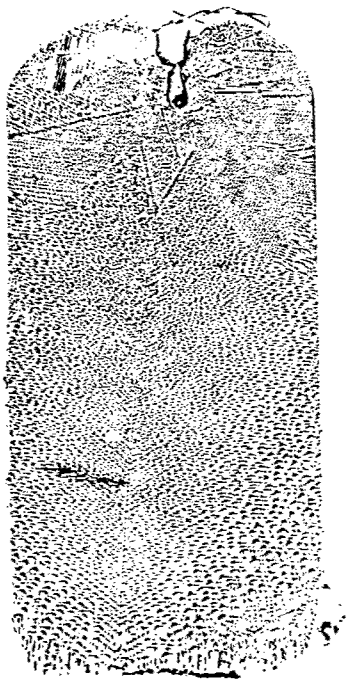

Figure 6

Figure 5: Initial $\Delta T = 5K$. Lead - 75 wt pct Sn. Sample size = 16mm long x 8mm diameter.

Figure 6: Initial $\Delta T = 5K$. Lead - 75 wt pct Sn. Sample size = 16mm long x 8mm diameter.

While microstructural observations from the metallographically prepared samples are found to be in qualitative agreement with the model the conclusions are still inferred. To gain insight regarding microstructural development in the Sn-Pb alloys direct observation and measurements of dendritic growth velocities, as a function of time, in undercooled mixtures were conducted[4]. Two videotape frames of the growing succinonitrile dendrites are reproduced in Figures 7 and 8.

Figure 7

Figure 8

Figure 7: Dendritic growth in succinonitrile - 1 wt pct water 6 seconds after induced nucleation. Initial undercooling = 4K.

Figure 8: As Figure 7, 15 seconds after nucleation.

Here, taking into account multiple dendrites from the initiation site, good agreement with the predicted growth velocities was found, Figure 9. Furthermore, at small initial undercoolings, it was found that the equiaxed region, such as seen in Figure 5, developed due to sinking, not nucleation, of secondary dendrite branches which initiated on the main stalk. It was subsequently[5] argued that the latent heat of fusion released upon solidification was sufficient to raise the temperature about those initial arms which upon dissociation, due to melting, began to sink.

## Conclusion

In a general conclusion, the rapid growth velocities which initiate in "bulk" size samples having large undercoolings quickly diminish. While directional growth in undercooled melts is essentially possible, rapid heating of the sample effects a rapid decrease in the dendrite growth velocity and a uniform microstructure is precluded.

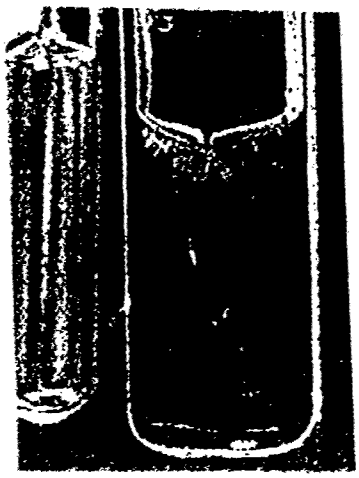

Figure 9

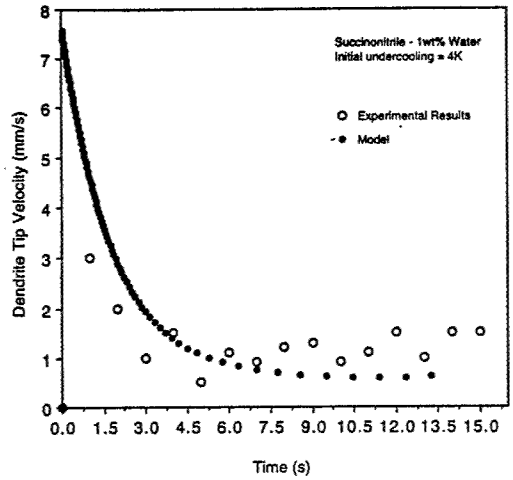


Figure 10

Figure 9: Dendritic growth in succinonitrile - 1 wt pct water 75 seconds after induced nucleation. Initial undercooling = 2K. Small dendrites, initially attached to the primary stalk, can be seen slowly singing to the bottom.

Figure 10: Comparison of the measured primary dendrite growth velocity with the predicted value as a function of time. Initial undercooling = 2K.

References

1. Fay Hua: Ph.D. Thesis, Vanderbilt University, Nashville, TN, August 1995.

2. Fay Hua and R.N. Grugel: "Microstructural Development in Undercooled Lead-Tin Eutectic Alloys." *Metallurgical and Materials Transactions*, 1995, vol. 26A, pp. 2699-2706.

3. Fay Hua and R.N. Grugel: Proceedings, "6th International Symposium on Experimental Methods for Microgravity Materials Science", R.A. Schiffman and J.B. Andrews, Eds., TMS, 1994, pp. 111-115.

4. Fay Hua and R.N. Grugel: "Direct Observation of the Columnar to Equiaxed Transition in an Undercooled Melt," *Scripta Materialia*, 1996, vol. 34, no. 4, pp. 573-577.

5. Fay Hua and R.N. Grugel: Presentation entitled "Development of Equiaxed Zones in Bulk, Undercooled Alloys." TMS Fall Meeting, 29 October - 2 November 1995, Cleveland, OH.

# NOVEL DIRECTIONAL SOLIDIFICATION PROCESSING OF HYPERMONOTECTIC ALLOYS

Richard N. Grugel
Universities Space Research Association
c/o Marshall space Flight Center
MS - ES75
Huntsville, AL 35812

telephone: (205) 544-9165
fax: (205) 544-8762
e-mail: richard.grugel@msfc.nasa.gov

## Statement of hypothesis, objective, and value

The basic hypothesis presumes if coalescence and settling of the Liquid II ($L_{II}$) phase, characteristic of hypermonotectic alloy compositions, can be eliminated than directional solidification will result in an aligned composite material with uniform incorporation and distribution of the excess Solid II phase. The proposed investigation has several scientific objectives which will be realized by conducting a systematic experimental investigation in conjunction with a thorough modeling effort. The objective of the theoretical study is to develop a semi-quantitative predictive model relating, microstructure to process parameters for the systems investigated experimentally. This will require close interaction with experiment in order to determine more precisely the role of the various dynamic processes induced by ultrasound in these monotectic systems. Experimentally, ultrasound will be utilized to suspend and maintain separation of the $L_{II}$ droplets which precipitate from the bulk liquid once the temperature drops below the miscibility gap boundary so that a uniformly aligned hypermonotectic composite might actually be produced by controlled directional solidification. Subsequent examination of the processed samples will promote our understanding of diffusion and coalescence processes, liquid-liquid interactions, wetting phenomena, and microstructural development. The liquid volume fraction ultrasonics can maintain dispersed versus the coalescing (settling) force imposed by gravity will be determined and then evaluated whether or not this could be improved upon in a microgravity environment. Consequently, the need for a microgravity investigation will also be demonstrated. Here the ground-based results will define and optimize the parameters required to ensure a successful microgravity experiment while concurrently establishing a base to which such experiments can be unequivocally compared and evaluated.

The value of this work, outside of actually producing a uniformly aligned hypermonotectic composite, will be a demonstration and mathematical characterization of a novel solidification processing technique. The knowledge acquired from investigating model alloys might then be applied to technologically relevant miscibility gap systems, e.g., superconducting Cu-Ba-Y, with the potential of producing novel composites having improved properties.

Review of relevant research

The binary miscibility gap system of interest, Figure 1, is characterized by 1) a region where two distinctly different liquids are in thermodynamic equilibrium and 2) the monotectic reaction, $L_I = S_I + L_{II}$. Microstructural development at the solid/liquid interface for these alloys has been theoretically discussed by Chadwick[1] and Cahn[2] and experimentally investigated by Livingston and Cline[3] and Grugel and Hellawell[4,5].

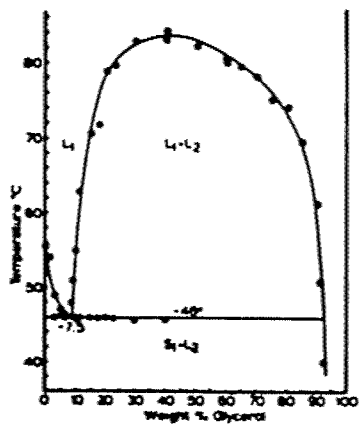


Figure 1:
The Succinonitrile-
Glycerol Phase Diagram[6].

Alloy compositions to the right of the monotectic reaction are termed hypermonotectic and, upon cooling, pass through the two liquid miscibility gap. Solidification of, for example Cu-Pb alloys for application as slide bearings is hampered by the inherent density differences between the $L_I$ and $L_{II}$ phases. This leads to rapid separation, coalescence and, consequently, a highly inhomogeneous structure. It was envisioned that processing in a microgravity environment would eliminate the density differences and yield a uniform composite of aligned or finely dispersed $L_{II}$ (eventually $S_{II}$) in the $S_I$ matrix could be produced. Unfortunately, microgravity experiments still resulted in highly macrosegregated structures. A number of explanations for these poor results have been posed. They include droplet coalescence by Ostwald ripening and/or thermocapillary convection and preferential wetting of the container by one of the liquid phases, factors which are both detrimental to microstructure and gravity *independent*.

Earlier experiments where hypermonotectic alloys were directionally solidified[7-9] served to demonstrate the detrimental effects of phase separation on microstructure. It is thus proposed to apply an ultrasonic field to the bulk liquid which, upon cooling, will initiate and maintain a

uniform dispersion of the precipitated liquid, $L_{II}$. The "imposed" microgravity environment would then serve to eliminate density differences, i.e., settling, between the liquids. With droplet coalescence minimized, controlled directional solidification should promote a uniformly aligned, composite microstructure.

The study of acoustic waves on initiating and maintaining suspensions in two-liquid systems is well established[10-13]. Some complementary experiments have been conducted in a microgravity environment[14-17]. These experiments examined metallic, miscibility gap systems from which microstructural development must be inferred after solidification is complete. This hindrance may be circumvented by using transparent materials which simulate solidification phenomena in metals and alloys, a technique that is well established and accepted[18]. With reference to the succinonitrile - glycerol phase diagram, Figure 1, consider the following experiment[19].

Briefly, hypermonotectic succinonitrile - 15 wt pct glycerol "alloys" were made and placed in test tubes having 12mm I.D. The samples were instrumented with a thermocouple and submerged in the water bath of a commercial ultrasonic cleaner, the initial bath temperature being ~90°C. When the bath, and sample, cooled to ~73°C precipitation of the excess $L_{II}$ phase (glycerol) initiates, Figure 2a. In Figure 2b, nine minutes later, $T \approx 67°C$, the slightly denser glycerol is seen condensing and settling to the sample bottom. After 45 minutes, ~51°C, the coalesced glycerol fully occupies the sample bottom, Figure 2c. Subsequent solidification results in a highly segregated structure. Figure 3a shows the same sample but subjected to ultrasonic energy during cooling. At ~50°C and 105 minutes after precipitation of the $L_{II}$ phase initiated, in contrast to Fig. 2c, a uniform dispersion of the excess liquid is maintained. Separation and coalescence is again obvious 30 minutes after the ultrasonic energy is stopped. Figure 3b ($T \approx 42°C$).

Justification for new microgravity research

There must be a limit to the liquid volume fraction ultrasonics can maintain dispersed before gravity imposed settling and coalescence occurs. This will be determined and then evaluated whether or not this could be improved upon in a microgravity environment. Microgravity processing will enable testing model predictions which can not be done on Earth and, utilizing the predicted parameters, could lead to novel composites with enhanced properties. Finally, a uniformly aligned hypermonotectic composite will *actually* be solidified in a microgravity environment. This will make a convincing demonstration when compared to past results and the inevitable failure of any similar future experiments.

## Without Ultrasound

**TEMPERATURE** [°C]

73.8 67.3 50.7

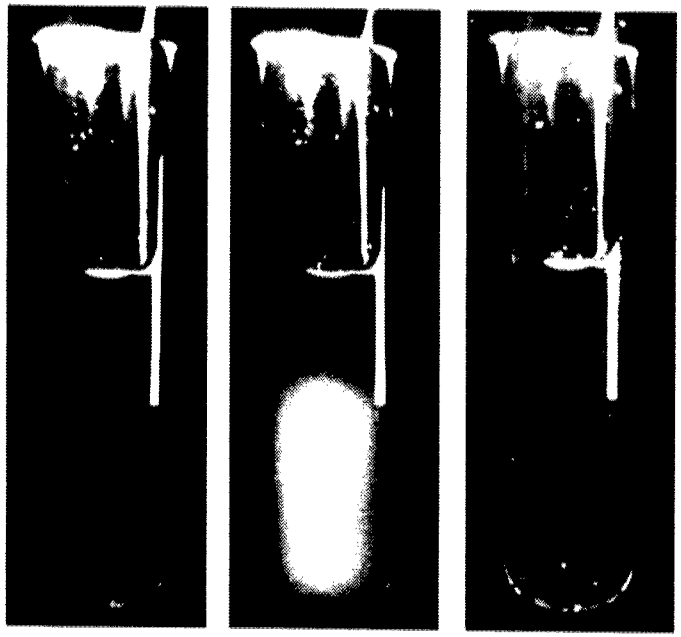

0 9 45

**TIME** [min]

Fig. 2a Fig. 2b Fig. 2c

## With Ultrasound

**TEMPERATURE** [°C]

50

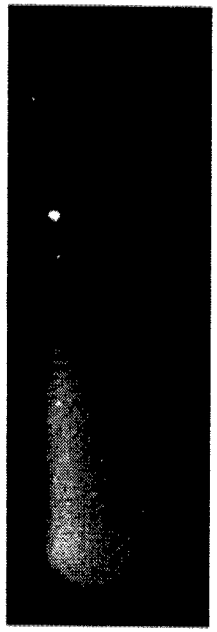

105

**TIME** [min]

Fig. 3a

## After Termination of Ultrasound

**TEMPERATURE** [°C]

42

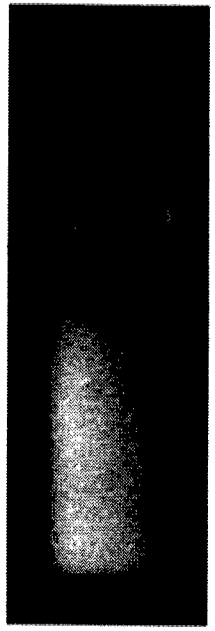

30

**TIME** [min]

Fig. 3b

Description of experimental or analytical method

The Pb-Ga, Zn-Bi, Al-In, and Al-Pb alloy systems exhibit miscibility gaps, are well characterized, and the thermophysical properties of the components are known. The systematic, controlled directional solidification, experimental investigation will utilize a series of alloy compositions ranging from the monotectic reaction to well into the miscibility gap. Two sample sets will be investigated, one in conjunction with ultrasonics and one, otherwise identically processed, without. An "off-the-shelf" ultrasonic processor will provide energy to the sample by either coupling with the crucible or by inserting a probe directly into the liquid. Metallographic examination will provide information regarding phase spacings, phase distributions, and volume fractions. Development aspects of the two-phase region will be followed and evaluated by serially sectioning along the length of the sample, i.e. from above the quenched in liquid, through the miscibility gap, through the $S_I + L_{II}$ zone, and into the $S_I + S_{II}$ region. Analysis of the data will 1) complement the parallel modeling effort and 2) provide valuable guidelines for optimizing a microgravity experiment. Ultrasonic vibrations are similar to sound waves but have higher frequencies (generally >500 MHz) and will influence hypermonotectic solidification by maintaining a uniform dispersion of $L_{II}$ droplets and by contributing heat to the system. A model which includes these effects will be formulated. Particular attention will be given to the nature of the ultrasonic waves, including reflection and refraction of longitudinal waves and the 2-liquid phase boundary, and on the importance of standing waves. Fluid motion due to the ultrasound will not be considered explicitly.

Collaborative effort

The Space Sciences Laboratory at MSFC is well equipped to conduct the ground-based research described above and to facilitate any future flight experiment. Furnaces and support facilities for alloying, directional solidification, data collection, and sample characterization, presently exist and are currently operational within the Laboratory. Marshall is also ideally located to house and conduct ground-based experiments with a potential flight capable furnace. The Center for Microgravity and Materials Research at the University of Alabama at Huntsville (Co-I Dr. J.I.D. Alexander) has an Ardent "Titan II" workstation with 850 megabytes of storage, a Silicon graphics Indigo (SGI) R4000 workstation with 96MB of memory and 1.2 gigabytes of disk space, and a gigabyte of disk space on a microvax 3000 workstation. In addition to other facilities there are also several Apple Macintosh, Macintosh II and IBM PC computers and peripherals available which are also networked for access to the CRAY XMP.

References


1. G.A. Chadwick: *Brit. J. Appl. Phys.*, 1965, vol. 16, pp. 1095-1097.
2. J.W. Cahn: *Metall. Trans. A*, 1979, vol. 10A, pp. 119-121.
3. J.D. Livingston and H.E. Cline: *Trans. TMS-AIME*, 1969, vol. 245, pp. 351-357.
4. R.N. Grugel and A. Hellawell: *Metall. Trans. A*, 1982, vol. 12A, pp. 669-681.
5. R.N. Grugel and A. Hellawell: Materials Research Soc., Proc., Elsevier Science Publishing Co., Inc., 1982, Vol. 19, pp. 417-422.
6. R.N. Grugel: Ph.D. Thesis, 1983, Michigan Technological University.
7. R.N. Grugel, T.A. Lograsso, and A. Hellawell: Mat. Proc. in the Reduced Gravity Environ. of Space, Mat. Res. Soc., Elsevier Publishing Co., New York, 1982, G.E. Ridone, ed., p. 553.
8. S. Shah, R.N. Grugel, and B.D. Lichter: *Metall. Trans. A*, vol. 19A, 1988, pp. 2677.
9. R.N. Grugel and Shinwoo Kim: *Adv. in Space Research*, 1993, vol. 13, no. 7, pp. 225-228.
10. R.W. Wood and A.L. Loomis: *Phil. Mag.*, 1927, vol. 7., p. 417.
11. W.T. Richards: *J. Amer. Chem. Soc.*, 1929, vol. 51, p. 1724.
12. K. Sollner et al.: *Kolloid-Zeit*, 1932, vol. 60, p. 263; *Trans. Far. Soc.*, 1935, vol. 31, p. 835.
13. G. Schmid et al.: *Zeit. fur Elecktrochem*, 1937, vol. 43, p. 869.
14. P.F. Clancy et al: Acta Astronautica, 1980, vol. 7, pp. 877-891.
15. P.F. Clancy et al: Proc. 4th Euro. Symp. on Mat. Sci. under Microgravity, ESA SP-191, 1983, p. 99.
16. P.F. Clancy, and W. Heide: Proceedings: Workshop on the Effect of Gravity on Solidification of Immiscible Alloys, ESA SP-219, 1984, p. 73.
17. T. Takahashi et al: *J. Japan Inst. Light Metals*, 1984, vol. 34, p. 479.
18. R.N. Grugel and R. Trivedi: Metallography: Past, Present, and Future (75th Anniversary Volume), ASTM STP 1165, G.F. Vander Voort et al, Eds., ASTM, Philadelphia, 1993, pp. 393.
19. R.N. Grugel: Unpublished research, Vanderbilt University, 1994.

# UTILIZING CONTROLLED VIBRATIONS IN A MICROGRAVITY ENVIRONMENT TO UNDERSTAND AND PROMOTE MICROSTRUCTURAL HOMOGENEITY DURING FLOATING-ZONE CRYSTAL GROWTH

Richard N. Grugel
Universities Space Research Association
c/o Marshall space Flight Center
MS - ES75
Huntsville, AL 35812

telephone: (205) 544-9165
fax: (205) 544-8762
e-mail: richard.grugel@msfc.nasa.gov

## Statement of the hypothesis, objective, and value of this research

Crystal quality should improve during float-zone processing if inherent convective flow within the liquid volume can be minimized. Consequently, the objective of this proposed experimental and theoretical investigation is to utilize vibration driven surface streaming flows in an effort to negate the detrimental effects of thermocapillary convection which arise during float-zoning of semi-conductor materials. The ground-based work would then be extended to the microgravity environment where the effect of thermocapillary flow on crystal homogeneity may be studied in an optimized floating-zone. The results of this study could well demonstrate a novel and inexpensive way of considerably improving crystal uniformity.

## Justification for new microgravity research

Gravity driven flow which occurs during float-zone processing is minimized in a microgravity environment and thus permits thermocapillary flow to be singularly investigated. Here, utilizing incremented and calibrated vibration, the consequence of flow velocities on microstructure can be controlled and systematically investigated, not just acknowledged. The microgravity environment will minimize unit-gravity induced biases such as static shape distortion and buoyancy flow; furthermore, sedimentation of tracer particles will be minimized. Here then is an opportunity to evaluate crystal growth and homogeneity in association with a stable and dimensionally optimized floating-zone.

Review of relevant research

The floating-zone technique for crystal growth of semiconductor materials has proven invaluable to the semiconductor industry. Advantages of this "containerless" processing technique include a reduced number of defects attributed to expansion (or contraction) at the solidification-crucible interface. Furthermore, the containerless aspect precludes the introduction of impurities into the crystal due to reactions between the crucible and the melt. Consequently, the floating-zone method of crystal growth is ideally suited for such germanium, silicon, and the group III-V materials. The vast number of investigative studies of these commercially significant crystals precludes a complete review of the scientific literature; see, for example, references 1-5.

Significant convective flow in the liquid, both natural and induced, is inherent to the process[1-6] and promotes non-uniform dopant distribution and crystal striations. Convection phenomena common to all floating-zone arrangements and pertinent to this proposal are: A) surface tension induced flow (Marangoni or thermocapillary) and B) gravity induced flow (buoyancy). The latter arises due to unstable density gradients of temperature and/or composition, while the former flow results from variations in surface tension at the liquid/vapor interface due to temperature and/or concentration gradients. It is relevant to appreciate that thermocapillary convection is *independent* of gravity level.

Consequently, in view of minimizing density driven flow by processing in space, a great number of investigations, both experimental and theoretical, have been conducted with the intent of understanding the influence of Marangoni convection on crystal uniformity. In view of the above observations a number of methods have been attempted or proffered to suppress or offset Marangoni convection and its deleterious consequences. While some improvement in crystal quality has been reported, these techniques generally induce other effects such as wandering growth axes and other flow patterns. Recently, a method for controlling fluid flow during Czochralski growth of crystals through the use of acoustic streaming has been proposed[7]. We intend to propose that controlled end-wall vibration of the float-zone could be utilized to ensure greater crystal homogeneity.

Some studies toward understanding the effect of vibration on float-zone processing have been conducted[8-11]. Simulation[8] of a floating half-zone was accomplished by placing silicone oil (DC 200; 20cS viscosity) between two vertical, 6.4mm diameter, aluminum rods which were separated by 2.5mm. Thermocapillary flow was initiated by imposing a temperature gradient (~20Kcm$^{-1}$) on the system via a small resistance heater attached to the upper rod to minimize buoyancy. Flow

was visualized by the addition of pliolite tracer particles (~50μm diameter) which were illuminated by a He-Ne (10mW) laser sheet 0.5mm thick. Also in conjunction with the bottom rod is a vibrator which, for the given system, operated at a frequency of 70 Hertz and oscillation amplitude of ~100μm. The induced surface streaming flow, due to end-wall vibration of the float-zone, counteracted the thermocapillary convection which, essentially, resulted in no flow. Here it is possible that the liquid at the vibrating surface is quiescent, a factor which ensures diffusion driven growth and promotes homogeneity in the resulting crystal. By increasing the vibration amplitude, the flow can be reversed. For this system a number of processing variables (e.g. zone length, temperature profiles, fluids) have also been characterized. Using a fine (0.1mm dia.) k-type thermocouple temperature profiles were taken in the liquid zone without and during induced vibration. In the latter case radial temperature gradients smoothed considerably, thus providing additional credence for this method as a means to control thermocapillary flow and thereby improve crystal quality.

This innovative approach of using end-wall vibration to promote crystal uniformity during float-zone processing has never been suggested or tested. In a feasibility study, the effort was expanded to investigate its effect in a traveling floating-zone of a model compound, sodium nitrate ($NaNO_3$)[9,10]. The choice of $NaNO_3$ has many advantages; it's transparency when liquid allows direct observation and recording of flow patterns, it has been successfully used in previous studies and some of the thermophysical parameters are similar to a germanium or silicon melt. Furthermore, with the surface tension of $NaNO_3$ (~120dycm$^{-1}$) being greater than the oil (~ 20dycm$^{-1}$) used earlier, taller float-zones, and thereby different aspect ratios, can be investigated. Here a traveling ring-heater assembly was constructed and used to float-zone process 6mm diameter rods of $NaNO_3$. Figure 1a is a photograph (0.5s exposure) which shows, via fine quartz particles, thermocapillary flow in the liquid zone. Figure 1b shows when vibration, at a frequency of ~1.5kHz and amplitude of ~10μm, to the liquid zone was induced through the upper $NaNO_3$ rod the corresponding interface improved, i.e., became essentially planar, and flow decreased considerably. Again, radial temperature profiles improved and it was found that increasing the frequency effectively reversed the flow.

With these encouraging results, it was sought to demonstrate improved microstructural homogeneity. The $NaNO_3$-$Ba(NO_3)_2$ system was re-evaluated[12] and found to have a eutectic point at ~18 wt pct $Ba(NO_3)_2$. "Alloys" of this composition were cast into 6mm diameter rods for float-zone processing with the intent of comparing distribution of the respective phases. Figure 2a is a cross-sectional micrograph of the eutectic which was solidified by the float-zone method, *without* vibration, at a rate ≈ 2.6mmhr$^{-1}$. The $Ba(NO_3)_2$ phase (white) is flake-like and

distinctly finer in the center whereas on the sample periphery it is branched and coarser. By analogy the former is characteristic of low temperature gradients and the latter by high, an observation that has been verified by *in-situ* temperature measurements[12]. When vibration is introduced to the system the solid/liquid interface, as in pure $NaNO_3$, flattens and subsequent examination reveals, Figure 2b, a uniformly coarse microstructure as a result of a uniform temperature gradient.

(a) (b)

Figure 1: (a) Thermocapillary flow in $NaNO_3$, (b) Cessation of flow and flattening of the upper solid-liquid interface after applying vibration, ~1.5kHz, amplitude ~10μm.

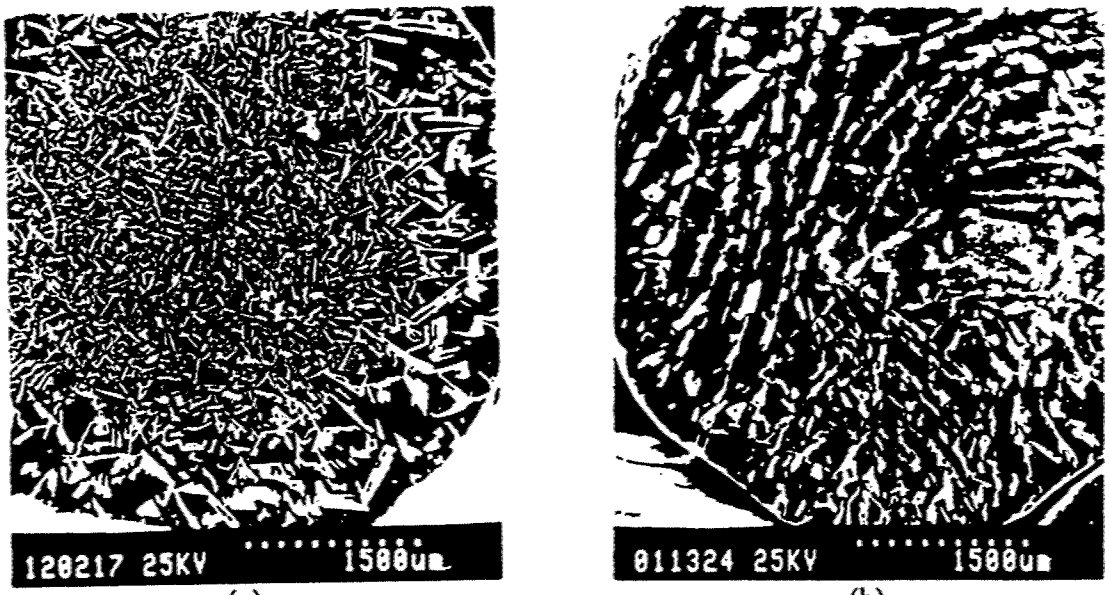


(a) (b)

Figure 2: (a) Transverse section of the eutectic microstructure solidified without vibration, (b) Microstructure with applied vibration, ~1.5kHz, amplitude ~10μm. Growth velocity ≈ 2.6mmhr$^{-1}$.

Description of Experimental and Analytical Method

The ground-based work will concentrate on defining the role various processing parameters play in promoting microstructural uniformity during floating-zone crystal growth. In particular float-zone dimensions, aspect ratios, oscillation frequency, and amplitude will be evaluated with the intent of understanding how thermocapillary flow is negated. To this end, work has already been initiated by utilizing the transparent nitrate model systems; further insight regarding crystal homogeneity will be gained by processing $NaNO_3$ crystals which have been doped with $AgNO_3$.

One particular ground-based investigation will concentrate on superposing vibration-driven surface-streaming flow (SSF) on thermocapillary convection, in a $NaNO_3$ half-zone, close to the critical point when temperature and flow oscillations are seen. It is well established that temperature oscillations cause striations in crystals. The questions then posed are: (i) can an opposing SSF lower the Marangoni number so that oscillatory thermocapillary flow becomes steady and, (ii) can a superposed SSF push steady thermocapillary flow into an oscillatory mode? These points will be addressed through well executed experiments and considerable insight will be gained regarding the strength and range of SSF.

In view of the successes described earlier, substantial effort will also be directed to negate thermocapillary flow in commercially viable materials, e.g., silicon and/or germanium-based semiconductors. Using Si and Ge-based materials is an advantage in that thermocapillary convection dominates and promotes microsegregation even in a microgravity environment. Furthermore, given their commercial importance, the crystals can be well characterized by utilizing a wide range of well established methods. Growth of the silicon and/or germanium-based semiconductors will be conducted in either the Single Ellipsoid Mirror Furnace, which was flown on the D1 mission, or the relatively new Paraboloid-Ellipsoid Mirror Furnace (Elli) which was specifically developed for growing crystals in space and used during the D2 mission.

A parallel effort will concentrate on modeling the SSF and its parameter range. It will be superposed on thermocapillary flow to study the balancing in a flow field, the latter represented on a grid scale. Trends from experimental observations and the developing theory will be evaluated and used to predict and optimize processing parameters for crystals of, for example, different scale or compositions. These predictions will be checked, and modified, against the results from crystals grown in the laboratory. The ground-based work will be invaluable in defining a flight experiment with the results serving to optimize the time available for microgravity processing while also providing a base to which the flight samples can be compared.

The crystals which are grown will be well documented in terms of the processing parameters. These include composition, translation rate, temperature profile, float-zone dimensions, aspect ratios, oscillation frequency, and amplitude and will be evaluated with the intent of optimizing microstructural homogeneity.

Collaborative Effort

Very briefly, the Crystal Growth and Solidification branch of MSFC has considerable experience in processing and characterizing semi-conductor crystals. Furthermore, it is ideally suited to house and conduct ground-based experiments with a potential flight capable furnace. Vanderbilt University (Co-I's. Prof. T.G. Wang and Dr. A.V. Anilkumar) is well equipped to facilitate the research described above. A traveling-ring heater for float-zoning of "model" materials used in previous studies[9-11] is available for further investigative purposes. The Crystallographic Institute of the Albert-Ludwigs-University (Co-I. Dr. A. Croll) has been involved in semiconductor growth and space experimentation since 1974. The Institute developed several mirror furnace prototypes which were later adapted for flight units onboard Spacelab and for sounding rockets. IBM's laboratory (Co-I. Mr. J. Hurd) brings to the proposed investigation not only scientific expertise, but also a world class analytical capability which can fully characterize and evaluate crystalline microstructural defects and solute distribution.

References


1. R.A. Brown: *AIChE Journal*, 1988, vol. 36, no. 4, pp. 881-911.
2. S. Eugen: Proceedings of IEEE, 1987, vol. 7, no. 7.
3. F. Rosenberger: Fundamentals of Crystal Growth, 1979, Springer, New York.
4. E. Kadis: Crystal Growth of Electronic Materials, 1985, North-Holland.
5. J.C. Brice: Crystal Growth Processes, 1986, Halsted Press, New York, pp. 157-162.
6. C.W. Lan and S. Kou: *J. Crystal. Growth*, 1991, vol. 108, pp. 1-7.
7. M.B. Barmatz and A.D. Morrison: *NASA Tech Brief*, 1988, vol. 12, No. 11, Item #66.
8. A.V. Anilkumar et al: *J. Appl. Physics*, 1993, vol. 73, no. 9, pp. 4165-4170.
9. X. Shen et al: Proc., "Microstructural Design by Solidification Processing", Materials Week '92, Chicago, IL, 1-5 November 1992, eds., E.J. Lavernia and M.N. Gungor, TMS, pp. 173-182.
10. R.N. Grugel et al: Proc., "The Inter. Work. on *g*-Jitter," Clarkston Univ., June 1993, p. 93.
11. R.N. Grugel et al: *J. Crystal Growth*, 1994, vol. 142, pp. 209-214.
12. R.N. Grugel, Fay Hua, and T.G. Wang: *J. Mat. Science Letters*, 1994, vol. 13, p. 1419.

# MICROGRAVITY PROCESSING OF OXIDE SUPERCONDUCTORS

William H. Hofmeister, Robert J. Bayuzick, and James R. Olive
Vanderbilt University
Nashville, TN 37235

N.B. Singh, Westinghouse Science and Technology Center, Pittsburgh, PA 15235
Marcus Vlasse, Marshall Space Flight Center, Huntsville, AL 35812
R. William McCallum, Ames Laboratory, Iowa State University, Ames, IA 50011

Since the discovery of superconductivity in lanthanide-based perovskite systems, considerable effort has been concentrated on the synthesis and characterization of these materials. The YBaCuO system has received the most intense study, as this material has shown promise for the application of both thin film and bulk materials. There are many problems with the application of bulk materials; weak links, poor connectivity, small coherence length, oxygen content and control, environmental reactivity, phase stability, incongruent melting behavior, grain boundary contamination, brittle mechanical behavior, and flux creep. The extent to which these problems are intrinsic or associated with processing is the subject of controversy. This study seeks to understand solidification processing of these materials, and to use this knowledge for alternative processing strategies, which, at the very least, will improve the understanding of bulk material properties and deficiencies.

In general, the phase diagram studies of the YBaCuO system have concentrated on solid state reactions and on the $Y_2Ba_1Cu_10_x$ + liquid $\rightarrow$ $YBa_2Cu_3O_{7-\delta}$ peritectic reaction. Little information is available on the complete melting relations, undercooling, and solidification behavior of these materials. In addition, rare earth substitutions such as Nd and Gd affect the liquidus and phase relations, increasing the width of the superconducting phase from a line compound to a solid solution. These materials have promising applications, but lack of information on the high temperature phase relations and the role of oxygen partial pressure has hampered research. In general, the understanding of undercooling and solidification of high temperature oxide systems lags behind the science of these phenomena in metallic systems. Therefore, this research investigates the fundamental melting relations, undercooling, and solidification behavior of oxide superconductors with an emphasis on improving ground based synthesis of these materials.

The difficulties of processing these materials in one g present a clear case for microgravity processing. For example, the large density differences in these multicomponent systems cause sedimentation in the melt. Also, $YBa_2Cu_3O_{7-\delta}$ has a very low thermal conductivity, such that moderate heating and cooling rates develop large thermal gradients in the melt, thereby driving convection. Furthermore, these materials react with all known containing media. The poor electrical conductivity at room temperature prevents the use of more conventional electromagnetic containerless processing techniques. For various reasons, other techniques for containerless processing are not appropriate because control of the processing environment is crucial to maintaining oxygen stoichiometry and preventing contamination by other gasses such as $CO_2$. Heat capacity, viscosity and surface tension measurements on the undercooled liquid melt cannot be done on earth but can be obtained in microgravity. Fundamental studies of the melting, undercooling, and solidification behavior under the highly controlled conditions possible in a microgravity environment will lead to a greater understanding of these materials. In addition, it will be possible to produce benchmark materials in space.

Significant progress has been made in understanding the above mentioned phenomena. The liquidus of the $YBa_2Cu_3O_{7-\delta}$ has been determined to be above 1800 °C, a considerably higher temperature than reported in the literature[1-2]. In addition, deep undercooling of these materials has been accomplished. In many cases tetragonal $ReBa_2Cu_3O_x$ was solidified directly from the melt, demonstrating that formation of the intermediate phases in these systems can be avoided by melt processing and undercooling.

Aero-Acoustic Levitation (AAL) experiments provide a means for direct observation of large (2.5 mm) samples during processing. The Ultra High Speed Thermal Imaging (UHSTI) system developed at Vanderbilt has proven to be useful for obtaining spatial thermal information during melting and solidification. Upon rapid solidification, several thermal events have been observed, most notably a low temperature (~1080 K) slow moving event which leads to a cellular structure with tetragonal $YBa_2Cu_3O_x$ being the primary solidification phase. When full melting of the sample is obtained, single phase tetragonal $YBa_2Cu_3O_x$ is formed upon recalescence.

Formation of tetragonal $YBa_2Cu_3O_x$ from the melt in AAL indicates that indeed it is possible to deeply undercool melts and avoid formation of the intermediate phases in these systems. However, with AAL, sample motions and large thermal gradients have continued to hamper diagnostics. Therefore, preliminary experiments have begun in collaboration with Space Systems/Loral using the Electrostatic Containerless Processing System (ESCAPES). This facility provides the advantage of excellent sample stability and improved diagnostic capabilities. The disadvantage is that processing atmospheres are limited. Electrostatic field continuity appears to be limited to extremely low pressures (< $10^{-3}$ Torr) or extremely high pressures (> 1520 Torr). In preliminary experiments under vacuum ($10^{-7}$ Torr), a dramatic recalescence event occurred at low temperature (~1000 °C). This event looks to be the same one encountered in AAL experiments.

Drop tube experiments at Vanderbilt University have concentrated on determining the high temperature phase relations in $YBa_2Cu_3O_{7-\delta}$, $NdBa_2Cu_3O_x$, $GdBa_2Cu_3O_x$, and combinations of each. These experiments involve melting small powders (< 400 μm) in a 2-meter drop tube which allows for control of processing environment and temperature. Table 1 lists the experiments performed to date.

| *Sample Material* | *Temp. (°C)* | *Atmosphere* | *Powder Size (μm)* |
|---|---|---|---|
| Y-123 | 1650 | 20 % $O_2$ / He | 44 - 295 |
| Y-123 | 1750 | 20% $O_2$ / He | 44 - 295 |
| Y-123, Nd-123, Gd-123 | 1720 | 20% $O_2$ / He | 75 - 400 |
| Y-123, Nd-123 | 1650-1800 | Pure $O_2$ and He | 100 - 150 |
| $Y_{.9}Nd_{.1}Ba_2Cu_3O_x$ | 1650-1800 | Pure $O_2$ and He | 100 - 150 |
| $Y_{.8}Nd_{.2}Ba_2Cu_3O_x$ | 1650-1800 | Pure $O_2$ and He | 100 - 150 |

**Table 1.** Drop Tube Experiments Performed to Date.

The earliest drop tube experiments revealed that the overall melting temperature in the $YBa_2Cu_3O_{7-\delta}$ system is considerably higher than that reported in the literature[1-2]. At 1650 °C, processed samples contained uniformly dispersed, faceted $Y_2O_3$ particles in a eutectic matrix,

indicative of an alloy heated into the solid + liquid region of the phase diagram and subsequently quenched. Experiments performed at 1750 °C exhibited a duplex microstructure, typical in samples that have been undercooled and rapidly solidified[3]. In these experiments, two new solidification phases were identified; a pseudocubic $YBa_2Cu_{3.2}O_x$, and tetragonal $BaCu_2O_x$. These solidification structures provide an alternate path to subsequent formation of superconducting orthorhombic $YBa_2Cu_3O_{7-\delta}$. Initial annealing experiments have produced materials with intragranular critical current densities as good as bulk materials processed by other means.

Drop tube experiments performed on Nd-123 and Gd-123 at 1720 °C revealed that the high temperature oxide phases in both of these systems have a lower melting point than that in the Y-123 system. X-ray diffraction and optical microscopy revealed that the smallest (75-100 μm) resultant spheres undercooled to below the superconducting phase peritectic and formed single phase tetragonal 123 in both cases. In the Y-123 samples, some of the sample morphologies consisted of a duplex structure where faceted $Y_2O_3$ particles existed along the outer surface of the drops. Others had large $Y_2O_3$ dendrites surrounded by a eutectic matrix of barium and copper oxides. In these experiments the presence of large faceted primary oxide particles is an indication that the highest temperature reached was in the liquid plus solid region of the phase diagram.

Experiments performed over a range of temperatures in pure $O_2$ provided a method for schematically mapping out the liquidus between pure Y-123 and pure Nd-123. The results are shown in figure 1. Here, it can be seen that at 1800 °C, Y-123 did not melt completely. At 1650 °C, single phase tetragonal Nd-123 is prominent. Substitution of slight amounts of Nd into $YBa_2Cu_3O_{7-\delta}$ tend to lower the melting point of the compound. In figure 1, the beginnings of a liquidus between Y-123 and Nd-123 can be seen. Experiments are planned to complete the definition of these phase relationships. This will provide valuable information as to the free energy of mixing due to substitution of other rare earths for yttrium.

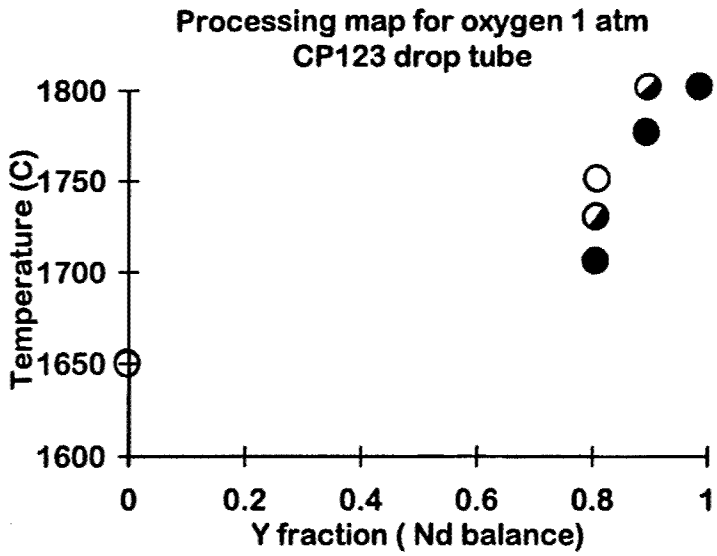


Figure 1: Summary of drop tube experiments. Open circles represent fully melted drops at the indicated temperature. Closed circles indicate the presence of faceted oxide particles and incomplete melting.

Experiments performed in pure helium revealed the large propensity for these compounds to release oxygen at elevated temperatures. In all cases, the materials began to decompose to the more stable metals almost immediately subsequent to processing. Experiments are planned to continue the fundamental high temperature phase relationships using the 2-meter drop tube at Vanderbilt. In addition, electrostatic levitation experiments will be performed on 2.5 mm drops to determine the viability of this technique for ground based containerless processing on these systems.

An additional goal of this program is to develop collaboration with other groups and provide access to the unique processing strategies developed by the microgravity program. Ultimately this research effort will lead to a proposed flight experiment where investigators from industry, national laboratories, and universities could participate in highly controlled experiments on the melting and solidification behavior of oxide superconducting systems.

References

1. R.S. Roth, K.L. Davis and J.R. Dennis, Adv. Ceram. Mater. 3B, v. 2, (1987) 303.
2. K. Osamura and W. Zhang, Z. Metallkunde 82, (1991) 408.
3. R. Mehrabian, Int. Met. Rev. 27, 185 (1982).

# DIMENSIONAL STABILITY OF SUPERMATRIX SEMICONDUCTORS

Douglas E. Holmes
Electronic Materials Engineering
829 Flynn Road
Camarillo, CA 93012

(805) 445-4500

Electronic Materials Engineering has established a unique research and development project focused on a new class of semiconductor materials for electronic and optoelectronic applications referred to as Supermatrix Semiconductors (SMS). SMSs are two-phase ìsingleî crystals, or "single double" crystals, in which the phases form in oriented, periodic, and crystallographically aligned arrays in 3 dimensions. SMSs are produced by a single-step solidification process under conditions where the two solids are in equilibrium with the melt at or near the eutectic composition (directional solidification of eutectics).

Motivation for investigating SMS materials and processing technology includes the potential to produce a 3-dimensional quantum superlattice, which would make possible for the first time new device structures based on the Quantum Cable. In addition, as composite materials, SMSs can exhibit properties not inherent to the respective component phases. For example, in the GaAs/CrAs rod-matrix system, the GaAs matrix is optically birefringent due to residual anisotropic stress. As a result, this material could have major technological applications in high speed nonlinear optical photonic devices needed for collecting, transmitting, storing, and analyzing large quantities of information in advanced commercial and DoD systems, such as C3I. Furthermore, virtual parallel processing of multi-phase materials offers several advantages compared to serial processing by epitaxy.

The application of SMS materials to device applications will generally require a microstructure with high dimensional stability. Dimensional stability refers to the degree of periodicity across the interface and the continuity of the microstructure along the direction of solidification. SMS materials have been produced by both the vertical Bridgman and the Czochralski methods.

It has been demonstrated that high dimensional stability is difficult to achieve under fluctuating conditions of microscropic solidification. Dynamical adjustments of the microstructure occurring under such conditions create microdefects in abundance. On the other hand, near photolithographic fidelity of an ideal, hexagonally packed rod-matrix microstructure has been achieved under conditions of effective diffusion-controlled segregation at high rates of solidification where the diffusion boundary layer is decoupled from velocity and temperature fluctuations in the melt.

Producing SMS material is therefore problematic because the solidification conditions necessary for dimensional stability also favor morphological instability (i.e., the maintenance of a planar, non-dendritic solidification front). The key to this dilemma is to substantially reduce hydrodynamical flows in the melt thus promoting near-diffusion-controlled segregation at reduced rates of solidification and morphological stability at reduced temperature gradients.

The overall mission of the program is to demonstrate that low gravity is an enabling environment for producing SMSs with high dimensional stability. Furthermore, a broader understanding of the cause-effect relationships between the microstructure of multi-phase materials and conditions of solidification shall be investigated. It is intended that quality research will lead to future space-flight experiments and that new technology so gained will be applicable to improved ground-based development and production of SMS materials.

Magnetic damping will be the cornerstone of the program, and the application of interface demarcation will provide a powerful research tool in understanding the dynamics of microstructural adjustment and in verifying the benefit of low gravity conditions.

Magnetically stabilized solidification of SMS materials shall be developed and compared to conventional processing methods. The program shall proceed initially by integrating an electro-magnet with Czochralski crystal growth equipment available at Electronic Materials Engineering. Ge/GeAs has been chosen as the demonstration vehicle because the physical-chemical properties are attractive for space-flight experimentation. In addition, a conventional process on which to base magnetic stabilization has already been established at the contractorís site.

The impact of magnetic stabilization on dimensional stability will be assessed by determining the dependence of microstructural features on magnetic field strength. Key features include the average and standard deviation of rod diameter and inter-rod spacing, the average length of continuous rods, and the incidence of terminations, nucleations, branching, and coalescence.

A fully developed growth system with magnetic stabilization and interface demarcation will serve as a SMS test bed to achieve a broader understanding of multi-phase solidification. Interface demarcation will enable the quantitative determination of macro- and microscopic interface shape and instantaneous rate of solidification. In addition, the injection of absolute time markers will provide a tool to quantitatively investigate the dynamics of morphological stability and microstructural adjustment to time and spatial fluctuations of solidification conditions. Thus the impact of low-gravity conditions on microstructure and optoelectronic properties can be evaluated. Quantitative empirical results will provide guidance for future theoretical assessments.

To assure thorough characterization of materials produced during the program, Professor Eike Weber of UC Berkeley will assist in providing structural (TEM, HREM) and optoelectronic (Hall effect, photoluminescence) measurements.

# NON-EQUILIBRIUM PHASE TRANSFORMATIONS

Kenneth A. Jackson
University of Arizona
4715 East Fort Lowell Road
Tucson, AZ 85712
(520) 322-2981
kaj@shadow.aml.arizona.edu

## Introduction

The goal of this research is to develop an understanding of the structure and properties of multi-component materials produced by phase transformations which occur under conditions which are far from equilibrium. The development of a sound physical understanding of non-equilibrium phase transformations in alloys or mixtures is perhaps the most important and challenging outstanding basic problem in materials science today. There have been many experimental studies designed specifically to explore this regime, but the underlying physical processes are not properly understood. Ad hoc equations have been used to fit experimental data and these have remained essentially unchanged for the past decade. We are using Monte Carlo modeling based on the Ising model, which played a major role in developing our understanding of the atomic level processes in the crystallization of pure materials, to study crystallization processes in alloys. The computer modeling provides a powerful tool to help us to understand the experimental results, to develop a detailed understanding of the processes involved, and as a predictive tool for guiding experiment.

Projects supported by NASA are making major experimental contributions to our understanding of nucleation and crystallization in the regime where these effects are important, including for example, the microstructure of rapidly solidified small droplets, and the distribution of the component elements resulting from nucleation and growth in containerless processing. Our simulations provide a new theoretical framework for the interpretation of these experiments.

Experimentally, we are pursuing measurements of the growth rate and orientation dependence of the segregation coefficient in InSb using a Bridgman apparatus, making use of atomic absorption and spreading resistance measurements to determine concentrations, and Peltier pulsing to determine growth rates. The orientation dependence of the segregation coefficient for a number of dopants in InSb has been reported, but the growth rate dependence has never been measured systematically. It must depend on growth rate since the equilibrium segregation coefficient cannot be orientation dependent. Our recent experimental results suggest that convection is a major problem, even though convection effects should be minimal in the Bridgman configuration. It is now apparent that experiments will have to be conducted in a convection free, reduced gravity environment in order to obtain reliable results. We plan to submit a proposal for flight experiments to complement our with ground-based experiments. The baseline capabilities of the MEPHISTO facility appear to be ideal for these experiments.

## Monte Carlo Modeling

In the conventional quasi-equilibrium model for crystal growth, the growth rate of a crystal is written as:

$$v = v_0\left[\exp\left(-\frac{L}{kT_M}+\frac{E_L}{kT}\right)-\exp\left(\frac{E_S}{kT}\right)\right] \tag{1}$$

Here $v_o$ is a temperature dependent prefactor, L is the latent heat of fusion, $E_L$ and $E_S$ are the internal energies of the liquid and solid respectively, T is the temperature in degrees Kelvin, $T_M$ is the melting point and k is Boltzmann's constant. This form assures that the growth rate is zero at $T = T_M$, since $E_L - E_S = L$. The internal energies should be replaced with enthalpies if that is appropriate. This expression is based on the thermodynamic type assumption that all growth sites are equivalent, and predicts that the growth rate is linear with undercooling near $T_M$. An expression for the growth rate which is very similar in spirit can be written as:

$$v = v_0\left[\exp\left(-\frac{L}{kT_M}-\frac{\Sigma\phi_L^i}{kT}\right)-\exp\left(-\frac{\Sigma\phi_S^i}{kT}\right)\right] \tag{2}$$

where the $\phi$'s are bond energies given by $L = E_L - E_S = (\phi_S - \phi_L)Z/2$, where Z is the number of nearest neighbors in the solid. The summation is over the nearest neighbors for each of the atoms at the interface. Eqn. 2 is conceptually very simple, and it is an embodiment of the classical Kossel-Stranski model for crystal growth. The two equations look similar, but the similarity is deceptive. For example, when $L/kT_M$ is large, the surface will be smooth, and there will only be isolated adatoms on the surface of the crystal, so the growth rate will depend on the rate of nucleation of new layers. This behavior is captured by Eqn. 2, but not by Eqn. 1. However, the summations in Eqn. 2 cannot be performed except for special cases, because the distribution of nearest neighbors depends in detail on the configuration of the atoms at the interface. But the physics of Eqn. 2 can readily be treated by Monte Carlo computer simulation where the configuration of each atom at the interface is stored in the computer. For simulations of alloys, the $\phi$'s depend on both the species of the nearest neighbors as well as whether they are in the solid or liquid.

The results derived from this model are in fact much more general than its deceptively simple assumptions suggest. The behavior of the system depends on the long range effects which are produced by the short range interactions between neighboring atoms. For example, even though each atom influences only its nearest neighbors, these interactions can produce large flat crystal surfaces. These long range effects are known as cooperative processes, and these cooperative processes depend strongly on the energy of the local interaction compared to the thermal energy, kT. At low temperatures the local interactions produces long range order, but at high temperatures the thermal energy overcomes the tendency to order. There is a critical temperature where a relatively abrupt transition from order to disorder occurs. This critical temperature depends on the details of the local interactions, but it has been found that the degree of order in a variety different systems depends only on the ratio $T/T_C$. Systems which have the same behavior relative to their critical points are said to belong to the same "universality" class. Surprisingly, members of the same uni-

versality class have in common only the number of components in their order parameter and the number of dimensions in which the system exists. The details of the local interactions determine $T_C$ but not the universality class. The ferromagnetic Curie point, order-disorder transitions, and even the liquid-vapor critical point all belong to the same universality class. These all belong to the universality class which bears the name Ising, since he first analyzed a model for the ferromagnetic Curie point based on a simple cubic lattice with interactions between spins on neighboring sites. This model correctly describes the critical point behavior of all the members of its universality class. Crystal growth from the vapor phase maps directly onto this model. It is not so obvious that it should apply equally well to growth from the liquid phase. But that is much less of a stretch than to understand why this universality class also includes the liquid-vapor critical point. The long range effects which are common within a universality class are independent of the details of the local interactions, provided that the behavior is scaled properly to the critical temperature which does depend on the details of the local interactions.

We have reported earlier [1, 2] on simulations for a "diffusionless" transformation, where the transformation takes place by the motion of the interface, but the atoms do not move: their position is fixed on lattice sites. These simulations correspond to a transformation where the interface moves very rapidly, such as, for example, in a "shear" or martensite-type transformation, where the atoms do not have time to make "diffusive" jumps as the transformation front passes.
The growth rate in the simulations of diffusionless growth was found to be zero on the $\mathbf{T_0}$ line for the alloy. On this line, the free energy of the solid alloy is equal to the free energy of the liquid alloy with the same composition. This is clearly the expected behavior for a diffusionless transformation. The equilibrium condition for a diffusionless transformation should depend on the difference between the free energies of the two phases, rather than on the difference between the chemical potentials of the species present in the two phases. For a diffusionless transformation, "freezing" or "melting" should be reversible at $\mathbf{T_0}$, depending on which phase has the lower free energy. These simulation results provided the first clear-cut confirmation of this expectation.

## Growth Rate Dependence of k

Data from simulations have been accumulated for a variety of different growth temperatures and with various diffusion coefficients [3]. The thermodynamic properties of bismuth in silicon have been used as a model system for many of these simulations since bismuth is a typical dopant in silicon and these alloys have been studied extensively experimentally. For the simulations a growth temperature is chosen and a normalized growth rate is calculated from the net number of atoms added to the crystal during the simulation. The variation of the distribution coefficient with normalized growth rate in two dimensional simulations of growth using a square lattice with growth in a <10> direction is plotted as **k** vs $\beta$ where $\beta = v^2/a\Gamma v^+ = av^2/4Dv^+$in Fig. 1. The diffusion coefficient is related to the diffusion jump rate by $\mathbf{D} = a^2\Gamma/4$, where **a** is the interatomic spacing. The **k**-value in the simulations does not depend linearly on the growth rate, **v**, divided by the diffusion coefficient, **v/D**, as has been suggested [4 -8]. Data derived from simulations like the one reported in [9] also fall on this same curve, even though the concentrations in those simulations was much smaller: less than 0.2%, rather than 5%. The solid line in Fig. 1 is $\mathbf{k} = (\mathbf{ke} + \mathbf{A}\beta)/(\mathbf{1}+\mathbf{A}\beta)$ with A = 63, fitted to the data for <10> oriented growth.

## Orientation Dependence of k

Also shown in Fig. 1 are data from simulations for growth in the <11> direction. The dashed line is a plot of $\mathbf{k} = (\mathbf{ke} + \mathbf{A}\beta)/(\mathbf{1}+\mathbf{A}\beta)$, with $\mathbf{A} = 5$, fitted to the <11> data. The only difference between the simulations labeled <10> and those labeled <11> was the orientation of the interface. There is a dramatic difference in the **k**-value for the two orientations at the same growth rate. Extensive measurements of the orientation dependence of the **k**-value have been reported for the incorporation of dopants into laser melted silicon [10, 11]. The incorporation of the dopants is greater for growth on the faceted (111) plane than on other orientations where the surface is rough. The measured orientation dependence of the **k**-value for several elements has been fitted with the "Aperiodic Stepwise Growth Model" [11]. Qualitatively similar result have been observed experimentally during the Czochralski growth of silicon crystals [12,13] and InSb [14], where this is known as the "facet effect". These simulation results are consistent with the suggestion that the step velocity determines the incorporation of dopants into the growing crystal [14, 15]. dependence of the **k**-value.

## Comparison with Experiment

Experimental data for the **k**-value for bismuth in (100) silicon as function of growth rate as observed in laser annealing experiments [16, 17, 18] are compared with the Monte Carlo data for growth in the <11> direction in Fig. 2. The line is the dashed line from Fig. 1. The (100) surface of melt grown silicon is rough, and it should have a step density similar to the <11> interface in our simulations. The correlation between the simulation data and the experimental data requires a correlation between the growth rates in the simulations and in the experiments, since the time unit used in the simulations is based on the rate at which atoms are added at repeatable step sites, and the corresponding rate in the real world depends on a number of factors. This correlation was made comparing the temperature dependence of the growth rate at small undercoolings in the present simulations with molecular dynamics simulations [19] as a model, and with experimental measurements. This resulted in an estimate of $\mathbf{v} = 0.12\ \Delta\mathbf{T}$ m/sec for the relationship between growth rate and undercooling at the interface for (100) growth of silicon at small undercoolings in the real world. The Monte Carlo data for <11> growth can be fitted with $\mathbf{v}/\mathbf{v}^+ = 1.6\times10^{-3}\Delta\mathbf{T}$, from which $\mathbf{v}^+ = 75$ m/sec. Using this value, and the value for the diffusion coefficient which was used by Aziz et al. [18] in the analysis of their depth profile data, $\mathbf{D} = 2\times10^{-4}$ cm$^2$/sec., gives $\beta = 5\times10^{-3}\mathbf{v}^2$, where **v** is the experimental growth rate in meters/second. This was used to plot the experimental data in Fig. 2. There are uncertainties in the value of this fitting constant deriving from the values of both $\mathbf{v}^+$ and **D** which were used, but the agreement with the data of both Baeri et al [16] and White et al. [17] is surprisingly good, and perhaps too good in view of the expected difference between the data for <11> and <10)> as discussed in the previous section. The velocity dependence of the data of Aziz et al. [18] differs from both of the other sets of data as well as from the simulation results. The reason for this discrepancy is not clear at present. It should be noted that changing the constant **A** which correlates $\beta$ to the experimental velocity does not improve the fit, it merely shifts the simulation curve horizontally with respect to the experimental data.

## Summary

These Monte Carlo simulations provide statistical information about the consequences of the simplest possible set of assumptions which can be made to model alloy crystallization. These assumptions lead to some very complex behavior which apparently includes many of the features found experimentally in rapid solidification studies. The simulation results indicate that the **k**-value depends on the growth rate squared divided by the diffusion coefficient. The **k**-value in these simulations depends on the orientation of the interface, as it does in experiment: the incorporation of an impurity is greater on a more closely packed surface. The simulation results agree with some of the experimental results for the growth rate dependence of the **k**-value in silicon. These simulations provide a very powerful framework for exploring the details of first order phase transformations in alloys.

## REFERENCES

[1] K. A. Jackson, G. H. Gilmer, D. E. Temkin, J. D. Weinberg and K. Beatty, J. Crystal Growth, **128** (1993) 127.

[2] K. A. Jackson, G. H. Gilmer, D. E. Temkin and K. Beatty, Proceedings of the East-West Surface Science Workshop '94.

[3] K. A. Jackson, G. H. Gilmer, D. E. Temkin, and K. M. Beatty, "Microsegregation *Far From Equilibrium*", J. Cryst. Growth **163** (1996) 461.

[4] M. J. Aziz, J. Appl. Phys. **53** (1982) 1158.

[5] M. J. Aziz, Appl. Phys. Lett., **43** (1983) 552.

[6] M. J. Aziz, MRS Symp. Proc. **23** (1984) 369.

[7] L. M. Goldman and M. J. Aziz, J. Mater. Res. **2** (1987) 524.

[8] M. J. Aziz and T. Kaplan, Acta Metall. **36** (1988) 2335.

[9] K. A. Jackson, G. H. Gilmer and D. E. Temkin, "Monte *Carlo Simulation of the Rapid Crystallization of Bismuth-doped Silicon*", Phys. Rev. Letters, **75** (1995) 2530.

[10] M. J. Aziz and C. W. White, Phys. Rev. Letters, **57** (1986) 2675.

[11] R. Reitano, P. M. Smith and M. J. Aziz, J. Appl. Phys., **76** (1994) 2359.

[12] T. Abe, J. Cryst. Growth, **24/25** (1974) 463.

[13] A. J. R. de Kock in *Crystal Growth and Materials*, ed. by E. Kaldis, North-Holland (1977) 693.

[14] J. B. Mullin, in *Compound Semiconductors*, ed. by R. K. Willardson and H. L. Goering, Reinhold, (1962) 365.

[15] R. Reitano, P. M. Smith and M. J. Aziz, J. Appl. Phys., **76** (1994) 2359.

[16] P. Baeri, G. Foti, J. M. Poate, S. U. Campisano, and A. G. Cullis, Appl. Phys. Lett. **38** (1981) 800.

[17] C. W. White, B. R. Appleton, B. Stritzker, D. M. Zehner and S. R. Wilson, in *Laser and Electron Beam Solid Interactions and Materials Processing*, ed. J. F. Gibbons, L. D. Hess and T. W. Sigmon, MRS Symp. Proc. 1 North-Holland (1981) 59

[18] M. J. Aziz, J. Y. Tsao, M. O. Thompson, P. S. Peercy and C. W. White, Phys. Rev. Letters 56 (1986) 2489.

[19] M. H. Grabow, G. H. Gilmer, and A. F. Bakker, MRS Symp. Proc. **141** (1989) 349.

# PHYSICAL PROPERTIES AND PROCESSING OF UNDERCOOLED METALLIC GLASS FORMING LIQUIDS

W.L. Johnson and D.S. Lee, Keck laboratory of Engineering, 138-78 California Institute of Technology, Pasadena, CA 91125

## Objective

The objective of this ground-base definition project is to carry out containerless measurements of several physical properties of undercooled glass forming liquid alloys and to develop a flight experiment which exploits the unique advantages offered by a microgravity environment. Understanding both the nucleation of crystalline phases from the melt, the related phase separation of the undercooled liquid, and the glass forming ability of bulk metallic glasses will be the scientific focus of the investigation The physical properties to be studied include specific heat, thermal conductivity, total hemispherical emissivity, viscosity, atomic diffusion, and liquid surface tension. Knowledge of these properties is critical to the understanding of solidification, crystallization, liquid phase separation, and glass formation. This knowledge will be used to understand experimentally determined TTT-diagrams (time-temperature-transformation diagrams) for crystal nucleation. The alloys under investigation include binary, ternary, and higher order alloys of the early transition metal elements Zr and Ti with the late transition metals Ni and Cu and the simple metals Al and Be. Containerless processing using ground-base electromagnetic and electrostatic levitation (EML and ESL) will be employed. The development of AC modulation calorimetry using a ground base ESL facility will be explored. Development of a flight experiment to measure atomic diffusion coefficients, viscosity, and surface tension in the undercooled melt is anticipated.

## Microgravity Relevance

The AC modulation calorimetry (ACMC) method has already been developed and implemented on the TEMPUS facility as part of the IML-2 mission. A second set of experiments is scheduled to be carried out as part of the MSL-1 flight (1997). The ACMC method as implemented on TEMPUS utilizes the separate electromagnetic positioning and heating coils of TEMPUS to stably position a liquid drop and separately control its temperature under high vacuum conditions. Ground-base EML systems are incapable of simultaneously levitating and undercooling a liquid in a high vacuum environment since steady state levitation requires heat input that results in a high temperature melt. To undercool on the ground requires active gas cooling of the liquid drop which then makes quantitative analysis of heat flow dynamics impossible. The ground-base ESL method offers the opportunity to overcome this problem by decoupling the levitation and heating functions. The implementation of the ACMC method on the ground-base ESL will be investigated.

Atomic diffusion measurements in glass forming melts are critical to understanding the kinetics of crystal nucleation and growth in the undercooled state. Very little data is presently available on liquid alloys in the undercooled state. Ground base studies suffer from convection driven transport effects. To overcome this limitation, one can employ capillary techniques. However, such experiments are hampered by chemical reactivity of the melt and the capillary wall. A containerless method is required for reactive liquids. The microgravity environment offers the possibility of eliminating both the effects of gravity driven convection and the container reaction, making possible the measurement of intrinsic

atomic diffusion constants in reactive liquids both in the stable and undercooled region . This concept will be developed as a possible flight experiment.

## Preliminary Results

The project has a start date of 10/96. As such only preliminary results are available. Experiments using the ground base ESL technique will be discussed. Measurements of TTT-diagrams for bulk glass forming alloys will be presented. Measurements of viscosity and diffusion in the deeply undercooled melt (near the glass transition temperature) using several ground-base methods will be presented and discussed and the need for data at higher temperatures will be emphasized. The plan for future work will be outlined.

# RESEARCH REPORT ON THERMO-PHYSICAL PROPERTIES OF METALLIC GLASSES AND UNDERCOOLED ALLOYS - AC MODULATION CALORIMETRY ON THE TEMPUS FACILITY

W.L. Johnson and D.S. Lee, Keck Laboratory of Engineering, 138-78,
California Institute of Technology, Pasadena, CA 91125
and
H.J. Fecht and R.K. Wunderlich, Technical University of Berlin, Metalphysics
and Technology, hardenbergstr. 36, PN 2-3
10623 Berlin, Germany

## INTRODUCTION

This report describes the AC Modulation Calorimetry experimental method (ACMC), its implementation on the TEMPUS facility in low earth orbit, results of the IML-2 flight, and the proposed MSL-1 flight experiment currently in progress. The ACMC modulation calorimetry technique was originally developed by two of the authors, Fecht and Johnson [1], as a method of measuring the heat capacity of a liquid drop under containerless conditions in high vacuum using electromagnetic heating of the droplet. The technique was implemented using the experimental hardware provided by the TEMPUS electromagnetic heating and positioning system. Experiments were carried out in low earth orbit for the first time aboard the space shuttle during the IML-2 mission. Two sets of samples were investigated during IML-2. These included samples from the Fecht/Wunderlich group (TU Berlin) and the Johnson/Lee group (Caltech).

## EXPERIMENTAL METHOD

The ACMC method as implemented on TEMPUS employs the separate positioning and heating coils of the TEMPUS facility together with the ultrahigh vacuum environment of TEMPUS. The TEMPUS hardware includes a silicon pyrometer as well as a two color InAs pyrometer. These are used to measure the sample temperature. Spectral emissivity measurements were carried out separately on the IML-2 samples by Dr. C. Krishnan at Containerless Research Inc. The spectral emissivity data at 663 nm from CRI and the measured optical transmission constants for windows and mirrors of the optical viewing path on the TEMPUS facility were used to calibrate the silicon pyrometer data from tempus.

The technique is described in detail in references [1] and [2]. An 8 mm sphere of the sample alloy is positioned in the coil assembly using an rf quadropole positioning coil operating at 200 kHz referred to as the positioner. The sample is heated by a 400 kHz rf dipole field provided by a separate heating coil. The different frequency and geometry; of the heating and positioning fields allows separation of the total power input in additive components from the heater and positioner $P_{tot} = P_{heater} + P_{pos}$. For heat

capacity measurements, a sinusoidal modulation of the heater current is applied which produces an AC temperature response of the sample. The heat capacity can be determined one the amplitude of the power modulation is known and the sinusoidal temperature response of the sample is measured. The power to the sample can be determined by from the coupling of the heating coil to the sample or by knowing the total hemispherical emissivity of the sample and measuring is steady state temperature at a given power input. Both methods provide a means of reducing the temperature modulation data to obtain heat capacity values. The reader is referred to reference [3] for more details.

## GOALS AND OBJECTIVES

The goals of the MSL-1 mission are:

(1) To evaluate the precision and accuracy to which specific heat capacity of a high temperature liquid can be measured using the ACMC technique as implemented on TEMPUS thus establishing a benchmark for liquid calorimetry on high melting point liquid metals and alloys.

(2) To provide accurate date for the temperature dependence of the specific heat of several glass forming metallic alloys both in the equilibrium and undercooled liquid states.

(3) Use this data to calculate the temperature dependence of the entropy and Gibbs free energy functions for these glass forming liquid alloys.

The samples to be studied on the MSL-1 mission include pure Zr metal (Johnson/Lee) , a binary $Zr_{64}Ni_{36}$ alloy (Fecht/Wunderlich), a ternary glass forming alloy $Zr_{60}Ni_{20}Cu_{20}$ (Johnson/Lee), and a quaternary bulk glass forming alloy $Ti_{34}Zr_{10}Cu_{48}Ni_{8}$ (Johnson/Lee), and quinary glass forming alloys of Zr-Ti-Ni-Cu-Al and Zr-Co-Ni-Cu-Al (both groups). This alloy series represents a progressively more complex sequence of alloys which exhibit progressively better glass forming ability. For instance, the binary alloy forms glass at cooling rates of $10^6$ K/s while the quinary alloys, at the opposite extreme, form metallic glasses at cooling rates as low as 10 K/s. Part of the motivation of the MSL-1 experiment is to determine if the enhanced glass forming ability of the more complex alloys can be related to the specific heat and thermodynamic functions of the equilibrium/undercooled liquid state. For example, the specific heat determines the temperature dependence of the entropy and Gibbs free energy of the liquid which in turn determines the driving force for crystallization of the undercooled melt. The entropy of the undercooled melt can be used to determine the Kauzmann temperature, which in turn can be related to the glass transition temperature, etc.

**RESULTS (MAINLY FROM IML-2 FLIGHT)**

Samples flown on the IML-2 mission included: pure Zr metal, $Zr_{76}Ni_{24}$, $Zr_{64}Ni_{36}$, and $Nb_{40}Nb_{60}$, and a $Zr_{72}Fe_{28}$ sample. Stability problems with the samples in TEMPUS during IML-2 limited the available processing time for samples. Reasonable amounts of ACMC data were obtained on the first three binary alloys. Little or no data was obtained on Zr or the Zr-Fe alloy. We briefly summarize some of the most complete results on one of the alloys below:

**$Zr_{64}Ni_{36}$** ( from ref. [3])

| Temperature (C) | Mod. Frequency (Hz) | Total Hemisph. Emissivity (at $T_m$) | Heat Capacity (J/mole-K) |
|---|---|---|---|
| 1215 | 0.05 | 0.37 | 43.7 +/- 0.8 |
| 1160 | 0.08 | 0.35 | 44.5 +/- 1.2 |
| | 0.10 | | 43.2 +/- 1.0 |
| 1038 | 0.05 | 0.33 | 43.9 +/- 1.0 |
| | 0.08 | | 44.2 +/- 1.0 |
| 1008 | 0.05 | 0.32 | 44.0 +/- 1.0 |
| | 0.10 | | 44.6 +/- 1.0 |
| 980 | 0.05 | 0.32 | 45.5 +/- 1.2 |

The results on this alloy are the most extensively analyzed of the IML-2 results. The alloy could not be significantly undercooled during the IML-2 mission due to contamination problems which arose with the samples during the flight. As such, data were limited primarily to the equilibrium liquid region (this eutectic alloy has a eutectic melting temperature of 1010 C). Data for slight undercooling to 980 C was the best obtained. These contamination issues have been extensively addressed and the TEMPUS sample holders and containment system has been modified to eliminate such problems during the MSL-1 mission. This should result in far more extensive undercooling of the samples to be studied.

The problems with sample stability during the IML-2 flight were analyzed and determined to have arisen from a misalignment of the heating and positioning coils. Corrective measures have also been taken to ensure that these problems do not occur during the MSL-1 mission.

The MSL-1 mission is expected to provide a far more extensive test of the ACMC method. Extensive undercooling of the samples is to be expected both on the basis of having eliminated sample contamination problems and on the basis of having chosen several superior glass forming alloys which have been demonstrated to exhibit extensive undercooling in ground base experiments using electrostatic levitation (ESL) methods. The ground base studies are being carried out using the High Vacuum Electrostatic Levitation Apparatus in collaboration with Dr. W.Q Rhim at Jet Propulsion Laboratory. The use of the ESL methods to characterize the MSL-1 specimens has

provided pre-flight characterization of the undercooling expected for the MSL-1 samples and has permitted better design of the time, temperature, profiles for the flight experiment.

## REFERENCES


1. H.J. Fecht and W.L. Johnson, Rev. of Sci. Instr., **62**, 1299 (1991)

2. R.K. Wunderlich, R. Willnecker, and H.J. Fecht, Appl. Phys. Lett., **62**, 3111 (1993)

3. R.K. Wunderlich, D.S. Lee, W.L. Johnson, and H.J. Fecht, "Non-Contact Modulation Calorimetry of Metallic Liquids in Low Earth Orbit", submitted to Phys. Rev. Lett., in press, (1996)

# DISLOCATION FORMATION DURING GROWTH OF SEMICONDUCTOR CRYSTALS

Dr. Monica L. Kaforey
Case Western Reserve University
10900 Euclid Ave. White 330
Cleveland, OH 44106
(216)368-4219
e-mail: mlk14@po.cwru.edu

In the ongoing efforts to produce higher quality semiconductor materials, there is a continuous search for ways to consistently make materials with fewer defects. Thus, improvements in the understanding of how and why defects form would be extremely beneficial. This research will examine one of the factors believed to affect dislocation formation during the growth of semiconductor crystals.

During directional solidification of semiconductor crystals, dislocations propagate from the existing crystal to the growing crystal at the melt/solid interface and from the solid/crucible surface into the growing crystal. Modeling efforts have shown that the interaction between the crucible wall and the sample in the region of the melt/solid interface has a significant effect on dislocation formation. Previous experimentation in microgravity has shown that when the melt is not in contact with the wall of the crucible, the resulting crystal will have a lower dislocation density. It is hypothesized that the increased ability of the crystal to relieve stresses is responsible for the lower dislocation density. The proposed work will investigate the effect of forced contact versus detachment of the melt from the crucible wall on dislocation structure during directional solidification of semiconductor crystals. The proposed experiments will be performed using germanium doped to $10^{18}/cm^3$ gallium (Ga/Ge).

## Background

Dislocations are one of the primary defects found in semiconductors. Dislocations can result in semiconductor crystals for a variety of reasons. Two of the main reasons are (1) propagation from the seed crystal, and (2) shear strains due to mechanical or thermal stresses[1].

One approach to reducing the dislocation density has been to dope the material such that the critical resolved shear stress (CRSS) is increased so that the applied stress will not exceed the slip threshold[2-6]. An alternate approach to reducing the dislocation density would involve decreasing the applied thermal stress. Stresses in crystals grown by the Czochralski method have been studied[7-12]. Rosch and Carlson[5] summarize the results of these studies by stating that for crystals smaller than one diameter in height, a significant amount of stress is located near the solid-liquid interface and near the seed crystal. For crystals longer than 2 diameters, all of the significant stress if found at the interface. Also, the stress is higher near curved rather than flat interfaces. Significant amounts of stress found at the perimeter and center of the interface will cause more dislocations to form in these regions, while fewer dislocations form in the intervening region. Experimental results agree with the modeling efforts; reducing the thermal stress resulted in a crystal with a lower dislocation density.

The third possible approach to reducing the dislocation density is to reduce the applied mechanical stress. There are two potential sources of applied mechanical stress for a crystal grown using the vertical Bridgman method in which the melt is in contact with the crucible. The first location is at the location of the melt-solid interface. Semiconductors expand upon solidification. Thus, if the melt is in contact with the crucible when it solidifies, the crystal will be constrained by the crucible. This results in a compressive stress on the crystal. This mechanical stress may be removed by processing in microgravity where the melt may form a free surface such that the melt is not in contact with the crucible wall at the melt-solid interface. If the melt is not in contact with the crucible wall, the solidifying crystal is free to expand without experiencing the compressive stress due to the crucible.

The second source of mechanical stress from the crucible occurs in cases where the crucible contracts more than the crystal upon cooling. In this case, the crucible applies a compressive stress to the crystal. If the crystal contracts more than the crucible, the crystal may stick to the crucible, partially stick, or detach from the crucible wall. Rosch and Carlson[5] computed stress fields in GaAs during vertical Bridgman growth. They found that the crystal-crucible interaction was the most important parameter in determining dislocation generation. This source of mechanical stress has been minimized in the proposed experiments through the use of a pyrolytic boron nitride (PBN) crucible. The germanium crystal will contract more than the PBN crucible upon cooling.

In ground based experiments, the melt will remain in contact with the crucible wall due to the pressure of the hydrostatic head during vertical Bridgman crystal growth. One method which eliminates contact with a crucible is float-zone crystal growth. In this method, the melt is held in place, in opposition to gravity, between two ends of a rod by surface tension. This limits the diameter of the crystals that can be grown to a few mm[13]. Vertical Bridgman growth can be used to grow much larger crystals.

## Hypothesis

It is hypothesized that during crystal growth in microgravity a free surface may form on the surface of the melt. If the free surface forms in the region of the melt-solid interface, the defect concentration in the resulting crystal is expected to be reduced from that found in a crystal grown with forced contact with the crucible.

## Objective

The objective of the proposed research is to comprehensively study the effect of free surface formation on the dislocation density of directionally solidified doped semiconductor crystals and to correlate these results with appropriate numerical modeling efforts.

## Justification for Microgravity Research

Traditionally, solidification experiments have been done in microgravity due to the significant reduction in buoyancy driven convection that can be achieved in this environment. In the current research, it is the desire to form a free surface in the region of the melt-solid interface that necessitates a microgravity environment. In a 1-g environment, the hydrostatic head of the melt is sufficient to keep the melt in contact with the wall of the crucible during vertical Bridgman crystal growth. In microgravity, the pressure on the melt is reduced or eliminated depending on the orientation of the acceleration vector. This can lead to the formation of a free surface on the melt. Ideally, this free surface will form in the region of the melt-solid interface and thus provide a crystal in which to study the effect of the free surface on defect formation.

## Experimental Plan

This experimental program was designed to be done in the Get Away Special (GAS) Payload developed at GTE during the GTE Labs/USAF/NASA GaAs Crystal Growth in Microgravity Program. This payload contains two gradient freeze furnaces. The proposed sample material is germanium doped to $10^{18}/cm^3$ gallium.

The current funding covers ground based research only. Ground based research will include confirming the sample-ampoule design and its interaction with the furnace. The characterization methods to be used on the samples will be developed, including a technique for determining the dislocation density in the samples. Numerical simulations will be performed by the Computational Materials Laboratory at NASA Lewis Research Center and will be compared to the experimental results. A framework for a student organization will be developed to be used if this program is selected for flight in the future.

Microgravity is necessary to investigate the case of a melt detached from the crucible wall. If this program is selected for flight in the future, two experiments are proposed to be done in microgravity. One of these experiments would employ a spring to prevent the formation of a

free surface on the melt. In this experiment, interface demarcation will be done using current pulsing to further identify the interactions between the interface and dislocation formation. The second experiment would be performed without the use of a spring. In this experiment, it is anticipated that the melt could detach from the crucible wall. Note that in all vertical Bridgman ground-based experiments, the pressure of the hydrostatic head will be sufficient to keep the melt in full contact with the crucible wall.

Corresponding Modeling Effort

Full scale numerical simulations of the experiment are an integral part of the proposed work. The full furnace/ampoule/charge assembly will be included in a finite element numerical model. Time dependent simulations will track the entire experiment from cold start to final cool down, allowing the determination of the solidification thermal history in the growing crystal under the different growth scenarios. The time dependent thermal history will then form the input data base for subsequent calculations of the stress field. Using a viscoplastic Haasan-Alexander full crystallographic constitutive model with different boundary conditions reflecting the crystal detachment/attachment to the crucible, we plan to compute the dislocation multiplication and resolved stresses in each individual crystallographic slip system. Effects of different wall contact conditions could then be directly traced to dislocation generation and resolved stresses in the growing crystal.

Value of Research

Dislocations are detrimental to the performance of semiconductors in device applications. Optical properties[13], hardness[14-16], and electrical properties such as electron mobility[17] are sensitive to the dislocation density in semiconductors. This study should result in a significant improvement in the understanding of dislocation formation during semiconductor crystal growth due to an applied mechanical stress. This knowledge could be used to improve terrestrial

processes so that they can consistently produce single crystal semiconductors with fewer defects.

The more specialized knowledge on the effect of using a spring to force a melt to remain in contact with a crucible wall will be useful in planning future space station experiments. Springs have been used in past experimentation to prevent the formation of a free surface and maintain electrical contact. However, alternative designs could be developed if it is known that the effect of the spring is detrimental.

## References


1. C. Elbaum, Prog. Met. Phys. **28**, 1959, p. 203.
2. Robert A. Brown, "Theory of Transport Processes in Semiconductor Crystal Growth from the Melt," in Microelectronics Processing, ed. by Dennis W. Hess and Klavs F. Jensen, 1989, American Chemical Society, Washington, D. C., p. 35-103.
3. G., Jacob, M. Dusuaux, J. P. Farges, M. M. B. Van den Boom, and P. J. Roksnoer: J. Cryst. Growth **61**, 1983, p. 417.
4. A. Jordan, A. Von Neida and R. Caruso, J. Crystal Growth **70**, 1984, p. 555.
5. William Rosch and Frederick Carlson, J. Crystal Growth **109**, 1991, p. 75-81.
6. H. Kohda, K. Yamada, H. Nakanishi, T. Kobayashi, J. Osaka, and K. Hoshikawa: J. Cryst. Growth **71**, 1985, p. 813.
7. J. Lambropoulos, J. Crystal Growth **80**, 1987, p. 245.
8. J. Lambropoulos and C. Delametter, J. Crystal Growth **92**, 1988, p. 390.
9. C. Schvezov, I. Samarasekera and F. Weinberg, J. Crystal Growth **84**, 1987, p. 219.
10. C. Schvezov, I. Samarasekera and F. Weinberg, J. Crystal Growth **85**, 1987, p. 142.
11. C. Schvezov, I. Samarasekera and F. Weinberg, J. Crystal Growth **92**, 1988, p. 489.
12. Shahryar Motakef, J. Crystal Growth **114**, 1991, p. 47-58.
13. W. R. Wilcox: AIAA 91-0507, 1990.
14. R. S. Feigelson and R. K. Route: J. Cryst. Growth **49**, 1980, p. 399.
15. J. C. Fisher: Dislocations and the Mechanical Properties of Crystals, 1957, Wiley, New York.
16. H. G. Van Bueren: Imperfections in Crystals, 2nd ed., 1961, North-Holland, Amsterdam.
17. J. R. Dale and J. C. Brice: Solid State Electronics **3**, 1961, p. 105.

# ROLE OF DYNAMIC NUCLEATION AT MOVING BOUNDARIES IN PHASE AND MICROSTRUCTURE SELECTION

A. Karma, Department of Physics, Northeastern University, Boston, MA 02115, and R. Trivedi, Ames Laboratory of the Department of Energy and Department of Materials Science and Engineering, Iowa State University, Ames, Iowa, 50011

## INTRODUCTION

Nucleation at moving boundaries and the growth competition between different phases play crucial roles in the selection of phases and solidification microstructures. Some important examples include the formation of layered structures in peritectic systems [1-8], the formation of banded structures in laser processing of alloys [5,9-11], the formation of metastable phases in highly undercooled droplets [12, 13], and the selection of phases and microstructures in strip cast stainless steels [14-16].

The prediction of phase and microstructure selection is currently based on: 1) heterogeneous nucleation on a static interface, and 2) comparing the relative growth rate of different phase/microstructures (planar, cellular, dendritic, or eutectic) under steady-state growth conditions. The formation of new phases, however, occurs via nucleation on, or ahead of, a moving boundary. In addition, the actual phase and microstructure selection is controlled by a complex interaction between the nucleation process and the growth competition between the nuclei and the pre-existing phase under non-steady-state conditions.

This research addresses the critical role of nucleation at moving boundaries in the selection of phases and solidification microstructures through experiments in peritectic and eutectic systems and the development of reliable theoretical models. Initial studies are carried out in peritectic systems which provide a unique opportunity to examine these issues under well controlled experimental conditions and by accurate modeling.

## BANDING IN PERITECTIC SYSTEMS

For a specific range of compositions in the two-phase region, a banded structure is observed in which two phases alternate perpendicular to the growth direction. The spacing and composition variations of these nearly planar phases are dictated by the nucleation at or ahead of the moving boundary and the relative growth rates of the nuclei and the pre-existing phase.

The basic mechanism of band formation [17] is shown schematically in Fig. 1 for a situation where the growth is purely diffusion-controlled. As the parent ($\alpha$) phase

forms and grows towards its steady state, the nucleation of the second ($\beta$) phase becomes possible so that the system, instead of reaching its steady-state growth condition, transforms into the second phase. This phase, in turn, grows towards its steady-state, but before it reaches the latter, the parent phase nucleates again, and the cycle of alternate band formation is then repeated.

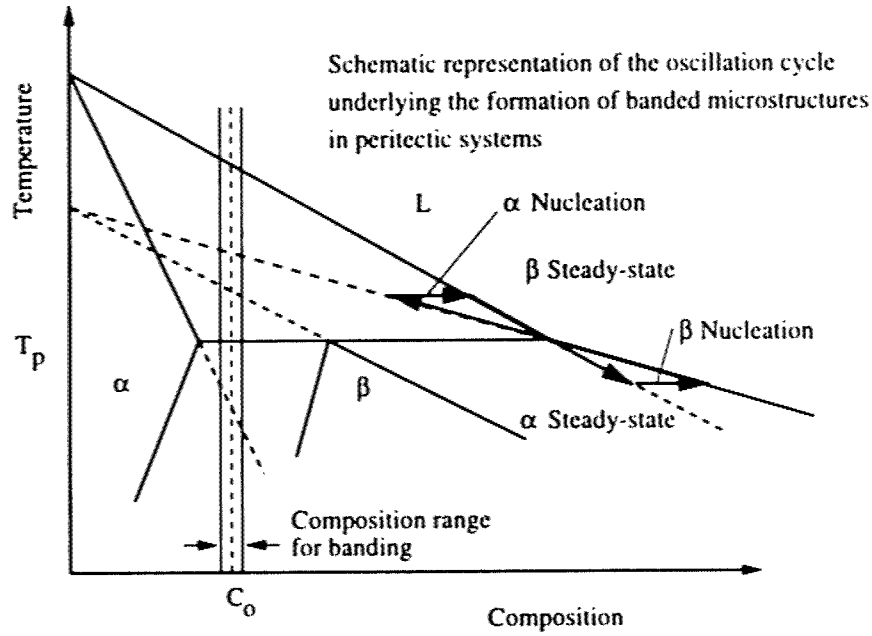


Figure 1: Schematic phase diagram of a peritectic system showing a nucleation controlled cycle of band formation in a purely diffusive regime.

## PRELIMINARY STUDY IN THE Pb-Bi SYSTEM

Ground based directional solidification experiments were carried out in a Bridgman furnace in Pb-Bi to establish the growth conditions and composition range for which layered structures can be formed as well as to make detailed measurements of composition and band spacings of the two phases. Examples of banded microstructures in this system are shown in Fig. 2.

A model was developed to describe banding under non-steady-state growth conditions in both diffusive and convective regimes. This model has been used to predict the nucleation undercooling of the first $\beta$-band and the amount of convection present in the system, as shown in Fig 3 below, and to study the effect of convection on the banding cycle, as shown in Fig. 4.

Experimental and modeling results so far have shown that:

1) Convection has an important effect on band formation:
   – It destabilizes band formation such that only a few bands are formed in a

Figure 2: Experimental micrographs showing band formation in the Pb-Bi system for a composition of 24%Wt Bi (left) and 33 %Wt Bi (right).

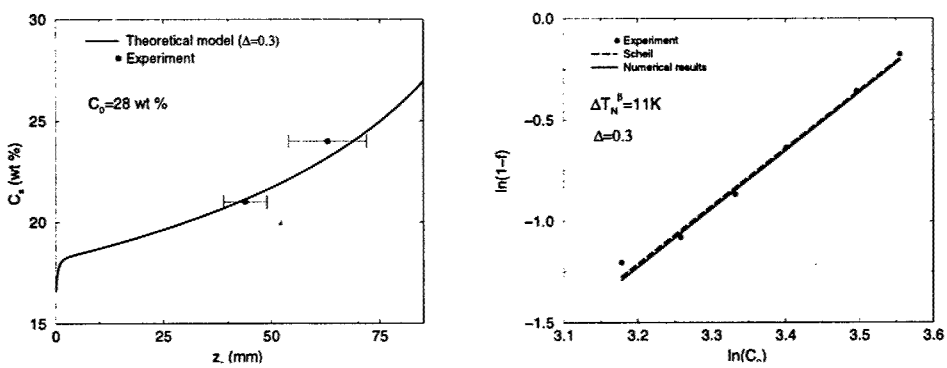


Figure 3: **Left:** Solid composition $C_S$ in the first $\alpha$ band as a function of distance in the sample $z_s$ predicted by the model. **Right:** Determination of the nucleation undercooling $\Delta T_N^\beta$ of the $\beta$-phase from the model. $f$ is the volume fraction of the first $\alpha$-band formed (i.e. the ratio of the length of this band to the length of the sample) and $C_o$ is the alloy composition. $\Delta T_N^\beta$ is defined as the difference between the stable $\beta$-liquidus temperature and the interface temperature when the first $\beta$-band is formed. $\Delta = dv_p/D$ where $d$ is the diffusion boundary layer thickness, $v_p$ is the pulling speed of the sample, and $D$ is the solute diffusivity. Also shown are the predictions of the Scheil equation which agree well with those of the numerical model because convection effects are large.

finite sample as shown by experiment in Fig. 2 and the model in Fig. 4.

– It introduces a large uncertainty in the determination of the nucleation undercoolings of the two phases because it causes the bands to depart from a planar morphology as shown in Fig. 2.

2) Only the first $\beta$-band forms by nucleation at the moving $\alpha$ phase. Subsequent $\beta$-bands are formed by growth from the edges.

3) The model predicts that $\alpha$-bands do not form by heterogeneous nucleation on the $\beta$-liquid boundary, as assumed in the idealized cycle of Fig. 1, but either by nucleation in the liquid ahead of the $\beta$-liquid interface, or by continuous regrowth of the $\alpha$-band. This is because, after the first $\beta$-band is nucleated, the interface temperature increases again, but up to a maximum temperature which is less than the peritectic temperature $T_p$. Hence, there is no driving force for heterogeneous nucleation of $\alpha$ after $\beta$ is nucleated the first time. The transient banding cycle shown in Fig. 4 occurs entirely below $T_p$ and was produced only under the condition that the $\alpha$ phase re-appears at some fixed temperature less than $T_p$.

## MICROGRAVITY RELEVANCE

Ground based experiments have shown that convection effects preclude the formation of regular banded structures over the entire length of the sample with a planar morphology. Thus, to perform a critical comparison of theory and experiment in a purely diffusive regime, where reliable quantitative modeling is possible, the effect of convection needs to be eliminated. Although convection can be minimized in thin samples, the presence of a meniscus curvature alters the diffusion field and potentially the dynamic nucleation process. Thus, to determine accurately the nucleation undercoolings of the two phases under non-steady-state growth conditions, microgravity experiments in bulk samples are required to obtain unambiguous results that can be compared accurately with the theoretical model developed for the diffusive regime.

## FUTURE DIRECTIONS

1) Identify peritectic systems where:

– Convection is reduced.

– Both phases form by dynamic nucleation at the boundary of the pre-existing phase.

– Bands form uniformly across the entire sample so that the mechanism of lateral growth is not operative.

2) Perform ground based experiments in thin samples and small capillary tubes to reduce convection.

3) Develop a phase-field model of peritectic solidification to study the nucleation process and the competitive growth of the nuclei with the pre-existing phase. Such

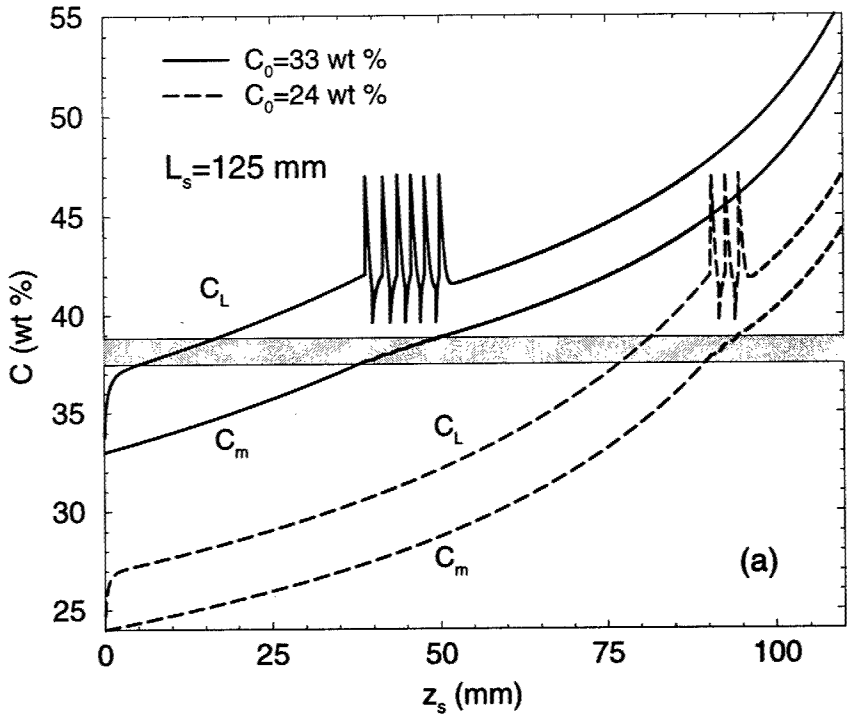


Figure 4: Results of the numerical model showing the liquid composition at the interface, $C_L$, and the melt composition outside the diffusion boundary layer, $C_m$, as a function of the position, $z_s$, of the solid-liquid interface along the sample. These results demonstrate that banding is destabilized by convection and only occurs when the melt composition $C_m$ traverses the composition range (shaded area) for stable band formation in a semi-infinite sample. For both compositions, the entire banding cycle occurs for interfacial temperatures below the peritectic temperature $T_p$. The $\alpha$-phase is taken to form at a fixed temperature below $T_p$, adjusted so as to produce the number of bands observed experimentally for $C_o = 33$ Wt% Bi. For this same temperature, fewer bands are then predicted to form for $C_o = 24$ Wt% Bi in agreement with what is observed experimentally. This is due to the fact that the rate of increase of $C_m$ with $z_s$ is larger at the end of the sample. Thus, the system spends a shorter period in a regime of stable band formation at 24 Wt% than 33 Wt%, thereby yielding fewer bands.

a model is currently being developed by extending the formalism used previously to construct phase-field models of eutectic growth [18, 19].

# References


[1] H.D. Brody and S.A. David, Int. Conf. Solidification and Casting, Sheffield, 139 (1977).

[2] A. Ostrowski and E.W. Langer, Int. Conf. Solidification and Casting, Sheffield, 144 (1977).

[3] N.J.W. Barker and A. Hellawell, Met. Sci. **8**, 353 (1974).

[4] W.J. Boettinger, Metall. Trans **5**, 2023 (1974).

[5] W. J. Boettinger, D. Shechtman, R. J. Schaefer, and F. S. Biancaniello, Metall. Trans. **15A**, 55 (1984). Acta Metall. **39**, 1431 (1991).

[6] H. Fredriksson, Scand. J. Met. **5**, 27 (1976).

[7] M. Bobadilla, J. Lacaze, and G. Lesoult, J. Cryst. Growth **89**, 531 (1988).

[8] T. Umeda and W. Kurz, "Phase and Microstructure Selection During Growth of Peritectic Systems" (to be published).

[9] W. Kurz and R. Trivedi, Acta Metall. **38**, 1 (1990).

[10] M. Zimmermann, M. Carrard, and W. Kurz, Acta Metall. **37**, 3305 (1989).

[11] M. Gremaud, M. Carrard, M., and W. Kurz, Acta Metall. **39**, 1431 (1991).

[12] J. H. Perepezko, Mat Sci. Eng. A**178**, 105 (1994).

[13] M. C. Flemings, NASA Workshop Presentation, Huntsville, AL. 1994.

[14] T. Takolo, N. Sutala, and T. Moisio, Metall Trans. **10**A, 1173 (1979).

[15] Y. Wu, T. J. Piccone, Y. Shiohara, and M. C. Flemings, Metall. Trans. **18**A, 915 (1987).

[16] T. Koseki and M. C. Flemings, "Phase and Microstructure Selection in Strip Cast Stainless Steels", in Proceeding of the U.S.-Japan Cooperative Science Program Seminar on Solidification Proces sing for the 21st Century, edited by M. C. Flemings, pp. 235-243 (1994).

[17] R. Trivedi, Metall. Mat. Trans. **26**A, 1583 (1995).

[18] A. Karma, Phys. Rev. E **49**, 2245 (1994).

[19] A.A. Wheeler, G.B. McFadden, and W.J. Boettinger, Proc. Roy. Soc. Lond. **452**, 495 (1996).

# Identification of Gravity-Related Effects on Crystal Growth from Melts with an Immiscibility Gap

**M. Kassemi*, A. Sayir**, S. Farmer*** and A. Chait*****

**NASA Lewis Research Center**
**Cleveland Ohio 44135**

## Abstract

This work encompasses a detailed experimental-numerical approach to study the effects of natural and Marangoni convections on solidification of single crystals from a silicate melt with a liquid-liquid immiscibility gap. Very little work has been done or published with regard to solidification from immiscible liquids. Preliminary experimental work in our laboratory has indicated that directional solidification of a single crystal mullite appears to be preceded by melt segregation where a liquid slightly enriched in $Al_2O_3$ is encapsulated in a $SiO_2$-rich liquid. This results in a unique growth configuration in which an alumina-rich crystal is adjoined by a silica-rich liquid and growth involves diffusion of solute from the encapsulated region through the stagnant layer to the solid-liquid interface. Disruption of the segregated state results in crystallization of a two phase structure. Therefore, in the $Al_2O_3$-$SiO_2$ system, the separation of the liquid phases is a desired result difficult to maintain on earth where mixing in the melt can disrupt single crystal growth. This is especially true when growing large diameter crystals, where mixing by the natural convective currents in the melt can only be eliminated by performing experiments under microgravity conditions. Determination of the necessary conditions for growing superior quality single crystals from the phase separated melt by isolating the effects of the various interacting transport processes is the desired outcome of this research effort.

## Introduction

Industrial use of crystals grown from silicate melts is becoming increasingly important in electronic, optical, and high temperature structural applications. Even the simplest silicate systems like $Al_2O_3$-$SiO_2$ have had, and will continue to have, a significant role in the development of traditional and advanced ceramics. A unique feature of crystals grown from the silicate systems is their outstanding linear electro-optic properties. They also exhibit exceptionally high optical rotativity. As a result, these crystals are attractive materials for dielectric, optical, and microwave applications.

In this work, we propose a combined experimental-numerical study of the role of gravity-driven convection on growth of single crystal mullites from the melt. High resolution digital images obtained in our laboratories at NASA Lewis demonstrate that mullite formation is preceded by a state of liquid-liquid immiscibility. To our knowledge, this is the first direct experimental evidence of liquid immiscibility reported for this system. Preliminary experimental results also reveal that mixing in the melt caused by density-driven convection can significantly affect the immiscibility of the liquid and result in different crystalline forms (stable or metastable crystalline phases; polycrystals or single crystals). On earth, the immiscible state has only been observed for small diameter crystals grown in float zone systems where natural convection is almost negligible. Therefore, it is anticipated that growth of large single crystals from silicate melts using the Bridgman technique proposed here would benefit from the microgravity conditions in order to eliminate mixing by natural convection which would be otherwise present in the 1-g environment.

The transport processes affecting concentration and temperature gradients in the melt and in the growing solid are quite complicated for silicate systems. The immiscibility of the liquid, segregation of dopant, and interface shape are not only directly affected by density-driven and Marangoni convection in the melt but are also indirectly influenced by a significant amount of radiation and conduction heat transfer through the

* Ohio Aerospace Institute
** Case Western Reserve University
*** NASA Lewis

semi-transparent solid. The interaction between the various transport processes are further complicated by the observed multi-layered fluid structure which brings about various mechanical and thermal couplings across the liquid-liquid interface. Consequently, determination of the necessary conditions for growing superior quality single crystals from phase separated melts is only possible by isolating the effects of the various interacting transport processes through a combined numerical-experimental approach.

During the course of this investigation, the effect of density-driven convection on the liquid-liquid immiscibility will be experimentally investigated in a series of controlled ground-based tests by growing crystals over a wide range of diameters (from 100 microns to 2 cm). This allows us to vary the intensity of natural convection by several orders of magnitude. The effect of surface tension forces will be studied by varying the Al/Si concentration of the materials and through dopant additions. The impact of thermal radiation on the liquid-solid interface shape and on the degree of homogenization in the melt will be studied by changing the dopant concentration (at fixed Al/Si compositions) which directly alters the transparency of the material. A comprehensive numerical model will be developed by formulating the simultaneous effects of natural and thermo-capillary convection, moving boundaries, and semi-transparent radiation heat transfer. The numerical model will be used in conjunction with the test results to isolate the interacting phenomena. Finally, the type and quality of crystal produced (void formation, ordering, dislocation density, and low angle grain boundaries) will be characterized using scanning electron, transmission electron, and atomic force microscopy. The crystal characteristics will be correlated to the growth conditions and their effect on the transport processes. By the end of this effort, the data and understanding acquired during the ground-based research will be used to design the *right* space experiment where long-duration microgravity conditions will be provided aboard orbiting space craft.

## Background

### Observation of the Immiscibility Gap during Mullite Solidification

Liquid-liquid immiscibility in the high $Al_2O_3$ compositions near stoichiometric mullite ($3Al_2O_3 . 2SiO_2$) has been predicted, but so far has not been unambiguously demonstrated. High resolution digital images captured during crystal growth at our facilities revealed that liquid adjacent to single crystal mullite was more transparent than liquid in the interior of the melt (Figs. 1, 2, and 3). Change in transparency occurs across a narrow spatial region. Reflected optical micrographs taken from longitudinal cross-sections of quenched molten zone specimens confirm that scattering intensity differences exist for the quenched-in features apparent in Figs. 1 and 2. We interpret these features as evidence for immiscibility in the liquid, due to compositional and/or structural differences in the melt. The two liquid phases remained separated for all compositions studied as long as they were kept above the monotectic temperature, TM, and below the convolution temperature, Tc. The liquid-liquid miscibility gap observations presented by Sayir and Farmer (1994) provide some of the first experimental evidence for liquid immiscibility for these compositions and temperatures. A brief description of the growth experiments follows.

Growth was initiated from polycrystalline seed material in all experiments, (Fig. 2). At the highest temperatures, growth of faceted single crystal occur from phase separated melts. The interface shape is planar and a region of Si-rich liquid adjoins the solid. At the onset of growth, polycrystalline seeded fibers are polycrystalline and the liquid/solid interface macroscopically very rough. By increasing the melt temperature, a planar liquid-solid interface is established at temperatures below Tc. Thus, single crystal growth was achieved without a complete monotectic invariant transition in the liquid state. We believe that the faster diffusion rates of Al through the Si-rich liquid achieved by increasing temperature may alter or override the effect of constitutional supercooling.

An image of single crystal mullite taken during growth is shown in Fig. 3. The melt position is not axially symmetric with respect to the crystal growth axis but is pulled to one side due to surface tension effects associated with the large side facet. Mullite single crystals grew with one or two facets, presumably (110) faces. The size of the facets varied during growth. Growth of single crystal mullite could be disrupted by agitation of the melt. Transition to polycrystalline growth in the absence of agitation occurs over time as the interface roughness increases. (This transition may be associated with Si evaporation losses-- a further complication to growth in this system.) It is interesting to note that although the starting compositions varied considerably, mullite single crystals have compositions of ~2 $Al_2O_3$-$SiO_2$, an anomaly which may relate to the occurrence of liquid immiscibility.

Interaction between Transport Processes in the Solidification of Mullite

The preliminary experimental investigations with mullite point out several interesting issues such as:

1. immiscibility gap in the melt and its effect on mullite formation
2. conditions for single crystal growth
3. effect of surface tension on faceting
4. effect of surface tension and Marangoni convection on striations.
5. effect of doping on radiation heat transfer and resulting interface shape.

All of these issues are intricately tied to the complex couplings between the different transport mechanisms and conditions at the interface.

In general, growth of crystals from melt is governed by a complex interplay between the various transport mechanisms for momentum, heat, and species. Optimization and control of the growth process is not possible unless the effects of these various mechanisms on the interfacial conditions are well understood. Unfortunately, in crystal growth from immiscible melts, these interactions are much more complex. The added complications are mainly caused by the mechanical and thermal couplings across the liquid-liquid interface as shown in Fig. 4. The liquid layers are mechanically coupled via transfer of momentum between the layers as determined by the continuity of tangential velocity and the balance of shear stress and surface tension at the interface. Likewise, the thermal coupling between the layers is achieved through the continuity of temperature and a balance of heat fluxes across the interface. These couplings distinguish the multi-layered problem encountered in mullite growth from the single-layer melt configuration traditionally addressed by the microgravity materials community.

The fluid motion in crystal growth is brought about by two co-existing and sometimes competing mechanism; natural convection induced by the volumetric buoyancy force and Marangoni convection driven by the interfacial stresses. Unlike natural convection which is driven by density differences generated by either temperature or concentration gradients in the bulk of the fluid, Marangoni convection is driven by surface tension forces brought about by temperature or concentration gradients (thermocapillary and solutocapillary convection, respectively) along the interfacial surfaces. On earth, the volumetric forces are dominant, especially, in systems with large volume to surface ratio. But in the reduced gravity environment of orbiting space craft, surface forces become more important and the effects of Marangoni convection become dominant. It is anticipated that on earth because of the dominance of natural convection and the resulting mixing, maintenance of the immiscible state in the silicate melt becomes nearly impossible especially for large diameter crystals. However in microgravity, the reduction of the buoyancy force might promote stable encapsulation of the liquid with the larger surface tension by the liquid with the lower surface tension. The fluid dynamics and heat transfer associated with both of these cases should prove to be extremely interesting.

During the solidification of mullite, heat is transferred through three interacting mechanisms of conduction, convection and radiation and affects the crystal growth process in two ways. First directly, by removing the latent heat from the interface. Second, indirectly, by modifying the convection patterns in the bulk of the fluid. In silicate systems, the process is not only complicated by the additional constraints imposed by the liquid-liquid interface, but because of the semi-transparency of the solid and the high operating temperatures of the growth process radiation can easily become the dominant heat transfer mode during growth. Indeed, prior experience with growth of other semitransparent crystals such as BSO and sapphire suggest that radiation loss from the interface through the solid dominates the energy balance at the interface as described by Kassemi and Naraghi (1994). The effects of radiation become even more important in microgravity, where convection is minimized and nonuniform radiation loss from the interface can easily determine the shape and the movement of the interface.

## Proposed Work

The main objective of this research is to isolate different mechanism essential to understanding mullite growth. This will be accomplished through a combined numerical-experimental analysis. The effects of natural convection, surface tension and the associated Marangoni convection and interactions caused by radiation heat transfer will be addressed. The objectives will be realized through completion of the following tasks.

Task 1: Natural Convection Effects

The effect of density-driven convection on the liquid-liquid immiscibility will be investigated in a series of ground based tests and numerical simulations. Crystals will be grown over a wide range of diameters from 100 microns up to 2.5 cm thereby changing the levels of natural convection by orders of magnitude.

The goal of this task would be to determine the effect of mixing caused by convection on the state of immiscibility of the liquid and on mullite crystal formation. The numerical simulations will be used to determine the relative contributions of the different transport mechanisms as the level of natural convection increases.

Task 2: Surface Tension Effects

Surface tension and its gradient will be modified by incorporating different levels of dopants. The objective of this task is twofold: 1) to study the effects of surface tension on faceting and 2) to study the effects of Marangoni convection induced by surface tension on the observed surface striations. Numerical models would be used to study the interaction between natural and Marangoni convection and its effect on stability of the liquid-solid interface. Detailed crystal characterization will be accomplished through scanning electron, transmission electron, and atomic force microscopy.

Task 3: Radiation Effects

Systematic dopant studies will be performed to change the radiative characteristic of the crystal from fully transparent to almost opaque. This then permits study of radiation effects on the curvature of the solid-liquid interface. Numerical models will be used to turn on and off radiation heat transfer thereby isolating its effect on interface curvature. Model predictions will be compared to high resolution digital images of the interface captured during growth.

Task 4: Design of Long Duration Space Experiments

During the last year of ground based experimentation, the acquired database will be analyzed to determine the relative contribution made by the separate phenomena affecting crystal growth from phase separated melts. After careful consideration, an appropriate long duration microgravity experiment will be designed to be carried out in the future.

## Closure

Little is known about the various interacting transport mechanisms which govern mullite growth from the immiscible melt. Unfortunately most of the work performed with respect to fluid mechanics and heat transfer of multi-layered immiscible fluids use model materials and idealized configurations which are not directly applicable to the real life solidification problem. Before the right space experiment can be designed the role of various transport mechanisms that affect the growth process must be elucidated. This will be accomplished through the combined experimental/numerical ground based investigation presented here. During the course of this investigation, the effect of density-driven convection on the liquid-liquid immiscibility will be experimentally investigated in a series of controlled ground-based tests by growing crystals over a wide range of diameters (from 100 microns to 2 cm). This allows us to vary the intensity of natural convection by several orders of magnitude. The effect of surface tension forces will be studied by varying the Al/Si concentration of the materials and through dopant additions. The impact of thermal radiation on the liquid-solid interface shape and on the degree of homogenization in the melt will be studied by changing the dopant concentration (at fixed Al/Si compositions) which directly alters the transparency of the material. A comprehensive numerical model will be developed by formulating the simultaneous effects of natural and thermo-capillary convection, moving boundaries, and semi-transparent radiation heat transfer. The numerical model will be used in conjunction with the test results to isolate the interacting phenomena. Finally, the type and quality of crystal produced (void formation, ordering dislocation density, and low angle grain boundaries) will be characterized using scanning electron, transmission electron, and atomic force microscopy on the crystals produced. The crystal characteristics will be correlated to the growth conditions and their effect on the transport processes. By the end of this effort, the data and understanding acquired during the ground-based research will be used to design an appropriate space experiment where long-duration microgravity conditions will provide the necessary conditions for maintaining the phase separated state.

## References


Sayir, A. and Farmer, S.C., 1995, in print, "Continuous Fiber Ceramic Composites, ed R. A. Lowden, Mat. Res. Soc. Proc. MRS.

Kassemi, M. and Naraghi M.H.N., 1993, Transport Phenomena in Solidification, ASME HTD-Vol. 284.


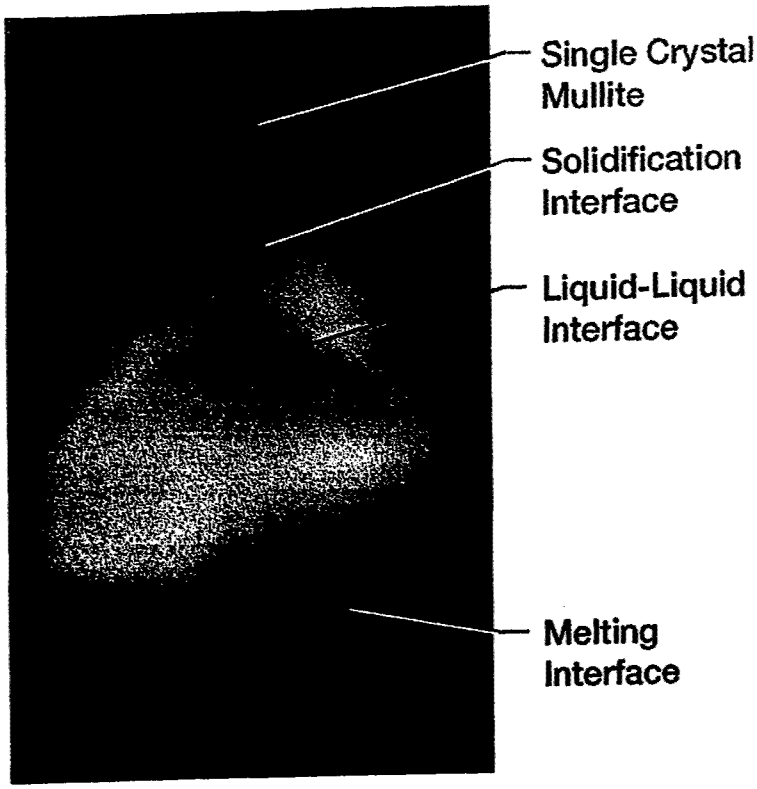


**Fig. 1** High resolution digital images captured during mullite crystal growth. Subsequent characterization of the quenched melt confirm that scattering intensity differences correspond to the phase separated liquid.

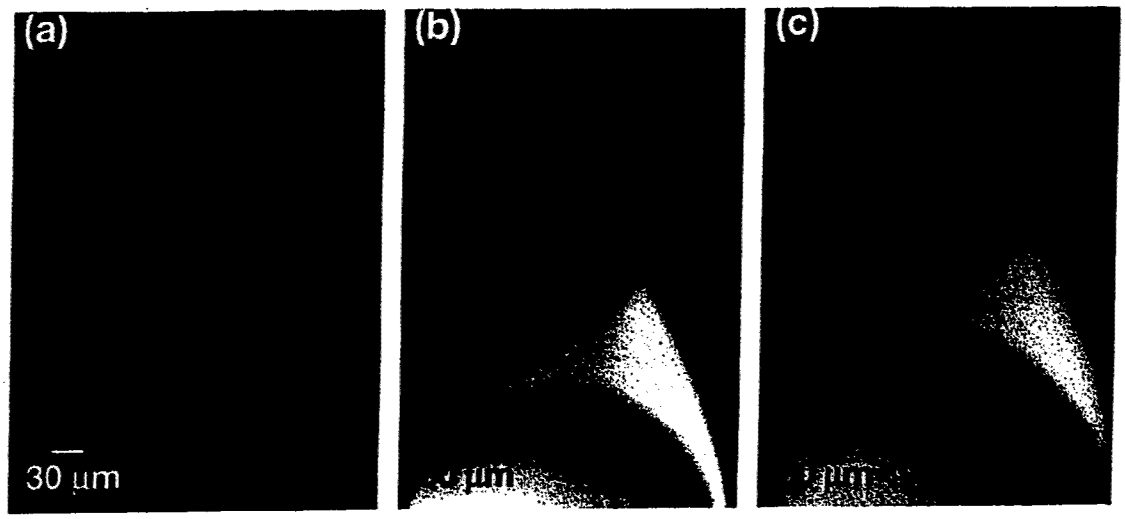


**Fig. 2** a) Initiation of single crystal growth. b) Subsequent occurrence of large facets. c) Non-centrosymmetric position of fiber relative to melt - a consequence of faceted growth.

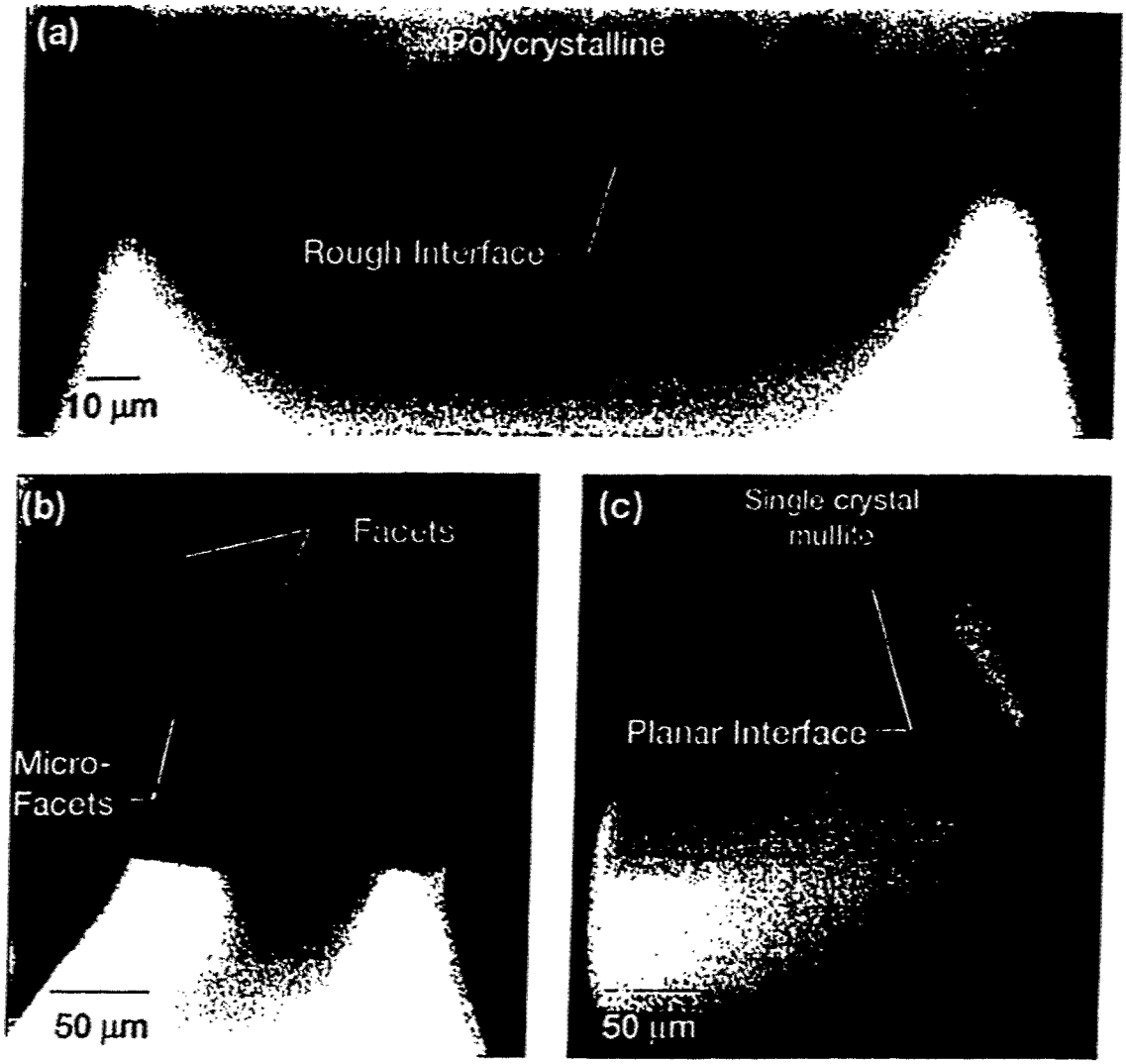


**Fig. 3** High resolution images of a) rough liquid solid interface in polycrystalline growth, b) strongly faceted single crystal growth from planar interface (note loss of axial symmetry) and c) faceted growth of single crystal, axial symmetry maintained.

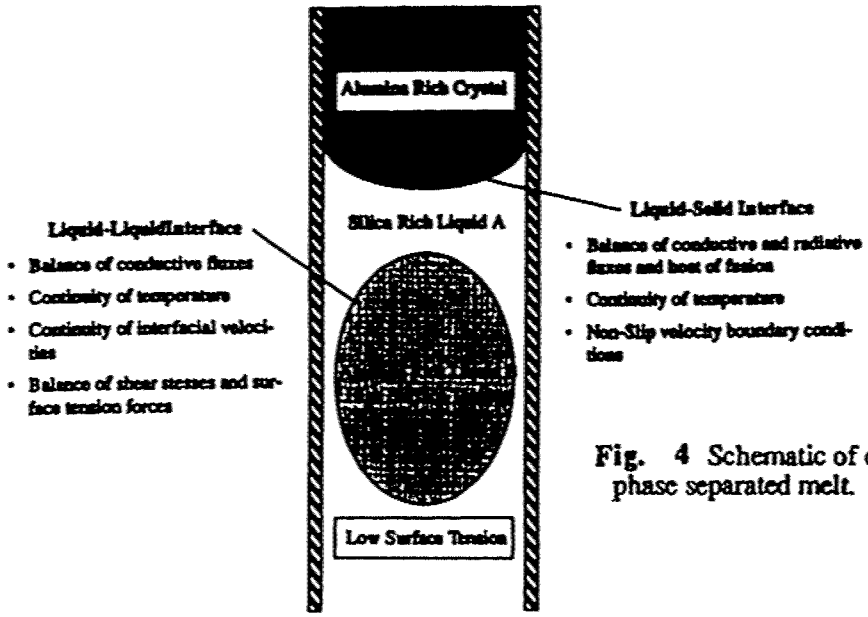


**Fig. 4** Schematic of crystal growth from phase separated melt.

# MEASUREMENT OF LIQUID-TO-SOLID NUCLEATION RATES IN UNDERCOOLED METALLIC MELTS

Joseph L. Katz
The Johns Hopkins University
Department of Chemical Engineering
Baltimore MD 21218
tel: 1-410-516-8484 e-mail: JLK@JHU.EDU

Aaron J. Rulison
Space Systems/Loral
Microgravity Programs, MS G-19
3825 Fabian Way
Palo Alto, CA 94303-4604

The main objective of this work is to obtain quantitative experimental measurements of liquid-to-crystal *homogeneous* nucleation rates in a variety of undercooled metallic melts. This apparatus will allow these measurements to be made in 1-g. However, in a version optimized to take advantage of microgravity, one will be able to extend the range of melt compositions and droplet sizes, and to increase the precision of droplet sizing measurements. Thus a second objective of this work is to obtain the information and experience needed for the design, construction, and use of a future space-based apparatus.

Industrial melt and resolidification processes involve nucleation phenomena. Some of those processes rely heavily on a detailed understanding and control of either heterogeneous or homogeneous nucleation rates to produce a desired phase or microstructure. Avoiding or delaying nucleation enables the materials scientist to produce fine dispersions of second phase particles, to extend solubility limits, to refine the microstructure to the nanometer size range, and to synthesize novel crystalline and amorphous phases.

Numerous researchers have made significant progress in theoretical descriptions of liquid-to-crystal nucleation. Unfortunately, these theories have not been adequately tested because of the experimental difficulties encountered when working with molten metals. In particular, it has not been possible to either eliminate or fully characterize the foreign surfaces presented to the melt by particles, by container walls, or by suspending liquids. Attempts to remove these surfaces by processing metals containerlessly introduces problems in measuring temperature with sufficient accuracy.

This study will use a novel experimental technique which allows a small metallic droplet to be formed, solidified, and remelted in high vacuum without physical contact. Temperature will be measured by pyrometry. The same experimental apparatus then can be very

effectively used to:

•expose droplets to controlled levels of gaseous reactants and/or particulate additives in order to make quantitative measurements of their influence on crystal nucleation;

•make quantitative measurements of critical cooling rates and time-temperature-transformation diagrams for metallic glass-forming alloys;

•investigate whether there is a correlation between overheating and the undercooling limit in germanium

This research will have several valuable outcomes: It will support the wide variety of solidification experiments of interest to microgravity investigators around the world. It will begin to confirm or deny theories for liquid-to-crystal nucleation in metallic melts, thereby filling a void in the current understanding of the ubiquitous phenomenon of liquid-to-crystal nucleation. It will quantify the effect of common trace impurities on crystal nucleation. In addition, this work, in conjunction with NASA's overall Microgravity Materials Science Program, will have a beneficial effect on almost countless industrial processes which involve the melting and resolidification of metals to produce a useful material.

Figures 1 and 2 show schematics of this experimental apparatus. Droplet forming, positioning, and processing all occur in a single, small evacuated chamber (Fig. 1). The chamber is constructed of ultrahigh vacuum stainless steel; the flanges are sealed with copper gaskets. A relatively inexpensive 6-way cross will provide the necessary optical access. This design ensures that windows are placed far enough from the droplet that coating of the windows by metal vapor is minimal. The entire chamber and all contents are bakeable. An oil-free turbomolecular pump backed with an oil-free diaphragm pump will be used. It should be possible to achieve at least $1 \times 10^{-9}$ Torr total residual gas pressure, which is low enough to allow sufficient processing time before a significant surface layer can form on the droplet.

Droplets are fabricated under ultrahigh vacuum by electrohydrodynamic atomization (Fig. 2). Molten droplets of various sizes in the micron range are ejected from the tip under the influence of the electric field which is established between the end of the sample stock rod and the top side of the top electrode. Initially, the atomizer is run briefly to eject the surface impurities inevitably deposited during installation. Afterwards, clean droplets are allowed to move through the hole in the top electrode and into the particle trap. The spray will contain a range of droplet sizes. A single droplet will be captured from the spray as described below. Note that the entire droplet fabrication procedure is accomplished in ultrahigh vacuum and *without* any physical contact.

Each droplet in the spray created in the atomizer moves downward, freezing at some point along its trajectory due to radiative cooling. Some of the frozen droplets move through a hole and into an electrodynamic levitator (EDL)[1] (Fig. 2). The EDL uses a vertical electric field to impart a counter-gravitational force on a charged particle. A simple feedback systems adjusts the top and bottom electrode potentials to keep the droplet vertically centered. An oscillating potential is placed on the center electrode to impart a centering force.

Electrodynamic levitation has a long history of successful use for a variety of particle studies [2,3,4,5,6,7,8,9]. It is exceedingly well-adapted to high vacuum work. In fact, in a manner very similar to that proposed here, it has been used to levitate small (solid) metallic particles in vacuum [9].

In ground-based studies, the droplet diameter will be determined by measuring the light scattering intensity resulting from illumination by a linearly-polarized HeNe laser [?]. Although relatively involatile metals will be studied, some evaporation of the more volatile metals will occur during the high temperature portions of the experiment. Therefore, each droplet will be sized before and after every quantitative nucleation measurement.

An alternative sizing method is electron stepping [10] which measures the droplet mass by adding or removing a single electron and noting the corresponding change in levitation potential. The accuracy of electron stepping is completely independent of any material properties. However, electron stepping is not accurate when the droplet holds more than about a hundred electronic charges since the addition or subtraction of an electron produces only a minor change in the levitation potential. As a result, electron stepping is not accurate in ground-based studies of 5 to 10 micron droplets. In a low-gravity environment, however, electron stepping would be a very accurate method of particle sizing. If a low-gravity version of this apparatus is to be built, electron stepping will almost certainly be utilized.

The droplets will be heated by a 150 mW argon-ion laser focussed through a quartz window and lens. Various laser power-time profiles will be selected to probe various aspects of nucleation. For example, to measure steady-state nucleation one would use a relatively slow continuous cooling, while to measure transient nucleation one would allow the droplet to cool rapidly. The maximum cooling rate is limited by radiative heat transfer from the particle. For example, for gold near its melting point the maximum cooling rate will be about $10^4$ K/s. Again, the droplet can be cooled at any rate less than or equal to the radiative cooling rate by supplying the appropriate laser heating power. (Note that even at the highest cooling rates, the droplets will remain nearly isothermal since the time scale for heat conduction within a 5

to 10 micron metallic particle is several orders of magnitude smaller than the time scale for radiative cooling.)

Although the accuracy of temperature measurement in optical pyrometry is limited by the current state of knowledge of material properties, the *time* at which certain events occur in a temperature-time trace can be measured to very high precision. These timings improve the precision of measurements needed for nucleation studies.

This experimental approach is useful for samples which can be fabricated by electrohydrodynamic atomization, can be laser-melted, have a low enough vapor pressure that their evaporation, while molten, is negligible, and emit measurable thermal radiation while molten.

Electrohydrodynamic atomization is a proven technology for producing micron and submicron particles from a wide range of materials including Ta, Mo, Ti, U, alloys, ceramics, and even ceramic-metal combinations. The material of interest need only be available in the form of a rod or wire.

Most metals have high reflectivities in the IR range but show a maximum absorbance in the visible. A 150 mW argon ion laser will provide ample heat to melt the proposed sample materials.

Some molten metals can have troublesomely high vapor pressures. For the experimental design presented here, the molten droplet evaporation rate should be small enough that its diameter does not decrease in size by more than about $10^{-4}$ microns/second. This constraint limits the choice of samples to those with sufficiently low vapor pressures in the vicinity of their melting temperatures.

To use IR-quartz optics and InAs detectors to measure temperature by optical pyrometry, the sample's melting temperature must be at least 1200 K. Otherwise, we will not be able to obtain a sufficiently strong signal with 5 micron droplets[7].

Some metals which satisfy all of these constraints are: germanium, gold, neodymium, praseodymium, and uranium.

This apparatus will result in much needed experimental data on homogeneous nucleation rates in undercooled metallic melts as a function of their temperature-time history. The first

materials to be studied are pure metals. Later, the study will be expanded to alloys, including glass-forming alloys. Subsequent studies will take advantage of the apparatus to expose the droplet to controlled levels of gaseous reactants and particulate additives in order to make quantitative measurements of their influence on crystal nucleation. This apparatus is a completely functional ground-based apparatus. We anticipate, however, that, a space-based apparatus would expand the versatility and reliability of droplet positioning and increase the precision of droplet sizing. The ground-based apparatus will establish the technical foundation and provide long-term support for future space-based studies of nucleation in liquid materials.


1. E. J. Davis,"Electrodynamic Levitation of Particles", in Aerosol Measurement, p. 452-470, edited by K. Willeke and P. A. Baron, Van Nostrand Reinhold, New York. (1993)

2. R. E. Spjut, A. F. Sarofim, and J. P. Longwell, "Laser heating and particle temperature measurement in an electrodynamic balance", *Langmuir* **1**, 355-360 (1985).

3. G. Sageev, J. H. Seinfeld, and R. C. Flagan, "Particle sizing in the electrodynamic balance", *Rev. Sci. Instrum.* **57**, 933-936 (1986).

4. T. D. Synder and C. B. Richardson, "A study of the nucleation of the solution-to-solid phase transition using levitated microscopic particles", *Langmuir* **9**, 347-351 (1993).

5. S. Arnold, "A three-axis spherical void electrodynamic levitator trap for microparticle experiments", *Rev. Sci. Instrum.* **62**, 3025-3028 (1991).

6. W. H. Hartung and C. T. Avedisian, "On the electrodynamic balance", *Proc. Royal Soc. Lond. A*, **437**, 237-266 (1992).

7. L. D. Hinkle and B. R. F. Kendall, "Brownian motion of a particle levitated in vacuum", *J. Vac. Sci. Tech.* **10**, 243-247 (1992).

8. J. R. Fincke, C. L. Jeffery, and R. E. Spjut, "Measurement of the emissivity of small particles at elevated temperatures", *Optical Engineering* **27**, 684-690 (1988).

9. R. F. Wuerker, J. H. Shelton, and R. V. Langmuir, "Electrodynamic Containment of Charged Particles", *J. Appl. Phys.* **30**, 342-349 (1959).

10. M. A. Philip, F. Gelbard, and S. Arnold, "An Absolute Method for Aerosol Mass and Charge Measurement", J. Colloid and Interface Science, **91**, 507 (1983).

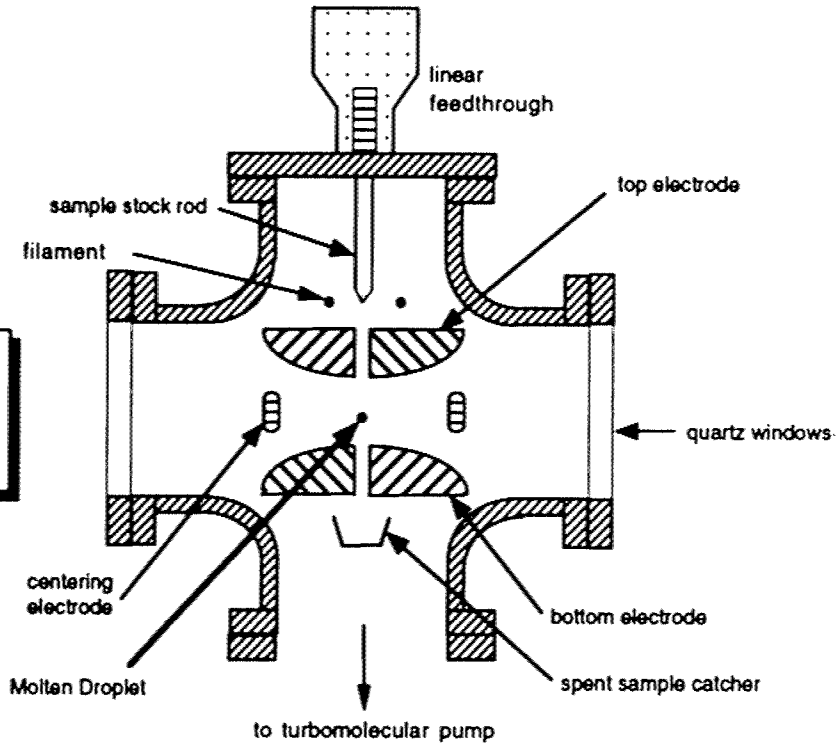


FIGURE 1. Molten Metal Droplet Levitator Concept Drawing

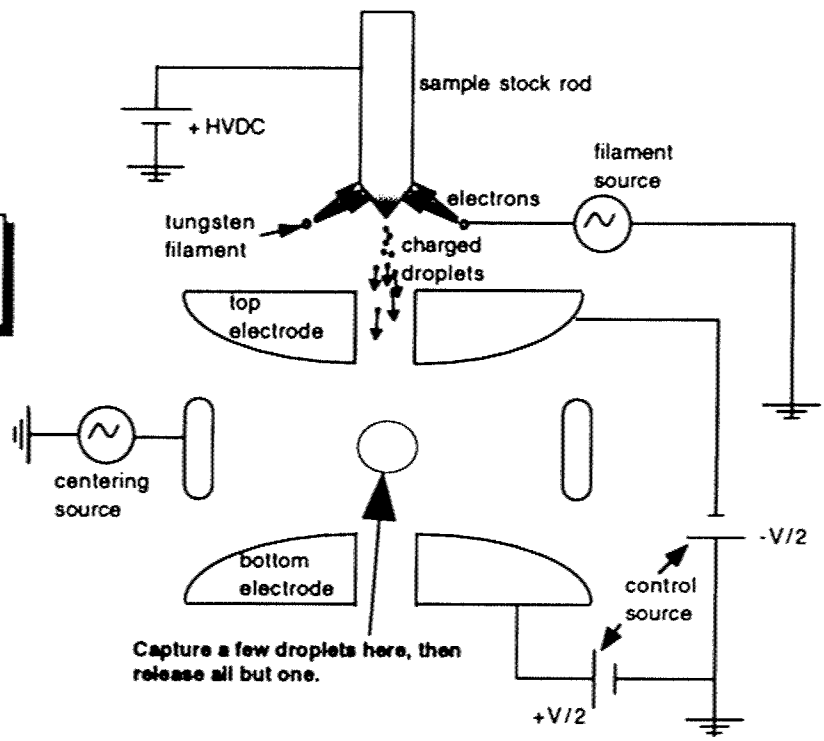


FIGURE 2. Electrical Connections

# PHASE FORMATION AND STABILITY: COMPOSITION AND SAMPLE-SIZE EFFECTS

Kenneth F. Kelton
Department of Physics
Washington University
St. Louis, MO 63130
USA
Phone - 314-935-6228
FAX - 314-935-6219
email: kfk@howdy.wustl.edu

## I. Introduction

Differential scanning calorimetry (DSC) and differential thermal analysis (DTA) are attractive for kinetic studies of phase transformations because they are relatively easy to make, the sample quantity required is small, and they can be automated in some cases. These features also make such experiments attractive for studies in a microgravity environment. Despite the broad popularity of calorimetric studies, however, few methods for quantitative data analysis exist. This is particularly true for nonisothermal data, where most methods are based on erroneous assumptions that generally result in misinformation. Even for isothermal studies, however, proper account is generally not taken of the transformation microstructure, making most interpretations suspect. Further, though DSC/DTA data are often obtained from quantities of fine powder, finite particle size effects are ignored. Finally, the initial and final phases frequently have different compositions; existing techniques have little validity there. Attempts at analysis are hampered by an incomplete knowledge of the composition dependence of the nucleation rate.

Under NASA support, we have developed computer-based methods for the quantitative analysis of calorimetric data, allowing estimates to be obtained of the time-dependent nucleation rate and cluster-size-dependent-growth rates for homogeneous- and heterogeneous-nucleation phase transformations involving no composition change (*i.e.* polymorphic transformations). We have recently extended the model to take the first account of finite-size effects. To extend these studies to the more common case of phase transformations involving solute partitioning (*i.e.* nonpolymorphic transformations), we present the first measurements of the compositional dependence of the time-dependent nucleation rate. These initial results are discussed in light of a new model for nucleation.

## II. Computer Models of DSC/DTA Scans in Polymorphic Transformations - Finite Size Effects

The basic computer model systematically follows the time-dependent development of clusters from the smallest sizes to macroscopic ones [1-3]. The time-dependent cluster density, $N_{n,t}$, is obtained by solving the coupled differential equations describing cluster growth:

$$\frac{dN_{n,t}}{dt} = N_{n-1}\, k^{+}_{n-1} - [N_{n,t}\, k^{-}_{n} + N_{n,t}\, k^{+}_{n}] + N_{n+1,t}\, k^{-}_{n+1}$$

where $k^+$ and $k^-$ are the forward and backward rate constants respectively, which are proportional to the diffusion coefficient in the initial phase[4]. The nucleation rate is defined as the flux in cluster-size space; in the most general case it is a function of both time and the cluster size at which it is measured,

$$I_{n,t} = N_{n,t}\, k^{+}_{n} - N_{n+1}\, k^{-}_{n+1}$$

Phase transitions are simulated by dividing the transformation time into a series of short isothermal intervals over which new nuclei appear and previously generated ones grow, assuming a size-dependent growth rate [2]. For nonisothermal transformations, the duration of the isothermal interval is inversely related to the scan rate, S. To model the small samples often used in DSC/DTA experiments (50 to 400 $\mu$m powders), finite-size effects are included by expressing the volume fraction transformed in terms of the scaled time, $\kappa$ [5],

$$x = 1 - \exp\left[-N\left(\kappa^3 - \frac{9}{14}\kappa^4 + m(N)\kappa^6\right)\right] \quad ,$$

where

$$\kappa = \frac{u(r)\,t}{R} \quad , \qquad m(n) = \max\,(5.26 - 0.26N\,,\,1.0) \quad ,$$

R is the average particle radius, and N is the average number of nuclei per particle. For many silicate glasses, the nucleation and growth are sufficiently well separated that all crystallites are approximately the same size, making the use of one value for R a valid assumption. Surface crystallization is also included. Based on optical microscopy studies of lithium disilicate glass (the glass studied here), the nucleation step for surface crystallization can be ignored. Calculating the

volume transformed by surface growth, and taking account of the overlap between surface, $x_s$, and volume, $x_v$, crystallization, the time-dependent volume transformed is given by

$$x(t) = x_s + x_v(1 - x_s) \quad .$$

Assuming that the rate of change of the enthalpy, dH/dt, and the rate of volume transformed scale linearly, the DSC/DTA signal can then be computed as a function of time and/or temperature as

$$DSC\ Signal \propto \frac{x(T_i + \delta T) - x(T_i)}{\delta T / S} \quad .$$

This model was used to investigate the effects of time-dependent nucleation and finite sample size on phase stability and transformation in lithium disilicate glass [3]. DSC/DTA peak parameters, such as peak temperature, $T_p$, and peak height, $I_p$, are strong functions of particle size [6] and sample history. Our computer-based approach is capable of taking both effects into account. As

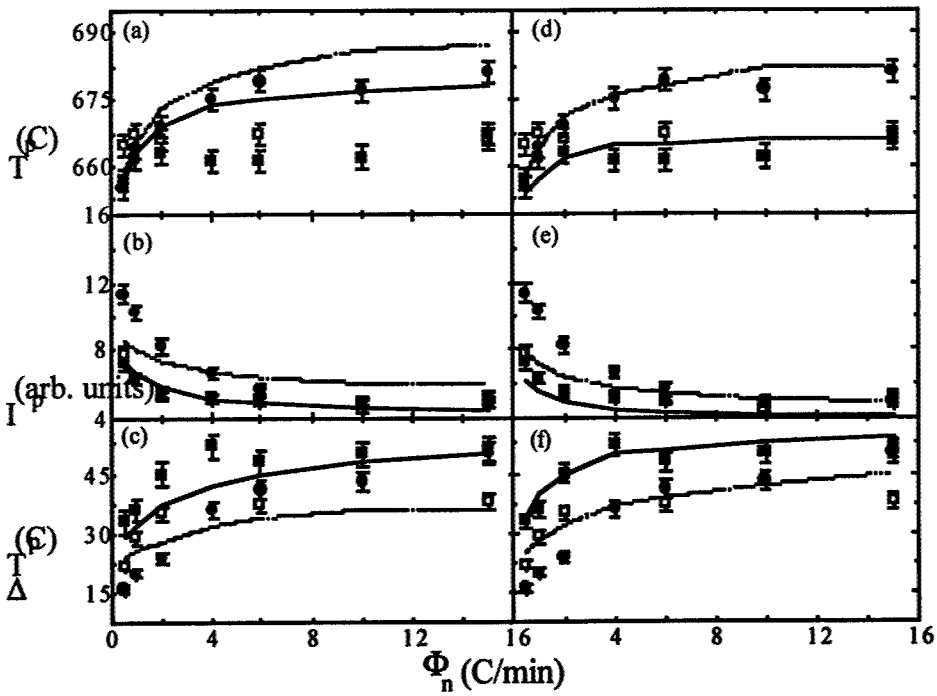


Fig. 1 The effect of scanning through the nucleation zone at different rates on the DSC/DTA peak parameters. 425-450 $\mu m$ particles; data - (■) and ( ); calculation - solid lines. 850-1170 particles: data (●); calculation - dashed line. Calculations in (a) - (c) are for spherical particles; (d) - (e) assume ellipsoidal particles with eccentricity (1,_,_) (from Ref. [5])

an example, Figure 1, compares the model predictions with experimental data for peak parameters for two sizes of spherical glass particles that were first scanned through the region in which the nucleation rate is significant (400°C to 500°C) at rates, $\Theta_n$, between 2 and 15°C/min, and were subsequently scanned through the crystallization peak at a rate, $\Theta_c$, of 15°C/min. Symbols are used for the data; the lines are the calculations. Results from two independent DSC/DTA measurements of these glasses are presented, providing a measure of the experimental error. Though the predicted trends for spherical particles (a)-(c) follow the data, slightly improved agreement is obtained if ellipsoidal particles are assumed (d)-(f). Optical microscopy studies of the particles show that this assumption is reasonable. It should be emphasized that these calculations were made with no fitting parameters.

Having established the validity of the model, it can be used to make meaningful evaluations of methods of analysis for DSC/DTA data. Two approaches are most common. The Kissinger analysis [7,8], which gives an estimate for the effective activation energy of the transformation, and the Ozawa method [9], which is used to estimate the Avrami coefficient, n, which can provide some information about the transformation mechanism. To check these methods, DSC/DTA data were calculated for glasses quenched at different rates using known thermodynamic and kinetic parameters [10]. Comparisons were made between calculations for infinite samples, and when surface and finite-size effects were included. Good fits to the Kissinger and Ozawa expressions were obtained. The activation energies calculated from the Kissinger analysis increase with increasing quench rate of the glass and decrease with increasing particle size. Since neither the nucleation rate nor the growth velocity have an Arrhenius temperature dependence, however, the precise meaning of these activation energies is unclear. A detailed examination demonstrates that the activation energies derived from the Kissinger analysis agree approximately with the local activation energy from growth in the range of the peak transformation temperatures. They do not reflect directly the temperature dependence of the nucleation rate in that temperature range.

## III. Measurements of the Nucleation Rates as a Function of Composition

The correct treatment for the nucleation of a cluster with a composition different from that of the parent phase is not clear. Here the embryo composition can change with cluster size and the chemical make-up of the regions surrounding the embryos will likely vary in a complicated manner, given the stochastic nature of cluster evolution. Based on the thermodynamic theory of fluctuations, the steady state rate of a binary phase of A and B atoms from a parent phase of different composition is expected to have the form,

$$I^s = A^* \exp\left(-\frac{W_{a,b}}{kT}\right)$$

where $W_{a,b}$ is the reversible work of formation of an embryo of size *n*, composed of *a*, A atoms and *b*, B atoms. As for the classical theory, the pre-term, $A^*$, must be determined from a kinetic analysis of nucleation.

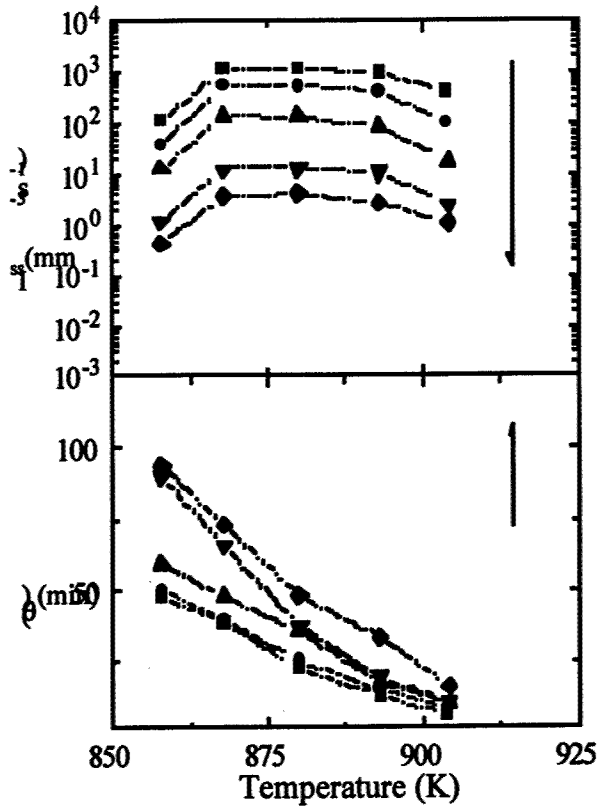


Fig. 2 (a) Nucleation rates and (b) induction times (θ) as a function of $SiO_2$ composition in $(Na_2O.2CaO)_{1-x}(SiO_2)_x$ glasses. $SiO_2$ concentration (at.%): (■) 49.6; (●) 50.0, the stoichiometric glass; (▲) 50.6; (▼) 52.0; (◆) 53.0. The arrows indicate the direction of increasing $SiO_2$

Figure 2 shows the first measurements of the nucleation rate and the induction time (a measure of the time required to reach the steady state nucleation rate) as a function of temperature and $SiO_2$ concentration in a $Na_2O.2CaO.3SiO_2$ glass. X-ray diffraction studies demonstrate that these data represent the nucleation of the stoichiometric crystalline phase. Interestingly, the nucleation rate drops by several orders of magnitude while the induction time rises by less than a factor of 2 with increasing $SiO_2$. That the measured growth velocity and the melting temperature, measured by DTA, change little suggests that these data cannot be explained by changes in the driving free energy or atomic mobility.

To better understand this behavior, we have developed a new model of nucleation for cases when diffusion in the parent phase is competitive with the interfacial attachment rate. Following earlier work by Russell [11], a cluster density, N(n,D), is specified by the number of atoms in the cluster, n, and in the region of the parent phase near the growing cluster, D. The cluster composition was held fixed at a value corresponding to that of the stoichiometric crystal. Cluster evolution was determined for the coupled fluxes of molecular attachment from the cluster neighborhood and diffusion in the parent phase to the cluster interface. The coupled differential equations describing cluster evolution are much more complicated than for the classical theory; their numerical solution was obtained by implicit methods, useful for solving stiff differential equations. The computed results are in qualitative agreement with the experimental results shown in Fig. 2, predicting both the decrease of the nucleation rate below its value for polymorphic crystallization and the increase of the induction time and the different scaling behavior of the two quantities. Work is underway to refine the model parameters, to explore the underlying kinetics more deeply by multi-step annealing studies and to investigate systems where a large compositional effect on the nucleation rate is expected on thermodynamic grounds, such as the crystallization of a quasicrystal from its melt. Undercooling experiments on Ti-based alloys are already underway using the NASA Drop Tube Facility at Marshall Space Flight Center.

* This work was partially supported by NASA under contracts NCC-849 and NCC 8-85

1. K. F. Kelton, A. L. Greer and C. V. Thompson, J. Chem. Phys., **79**, 6261 (1983).
2. K. F. Kelton and A. L. Greer, J. Non-Cryst. Solids, **180**, 17 (1986).
3. K. F. Kelton, J. Non-Cryst. Solids, **163**, 283 (1993).
4. K. F. Kelton in *Solid State Physics*, 1991, Academic Press, New York, p. 75-177.
5 K. F. Kelton, K. L. Narayan, L. E. Levine, T. C. Cull and C. S. Ray, "Computer Modeling of Nonisothermal Crystallization," J. Non-Cryst. Solids (in press).
6. W. S. Huang, C. S. Ray, D. E. Day, K. L. Narayan, T. C. Cull and K. F. Kelton, "Nonisothermal Calorimetric Studies of the Crystallization of Lithium Disilicate Glass," J. Non-Cryst. Solids (in press).
7. H. E. Kissinger, J. Res. Nat. Bur. Stand., **57**, 217 (1956).
8. D. W. Henderson, J. Non-Cryst. Solids, **30**, 301 (1979).
9. T. Ozawa, Polymer, **12**, 150 (1971).
10. K. F. Kelton, "Kinetic Analysis of Nonisothermal Crystallization," Proceedings of the MRS, Boston, November, 1995.
11. K. C. Russell, Acta Metall., **16**, 761 (1968).

# INFLUENCE OF NATURAL CONVECTION AND THERMAL RADIATION ON MULTI-COMPONENT TRANSPORT AND CHEMISTRY IN MOCVD REACTORS

Anantha Krishnan & Sam Lowry
CFD Research Corporation
3325 Triana Blvd.
Huntsville, AL 35805
Phone: (205) 536-6576
Email: ak@cfdrc.com

Ivan Clark
NASA-Langley Research Center
Hampton, VA 23681
Phone: (804) 864-1500
Email: i.o.clark@larc.nasa.gov

## 1. RESEARCH PROJECT DESCRIPTION

### 1.1 Introduction

The development of advanced epitaxial growth techniques has enabled the extensive use of compound semiconductors in the electronics and the optoelectronics industry. High purity materials in ultra-thin multi-layer structures have been produced using these techniques. In this regard, Metalorganic Chemical Vapor Deposition (MOCVD) has emerged as the most viable technique for producing devices with stringent quality requirements. MOCVD allows for the control over the composition and doping of epitaxial semiconductors ranging in size from microns to atomic dimensions. Also, it can be extended to a wide range of heteroepitaxial systems. Conventional MOCVD involves the reaction of a metal alkyl (*e.g.*, Trimethyl Gallium-TMG), with a hydride of the non-metal component (*e.g.*, Arsine) in order to produce the compound semiconductor (*e.g.*, GaAs) which is then deposited on the substrate.

Some of the important issues relating to compound semiconductor growth by MOCVD are:

**1. The Growth Process:** The gas phase deposition of the compound semiconductor requires supersaturation of both the metal and the non-metal components in the gas in excess of the amount required for equilibrium. These components are produced through the decomposition of the reactants. The concentration of reactants must therefore be high enough to guarantee supersaturation so that the growth surface remains compositionally stable at the growth temperature.

**2. Fluid Flow:** The fluid flow in the reactor has a significant influence on the uniformity and the efficiency of the growth process. The mixing and convective transport of the reactants to the substrate surface are determined by the flow field. Boundary conditions, such as susceptor rotation coupled with natural convection, result in complex flow patterns which alter the deposition characteristics substantially.

**3. Mass and Energy Transport:** The temperature distribution in the reactor determines the extent of gas phase decomposition of the reactants as the mixture flows over the substrate. Also, the presence of a mixture of various species in the reactor results in phenomena such as multi-component diffusion, thermodiffusion (the Soret Effect) and the Dufour effect. These physical effects result in complex interactions between the flow, the temperature and the species fields that can significantly influence the deposition process.

**4. Surface Phenomena:** The group V constituent is usually present in excess over the metal alkyl. A number of processes occur in sequence during the epitaxial growth. The reactants are transported to the substrate surface where they undergo chemical reactions. The main product of the reaction (GaAs) is incorporated into the growth surface and the reaction by-product ($CH_4$) is transported away from the surface. The by-product of $CH_4$ is one-sixth as dense as the original nutrient $Ga(CH_3)_3$, creating a strong potential for buoyancy driven convection.

The substrate temperature is usually held high enough to ensure rapid decomposition of the reactants near the surface. This ensures that the growth process is diffusion limited since the reactions are extremely fast. It also creates high thermal gradients near the interface which increases the tendency for natural convection. High thermal gradients also increase the Soret effect.

**5. Chemistry:** The MOCVD precursors undergo a series of gas phase (homogeneous) and surface (heterogeneous) reactions during the growth process. Many of these reactions have been identified for the conventional MOCVD process involving TMG and arsine.

The complexity of the above mentioned physical phenomena and their mutual interactions makes the analysis of MOCVD systems difficult. Although MOCVD is being applied widely, the technique has not yet realized its large scale production potential due to the lack of understanding of these interactions over a range of conditions.

The objective of the proposed study is to perform comprehensive experimental/computational analysis of transport and chemistry in MOCVD reactors and to specifically quantify the roles of natural convection and thermal radiation under ground-based and microgravity environments. The experiments will be performed at NASA-LaRC and the computations will be done at CFD Research Corporation (CFDRC).

## 1.2 Description of Analytical Method

The general purpose commercial Computational Fluid Dynamics (CFD) code, CFD-ACE (developed and marketed by CFDRC), has been upgraded under recent contracts from ARPA, NASA, SEMATECH and private industry to include the following models for specific application to materials processing:

**a. Multi-Component Transport Model**: A comprehensive multi-component transport model (based on the low pressure kinetic theory of gases) is available in CFD-ACE to compute mass, momentum and energy transport in three-dimensional reactor configurations. Additional effects such as thermodiffusion (the Soret Effect) are also resolved. The formulation is general and is applicable to non-unity Lewis number flows.

**b. Multi-Step Finite Rate Chemistry:** CFD-ACE has a generalized model for multi-step gas and surface reactions. The model can handle systems of highly stiff chemical equations. Currently, the code can accommodate 50 gas phase reactions and 20 surface reactions. The reaction rates are accepted in the generalized Arrhenius form.

**c. Thermal Radiation Model:** A comprehensive radiation model (based on the discrete ordinate

method) in three-dimensional, non-orthogonal, body-fitted-coordinates (BFC) is available in CFD-ACE. The model can simulate radiation heat transfer through dissimilar, semi-transparent, participating media. The gray approximation is used in the model currently. However, a non-gray model is under development and will be used to assess the influence of non-gray effects in the MOCVD system.

**d. Geometry and Scientific Visualization Models:** CFD-ACE is coupled to a geometry/grid generation software (CFD-GEOM) and an interactive scientific data visualization package (CFD-VIEW). Currently, these packages are being integrated into a virtual design environment to enable quick synthesis and evaluation of different reactor designs and operating conditions.

## 1.3 Description of Experimental Method

The following experimental facilities are available at NASA-LaRC for performing the proposed work:

**a. MOCVD Reactor:** The experimental reactor has a circular inlet section that merges into a tapered rectangular duct with an aspect ratio (width to height) of 2.22. The graphite susceptor is mounted in a fused silica sled which is inserted into the flow channel. The susceptor and sled are tilted at an angle of nine degrees with respect to the horizontal. The graphite susceptor is heated by rf induction coils wound around the fused silica channel.

**b. Laser Velocimetry:** The three-dimensional velocity flow field in the reactor will be measured using the laser velocimetry (LV) system of the Chemical Vapor Deposition Facility for Reactor Characterization (CVDF) at LaRC. This LV system is capable of measuring the three components of velocity with a spatial resolution of 150 microns. By translating this sample volume through the reactor volume, a full quantitative mapping of the velocity flow field is achieved. In addition, CVDF includes flow visualization capabilities for a qualitative measurement of the overall flow field. Both the LV and flow visualization techniques employ tracer particles. Small particles, on the order of 1 micron in diameter are introduced into the flow upstream of the reactor.

**c. Infrared Imagery:** An Inframetrics model 6000 IR camera will be used for the experiments. The camera is mounted above the reactor vessel, and a pair of gold-plated mirrors is deployed to

enable simultaneous observation of both sides and top of the vessel. IR imagery is recorded digitally on VHS tape, with a total of 128 gray scale levels.

Experimental runs will be performed with reactant gases flowing at 8.0 lpm. Susceptor temperature will be either 600°C or 700°C, achieved by radio-frequency (RF) inductive heating. Optically, fused quartz is opaque at wavelengths above about 4 microns, so the IR sensor is seeing the outside surface only. The emissivity is calculated to be 0.8. Digital imagery data is processed to produce a pixel file of temperature data in a 378 by 206 array. This file contains the three views. Reference markings will be produced in IR image by placing thin copper rods (about 2mm diameter) atop the reactor so as to appear in both top and side views. These rods are gently heated by a blower so as to be visible in the IR images. These rods provide the necessary axial positioning information in the images. Vertical and transverse positioning information is achieved by the ability to see the reactor edges in the images. The result is a set of three reference points in each view corresponding to known points in object space. A general coordinate transformation based on these points is used for each view of the vessel (i.e. top and two sides).

## 1.4 Data Analysis/Research Plan

**Year 1:** A series of experimental and computational studies will be performed using nitrogen and hydrogen as inlet gases. Using a pure component such as hydrogen or nitrogen will make it possible to analyze flow and heat transfer without taking chemistry and multi-component diffusion/thermodiffusion into account. The modeling studies will be used to identify conditions that will result in the best flow and temperature uniformity on the substrate. Detailed measurements of flow velocities and wall temperature distributions will be used to validate the model.

**Year 2:** The studies will be extended to nitrogen/hydrogen mixtures thus bringing in the additional effects of multi-component diffusion and thermodiffusion (Soret Effect). The computational studies will focus on determination and minimization of the effects of natural convection on flow and temperature uniformity. The parameters that will be used in this study are reactor orientation, reactor pressure, susceptor heating rate and mixture composition. The practical lower limit of $Gr/Re^2$ achievable on the ground will be determined. Simultaneously, the feasibility of establishing laminar forced flows without significant natural convection in ground-based configurations will be

determined. If microgravity is necessary to achieve the laminar forced flow dominated regime, preliminary science requirements and conceptual designs for a flight experiment will be developed.

In parallel with the convection analysis, the study will be extended to a GaAs or InP growth system. Model predictions of deposition rate/uniformity under different operating conditions will be verified through experimentation.

**Year 3**: Advanced models for the MOCVD chemistry involving several gas phase and surface reactions will be tested using the computational model. The non-gray radiation model (developed and tested under other concurrent projects) will be applied to assess the influence of non-gray effects on the MOCVD process. The model predictions will be validated using experimental data. The models will be used to estimate the impact of radiative heat transfer under microgravity/low $Gr/Re^2$ conditions. If appropriate, the definition of the flight experiment will continue.

**Year 4**: The effects of microgravity (Low $Gr/Re^2$) on deposition rates and uniformity for a "real" system will be quantified using the numerical model.

The matrix of test conditions will be completed and the experimental data consolidated to provide a knowledge base of the effects of natural convection and thermal radiation on substrate quality and deposition rate as a function of operating conditions. If applicable, the design of the flight hardware and definition of the science requirement in preparation for a flight experiment will be completed.

# CONTAINERLESS OPTICAL PROPERTY MEASUREMENTS ON HIGH TEMPERATURE LIQUIDS

Shankar Krishnan and Paul C. Nordine
Containerless Research, Inc., 906 University Place, Evanston, IL 60201, USA

Abstract:

The major goal of this NRA research was to obtain experimental measurements of the optical properties and spectral emissivities of liquid metals and alloys as functions of temperature, wavelength and composition. A second goal was to provide emissivity and optical property results on materials investigated in the TEMPUS IML-2 mission. To facilitate these objectives, we constructed a novel, high precision pulsed-dye laser spectroscopic ellipsometer that operated in the energy range of 1 - 3.5 eV ($\lambda \approx 1000$ - 350 nm). All of the materials were investigated using electromagnetic levitation to position and melt the specimens and to eliminate any container-derived impurities. This approach yielded extremely clean liquid surfaces on which spectroscopic ellipsometry was conducted. The complex dielectric functions and spectral emissivities were obtained on liquids as functions of temperature, wavelength, and composition. The optical properties obtained in this work in combination with radiometric measurements have been used to derive accurate temperature measurements and approximate values of the total hemispherical emissivity for high temperature liquid metals and alloys. Our NRA research work has directly supported flight experiments on TEMPUS IML-2 mission. We outline below some of the key accomplishments of the research.

## Experimental Methods:

Electromagnetic levitation and heating were used to suspend and melt the liquid specimens of the different materials investigated. A 5 kW radio frequency generator that operated at *ca.* 450 KHz with a 4:1 step-down transformer supplied power to the levitation coil. The samples were levitated and melted in a high vacuum chamber under high purity argon and helium mixtures. The specimens were levitated in the gap between the upper and lower turns of the levitation coil. Cw $CO_2$ laser heating was used to extend the temperature range for some materials. Apparent specimen temperatures were measured using two calibrated optical pyrometers whose operating wavelengths were 650 nm. For measurements on the TEMPUS materials, a special infrared pyrometer with a bandpass similar to the infrared flight pyrometer was employed. Figure 1 shows a schematic of the experimental apparatus.

The first major accomplishment of the NRA research was the construction of a pulsed-dye laser spectroscopic ellipsometer for optical property measurements. The ellipsometric measurements utilized a dual-detector rotating analyzer design [1]. Simultaneous intensity measurements for orthogonal components of polarization were obtained to overcome inherent light level variations due to laser intensity and specimen shape fluctuations. A Molectron

UV-24 nitrogen laser pumped a Molectron DL-II dye-laser to provide laser radiation at wavelengths from 360-990 nm, 3.44-1.25 eV. The laser had a pulse width of 7 ns and was at a repetition rate of 20 Hz. The detector outputs were measured using a pair of gated integrators and digitized by a dedicated laboratory computer. A total of 24 laser dyes were used to obtain radiation over all but a few narrow wavelength regions, with a spectral resolution approximately 10 GHz. Incident laser pulse energies were adjusted to 1 mJ or less in a 0.5 cm diameter beam with the aid of an attenuator. The computer operated the motorized rotating analyzer and the scan control functions of the dye laser. Figure 1 includes a schematic of the spectroscopic ellipsometer system.

The specimens were first purified by heating to temperatures sufficient to evaporate oxides or decompose nitride impurities and to evaporate small amounts of metal which served as a getter. The vapor pressure and vaporization rate of the elements determined the maximum temperatures at which ellipsometry could be conducted. Optical properties were measured for liquid Al at 1550K, Zr at 2335K, Ni at 1765K, Ni-75%Zr at 1500K, and Fe at 1890K and *vs* temperature at selected wavelengths. Some optical property measurements were conducted on the undercooled liquids by allowing helium gas into the chamber to increase convective heat loss and lowering the specimen temperature. Measurements were obtained on additional nickel-based alloys Ni-25%Sn, Ni-32.5%Sn, Ni-40%Nb, and Ni-75%Zr. The effects of oxygen and nitrogen on the optical properties of liquid Zr were measured.

Results:

Spectroscopic ellipsometry (SE) allows direct measurements of the complex dielectric functions of materials. The data derived from SE include the optical conductivity($\sigma$), the polarization ($\epsilon_1$), the real and imaginary parts of the index of refraction (n and k respectively), and the normal ($\epsilon_\lambda$) and hemispherical ($\epsilon_{\lambda,2\pi}$) spectral emissivities. In this research report, we give example results of these property measurements for the liquids investigated. All of the results from this NRA research can be found in the literature [1-6].

Figure 2 shows the optical conductivity results for liquid aluminum. The data reveal that clean liquid aluminum exhibits an absorption peak at ca. 1.4 eV [1]. Since the optical property data exhibit a shape and form quite similar to the solid, the Ashcroft-Sturm model [7] of parallel band absorption was used as an empirical means for fitting the data. The model requires that four physical parameters be determined. These parameters are $m_o\tau$, $\tau_i$, $|U_{111}|$, and $|U_{200}|$, which describe inter- and intra-band relaxation times and pseudo-potential energies (along the [111] and [200] zone directions in the solid), respectively. The model fit [2] is shown by a solid line in Fig. 2. The derived pseudo-potential energies provide an indirect view of the structure and bonding in the liquid. The liquid and solid have very similar electronic structures and optical properties, implying that the liquid contains a high degree of order (or clustering). This research has provided the first successful physical modelling of optical properties for a liquid metal. With measurements at a few additional temperatures and wavelengths, the model would allow accurate calculation of all of the spectral, hemispherical, and total emissivities and the optical properties of liquid aluminum over wide wavelength and temperature ranges.

Figure 3 presents the wavelength dependence of emissivity for liquid Al [1], Zr [3], Fe [4], Ni [4], Ni-75%Zr [5] and Gd. These results illustrate the differences in emissivity exhibited by liquid metals in the visible and near infrared spectral regions. The temperatures at which these results were obtained are listed in the figure legend. The emissivity variation for liquid aluminum near 800 nm arises due to the strong absorption that is more clearly resolved by the optical conductivity data presented in Figure 2. Liquid Zr [3] and Ni-75% Zr [5] show similar slopes for their emissivity *vs* wavelength functions and similar emissivity values. The properties of liquid Gd are also shown in the same plot. The transition metal liquids, Zr, Ni and Fe, exhibit a emissivity *vs* wavelength dependence similar to their solid counterparts.

The NRA research has facilitated spectral emissivity measurements in the visible and infrared and a detailed analysis of errors in pyrometry associated with the TEMPUS flight pyrometer. Measurements of the normal spectral emissivity and the infrared radiance temperature were obtained as functions of true temperature for liquid Ni and several Ni-based alloys. Figure 4 plots the infrared radiance temperature (bandpass 1-2.5 $\mu$m) *vs* true temperature for pure Ni and several Ni-based alloys [5]. This plot allows the true temperature to be derived from the radiance temperatures measured in space during the TEMPUS IML-2 mission. Figure 5 plots values of the emissivity *vs* wavelength for the nickel alloys, liquid zirconium and a typical solid metal, tungsten. In addition to optical property measurements, we have analyzed the errors associated with the infrared channel of the TEMPUS pyrometer [8].

The effects of oxygen and nitrogen contamination on the optical properties of liquid Zr were measured in collaboration with scientists at Vanderbilt University. In these studies, the optical constants of the liquid were measured as a function of the oxygen/nitrogen concentration. Oxygen or nitrogen gas was allowed to flow into the levitation chamber using precision mass flow controllers. The optical properties were measured up to the supersaturation limits of the oxygen and nitrogen concentrations. An empirical model precisely describes the results for both Zr-O and Zr-N liquids [6]. This model is illustrated in Fig. 6, where the imaginary part of the dielectric constant, $\epsilon_2 = 2nk$, (proportional to the optical conductivity), is plotted *vs* the electron/atom ratio. A single function describes both Zr-N and Zr-O results, showing that the conduction electron concentration in the solution is the primary factor that governs the optical response of the liquid.

## References


1. S. Krishnan and P. C. Nordine, *Phys. Rev. B*, **47**, 11780 (1993).
2. S. Krishnan and P. C. Nordine, *Phys. Rev. B.*, **48**, 4160 (1993).
3. S. Krishnan, C. D. Anderson, and P. C. Nordine, *Phys. Rev B.*, **49**, 3161 (1994).
4. S. Krishnan, K. J. Yugawa, and P. C. Nordine, Submitted to *Phys. Rev. B.*, 1996.
5. S. Krishnan and P. C. Nordine, In press, *J. App. Phys.*, Aug. 1, 1996.
6. S. Krishnan, J. K. R. Weber, C. D. Anderson, P. C. Nordine, C. T. Morton, W. H. Hofmeister, and R. J. Bayuzick, In press, *Materials Science and Engineering A.*, 1996.
7. N. W. Ashcroft and K. Sturm, *Phys. Rev. B.*, **3**, 1898 (1971).
8. W. H. Hofmeister, R. J. Bayuzick and S. Krishnan, Paper in Preparation.

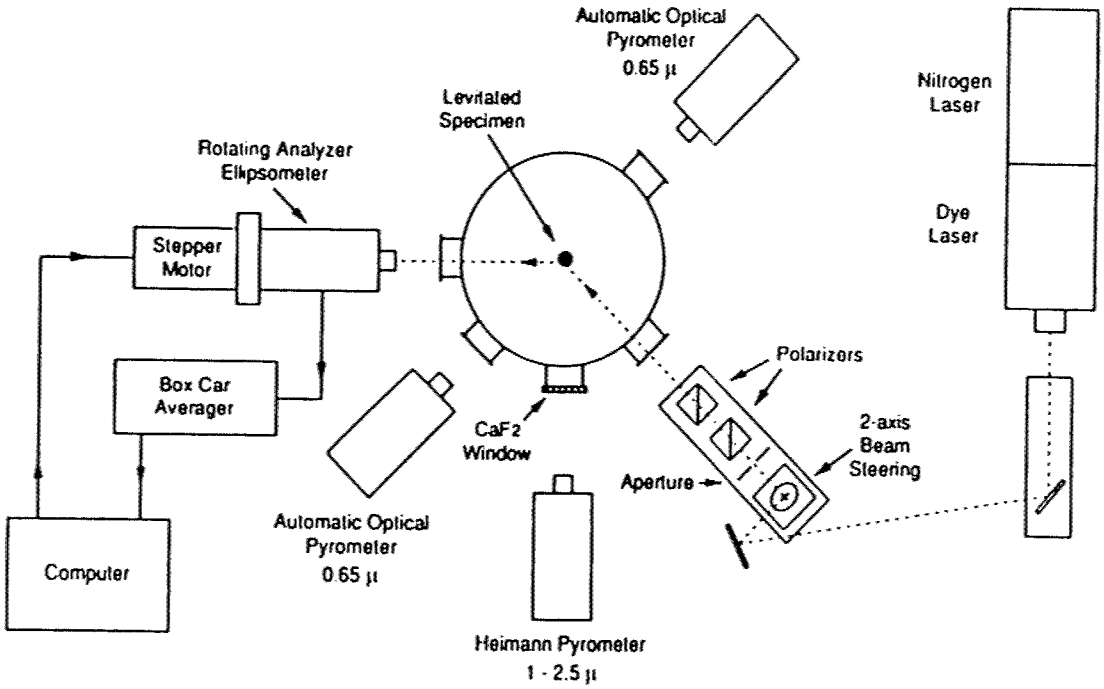


Figure 1. Schematic of the experimental apparatus for optical property measurements on levitated liquid metals and alloys.

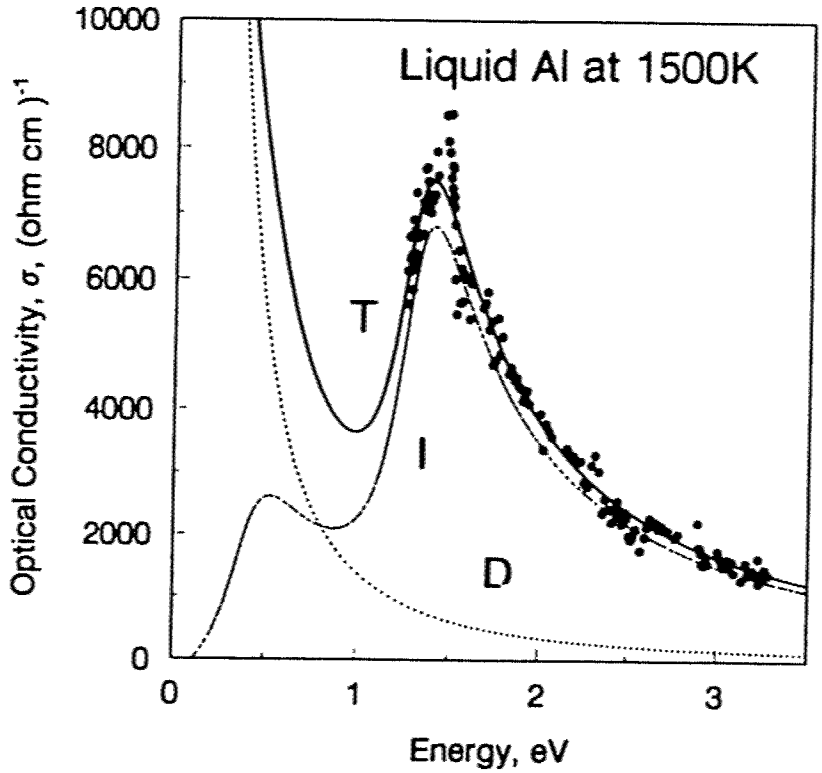


Figure 2. Measured optical conductivity values (●) and calculated fit for the parallel-band absorption model. Drude (D), Interband (I), and total (T) conductivities are shown.

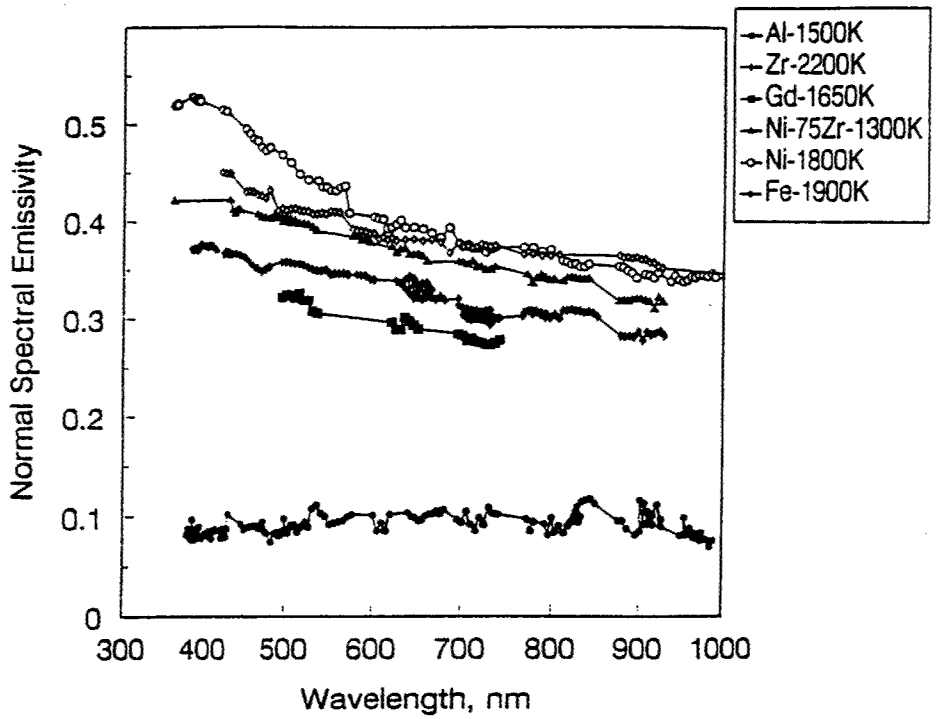


Figure 3. Normal spectral emissivities *vs* wavelength for liquid Al, Zr, Gd, Ni, Ni-75%Zr, and Fe at temperatures given in the legend box.

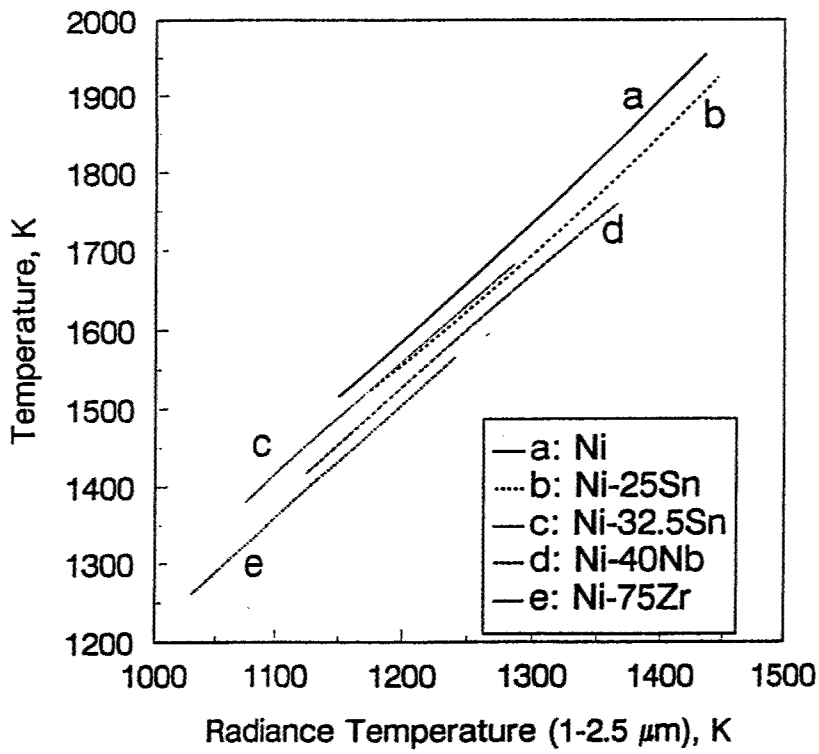


Figure 4. True temperature of metals and alloys investigated in the TEMPUS IML-2 space-based experiments as a function of radiance temperature measured with an infrared pyrometer, with the same bandpass as the pyrometer used in the flight.

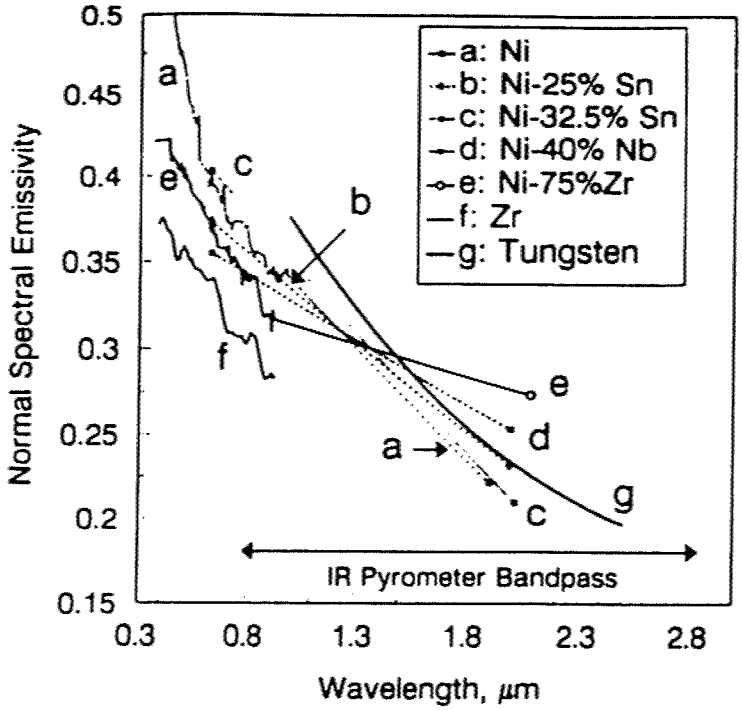


Figure 5. Normal Spectral emissivities as a function of wavelength for materials investigated in the TEMPUS IML-2 space-based experiments. Tungsten data are shown for comparison.

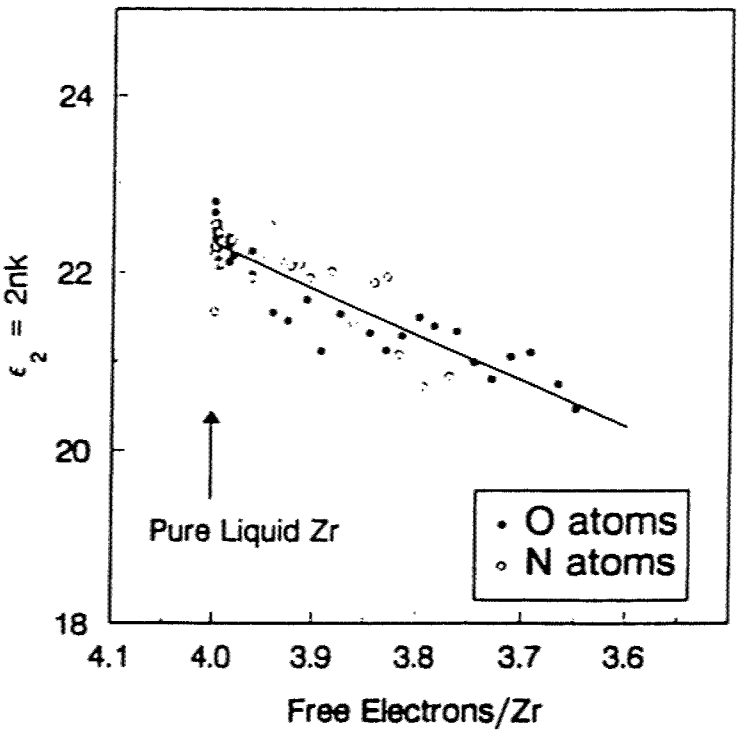


Figure 6. Imaginary part of the dielectric constant of Zr-O and Zr-N solutions as a function of the conduction electron concentration in the solution. Solid line is a least-squares fit.

# ORBITAL PROCESSING OF EUTECTICS

Dr. David J. Larson, Jr.
Materials Science & Engineering
318 Engineering
University at Stony Brook,
Stony Brook, NY 11794-2275
(516) 632-8485
(516) 632-8052 FAX
dlarson@ccmail.sunysb.edu

## Objective

The technical objective of this program is to utilize the orbital microgravity environment to evaluate convective influence(s) on the solidification of eutectic alloys.

## Approach

This program is a coordinated research effort involving both space and ground-based research and includes French joint participation. We will extend the application of flight furnace and diagnostic capabilities. Seebeck interfacial temperature, interface velocity, and compositional measurements will be applied to the low volume fraction eutectic case, for the first time. Peltier pulsing will be utilized to investigate eutectic kinetic stability, morphological stability, and the extended cooperative growth region during eutectic growth with interfacial undercooling.

## Results

Our effort builds on a substantive one-g and μ-g baseline. Microgravity results have demonstrated: substantial refinement of the Bi/MnBi and NiSb/InSb rod microstructures, expansion of the $Al_3Ni$/Al rod microstructure, and unchanged $Al_2Cu$/Al equivolumetric lamellar microstructure. Convection levels have been altered using applied magnetic fields to damp buoyancy convection and accelerated crucible rotation to introduce forced convection at the solidification interface. Each of these investigations demonstrated substantive convective influence on the Bi/MnBi eutectic microstructure on damping (refinement), or under forced convection conditions (expansion). The well established Jackson-Hunt Theory for eutectic solidification and the complementary Verhoeven sensitivity analysis for convective influence predict insensitivity to convection.

The Jackson-Hunt Theory will be investigated with respect to kinetic effects at the solidification interface. Theory has been advanced that suggests that the interface composition may be unequal to the bulk eutectic composition, in some cases. This, in turn, can lead to interaction with the macroscopic fluid flow field. This theory includes interface undercooling which is velocity dependent. The 'advanced' theory predicts convective influence resulting in compositional and structural refinement. The 'advanced' theory will be experimentally validated in the interest of developing a 'universal' theory that can explain all of the microgravity results and which can be used to predict results of future experiments in one-g and μ-g.

Limited measurements on Bi/MnBi eutectic samples solidified in μ-g on Space Processing Applications Rocket (SPAR) flights indicated that the solid composition solidified in orbit differed from that terrestrially, though a total mass balance could not be accomplished in the limited μ-g regions. Extensive eutectic Bi/MnBi one-g and μ-g damping experiments demonstrated that interface undercooling was velocity dependent and increased significantly with damping. These

thermocouple measurements were not as precise as necessary to test the theory because of the spatial volume of the sensors. The precision of these temperature measurements will be extended by an order of magnitude by the unique application of Seebeck measurements at the low-volume-fraction eutectic interface. Complementary measurements will provide interface velocity, quantitative morphological data, and composition data, which are necessary to the testing of the theories.

The Bi/MnBi rod cross-section has also been shown to be velocity dependent. It varies from a finely faceted cylinder at high velocities, to triangular cross-sections at intermediate velocities, to fragmented hexagonal prismatic segments at low velocities. Rod cross-sections measured at 'instantaneous' or programmed furnace rate changes proved to be rate-limited by heat transfer across the interface, erroneously suggesting kinetic limitations at the interface. Peltier interface demarcation, used to instantaneously vary the interface solidification velocity, showed that the non-faceted/faceted Bi/MnBi microstructure was not limited kinetically, achieving a new eutectic distribution pattern without a measurable microstr ctural transient. Post-pulse recovery microstructures also demonstrated whether the local eutectic composition was within the extended region of the cooperative growth regime, or not. Within the cooperative regime, no recovery compositional transient was noted, whereas a strong Bi-rich transient was noted in recovery from the non-cooperative regime. We can thus use Peltier interface demarcation uniquely to probe interface stability and nterface kinetics. Peltier interface demarcation cannot be exploited terrestrially in damping magnetic fields due to strong interactive effects between the p lse and the applied magnetic field. These damped experiments are thus unique to the μ-g investigation.

## Conclusion

These experimental results strongly suggest that convection influences the solidification of this important class of materials, whereas conventional theory predicts otherwise. This program uniquely applies Peltier interface demarcation and the Seebeck effect orbitally to address kinetic stability and morphological stability of these eutectic composites. Further, the unique Peltier interface demarcation and Seebeck effect results will be complemented by compositional, and metallographic measurements to provide a unique quantitative basis for comparing and validating eutectic theories, with and without convective influence.

# ORBITAL PROCESSING OF HIGH-QUALITY Zn-ALLOYED CdTe COMPOUND SEMICONDUCTORS

Dr. David J. Larson, Jr.
Materials Science & Engineering
318 Engineering
University at Stony Brook
Stony Brook, New York 11794-2275
(516) 632-8485 Phone
(516) 632-8052 FAX
dlarson@ccmail.sunysb.edu

## Introduction

This program conducted experiments in the Crystal Growth Furnace (CGF) during USML-1 (STS-50) and USML-2 (STS-73) missions. Chemical homogeneity, and defect distribution, defect type, and defect density were investigated for gravitational influence.

## Objectives

The objectives of this program are to investigate, quantitatively, the influences of gravitationally-dependent phenomena, both hydrostatic and buoyant, on the growth and quality of alloyed CdZnTe compound semiconductors grown by the seeded Bridgman-Stockbarger process. Of particular interest to this program is chemical homogeneity and defect distribution and density.

## Low-g Rationale

Prior experiments demonstrated that the microgravity environment can effectively damp thermo-solutal convection, achieving diffusion-controlled conditions during crystal growth. Scaling analyses for this alloy system suggested that similar growth conditions were achievable within this system, suggesting that chemically homogeneous material could be grown. Further, prior art suggested that the defect density within microgravity processed crystals that solidified without wall contact was greatly reduced. This program attempted to confirm and explain that intriguing result and to maximize the volume of material that solidified without wall contact.

## Results

Four CdZnTe crystals grown in microgravity (μ-g), using a seeded Bridgman-Stockbarger crystal growth technique, were analysed to elucidate gravitationally-dependent hydrostatic and buoyant gravitational influences. Characterization was conducted utilizing: optical and infrared microscopy, differential chemical etching, FTIR spectroscopy, x-ray double crystal rocking curve mapping, precision lattice parameter mapping, triple crystal x-ray diffraction analysis, and x-ray synchrotron topography. It was found that in the absence of hydrostatic pressure the liquid separated from the ampoule walls, depending on influences including: volumetric fill-factor, level of constraint, residual g-vector, ampoule geometry and growth conditions. Regions solidified without wall contact were found to virtually

eliminate twinning, which is pervasive terrestrially. This suggests that many of the twinning defects are surface nucleated, and nucleation and/or multiplication is furthered by stiction at the ampoule/crystal wall. Further, regions solidified without wall contact showed dramatic reductions in (111)[110] dislocation density, from 800,000 ± 400,000 (1-g) to 800 ± 400 (μ-g) epd. This was attributed to reduction in hoop stresses within the flight samples during growth and post-solidification cooling. Regions of partial wall contact showed defect gradients, with high densities on the wall side and low densities on the free surface side. These results are consistent with our original experiment hypotheses and are in excellent agreement with predictions from our high-fidelity thermal and thermo-mechanical stress models. Synchrotron reflection topographs of the sample surfaces, synchrotron transmission and reflection topographs of selected chemo-mechanically polished wafers, and Bragg contour maps of the residual strains within the one-g and μg crystals will be presented and explained on the basis of the thermo-mechanical process model. Implications of these results with respect to twin and dislocation reduction orbitally and terrestrially, will be presented.

# CRYSTAL GROWTH OF SELECTED II-VI SEMICONDUCTING ALLOYS BY DIRECTIONAL SOLIDIFICATION

Dr. Sandor L. Lehoczky, Principal Investigator, ES75/NASA Marshall Space Flight Center (MSFC)
Phone: (205) 544-7758, e-mail: Sandor.Lehoczky@ssl.msfc.nasa.gov, Fax.: (205) 544-8762

Co-Investigators:
Dr. Frank R. Szofran, Dr. Ching-Hua Su, NASA Marshall Space Flight Center (MSFC)
Dr. Rosalia N. Scripa, University of Alabama at Birmingham (UAB)
Dr. Yi-Gao Sha, Universities Space Research Association (USRA)

This research study is investigating the effects of a microgravity environment during the crystal growth of selected II-VI semiconducting alloys on their compositional, metallurgical, electrical and optical properties. The on-going work includes both Bridgman-Stockbarger and solvent growth methods, as well as growth in a magnetic field. The materials investigated are II-VI $Hg_{1-x}Cd_xTe$, $Hg_{1-x}Zn_xTe$, and $Hg_{1-x}Zn_xSe$ ($0 \leq x \leq 1$), with particular emphasis on x-values appropriate for infrared detection and imaging in the 5 to 30 μm wavelength region. Wide separation between the liquidus and solidus of the phase diagrams[1] (Fig. 1) with consequent segregation during solidification and problems associated with the high volatility of one of the components (Hg), make the preparation of homogeneous, high-quality, bulk crystals of the alloys nearly an impossible task in a gravitational environment.

The three-fold objectives of the on-going investigation are as follows: 1. to determine the relative contributions of gravitationally-driven fluid flows to the compositional redistribution observed during the unidirectional crystal growth of selected semiconducting solid solution alloys having large separation between the liquidus and solidus of the constitutional phase diagram, 2. to ascertain the potential role of irregular fluid flows and hydrostatic pressure effects in generation of extended crystal defects and second-phase inclusions in the crystals, and 3. to obtain a limited amount of "high-quality" materials needed for bulk crystal property characterizations and for the fabrication of various device structures needed to establish ultimate material performance limits.

The flight portion of the study was to be accomplished by performing growth experiments using the Crystal Growth Furnace (CGF) manifested to fly on various Spacelab missions. The investigation complements the experiments being done on the crystal growth of $Hg_{1-x}Cd_xTe$ using the Advanced Automatic Directional Solidification Furnace (AADSF) flight instrument. The main emphasis of the study involves the $Hg_{1-x}Zn_xTe$ and $Hg_{1-x}Zn_xSe$ alloys. The investigation consists of an extensive ground-based study followed by flight experimentation and involves both experimental and theoretical work. Just as for the AADSF-related studies, both melt and solvent growth methods are being pursued, with the melt growth being the primary emphasis of the initial flight experiments. The combination of the two studies provides the basis for the evaluation of the influence of alloy property variations on the relative importance of various gravity- and non-gravity related effects. Several alloy properties including the effective diffusion coefficient, segregation coefficient, thermal conductivity, microhardness, etc. are known to vary substantially with composition and from alloy system to alloy system. For example, the "effective" mass diffusion coefficients deduced from directional solidification

compositional redistribution data differ by about a factor of 10, from that of $Hg_{1-x}Cd_xTe$ being the largest and $Hg_{1-x}Zn_xTe$ being the smallest.[2] These variations will cause non-gravity-related effects to be more significant in some cases than in others.

A series of HgZnTe crystal ingots has been grown form pseudobinary melts by Bridgman-Stockbarger type directional solidification using the CGF Ground Control Experiment Laboratory (GCEL) furnace, as well as MSFC heat pipe furnaces. Several ZnTe crystals were also grown using a Te-solvent zone growth method. Various thermal boundary conditions and growth rates were employed and several of the ingots were rapidly quenched during the steady-state portion of growth to establish correlation between thermal conditions and melt/solid interface shapes. These experiments also indicated that the ingots can be successfully quenched and back melted to allow a rapid return to steady-state growth.[2-5] The fitting of the measured crystal compositional distributions to appropriate theoretical models was used to obtain an estimate of the effective HgTe-ZnTe liquid diffusion coefficient. To assist the modeling of the pertinent heat and mass transport processes, selected portions of the pseudobinary phase diagram,[1] thermal diffusivity[6] and melt viscosity[7] have been measured. A microscopic theoretical model for the calculation of point defect energies[8], charge-carrier concentrations, Fermi energy, and conduction-electron mobility as functions of x, temperature, and both ionized and neutral defect densities has been developed [9-12] and some of the pertinent materials properties were measured.[13,14] Theoretical models have also been developed for the axial and radial alloy segregation as functions of alloy composition, growth rate, thermal gradient and growth interface curvature. The calculated results agreed well with experimental data and indicated that the axial alloy composition is limited by diffusion-like behavior (Fig. 2) and the radial segregation by fluid flow effects (Fig. 3). Further numerical modeling including the detailed sample, experiment container and furnace system is in progress to further assess the role of gravity in the overall solidification process.

A ground preprocessed and quenched sample was successfully back-melted and partially regrown in the CGF instrument during the first United States Microgravity Laboratory (USML-1) mission.[3,4,15-17] The meltback interface was within 0.5 mm of the desired value. Because of the loss of power to the CGF, the experiment was prematurely terminated after approximately 39 hours into the planned 150 hour growth period. About 5.7 mm of sample had been grown at that point. Surface photomicrographs of the sample clearly showed significant topographical differences between the space- and ground-grown portions. Compositional measurements along the sample axis indicated that the desired steady-state growth for the axial composition was reached at about 3 mm into the growth because of the quenched in melt composition for steady state growth. An x-ray diffraction and SEM survey of the sample showed that both the ground- and flight-portions of the ingot contained only a few grains, i.e., were nearly single crystals, and the crystallographic orientation was maintained following back-melting and space growth. The interface shape, radial compositional variations, and the quenched-in dendretic structures of the flight sample all have shown an asymmetric behavior. The compositional data strongly suggest that the most likely cause was unanticipated transverse residual accelerations.

A new seeded method has been developed for the growth of HgZnTe crystal ingots from pseudobinary melt by the Bridgman-Stockbagrer type directional solidification for the Second United States Microgravity Laboratory (USML-2) mission.[18] A physical vapor transport method developed by us[19-22] was used to grow 2 cm ZnTe seed crystals in the fused silica ampoules. Then a stack of precast pseudobinay alloys of varying compositions were loaded in the remaining ampoules. The alloy

compositional variation in the stack was chosen to correspond to the expected melt composition variation along the growth axis for steady-state diffusion-controlled growth conditions (Fig. 4). Composition analysis on the grown crystals confirm that steady-state growth was achieved from the beginning of the growth process (Fig. 5). A series of $Hg_{0.84}Zn_{0.16}Te$ and $Hg_{0.88}Zn_{0.12}Te$ crystals were then grown using the CGF Ground Control Experiment Laboratory (GCEL) furnace, as well as in heat-pipe furnaces. Several crystals were also grown under the influence of a 5 T axial magnetic field[22] and 0.5 T transverse magnetic field[23]. Detailed compositional and microstructural characterization of the samples indicated that the alloy stacks could be successfully back-melted within 0.5 mm of the seed interface to assure that growth begins under nearly steady-state growth conditions. The applied magnetic fields had a significant influence on radial alloy segregation (Fig. 6) and interface constitutional supercooling breakdown demonstrating the importance of gravity-induced fluid-glow effects.

Two $Hg_{0.88}Zn_{0.12}Te$ seeded ampoules were chosen for processing in the CGF during the Second United States Microgravity Laboratory (USML-2) mission. The results from a similar experiment that was inadvertently terminated during the previous USML-1 mission strongly indicated that residual accelerations transverse to the growth axis are detrimental for achieving the primary experiment objectives. Thus a Shuttle flight attitude that minimizes such accelerations was requested for the USML-2 mission. Just prior to launch the attitude was disallowed because of programmatic constraints and a decision was made not to perform the flight portion of the experiment under unfavorable growth conditions.


1. Su, C.-H., Y.-G. Sha, K. Mazuruk, and S. L. Lehoczky, "Phase Diagram, Density, Heat Capacity and Enthalpy of Mixing of Pseudobinary $Hg_{1-x}Zn_xTe$ Melts," J. Appl. Physics, 80 (1), 137-142, July 1, (1996).
2. Su, C.-H., S. L. Lehoczky, and F. R. Szofran, "Growth of HgZnTe Alloy Crystals by Directional Solidification," J. Crys. Growth, 86, 87-92 (1988).
3. Lehoczky, S. L., F. R. Szofran, D. C. Gillies, S. D. Cobb, C.-H. Su, Y.-G. Sha, and R. N. Andrews, "Crystal Growth of Selected II-VI Semiconducting Alloys by Directional Solidification," Proceedings of the Joint Launch and One Year Science Review of USML-1 and USMP-1 with the Microgravity Measurement Group, N. Ramachandran, D. O. Frazier, S. L. Lehoczky, and C. R. Baugher, eds., NASA Conference Publication 3272, Vol. 1, 163-222 (1994).
4. Su, C.-H., S. L. Lehoczky, F. R. Szofran, D. C. Gillies, S. D. Cobb, Y. G. Sha, and R. N. Andrews, "Crystal Growth of Selected II-VI Semiconducting Alloys by Directional Solidification in Microgravity," Proceedings of the 3rd International Union of Materials Research Society (IUMRS) International Conference on Advanced Materials, ed. By S. Somiya, M. Doyama, M. Hasegawa, and S. Yamada, Trans. Met. Res. Soc. Jpn., 16A, 699-706 (1994).
5. Su, C.-H., Y.-G. Sha, S. L. Lehoczky, F. R. Szofran, D. C. Gillies, S. D. Cobb, and R. N. Scripa, "Crystal Growth of Selected II-VI Semiconducting Alloys by Directional Solidification 1. Ground-Based Experiments," J. Materials Sci., submitted (1995).
6. Lehoczky, S. L. and R. R. Szofran, "Growth of Solid Solution Single Crystals," in The Nation's Future Materials Materials Needs, International SAMPE Technical Conference Series, eds., T. Lynch, J. Persh, T. Wolf, and Rupert (SAMPE: Convina, CA), Vol. 19, p. 332

(1987) (proceedings 19th International SAMPE Technical Conference, Arlington, VA, October 13-15, 1987).

7. Gillies, D. C., S. L. Lehoczky, F. R. Szofran, G. L. E. Perry, and C.-H. Su, "Interface Demarcation in Bridgman-Stockbarger Crystal Growth of II-VI Compounds," to appear in Proceedings, Vol. 1557, SPIE's Symposium on Growth and Characterization of Materials for Infrared Detectors and Nonlinear Optical Switches (held Orlando, FL, April 1-5, 1991).
8. Li, W., and J. D. Patterson, "Deep Defects in Narrow-Gap Semiconductors," Phys. Rev., B50, 14903 (1994).
9. Abdelhakiem, W., J. D. Patterson, and S. L. Lehoczky, "A Comparison Between Electron Mobility in N-Type $Hg_{1-x}Cd_xTe$ and $Hg_{1-x}Zn_xTe$," Materials Letters, 11(1,2), 47-51 (1991).
10. Patterson, J. D., W. A. Gobba, and S. L. Lehoczky, "Electron Mobility in n-Type $Hg_{1-x}Cd_xTe$ and $Hg_{1-x}Zn_xTe$ Alloys," J. of Materials Research, 7(8), 2211-2218 (1992).
11. Gobba, W. A., J. D. Patterson, and S. L. Lehoczky, "A Comparison Between Electron Mobilities in $Hg_{1-x}Mn_xTe$ and $Hg_{1-x}Cd_xTe$," Infrared Phys., 34(3), 311-321 (1993).
12. Patterson, J. D., and S. L. Lehoczky, "The Second Born Approximation and the Friedel Sum Rule," Physics Lett. A, 137(3), 137-138 (1989).
13. Volz, M. P., F. R. Szofran, S. L. Lehoczky, and C.-H. Su, "Lattice Vibration Spectra of $Hg_{1-x}Zn_x$ Alloys," Solid State Comm., 75(12), 943-947 (1990).
14. Volz, M. P., C.-H. Su, S. L. Lehoczky, and F. R. Szofran, "Vibronic Spectra of $Cu^{2+}$ in ZnTe," Phys. Rev. B, 46(1), 76-82 (1992).
15. Su, C.-H., D. C. Gillies, F. R. Szofran, and S. L. Lehoczky, "The Influence of Reduced Gravity on the Crystal Growth of Electronic Materials," Proceedings of the 6th International Space Conference of Pacific Basin Societies (6th ISCOPS), Marina del Rey, CA, December 1995, AAS, 95-590, 351-363 (1996).
16. Su, C.-H., Y.-G. Sha, S. L. Lehoczky, F. R. Szofran, D. C. Gillies, S. D. Cobb, and R. N. Scripa, "Crystal Growth of Selected II-VI Semiconducting Alloys by Directional Solidification 2. Experiments in Low Gravity Environment," J. Materials Sci., submitted (1995).
17. Gillies, D. C., D. J. Larson, S. L. Lehoczky, F. R. Szofran, Y.-G. Sha, C.-H. Su, and A. Alexander, "Bulk Growth of II-VI Crystals in the Microgravity Environment of USML-1," Proceedings, 1993 SPIE Symposium on Optical Instrumentation and Applied Science (San Diego, California, July 11-16, 1993), 2021, 11-21 (1993).
18. Sha, Y.-G., C.-H. Su, H. A. Alexander, S. L. Lehoczky, and J.-C. Wang, "Seeded Growth of HgZnTe by Directional Solidification Using an Initial Compositional Profile Simulating a 'Diffusion-Boundry'Layer", J. Crystal Growth, submitted (1996).
19. Su, C.-H., S. L. Lehoczky, and F. R. Szofran, "Growth and Characterization of CdS Crystals," J. Crys. Growth, 101, 221-225 (1990).
20. Zhou, W., J. Wu, M. Dudley, C.-H. Su, M. P. Volz, D. C. Gillies, F. R. Szofran, and S. L. Lehoczky, "Characterization of Growth Defects in ZnTe Single Crystals," in Proceedings of the First Symposium on Semiconductors for Room-Temperature Radiation Detector Applications, Vol. 302, pp. 451-456 (1993) (Materials Research Society: Pittsburgy, PA) (proceedings of meeting held San Francisco, CA, April 12-16, 1993).

21. Zhou, W., M. Dudley, J. Wu, C.-H. Su, M. P. Volz, D. C. Gillies, F. R. Szofran, and S. L. Lehoczky, "Synchrotron Topography Characterization of ZnTe Single Crystals," Materials Science & Engineering, B27, 143-153 (1994).
22. Sha, Y.-G., C.-H. Su, and S. L. Lehoczky, "Growth of HgZnTe by Directional Solidification in a Magnetic Field," J. Crys. Growth, submitted (1996).
23. Su, C.-H., S. L. Lehoczky, and F. R. Szofran, "Directional Solidification of HgCdTe and HgZnTe in a Transverse Magnetic Field," J. Crys. Growth, 109, 392-400 (1991).

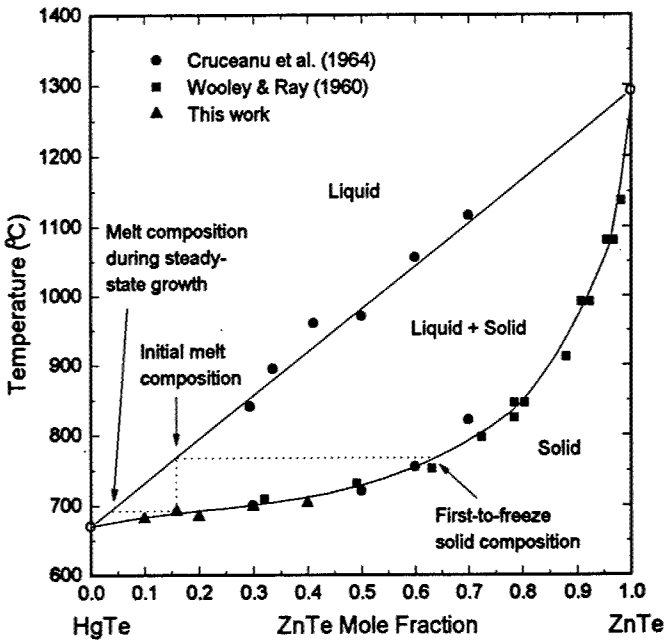


Fig. 1 Phase diagram of HgTe-ZnTe pseudobinary system.

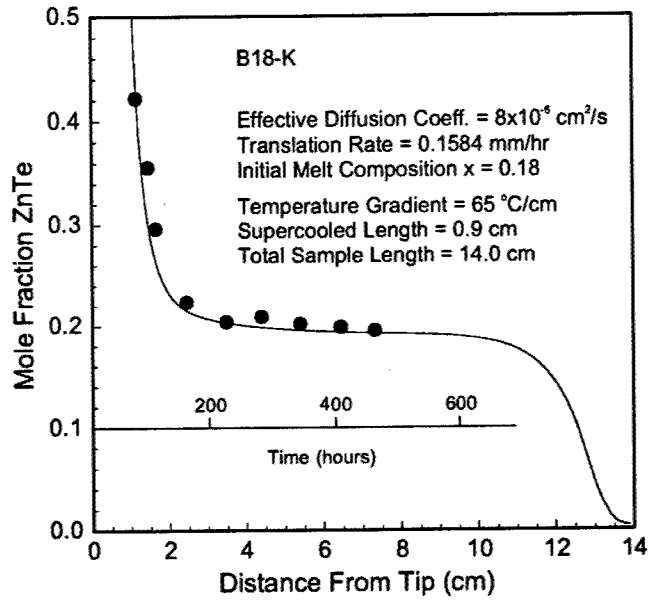


Fig. 2 Measured and calculated axial composition variation in a HgZnTe crystal. The time scale indicates the time needed for growth.

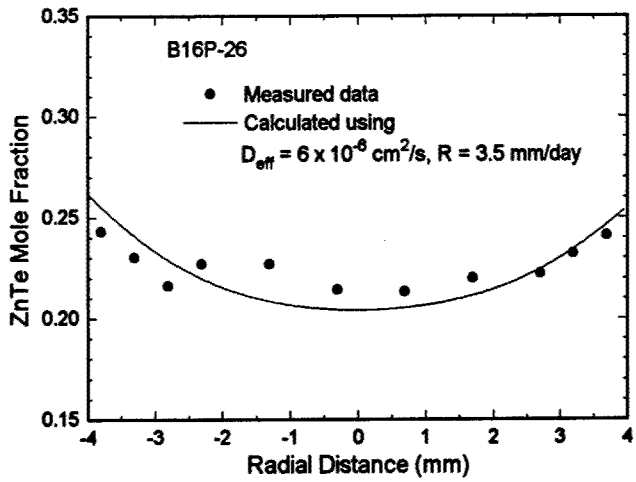


Fig. 3 Radial composition distributions measured by EDS. The solid line is calculated using a two-dimensional diffusion limited model.

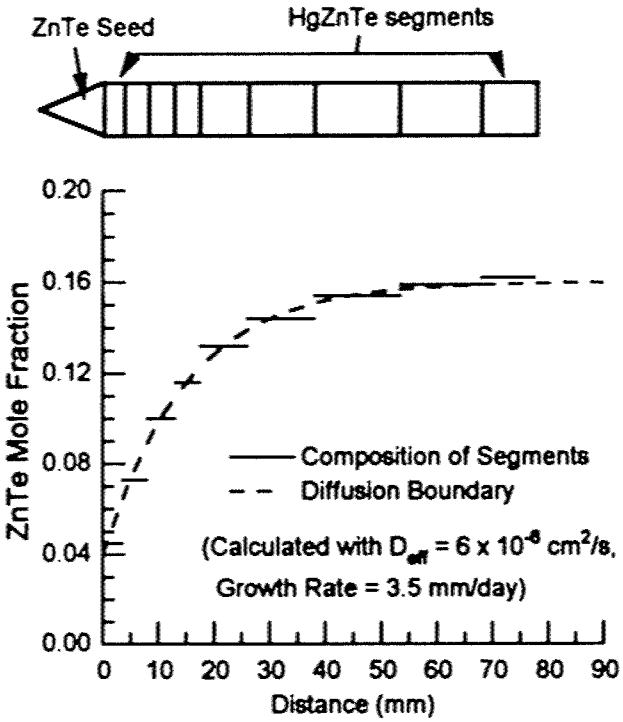


Fig. 4 Sample configuration and typical composition profile in HgZnTe segments used for seeded growth experiments.

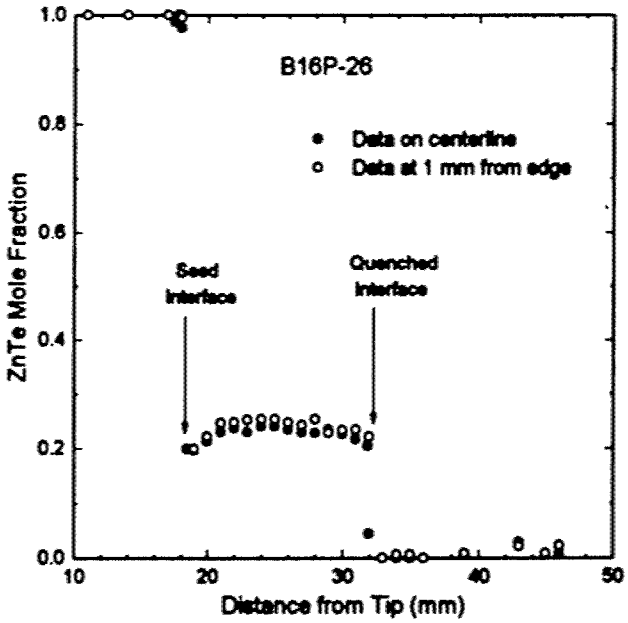


Fig. 5 Composition distributions measured by EDS along the growth direction.

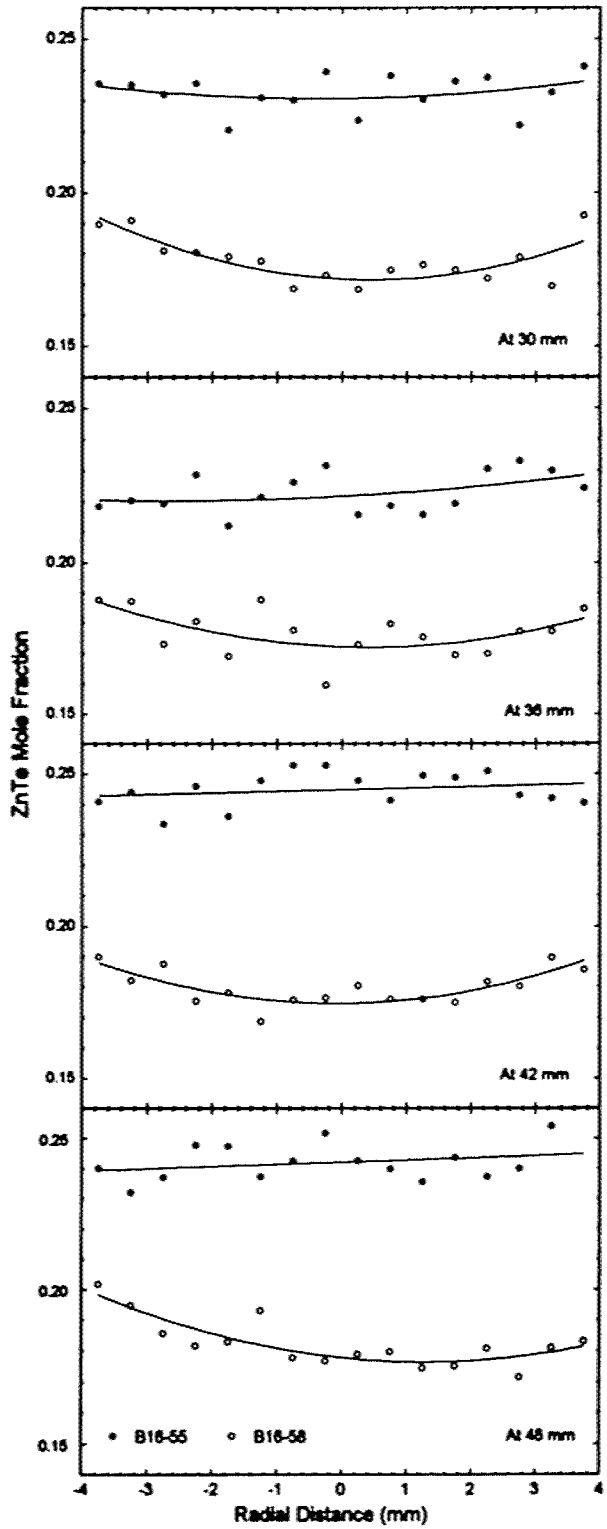


Fig. 6 Radial composition profiles measured by EDS for samples grown with (B16-55) and without (B16-58) a magnetic field.

# GROWTH OF SOLID SOLUTION SINGLE CRYSTALS

Dr. Sandor L. Lehoczky, Prinicipal Investigator, ES75/NASA Marshall Space Flight Center (MSFC); Phone (205) 544-7758, e-mail Sandor.Lehoczky.msfc.nasa.gov

Co-Investigators: Dr. Frank R. Szofran, Dr. Donald C. Gillies, Mr. Dale A. Watring, NASA Marshall Space Flight Center (MSFC)

The objective of the study is to establish the effects of processing semiconducting, solid solution, single crystals in a microgravity environment on the metallurgical, compositional, electrical, and optical characteristics of the crystals. The alloy system being investigated is the solid solution semiconductor$Hg_{1-x}Cd_xTe$, with x-values appropriate for infrared detector applications in the 8 to 14 μm wavelength region. Both melt and Te-solvent growth are being performed. The study consists of an extensive ground-based experimental and theoretical research effort followed by flight experimentation where appropriate. The objectives of the ground-based research effort are to: (1) obtain the experimental data and perform the analyses required to define the optimum growth parameters for the flight samples, (2) quantitatively establish the characteristics of the alloy crystals grown in a 1-g environment as a basis for subsequent comparative evaluations of the alloy crystals grown in microgravity, and (3) develop theoretical and analytical methods required for such evaluations. The ground-based portion of the investigation also includes the evaluation of the relative effectiveness of stabilizing techniques, such as applied magnetic fields, for suppressing convective flow during the melt growth of the crystals.

The difficulty of growing bulk crystals, with both radial and axial homogeneity of significant lengths in Earth's gravity is well documented.[1-9] Because the HgTe-rich component rejected during solidification is more dense, the vertical Bridgman-Stockbarger growth process would appear to be both gravitationally and thermally stable against convection, but this is not generally true. Due to the peculiar relationships between the thermal conductivities of the melt, solid, and ampoule, it is practically impossible to completely avoid radial temperature gradients in the growth region.[3,29-31] In general, the presence of radial temperature gradients near the growth region will cause a curvature in the solid-liquid interface which need be neither an isothermal nor an isoconcentrational surface. Furthermore, the growth of high quality crystals usually requires a slightly convex growth interface as viewed from the melt. Under the influence of stable growth conditions, such interface geometries readily lead to lateral alloy segregation because of the tendency of the more dense HgTe-rich liquid to settle at the portions of the surface having the lowest gravitational potential. Because the alloy solidus temperature decreases with increased HgTe content,[17] the interface temperature will be lowered in this region, causing the interface curvature to increase. Although lateral diffusion will tend to drive the interfacial melt compositions to some equilibrium values, most ground-based melt-growth experiments show large radial compositional variations that are probably a direct consequence of such an interfacial fluid flow phenomenon.[7,49] In low gravity it is expected that the highly desired slightly convex growth surfaces will be easier to maintain because of the reduced tendency for stratification of the denser (HgTe rich) fluid component. At the same time, the near-elimination of radial temperature gradient-driven convection is expected to provide for a better control of the lateral compositional distribution in the melts. It is thus expected that by growing

under the influence of low-gravity conditions ($g \leq 10^{-6} g_0$), crystals with significantly improved crystallinity and compositional homogeneity can be prepared as compared to the best crystals that can be produced on Earth. It is also reasonable to expect that careful characterization of both the space- and ground-grown materials will lead to better insights into the peculiarities of the various growth mechanisms that will permit improvements in Earth-based processing of $Hg_{1-x}Cd_xTe$ and other commpound semiconductor alloy systems.

It is believed that CdTe, $Hg_{1-x}Cd_xTe$, etc. probably possess extremely small yield strengths near their growth temperatures. If this is the case, the high dislocation density ( $\sim 10^5$ $cm^{-2}$) usually seen in these crystals could be due at least in part, to stresses induced by the samples own weight, that is, self-induced stresses. Therefore, a second goal of these experiments is to assess the validity of this hypothesis.

Over the past several years, a detailed evaluation has been performed on the effects of growth parameters on the axial and radial compositional uniformity, defect density, and optical properties in directionally solidified $Hg_{1-x}Cd_xTe$ and other similar compounds and pseudo-binary alloys.[1-49] A series of $Hg_{1-x}Cd_xTe$ alloy ingots ($0 \leq x \leq 0.6$) has been grown from pseudobinary melts by a vertical Bridgman-Stockbarger method using a wide range of growth rates and thermal conditions.[1-16] Several of the experiments were performed in transverse and axial magnetic fields of up to 5T[14-16]. Precision measurements were performed on the ingots to establish compositional distributions and defect density distributions for the ingots. Correlation between growth rates and thermal conditions and growth interface shapes have been established for the alloy system. To assist the interpretation of the results and the selection of optimum in-flight growth parameters, the pseudobinary phase diagram ($0 \leq x \leq 1$),[17] liquid and thermal diffusivities ($0 \leq x \leq 0.3$)[19] melt viscosity,[20] and the specific olumes as a function of temperature ($0 \leq x \leq 0.15$)[21,22] have been measured. From these measurements and other available data, the heat capacity, enthalpy of mixing, and the thermal conductivity of pseudobinary melts have been calculated using a regular associated solution model for the liquid phase.[23] A one-dimensional diffusion model that treats the variation of the interface temperature, interface segregation coefficient, and growth velocity has been used to establish effective diffusion constants for the alloy system.[1,3,24,25] Theoretical models have been developed for the temperature distribution and the axial and radial compositional redistribution during directional solidification of the alloys.[5,26-31] These were used along with the experimental results to select the parameters for the first flight experiment flown on the Second United States Microgravity Payload (USMP-2) mission. A microscopic model for the calculation of point-defect energies, charge-carrier concentrations, Fermi energy, and conduction-electron mobility as functions of x, temperature, and both ionized and neutral defect densities has been developed.[1,2,32-37] For selected samples, measurements were performed of electron concentration and mobility from 10-300K. The experimental data were in reasonably good agreement with theory and were successfully analyzed to obtain donor and acceptor concentrations for various processing conditions.[1,2,32] Microhardness measurements were performed for a series of HgCdTe and HgZnTe alloy compositions to assess the effect of alloying on lattice stabilities and strengths.[38] A regular associated solution formulation was used to calculate the vapor pressures over the pseudobinary melts and to obtain estimates of species concentrations in the liquid phase.[1,34] Extensive development tests were conducted to establish temperature limits for safe use of fused silica ampoules for the growth of the HgCdTe alloy system in a crewed

in a crewed environment[40] and preliminary measurements were performed of the electrical conductivities in HgTe melts.[44]

A five zone Bridgman-Stockbarger type "Advanced Automatic Direction Solidification Furnace (AADSF)" has been designed and developed for the flight portion of the investigation.[48]The AADSF was successfully flown on the USMP-2 mission in March 1994 during which a 15 cm long and 0.8 cm diameter $Hg_{0.8}Cd_{0.2}Te$ alloy crystal was grown under precisely controlled residual acceleration conditions over a period of approximately 11 days. Detailed microstructural and compositional analysis has been performed for the crystal.[50] A rate change inserted into the growth timeline sequence produced in the crystal an effective time marker for correlating orbital and residual accelerations to various crystal features and alloy compositional changes. This allowed a detailed evaluation of the effects of the magnitude and direction of residual acceleration[53] on crystal homogeneity and perfection to be made for the first time.(Figs. 1 and 2) Circumferential variation of composition and topographic features around the boule indicated that residual acceleration vectors were present and have a large effect on the growth process.[48,50-52] The magnitude of the measured transverse compositional variations along the growth axis showed a high degree of correlation to the direction of the residual acceleration vectors. Preliminary x-ray topographs of the portion grown in the most favorable attitude (-XLV, -ZVV) indicate that this region is of significantly higher quality than usually grown on the ground. The Orbital Acceleration Research Experiment (OARE) acceleration measurement instrument record of residual acceleration vectors proved to b in excellent agreement with our results, as evidenced by the surface features of the boule. Certain attitude maneuvers of the orbiter can dramatically affect the growth stability. This is illustrated by the roll-around in tail-down attitude which reversed the direction of the residual acceleration perpendicular to the interface and caused thick compositional striations at 11 cm along the crystal. Further microstructural, optical, and electrical characterizations of the crystal promise to provide a wealth of additional information on the growth in low Earth orbit of solid solution alloy crystals having a large separation between their liquidus and solidus. A series of $Hg_{0.8}Cd_{0.2}Te$ crystals were also grown under the influence of axial magnetic fields up to 5T[16] The application of the magnetic fields greatly reduced the radial compositional variations in the crystals, further underlining the importance of gravitationally-induced fluid flows. The observed radial segregation agreed well with theoretically predicted results.


1. Lehoczky, S. L., F. R. Szofran, and B. G. Martin, "Advanced Methods for Preparation and Characterization of Infrared Detector Materials," NASA CR-161598, July 5, 1980.
2. Lehoczky, S. L. and F. R. Szofran, "Advanced Methods for Preparation and Characterization of Infrared Detector Materials," NASA CR-161949, September 30, 1981.
3. Lehoczky, S. L. and F. R. Szofran, "Directional Solidification and Characterization of $Hg_{1-x}Cd_xTe$ Alloys," in Materials Research Society Proceedings, Materials Processing in the Reduced Gravity Environment of Space, ed., G. E. Rindone (Elsevier: New York), 9, 409-420 (1982).
4. Lehoczky, S. L., and F. R. Szofran, "Growing Crystals for Infrared Detectors," NASA Tech Briefs 8, 136 (1983).
5. Szofran, F. R. and S. L. Lehoczky, "A Method for Interface Shape Control During Bridgman Type Crystal Growth of HgCdTe Alloys," J. Crys. Growth, 70(1/2), 349-355 (1984).
6. Szofran, F. R., D. Chandra, J. C. Wang, E. K. Cothran, and S. L. Lehoczky, "Effect of Growth Parameters on Compositional Variations in Directionally Solidified HgCdTe Alloys," J. Crys. Growth, 70(1/2), 343-348 (1984).

7. Lehoczky, S. L. and F. R. Szofran, "Growth of Solid Solution Single Crystals," NASA TP-2787, December 1987.
8. Szofran, F. R. and S. L. Lehoczky, "Bridgman Growth of Mercury Cadmium Telluride Alloys," in Processing of Electronic Materials, eds., C. G. Law, Jr. and R. Pollard (American Institute of Chemical Engineers: New York), pp. 342-348 (1987) (proceedings of First International Conference on Processing of Electronic Materials, held Santa Barbara, CA, February 23-28, 1986).
9. Lehoczky, S. L. and F. R. Szofran, "Growth of Solid Solution Single Crystals," in The Nation's Future Materials Needs, International SAMPE Technical Conference Series, eds., T. Lynch, J. Persh, T. Wolf, and N. Rupert (SAMPE: Covina, CA), Vol. 19, p. 332 (1987) (proceedings 19th International SAMPE Technical Conference, Arlington, VA, October 13-15, 1987).
10. Lehoczky, S. L., F. R. Szofran, C.-H. Su, S. D. Cobb, and R. N. Andrews, "Crystal Growth of Solid Solution Systems by Directional Solidification," Proceeding of ASM International '87 Materials Congress (held Cincinnati, Ohio, October 12-15, 1987).
11. Andrews, R. N., F. R. Szofran, and S. L. Lehoczky, "Growth and Characterization of $Hg_{1-x}Cd_xSe$ Alloys," J. Crys. Growth, 92(3/4), 445-453 (1988).
12. Andrews, R. N., F. R. Szofran, and S. L. Lehoczky, "Internal Temperature Gradient of Alloy Semiconductor Melts from Interrupted Growth Experiments," J. Crys. Growth, 86(1-4), 100-105 (1988).
13. Lehoczky, S. L. and F. R. Szofran, "Method of Preparing Radially Homogeneous Mercury Cadmium Telluride Crystals," U.S. Patent No. 4,863,553, September 1989.
14. Su, C.-H., S. L. Lehoczky, and F. R. Szofran, "Directional Solidification of HgCdTe and HgZnTe in a Transverse Magnetic Field," J. Crys. Growth, 109, 392-400 (1991).
15. Price, M. W., R. N. Andrews, C.-H. Su, S. L. Lehoczky, and F. R. Szofran, "Effect of Transverse Magnetic Field on the Microstructure of Directionally Solidified CdTe," J. Crys. Growth, in press (1994).
16. Watring, D.A., and S.L. Lehoczky, "Magneto Hydronamic Damping of Convection During Vertical Bridgman-Stockbarger Growth of HgCdTe," J. Crystal Growth (in press).
17. Szofran, F. R. and S. L. Lehoczky, "The Pseudobinary HgTe-CdTe Phase Diagram," J. Electronic Matls., 10, 1131-1150 (1981).
18. Szofran, F. R. and S. L. Lehoczky, "Liquidus Temperatures of Hg-Rich Hg-Cd-Te Alloys," J. Electronic Matls., 12(4), 713-717 (1983).
19. Holland, L. R. and R. E. Taylor, "Measured Thermal Diffusivity of $Hg_{1-x}Cd_xTe$ Solids and Melts," Journal of Vacuum Science Technology, A1, 1615 (1983).
20. Mazuruk, K., C.-H. Su, S. L. Lehoczky, and F. Rosenberger, "Viscosities of Molten HgTe and $Hg_{0.8}Cd_{0.2}Te$," J. Appl. Phys., in press (1995).
21. Chandra, D. and L. R. Holland, "Density of Liquid $Hg_{1-x}Cd_xTe$," Journal of Vacuum Science and Technology, A1, 1620 (1983).
22. Chandra, D., "Anomalous Volume Expansion in $Hg_{1-x}Cd_xTe$ Melts: An Analysis Employing the Inhomogeneous Structure Model," Phys. Rev. 331, 7706 (1985).
23. Su, Ching-Hua, "Heat Capacity, Entalphy of Mixing and Thermal Conductivity of $Hg_{1-x}Cd_xTe$ Pseudobinary Melts", J. Cryst. Growth 78, 51 (1986).
24. Clayton, J. C., "Transient and Diffusion Analysis of HgCdTe," NASA CR162049, 1982.
25. Clayton, J. C., M. C. Davidson, D. C. Gillies, and S. L. Lehoczky, "One Dimensional Analysis of Segregation in Directionally Solidified HgCdTe," J. Crys. Growth, 60, 374 (1982).
26. Naumann, R. J., "An Analytical Approach to Thermal Modeling of Bridgman-Type Crystal Growth I. One-Dimensional Analysis," J. Cryst. Growth 58, 554-568 (1982).
27. Naumann, R. J., "An Analytical Approact to Thermal Modeling of Bridgman-Type Crystal Growth II. Two-Dimensional Analysis," J. Cryst. Growth 59, 569-584 (1982).
28. Cothran, E. K., "An Analytical Approach to Thermal Modeling of Bridgman-type Crystal Growth: One Dimensional Analysis, COmputer Program Users Manual," NASA TM82487, May 1982.
29. Naumann, R. J. and S. L. Lehoczky, "Effect of Variable Thermal Conductivity on Isotherms in Bridgman Growth," J. Crys. Growth, 61, 707-710 (1983).
30. Jasinski, T. and R. J. Naumann, "One-Dimensional Modeling of Vertical Bridgman-Type Crystal Growth", J. Cryst. Growth 66, 469 (1984).
31. Dakhoul, Y. M., R. Farmer, S. L. Lehoczky, and F. R. Szofran, "Numerical Simulation of Heat Transfer During the Crystal Growth of HgCdTe Alloys," J. Crys. Growth, 86, 49-55 (1988).

32. Lehoczky, S. L., C. J. Summers, F. R. Szofran, and B. G. Martin, "Electrical Characterization of $Hg_{1-x}Cd_xTe$ Alloys," in Materials Research Society Proceedings, Materials Processing in the Reduced Gravity Environment of Space, ed., G. E. Rindone (Elsevier: New York), 9, 421-431 (1982).
33. Patterson, J. D., and S. L. Lehoczky, "The Second Born Approximation and the Friedel Sum Rule," Physics Lett. A, 137(3), 137-138 (1989).
34. Abdelhakiem, W., J. D. Patterson, and S. L. Lehoczky, "A Comparison Between Electron Mobility in N-Type $Hg_{1-x}Cd_xTe$ and $Hg_{1-x}Zn_xTe$," Materials Letters, 11(1,2), 47-51 (1991).
35. Patterson, J. D., W. A. Gobba, and S. L. Lehoczky, "Electron Mobility in n-Type $Hg_{1-x}Cd_xTe$ and $Hg_{1-x}Zn_xTe$ Alloys," J. of Materials Research, 7(8), 2211-2218 (1992).
36. Gobba, W. A., J. D. Patterson, and S. L. Lehoczky, "A Comparison Between Electron Mobilities in $Hg_{1-x}Mn_xTe$ and $Hg_{1-x}Cd_xTe$," Infrared Phys., 34(3), 311 (1993).
37. Li, W., and J.D. Patterson, "Deep Defects in Narrow-Gap Semiconductors," Phys. Rev. B 50, 14903, (1994).
38. Andrews, R. N., S. D. Walck, M. W. Price, F. R. Szofran, C.-H. Su, and S. L. Lehoczky, "Microhardness Variations in II-VI Semiconducting Compounds as a Function of Composition," J. Crys. Growth, 99, 717-721 (1990).
39. Kelley, J. D., B. G. Martin, F. R. Szofran, and S. L. Lehoczky, "Applications of the Regular-Associated-Solution Model to the Cd-Te and Hg-Te Binary Systems," J. Electrochem. Soc., 129, 2360-2365 (1982)
40. Holland, L. R., "Sealed Silica Pressure Ampules for Crystal Growth", J. Cryst. Growth 66, 501 (1984).
41. Gillies, D. C., "Analysis of Mercury Cadmium Telluride by Energy Dispersive Analysis," J. Electronic Mat. 11, 689 (1982).
42. Lehoczky, S. L. and F. R. Szofran, "Further Comments on Segregation During Bridgman Growth of $Hg_{1-x}Cd_xTe$," J. Crys. Growth (Lett.), 69, 201-203 (1984).
43. Szofran, F. R. and P. N. Espy, "Automated ac Galvanomagnetic Measurement System," Review of Scientific Instruments 56, 1363 (1985).
44. Lehoczky, S. L., and Frank R. Szofran, "HCT Crystal Growth Method," U.S. Patent No. 4,545,848, October 1985.
45. Su, C.-H., S. L. Lehoczky, and F. R. Szofran, "A Method to Eliminate Wetting During the Homogenization of HgCdTe," J. Appl. Phys., 60(10), 3777-3778 (1986).
46. Szofran, F. R., Gretchen L. E. Perry, and S. L. Lehoczky, "Highly Automated Transmission-Edge Mapping," J. Crys. Growth, 86, 650-655 (1988).
47. Su, C.-H., G.L.E. Perry, F. R. Szofran, and S. L. Lehoczky, "Compositional Redistribution During Casting of $Hg_{0.8}Cd_{0.2}Te$ Alloys," J. Crys. Growth, 91, 20-26 (1988).
48. Lehoczky, S. L., D.C. Gillies, F. R. Szofran, F.A. Reeves, J.D. Sledd, J.M. Cole, T.K. Pendergrass, D.A. Watring, C.R. Coppens, J.E. LeCroy, and D. Popok, "Crystal Growth of HgCdTe in the AADSF on the USMP-2 Mission," 33rd Aerospace Sciences Meeting and Exhibit, January 9-12, 1995, Reno, NV, Paper AIAA 95-0609.
49. Szofran, F. R. and S. L. Lehoczky, "High Temperature Electrical Properties of HgTe," Bull. APS, 28, 1313 (1983).
50. Lehoczky, S. L., F. R. Szofran, and D. C. Gillies, "Growth of Solid Solution Single Crystals," Launch + One (L+1) Report, Second United States Microgravity Payload (USMP-2) Mission, NASA Technical Memorandum 4737, April 1996.
51. Gillies, D. C., S. L. Lehoczky, F. R. Szofran, D. A. Watring, "Effect of Residual Acceleration during Microgravity Directional Solidification of Mercury Cadmium Telluride on the USMP-2 Mission," Proc. Tenth American Conf. On Crystal Growth, Aug. 4-9, 1966 Vail, CO, J. Crystal Growth, submitted.
52. Gillies, D. C., S. L. Lehoczky, F. R. Szofran, D. A. Watring, , H. A. Alexander and G. A. Jerman, "Directional Solidification of Mercury Cadmium Telluride During The Second United States Microgravity Payload Mission (USMP-2), Proc. Of SPIE Space Processing of Materials, Aug. 4-5, 1996, Denver, CO, in press.
53. Rogers, M. J. B., and R. DeLombard, "Summary Report of Mission Acceleration Measurements for STS-62", NASA TM 106773, November 1994.

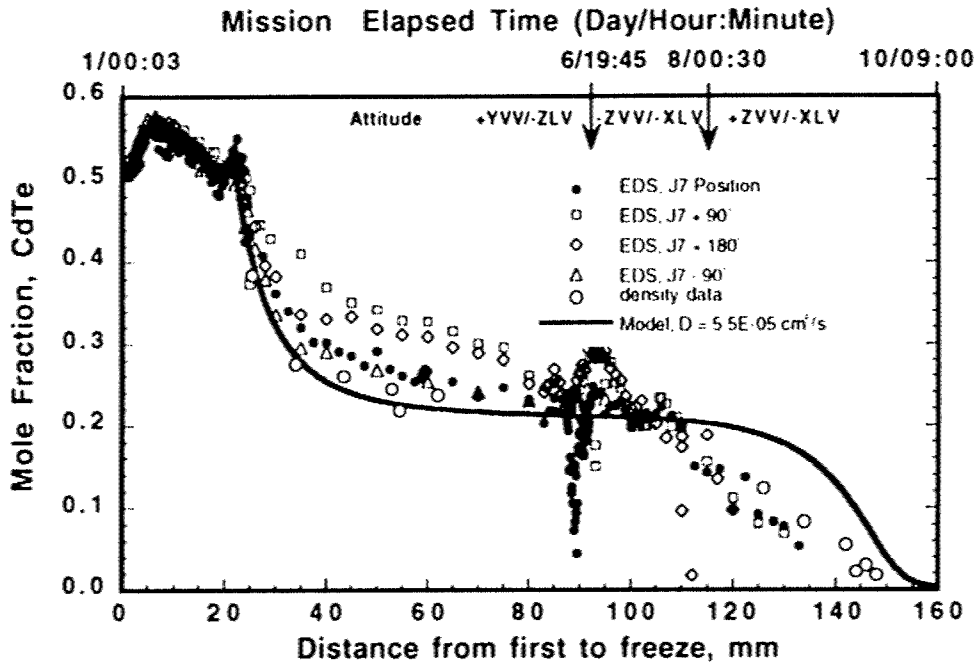


Figure 1. Mission timeline for USMP-2 showing composition of crystal growth

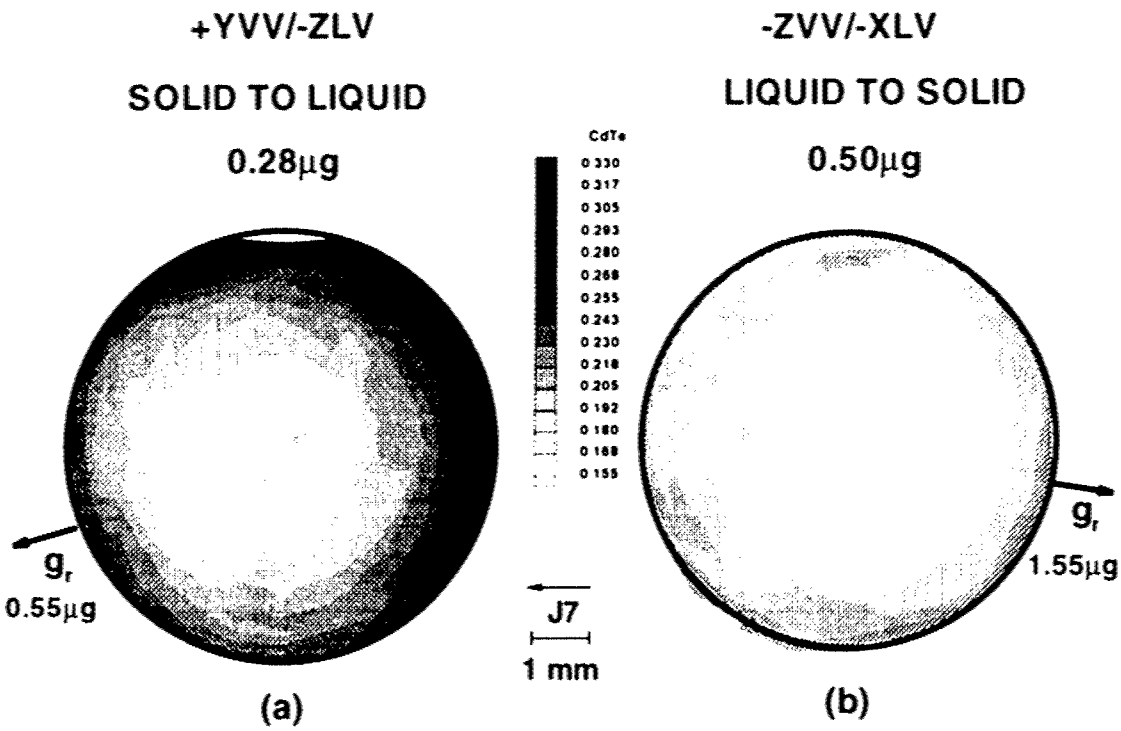


Figure 2. Composition of material grown during two attitudes of the orbiter, (a) 62 mm, (b) 106 mm from first to freeze

# STUDY OF MAGNETIC DAMPING EFFECT ON CONVECTION AND SOLIDIFICATION UNDER G-JITTER CONDITIONS

Ben Q. Li
Department of Mechanical Engineering
Louisiana State University
Baton Rouge, LA 70803
Phone: 504-388-6488
Fax: 504-388-5924
Email: meli@me.lsu.edu

and

H. C. de Groh III
NASA Lewis Research Center
Cleveland, OH 44135
Phone: (216)433-5025
Fax: (216)433-5033
Email: henry@sarah.lerc.nasa.gov

## ABSTRACT

As shown by NASA resources dedicated to measuring residual gravity (SAMS and OARE systems), g-jitter is a critical issue affecting space experiments on solidification processing of materials. This newly-funded study aims to provide, through extensive numerical simulations and ground based experiments, an assessment of the use of magnetic fields in combination with microgravity to reduce the g-jitter induced flow in space processing systems. The project was funded about one month ago and is now in good progress. We have so far completed asymptotic analyses based on the analytical solutions for g-jitter driven flow and magnetic field damping effects for a simple one-dimensional parallel plate configuration. Some useful findings have been obtained from the analyses and the results showed that the amplitude of the oscillating velocity decreases at a rate inversely proportional to the g-jitter frequency and with an increase in the applied magnetic field. The induced flow oscillates at the same frequency as the affecting g-jitter, but out of a phase angle. The phase angle is a complicated function of geometry, applied magnetic field, temperature gradient and frequency. Results also suggest that while a magnetic field can be applied to suppress oscillating flows associated with g-jitter, the damping effect is more effective for low frequency flows. Besides analytical analyses, we have also completed the modification of our existing finite element program and are in a position to carry out detailed numerical simulations for a 2-D geometry. Additional work planned in the project will involve extensive ground based

experimental measurements and numerical model development and simulation to obtain information useful for both fundamental understanding of magnetic damping phenomena and designing of damping facilities for microgravity applications.

## I. INTRODUCTION

Microgravity and magnetic damping are two mechanisms applied during the melt growth of semiconductor or metal crystals to suppress buoyancy driven flow so as to improve macro and micro homogeneity of the crystals. As natural convection arises from gravity effects, microgravity offers a plausible solution to reduce the convective flow. However, recent flight experiments indicated that residual accelerations during space processing, or g-jitter, can cause considerable convection in the liquid pool, making it difficult to realize a diffusion controlled growth, as originally intended, when experiments were conducted in microgravity [1]. Further studies showed that g-jitter is a random phenomenon associated with microgravity environment and has both steady state and transient effects on convective flow [2-7].

The fact that molten metals and semiconductor melts are electrically conducting opens one more avenue to control the convective flow. Less obvious than gravity, this approach is based on the interaction of the liquid motion with an externally applied magnetic field. This interaction gives rise to an opposing Lorentz force that results in a reduction (or damping) of melt flow velocities. While magnetic damping has been well understood for terrestrial conditions [8,9], its effect in g-jitter environment is still embedded in the governing equations and has not yet been fully appreciated. There appears to have been neither theoretical nor experimental work on the subject.

The objectives of this newly-funded MSAD/NASA project are to: (1) determine the behavior of g-jitter induced convection in a magnetic field, (2) assess the abilities of magnetic fields to suppress the detrimental effects of g-jitter during solidification and (3) develop an experimentally verified numerical model capable of simulating transport processes and solidification phenomena under g-jitter conditions with and without a magnetic field. These goals will be achieved through both theoretical analyses and ground based laboratory experiments. By now the project has been in place for about one month. During this period of time, we have carried out some asymptotic analyses based on the analytical solutions for g-jitter driven flow and magnetic field damping effects for a simple one-dimensional parallel plate configuration. The analyses showed that the amplitude of the oscillating velocity decreases at a rate inversely proportional to the g-jitter frequency and with increase in the applied magnetic field. The induced flow oscillates at the same frequency as the affecting g-jitter, but out of a phase angle. The phase angle depends on geometry,

applied magnetic field, temperature gradient and frequency. A magnetic field can be applied to suppress oscillating flows associated with g-jitter; it is more effective in damping low frequency flows but only has a moderate damping effect on the flow induced by high frequency g-jitter.

In addition, a 2-D finite element model has been developed and preliminary numerical results compared well with available results on g-jitter driven flow. We now are further refining the 2-D model and conducting extensive numerical simulations with g-jitter data obtained from flight experiments. Our future work involves incorporating the adaptive algorithm into the 2-D model to account for moving boundary shapes associated with solidification under g-jitter conditions and magnetic damping effects in microgravity conditions. The 3-D numerical models will be further developed. Laboratory experiments on magnetic damping of oscillating flow generated in mercury pool by appropriate thermal boundary conditions will be conducted. Further experiments will be carried out at NASA Lewis Research Center to verify the numerical model predictions.

## II. ANALYTICAL SOLUTION FOR A ONE-D SIMPLE SYSTEM

This simple one dimensional analysis is intended to provide some perspective on asymptotic behavior of the magnetic damping effects on g-jitter induced flow. Figure 1 shows the geometry for our analyses. The analyses consider a steady state flow with otherwise time harmonic oscillation. Some simplifications have been made to make the analyses feasible. These include the following: (1) the parallel plates are infinitely long, (2) g-jitter oscillates with a single frequency (of course, multiple frequency can be readily incorporated into the analyses), (3) the temperature field is controlled by diffusion, and (4) g-jitter frequency sufficiently small that its time oscillating nature will not affect the imposed DC magnetic field. With these simplifications and with the use of phasor notation for time harmonic analyses, the Maxwell equations and fluid flow equations can be reduced to a set of one dimensional ordinary differential equations and thus readily solved.

Some results are selectively presented in Figures 2 to 4. Figure 2 shows the natural convection distribution across the width of the channel induced by g-jitter without an applied magnetic field for different times. The quantity plotted along the vertical axis shows the velocity in the channel driven by a single frequency g-jitter component. The flow oscillates about zero and changes direction, as expected. It is noticed that at around $\Omega\tau=5\pi/4$ the velocity profile also oscillates along the width of the channel but for other times the velocity profile is approximately parabolic.

Figure 3 depicts the flow behavior at a fixed position (Y=0.5) with and without an imposed magnetic field. As a reference, the g-jitter oscillation responsible for the natural convective flow is

also plotted but scaled down by a factor of 0.1 for the sake of comparison. It is seen that the flow oscillates at the same frequency as the g-jitter with or without the presence of a magnetic field. There exists a phase change, however, between the driving g-jitter and the flow. The phase angle is strongly affected by the magnetic field. It is also clear that application of the magnetic field helps to suppress the flow, and indeed the flow intensity is damped by more than 50% when the Hartmann number increases from 0 to 5.

The damping effect of the magnetic field on the g-jitter induced flow is further illustrated in Figure 4, where the flow distribution is plotted as a function of the Hartmann number. As a limit, the flow can be damped entirely if a large enough magnetic field is applied, as indicated by the horizontal line across U=0. It is apparent that a magnetic field is effective in damping flows induced by g-jitter. In fact, it is more effective in suppressing the flows associated with g-jitter with lower frequencies but only has a moderate effect on the high frequency g-jitter flows. At Ha=15 and beyond, the curves converge to virtually the same line, indicating that the frequency becomes basically irrelevant and the rate of damping is reduced.

## III. DEVELOPMENT OF 2-D FINITE ELEMENT MODEL

We have completed modifying our existing finite element fluid flow and heat transfer code to study the g-jitter induced flow and magnetic damping effects. Our finite element code, during the course of its development, has been extensively compared with various commercial packages including FIDAP, FLOW3D, and FLUENT. Some preliminary results have been obtained for natural convective flows driven by some idealized sinusoidal oscillating g-jitter in a cavity. The results compared well with those on g-jitter driven flow reported in literature [4-6]. Our current effort is on the refinement of this 2-D model by comparing with the analytical solutions obtained for parallel plates as described above for both magnetic damping effects and g-jitter oscillating flows and is on developing an adaptive algorithm and incorporating the algorithm, along with deforming elements for solidification modeling, into the existing 2-D model.

## IV. FUTURE WORK

The planned work involves extensive experimental measurements and numerical simulations to enhance our fundamental understanding of magnetic damping effects on g-jitter induced flow and solidification phenomena in space processing systems and to help design damping facilities for microgravity applications.

Experiments will be conducted in an experimental setup in which mercury will be used as a testing fluid. The oscillating flow, which is intended to simulate the effect of single frequency g-jitter, is generated in the mercury by applying an oscillating temperature boundary condition. External magnetic fields are be applied and their effects on the damping of the oscillating convective flows are studied. The flow velocities in the mercury pool will be measured using hot film anemometers with and without the presence of an applied magnetic field. These experiments are intended to provide a basic understanding of the behavior of the gravity-induced oscillating convective flow with and without an applied magnetic field. Further experiments of magnetic damping during unidirectional solidification will be conducted in NASA's magnetic damping furnace at the NASA Lewis Research Center. Both the laboratory and NASA's Lewis magnetic damping experiments will be used to verify and refine numerical models, as described below, and to assess the effectiveness of a magnetic field in damping the deleterious effects associated with g-jitter.

Two-D and three-D mathematical models will be developed to represent the complex phenomena associated with magnetic damping during solidification in space, such as the induced Lorentz force distribution, fluid flow and temperature distribution in melts under g-jitter conditions. The numerical predictions will be compared with measurements taken on the mercury model and on the magnetic damping furnace at NASA Lewis. The numerical models will be refined in light of the comparison. With the experimental setups and mathematical models, the melt flow under the influence of a magnetic field will be studied as a function of operating conditions for space experiments, including (1) gravity orientation, (2) magnetic field strength, and (3) oscillation frequency. Both steady state and transient conditions will be studied. Experience gained from the physical and mathematical models will be applied to develop an integrated numerical model to determine magnetic damping effects on velocity distribution, temperature distribution, solid-liquid interface and solute distribution during solidification under g-jitter conditions.

## V. REFERENCES


[1] Lehoczky, S., Szofran, F. R. and Gillies, D. C. (1994). Growth of solid solution single crystals. Second United States Microgravity Payload, Six Month Sciences Report, NASA MSC.

[2] Alexander, J. I. D. (1990) *Microgravity Sci Tech.*, vol. 3, P. 52.

[3] Alexander, J. I. D. (1994). *Microgravity Sci. Tech.*, Vol. 2, p.131.

[4] Alexander, J. I. D., Amiroudine, S., Quazzani, J. and Rosenberger, F. (1991) *J. Crystal Growth*, Vol. 113, p.21.

[5] Chen, H., Saghir, M. Z., Quon, D. H. H. and Chehab, S. (1994). *J. Crystal Growth*, Vol. 142, p. 362.

[6] De Groh, H. C. and Nelson, E. S. (1994). On residual acceleration during space experiments. ASME Winter Annual Meeting, Chicago, IL, HTD-Vol. 290, p. 23.

[7] Nelson, E. S., (1991). An examination of anticipated g-jitter on space station and its effects on materials processes. NASA TM 103775.

[8] Langlois, W. E., (1981). *Comput. Methods. Appl. Mech. Eng.*, Vol. 25, p.315.

[9] Sabhapathy, P. and Salcudean, M. E. (1991). *J. Crystal Growth*, Vol. 113, p. 164.

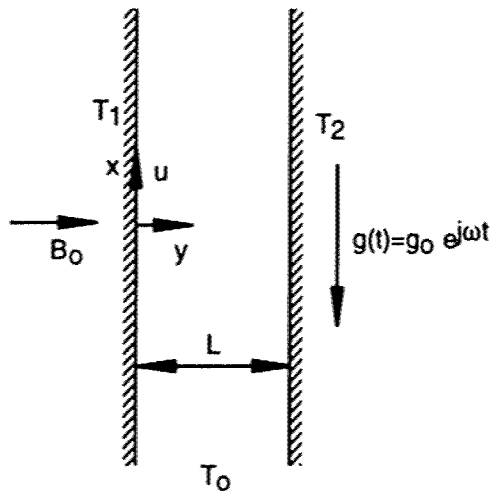


Fig. 1. Schematic representation of g-jitter induced free convection problems and coordinate system used for calculations.

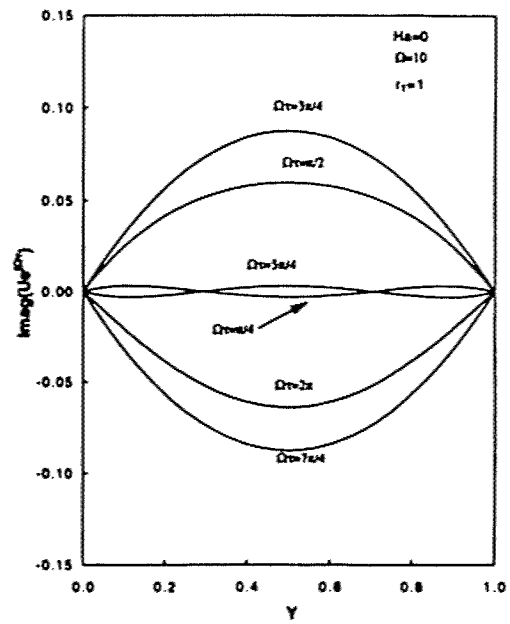


Fig. 2. Velocity distribution of oscillating free convection induced by g-jitter. The vertical axis represents the measurable oscillating velocity. Ω=frequency, τ=time, U=velocity, H=Hartmann number and $r_T$=temperature difference across the channel, all being nondimensionalized.

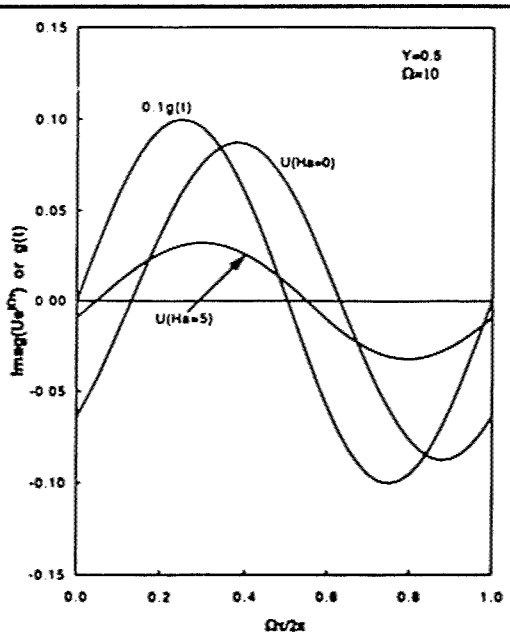


Fig. 3. G-jitter induced free convection variation over a cycle of oscillation. Variables are given in Fig. 2.

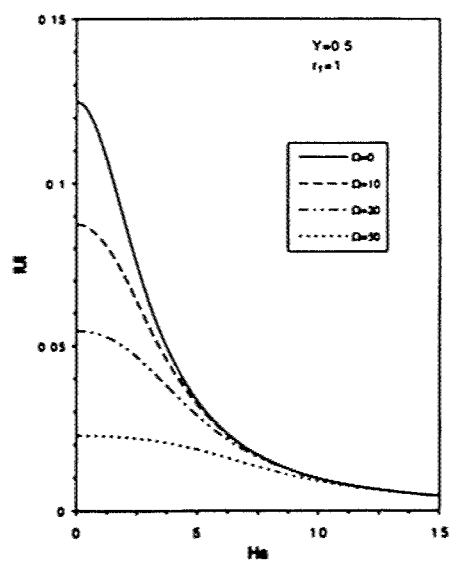


Fig. 4. Decrease of velocity amplitude |U| as a function of applied magnetic field strengths. Other variables are given in Fig. 2.

# MICROSTRUCTURAL DEVELOPMENT DURING DIRECTIONAL SOLIDIFICATION OF PERITECTIC ALLOYS

K. L. Zeisler-Mashl and T. A. Lograsso
Institute for Physical Research and Technology
Iowa State University
Ames, Iowa 50011
(515) 294-6529 and (515) 294-8425
kzeisler@iastate.edu and lograsso@ameslab.gov

## Introduction

A thorough understanding of the microstructures produced through solidification in peritectic systems has yet to be achieved, even though a large number of industrially and scientifically significant materials are in this class. One type of microstructure frequently observed during directional solidification consists of alternating layers of primary solid and peritectic solid oriented perpendicular to the growth direction [1-10]. This layer formation is usually reported for alloy compositions within the two-phase region of the peritectic isotherm and for temperature gradient and growth rate conditions that result in a planar solid-liquid interface. Layered growth in peritectic alloys has not previously been characterized on a quantitative basis, nor has a mechanism for its formation been verified. The mechanisms that have been proposed for layer formation can be categorized as either extrinsic [1,4,10] or intrinsic [2,3,5,11] to the alloy system. The extrinsic mechanisms rely on externally induced perturbations to the system for layer formation, such as temperature oscillations, growth velocity variations, or vibrations. The intrinsic mechanisms approach layer formation as an alternative type of two phase growth that is inherent for certain peritectic systems and solidification conditions. Convective mixing of the liquid is an additional variable which can strongly influence the development and appearance of layers due to the requisite slow growth rate. The first quantitative description of layer formation

is a model recently developed by Trivedi based on the intrinsic mechanism of cyclic accumulation and depletion of solute in the liquid ahead of the interface, linked to repeated nucleation events in the absence of convection [12]. The objective of this research is to characterize for the first time the layered microstructures developed during ground-based experiments in which external influences have been minimized as much as possible and to compare these results to the predictions of the model. Also, the differences between intrinsic and externally influenced layer formation will be explored.

## Materials and Procedure

The Sn-Cd system was selected for study, in part because this low melting point system has been reasonably characterized and previously observed to form layered microstructures. In addition, the solute element Cd is expected to be more dense in the liquid state than Sn, which should minimize density-driven convection in ground-based experiments when solidification occurs upward. A review of the phase diagram literature revealed a discrepancy in the position of the peritectic phase field at the peritectic temperature. Directional solidification experiments in conjunction with compositional analyses using an electron microprobe confirmed the version in the most recently published phase diagram evaluation drawn in Figure 1 [13]. Alloy compositions used in this research extended across the entire peritectic isotherm between the primary solid and liquid compositions. Alloy rods of the desired composition and approximately 6 mm in diameter and 100 mm in length were directionally solidified upward for roughly 50 mm prior to quenching to preserve the shape of the solid-liquid interface. The temperature gradient in the liquid ahead of the interface was 17°C/mm. The range of growth velocities utilized was between 1 and 10 μm/sec. External perturbations were checked and maintained at the lowest practical levels for the majority of the experiments. Certain samples were solidified in the presence of an oscillating furnace temperature.

## Summary and Conclusions

Most of the experimental work reported here has focused on an alloy composition slightly higher in solute than the peritectic solid composition at the peritectic temperature, namely 1.4 wt.% Cd. The model does not anticipate layer formation for alloy compositions outside the range between the primary and peritectic solids at the peritectic temperature. Nonetheless, layer formation was observed for these compositions; however, the layers developed did not fill the entire sample cross section (see Figure 2). Furthermore, they were accompanied by a non-uniform cross-sectional composition, with the result that the overall composition in the layered regions was estimated to be within the two-phase region. These layered microstructures were characterized in terms of layer compositions and layer lengths measured parallel to the growth direction as a function of growth velocity. The composition gradients within individual layers predicted by the model were not observed experimentally; these gradients are most likely below the resolution limit of the measurement technique utilized. The individual layer compositions and lengths did not vary with solidification distance, which agrees with the model and with the experimentally verified minimal long range mixing in the liquid. The average layer compositions were not a function of growth velocity, which is as the model predicts. The $\alpha$ layer composition was 0.4 wt.% Cd and the $\beta$ layer composition was 1.0 wt.% Cd within $\pm 0.1$ wt.% Cd at 95% confidence limits. However, the average layer lengths showed a different dependence on growth velocity than that expected from the model; the measured lengths were proportional to the inverse square root of velocity rather than to the inverse of velocity (see Figure 3). The differences between experimental observations and model predictions are most likely related to two features of layer formation in the Sn-Cd system which contradict assumptions of the model: 1) continuity between the solid phases which negates the requirement for repeated nucleation events and 2) a non-uniform cross-sectional composition throughout the directionally solidified length, which implies non-uniform conditions for nucleation and growth of the two solid phases. Some of these issues are being currently addressed in the work of Karma et al. [15]. The measurements of layer compositions and lengths as a function of growth velocity are being repeated for an alloy of lower solute content to determine the effect of composition on layer formation.

To investigate the differences between intrinsic layer formation and externally influenced layer formation in the Sn-Cd system, controlled interface velocity variations were induced through hot zone temperature oscillations. Preliminary results show that the layer periodicity matches with the periodicity of the temperature changes. The layers differ in appearance from the previously obtained microstructures and are very regular. Experiments are being conducted for a range of alloy compositions both with and without the induced oscillations.

## References


1. N. J. W. Barker and A.Hellawell: *Met. Sci.*, 1974, vol. 8, pp. 353-356.
2. W. J. Boettinger: *Metall. Trans.*, 1974, vol. 5, pp. 2023-2031 .
3. A. P. Titchener and J. A. Spittle: *Acta Metall.*, 1975, vol. 23, pp. 497-502.
4. A. Ostrowski and E. W. Langer: in *Solidification and Casting of Metals*, The Metals Society, London, 1979, pp. 139-143.
5. H. D. Brody and S. A. David: in *Solidification and Casting of Metals*, The Metals Society, London, 1979, pp. 144-151.
6. D. J. Larson, R. G. Pirich, and W. R. Wilcox, Annual Report on Contract NAS8-32998, Marshall Space Flight Center, 1981.
7. B. C. Fuh: Ph.D. Dissertation, Iowa State University, Ames, IA, 1984.
8. B. F. Oliver and B. Kad: *J. Less-Common Met.*, 1991, vol. 168, pp. 81-90.
9. J. H. Lee and J. D. Verhoeven: *J. Cryst. Growth*, 1994, vol. 144, pp. 353-366.
10. J. W. Rutter, M. G. Julien, and G. R. Purdy: *Mater. Sci. and Technology*, 1995, vol. 11, pp. 1233-1240.
11. M. Hillert: in *Solidification and Casting of Metals*, The Metals Society, London, 1979, pp. 81-87.
12. R. Trivedi: *Metall. and Mater. Trans. A*, 1995, vol. 26A, pp. 1583-1589.
13. K. L. Zeisler-Mashl and T. A. Lograsso: *J. Phase Equilibria*, 1996, vol. 17, pp. 7-9.
14. J. Dutkiewicz, L. Zabdyr, Z. Moser, and J. Salawa: *Bull. Alloy Phase Diagrams*, 1989, vol. 10, pp. 223-229.

15. A. Karma, W. Rappel, and R. Trivedi: The Role of Dynamic Nucleation at Moving Boundaries in Phase and Microstructure Selection, Microgravity Conference, Huntsville, AL, 1996.

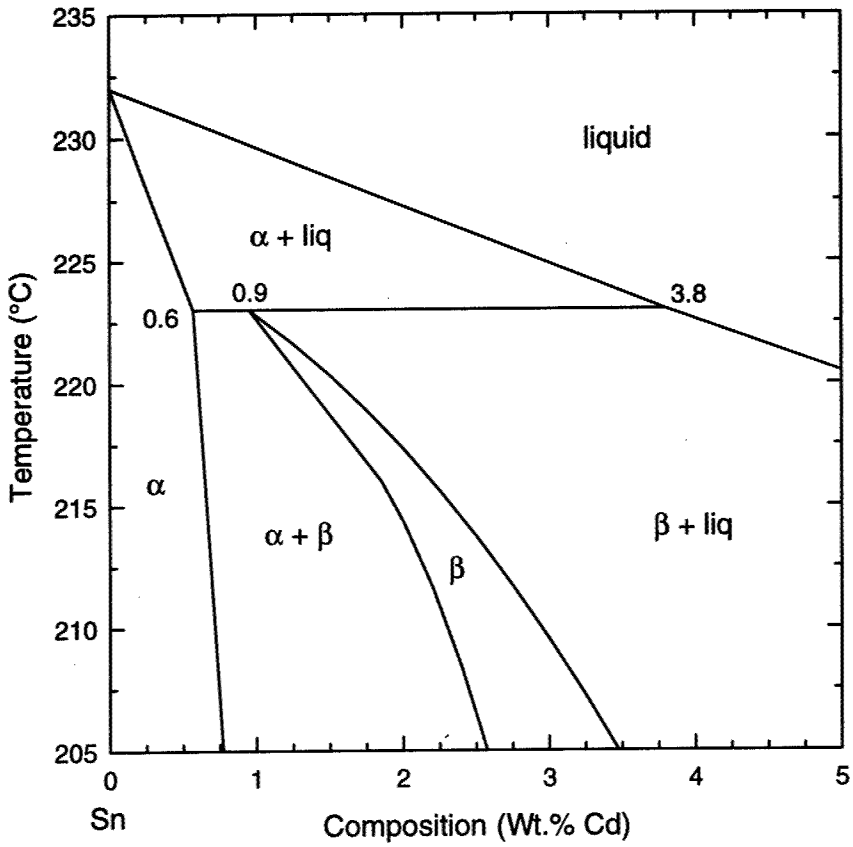


Figure 1: Section of the Sn-Cd phase diagram containing the peritectic reaction drawn from Reference 14.

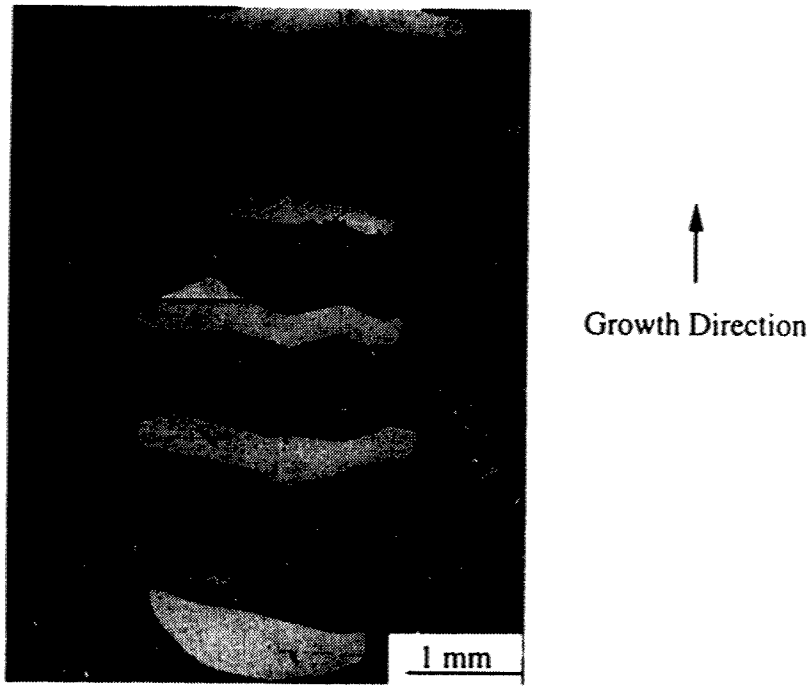


Figure 2: Optical micrograph of a longitudinal section near the center of a Sn-1.4 wt.% Cd sample directionally solidified at 3.8 μm/sec. Alpha is the light phase and β is mottled.

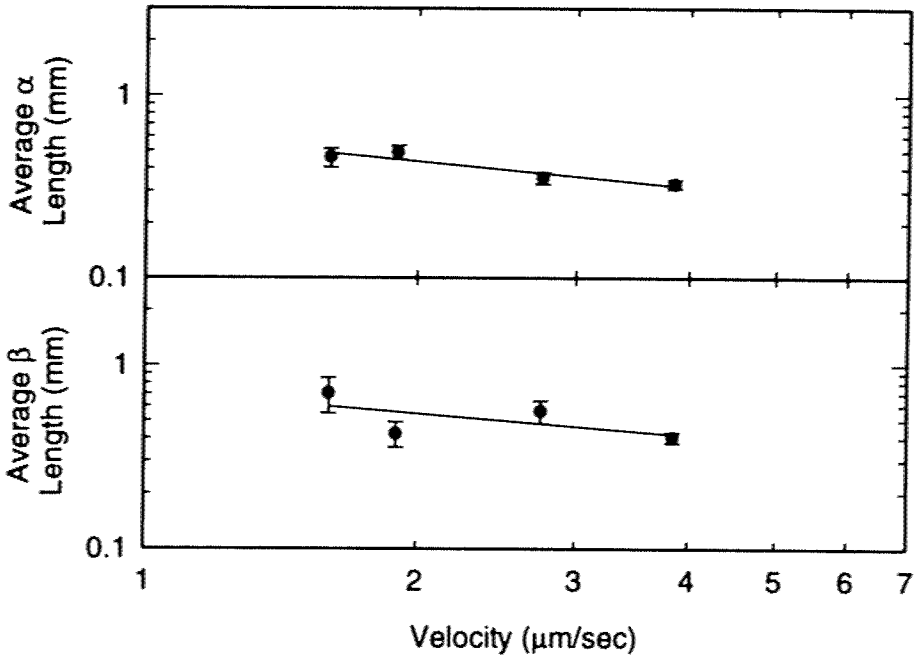


Figure 3: Average lengths of the α and β layers in Sn-1.4 wt.% Cd samples as a function of growth velocity with a linear regression of the data. Error bars represent 95% confidence limits.

# DIFFUSION PROCESSES IN MOLTEN SEMICONDUCTORS

Professor D.H. Matthiesen
420 White Building
Case Western Reserve University
10900 Euclid Avenue
Cleveland, OH 44106
(216) 368-1366 voice
(216) 368-3209 FAX
DHM5@po.cwru.edu E-mail

## 1. Description of Experiment

For the MSL-1 flight of opportunity, this program of study is directed at the fundamental and applied issues pertaining to diffusion of mass in the liquid state as driven by concentration gradients (Fickian diffusion). The fundamental material systems of interest for the MSL-1 mission are the dilute binary systems of gallium (Ga), silicon (Si) and antimony (Sb) into germanium (Ge). This research program consists of three major components: an experimental measurement portion, a continuum numerical simulation portion and an atomistic numerical simulation portion.

The experimental measurement portion is designed to provide definitive measurements of the purely diffusive component of mass transfer in molten semiconductor systems. The shear cell technique will be used to directly measure the diffusion coefficients in semiconductor melts. For the Fickian diffusion case, isothermal measurements will be used to determine the diffusion coefficients. An experimental matrix will be used to determine the dependence of the diffusion coefficients on temperature, dopant type and column diameter. For the MSL-1 mission, the experiments will contain a "check" to quantify, if any, the amount of Soret diffusion driven by the small thermal gradients in the LIF.

The shear cell technique consists of two columns of different liquids which are brought into contact with one another, allowed to diffuse, and then these columns are sheared into segments. Following solidification, the average concentration level of each segment is measured enabling the construction of a diffusion profile. From that concentration profile, the diffusion coefficients can be computed, and possible diffusion mechanisms may be verified.

An extensive ground based experimental matrix is currently being pursued. However, each of these experiments measures an effective diffusion coefficient, which will be a combination of a purely diffusive transport and convective transport. By reducing the sample diameter, the convective transport term can be minimized. However, if the sample diameter is too small, an addition transport term due to wall effects becomes important. From the data in the literature, the wall effect term is negative (i.e. decreasing the effective diffusion coefficient relative to the purely diffusive diffusion coefficient) and is functionally dependent on the column diameter. In the microgravity environment of near earth orbit, the convective term can be minimized and the sample diameter can be increased to minimize the wall effect, thus measuring the purely diffusive diffusion coefficient.

Post flight characterization will consist of providing a precise spatial map of solute distribution in each segment via Spreading Resistance Measurement technique (SRM). This is an electrical characterization technique and allows a very large number of measurements to be taken on each sample. The average concentration of each segment will be determined via Inductively Coupled Plasma/Atomic Emission Spectroscopy (ICP/AES) for Ga and Si, and Inductively Coupled Plasma/Mass Spectroscopy (ICP/MS) for Sb. In both the ICP/AES and ICP/MS techniques, the sample is digested and a small number of measurements are taken from each sample. Statistical analysis of these measurements are being done to determine the precision and accuracy of these measurements. In addition, a statistical model of a perfect diffusion profile has been developed. Known error has been added to this model to determine the exact precision for which the value of diffusion coefficients can be differentiated.

Extensive continuum numerical simulation experiments will be performed using a complete thermal model of the furnace, combined with a three dimension model of the shear cell. These simulations (together with verification experiments) will be used to determine the input control parameters for the isothermal furnace.

A second class of continuum numerical simulations have been used to directly predict the mass diffusion behavior of an experiment. These predictions will be used to determine the diffusion coefficients by direct comparison with experimental data of the concentration profile. Another purpose of these simulations is to isolate the functional temperature dependencies by comparing the measured concentration profile shapes for the Ga, Si, and Sb doped Ge with predicted behavior.

The atomistic numerical simulations will model diffusion on an atomistic level to predict possible diffusion mechanisms. It is intended that these modeling efforts will provide a scientific

explanation of the measured dependencies of temperature and dopant type as well as the wall effect phenomena. It is hoped that these simulations will lead to an analytical expression for the diffusion coefficient as a function of temperature, atomic size differential, atomic charge differential for other dopant material in other matrix materials.

## 2. Scientific Knowledge to be Gained

The fundamental mechanisms of mass diffusion in the liquid state are still unclear to the degree necessary for the prediction of diffusion of one species into another or even within itself. This observation is especially true with respect to the dependence of diffusion mechanisms on temperature as well as on the dopant type. Present estimates of diffusivity in molten semiconductors can typically provide an order of magnitude estimate only, without any information on their dependency on type and temperature

The availability of these data is of paramount importance for practical reasons as well. The relevancy of numerical modeling for the analysis and design of ground based and space experiments is directly dependent upon the accuracy of the fundamental material properties used in these simulations. These data are also important for the correct characterization and interpretation of experimental results from ground based and space experiments.

## 3. Value of Knowledge to Scientific Field

The subject of how a mass of one species diffuses through a matrix of another is, at the same time, both a very old and very new research area. That this area can encompass the small, i.e., movement of electrons in a plasma, to the very large, i.e., the depletion of the global ozone layer, merely serves to emphasize the fundamental aspects of this subject. Most manufacturing technologies at some stage, rely on diffusion processes in the solid, liquid or gas.

The need for precise measurements of the diffusion coefficients in molten semiconductors has been repeatedly pointed out. These data are required both to interpret the experimental results from previous space-based (and Earth-based) experiments and also to optimize newly envisioned experiments. Difficulties in experimental techniques and theoretical interpretations are cited for the lack of these data. This is a comprehensive program which addresses both of these issues.

## 4. Justification of the Need for Space Environment

Terrestrial experiments designed to measure diffusion coefficients in the liquid state are hampered by convection in the melt and convection during the solidification process, both of which typically confound data interpretation. This has resulted in wide variations in the few reported data in the literature. Arnold and Matthiesen have predicted, based on numerical simulations, that for the Ga-doped Ge system, convection effects increase the measured diffusion coefficient and are expected for capillary diameters greater than 2 mm and may be present for capillary diameters less than 2 mm. The experimental data combined with the numerical simulations of convective effects predict a nonexistent range of capillary diameters that allow the measurement of the actual diffusion coefficient on Earth. As a result, the microgravity environment, in which convective effects are minimized, is required.

## 5. Summary of Ground Based Tests

The table below lists the summary of ground based testing.

| Capillary Diameter (mm) | Diffusion Coefficient | errors |
|---|---|---|
| 1.6000 | 2.2200 | 1.1900 |
| 1.6000 | 1.6000 | 0.090000 |
| 1.6000 | 1.7500 | 0.11000 |
| 3.0000 | 2.7600 | 0.37000 |
| 3.0000 | 3.1200 | 0.14000 |
| 1.0000 | 1.5900 | 0.50000 |
| 2.0000 | 0.92500 | 0.13800 |
| 3.0000 | 0.76300 | 0.12800 |
| 1.6000 | 1.6400 | 0.11000 |
| 3.0000 | 2.6400 | 0.41300 |
| 1.6000 | 1.7900 | 0.41300 |

Table 1. Summary of diffusion measurements in Ga-doped Ge.

These data are plotted below.

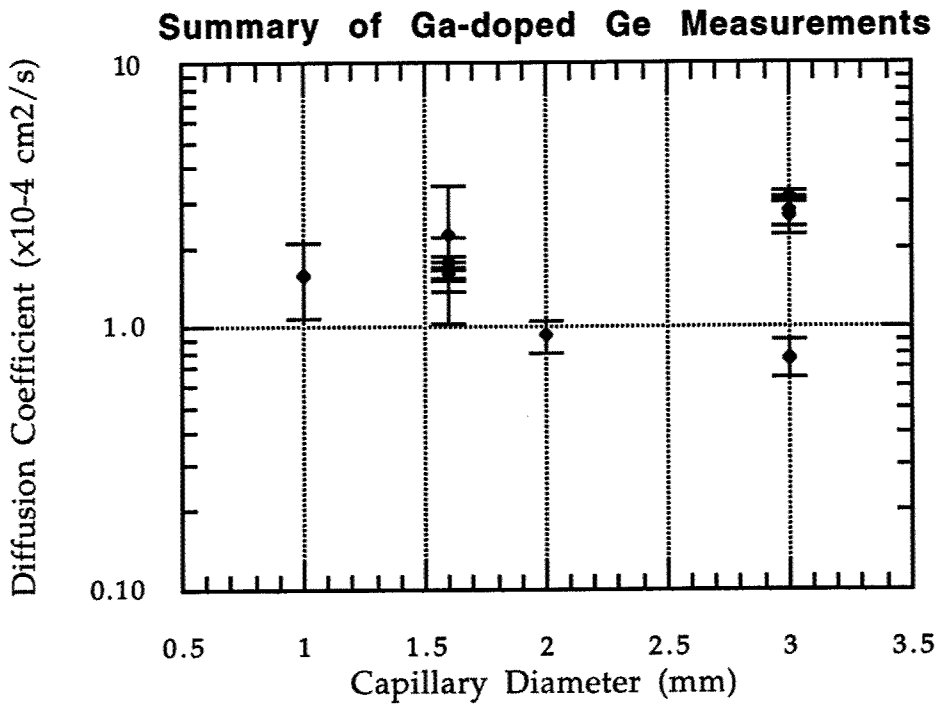


Figure 1. Plot of diffusion coefficients as a function of capillary diameter for Ga-doped Ge.

As can be seen in Fig. 1., the diffusion coefficient does increase as the capillary diameter increases, which is indicative of convection in the column.

## 6. Conclusions

The shear cell technique has been used to successfully measure the diffusion coefficients for Si, Ga and Sb doped germanium. Capillary diameters of 1, 1.6 and 3.0 mm have indicated an increase in the diffusion coefficient with increasing capillary size. This is indicative of convection being present in the diffusion column.

# THE STUDY OF DOPANT SEGREGATION BEHAVIOR DURING THE GROWTH OF GaAs IN MICROGRAVITY

Professor David H. Matthiesen
420 White Building
Case Western Reserve University
10900 Euclid Avenue
Cleveland, OH 44106
(216) 368-1336
dhm5@po.cwru.edu

## 1. Description of Experiment

The original proposal for the study of dopant segregation behavior during the growth of gallium arsenide (GaAs) in microgravity was a program to investigate techniques for obtaining complete axial and radial dopant uniformity during crystal growth of selenium doped gallium arsenide (Se/GaAs). The primary goal of the reflight opportunity on the Second United States Microgravity Laboratory (USML-2) was to characterize and, if possible, controllably modify the melt-solid interface shape during the growth of Se/GaAs to achieve uniform radial segregation of the dopant. The reduced effective gravitational accelerations in a microgravity environment can reduce or eliminate the driving force for buoyancy driven convection. As the level of convection is reduced, axial segregation approaches that of diffusion controlled growth. An axial segregation profile due to diffusion controlled growth will have a uniform steady state region after an initial transient. Radial segregation during diffusion controlled growth, however, is controlled by the shape of the melt-solid interface. In these experiments, the booster heater and gradient zone configuration of NASA's Crystal Growth Furnace (CGF) were utilized in an attempt to achieve a near planar interface shape in order to minimize radial dopant variation.

Each of the experiments used a Se/GaAs crystal grown using the Liquid Encapsulated Czochralski (LEC) technique. Each crystal was machined to a diameter of 1.5 cm and inserted into a pyrolytic boron nitride (PBN) sleeve. A graphite cup supports the cold end of the crystal. At the hot end of the crystal is a spring composed of a stack of PBN leaf springs inside a graphite spring chamber. This spring expands when the GaAs melts and maintains electrical contact with the melt surface. The expansion of the spring also keeps the melt in contact with the wall of the container and

prevents the formation of a free surface on the melt. This entire assembly is hermetically sealed inside a quartz ampoule. Electrical current is passed through the quartz ampoule using molybdenum feedthroughs. The CGF was modified to include a Current Pulse Interface Demarcation (CPID) system. This allows a current pulse to be sent through the solidifying crystal. Peltier cooling results in the incorporation of a portion of the solute boundary layer. This change in the composition of the solute can be seen as a demarcation line when a slice of the final crystal is viewed in infrared transmission. The demarcation lines show the interface shape and position at known points in time.

## 2. Justification for Microgravity Research

During ground based experimentation, buoyancy driven convection mixes the melt and results in a dopant distribution profile that may be described by the complete mixing theory. During experimentation in microgravity, buoyancy driven convection may be reduced such that diffusion is the dominant driving force for movement of the Se within the liquid GaAs. If this is the case, the Se distribution profile will be that of the diffusion controlled growth theory. Diffusion controlled growth results in a concentration profile with initial and final transients and a long steady state region of constant composition in between the transients. The duration of these experiments is on the order of days. Thus, the microgravity environments available in drop towers and aircraft flying parabolic arcs are insufficient and it is necessary to do these experiments in a space environment.

## 3. Value of Research

The technological aspects of interface control and of transient versus steady state growth are important issues in ground-based processing of GaAs and other semiconductor materials. Experimental programs such as this one are providing an improved understanding of the interactions between process controls, such as furnace temperatures and translation rates, and the growth process, as seen via the observed interface shape and growth rate, on the resulting microstructure and material properties. Improvements in the fundamental understanding of crystal growth, whether gained during ground-based or space-based experiments, can be used to improve terrestrial crystal growth processes. Knowledge gained from this experimental program will also lead to the design of better experiments for future space station programs.

## 4. Ground-based Experimentation

Six crystals of Se/GaAs were successfully grown during ground-based experiments. These crystals have been examined using optical and electrical characterization techniques. The Current Pulse Interface Demarcation (CPID) system that was added to the CGF could be used to successfully mark the interface position in the crystal at a known point in time. This position and time could later be used to calculate the actual growth rate of the crystal. The growth rate of the crystals was equal to the translation rate of the furnace for translation velocities of less than 1.5mm/s. The melt-solid interface position could be moved, relative to the gradient zone of the furnace, but the interface remained concave into the solid at all positions in the furnace. The dopant distribution profiles of these crystals matched the complete mixing theory as expected.

## 5. Flight Experiments

Two Se/GaAs samples (primary and secondary) were processed during the USML-2 mission. The experiments were designed to minimize natural convection by processing in microgravity and to minimize surface tension driven convection through the use of a spring loaded piston designed to prevent the formation of a free surface on the molten gallium arsenide. One piece single crystals were partially melted and regrown in microgravity. The primary sample was processed for 67 hours, 45 minutes and included 19 hours of growth at 0.5 mm/s to grow 3.42 cm and 5 hours of growth at 1.5 mm/s to grow 2.7 cm. During the second experiment, the furnace temperature was adjusted to move the melt-solid interface position towards the hot end of the furnace in order to flatten the interface shape. The second sample was processed for 50 hours, 10 minutes and included 11 hours of growth at 0.5 mm/s to grow 1.98 cm and 1 hour, 25 minutes of growth at 5.0 mm/s to grow 2.6 cm. This sample provides an order of magnitude change in growth rate and reproduces one of the growth rates used during the USML-1 mission. The cartridges containing the samples were x-rayed at Marshall Space Flight Center. The x-rays show that the crystals are in contact with the container along the length of the crystals and no voids were formed in the crystals.

The x-rays were also used to measure the position of the 6 thermocouples that were inside the cartridge during processing. This data is essential to correctly interpret the thermal data. Preliminary data indicate that the thermal profiles that were desired were achieved. The absence of voids in these two samples is a result that differs from the results of USML-1. It is now believed that the voids found in the crystals grown on USML-1 resulted from the use of multipiece initial

samples. The ampoules have been removed from the USML-2 cartridges and no devitrification or gross deformities were observed. The ampoules will be opened in a mass spectrometer to check for any residual gases. The samples will be removed from the ampoules, cut, and polished. Sections of the crystals will be analyzed using an array of characterization methods including electrical, chemical, and optical techniques. Electrical techniques will include Hall effect and capacitance-voltage measurements. Optical measurements will include quantitative infrared microscopy and Fourier transform infrared spectroscopy. The data from these measurements will be compared to current analytical and computer model based theories of crystal growth.

## 6. Corresponding Modeling Effort

Numerical modeling in support of the experimental program was done at the Computational Materials Laboratory at NASA Lewis Research Center. The numerical modeling results were very helpful in predicting the location of the melt-back interface relative to the furnace position for a variety of furnace temperatures. The model also predicts the shape of the interface and was used to determine the best temperature setpoints to optimize the results of the experiments. The model results predicted that the interface shape would remain concave into the solid at all positions in the furnace. This is the result that was seen in the experiments.

## 7. Conclusions

Ground-based experimentation demonstrated that the Current Pulse Interface Demarcation (CPID) system could be used to successfully demark the interface position in the crystal at a known point in time. This position and time could later be used to calculate the actual growth rate of the crystal. The growth rate of the crystals was equal to the translation rate of the furnace for translation velocities of less than 1.5mm/s. The melt-solid interface position could be moved relative to the gradient zone of the furnace, but the interface remained concave into the solid at all positions in the furnace. Numerical modeling also predicts this behavior. Preliminary results from the USML-2 flight indicate that two crystals were grown successfully and that no free surfaces were formed at the surface of the crystals during the growth process. The absence of voids in either sample indicates that growth rate changes alone were not responsible for the formation of the voids seen in the USML-1 samples.

# NUMERICAL AND LABORATORY EXPERIMENTS ON THE INTERACTIVE DYNAMICS OF HELE-SHAW FLOWS AND DIRECTIONAL SOLIDIFICATION

E. Meiburg[1], T. Maxworthy[2], M. Zhang[2], and S. Buddhavarapu[1]
[1]Department of Aerospace Engineering
[2]Departments of Aerospace and Mechanical Engineering
University of Southern California
Los Angeles, CA 90089-1191
Tel: (213) 740-5376 (EM), (213) 740-0481 (TM)
Fax: (213) 740-7774
E-mail: eckart@spock.usc.edu (EM), maxworth@mizar.usc.edu (TM)

## Introduction

Over the last decade, the effect of convective melt motion on the growth of morphological instabilities during crystal growth has been the focus of increased research efforts. While the bulk of investigations to date have addressed questions of linear stability, relatively little attention has been devoted to experiments and numerical simulations, cf. the recent comprehensive reviews provided by Glicksman et al. (1988) and Davis (1990, 1992, 1993). In the absence of flow, morphological changes in the solid-liquid interface are controlled by heat conduction and the diffusion of rejected solute. Fluid flow, either forced or naturally occurring, can dramatically affect these processes by redistributing heat and solute, thereby changing the intrinsic morphological development and, at the same time, produce new morphologies. Both stabilization and destabilization have been observed as a result of convective motion in the melt. In the simplest case, the interfacial stability in an imposed linear temperature gradient is controlled by two dimensionless parameters, a morphological number which represents the ratio of concentration and temperature gradients at the interface, and a surface energy parameter.

Within the present investigation, we are interested in the effect that flow can have on this instability. Traditionally, the goal has been to minimize the flow in order to avoid impurities. However, some recent investigations, for example by Coriell et al. (1984) as well as Forth and Wheeler (1989), predict a stabilization by flow parallel to the interface. When the applied flows are non-parallel, e.g. stagnation point flow, Brattkus and Davis (1988) have found a new flow-induced morphological instability that occurs at long wavelengths and consists of waves propagating against the flow. As far as we are aware, there have been no physical or numerical experiments to investigate such effects.

In the realm of competing instabilities, e.g. the interaction of solute and thermally generated convection and morphological instability, there has been a substantial amount of theoretical work. Under circumstances of interest here, i.e. when the temperature field is known and stabilizing, double-diffusive convection is driven by solute rejection. As the pulling speed increases, the thickness of the solute layer decreases, so that the effective Rayleigh number of the convection decreases, while the morphological instability occurs at smaller values of the morphological number. Davis (1992) as well as Mehrabi and Brown (1992) describe circumstances under which a strong coupling is possible with convection generating an interface shape susceptible to morphological instability.

The present experimental and computational investigation represents an extension of ealier work on directional solidification in thin films in a linear temperature profile without flow

(e.g. Eshelman and Trevedi 1987, Eshelman et al. 1988, Seetharamman et al. 1988, Lee and Brown 1993). The only study we know of with flow is the recent one of Huang et al. (1993), in which flow was induced by a rotating impellor. However, this flow may be hard to control, in addition to being unsteady. We make use of the fact that steady forced flow in such a thin cell obeys the Hele-Shaw equations with a potentially variable viscosity. Furthermore, convection can be minimized by suitable adjustment of the gap width or by tilting the apparatus at an angle to the horizontal. The goal is to develop a more complete understanding of the flow's dynamical interplay with the growing crystal, so that strategies can be developed for how to limit its negative side effects and, if possible, obtain some benefits by artificially imposing a controlled flow field.

## Experimental Investigation

The apparatus being used in this investigation was built over the past 18 months with funds from NASA Grant No. NAG3-1621. It consists of three sub-systems surrounding the test cell. The latter consists of two accurately flat quartz plates, 1/8" thick, 22cm long and 6cm wide, maintained accurately parallel at a spacing of 500μm. A hole pattern is drilled into the top plate, and each hole is connected to a fluid supply/removal tube. The cell is mounted on a translating stage moved by a lead screw and feed-back controlled DC motor (Newport Model 850A-2). The flow system consists of a reservoir to store the material to be solidified, a piston pump, driven by a lead screw-DC motor combination, and a number of valves to manipulate the flow path. Some of the details are given in figure 1a, where the valve settings to produce a stagnation-point flow and a shear-flow, parallel to the interface, are indicated. The heat-transfer sub-system consists of an electrically heated block coupled, thermally, to a water cooled block, by an aluminum strap. A linear temperature profile is maintained in the strap, which is in intimate contact with the test cell. The heat-transfer to the cell is enhanced, allowing a large pulling speed while maintaining the linear profile along the cell. The solidifying interface and the concentration field are imaged through a Leitz Interferometric Microscope, the optical path of which is shown in figure 2, together with some detail of the cell geometry and the heater location. Finally the whole apparatus and support structure are shown in figure 3. The latter allows the accurate movement of the whole system in three mutually perpendicular directions under the fixed microscope. The materials employed are: I) an organic alloy succinonitrile-acetone (SCN-Ac) that is transparent and has been used in numerous studies as a substitute for metallic alloys, since it mimics many of the effects found in the latter. For a full justification, the reader is referred to Jackson and Hunt (1966). II) a dilute NaCl-water system, which is very important from a geophysical point of view. The question of ice formation and morphology in the polar regions is of great interest to a wide range of potential applications. At the time of writing this report a few preliminary tests had been run, mainly to familiarise the operator with the techniques necessary to fill the cell and set the appropriate flow pattern. It is anticipated that experiments under full operating conditions will have begun by June 1996.

## Linear Stability Analysis

Based on the governing equations for directional solidification, as reviewed by Davis (1992), we can perform a linear stability analysis for the case of uniform Hele-Shaw flow parallel to the solid/liquid interface. The analysis is similar in spirit to the original stability investigation by Mullins and Sekerka (1962) for the case without flow, with one additional dimensionless parameter indicating the ratio of fluid velocity to pulling speed. A complex, nonlinear algebraic equation is obtained, which can be solved by a Newton iteration

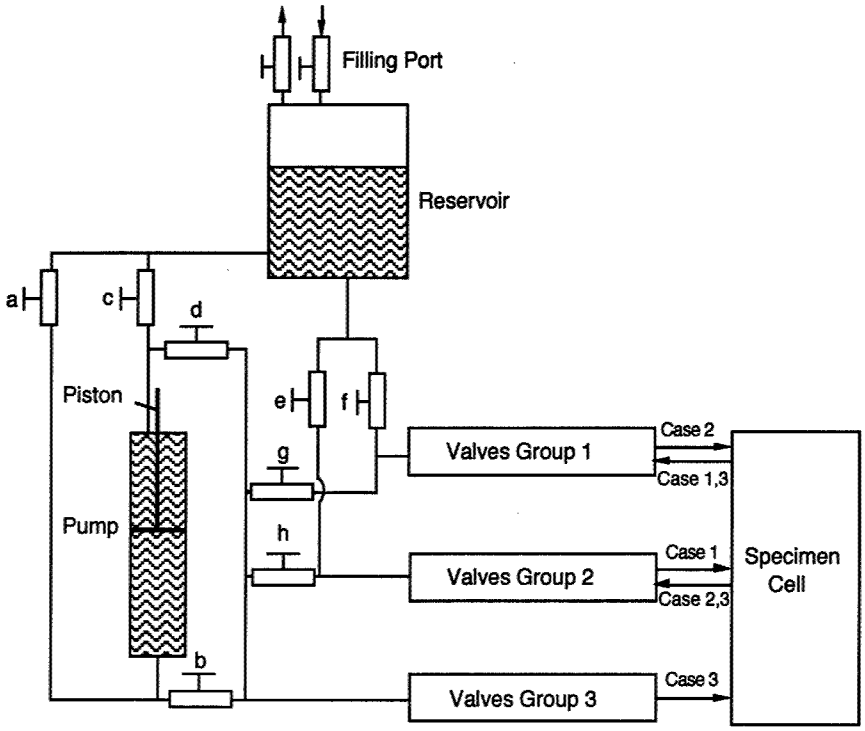


Figure 1a. Schematic Diagram of Flow Control System

Piston Down: a,d OFF; b, c ON
Piston Up: b,c OFF; a, d ON

| | | | |
|---|---|---|---|
| Case 1 | Shear Flow | valves group 3 closed, group 2 in and group 1 out | e,g OFF; f,h ON |
| Case 2 | Shear Flow | valves group 3 closed, group 1 in and group 2 out | f,h OFF; e,g ON |
| Case 3 | Stagnation Point Flow | valves group 3 in, valves group 1 and 2 out | g,h OFF; e,f ON |

Note: " in " and " out " are relative to the specimen cell

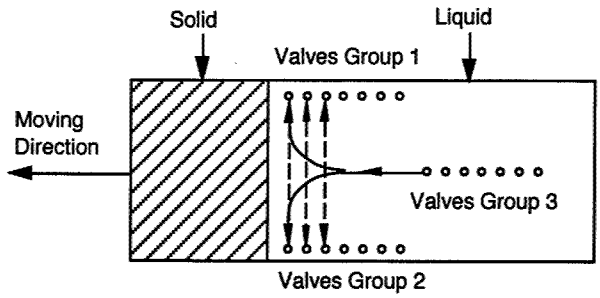


Figure 1b. Top View of Specimen Cell

Solid Lines: Stagnation Point Flow
Dashed Lines: Shear Flow

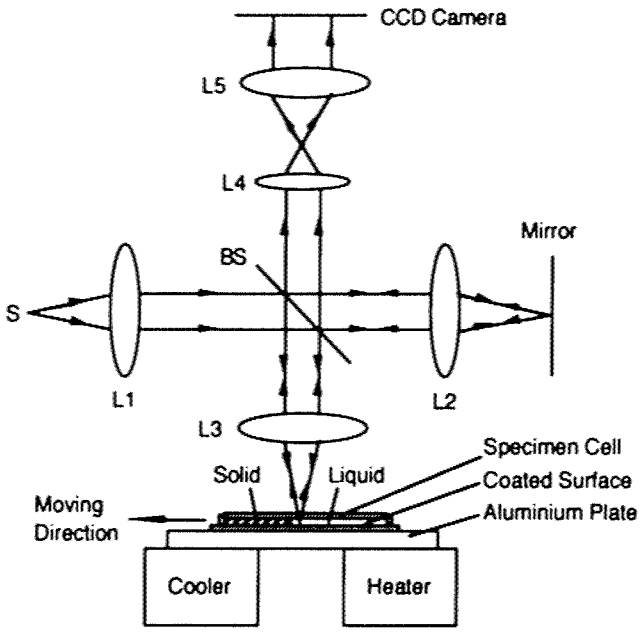


Figure 2. Schematic Diagram of Optical and Solidification Systems

S: Light Source; BS: Beam Spliter; L: Lenses

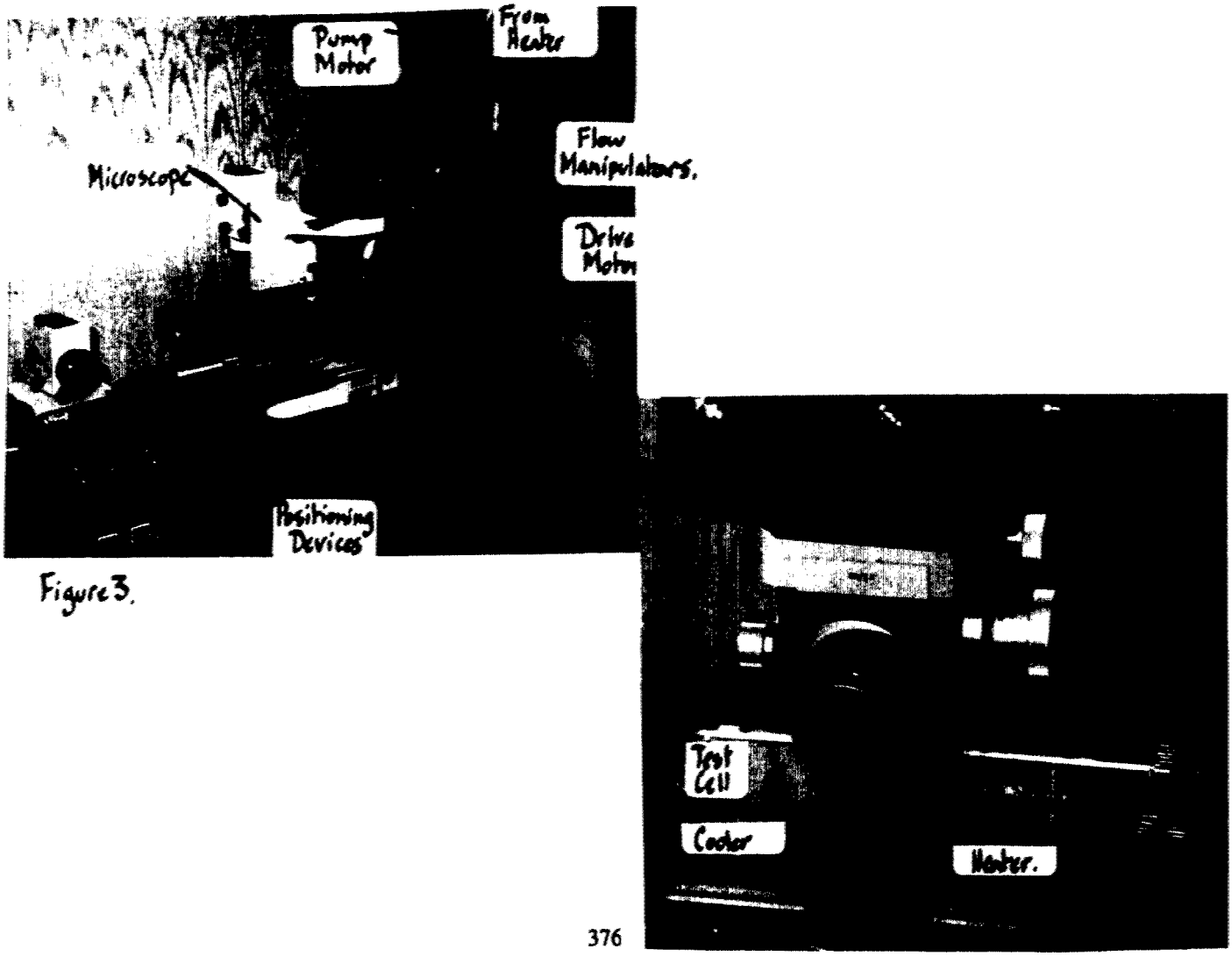


Figure 3.

procedure to yield the instability growth rate as well as the wave propagation velocity. The results show that, in the presence of flow, the instability wave propagates *against* the direction of the melt motion, similarly to the earlier findings for similar flows by Brattkus and Davis (1988) as well as Forth and Wheeler (1989). The growth rate can be increased or decreased as a result of the flow, depending on the wavenumber and the value of the morphological number.

## Computational Investigation

In order to accurately represent the variety of linear and nonlinear mechanisms whose interplay governs the growth of the liquid/solid interface, it is mandatory to employ highly accurate computational procedures. Consequently, we have developed over the last 18 months under NASA Grant No. NAG3-1619 a numerical approach that employs a combination of a Fourier spectral method (Gottlieb and Orszag 1977) in the periodic direction and a high-order compact finite difference method (Lele 1992) in the pulling direction. Away from the boundaries, we employ discrete approximations of central kind and sixth order accuracy, whereas near the boundaries one-sided stencils of third order accuracy are used. These compact finite difference discretizations allow the evaluation of spatial derivatives in the pulling direction with high accuracy as well. The calculation is advanced in time by means of a low-storage third order Runge-Kutta scheme (Wray 1991). This combination, in conjunction with an analytical conformal mapping procedure (Pope 1978), leads to excellent accuracy.

In order to demonstrate the accuracy of our computational approach, and to test the computational code, we have performed test calculations in which the growth of small amplitude perturbations with time is calculated for different values of the governing parameters. In these test calculations, we have typically employed 32 Fourier modes in the spanwise direction, and 32 finite difference gridpoints in the direction of the crystal motion, a rather coarse discretization. The surface energy was set to zero, the Peclet number had values of 1 and 10, respectively. The morphological number was chosen to be 10, and the segregation coefficient had a value of 0.9. We conducted a detailed comparison between the computationally obtained growth rates and the analytical ones given by Mullins and Sekerka. For all wavenumbers tested, the agreement is better than one tenth of one per cent, which reflects the overall accuracy of our computational approach.

While the above tests concern situations without flow, we have, more recently, extended the numerical code to account for forced convection. As a first case, we consider uniform flow parallel to the nominal interface. Preliminary results confirm that this flow results in the migration of the wavy interfacial perturbation against the direction of the flow, in agreement with the stability analysis described above. The wave propagation velocity depends on the strength of the imposed flow. For the few cases considered so far, the instability growth rates do not appear to be strongly affected by the flow.

## References

Brattkus, K. and Davis, S.H. 1988 Flow induced morphological instabilities: Stagnation point flow. J. Cryst. Growth 89, 423.

Coriell, S.R., McFadden, G.B., Boisvert, R.F., and Sekerka, R.F. 1984 The effect of forced Couette flow on coupled convection of morphological instability during directional solidification. J. Cryst. Growth 69, 15.

Davis, S.H. 1990 Hydrodynamic interactions in directional solidification. J. Fluid Mech. 212, 241.

Davis, S.H. 1992 Microscale coupling of solidification and flow. Proc. of the Symp. on Interactive Dynamics of Convection and Solidification. Kluwer Academic Press.
Davis, S.H. 1993 Effects of flow on morphological stability. Handbook of Crystal Growth, vol. 1. Elsevier Science Publishers.
Eshelman, M.A. and Trivedi, R. 1987 The planar to cellular transition during the directional solidification of alloys. Acta Metall. 35, 2443.
Eshelman, M.A., Seetharaman, V., and Trivedi, R. 1988 Cellular spacing I: Steady-state growth. Acta Metall. 36, 1165.
Forth, S.A. and Wheeler, A.A. 1987 Hydrodynamical and morphological stability of the unidirectional solidification of a freezing binary alloy: A simple model. J. Fluid Mech. 202, 339.
Glicksman, M.E., Coriell, S.R., and McFadden, G.B. 1986 Interaction of flows with the crystal-melt interface. Ann. Rev. Fl. Mech. 18, 307.
Gottlieb, D. and Orszag, S.A. 1977 Numerical analysis of spectral methods. SIAM, Philadelphia.
Huang, T., Liu, S., Yang, Y., Lu, D., and Zhou, Y. 1993 Coupling of Couette flow and crystal morphologies in directional freezing. J. Cryst. Growth 128, 167.
Jackson, K.A. and Hunt, J.D. 1966 Trans. Metall. Soc. AIME 236, 1929.
Lee, J.T.C. and Brown, R.A. 1993 Experimental study of the planar to cellular transition during thin-film directional solidification. Phys. Rev. B 47, 4937.
Lele, S.K. 1992 Compact finite difference schemes with spectral-like resolution. J. Comp. Phys. 103, 16.
Mehrabi, R. and Brown, R.A. 1992 Nonlinear analysis of morphological interactions between flow and interface shape in the directional solidification of a binary alloy. Proc. of the Symp. on Interactive Dynamics of Convection and Solidification. Kluwer Academic Press.
Mullins, W.W. and Sekerka, R.F. 1964 Stability of a planar interface during solidification of a dilute binary alloy. J. Appl. Phys. 35, 444.
Pope, S.B. 1978 The calculation of turbulent recirculating flows in general orthogonal coordinates. J. Comp. Phys. 26, 197.
Seetharaman, V., Eshelman, M.A., and Trivedi, R. 1988 Cellular spacings II: Dynamical studies. Acta Metall. 36, 1175.
Wray, A.A. 1991 Minimal storage time-advancement schemes for spectral methods. Preprint.

# SPACE- AND GROUND-BASED CRYSTAL GROWTH USING A MAGNETICALLY COUPLED BAFFLE

Aleksandar G. Ostrogorsky, Rensselaer Polytechnic Institute, Troy, N.Y. 12180,
Tel.: (518)-276-6975; Fax.: (518)-276-6025; e-mail: ostroa.rpi.edu

Thierry Duffar (Co-Investigator), Centre d'Etudes Nucleaires, Grenoble, France;
Tel.: 33-76-88-38-36; Fax: 33-76-88-51-17; e-mail: td@ecrins.ceng.cea.fr

This definition-phase flight research (to be conducted in the period 7/1/96 to 6/30/00) is a follow-up of the ground based research entitled "Crystal Growth and Segregation using the Submerged Heater Method", sponsored by NASA in the period 2/1/93 to 5/31/96 (NAG8-952).

The use of a submerged disk-shaped device to control heat and mass transfer in Vertical Bridgman Configuration was proposed by Ostrogorsky [1]. In experiments carried on since, powered devices, (i.e., "submerged heaters", [1]) and unpowered devices (i.e., baffles, [2-4] were used. The submerged baffle:

- drastically reduces the undesirable natural convection at the solid/liquid interface;
- acts as a partition, separating a small melt zone adjacent to the interface from the large "bulk" melt, (which replenishes the material absorbed at the phase boundary);
- contains thermocouples which permit temperature measurement and control ~1 cm from the solid /liquid interface;
- provides a method for vigorous melt mixing (i.e., homogenization) prior to solidification.

A multi-zone tubular heater controls the radial heat flow and thus the shape of the phase boundary, Fig. 1. In the melt zone adjacent to the interface, the radial temperature gradients are readily reduced to $\partial T/\partial r \sim 0.1$ K/cm, yielding close to purely axial heat flow. The melt is solidified by lowering the crucible. While the crucible is lowered, the large top melt feeds the zone melt. During growth, the temperature of the baffle is held constant at $\approx 10$ K above $T_m$, the melting point of the charge. As a result, the freezing interface is at a small constant distance below the baffle.

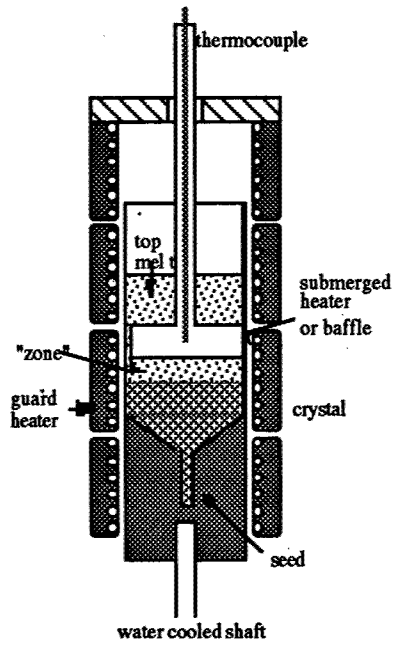


Fig.1 Schematic of vertical Bridgman growth with the submerged baffle.

By using the baffle in Vertical Bridgman melts, we were able to study segregation under conditions of very low convection and effectively simulate several previous space experiments [2, 3]. Our experiments and finite element simulations demonstrate that:

(i) The equilibrium segregation coefficient k is the key parameter influencing convective interference with segregation in space experiments. Solidification of solvent-solute systems with $k \sim 0.5$ (eg. Te-doped InSb) is not affected by significant levels of melt convection. Velocities in the melt of the order of $V \sim 10\ \mu m/s$ will not cause convective interference with segregation (Fig. 2a). In contrast, the having $k \ll 1$ (eg. Sn-doped InSb) are sensitive to very low levels of convection (Fig. 2b). The only difference between the Figs. 2a and 2b is in the value of k, which is one order of magnitude lower for Sn (k=0.06). This explains why all space-grown semiconductor crystals, except Te-doped InSb, provided evidence of convective interference with segregation, and did not approach the ideal steady-state growth.

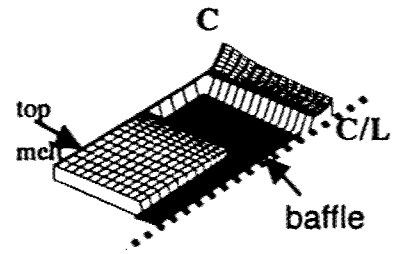

a) Te - doped InSb (k=0.5)

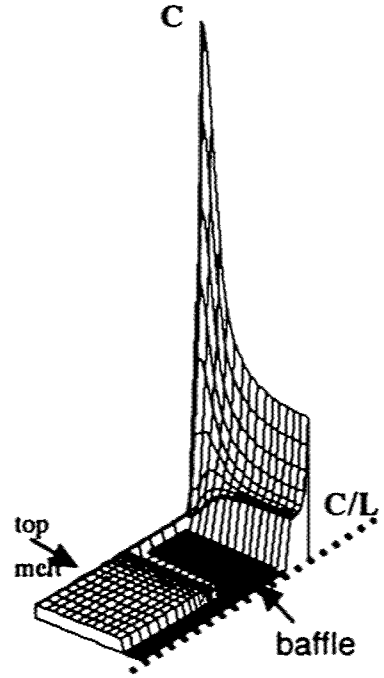

b) Sn - doped InSb(k=0.06)

Fig. 2 Te and Sn concentrations in InSb. $V_S = 3.1\ \mu m/s$ for both dopants. Both dopants are carried (convected) by the same velocity field.

(ii) The solutal Peclet number can not be successfully used to predict whether segregation of a particular solvent-solute system, will be affected by melt convection. Instead, we proposed a new non-dimensional parameter named the Segregation number, obtained by scaling the amount of solute removed from the interface by convection $J_{conv}$ to the amount of solute absorbed in the solid $J_{solid}$, Fig. 3,

$$Se = \frac{J_{conv}}{J_{solid}} \qquad (1)$$

$J_{conv}$ and $J_{solid}$ are determined using the order-of-magnitude analysis [5,6] and substituted in (1), yielding,

$$Se = \frac{V}{V_S^2}\frac{D}{L}\cdot\frac{1-k}{k} \qquad (2)$$

where V is melt velocity, $V_S$ is the growth rat, D is the diffusion coefficient, L is the characteristic length and k is the equilibrium segregation coefficient.

Reduction of Convection in Microgravity Using the Baffle

When the baffle is used for crystal growth in space laboratories, buoyancy driven convection will be extremely low because : (i) gravitational acceleration is reduced and, (ii) because the baffle hinders convection.

Our calculations indicate that indeed significant convection is produced in microgravity if residual acceleration acts normal to ampule axis Therefore, the "horizontal Bridgman" growth, is the limiting case ("worst case scenario") that should be considered in planing and designing space experiments. Our three-dimensional calculations agree well with calculations of Alexander et al. [10] . For example, Figure 4 shows a three-dimensional calculation of the velocity field in the melt with and without the baffle, calculated using FIDAP [11]. Almost identical results (not shown) were obtained by NEKTON [12]. At $10^{-4}$ $g_0$, the maximum velocity in the melt is ~ 14 $\mu$m/s. However if the baffle is used at $10^{-4}$ $g_0$, the velocity in the zone melt drops to 2 $\mu$m/s, a situation equivalent to $10^{-5}$ $g_0$, without the baffle, Fig. 4b. However, if the baffle is used at $\geq 10^{-5}$ $g_0$, maximum melt velocity in the zone melt drops to ~ 0.2 $\mu$m/s, (Fig. 4 b) so that most of the doped semiconductors can be grown under diffusion-controlled conditions [6].

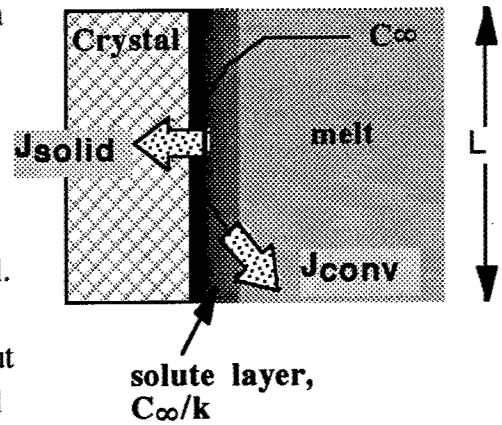


Fig. 3 Segregation number, Se ~ $J_{conv}/J_{solid}$ Diffusion controlled segregation is achieved for $J_{conv} << J_{solid}$) [5,6].

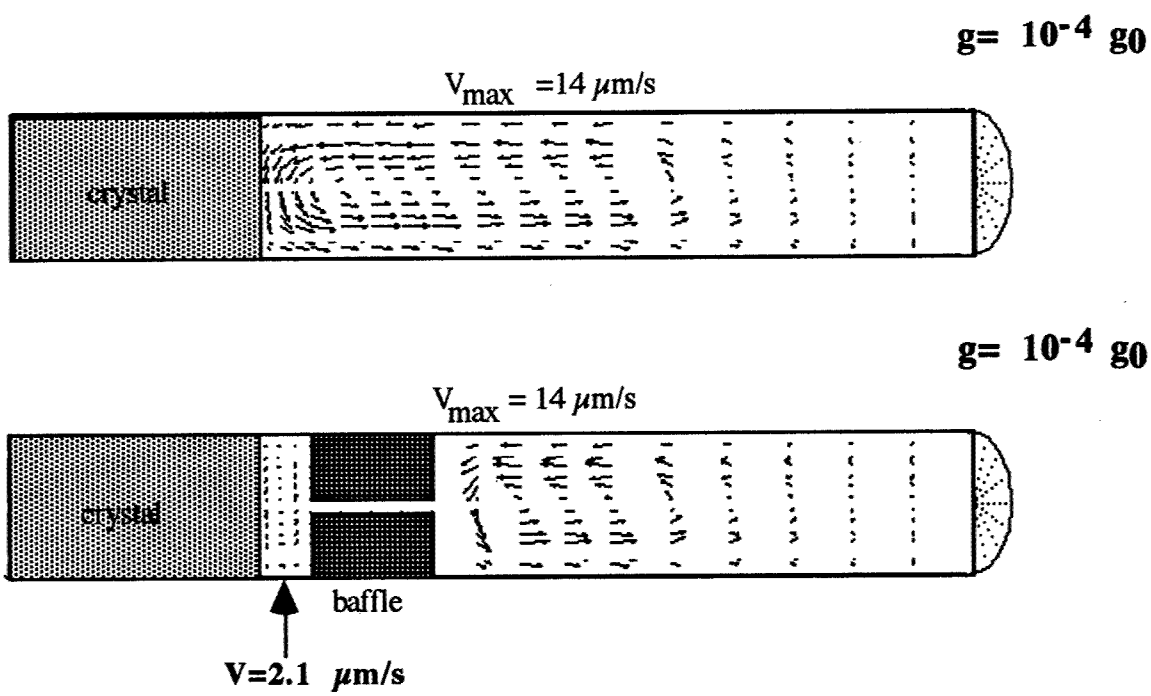


Fig. 4 a) Three-dimensional calculation of the velocity field in the melt with the baffle calculated using FIDAP [11]. The residual acceleration is normal to ampule axis.

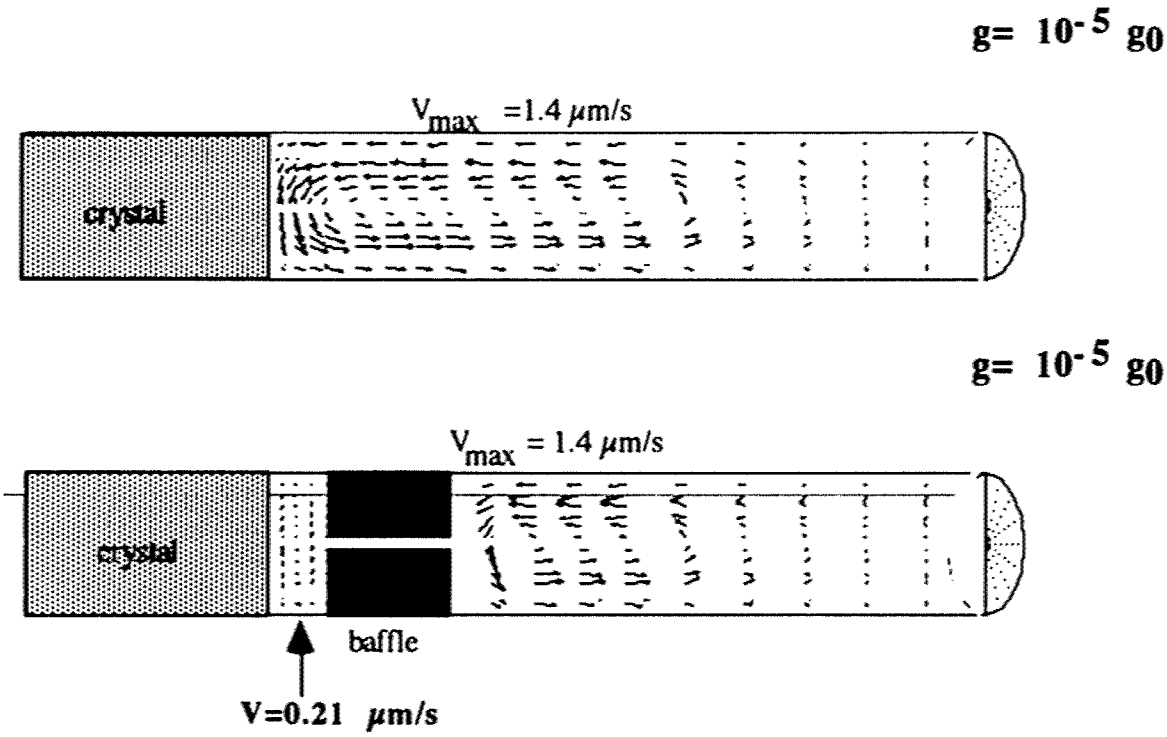


Fig. 4 b) Three-dimensional calculation of the velocity field in the melt with the baffle calculated using FIDAP[11]. The residual acceleration is normal to ampule axis.

The shaft that we currently use to suspend the submerged baffle, and for thermocouple feeds, does not allow growth from sealed ampules. Since growth in sealed ampules is essential for space experiments and may have additional advantages , we will modify our furnaces to set up growth with the baffle suspended by magnetic coupling. The use of magnetic coupling to a high Curie temperature alloy slug sealed within the quartz pulling road, was first reported by Gremmelmeier [13]. A sketch of the preliminary design of the baffle is shown in fig. 5. The baffle with the high Curie point core (eg. Cobalt, which retains good magnetic properties up to 1075) will be used to premix the melt and subsequently used to minimize melt convection. Relative motion will be achieved by translating the ampule (or the magnet). Other options that will be explored are: rotation of the ampule or the magnet.

It is important to note, that in space laboratories, the weight and the buoyancy forces of the baffle are reduced by at least a factor of $10^4$ in space laboratories. Therefore, magnetic coupling should perform particularly well in space. The use of highly conductive metal discs or even heat pipes will be considered in both Bridgman and zone melting configurations. A second silica baffle with a high Curie point core but without a central passage, will be located at the free surface of melt. It will be used to impose a desired level of static pressure (to be determined) on the melt. This will prevent de-wetting and Marangoni convection.

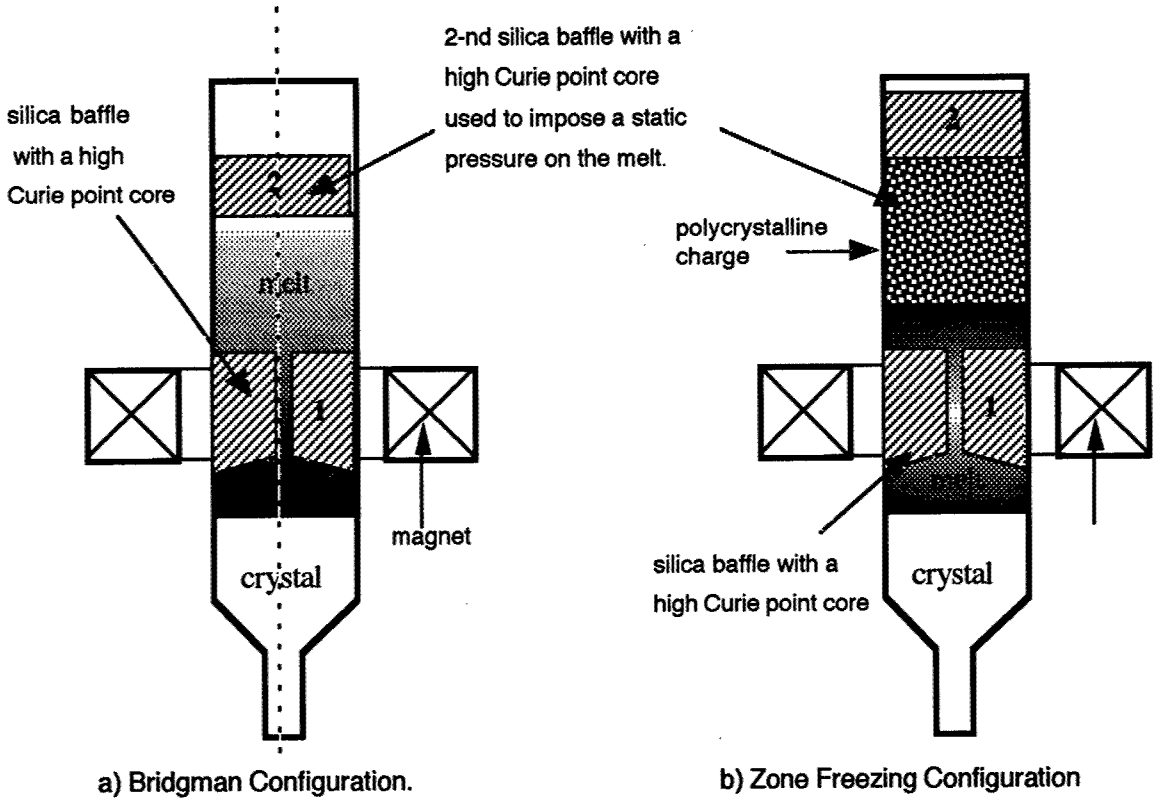


Fig.5 Schematic of the baffle, suspended by magnetic coupling to a high Curie temperature alloy slug.

A sketch of the zone-melting configuration (which is also being considered) is shown in fig. 5b. Again, the baffle with the high Curie point core is used to premix the melt and subsequently used to minimize melt convection. Note that the undesirable high radial temperature gradients typical of zone melting will be minimized, because most of the heat will be transferred (i) radially from the heater to the baffle, (ii) radially through the baffle, and (iii) released axially into the melt.

## Objectives of the Definition-Phase Flight Research

The scientific and technical objectives of the proposed research are:

- to design a *simple and reliable* baffle that can be used to grow the semiconductor crystals *in sealed silica ampules*, in microgravity.
- test the design by growing semiconductor crystals in sealed silica ampules; both *Bridgman growth* and *zone freezing* will be considered;
- to verify that the magnetically coupled baffle provides means for vigorous melt mixing.
- to optimize the temperature field and the growth procedure to minimize convective interference with segregation.

The above objectives will be achieved by conducting ground based experimental studies and three-dimensional finite element simulations of growth, convection and segregation. Furthermore, it is proposed that two ampules with doped GaSb (one with the baffle and one, for comparison, without the baffle) are solidified in microgravity. The goal of these experiments are to verify :

- that the developed method for crystal growth (using magnetically coupled baffle), is less sensitive to residual acceleration in space laboratories then the conventional methods(Bridgman and zone freezing);

- that by using the developed in space laboratories, important semiconductor crystals can be grown under the ideal steady-state conditions, resulting from diffusion controlled solidification;

- that by using the magnetically coupled baffle in space laboratories to (i) premix the melt and (ii) to eliminate convection, semiconductors of exceptional crystalline and chemical perfection can be grown;

- to test the non dimensional parameter named the Segregation number, Se which can be used to select dopants and growth parameters for space experiments.


[1] A.G. Ostrogorsky, J. Crystal Growth 104 (1990) 233.

[2] A.G. Ostrogorsky, H.J. Sell, S.Scharl and G. Müller, J. Crystal Growth 128 (1993) 201 206.

[3] A.G. Ostrogorsky, F. Mosel and M.T. Schmidt, J. Crystal Growth 110 (1991) 950-954.

[4] A.G. Ostrogorsky and G. Müller, J. Crystal Growth 137, (1994) 64-71.

[5] A.G. Ostrogorsky, Z. Dagojlovic, *Transport Phenomena in Solidification*, ASME HTD-Vol.284/AMD-Vol.182, (1994) 255-263

[6] A.G. Ostrogorsky, Z. Dagojlovic, Proceedings of the International Aerospace Congress, Moscow (1994).

[7] A.G. Ostrogorsky and G. Müller, J. Crystal Growth 121 (1992) 587-598.

[8] A.G. Ostrogorsky and G. Müller, J. Crystal Growth 128 (1993)207-212.

[9] G. Müller and A.G. Ostrogorsky, Chapter 13 of the Handbook of Crystal Growth, Vol.2, North-Holland/Elsevier, (1994) p. 708-820.

[10] J.I.D. Alexander and F, Rosenberger, Progres in Astro. and Aeronautics 130, (1990) p.87

[11] FIDAP 7.5 Users Manual, (1994).

[12] NEKTON 2.85 Users Manual, (1994).

[13] R. Gremmelmeier, *Z. Naturforsch. 11a*, (1956) 511.

Gravitational Effects on the Morphology and Kinetics of Photo-Deposition of Polydiacetylene Thin Films from Monomer Solutions

Mark S. Paley, PI

Universities Space Research Association
Huntsville, Alabama

## INTRODUCTION

Polydiacetylenes (see structure below) are a class of highly conjugated organic polymers that are of considerable interest because of their unique chemical, optical, and electronic properties. They have been studied extensively as organic conductors and semi-conductors, as well as nonlinear optical materials. Many of these applications require the formation of high quality thin polydiacetylene films; i.e., films possessing minimal defects such as impurities, inhomogeneities, light scattering centers, etc.

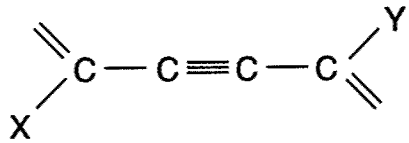


**STRUCTURE OF POLYDIACETYLENE REPEAT UNIT**

We have discovered a novel process for the formation of thin amorphous polydiacetylene films using photodeposition from monomer solutions onto transparent substrates (U.S. patent #5,451,433). Specifically, we have directly synthesized a polymeric film from a diacetylene monomer (DAMNA) derived from 2-methyl-4-nitroaniline (MNA) that only sluggishly polymerizes when the crystalline monomer is irradiated. We have found that thin polydiacetylene (PDAMNA) films can be obtained readily from solutions of DAMNA in 1,2-dichloroethane by irradiation with long wavelength UV light through a quartz or glass window, which serves as the substrate. This simple straightforward process yields transparent films with thicknesses on the order of a micrometer.

Thin PDAMNA films obtained in this manner are glassy, yellow-orange in appearance, suggesting an amorphous nature. Both refractive index measurements and electron-beam diffraction studies indicate that the films are indeed amorphous. When viewed under an optical microscope, PDAMNA films grown by photodeposition exhibit small particles embedded throughout the films. The particles range in size from 0.01 to 1.0 microns. These particles are defects that can

scatter light and thus hinder the usefulness of the film for technological applications. They form when growing polymer chains in the bulk solution collide, coalesce into solid particles, and then precipitate out. Because the particles are small they do not readily sediment out of the solution. Convection, which results from uneven heating of the monomer solution by the UV radiation, then transports the particles to the surface of the growing polydiacetylene film where they can become incorporated into the film. Additionally, there is some evidence to suggest that convection may play a role in affecting the molecular orientation in the films. This is significant because ordered films are preferable, and in some cases, required, for many applications. Thus reducing convection could be an important step in improving the quality of these polydiacetylene films.

The thrust of this work is to investigate the effects of buoyancy-driven convection on the photodeposition of polydiacetylene thin films from solution. Specifically, we are interested in how convection affects transport and incorporation of defects in PDAMNA films grown from solution. Additionally, we are interested in how convection may affect the growth kinetics, and thereby, the morphology, microstructure and properties of the films.

## EFFECTS OF CONVECTION

Special chambers were constructed for carrying out photodeposition of PDAMNA thin films from solution onto small round substrate disks. These chambers are cylindrical in shape, closed at one end, with approximate dimensions of 0.5cm depth and 1.0cm inside diameter. The substrate comprises the other end of the cylinder. To grow thin films onto quartz disks (or any transparent substrate), the chambers are filled with a solution of DAMNA in 1,2-dichloroethane and irradiated through the substrate with long wavelength (365nm) UV light. As the solution is irradiated a photo-polymerization reaction occurs and a thin polydiacetylene (PDAMNA) film is deposited on the inside surface of the substrate. Masking experiments have demonstrated that film deposition occurs only where the substrate is directly irradiated. The thickness of the film is determined by the intensity of the radiation and the duration of exposure.

### Fluid Dynamic Analysis

Both the monomer solution and the film generate heat due to absorption of UV radiation. The radiative heating, along with the thermal boundary conditions of the walls of the thin film growth chamber, will give rise to a complex temperature pattern in the solution. Due to the lack of thermodynamic equilibrium, the solution will possess temperature and concentration gradients, and therefore density gradients. It is well-known that these gradients, under the

influence of gravity, can induce convective fluid flows in the solution (buoyancy-driven convection).

The onset of thermal convection is determined by a stability parameter known as the Rayleigh number, Ra, defined as:

$$Ra = \frac{\alpha g d^3 \Delta T}{\nu \kappa},$$

where $\alpha$ is the coefficient of thermal expansion of the solution, g is the acceleration due to gravity, $\Delta T$ is the temperature difference across distance, d, in the solution, $\nu$ is the kinematic viscosity, and $\kappa$ is the thermal diffusivity. For photodeposition of PDAMNA films, the value of $\Delta T$ (over a distance of less than 1 mm) can vary from a only a few tenths of a degree to several degrees, depending on the intensity of the UV radiation. In order to grow thicker films (> 1 micron), higher intensity radiation is necessary, making large temperature gradients unavoidable. The intensity and flow pattern of convection can be predicted when the Rayleigh number is known. For instance, for an infinite fluid layer in the horizontal direction with a temperature gradient in the vertical direction (co-linear with gravity), convective motion will occur in the form of rolls with axes aligned horizontal when Ra > 1708 (the critical Rayleigh number), while no convection will occur if Ra < 1708. The exact value can only be determined by numerical solution of the fluid flow in the chamber. In the case of horizontal temperature gradients (orthogonal to gravity), all values of the Rayleigh number lead to convection, and the magnitude of the velocity of the fluid flow is proportional to the square root of the Rayleigh number.

Density gradients can also arise in the solution due to variations in the concentrations of the chemical species in the solution. Such solutal gradients, along with the temperature gradients, can give rise to double-diffusive convection. This complicated convective motion is usually analyzed with the aid of the solutal Rayleigh number, in addition to the thermal Rayleigh number. The solutal Rayleigh number, $Ra_s$, is defined as:

$$Ra_s = \frac{\beta g d^3 \Delta C}{\nu D},$$

where $\beta$ is the coefficent of concentration expansion, $\Delta C$ is the concentration difference across distance, d, in the solution, and D is the diffusion coefficient. Double-diffusive convection flows can be far more complex than simple thermal convection flows. Fortunately, in our case, the solutions are very dilute and exhibit very little volume change with concentration, so $\beta$ is quite small. Thus solutal convection may only be a minor contributor to the fluid flow.

Hence we see that convection can arise by several means during polydiacetylene film photodeposition from solution. Also, it is apparent from this discussion that there is no configuration of the growth chamber that will completely eliminate convection in 1-g. The extent of convection, and its intensity and structure can only be understood through accurate numerical modeling of the fluid motion and thermodynamic state of the system.

Transport of Particles from Bulk Solution

To study the effects of convection on the incorporation of particles into the films, the growth chamber was placed in different orientations with respect to gravity in order to vary the fluid flow pattern. PDAMNA films were grown both with the chamber vertical (irradiating from the top) and with the chamber horizontal (irradiating from the side). In the case when the chamber is vertical and the solution is irradiated from the top, the axial temperature gradient is vertical with respect to gravity, and the bulk solution is stably stratified because warmer, less dense solution is above cooler, more dense solution. Thus in this orientation convection should be minimal. In the case when the chamber is horizontal and the solution is irradiated from the side, the axial temperature gradient is horizontal with respect to gravity, which makes the density gradients less stable. Hence convection should be much more pronounced in this orientation. Preliminary numerical simulations of the fluid flows support these expectations.

The distribution of solid particles observed in the PDAMNA films grown in the two different orientations is consistent with the above analysis. Films grown with the chamber horizontal clearly contain a greater concentration of particles than films grown with the chamber vertical. In other words, films grown under increased convection contain more particles than those grown under less convection. Waveguiding experiments with these films demonstrate that the films containing more particles exhibit greater light scattering than those containing fewer particles. However, even the film grown in the vertical orientation, where convection is minimized, still contains some particles. This suggests that while convection is lessened in this case, it is not eliminated. Hence even under optimum conditions in 1-g, some convection may still be present during polydiacetylene thin film photodeposition from solution, resulting in particles in the films.

We recently conducted an experiment aboard the Space Shuttle Endeavor (CONCAP-IV) in which photodeposition of PDAMNA films from solution was carried out in microgravity. In this environment buoyancy-driven convection can essentially be eliminated. Because of unplanned orbiter maneuvers during the mission, leading to extraneous accelerations, and limitations of the flight hardware, results varied somewhat among samples. However, the best space-grown film

clearly exhibits fewer particles than the best ground-based films. These few particles may have resulted from slight mixing in the solution caused by the orbiter motions, or possibly, they may have nucleated on the surface the film itself. Nonetheless, the initial results are very encouraging; it appears that the lack of convection can indeed lead to PDAMNA films with significantly fewer defects, and thus greater optical quality. Further characterizations of the space-grown films are currently underway.

Effects on Kinetics, Morphology, and Microstructure

Once the convective patterns that develop during photodeposition of polydiacetylene thin films are reasonably well understood, the next question is how does this convection affect the dynamics of film deposition and the nature and properties of the films obtained. We have already discussed how convection can transport particles of solid polymer precipitated from the bulk solution into the films. However, convection can also affect film deposition at the molecular level. To gain some insight into these effects, it is necessary to understand the kinetics of film deposition.

The rate of polydiacetylene film photodeposition from solution can be given by the expression:

$$\frac{dl}{dt} = k I^m C^n,$$

where l is film thickness, t is time, I is the intensity of the UV radiation, C is monomer concentration, m and n are the orders of the reaction in radiation intensity and monomer concentration, respectively, and k is the rate constant. Initial results obtained in our laboratory indicate that, for photodeposition of PDAMNA films from 1,2-dichloroethane at ambient temperature (25°C), m = 1.0, n= 0.5, and $k = 3.2 \times 10^{-7}$ (mks units).

Additionally, it can be shown from the principles of chemical kinetics (Arrhenius equation) that the rate constant (k) is given by:

$$k = A e^{-E/k_b T},$$

where E is the activation energy of the reaction, $k_b$ is Boltzman's constant, T is temperature, and A is a pre-exponential factor related to the frequency of collisions of molecules with the surface of the growing film.

The equations above clearly show how the rate of polydiacetylene film photodeposition from solution depends on variables such as temperature and monomer concentration. The effects of convection can also be gleaned from these

equations. We know that convection affects heat and mass transport to and from the surface of the growing film, which is reflected in the temperture and concentration profiles along the surface. Variations in these parameters along the surface of the film, in accordance with the above equations, will cause variations in the rate of film deposition, leading to uneven film growth. This will be especially pronounced if the fluid flow along the surface varies drastically, or is turbulent. Thus we see how convection can directly affect the kinetics of polydiacetylene film photodeposition from solution, and thereby affect the morphology (thickness and surface roughness) of the films.

Lastly, convection could also play a role in affecting the microstructure of the films, specifically, the molecular orientation of the polydiacetylene chains. Preliminary studies we have conducted using atomic force microscopy and X-ray photo-electron spectroscopy indicate that films photodeposited onto quartz (in 1-g) for very short durations of time (a few minutes) appear to have their polymer chains aligned, while films grown for longer durations show a random arrangement of the chains. Thus in the early stages of deposition there appears to be some tendency for polymer chain orientation, which becomes lost as the reaction proceeds and the chains grow. This may be a result of convection. The turbulent and chaotic molecular motions that occur during convection can cause the chains to become entangled and matted around each other as they grow longer. Also, variations in temperature and monomer concentration along the film surface, affected by convection, can influence molecular orientation, and possibly even polymer chain packing densities. Of course this is somewhat speculative at present; however, discerning the role that convection plays in affecting molecular orientation is an essential part of any fundamental study of polydiacetylene film photodeposition from solution.

# INVESTIGATION OF CONVECTIVE EFFECTS IN CRYSTAL GROWTH BY PHYSICAL VAPOR TRANSPORT

Witold Palosz
Universities Space Research Association
NASA, Marshall Space Flight Center, ES75
Huntsville, AL 35812
ph. (205) 544-1272
e-mail palosz@ssl.msfc.nasa.gov

## 1. General objectives of the investigation

Development of a Physical Vapor Transport (PVT) growth system and selection of optimum experimental conditions suitable for a conclusive and meaningful assessment of convection and its effect on the quality of the grown crystals:

- determination of the dependence of convective effects on fluid dynamic parameters;
- evaluation of the effects of concentration gradient(s) on the c-v interface stability and related morphology of the crystals with respect to convective flow;
- assessment of practical limitations of the effects of convection on uniformity and interfacial stability of the growing crystals.

## 2. Relevance to microgravity

Growth of crystals in the absence of convection:

- effect of gravity-dependent convection on growth and quality of crystals in PVT system(s).

## 3. Significance

Advanced investigation of convective effects:

- assessment of convection independent of the crystal morphology;
- advanced numerical simulations of fluid dynamics phenomena in crystal growth systems;

- improved match between the experimental system and the fluid dynamics model used for numerical simulations.

## 4. Technical approach

### *4.1 Tasks.*

To achieve the objectives of the research, the following tasks will be performed:

- investigation of the dependence of the c-v interface shape on the geometry, temperature field, and thermal properties of the materials in the growth systems;
- investigation of the conditions required for growing different crystals under the same thermal field and system geometry and with the same growth rate, but under different fluid dynamics conditions;
- development of a thermochemical model of PVT of (Pb, Sn)Te in a closed system;
- experimental studies on transport of (Pb, Sn)Te by PVT in a closed system;
- studies on transport of selected dopants during physical vapor transport of (Cd, Zn)Te and (Pb, Sn)Te in closed ampoules.

### *4.2 C-v interface shape.*

In typical PVT systems where the total pressure is low (below 100 Torr), a convective flow may lead to only a small increase in the mass transport rate and the presence of convection may require quite subtle methods of assessment. The problem is particularly difficult for high temperature processes to be conducted in space: currently available flight furnaces suitable for crystal growth at such temperatures limit the maximum diameter of the ampoules to less than 20 - 25 mm. Effect of gravity on convection in such ampoules at lower pressures may be low. One of the resulting technical problems is the identification of the effects related to (gravitational) convection, as opposed to those dependent on factors like the geometry of the ampoule and the solid-vapor interfaces, or the thermal field alone. For example, a conical-cylindrical geometry of the gaseous space might possibly lead to a formation of vortices caused by a change in the mass flow velocity with change in the ampoule cross-section area. Non-planar, particularly faceted c-v interface may lead to local flow patterns that change with change in the c-v interface shape and have a variable, unpredictable and non-reproducible effect(s) on the growth conditions and the quality of the growing crystals. Such effects overlap with convective contributions to the flow and may make a meaningful and conclusive analysis of the results practically impossible. In addition, a comparison with the results of a relatively simple numerical modeling (i.e. the one that is feasible at this time) would be of little, if any, use. For

the above reasons it is important that the growth system used to assess gravitational effects has a simple cylindrical geometry of the gaseous space, particularly in the growth region. The crystal-vapor interface should be flat and remain such throughout the growth experiment with all the main growth parameters (temperature of the source and crystal, temperature field in the gas phase and at the c-v interface) remaining essentially unchanged. The shape of the c-v interface depends, under mass transport limited conditions, primarily on the temperature field at the interface and is strongly dependent on the differences in thermal properties of the growing crystal and the growth capsule. In this project, we will investigate the conditions necessary to maintain a flat c-v interface for a period required to grow a crystal of the length suitable for a meaningful evaluation of convective contribution(s) to the growth process (a few mm). Silica glass ampoules, most suited for crystal growth of electronic materials at high temperatures, will be used in the investigation. To enhance convective effects, experiments will be performed in ampoules of a maximum diameter possible in flight experiments (about 20 mm). The effects of: (i) the ampoule wall thickness and shape, (ii) crystal pedestal size and material (silica, sapphire, $BaF_2$), (iii) heat sink at the growth end, (iv) the furnace temperature profile, (v) (vacuum) envelope around the ampoule, (vi) the length of the crystal, (vii) the growth rate, and other growth conditions will be investigated. Application of a tubular shield made of polymeric carbon and used as a thermal insulator (reflector) to reduce radial gradients in the crystal will be tested.

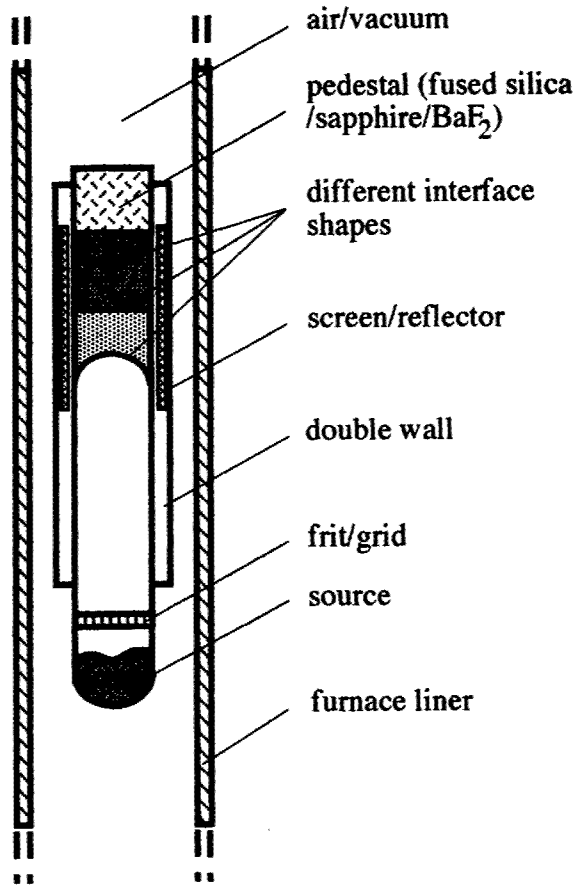


Fig.1 Schematic graph of the ampoule-furnace configuration

*4.3 Different fluid dynamic conditions*

The second main feature of the test growth system that is the target goal of this research is to grow different samples under the same conditions except for those important for gravitational

convection. In addition, for the sake of the most direct conclusions, we envision such comparison in the future under microgravity conditions. It is known that gravitational convection is dependent on the Grashof number, $Gr = \beta g d^3 \Delta T \rho^2/\eta^2$ ($\beta$ - thermal expansion coefficient, g - acceleration, d - the system specific dimension, $\Delta T$ - undercooling, $\rho$ - density, $\eta$ - viscosity). For a given source material and its temperature, constant acceleration level, and fixed undercooling, convective contribution to the growth process can be affected (and investigated) by a change in the system diameter and/or a change in the ambient (or excess) pressure ($Gr \propto \rho^2 \propto P^2$). Change in the total pressure has only little effect on the thermal field in the ampoule but it changes the mass transport rate (crystal growth) and may affect the growth process by a change in the rate of the latent heat release and possible effects on the growth kinetics. In the proposed research, the growth rate and related phenomena will be maintained constant under different total pressure conditions by an appropriate modification of the ampoule geometry. The modification, a constraint in the form of a system of capillaries or a frit/grid, will be made in the source region of the ampoule (Fig. 1) such as to minimize its effect on the growth conditions at the c-v interface. It will also assure a simple cylindrical geometry in the source region making the system more compatible with the model used for our numerical simulations.

### *4.4 Source materials*

The proposed investigation of convective effects by a change in the total pressure requires a system which: (i) has a sufficiently high growth rate even at excess pressures exceeding the minimum pressure of the constituent components, (ii) the source material has a nearly congruent sublimation composition, and (iii) the amount of residuals from the source and the ampoule material is very low and allows for a significant difference in the total pressure between the related (i.e. with and without intentional excess pressure) experiments. Cadmium telluride can meet these requirements. Lead telluride is expected to be a suitable material too; systematic studies on the mass transport of PbTe and its dependence on the pretreatment procedures is a part of this investigation. The materials are also suitable with respect to our goal of achieving a flat c-v interface: the shape of the c-v interface is strongly dependent on the thermal properties of the deposited material, particularly with respect to those of the growth capsule. Cadmium telluride has a thermal conductivity lower than that of fused silica (the ampoule material) at the growth temperature. As a result, crystals of (Cd, Zn)Te have a tendency to assume a concave shape of its free surface during growth. On the other hand, lead telluride has a thermal conductivity higher than that of fused silica and tends to assume the opposite, convex shape of the c-v interface. Experimenting with both materials will provide a flexibility with selection of optimum conditions for growth of crystals with a flat c-v interface.

To detect convective effects in our growth systems, we will be using doped and/or ternary source materials. As the third constituent element we will be using Zn ($Cd_{1-X}Zn_XTe$) and Sn ($Pb_{1-X}Sn_XTe$). The selection of dopants will be based on their thermochemical properties (volatility of respective tellurides) and an absence, or a relatively low content of the dopant element in the original (undoped) source material.

### *4.5 Mass transport of (Pb, Sn)Te by PVT*

A theoretical model of the mass transport in the (Pb, Sn)Te PVT system will be developed using a one-dimensional approximation. The results of this thermochemical analysis will be used to predict conditions for a steady-state (particularly with respect to crystal composition) growth of (Pb, Sn)Te crystals. After experimental verification, the parameters for steady-state transport of lead-tin telluride will be incorporated into our model of fluid dynamics simulations of this growth system. The procedures of the material synthesis, purification, and refinement will be established to assure high purity and stoichiometry of the material as necessary for the purpose of this investigation.

### *4.6 Crystal characterization*

For composition profiling/mapping, usefulness of several different techniques will be evaluated: (1) energy dispersive spectroscopy (EDS), (2) wavelength dispersive spectroscopy (WDS), (3) Fourier transform infrared spectroscopy (FTIR), (4) photoluminescence (PL) and spatial resolve photoluminescence measurements (SRPL), (5) secondary ion mass spectroscopy (SIMS), (6) electron spectroscopy for elemental analysis (ESCA), and (7) time dependent charge measurements (TDCM) techniques.

As the primary objective of the composition mapping is to determine the symmetry of the dopant/constituent elements in the crystal, the absolute accuracy of the measurements or the absolute concentration of the tracer elements are of a lesser importance. Also, no arbitrary dopant(s) has to be used for that purpose. That will allow for a significant flexibility in the selection of dopant(s) for that purpose. The techniques to be tested allow for mapping the distribution of both lighter and heavier dopants, both at lower and higher concentration levels. The dopant(s) and related profiling (mapping) techniques found to be most suited for this research (good reproducibility and precision) will be selected for the final crystal growth experiments on fluid dynamics effects in our test growth systems.

The experimental results on the distribution of dopant(s) and/or constituent elements in the grown crystals will be combined with crystal characterization in terms of morphology and crystallographic perfection. Spatial correlation between these two groups of crystal characterization results, i.e. composition mapping and crystal quality, will be used to differentiate between gravity-dependent and gravity-independent phenomena.

### *4.7 Computational fluid dynamics simulations*

Numerical modeling of crystal growth in a multicomponent PVT system will be based on solving 3-dimensional equations governing heat and mass transfer in the growth ampoule and its surroundings. The full Navier-Stokes equations will be solved with second order in time, and third order in space control volume formulations. Extensive parametric studies will be performed to evaluate the effect of the furnace temperature profile, ampoule geometry, properties of the materials, and other factors on the process and to optimize the volume of the experimental effort.

## 5. Investigation plan

The research will start with numerical modeling of the thermal and flow fields in the ampoule. Fluid dynamics parametric studies will be performed to predict optimum conditions required to grow crystals with a flat c-v interface. The results will be used to select/fabricate a furnace for subsequent growth experiments. At the same time a basic thermochemical and experimental study of the PbTe-SnTe PVT system will be conducted. The fluid dynamics studies will be followed by appropriate experiments to verify and modify (if necessary) the theoretical predictions. Based on the results of the above investigations, a selection of the growth conditions and related ampoule geometry for experiments on convective effects will be made. The growth experiments will be performed and will include tests with appropriate angular and radial displacement of the ampoule in order to identify and quantify the thermal field asymmetry and its effect on the growth process. The grown crystals will be characterized in terms of a distribution of the minority constituents and/or dopants, and of the morphology of the surface and bulk of the material. The (radial) distribution of the components in the crystal and their dependence on the pressure in the ampoule will be used to assess the presence and origin of convection in the system. The results of the investigation will be used to design a corresponding set of experiments to be performed under microgravity conditions.

# ANALYSIS OF CONTAINERLESS PROCESSING AND SOLIDIFICATION MICROSTRUCTURES

J.H. Perepezko, University of Wisconsin-Madison, 1509 University Avenue, Madison, WI 53706
phone: (608) 263-1678; e-mail: perepezk@nucleus.msae.wisc.edu

## Objective and Application to Microgravity Knowledge Base

The main research objective is the evaluation and analysis of the undercooling and resultant solidification microstructures in containerless processing, including drop tube processing and levitation melt processing of selected alloys. The results are intended for use as an experience base for the design of space-based microgravity experiments.

Containerless processing in ground-based drop tubes may simulate the microgravity conditions via solidification of liquid droplets under free fall conditions. The containerless solidification processing of materials in space requires an understanding of the critical variables affecting solidification. Perhaps the most fundamental parameter in solidification processing is the level of melt undercooling prior to solidification. The containerless environment removes a major source of impurities and heterogeneous nucleation sites, allowing for a large melt undercooling. This enhanced liquid undercooling exposes alternate solidification pathways, allowing for the formation of novel microstructures. Controlling the undercooling level provides some control of the operative solidification pathway and the resultant microstructure. The novel structures that may be produced in a ground-based containerless processing facility preview the wide range of possible materials processing experiments that may be conducted in a space-based laboratory. The results of the ground based drop tube study will be used to identify critical experimental variables in microgravity processing, and the analysis may be used to design and predict the science requirements for space experiments.

## Research Task Description and Progress to Date

The proposed program represents a balanced experimental and analysis effort directed toward the investigation of drop tube and levitation containerless processing methods in ground based studies. The investigation will focus on the understanding and analysis of microstructural evolution during solidification of undercooled melts. The degree of liquid undercooling attainable in a laboratory scale (3 m) drop tube and levitation melting system can be altered through the variation of processing parameters such as alloy composition, melt superheat, sample size and gas environment. The solidification behavior will be evaluated through metallography, thermal analysis and x-ray diffraction in conjunction with calorimetric measurements of falling droplets and a heat flow model of the processing conditions to judge the sample thermal history.

The analysis of microstructural development requires an analysis of kinetic competition between the possible phases and structure morphologies. The classification of these kinetic transitions has been discussed previously [1-3]. Some examples include the transition from growth- to nucleation-controlled microstructure development in laser-processed Al-Si alloys [4] and the formation of the metastable, ferromagnetic $\tau$ phase in the Mn-Al system during drop tube processing [5-7].

One of the main components of the proposed investigation will focus on new directions for the control of microstructural evolution in Ni-V, Co-Al, and related alloy systems through the high undercooling levels provided by containerless processing. Solidification processing of eutectic alloys at high rates and large undercoolings has yielded varying degrees of solute trapping; but with very high undercooling only one of the solid phases typically forms partitionlessly. In contrast to this usual observation, high undercooling solidification of Ni-V alloys over a range of compositions has yielded a duplex partitionless structure of fcc and bcc phases [8,9]. Because of the short solidification time available and the vastly different nucleation and growth rates which may be expected for the two different phases over a range of compositions, it is difficult to comprehend how this structure may develop at all. Therefore the analysis of a duplex partitionless structure can reveal new fundamental information about the nucleation and growth

kinetics of competing phases and contribute to an understanding of this novel microstructural class. The development of a heterogeneous nucleation kinetics model for rapidly quenched large (mm size) droplet samples agrees well with the experimental results [9]. The model is currently undergoing further refinement to include transient effects as well as the influence of heat flow on microstructural development. The nucleation kinetics model developed for laser processed Al-Si alloys [4] has provided the basis for the current analysis. Cross-sectional TEM analysis of the containerlessly processed foil samples are underway to further characterize the phase selection behavior.

Collaboration with Dr. Dieter Herlach at the Institut für Raumsimulation in Köln, Germany has also revealed information on the phase selection in bulk undercooled Ni-V alloys during containerless processing [10]. A transition from stable fcc phase to metastable bcc phase was observed for near-eutectic compositions with increasing undercooling. A nucleation kinetics model suggested a specific range of catalytic potency necessary to support duplex reaction.

Analysis of phase selection in the Co-Al system extends the foundation of results of the Ni-V system to show the generality of the kinetics analysis approach. High undercooling solidification of Co-Al alloys has also yielded a duplex partitionless structure of fcc and B2 (ordered bcc) phases. Phase selection will be studied in both large (mm size) and small (μm size) droplets. The nucleation kinetics for the competing fcc and B2 fcc phases will be analyzed to determine the conditions needed to produce the structure. Moreover, the analysis approach will be developed further to allow for the construction of a processing map that will be essential in the design of a space experiment. This investigation will contribute to the understanding of terrestrial solidification processing and will demonstrate that microgravity materials processing can yield novel microstructures and phases that have not been observed previously with conventional terrestrial processing approaches.

Another central component of the proposed program addresses the use of containerless processing together with an undercooled melt and incorporated particles to develop a critical evaluation of solidification front-particle interactions. Numerous models for the interaction

behavior have been proposed, but critical tests are lacking in many cases due to confounding gravitational effects. A common concept in the interaction models is the critical velocity for particle incorporation. The research plan includes a novel experimental design based upon an undercooled melt with particles to distinguish particle incorporation effectiveness as a function of interface velocity in the presence of a distribution of particle sizes. The experimental strategy will allow for an assessment of various models and governing conditions that have been proposed for particle incorporation.

Model systems of nickel with discontinuous reinforcement particles of aluminum oxide or titanium carbide are being studied with containerless processing to isolate effects caused by the forces of gravity and of the containing crucible. Initial experiments have resulted in undercoolings of 20-30 K for Ni/TiC, with apparent uniform particle incorporation into the melt. Microstructural analysis shows a transition zone from higher to lower particle density around shrinkage cavities or edges of the sample (i.e., near the point of final solidification of the sample). These results appear to demonstrate the transition from particle incorporation to particle pushing, perhaps caused by a decrease of solidification front velocity. Results also suggest a critical velocity below which particle engulfment is unfavorable. Evaluation of the microstructure and the time required to complete solidification provides estimates of this critical velocity. Further study has identified the copper-aluminum oxide system; the aluminum oxide particles do not appear to act as potent nucleant sites for copper, thus allowing for undercooling to be used effectively as a tool for controlling the rate of solidification.

Reliable evaluation of thermal history during containerless processing is central to the proper interpretation of a solidification microstructure. In the intended studies thermal measurement of a falling droplet will be conducted using a calorimetric method. With a given level of superheat, the heat content of a droplet will be determined at the time of impact with the calorimeter by means of a simple heat balance. The method has been successfully implemented with pure tin droplets and will be used to analyze alloy droplets in future work.

Experimental results in the metastable yield analysis of powders have defined three critical parameters in the alteration of solidification pathway development: melt superheat, processing environment, and particle size. By using particle size as a reference, the relative effect of other process parameters can be calculated and experimentally verified. In particular, the relative effect of the processing environment on metastable yields can be isolated to three factors: nucleant type, gas conductivity, and nucleant density. Statistical analysis of metastable yield in the droplet population as a function of processing conditions will provide a basis for greater control of solidification structure. These results will then be considered in the nucleation and growth kinetics analysis for metastable phase formation.

As a further aid, droplet solidification microstructures will be used to establish the relationship between microstructural scale and level of undercooling as an in situ probe for sample thermal history. A microstructural probe provides an effective evaluation technique to correlate microstructure to direct or non-contact temperature measurements; this correlation may then be applied to situations for which experimental temperature measurement is difficult, such as a small droplet in flight. Moreover, the in situ probe concept allows for the systematic analysis of disturbances such as external positioning fields on solidification behavior during the containerless processing of materials in space. The experimental determination of undercooling level through non-contact temperature measurement in the investigation will provide a test of the solidification and heat flow models that were developed to yield insight into the mechanisms of solidification microstructure development. While these methods are useful a direct thermal history capability is planned when budget resources are available. Moreover, this ground-based experience will also be of value in designing the science and hardware requirements for a space experiment.

[1] "Solidification Reactions in Undercooled Alloys", J.H. Perepezko, Materials Science and Engineering A179/180, 52 (1994).

[2] "Kinetic Competition in Undercooled Liquid Alloys", J.H. Perepezko and D.R. Allen, Thermodynamics and Kinetics of Phase Transformations, Proceedings of the Materials Research Society Symposium, edited by J.S. Im, B. Park, A.L. Greer, and G.B. Stephenson, in press.

[3] "Kinetic Competition in Undercooled Liquid Metals", J.H. Perepezko, Mat. Sci. Forum 179-181, 701 (1995).

[4] "The Development of Nucleation Controlled Microstructures During Laser Treatment of Al-Si Alloys", M. Gremaud, D.R. Allen, M. Rappaz, and J.H. Perepezko, Acta Mat., in press.

[5] "The thermodynamics and competitive kinetics of metastable τ phase development in MnAl-base alloys", Y.J. Kim and J.H. Perepezko, Mat. Sci. and Eng., A163 (1993) 127.

[6] "Formation of a Metastable Ferromagnetic τ Phase During Containerless Melt Processing in Mn-Al-C Alloys", Y.J. Kim and J.H. Perepezko, 31st Aerospace Sciences Meeting and Exhibit, American Institute of Aeronautics and Astronautics, (1993) 1.

[7] "The Formation of a metastable ferromagnetic τ phase during containerless melt processing and rapid quenching in Mn-Al-C alloys", Y.J. Kim and J.H. Perepezko, J. Appl. Phys. 71, 676 (1992).

[8] "Kinetic Competition During Duplex Partitionless Crystallization", D.R. Allen, S. Das, and J.H. Perepezko, Ceramic Transactions 30, 343 (1993).

[9] "Kinetic Competition During Duplex Partitionless Solidification in Ni-V Alloys", D.R. Allen and J.H. Perepezko, Thermodynamics and Kinetics of Phase Transformations, Proc. Mat. Res. Soc. Symp., edited by J.S. Im, B. Park, A.L. Greer, and G.B. Stephenson, in press.

[10] "Phase Selection Processes in Undercooled Ni-V Melts", J. Schroers, T. Volkmann, D.M. Herlach, D.R. Allen, and J.H. Perepezko, International Journal of Rapid Solidification, in press.

# COMPARISON OF STRUCTURE AND SEGREGATION IN ALLOYS DIRECTIONALLY SOLIDIFIED IN TERRESTRIAL AND MICROGRAVITY ENVIRONMENTS

D.R. Poirier, Principal Investigator, Department of Materials Science and Engineering, The University of Arizona, Tucson, AZ 85721. Phone 520-621-6072; FAX 520-621-8059; poirier@ccit.arizona.edu

S.N. Tewari, Co-Investigator, Chemical Engineering Department, Cleveland State University

J.C. Heinrich, Co-Investigator, Department of Aerospace and Mechanical Engineering, The University of Arizona

## Introduction

The primary purpose of the research is to compare the structure and segregation in binary metallic alloys that are directionally solidified in terrestrial and low gravity environments. In addition the grant was awarded to define flight experiments to guide the development of an experimental apparatus for carrying out directional solidification of a dendritic alloy in microgravity. Since this grant only began on June 1, 1996, there is no progress to report as of this writing. Consequently, the objectives of the research, relevant results of a prior grant, and justification for long-term microgravity are given.

Models of dendritic solidification that are used to predict the undercooling during growth of alloys rely on the assumption of diffusional transports of both heat and solute. An important feature of the models is a prediction of the dendrite tip radius. However, the thermosolutal convection of liquid in, from, or close to the solid plus liquid region of solidifying alloys masks the diffusional processes at the dendrite tips and is responsible for most macrosegregation in castings and ingots. Availability of microgravity provides an opportunity to obtain experimental data, where thermosolutal convection is negligible. With the new grant, growth conditions for such

microgravity experiments will be defined by combining mathematical modeling and simulation with the results of terrestrial experiments. Thermosolutal convection will be significantly reduced in microgravity, and thus we can compare microsegregation and microstructure in specimens terrestrially solidified and those solidified in microgravity.

## Objectives

This is a program to conduct experiments in a long-duration microgravity environment, with the objective of studying dendritic microstructures and segregation in directionally solidified dendritic alloys. The research builds on our previous grant in which we generated an extensive data base on directionally solidified Pb-Sn alloys and simulated solidification of the alloys using continuum theory of porous media. Based on our previous research, it is clear that thermosolutal convection strongly affects diffusional transport during solidification and also leads to macrosegregates known as freckles. We are convinced, therefore, that with terrestrial experiments, diffusive and convective phenomena occur simultaneously, which complicate the study of dendritic growth. In microgravity, however, it will be possible to effect directional solidification with no thermosolutal convection. Our hypotheses are the macrosegregation is eliminated and the dendritic microstructure is greatly altered in microgravity.

The opportunity to carry out experiments in microgravity would enable us to gain scientific data on dendritic microstructures that would be beneficial in materials processing and would provide benchmark data of dendritic microstructures grown without thermosolutal convection. We will characterize dendrite arm spacings, volume fraction of interdendritic liquid, and both macrosegregation and microsegregation in directionally solidified samples. The design of the microgravity experiments will be guided by terrestrial experiments and computer simulations, in order to identify the growth conditions and the effect of g-jitter in long-duration microgravity experiments.

Relevant Results from Prior Grant

Under the auspices of our prior NASA grant, segregation and microstructures in Pb-Sn alloys were extensively studied.[1-3] Thermal gradients in the range of 17 to 81 K $cm^{-1}$ and solidification rates of 1 to 64 μm $s^{-1}$ were employed in directionally solidified castings with a diameter of 7 mm. It had been established that the extent of macrosegregation along the length of the castings varied with Sn content, with little macrosegregation at 10 and 58 wt pct Sn and the maximum macrosegregation at 33 wt pct Sn.[4] In castings that exhibited cellular morphology, the macrosegregation was exacerbated.[1] This was attributed to the thermosolutal convection driven by the greater solute buildup at the advancing tips and the reduction in the length of the mushy zone that are associated with cellular growth compared to dendritic growth.

Figure 1 illustrates the macrosegregation along the length of directionally solidified Pb-Sn alloys. The fraction solid on the abscissa is the distance along the solidified casting measured from the position where solidification commenced. The obvious segregation indicates the prominent role of convection. Hence, there is a net convective transport of Sn from the mushy zone to the overlying liquid, which results in the extensive macrosegregation.

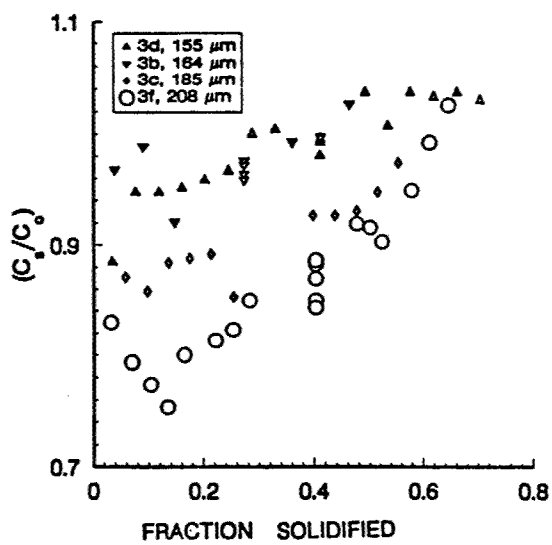


Fig. 1: Macrosegregation in directionally solidified castings of Pb-Sn alloys with various primary dendrite arm spacings.[3] $C_S$ is the concentration of Sn and $C_o$ is the concentration of Sn in the melt before solidification.

There is also evidence indicating that the primary arm spacing depends on the extent of convection, Figure 2. Using the theory of Hunt[5] to predict the primary dendrite arm spacing, we see that when the measure of segregation is less than 4 wt pct Sn, then the measured and theoretical values of the primary arm spacings show reasonable agreement. Hunt's model only accounts for thermal and solutal transport by diffusion but without advection; so with more segregation (*i.e.*, more thermosolutal convection) the agreement is poor.

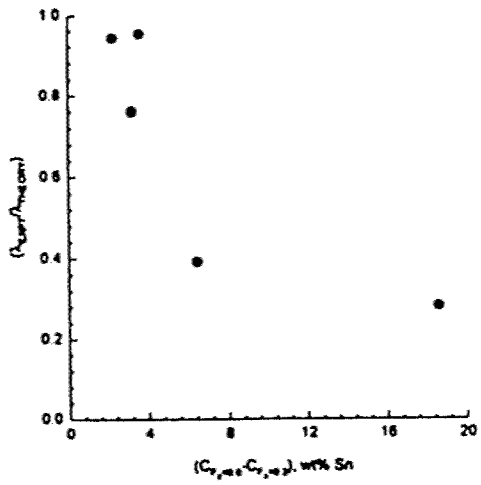


Fig. 2: The ratio of experimental to theoretical primary dendrite arm spacings *versus* a measure of macrosegregation in directionally solidified Pb-Sn castings.[3]

An example of a computer simulation of Pb-23.2 wt pct Sn alloy solidified at 6 μm $s^{-1}$ with a maximum thermal gradient of 7700 K $m^{-1}$ is presented as Fig. 3.[6] After 4000 s, the overlying liquid is above 2.2 cm, and the casting is completely solid below approximately 0.9 cm. Thermosolutal convection in the overlying liquid is shown in Figure 3a. Near each side wall the liquid flows upward, and there is a counterclockwise cell just above the advancing mushy zone. Also there are several smaller cells aligned horizontally and just above the dendritic tips.

Not shown in the figure is the convection in the mushy zone, which is much weaker but nevertheless responsible for much of the transport of solute. This is obvious when Figures 3b and 3c are viewed. In Figure 3b, the volume fraction liquid is shown; near each side wall there is a channel of liquid, and intrusions of liquid near the dendrite tips are evident. There are also two

pockets of enriched liquid in the lower part of the mushy zone. Macrosegregation resulting from the convection is depicted in Figure 3c. Where the alloy has solidified completely, freckles remain. In the experimental casting made by Tewari and Shah,[4] there were in fact two to three freckles along the surface.

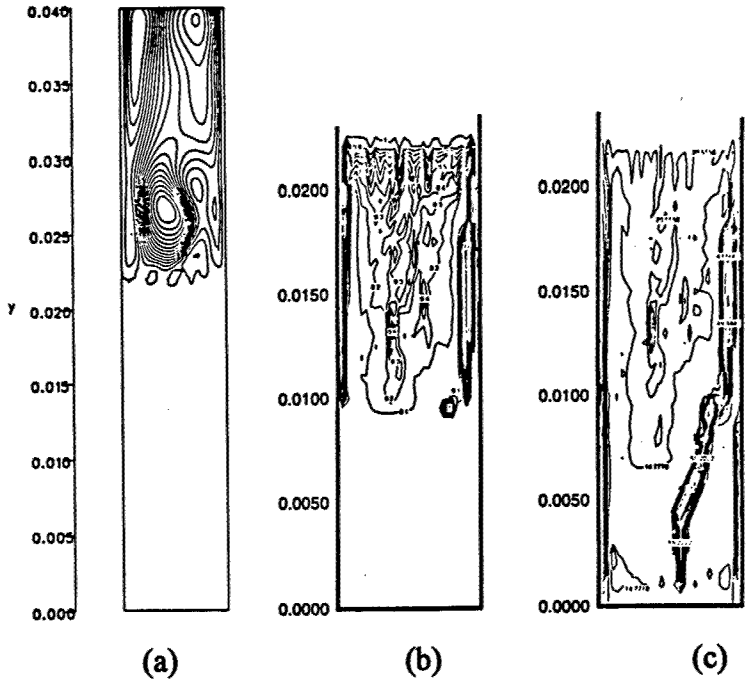


Fig. 3: Convection and macrosegregation in directionally solidified Pb-23.2 wt pct Sn alloy: (a) streamlines; (b) volume fraction liquid; (c) concentration of Sn.

## Justification for Microgravity

In terrestrial experiments, dendritic solidification is difficult to study because specimens are often plagued with severe forms of macrosegregation caused by thermosolutal convection, including: 1) continuous segregation from end-to-end; 2) occurrence of localized segregates referred to as freckles; and 3) dendrite clustering. In the microgravity environment, the thermosolutal convection will be greatly diminished, and the convection will be confined mainly to the minor flows of interdendritic liquid required to satisfy solidification shrinkage and possibly due to

1) continuous segregation from end-to-end; 2) occurrence of localized segregates referred to as freckles; and 3) dendrite clustering. In the microgravity environment, the thermosolutal convection will be greatly diminished, and the convection will be confined mainly to the minor flows of interdendritic liquid required to satisfy solidification shrinkage and possibly due to "g-jitter." Morphological features, metrics, and segregation in samples directionally solidified in an earth-based furnace and in samples grown in the microgravity are expected to be quite different.

In terrestrial solidification experiments on binary metallic alloys, whether growth is upward or downward growth, whether with the heavy solutes or light solutes, or whether they are conducted with an applied magnetic field or without, solidification is always accompanied by natural convection. It has not been possible to eliminate the convective transports and the associated problems in order to obtain the dendrite shapes which are truly determined by the diffusive transports. Only microgravity directional solidification (DS) of metallic alloys can yield the four critical parameters for evaluating dendrite growth theories in DS arrays: the growth speed, the tip radii, the thermal gradient, and the solutal gradient near the dendrite tips.

## References


1. S.N. Tewari, R. Shah and M.A. Chopra: *Metall. Trans. A*, 1993, vol. 24A, pp. 1661-9.
2. S.N. Tewari, R. Shah and H. Song: *Metall. Trans. A*, 1994, vol. 25A, pp. 1535-44.
3. S.N. Tewari and R. Shah: "Macrosegregation during Dendritic Arrayed Growth of Hypoeutectic Pb-Sn Alloys: Influence of Primary Arm Spacing and Mushy Zone Length," *Metall. Mater. Trans. A*, 1996, vol. 27A, in press.
4. S.N. Tewari and R. Shah: *Metall. Trans. A*, 1992, vol. 23A, pp. 3383-92.
5. J.D. Hunt: "Cellular and Primary Dendrite Spacings," in *Solidification and Casting of Metals*, The Metals Society, London, 1979, pp. 3-11.
6. H.-W. Huang, J.C. Heinrich and D.R. Poirier, "Simulation of Directional Solidification with Steep Thermal Grandients," *Model. Simul. in Mater. Sci. Eng.*, 1996, in press.

# THE EFFECTS OF GRAVITY, REACTION ENVIRONMENT, AND COMPOSITION ON THE COMBUSTION SYNTHESIS OF THE $TiB_2$-$TaB_2$ SYSTEM

J. A. Guzman, C. Lantz, J. J. Moore, D. W. Readey
Colorado Center for Advanced Ceramics
Colorado School of Mines
Golden, CO 80401
(303) 273-3437
dreadey@mines.edu

## Abstract

The effect of conducting combustion synthesis reactions in a low gravity environment was examined. The atmospheric pressure of the reaction vessel and inert dilution ($TiB_2$) of reactant compact were varied. Macrostructural and microstructural differences were found in the different environments. The composition was varied between pure $TiB_2$ and pure $TaB_2$. The reaction characteristics changed dramatically in different environments such that the reactions conducted in low gravity exhibited a substantial increase in the combustion temperature.

## Introduction

Self propagating high-temperature synthesis (SHS), or combustion synthesis, is a relatively new processing technique which is being used to rapidly and efficiently synthesize ceramics, ceramic composites, and intermetallic compounds[1]. Combustion synthesis relies on the exothermicity of certain chemical reactions to sustain a reaction once it is initiated. Most solid-solid combustion synthesis reactions have such high exothermicities, that the highest temperature of the reaction, the combustion temperature ($T_c$), usually exceeds $2000^{\circ}$ C[2]. Such an excessive

heat release can have disadvantages since it results in high levels of porosity and mass loss. However, SHS has many potential advantages; such as, savings in processing time and energy, and production of metastable products. [3].

In combustion synthesis, there are two modes of reaction: the propagation mode or the simultaneous combustion mode. The propagation mode results in reactions that are very exothermic and have adiabatic combustion temperatures higher than 1800°C[4]. Since these reactions are highly exothermic, only a local heat source is used to initiate or ignite the reaction at one end where a combustion wave forms and travels through the powder compact, leaving behind the product material. In the simultaneous combustion mode, the reaction is not exothermic enough to be self sustaining, thus the whole powder compact is heated and reacts simultaneously. Both these processing routes still rely on very exothermic reactions. A typical time-temperature history of a combustion synthesis reaction is shown in Figure 1. The reaction is initiated at at the ignition temperature ($T_{ig}$), and the maximum temperature is the combustion temperature ($T_c$). By examining the thermochemistry of the reaction system, the adiabatic temperature is calculated and yields information about the control of the reaction. An enthalpy-temperature diagram for the SHS reaction:

$$Ti + 2B = TiB_2$$

is shown in Figure 2. The initial temperature ($T_o$), combustion and adiabatic temperatures ($T_c$ and $T_{ad}$, respectively) are shown. The adiabatic temperature results from no heat losses. However due to heat losses ($\Delta H$) the maximum temperature is usually less. The adiabatic temperature for this reaction is 3200 K, coincident with melting point of $TiB_2$.

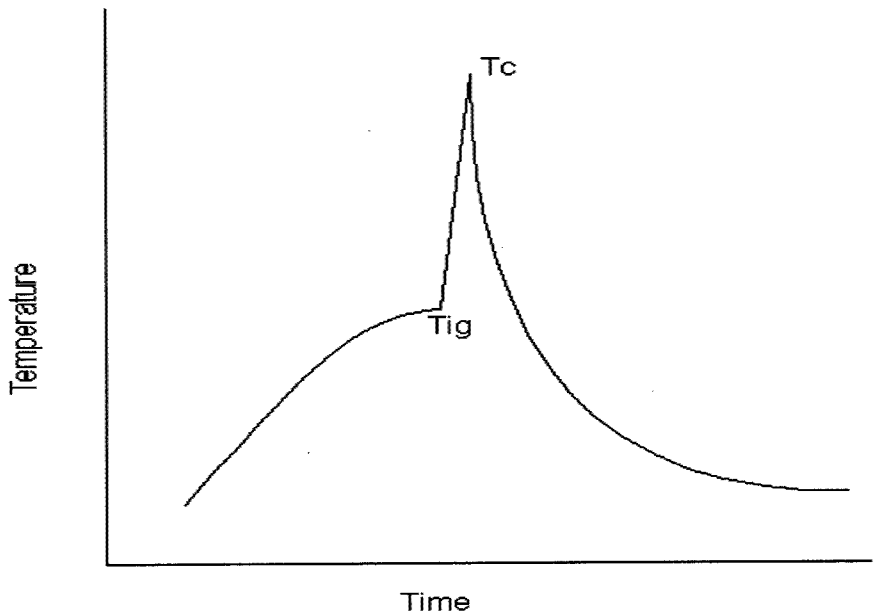


Figure 1: Typical time-temperature history for a combustion synthesis reaction.

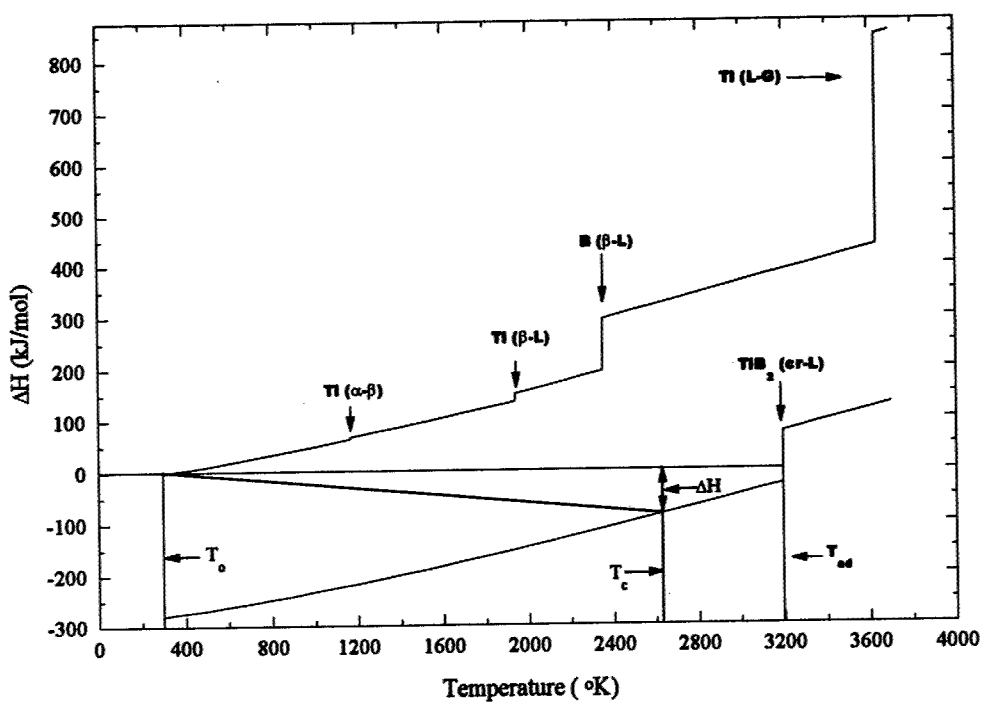


Figure 2: Enthalpy diagram for the $TiB_2$ reaction system showing phase changes and reaction temperatures.

The addition of tantalum to the $TiB_2$ reaction is to investigate the effect of different amounts and density of metal liquids at the reaction front. Munir[4] and others have shown that titanium melts during the formation of TiC and $TiB_2$. Titanium and tantalum form a complete solid solution at all compositions. Therefore, by adding tantalum, the amount of metal liquid decreases, while the density of the metal liquid increases.

Examination of the effects of gravity on combustion synthesis reaction has been limited. Recent studies of composite systems in microgravity environments have shown that gravity conditions can considerably affect the product morphologies especially when liquid or gaseous specie(s) are generated or present at and/or ahead of the SHS reaction front. [5-7 ] The purpose of this current research program is to examine the effects of gravity on the combustion synthesis of titanium diboride ($TiB_2$), tantalum diboride ($TaB_2$) systems with different liquid densities.

## Results and Discussion

Conducting SHS reactions in a low gravity environment had significant effect on the combustion synthesis reactions. For the process variables examined in low gravity and, the combustion temperatures were higher, and closer to adiabatic conditions, than the combustion temperatures measured in normal gravity conditions. Figure 3 is a plot combustion temperature versus gravity. There is a large increase in the combustion temperature for low gravity conditions. The measured combustion temperatures indicated that the product is closer to adiabatic conditions. Conduction between the sample and the environment is negligible since the contact between the pellet and the table was minimized, and convection is eliminated or minimized in low gravity. The main heat loss process is radiation heat transfer. Therefore, a rapid diffusion, sintering, or even viscous flow process is expected to some extent. Microstructures of normal gravity samples are well defined grains (individual crystals), while low gravity microstructures rounder edges and bulbs on individual grains, which appears to be non-faceted grain growth. When tantalum was added to the $TiB_2$ system, the combustion temperature decreased as expected. However, the same trend of increased combustion temperature in low gravity is observed. Also,

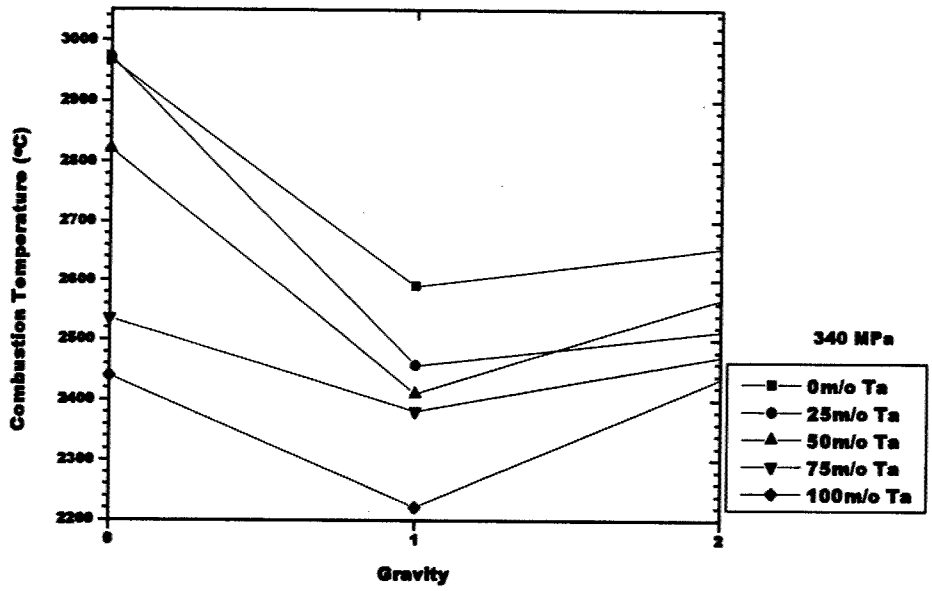


Figure 3: Plot of the combustion temperature versus gravity for various amounts of tantalum additions.

in low gravity, the combustion temperature decreases with tantalum addition. Figure 4 is an X-Ray diffraction pattern of a sample having 50 m/o tantalum addition. The first two patterns are standards for pure $TiB_2$ and pure $TaB_2$, respectively. The X-Ray diffraction pattern indicates that product is a solid solution diboride with the two metal elements. Typical microstructures are rounded grains with bulbous growths, which is non-faceted. Thus grain growth has occurred.

## Conclusion

Low gravity has a large effect on the combustion synthesis of $TiB_2$ and $TaB_2$ systems. The combustion temperature is higher in low gravity for all the different compositions. There microstructure for low gravity samples seem to show non-faceted grain growth, which tends to occur at high temperatures. Samples with tantalum and titanium form a solid solution of the diboride. Lastly, since such differing microstructures are achieved with process variables, there is the opportunity to "tailor" microstructures using the process variables.

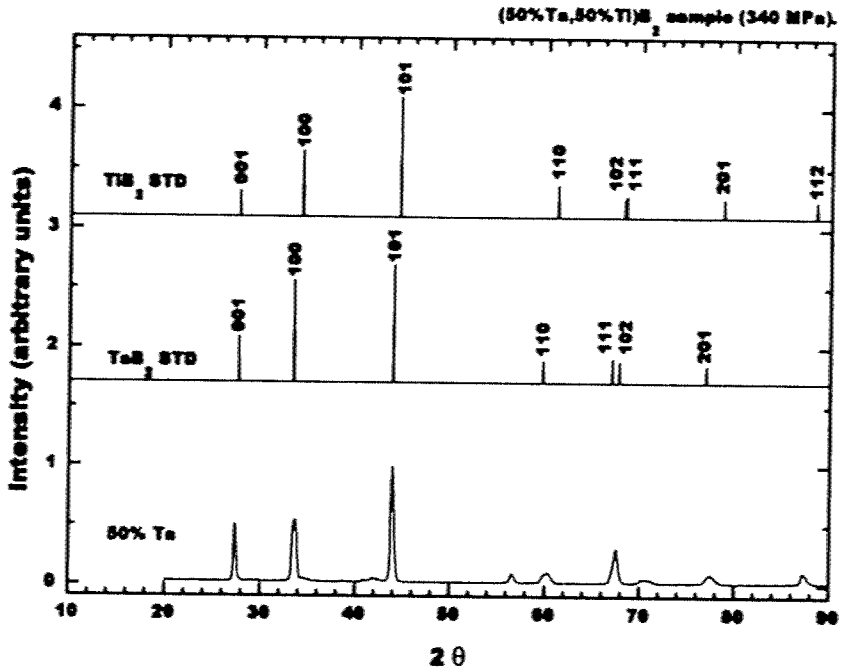


Figure 4: X-Ray diffraction pattern for sample with 50m/o tantalum addition.

## References


1. Yi, H.C., and Moore, J.J., Journal of Materials Science, 25, pp. 1159-1168 (1990).

2. Holt, J.B., Kingman, D.D., and Bianchi, G.M., Materials Science and Engineering, 71, 321-327 (1985).

3. Moore, J.J., Minerals and Metallurgical Processing, August 1991, pp. 152-159.

4. Munir, Z.A., and Anselmi-Tamburini, U., Materials Science Reports, May 1989, pp.277-365.

5. Odawara, O., Mori, K., Tanji, A., and Yoda, S., Journal of Materials Science Reports, 2, (1992).

6. Hunter, K.H., 1993 M.S. Thesis, Colorado School of Mines, Department of Metallurgical and Materials Engineering.

7. Shteinberg, A.S., Sjcerbakov, V.A., and Martynov, V.V., Proceedings of the First Soviet-American Symposium on the Study in Microgravitational Conditions, pp. 13-17 (1991).

# THE EFFECTS OF MICROGRAVITY ON VAPOR PHASE SINTERING

D. J. Aldrich, J. C. Westhoff, and D. W. Readey
Colorado Center for Advanced Ceramics
Colorado School of Mines
Golden, CO 80401
(303) 273-3437
dreadey@mines.edu

## Abstract

Vapor transport during sintering of ceramics can have a profound effect on microstructure. It can decrease the rate of densification by reducing surface curvature. At the same time, it can greatly enhance grain growth at all porosities further decreasing the rate of densification. On the other hand, vapor transport can be advantageously used to produce ceramics of controlled porosity and pore sizes which have potential for a number of applications, including filters. Some systems fit the existing particle growth models well and others do not. The reason for this is thought to be the competition between normal grain boundary motion and transport via the vapor phase. Microgravity offers the potential for experiments of relatively dispersed, unconstrained particles for which boundary motion will not play a role. Comparison between particle coarsening of dispersed particles in microgravity and those in a powder compact can provide information about the relative roles of vapor transport and grain boundary motion. Low temperature, non-toxic, high vapor pressure surrogate materials are being sought for microgravity experiments. In addition, multiphase systems were studied to determine the effect of particle connectivity.

## Vapor Transport and Sintering

The two-sphere model,[1 ] Figure 1, is useful to illustrate the potential effects of enhanced vapor transport. Bulk diffusion and grain boundary diffusion involve the removal of material from

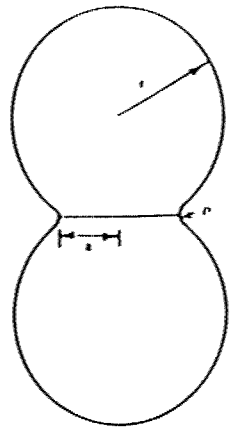

Figure 1 - Two sphere model used to describe the initial stages of sintering.[1]

between the particle centers which results in densification. Surface diffusion and vapor transport, on the other hand, only move material from the surface to the neck region. Since no material is removed from between particle centers, no densification occurs. It has been shown that partial pressures on the order of $10^{-4}$ atmospheres are sufficient to cause vapor transport to dominate mass transport for materials with diffusion coefficients less than $10^{-10}$ $cm^2/s$.[2] For diffusion through the gas phase, the model predicts that neck size should grow as:

$$x^3 = \frac{12D\gamma}{\pi}\left(\frac{\Omega}{RT}\right)^2 p_o t \qquad (1)$$

For systems in which vapor transport dominates, particle coarsening can also occur and can be described by Ostwald ripening kinetics.[3]

$$r^3 - r_o^3 = \frac{8}{9} D\gamma\left(\frac{\Omega}{RT}\right)^2 p_o t \qquad (2)$$

Where D = gas diffusion coefficient, $\gamma$ = surface energy, $p_o$ = equilibrium partial pressure, t = time, $r_o$ = initial particle radius, $\Omega$ = molar volume, R = gas constant, and T = temperature. While the kinetics of this process have been well demonstrated for many systems (for example: $Fe_2O_3$[4], $TiO_2$[5], and $Al_2O_3$[6]) Figure 2 shows an example of particle coarsening in $Fe_2O_3$ sintered in HCl[4]. However, there is still some question as to the limiting constraint that controls the coarsening which is thought to be the surrounding nearest neighbors in a powder compact.[6] To alleviate the constraint of multiple particle contact, it is proposed to study vapor phase sintering in microgravity in which particles are dispersed or, at least, less densely agglomerated or packed.

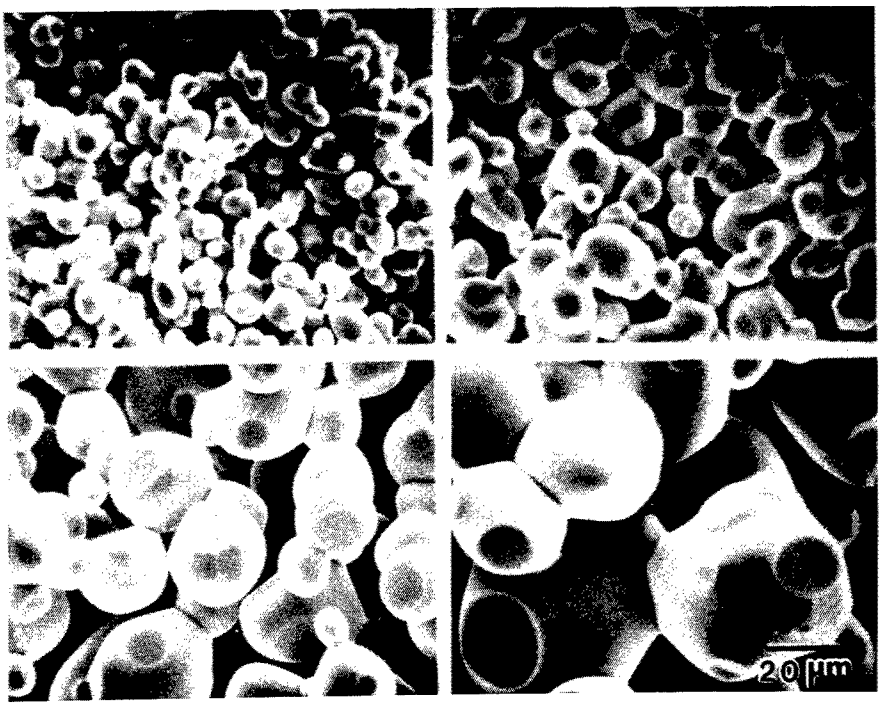


Figure 2. Coarsening of $Fe_2O_3$ in HCl at 1200 °C. Top: left, 10 min.; right, 30 min. Bottom: left, 100 min.; right, 300 min.

Surrogate Materials

One part of this program has been to find a surrogate material having ideal properties of: high vapor pressure, low melting point, simple crystal structure, non-toxic, small particle size (< 10 μm), does not densify, shows vapor phase coarsening, and does not completely fit the simple coarsening models. Some 200 organic and inorganic compounds were evaluated and experiments were carried out on about ten systems. The ideal material was found to be ZnS which shows coarsening at low temperatures and does not densify, Figure 3.

Multiphase Systems

Experiments were carried out in the systems: $NiO$-$Fe_2O_3$-HCl, $NiO$-$Al_2O_3$-HCl, and $Fe_2O_3$-$Al_2O_3$-HCl to determine the effects of phase connectivity and different grain boundary types on

Figure 3. Polished sections of 55% dense ZnS samples sintered at 1100 °C in hydrogen for, from left to right: 0 min., 100 min., and 10,000 min.

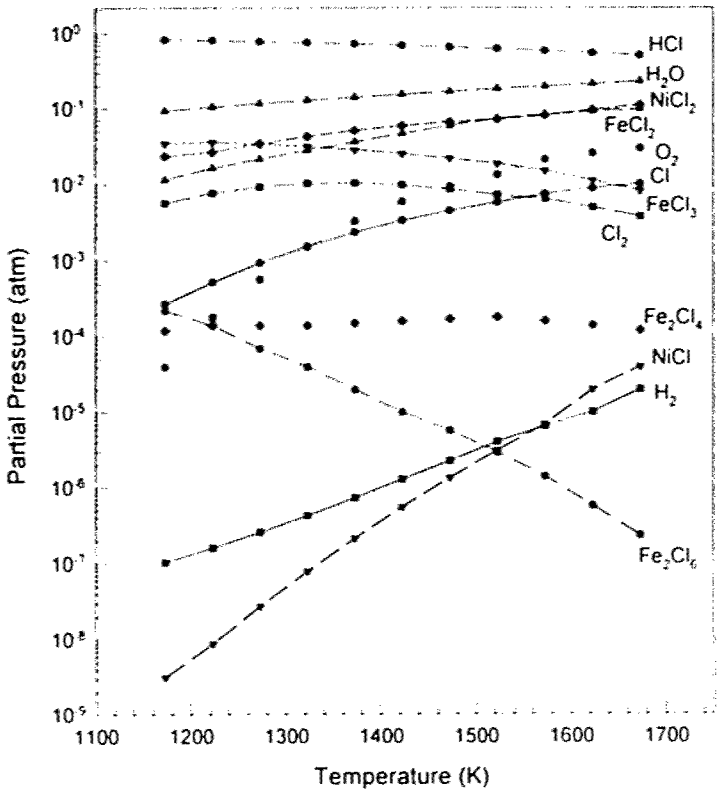


Figure 4. Calculated partial pressures for the system $NiO$-$Fe_2O_3$-HCl.

coarsening. As an example of one of the effects observed in these multicomponent systems, Figure 4 shows the calculated[7 ] pressure variation with temperature for the system $NiO-Fe_2O_3-HCl$. This demonstrates that both oxide components have volatile species with pressures above $10^{-3}$ atmospheres indicating that vapor transport will occur for both. Indeed, coarsening occurs in all three compounds in the system, NiO, $Fe_2O_3$, and $NiFe_2O_4$. However, they coarsen at different rates as shown in Figure 5 suggesting different effects of grain boundary mobility.

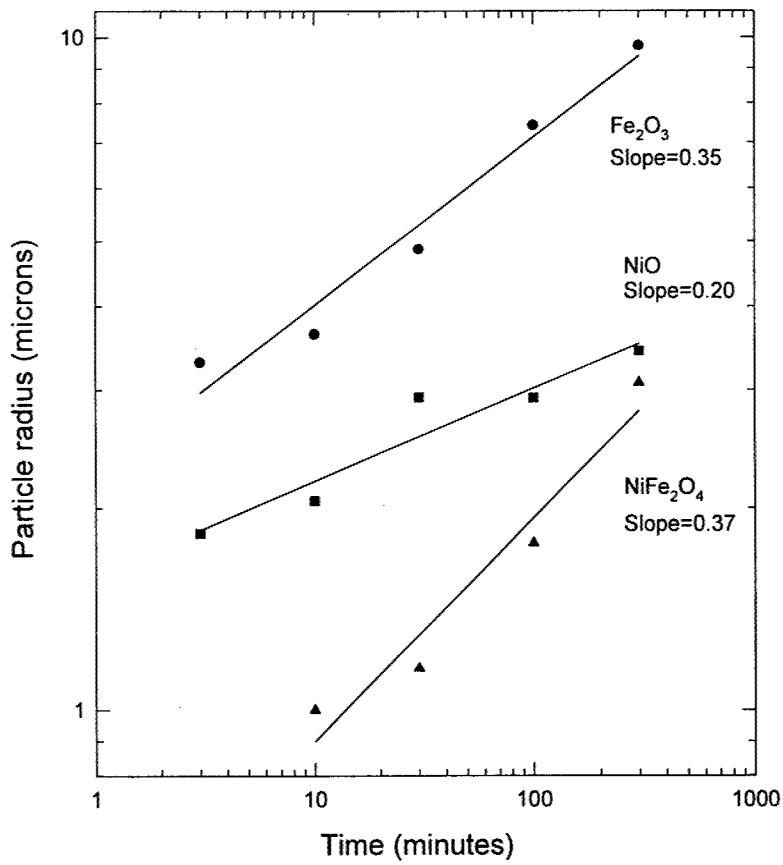


Figure 9 - Coarsening data for the system $NiO-Fe_2O_3-HCl$ at 1200 °C.

## Conclusions

A surrogate material appropriate for microgravity was found to be ZnS. Sintering experiments in multiphase systems reinforced the importance of the role of grain boundary mobility on coarsening or grain growth during vapor phase sintering of ceramics.

References


1. G. C. Kuczynski, "Self-Diffusion in Sintering of Metallic Particles," Trans. AIME, 185 [2] 169-78 (1949).

2. D. W. Readey, D. J. Aldrich, and M. A. Ritland, "Vapor Transport and Sintering," to be published in the Conference Proceedings of Sintering '95 (1996).

3. C. Wagner, "The Aging of Precipitates by Dissolution," (in Ger.), Z Elektrochem, 65 (718) 581-91 (1961).

4. J. Lee and D. W. Readey, "Microstructure Development in $Fe_2O_3$ in HCl Vapor"; pp. 145-57 in Materials Science Research, Volume 16, Sintering and Heterogeneous Catalysis. Edited by G. C. Kuczynski, A. E. Miller, and G. A. Sargent. Plenum, New York, 1984.

5. M. J. Readey and D. W. Readey, "Sintering $TiO_2$ in HCl Atmospheres," J. Am. Ceram. Soc., 70 (12) C-358-61 (1987).

6. Marc A. Ritland and Dennis W. Readey, "Alumina-Copper Composites by Vapor Phase Sintering," Ceramic Engineering and Science Proceedings, 14 (9-10) 896-907 (1993).

7. T. Bessman, "A Computer Program To Calculate Relationships in Complex Chemical Systems," (Report ORNL/RM-5775, Oak Ridge National Laboratory, Oak Ridge, Tn, 1977)

# DETACHED SOLIDIFICATION: STEADY STATE RESULTS

Liya L. Regel, Dmitri I. Popov and William R. Wilcox
International Center for Gravity Materials Science and Applications
Clarkson University, Potsdam, NY 13699-5814, USA
Phone 315-268-7672, e-mail: regel@agent.clarkson.edu

Abstract.

The goal of our research is to achieve a complete understanding of detached solidification, in order to be able to produce it reproducibly. This is necessary because of the better quality of crystals produced by detached growth. The objectives of the current project are to provide the theoretical description of the model proposed in [1], and to develop concepts for flight experiments based on the obtained results. To carry out this plan, the following is required: find the conditions in a directional solidification experiment for detached growth to occur; determine the transient behavior of the gap and the meniscus immediately after detachment; find the parametric dependence and stability conditions of the steady-state detached configuration. In the present report, the results for steady state detached growth are discussed.

## Introduction

Many directional solidification experiments in space gave ingots which were not in contact with the ampoule wall [1]. Their surfaces were not smooth, but wavy, often with small ridges. Several possible explanations have been proposed, often in contradiction with some experimental results. An attempt to fit the experimental results qualitatively was made in the model proposed in [1]. In this model, a small gap forms between the growing crystal and the ampoule wall. A meniscus contacts the growth interface with the ampoule wall. While the meniscus and the wetting conditions of the melt and ampoule materials have been also considered in the other models [2], the inherent feature of this model is a volatile component or dissolved gas, which is always present in a sealed ampoule. The volatile component is rejected by the growing interface and liberated through the meniscus into the gap, maintaining the pressure in the gap and affecting the meniscus shape. Steady-state detached growth takes place when the transport of volatile species

across the meniscus is sufficient to satisfy the conditions of mechanical equilibrium of the meniscus.

Theoretical model and method of solution

We numerically modeled steady-state detached solidification of InSb in microgravity. We obtained dependence of the steady state gap width on the solidification rate and residual gas pressure in the ampoule, as well as the stability conditions for steady-state detached growth. First, the meniscus line (in axisymmetric case) was determined. To maintain a gap width constant requires a certain flux of volatile species across the meniscus. Gas, initially dissolved in the melt, is transported into the gap across the meniscus, affecting the pressure in the gap and the gap width. Initially, gas remains in the ampoule before sealing due to residual or back-filled gas in the ampoule, such as argon or hydrogen. At steady state, the volatile species diffuses across the meniscus into the gap at exactly the correct rate to fill the new volume of the gap created by growth, while maintaining the gap pressure $P_g$. For the purpose of calculating this diffusion gas flux, the steady-state velocity field was obtained in the reference frame of the interface, which moves at freezing rate $V_c$. The concentration $C$ of gas dissolved in the melt was assumed to satisfy the steady state mass transfer equation with convection. The concentration along the freezing interface was found by solving simultaneously the mass transfer equation and the usual interfacial material balance.

The calculation of the steady state gap width was iterative. First, a gap width $e$ was assumed. Then the velocity field and the concentration field in the melt were solved. The gas flux into the gap was obtained. This flux yielded a new value for gap width. The iterations proceeded until the calculated gap width equaled the assumed gap width.

It has been recognized [3] that the stability of the gap must be related to that of the meniscus shape. A change in the meniscus shape is affected by the change in the gap width and the pressure in the gap. Crystal growth and gas transport across the meniscus are the mechanisms that cause this change. Stability analysis of the steady state detached configuration was carried out considering an infinitesimal perturbation in the gap width $e$ and the pressure in the gap $P_g$ from the state of mechanical equilibrium. Thus, if a steady-state crystal growth was perturbed, the angle between the meniscus and the ampoule axis is not the growth angle $\alpha$ any more (Fig.1). In this case the pressure balance in the gap would be disturbed and the gap width would change. The

analysis was done taking into consideration a constant growth rate with gas mass transfer across the meniscus. We excluded from the shape stability analysis the effects of thermal field in the melt-crystal-gap system.

Results

At steady state, the volatile species diffuses across the meniscus into the gap due to the gradient of concentration near the meniscus. The total molar flux $J_{mole}$ into the gap was calculated by integrating the diffusion molar flux, obtained from the numerical calculations, over the total surface of the meniscus. In axisymmetric case the integration can be carried out along the meniscus line. In this case, the steady state gap width was determined to be:

$$e_{st} = \frac{RT\frac{D}{V_c}\int_0^{l_a}(-\frac{\partial C}{\partial n})dl - 2\sigma\cos(\frac{\alpha-\theta}{2})\cos(\frac{\alpha+\theta}{2})}{P_m} \qquad (1)$$

where R is the ideal gas constant, T is the temperature of the gas in the gap, D is diffusion coefficient of dissolved gas in the melt, $\sigma$ is the melt/gas surface tension, $\alpha$ is the growth and $\theta$ is the contact angle of the melt with the ampoule. The gap width from our calculations is on the order of 1 mm, which agrees with experimental observations. Steady state curves were obtained for a range of solidification rate $V_c$ (Fig.2) and residual gas pressure in the ampoule $P_m$ (Fig.3). It was found that a steady state gap width can be obtained only if the solidification rate is not large and the residual gas pressure in the ampoule is not small. The critical values of $V_c$ and $P_m$, , beyond which detached solidification cannot be obtained, depend on the physical properties of the melt and the solubility of the gas dissolved in it. From equation (2) it can be concluded that the steady state gap width will be larger for materials with larger growth angle and contact angle. On the other hand, the steady state gap width will decrease for materials with larger value of melt/gas surface tension.

Marangoni convection makes little difference to the gap width, in spite of its dramatic influence on the velocity and concentration fields near the meniscus. The primary influence of gravity on the transport of volatile species is buoyancy-driven convection, which provides global

mixing of the melt. This mixing leads to decrease of dissolved gas concentration near the meniscus, and, therefore, to a reduction of the gas flux.

With the use of Liapunov stability concepts, in a system with two degrees of freedom, small deviations from equilibrium value of a steady state gap width $e$ and pressure in the gap $p$ were described by a system of coupled differential equations:

$$(\delta\dot{e}) = a_{ee}(\delta e) + a_{ep}(\delta p)$$
$$(\delta\dot{p}) = a_{pe}(\delta e) + a_{pp}(\delta p) \qquad (2)$$

where $\delta e$ is the perturbation in the gap width, $\delta p$ is the perturbation of pressure in the gap, and the coefficients $a_{ij}$ are obtained from variation of the growth angle $\alpha$ and molar gas flux $J_{mole}$ near their equilibrium values. From this stability analysis it was found that stable detached growth is achieved for larger gap widths, whereas smaller gaps are always less stable. Stability is reached only for small solidification rates at the beginning of detached solidification. With continued detached growth the stability deteriorates (Fig.4).

## Conclusion.

In this paper we have shown that the model proposed in [1] can reasonably describe steady-state detached solidification. It seems likely that the influence of heat transfer, which changes the solidification rate when the gap width or the meniscus shape change, must be considered in order to understand the stability of steady-state detached solidification over a long distance.

## References

[1]. W.R. Wilcox and L.L. Regel, "Detached Solidification," Microgravity Sci. Technol. 8, 56-61(1995)

[2]. T. Duffar, C. Potard, P. Dusserre, "Crucible De-Wetting During Bridgman Growth of Semiconductors in Microgravity," J.Crystal Growth, 100,171(1990)

[3]. T. Surek, "Theory of Shape Stability in Crystal Growth from the Melt," J.Appl.Phys., 47,4384(1976)

Acknowledgment.

This project is supported by NASA's Microgravity Science and Applications Division under grant NAG8-1063.

Figure captions

Fig.1 Physical domain used in the numerical calculations. Meniscus region is exaggerated.

Fig.2 The dependence of the calculated steady state gap width on inverse diffusion length $V_s/D$. Residual gas pressure $P_m = 10^{-4}$ MPa; segregation coefficient k=0.03. The solid lines are the iteration curves obtained in the numerical calculations; the dashed lines - initial values. The thick solid line is the steady state gap width.

Fig.3 The dependence of the steady state gap width on residual gas pressure. Inverse diffusion length $V_s/D=10$; segregation coefficient k=0.03; see explanation in caption for Fig.2.

Fig.4 Stabilization of the detached configuration by gas transport (solid lines). Dashed line - no gas transport included. Gap width e=0.15 cm. Two cases are considered: with both curvatures of the meniscus taken into account and with one of the curvatures, the ampoule radius is neglected.

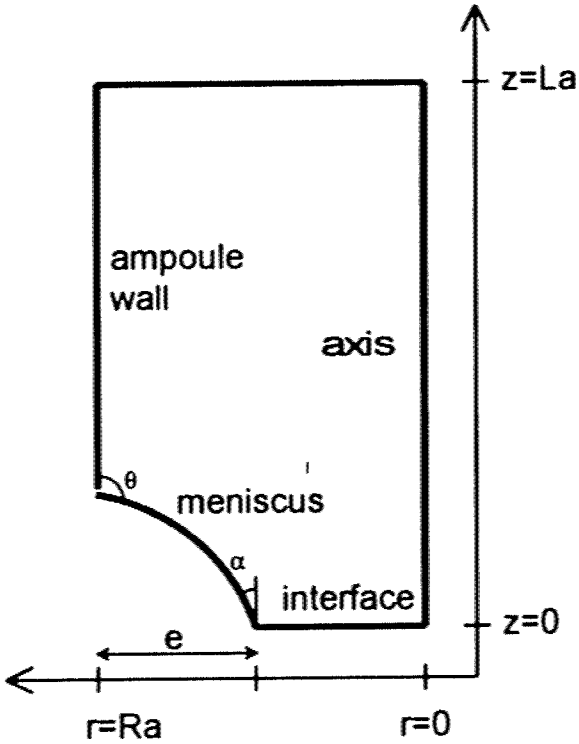


Figure 1

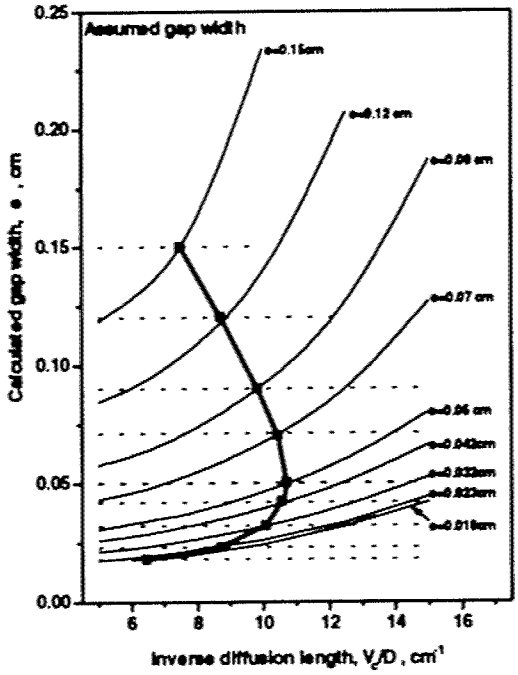


Figure 2

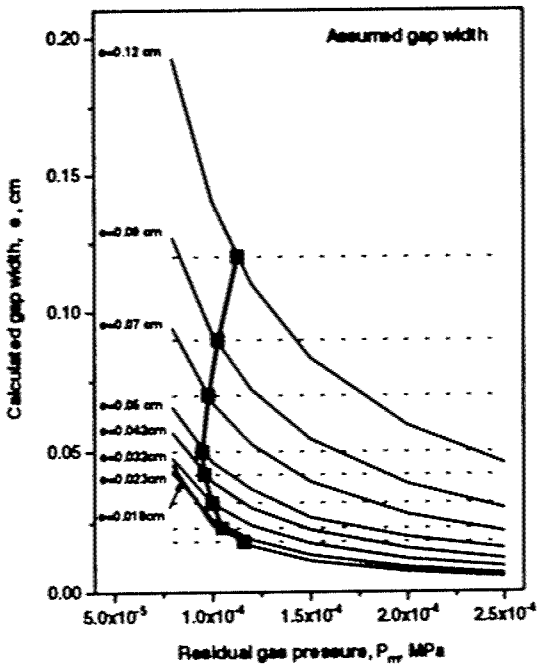


Figure 3

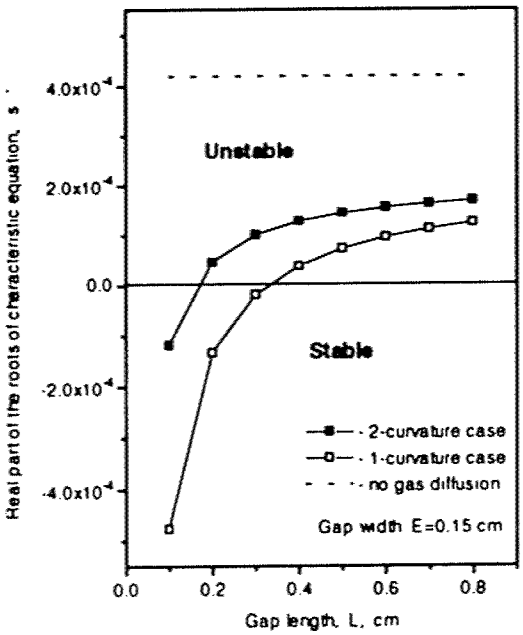


Figure 4

# THERMOPHYSICAL PROPERTY MEASUREMENTS OF MOLTEN SEMICONDUCTORS

Won-Kyu Rhim
Jet Propulsion Laboratory, California Institute of Technology, 4800 Oak Grove Drive, Pasadena, California 91109 Mail Stop 183-401, (818) 354-2925, e-mail: won-kyu.rhim@jpl.nasa.gov

## Research Objectives

As the dimensions of semiconductor devices continue shrinking, the understanding and the control of the formation kinetics of a variety of crystal imperfections such as point defects, non uniform distribution of doping atoms, and impurity atoms in the growing crystals have become very important. To achieve this objective a theoretical modeling of the crystal growth process is an essential step. In order to obtain reliable modeling results, input parameters, i.e. various thermophysical parameters, must be accurate. However, in an environment where accurate thermophysical properties are lacking, crystal growth remains an 'art' instead of 'science'. For instance, the total hemispherical emissivity has a dramatic impact on the thermal environment. It determines the radiative emission from the surface of the melt controlling to a large extent the profile of the solidified crystal. In order to understand convection and turbulence in the melt, viscosity becomes an important parameter. The liquid surface tension determines the shape of the liquid-atmosphere interface near the solid-liquid-atmosphere triple point. Currently used values for these parameters are very inaccurate, and this program intends to provide more reliable thermophysical properties. Thus, the objective of this program is the accurate measurement of various thermophysical properties which can be reliably used in the modeling of crystal growth processes.

Many molten semiconductors are chemically reactive with crucibles and a minute amount of impurities in the melts tends to substantially modify the properties of the semiconductors. Sample levitation done in a vacuum clearly helps to maintain the sample purity by isolating it from container walls. However, all gravity-caused effects such as convection, sedimentation and buoyancy will still take place in the sample. In addition, large forces needed to levitate the sample in the presence of gravity can cause additional flows in the melt. Although considerably less flows are expected in the High Temperature Electrostatic Levitator (HTESL), which is a new levitation technique developed at JPL, little is known about the flows induced by the electrostatic forces. Most seriously affected by the flows might be those measurements of transport properties such as atomic diffusion, viscosity, and thermal diffusivity. Therefore, the second objective of this

program is to define the limits of the HTESL technology as various thermophysical properties of molten semiconductors are measured in ground-baseed laboratories. This program also promotes national as well as international collaboration for the accurate thermophysical property measurements of various molten semiconductors. A Japanese team, for example, is in the process of constructing an electromagnetic levitator which will measure thermophysical properties of molten semiconductors as it attains reduced-g condition in the 10 second drop-shaft in Hokkaido, Japan. The measurements of thermophysical properties which require reduced-g condition will become clear as the results from the two different g-conditions are compared.

Specific Objectives:

In this program, thermophysical properties of molten semiconductors, such as Si, Ge, Si-Ge, and InSb will be measured as a function of temperature using the High Temperature Electrostatic Levitator . Each material will be doped by different kinds of impurities at various doping level. The thermophysical properties which will be measured include:

Density,
Thermal expansion coefficient,
Surface tension,
Viscosity,
Specific Heat,
Hemispherical total emissivity, and tentatibly
Electrical conductivity.

The results obtained with the electrostatic levitator will be compared with (or complement) the results obtained by collaborators both in 1-g as well as in the reduced-g environments. Research cooperation will be mainly with the Japanese team led by Mr. Norio Suzuki, who will use various methods to measure a given thermophysical property. Micro-g experiments will be done primarily by an electromagnetic levitator as it is dropped in the 10 second drop-shaft in Hokkaido, Japan. Various apparatuses available at Purdue University (Professor Raymond Taylor's group) may well be utilized for an added dimension. Such comparitive studies will help identify those thermophysical properties which are difficult to measure on Earth due to the convective flows in the melts, and, at the same time, one may be able to identify the most reliable technique which will consistently produce accurate results.

## Experimental Facility

The main work horse for this program is the High Temperature Electrostatic Levitator (HTESL)[1] which was recently developed at JPL. In the HTESL, samples are melted while in levitation in a high vacuum condition. Charged sample is levitated electrostatically by a set of electrodes connected to high voltage amplifiers. The sample is charged initially by a capacitive charging. Once the sample is levitated, the sample charge is maintained either by thermionic emission or by photoemission. A schematic diagram of HTESL is shown below. The levitation chamber contains the electrode assembly and optical components to direct the heating beam to the levitated sample, and various equipment surrounding the chamber which are required for the levitator operation. The sample position is optically sensed, and feedback loop controls the high-voltage level to maintain the sample at a desired position. The largest sample that can be levitated is approximately 200 mg, which corresponds to a lead sample approximately 3 mm in diameter. The chamber is evacuated to an ultimate vacuum of $5 \times 10^{-8}$ torr. A 1000 watt xenon-arc lamp is used to heat the sample up to approximately 2300 K. Non contact techniques which are required for a specific thermophysical property will be described in the following sections.

## Technical Approaches

Mass Density and Thermal Expansion Coefficient Measurements: Density is one of the fundamental parameters which affect measured thermodynamic quantities. However, when it comes to the density of undercooled high temperature liquids, data are very scarce, or if available, are rather inaccurate. The density measurement system[2] built around the HTESL is consisted of a high quality tele-microscope for magnified side view of levitated drop, a CCD video camera attached to the microscope, and a micro-computer for image digitization and analysis. Image analysis software was also developed to extract the image area accurately. Preliminary density results for molten silicon[3] are shown in Figure 2. These are the first density data of there kind showing the density of molten silicon over more than a 250 K-wide undercooled region. Currently this technique can measure density less than 0.5 % uncertainty.

Heat Capacity and Total Hemispherical Emissivity: In spite of their importance, the specific heat capacity $c_p$ and the total hemispherical emissivity $\varepsilon_T$ are known for very few high-temperature liquids. Data are particularly scarce for undercooled liquids. Once the heating beam is completely blocked, the levitated melt cools radiatively satisfying the radiative heat transfer equation. Figure 3 shows a typical cooling curve of a levitated molten silicon. It shows approximately 300K

undercooling, and also a large shift in the emissivity upon solidification. Since both T and dT/dt can be obtained from this curve, the specific heat to the emissivity ratio[4] can be readily obtained from the radiative heat transfer equation:

$$\frac{c_p}{\varepsilon_T} = -\frac{6\sigma_{SB}(T^4 - T_R^4)}{\rho d \frac{dT}{dt}} \quad , \tag{1}$$

where $\sigma_{SB}$ is the Steffan-Boltzman constant, $m$ is the sample mass, $T_E$ is the temperature of surrounding environment and d is the sample diameter assuming spherical sample shape. Strictly speaking $\varepsilon_T$ has to be independently measured over the entire undercooling temperature to determine $c_p(T)$. (The technology development for independent $\varepsilon_T(T)$ measurement is in progress at Caltech[5]). However, $c_p(T_m)$ at the melting temperature is often available or it can be readily measured using a conventional calorimeter, while $\varepsilon_T(T_m)$ is sensitive to surface contamination. In that case, $\varepsilon_T(T_m)$ is determined using available $c_p(T_m)$.

Surface Tension and Viscosity Measurements: As a commonly used non-contact technique, drop oscillation method is established on the basis of theoretical understanding of drop shape oscillations[6,7]. The theory was further refined to account for more realistic coditions such as quiescent drop deformation and non-uniform charge distribution which are encountered in the electrostatic levitation in the presence of gravity. In an ideal situation where a charged drop maintains spherical equilibrium shape in the absence of external fields, the the surface tension in the small viscosity limit can be determined by measuring the resonance frequency of its lowest resonance mode

$$\sigma = \frac{r_o^3 \rho}{8}\left(\omega_2^2 + \frac{Q_s^2}{8\pi^2 r_o^6 \rho \varepsilon_o}\right), \tag{2}$$

and the viscosity can be determined by

$$\eta = \frac{\rho r_o^2}{5\tau_2}, \tag{3}$$

where $r_o$ is the radius of the drop, $\rho$ is the density of the drop, $\omega_2$ is the fundamental resonance frequency, $Q_s$ is the drop charge, $\varepsilon_o$ is the permittivity of vacuum, and $\tau_2$ is the damping constant of the oscillation. Strictly speaking, however, a sample drop in an electrostatic levitator cannot maintain the spherical equilibrium shape, rather, it deforms into a prolate shape due to the external electric field. The asymptotic correction to the drop oscillation characteristics when the static drop deformation is accounted for has recently been obtained by Feng and Beard[8] with a multiple-

parameter domain-perturbation technique. The results of Feng and Beard will provide more accurate interpretation of experimental measurements of surface tension based on drop oscillation method.

## Summary

This is the first year of this program. It attempts to make accurate measurements of various thermophysical properties in molten semiconductors. The HTESL will levitate molten samples, and various non contact techniques will be used for each property measurement. The processing environment will be a high vacuum, therefore, the sample materials will be limited to those with relatively lower vapor pressure. Both national and international cooperations are being sought to increase the understanding of the effects of the gravity when a given thermophysical property is measured using different measurement techniques.

## References

1. W. K. Rhim, S. K. Chung, D. Barber, K. F. Man, Gary Gutt, A. Rulison, R. E. Spjut.: "An Electrostatic Levitator for High Temperature Containerless Materials Processing in 1-g." Rev. Sci. Instrum .64, 2961, 1993.
2. S. K. Chung, D. Thiessen, Y. J. Kim, and W. K. Rhim: "A non contact measurement technique for the density and thermal expansion of molten materials." Rev. Sci. Instum. in press.
3. W. K. Rhim and A. J. Rulison: "Thermophysical properties of molten silicon", Int. J. Thermophysics (in press).
4. A. J. Rulison and W. K. Rhim: "Constant pressure specific heat to hemispherical total emissivity ratio for undercooled liquid nickel, zirconium, and silicon." Metal. and Materials Trans. B, 26, 503, 1995.
5. W. L. Johnson: (private communication)
6. J. W. S. Rayleigh: Phil. Mag. 14, 184-186, 1882.
7. H. Lamb, Hydrodynamics, 6th ed., Cambridge University Press, 473-639, 1932
8. J. Q. Feng and K. V. Beard: Proc. R. Soc. London. A. 430, 133, 1990
9. W. K. Rhim and A. J. Rulison: "Surface tension and viscosity measurements of molten materials by electrostatic levitation." JPL New Tech. Report, Item No. 9063, Docket No. 194582.

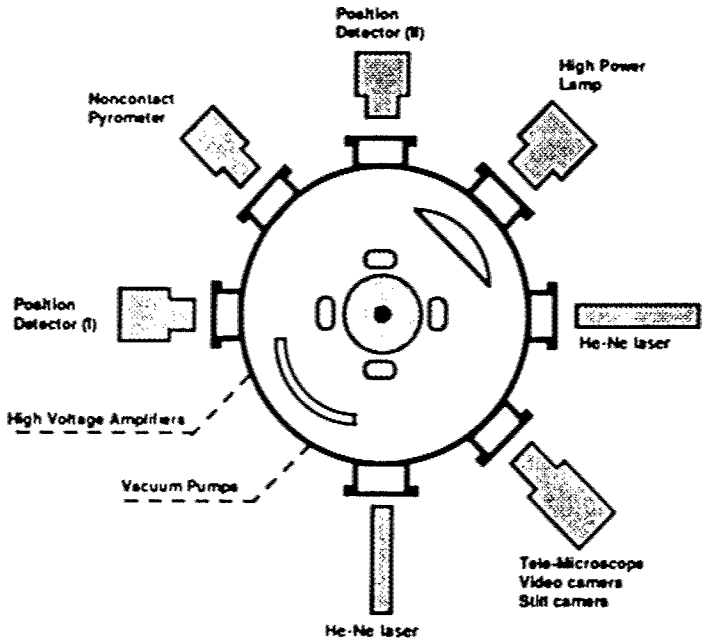


Fig. 1. A schematic diagram of the high temperature electrostatic levitator designed for the ground base applications.

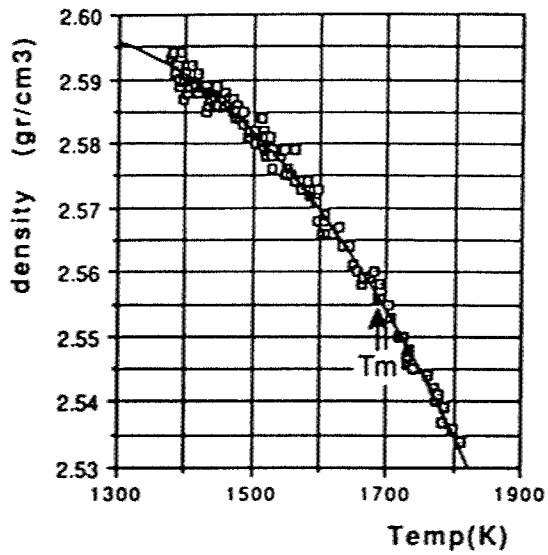


Fig. 2. Density of a molten silicon measured by the HTESL assisted by a newly developed imaging and processing techniques.

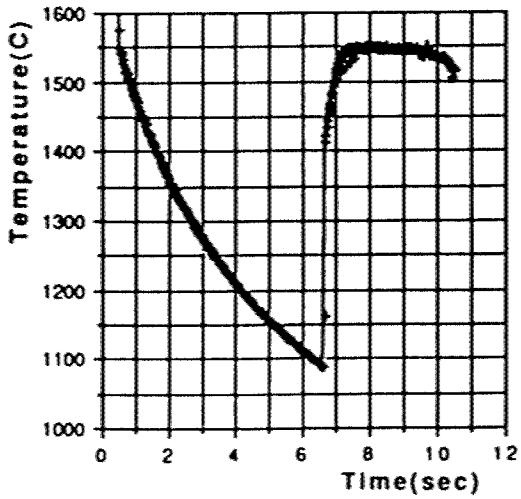


Fig. 3. A typical cooling curve of molten silicons as they are subjected to a purely radiative cooling with the heating beam blocked.

# UNDERCOOLING LIMITS AND THERMOPHYSICAL PROPERTIES IN GLASS-FORMING ALLOYS

Won-Kyu Rhim, Principal Investigator
Jet Propulsion Laboratory, California Institute of Technology
4800 Oak Grove Drive, Pasadena, California 91109 Mail Stop 183-401, Tel: (818) 354-2925,
e-mail: won-kyu.rhim@jpl.nasa.gov

Prof. R.Erik Spjut, Co-Investigator
Harvey Mudd College, Claremont, CA 91711, Tel: (909) 607-3890

Dr. Kenichi Ohsaka, Co-Investigator
Jet Propulsion Laboratory, California Institute of Technology, Mail Stop 183-401,
Tel: (818) 354-3111

## Introduction

Glass formation from the molten state requires undercooling to a characteristic temperature known as the glass transition temperature $T_g$, while avoiding the nucleation of crystallites. If the liquid can be cooled to Tg without appreciable crystallization, a glass is formed. The glass-forming ability of melts is greater for higher values of the reduced glass transition temperature $T_{rg}$ ($=T_g/T_m$) which is typically in the range of 0.5 - 0.67. For marginal glass formers, with low $T_{rg}$, rapid quenching is used to form glasses. However, it is known from devitrification experiments that nucleation is not totally avoided during rapid quenching. The material remains amorphous because there is insufficient time for significant crystal growth. On the other hand, for good glass formers (e.g. PdNiP alloy with $T_{rg}$=0.67), the population density of internal nucleation sites can be very low with most crystal nucleation coming from the sample surface. In these materials the homogeneous nucleation frequency is so low that a clean processing, in particular, the containerless processing, can dramatically reduce the critical cooling rate by eliminating most heterogeneous nucleation sites.

There are several factors which are known to influence the maximum undercooling. These are the mean sample size, the nature of the sample surface, the cooling rate, the melt superheat, and the composition of the sample. A number of different methods, such as the drop dispersion

technique, the fluxing technique, the drop tube technique, and various levitation techniques, have been devised to control some, if not all, of these factors. The most notable of these methods, the droplet emulsion technique has succeeded in achieving remarkable undercooling. As low as $0.5T_m$ has been reached, and thermodynamic properties of various undercooled liquids have also been successfully measured.[1] However, because of the volatility and instability of most carrier fluids, this method has a rather limited temperature range. Alternative methods to undercool bulk samples are fluxing techniques where the liquid is encased in inorganic glasses. This method has been successful in undercooling bulk samples[2]. Kui et.al.[3] has demonstrated the glass formation of Pd-Ni-P melts embedded in liquid $B_2O_3$ with cooling rare as low as 1 K/s. In this method, however, the melt is in contact with fluxing material which might change the surface property of the melt due to dissolution of impurities and due even to the flux itself.

The drop-tube method is basically a containerless method using the reduced gravity conditions during free fall. Turnbull and his co-workers used this method for nucleation studies in undercooled $Pd_{83}Si_{17}$ and $Pd_{82}Si_{18}$ droplets of 50-370 μm in size[4]. Similar experiments have also been conducted by Steiberg et.al.[5] using the 32 m drop tube at NASA's Marshall Flight Center with $Pd_{77.5}Si_{16.5}Cu_6$ alloy. They found that a sample size as large as 1.5 mm could be cooled to an amorphous state at an estimated cooling rate 500 K/s. The main drawback of this method is that it is impossible to follow the sample temperature during the fall. Without accurate temperature data it is impossible to gain a quantitative knowledge about the experiment.

The main motivation for this program is to revisit undercooling and glass forming under conditions where the sample can be accurately monitored, and where accurate measurements of the thermodynamic and kinetic properties of the sample can be performed *in situ*. The High Temperature Electrostatic Levitator (HTESL)[6] at JPL will be the main apparatus by which most thermophysical properties of the undercooled liquids will be measured. A single levitated sample can be subjected to repeated thermal cycling for increased statistical accuracy. For the studies of undercooling limits, we plan to construct a separate electrostatic levitator for small samples operating in ultra-high-vacuum conditions. With this small-sample levitator the sample-size dependence of the undercooling limit will be studied with sample diameter varying from 10 μm to 1000 μm. By combining these two levitators, all the factors which affects undercooling (the sample size, the nature of the sample surface, the cooling rate, and the melt superheat) can be controlled for a rigorously quantitative investigation of undercooling and the nucleation/glass-formation processes.

## Research Objectives

This program has two groups of research activities, one following the other in their order of implementation. Initially, thermophysical properties and critical cooling rates of easy glass-forming alloys will be measured using the existing HTESL. Then, upon completion of the small droplet levitator, the studies of undercooling limits, nucleation mechanisms, and the glass-formation process will be carried out with increasingly reluctant glass formers.

The research objectives can be summarized as follows:

(i) Investigation of undercooling limits in glass-forming alloys, as those factors that limit undercooling are systematically controlled. Factors that are examined are sample surface condition, sample volume, cooling rate, and material-dependent factors such as viscosity and interfacial energy between solid and liquid, etc.

(ii) Thermophysical property measurements and investigation of the validity of the classical nucleation theory and other existing theories in the extreme undercooled states. Thermophysical quantities that will be measured as a function of undercooling level are heat capacity, hemispherical total emissivity, surface tension, viscosity, mass density, and thermal expansion coefficient.

(iii) Investigation of morphological and micro-structural development during solidification from deeply undercooled melts. Factors which are investigated through analysis of processed samples are the morphology of metastable crystalline or amorphous phase, and the dependence of microstructure on undercooling level, etc.

(iv) Evaluation of the limits of applicability of electrostatic levitation for containerless materials processing in the 1-g environment. Although considerably less flows are expected with the HTESL, little is known about the flows induced by the electrostatic forces. Most seriously affected by the flows might be those transport properties such as atomic diffusion, viscosity, and thermal diffusivity. In this ground based program, we will define the limits of the HTESL technology as various thermophysical properties are measured.

(v) Development of a Small Particle Electrostatic Levitator (SPESL) to change the sample volume by 6 orders of magnitude. Design and tests of several basic technologies such as the structure of electrode assembly, sample launch and position detection systems, and the particle charging and heating systems will be conducted. These are the core technologies for the construction of a SPESL. Actual construction of a SPESL should wait for the availability of additional funding.

Technical Approaches

The main work horse for this program is the High Temperature Electrostatic Levitator (HTESL)[6] which was recently developed at JPL. In the HTESL, samples are melted while in levitation in a high vacuum condition. The charged sample is levitated electrostatically by a set of electrodes connected to high voltage amplifiers. The sample is charged initially by capacitive charging. Once the sample is levitated, the sample charge is maintained either by thermionic emission or by photoemission. Figure 1 shows a schematic diagram of the electrode assembly. The levitation chamber contains the electrode assembly and optical components to direct the heating beam to the levitated sample, and various equipment surrounding the chamber which are required for the levitation. The sample position is optically sensed, and feedback loop controls the high-voltage level to maintain the sample at a desired position. The largest sample mass that can be levitated is approximately 200 mg, which corresponds to a lead sample approximately 3 mm in diameter. The chamber is evacuated to an ultimate vacuum of $2 \times 10^{-8}$ torr. A 1000 watt xenon-arc lamp is used to heat the sample up to approximately 2300 K. Measurement of a specific thermophysical property requires an additional non-contact diagnostic instrument. In this program we are investigating the undercooling behavior of a single droplet which is levitated in an ultra-high vacuum. A stably levitated sample will go through a certain predetermined thermal (or mechanical excitation) cycles while the drop response is accurately monitored.

Advantages of this approach are:

a) By conducting experiments in an UHV condition, the sample will be well protected from contamination. Furthermore, the sample materials may even be purified as volatile impurities evaporate as the sample goes through repeated thermal cycle.

b) Samples are no longer limited to low-melting materials unlike the droplet emulsion and fluxing techniques. In fact, if the drop size is small, most refractory materials can be melted with affordable laser power.

c) Unlike the drop tube technique, the sample stays at a fixed point in space for practically indefinite period of time. In fact the whole statistical behavior of nucleation events can be obtained using a single sample particle.

d) Thermophysical properties such as the mass density and volume expansion coefficient[7], the specific heat capacity to the hemispherical total emissivity ratio[8], the surface tension[9,10] and the viscosity can be measured at the present time. Figure 2 is a typical damped oscillation obtained from a freely oscillating molten drop. The surface tension and viscosity can be obtained from the observed resonance frequency and the damping time constant, respectively.

e) Critical cooling rates for glass formations can be determined along with the Temperature-Time-Transformation (TTT) or the Continuous Cooling Nucleation (CCN) curve. Indeed, the feasibility of glass formation in a levitated alloy was successfully demonstrated recently at JPL along with the determination of its critical cooling rate[11].

f) Using the Small Droplet Electrostatic Levitator the droplet size along with the cooling rate can be changed by two orders of magnitude. This means that the number of heterogeneous nucleants in the drop can be varied by 6 orders of magnitude, and those on the drop surface by 4 orders of magnitude.

## Summary

This is the first year of this program. This program will focus on amorphous-phase formation in glass-forming alloys with particular emphasis on their thermophysical properties, factors that limit their undercooling, and their critical cooling rates to reach glass states. This work is being carried out in collaboration with Professor William Johnson at Caltech and Professor Robert Bayuzick at Vanderbilt University. Identifying the limits of the HTESL in the gravity environment for its capability of measuring various thermophysical properties is also an important part of this program.

## References


1. J. H. Perepezko and W. H. Allen: Proc. 3rd Int. Colloq. on Drops and Bubbles, AIP Cof. Proc. 197, p289, 1989, ed. by T. Wang
2. T. Z. Kattamis and M. C. Flemings: Trans. AIME, 236, 1523, 1966
3. H. W. Kui, A. L. Greer, and D. Turnbull: Formation of Bulk Metallic Glass by Fluxing, Appl. Phys. Lett. 45, 615, 1984
4. A. J. Drehman and D. Turnbull: Solidification Behavior of Undercooled $Pd_{83}Si_{17}$ and $Pd_{82}Si_{18}$ Liquid Droplets. Scripta Metall. 15, 543, 1981
5. J. Steinberg, A. E. Lord, Jr., L. L. Lacy, and J. Johnson: Production of Bulk Amorphous $Pd_{77.5}Si_{16.5}Cu_6$ in a containerless low-gravity environment, Appl. Phys. Lett. 38, 135, 1981
6. W. K. Rhim, S. K. Chung, D. Barber, K. F. Man, Gary Gutt, A. Rulison, R. E. Spjut.: An Electrostatic Levitator for High Temperature Containerless Materials Processing in 1-g, Rev. Sci. Instrum .64, 2961, 1993.

7. S. K. Chung, D. Thiessen, and W. K. Rhim: "A non contact measurement technique for the density and thermal expansion of molten materials." Rev. Sci. Instrum. in press.
8 A. J. Rulison and W. K. Rhim: "Constant pressure specific heat to hemispherical total emissivity ratio for undercooled liquid nickel, zirconium, and silicon." Metal. and Materials Trans. B, 26, 503, 1995.
9. W. K. Rhim and A. J. Rulison: "Surface tension and viscosity measurements of molten materials by electrostatic levitation." JPL New Tech. Report, Item No. 9063, Docket No. 194582.
10. W. K. Rhim and A. J. Rulison: "Thermophysical properties of molten silicon", Int. J. Thermophysics (in press).
11. Y. J. Kim, R. Busch, W. L. Johnson, A. J. Rulison, and W. K. Rhim: Appl. Phys. Letts. (in press)

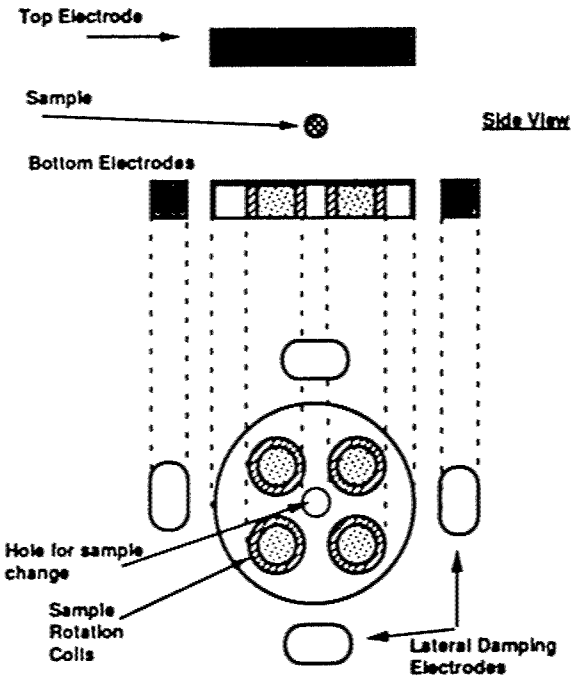


Fig. 1 Schematic diagram of an electrode assembly. Four side electrodes control the lateral position stability.

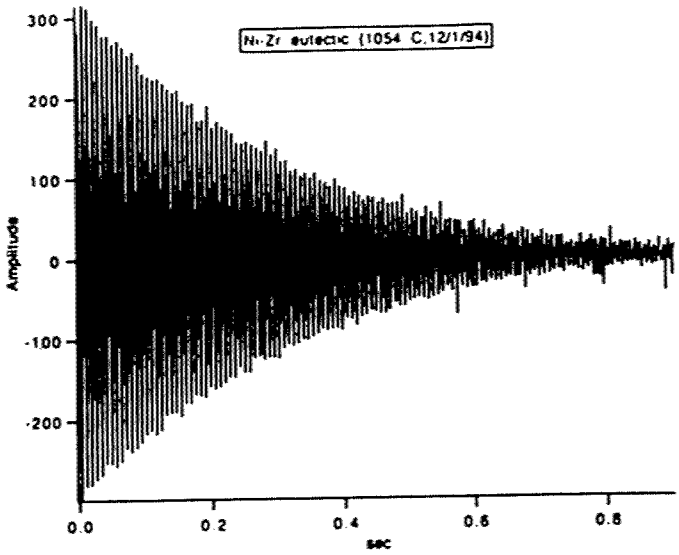


Fig. 2. A free oscillation taken from a molten Zr-Ni alloy.

# A STUDY OF THE UNDERCOOLING BEHAVIOR OF IMMISCIBLE METAL ALLOYS IN THE ABSENCE OF CRUCIBLE-INDUCED NUCLEATION

T. J. Rathz
University of Alabama in Huntsville
Huntsville, AL 35899
205-544-1409; tom.rathz@msfc.nasa.gov

M. B. Robinson
NASA/Marshall Space Flight Center
Huntsville, AL 35812
205-544-7774; mike.robinson@msfc.nasa.gov

## Introduction

Previous studies[1-6] have shown that the amount of undercooling in liquid immiscible metals is determined by the relative volume fraction of the components and, in particular, the minority phase's wettability and separation at the container/sample interface. Several theories[7,8] have predicted an asymmetry about the critical composition ($C_c$) in the wetting versus composition diagram and in the amount of undercooling. However, the degree of undercooling predicted from theory varies significantly from that minuscule amount of available experimental data. There has been only one reported investigation of low-gravity AND true containerless solidification of metal immiscibles.[9] This study showed promising results for attaining a dispersed morphology of minority phase droplets and some undercooling.

The primary objective of this work is to determine if processing immiscible metals in a containerless environment will alter the surface wetting mechanism and the extent to which this will lead to changes in the subsequent nucleation kinetics. The 105-meter Drop Tube Facility at Marshall Space Flight Center provides a low-gravity, containerless, and quiescent environment for this study.[10] Several metal systems will be discussed here that have been initially examined after processing in the Drop Tube.

## Experimental Method

In the belljar atop the Drop Tube, the samples were melted in a levitation coil powered by a 10 kW Lepel generator. Temperatures in the belljar were measured with an Ircon Modline 2-color pyrometer. Six-nines pure argon or helium gas was used for forced-convective cooling or to prevent the coil from arcing in a vacuum when the sample was too vaporous. The incandescence of the falling drops was monitored with Si photodiodes spaced every 7.4 meters along the Drop Tube's length and with a time-marked CCD camera. Recalescence could then be determined as a function of free-fall time from which calculated undercoolings can be obtained. Post-processing analysis was performed with a Hitachi Model S4100 field emission scanning electron microscope (SEM) with energy dispersive spectroscopy (EDS) capability.

All starting materials were made from bulk supplies of at least 3-nines purity. The vanadium had to be etched to remove an oxide layer. All materials were then arc-melted into alloy pellets about 5mm diameter. As expected, all arc-melted samples showed a distinct separation of the two constituents which prompted little analysis at this time.

## Preliminary Results

Several systems of immiscible metals were selected for initial study, one of which was Sn-Cr(59w/o). The phase diagram can be found in Figure 1a. When samples of these materials were melted in a gas atmosphere, significant vaporization occurred creating a plume which sometimes blocked the pyrometer view; or, if processed in a vacuum, arcing of the levitation coil occurred. Additionally, the sample did not remain stable within the coil as it was being heated through the liquid-liquid region of the miscibility dome: the samples either sheared themselves apart from uncontrolled spinning or fell out of the coil with a large horizontal velocity component which made them hit the Tube walls. However, several samples were controlled and heated above the critical consolute temperature ($T_c$ ~1485°C) before release. One sample reached 1690°C before losing its levitability and falling out of the coil. For this sample, recalescence was observed after ~1.5 second of free-fall.

Internal examination of this spherical sample made by the SEM indicated an overall chemical composition of 66 w/o Sn. From the original composition, this indicates a significant loss of Cr had occurred in the arc-melting and/or the Drop Tube processing. This composition was still well within the immiscibility dome range (40-74 w/o Sn) and just slightly hyper-critical ($C_c$ ~62 w/o Sn). Figure 2 is the SEM photograph of the microstructure showing a uniform distribution of dendritic clusters. The dendrites are composed of 97 w/o Cr ($\alpha$-phase) resting in a 2-nines pure Sn matrix, as predicted by the equilibrium phase diagram. Solidification must not have been rapid enough to cause any extension of the solubility of the $\alpha$-phase.

Samples of Ti-Ce(74 w/o) composition, were also processed. The Ti-Ce phase diagram can also be found in Figure 1b. Due to cerium's extremely small equilibrium oxygen partial pressure(less than $10^{-30}$ atmospheres at 1000°K), great care was taken in sample preparation. Flowing argon in a glovebox was used for cutting and weighing the materials, and the cerium and alloys were stored under ethanol. These samples were then processed in a 630 Torr He atmosphere resulting in very little vaporization. However, most of the samples that were retrieved from the Tube had a yellowish tint on the surface indicating oxidation.

One sample that was released at a temperature of about 260 degrees above $T_c$ (~1660°C) appeared to have recalesced about 1.7 seconds into free-fall. Figure 3 shows the internal morphology of this sample. The constituents have almost completely separated into the concentric sphere configuration. The inner large sphere consist of Ti(78 w/o) and the smaller satellite spheres of Ti(82 w/o). The outer shell is 3-nines pure Ce. A noticeable

separation exists between the outer shell and inner sphere indicating a lack of wetting at the interface between the two phases. Since the Ti coalesced and solidified before the Ce solidified, the temperature would have dropped from the release temperature of 1920°C to the monotectic temperature of 1450°C within the first two seconds of free-fall.

Oxygen analysis of the Ti-Ce materials was performed by Leco Corporation and is presented in Table 1. The Drop Tube samples had 1000 ppm more of oxygen than the sum of that found in the original constituents but less than that found in the samples which had only undergone the arc-melting process. This might be attributable to the amount of Ce surface area exposed from severely separated arc-melted samples versus the Drop Tube sample.

Table 1. Oxygen Concentration, ppm, in 99.99% Ce and 99.99+% Ti.

| | Manufacturer's Specifications | LECO Analyzed | | |
|---|---|---|---|---|
| | Pure | Pure | Arc-Melted Alloy | Drop Tube Alloy |
| Ce | NA | 690 | 6700 | 2860 |
| Ti | 400 | 1170 | | |

Future Plans

Of those materials initially studied in this work it was found that the levitation coils and processing conditions need to be optimized to attain more stable levitation and good pyrometry. This is a known problem when trying to overheat liquid metals in levitation coils which lowers the viscosity and causes instability. If stable levitation can be accomplished, then it has been shown that quantifiable undercooling can be observed. If the following cannot be achieved, then other furnace capabilities such as a dripper furnace may be needed to eliminate the vapor loss and allow stable heating through the immiscible dome of systems yet to be attempted.

From the initial research presented herein, it has been shown that the objectives of this research should be attainable. The objectives of this research may also be reached in a less-arduous manner by performing low-temperature experiments in other facilities. These experiments could be performed in most levitation devices (one-g). However, for the low-g experiments the longer cooling times needed for lower temperatures may rule out the use of all microgravity facilities except the long-duration capability of the Shuttle. A low temperature apparatus such as the Microgravity Electromagnetic Levitation (MEL) system or the Electrostatic Levitator would provide direct and distance-invariant optical observation of the drop and its temperature. Also, since heating and levitation are independently controlled, this would provide heating the liquid-liquid immiscible through the miscibility dome while independently eliminating the destructive spinning or oscillations that occur in other levitation systems.

References

1. Gelles S. H. and Markworth A. J., 15th AIAA Conf., Los Angeles 1977, paper 77-122.
2. Potard C., 17th AIAA Conf., New Orleans 1979, paper 79-0173.
3. Ahlborn, H., Lohberg, K., 17th AIAA Conf., New Orleans 1979, paper 79-0172.
4. Perepezko J. H., Galup C., Cooper K.P., in **Materials Processing in the Reduced Gravity Environment of Space** (Guy Rindone, ed., Elsevier Science Pub. Co., Amsterdam, 1982), p. 491.
5. Uebber N. and Ratke L., Scripta Mettall., 25, 1133(1991).
6. Granasy L. And Ratke, L., Scripta Mettall., 28, 1329(1993).
7. Cahn J. W., J. Chem. Phys., 66(8), 3667(1977).
8. Teletzke G. E., Scriven L. E., Davis T. H., J. Colloid Interface Sci., 87(2), 550(1982).
9. Andrews J. B., Briggs C. J., Robinson M. B., in Proc. 7th European Symposium on **Materials and Fluid Sciences in Microgravity** (Oxford, UK, ESA SP-295, 1989), 121.
10. Rathz, T.J., Robinson, M.B., Hofmeister, W.H., Bayuzick,R.J.,"The Marshall Space Flight Center Drop Tube Facility", Rev. Sci. Instrum.,61(12), 3846 (1990).


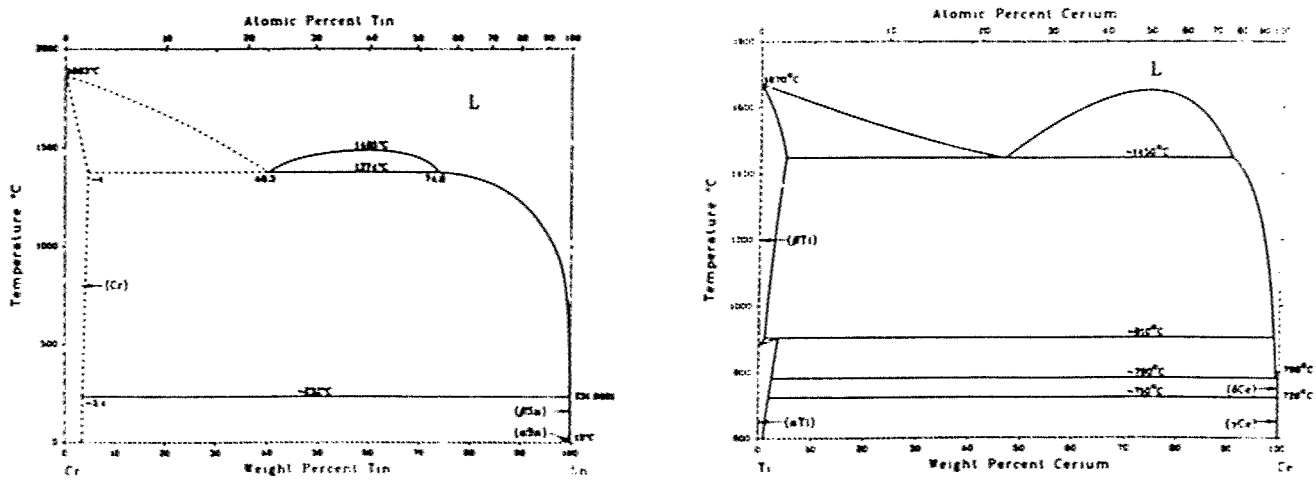


(a) (b)

Figure 1. The phase diagrams of (a) Cr-Sn and (b) Ti-Ce.

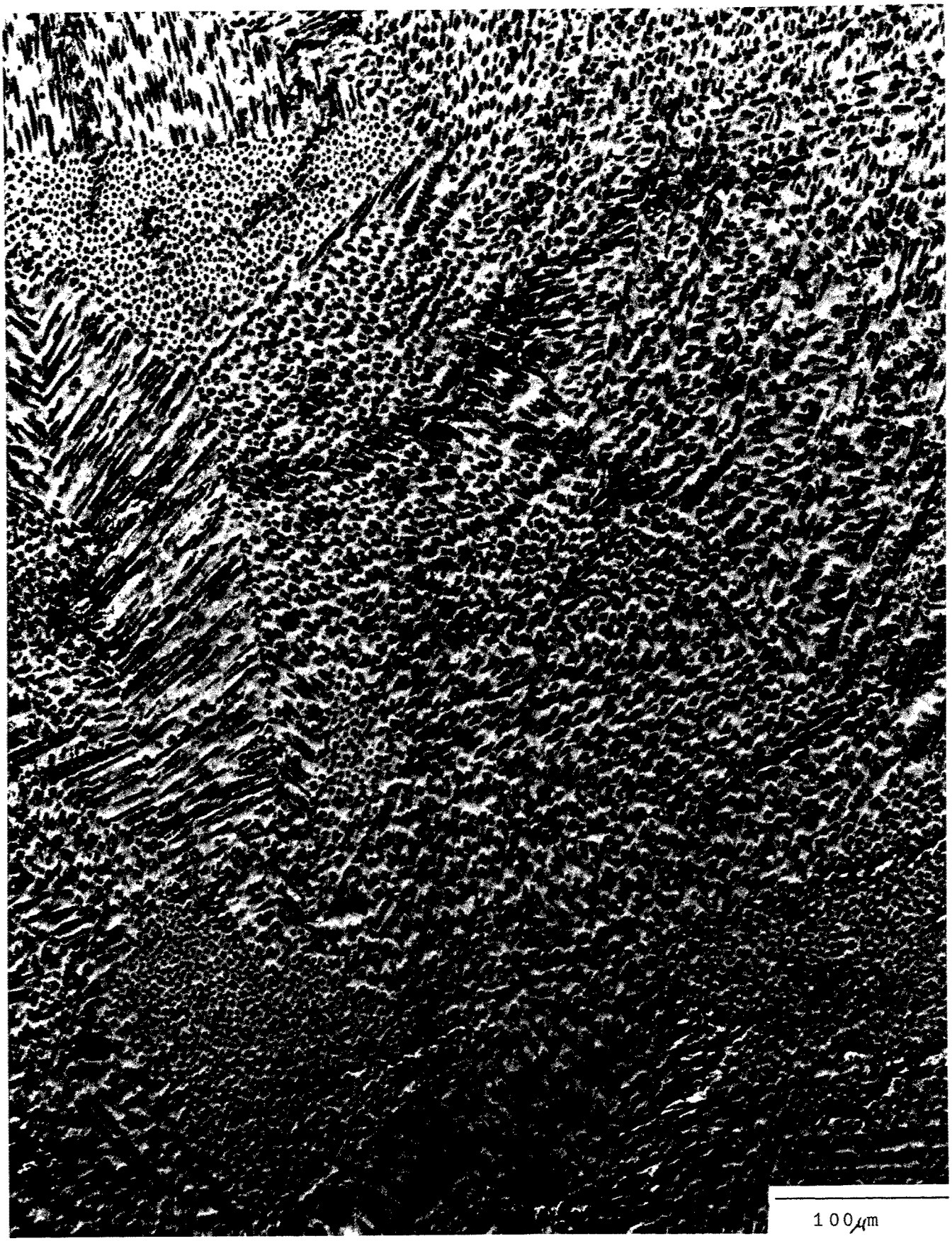


Figure 2. SEM image of Drop Tube processed Sn-Cr sample.

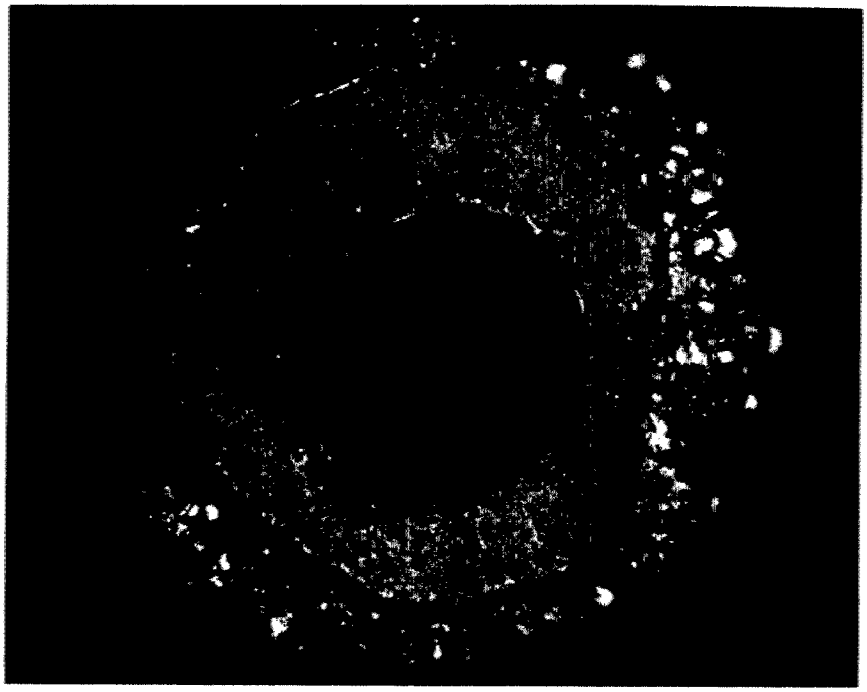

(a)

(b)

Figure 3. Drop Tube processed Ti-Ce. Dark areas are Ti; lighter, Ce. (a) Optical microscope view at 16x magnification showing Ti spheres contained within a Ce shell. Dark "bubbly" area outside Ce shell is mounting material. (b) SEM 500x @ 300dpi view of the Ti-Ce interface.

# SELF-DIFFUSION IN LIQUID ELEMENTS

Franz Rosenberger, R. Michael Banish, J. Iwan D. Alexander,
Lyle B. Jalbert and Ricky J. Roberson
Center for Microgravity and Materials Research
University of Alabama in Huntsville
Huntsville, Alabama 35899, USA
phone:(205) 895-6050, e-mail: fros@cmmr.uah.edu

## Background

With increasing insight into transport and segregation in solidification and crystal growth, reliable data for diffusivities in liquid metals and semiconductor have become essential for guidance in process development. However, at this point even *self*-diffusion in elemental liquids is not well understood, let alone binary and ternary diffusion. In particular, there is little insight into the temperature dependence of diffusivities and its correlation to the temperature-dependent liquid structure of an element. Currently, the differences between several theoretical predictions are often less than those between different sets of data for the same system. Hence, for both theoretical and technological developments, there is a clear need for diffusivity measurements of improved accuracy and precision for a large variety of elements over wide temperature ranges.

The exclusion of convective contamination in liquid diffusion studies is difficult. Measurement techniques, such as nuclear magnetic resonance and inelastic neutron scattering, that probe the rapid molecular motion are insensitive to convective contributions, but are not as precise as macroscopic, averaging techniques. However, all macroscopic measurement techniques yield diffusivity data prone to be contaminated by gravity-driven convection. The use of narrow capillaries to suppress convective transport has revealed poorly understood wall effects. Magnetic fields, widely used for suppressing convection in conducting liquids, modify the diffusive motion itself. Earlier liquid metal diffusion studies conducted on spacecraft have demonstrated the *gain in precision* resulting from the drastic reduction of convection in a low-gravity environment. However, by comparison with ground-based experiments, these data appear rather *inaccurate*. Hence, there is a need for well defined liquid diffusion studies under low gravity.

## Objectives

The scientific objectives of this research project include the

- accurate measurement of self-diffusivities of liquid elements (selected for their class-like structure properties) and their temperature dependence;
- interpretation of the measured diffusivities in terms of diffusion mechanisms and associated classes of liquid structures;
- investigation of the "wall effect" believed to contaminate diffusivity measurements in capillaries;
- characterization of convective contamination of the diffusivity measurements on Earth through numerical modelling;

The technical objectives consist of the

- development of an efficient technique for dynamic *in-situ* measurements of diffusivities in melts as a function of temperature;
- design and construction of flight-certified hardware for automated measurement of diffusivities at several temperatures per sample.

## Experiment Concept and Approach

We have developed a novel technique for the measurement of diffusivities in liquids. In this approach, as schematically depicted in Fig. 1a, the cylindrical diffusion sample consists of a pure

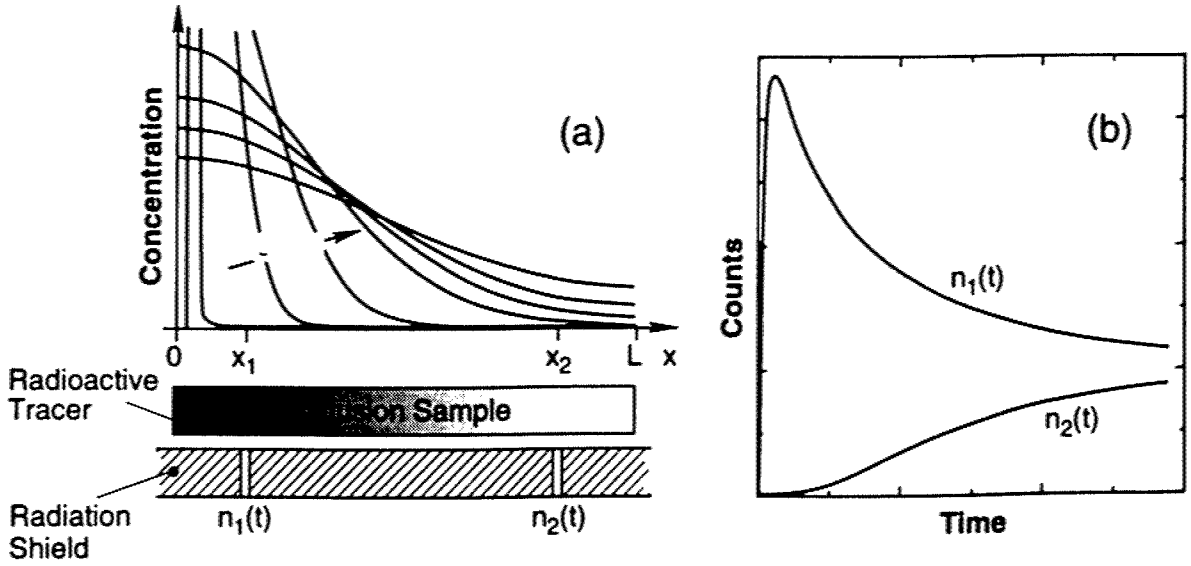


Fig. 1. Schematic of real-time diffusivity measurement technique and signal output.

material, with an activated isotope, initially located at one end, as the diffusant. The sample is positioned in a concentric isothermally heated radiation shield, with two bores that act as radiation collimators. These bores are located x = L/6 and 5L/6 to satisfy the requirement of the numerical scheme used to evaluate the diffusivity [Codastefano et al., Rev. Sci. Instr. 48 (1977) 1650]. After melting of the sample, the intensity of the radiation emitted through the collimators is monitored throughout the experiment with solid state detectors and associated energy discrimination electronics. Corresponding signal traces $n_1(t)$ and $n_2(t)$ obtained at a given temperature are plotted in Fig. 1b. The diffusivity, D, is calculated from the difference of the signals using Codastefano et al.'s relation

$$\ln [n_1(t) - n_2(t)] = \text{Const} - (\pi/L)^2 D t .$$

Since the data are obtained in real time, diffusivities can be consecutively determined at several temperatures during the spreading of the concentration profile in one sample. This is advantageous for experiments under reduced gravity, particularly given the limited flight opportunities and flight time of space craft.

By employing an isotope which emits photons at two sufficiently different energies and, thus, different self-absorption behavior, transport in the bulk of the sample and near the container wall can be distinguished to some extent. As an illustration of this approach, Fig. 2 presents for two different emission energies the fraction of the total radiation measured outside a sample of In *vs.* the thickness of the sample. One sees that the 24 keV photons received originate in essence only from a 300 μm deep surface layer. The 190 keV photons, on the other hand, stem from throughout the sample. Thus, using an appropriate detector circuit with energy discrimination capability, some distinction between transport near the wall of the sample container and in the sample bulk can be made in real-time.

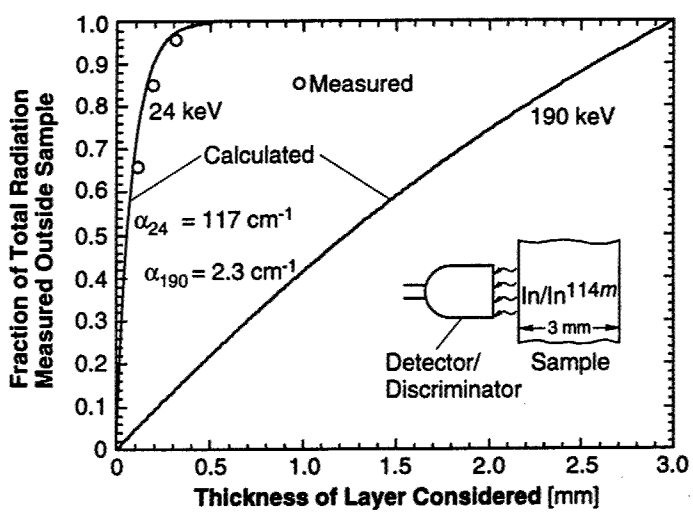


Fig. 2. Emission depth limitation in indium due self absorption.

Numerical simulations of convective contamination in diffusivity measurements

In order to provide guidance for our, and other, experimental work, we have numerically modeled the time-dependent and three-dimensional diffusive-convective transport in typical diffusion experiment geometries with slightly asymmetric thermal boundary conditions. We found that even in capillaries, very small temperature nonuniformities across the sample result in convective transport that largely exceeds diffusion. This is illustrated in Fig. 3 for transport in a vertical cylinder of liquid indium (diffusant of same mass density as that of the sample initially contained in a 0.3 mm high bottom layer) for a horizontal temperature gradient of 0.1 K/mm. Note that the diffusivity, deduced from the signal traces that represent the evolution of the radially averaged concentration values, is almost 3 times larger than the input diffusivity. Most strikingly, the diffusive-convective transport results under these conditions in profiles of the radially averaged concentration values that are analytically indistinguishable from pure diffusion profiles. This can be seen from the perfect linearity obtained in the ln $[n_1(t) - n_2(t)]$ plot in Fig. 3. This finding casts considerable doubt on various "straight line" or "exponential profile" criteria previously used to demonstrate the absence of significant convective contamination in diffusivity data plots.

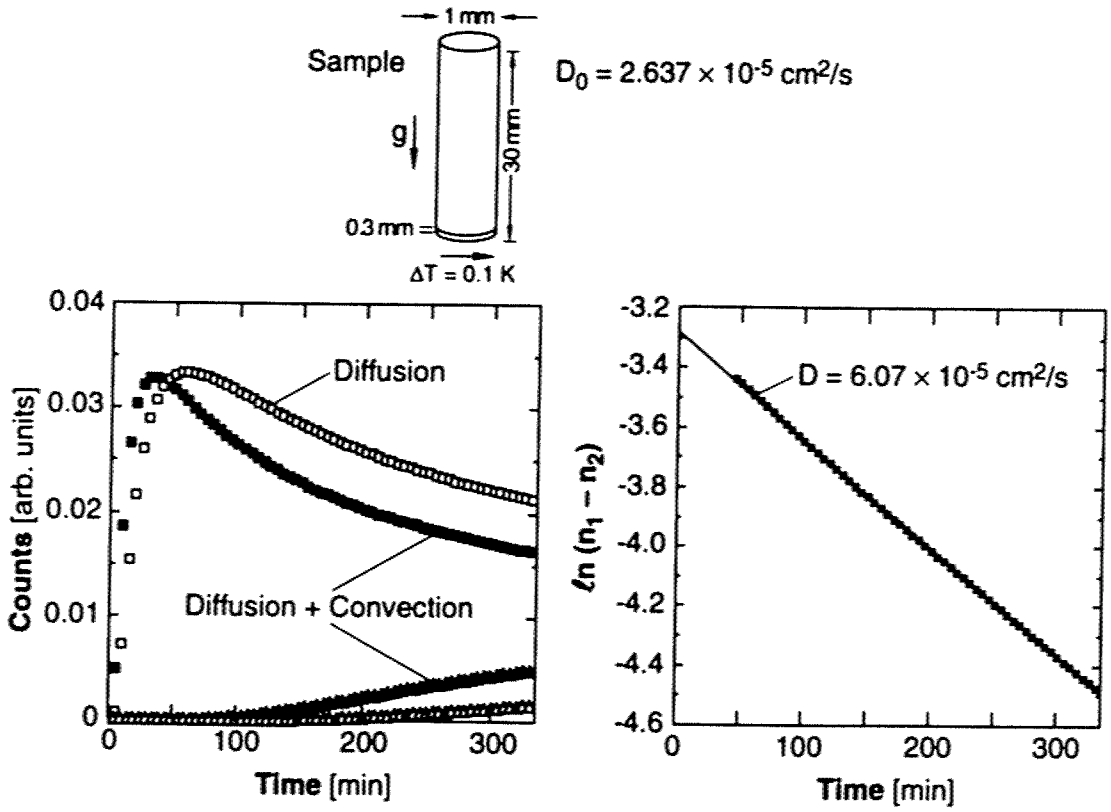


Fig. 3. Three-dimensional simulation of ground-based diffusivity measurement in sample with slight temperature nonuniformity.

## Hardware Development

In response to an imminent flight opportunity aboard MIR utilizing the Microgravity Isolation Mount (MIM), we have developed and constructed a low temperature (200 °C) version of our wide-temperature-range diffusion experiment instrumentation to be flown later on either the Shuttle or the Spacestation. Measurements to be conducted with $In/In^{114m}$ on the MIM in early 1997 under defined residual accelerations will provide data for comparison with our numerical modeling results as well as guidance for the planned high temperature experiments. Fig. 4 represents cross-sectional views of (a) the diffusion sample cartridge and (b) the diffusivity measurement apparatus with sample exchange carousel.

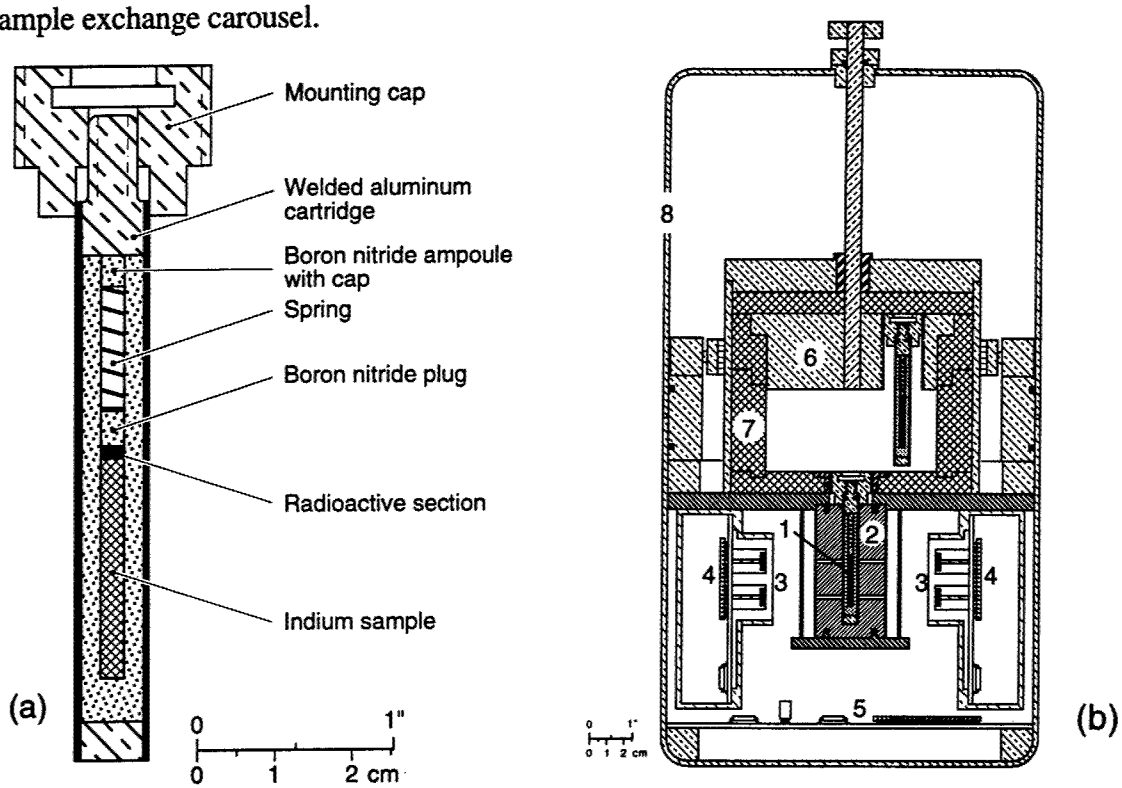


Fig. 4. Cross-section through components of semi-automatic diffusivity measurement apparatus. (a) Cartridge with spring-loaded diffusion sample. (b) Complete payload with 1: Diffusion sample in cartridge inside heated isothermal liner/ radiation shield 2. 3: CdZnTe detector pairs with preamplifier/discriminator circuits 4. 5: Circuit boards for experiment control, programming and data storage. 6: Carousel with 4 additional sample cartridges. 7: Lead pig. 8: Sealed housing.

## Diffusivity Measurements

Fig. 5 presents data obtained with the above low temperature apparatus for $In/In^{114m}$ on Earth. The values for the diffusivity given in Fig. 5b illustrate the high precision of this novel diffusivity measurement technique.

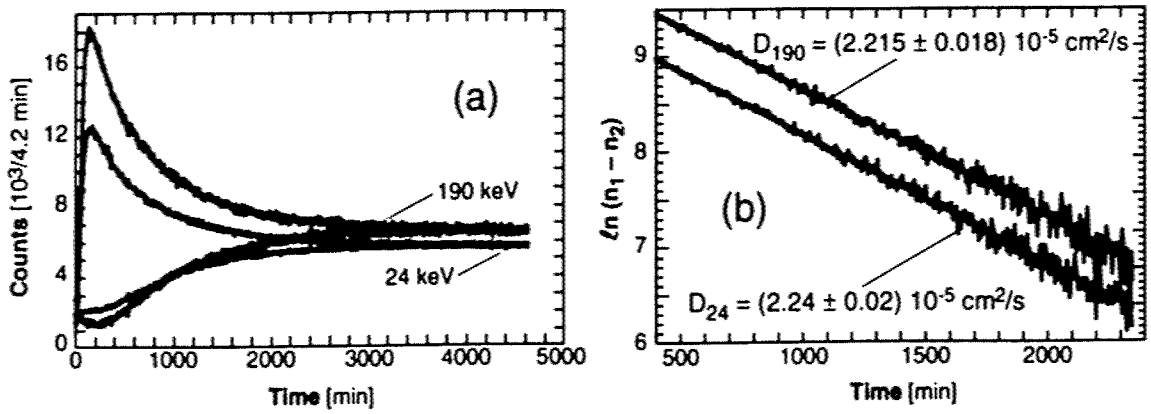


Fig. 5. Ground-based results of diffusion measurements with In/In$^{114m}$.

## Choice of Elements

Based on diffraction data, one can distinguish between elements that are known to or can be expected to undergo structural changes at temperatures above their melting points, and elements that do not undergo such changes. Such "second liquid structures" occur in elements that are dominantly covalently-bound in their solid form. Diffusivity studies of a few of the elements with such transitions have revealed pronounced nonmonotonic temperature dependencies D(T). By analogy, we expect all other elements in this category to show structure-change revealing D(T)'s when measured over a wide temperature range. Hence, as indicated in the following partial Periodic Table, we have grouped, for the first time, the relevant elements into those with expected monotonic and nonmonotonic D(T) behavior, indicated by open and full symbols, respectively. In addition to the behavioral predictions, the table contains the melting and boiling points, the radioactive isotope suitable for diffusion studies with their half-life and photon energy. If an isotope possess two different photon energies, that is also indicated. Based on these considerations, we plan to study In, Na, Cd, Ga, Sn, Te and S.

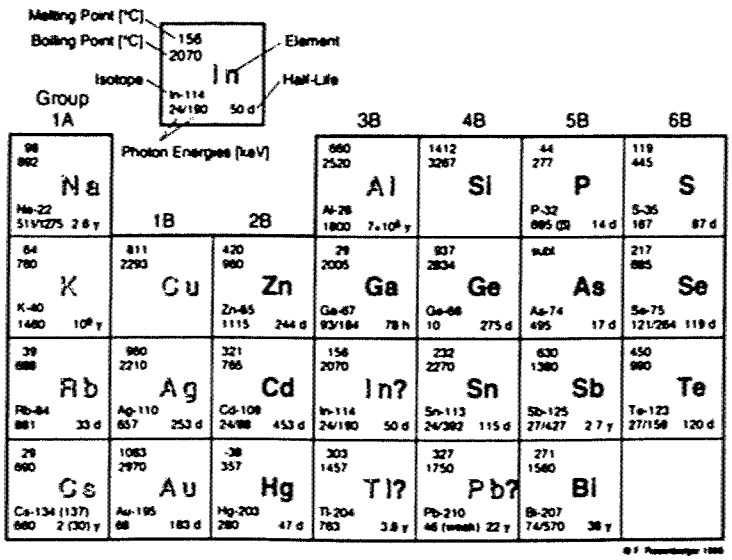

# DETERMINATION OF THE SURFACE ENERGY OF SMECTIC LIQUID CRYSTALS FROM THE SHAPE ANISOTROPY OF FREELY SUSPENDED DROPLETS

Charles Rosenblatt and Philip L. Taylor
Department of Physics
Case Western Reserve University
Cleveland, Ohio 44106-7079 USA
Tel: 216-368-4125 (CR) and 216-368-4044 (PLT)
E-mail: cxr@po.cwru.edu (CR) and plt@po.cwru.edu (PLT)

## Background

We plan to undertake a program of ground-based experimental studies of the surface shape of droplets of nematic and smectic liquid crystals suspended in an intense magnetic field gradient. This experimental arrangement mimics microgravity in a ground-based system, and facilitates the levitation of nearly all organic materials. The initial goal of this work will be to determine the fundamental properties of these materials by determining the anisotropy in their surface energy. The ultimate goal will be to determine how best to design flight experiments that can yield the same information when the perturbing effects of magnetic field used for levitation are absent.

This research will include an experimental and a theoretical component. The experimental work will be concerned with the magnetic levitation of droplets of liquid crystals in a carefully designed magnetic field gradient and the associated measurements of their shape and curvature. The theoretical component will be devoted to the interpretation of the shape measurements in terms of the anisotropy of the surface energy of the materials.

The principal advantage of measurements on levitated droplets is the absence of the perturbing effects of the solid substrate on which the material would otherwise rest in a ground-based experiment. It is the long-range orientational ordering of liquid crystal molecules that is responsible for the fact that the molecular orientation in a droplet will generally be dominated by any contact the material has with a solid surface.

The motivation for this work arises from the fundamental scientific issues of surface tension in anisotropic systems, as well as the great importance of liquid crystals in the design and manufacture of flat-panel display devices. In order to design new systems and devices it will be necessary to have a complete understanding of the intrinsic properties of liquid crystals. Only by removing the perturbing effects of containers and substrates can we measure the coefficients that describe the behavior characteristic of a particular material. A levitating magnetic field is one way of removing the effects of contact with solid surfaces, although the magnetic field itself does add its own distortion of the droplet shape. The use of a microgravity environment would be the ideal means with which to perform these measurements.

## Concepts

When a sample of anisotropic material is in equilibrium with the isotropic phase of the same substance, the shape of the interface is determined by the variation of the surface free energy with orientation. Thus it is possible to study the anisotropic surface free energy by measuring the local curvature of a free surface. This type of measurement is readily possible in the presence of gravity for the case of a crystalline solid in equilibrium with its vapor, as the solid crystal generally has a binding energy per atom that is much greater than any gravitational potential energy.

Liquid crystals, however, form a special class of substances for which such measurements are difficult. In ground-based experiments the liquid crystal rests on a surface, and this surface imposes its geometry on the orientation of the liquid crystal molecules. This process is known as anchoring. One thus does not have access to a free surface unaffected by the influence of other materials.

These considerations become even more important when one wishes to observe dynamic effects related to rheological properties. The modes of oscillation of a freely suspended droplet are comparatively simple for an isotropic liquid, but become much more complex in the case of even as simple a liquid crystal as a nematic. For a smectic liquid crystal one finds that there are many components to the viscosity, and this makes interpretation of oscillations of a freely suspended droplet a complex (but feasible) operation. However, the presence of an anchoring substrate makes the analysis appear too complex for practical analysis. There is thus a great incentive to perform experiments on freely suspended droplets if one is to obtain some needed information about these technologically important materials.

Ideally, experiments to measure the surface curvature and normal-mode frequencies and damping times should be conducted in a microgravity environment. Before space-based studies are undertaken, however, we intend to begin with a series of ground-based investigations in a magnetic field that may approximate microgravity conditions. The diamagnetic susceptibility of most liquid crystals allows one to levitate droplets if one has access to a sufficiently large magnetic field gradient. While this has the disadvantage of introducing a new type of anisotropy into the system, it does completely eliminate the perturbing effects of the substrate, with all its attendant complications. It will thus provide an excellent test system in which to prepare for the later phases of the work, in which the effects of gravity can be removed without the need for a magnetic field gradient.

The goal of our work is to understand the anisotropic surface free energy (surface tension) of liquid crystals in the absence of a substrate. This is a particularly important problem both from a purely scientific and from a technological standpoint. Scientifically, the effects of orientational anisotropy and smectic layering on the surface energy are not well understood. For example, recent work on anchoring in smectic liquid crystals [1] claims to measure a molecular-based anisotropy in the surface tension. Nevertheless, the role of long-range smectic layering is not all clear. Even in the nematic phase, one fully expects surface-induced smectic order, as has been observed in high magnetic field Freedericksz experiments by one of us. [2]. An understanding of this effect in liquid crystals would additionally have a beneficial impact on such other fields as biomembranes and soap films [3]. From a technological perspective, liquid crystal display devices currently comprise a $10 billion worldwide market, and every such device must be housed in a sandwich between two pieces of optically transparent substrate material. The liquid crystal-substrate interaction may be characterized by an "anchoring strength" coefficient W, such that the energy cost associated with a reorientation by angle $\theta$ of the liquid crystal molecules from their equilibrium axis at the surface is given to lowest order in $\theta$ by $\frac{1}{2}W\theta^2$. Although often measured, this quantity is neither well understood nor well controlled [4]. This is a particularly unfortunate situation, because the performance characteristics (such as gray-scale and threshold voltage) of most liquid crystal displays are very sensitive to W. Thus clean measurements of the surface energies associated with the free liquid crystal-air interface will provide us with a much clearer picture of the surface properties of the material, as well as possible methods to control it.

## Experimental

The principle behind magnetic levitation is completely analogous to that used in the Faraday susceptometer. Given a material with a magnetic susceptibility (per unit mass) $\chi$, the energy U of this mass in a magnetic field H is $U = -\frac{1}{2}\chi H^2$. Thus, if there exists a spatial gradient $\nabla H$ in the field, there is an associated force $F_{magnetic}$ (per unit mass) equal to $F_{magnetic} = -\nabla U = \chi H \nabla H$. In a Faraday

susceptometer, which measures $\chi$, an electromagnet with specially shaped pole pieces is used to maximize both the magnitude and uniformity of the quantity $H\nabla H$. The sample, which is housed in a small bucket, is suspended from a very sensitive balance — typical sensitivity is $1\mu g$ — and the total force (per unit mass) $F_{tot} = F_{gravity} + F_{magnetic}$ is measured in the presence and absence of the magnetic field. The difference $\Delta F$ between these two measurements corresponds to the magnetic force $F_{magnetic}$. The desired quantity, the susceptibility per unit mass $\chi$, is simply $\Delta F/H\nabla H$. Both the magnetic field and its gradient may be measured with a standard Hall probe or, alternatively, $H\nabla H$ may be obtained empirically by measuring $\Delta F$ for a material whose susceptibility is available in the literature. We have for many years successfully performed these sorts of measurements to determine $\chi$ as a function of temperature.

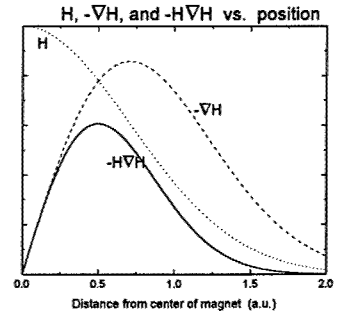


Most Faraday susceptometers rely on magnetic field strengths of order 10kG( =1T) in field gradients of order 1000 G $cm^{-1}$. For typical diamagnetic materials, e.g. benzene or water, the susceptibility per mass is $\chi \sim -0.7 \times 10^{-6}$ cgs. The magnetic forces experienced by these materials are therefore approximately two orders of magnitude smaller than the gravitational forces, and thus a very sensitive balance is clearly needed to determine $\chi$.

Instead of using a standard 10 kG laboratory magnet, however, one might consider using a significantly larger field and field gradient. For these same materials, one may exert a magnetic force *equivalent* to $F_{gravity}$ if $H\nabla H \sim 1.4 \times 10^9 G^2 cm^{-1}$. If the magnetic force is directed downward it will add to gravity; on the other hand, if the force is directed upward, the sample will experience the equivalent of *a vanishingly small gravitational field.* The necessary fields and gradients can be achieved with Bitter or superconducting magnets having a maximum field strength of 100 kG or more. [Alternatively, lower field magnets — to approximately 70 kG — may be effectively used with the insertion of a pole piece]. Although the total force vanishes in a mathematical plane, one can achieve uniformity of $H\nabla H$ to a few percent over millimeters. Thus, one may obtain experimental volumes in which the total force per unit mass is of order 10 dyn $g^{-1}$, and even much smaller over more limited volumes. Using this technique we have often "levitated" sample materials such as water in a 100 KG Bitter magnet. An alternative may involve studying the liquid crystal in an immiscible fluid, as the uniformity of the force may be increased and the required fields decreased.

Experimentally, we shall use an 85kG superconducting magnet. This magnet possesses a 5.4 cm diameter gap running along the z-axis over the entire length of its helium dewar, as well as a pair of 1 cm optical ports along the x- and y-axes of the dewar. (The x- and y- ports pass through the center of the split coil.) In the absence of a pole piece the maximum achievable value of $H\nabla H$ is approximately $5 \times 10^8$ $G^2cm^{-1}$, about a factor of three too small to achieve a "microgravity" environment. Insertion of a pole piece can easily rectify this circumstance. Calculations for the field gradient $\nabla H$ performed by Robert Weggel of the Francis Bitter National Magnet Laboratory magnet design group show that on insertion of a 2 cm diameter cylindrical piece of soft, the field gradient is increased by approximately a factor of three from its value in the absence of a pole piece. An increase in the actual field also occurs, although the relative change is somewhat smaller. Thus, a simple design involving a cylindrical pole piece is easily sufficient to create a microgravity-mimicking environment in our magnet. Weggel notes that a more complex design involving a tapered pole piece will further improve the performance, not only in terms of the maximum value of $H\nabla H$, but in terms of the uniformity of this quantity as well.

To accomplish our goal we intend to study liquid crystal droplet shape in a variety of phases in a microgravity environment. First, we note that $\chi < 0$ and therefore the liquid crystal is repelled from the core area of the magnet. Thus, using a pole piece centered about the magnet's midplane (with the top of the pole piece located at the position where $H\nabla H$ *in the absence of the pole piece* would be

maximum), our 85 kG superconducting magnet will provide such an environment. The quantity $H\nabla H$ at the top of the pole piece will be adjusted so that $H\nabla H > g/|\chi|$, thus causing a slight upward force on a sample which is located at the top of the pole piece. As the sample rises under this magnetic force, $F_{magnetic}$ will decrease, so that the total force $F_{tot}$ vanishes at one position $z_0$. On the other hand, for samples located at $z > z_0$ the net force will be downward; the material will fall to the position $z_0$ where the total force vanishes. Clearly, $z_0$ is a position of stability, and the material may be suspended at or near $z_0$ indefinitely.

The material itself will be injected into the test cell by means of an atomizer (to obtain small liquid crystal droplets), or by means of a microsyringe to obtain larger droplets. Temperature will be maintained by an electrical heating system, with control to better than 10 mK. The droplets will be imaged using a boroscope and CCD camera, with a computerized image grabber. This technique will allow us to study temporal changes in the droplet, as well as size and shape information about droplets.

Experiments will be performed in several liquid crystalline phases, especially those of technological relevance, with different categories of liquid crystal materials. In particular, the isotropic, nematic, smectic A, and smectic C phases will be probed. The isotropic phase, of course, has no long range order, although we may find a nonzero value of $< P_1(\cos\theta) >$ at the symmetry-breaking surface. Here $\theta$ is the orientation of the liquid crystal "director." This phase is of more scientific curiosity than of practical importance, although an important technological consideration is that most liquid crystal device cells are filled in the isotropic phase. In fact, the problem of cell voids (air bubbles), which appear in cells subjected to *large* gravitational-like forces (e.g., military aircraft), are often the result of difficulties during the initial filling process in the isotropic phase. The nematic phase is, of course, the most technologically important phase, as most current displays (e.g., the twisted nematic and supertwisted nematic) are based on this phase. The smectic A phase, in which the molecules lie in layers, is the simplest phase in which layering occurs. As there are at least fifteen smectic phases at last count [5], the smectic A is thus the simplest phase in which one can study the effects of layering on the surface energy. The smectic C phase, which is similar to a smectic A phase except that the molecules are tilted with respect to the layers, shows a number of interesting symmetries and is also associated with ferroelectricity. Currently, there is a growing interest in these materials as ferroelectric display devices, which tend to switch on and off quite rapidly.

In terms of materials, most liquid crystalline molecules can be divided — although not very cleanly — into two classes: strongly polar and weakly polar. The polar molecules, *e.g.*, the cyanobiphenyl series of molecules which possess a terminal $C \equiv N$ group, exhibit a nonzero $< P_1(\cos\theta) >$ at the surface [5]. A crucial question is how this polar group affects the surface tension. One might expect a much more strongly anchored homeotropic arrangement, in which the molecules are perpendicular to the surface, than for a nonpolar molecule. A systematic study of this class of molecules will be undertaken, and compared to results from the class of alkoxyphenylbenzoates. The latter series is not polar, and exhibits weak anchoring and even a temperature-dependent anchoring transition[6] in the nematic phase. Additionally, we intend to investigate chiral species, as molecules of this symmetry class may exhibit a polarization component transverse to the molecule and in the plane of the interface[7,8]. To date only one paper has appeared on the subject of chirality and anchoring [9], although it is a subject of both scientific and technological relevance [10].

## Theory

The value of the experimental measurements will be governed largely by their interpretation in terms of the fundamental properties of the materials. We therefore will develop a program to compute the surface energy anisotropy from the droplet shapes. Fortunately, there already exists a considerable body of formalism which we plan to extend as follows.

We intend to study the surface free energy of liquid crystals via an inversion of a generalized "Wulff construction." The Wulff construction was first introduced by Wulff [11] in 1901 from the idea of minimization of the surface free energy for a fixed volume. The full proof of Wulff's theorem by Liebman [12] did not come out until 1914; it was then further developed by many other people [13-16]. The basic idea of the Wulff construction is simply that the surface free energy of any body is an integral of the form

$$\int \gamma(\hat{p})dS \qquad (1)$$

extended over the surface of the body, where the specific surface free energy $\gamma$ is, for anisotropic bodies, a function of the orientation of the unit outward normal $\hat{p}$ at each surface point. Assuming that the bulk of the body is already in the lowest free energy structure, then all one needs to do is to minimize the surface free energy in order to get the equilibrium shape of the body, which in the past has generally been assumed to be crystalline.

After making some mathematical manipulations, one obtains the following geometrical construction: Make a three dimensional radial plot $r = \gamma(\hat{p})$; one obtains a two dimensional surface which may contain cusps. At each point of this radial plot one can construct a plane perpendicular to the radius vector at that point. Finally, the volume reached from the origin without crossing any of the planes is, according to Wulff, geometrically similar to the "ultimate equilibrium shape" for the crystal; *i.e.,* the shape that minimizes Eq.(1) for fixed volume.

When one deals with a crystal in a nearly equilibrium condition all one has to do is to invert the construction process to get the radial plot of the surface energy. In general, it is not easy, as predicted by Gibbs[17], to bring a crystal into equilibrium with the surrounding vapor or melt if the size of the crystal is large. The reason for this is that it will take a very long relaxation time for a constituent particle to move to the place where the free energy is a global minimum if the size of the crystal is large. Nevertheless, people have been successful in bringing small crystals into equilibrium with their vapor or melt [18-19].

For the liquid crystal droplet, we will need a generalized version of the Wulff construction. The reasons for that are twofold: First, the intermolecular interaction is in general much weaker than in the crystalline case; therefore it is very possible to have a director field deformation inside the droplet, which results in a free energy increase proportional to the volume, and which is non negligible. Second, the possibility of director field deformation will invalidate the assumption that the surface tension depends only on the direction of the surface normal.

An encouraging recent work by Oswald *et al.* [20] shows that in the case of a quasi-two-dimensional smectic A - smectic B interface, application of the Wulff construction seems to be successful. This shows that we might use the result of the "Wulff Theorem" as our zeroth-order approximation and develop corrections afterwards.

Although some recent work [21] has been done to measure the surface tension of a free-standing smectic film, this study was limited to finding the surface tension when the surface normal was actually perpendicular to the smectic layers. Our objective, on the other hand, is to obtain the anisotropic surface tension.

To incorporate the contribution from the director field deformation inside the droplet, we write down formally the total free energy of a liquid crystal droplet:

$$F = \int_V f(\hat{n})dV + \int_S \gamma(\hat{p}, \hat{n})dS \qquad (2)$$

where $\hat{n}(\bar{r})$ is the director field inside the droplet and the surface tension $\gamma$ now is a function of the surface normal $\hat{p}$ as well as a functional of the director field $\hat{n}(\bar{r})$. We then minimize the free energy with the constraint that the total volume be fixed, *i.e.*, $\int_V dV$ be constant. If we regard the Lagrange multiplier associated with this constraint as the density multiplied by some factor, we may also regard the constraint as fixing the total liquid-crystal mass.

Formally, we can write down the equation from the variation:

$$\frac{\delta\tilde{F}}{\delta\hat{n}(\bar{r})} = 0 \quad \text{and} \quad \frac{\partial\tilde{F}}{\partial\hat{p}} = 0 \tag{3}$$

where $\tilde{F} = F - \rho\int_V dV$. These equations are in general difficult to solve. We plan to solve them perturbatively using the original Wulff construction as the zeroth order approximation.

Once this is done, we can proceed to analyze the surface tension from the experiments. At the same time we must recall that another complication arises from the presence of the magnetic field. This will introduce the H field dependence into the bulk free energy density, so that $f(\hat{n}) \longrightarrow f(\hat{n}, H)$. Because almost all liquid crystal molecules have an anisotropic magnetic susceptibility, the molecules will tend to line up either parallel or perpendicular to the field. This factor introduces an additional anisotropy to the droplet shape through the change in the free energy, but this can be allowed for in the calculation. In the case of experiments performed in a true microgravity environment (as distinct from a microgravity-mimicking magnetic environment) this added correction would not be necessary.

References


1. Z. Li and O. D. Lavrentovich, Phys. Rev. Lett. 73, 280 (1994).
2. C. Rosenblatt, Phys. Rev. Lett. 53, 791 (1984).
3. G. Cevc and D. Marsh, *Phospholipid Bilayers*, John Wiley, New York (1987).
4. B. Jerome, Rep. Prog. Phys., 54, 391 (1991).
5. S. Chandrasekhar, *Liquid Crystals*, Cambridge Univ. Press, Cambridge (1993).
6. G. A. DiLisi, C. Rosenblatt, A. C. Griffin, and U. Hari, Liquid Crystal 7, 353, (1990).
7. R. B. Meyer, L. Liebert, L. Strzelecki, and P. Keller, J. Physisque Lett. 36, L69 (1975).
8. S. Tripathi, M.-H. Lu, E. M. Tarentjev, R. G. Petschek, and C. Rosenblatt, Phys. Rev. Lett. 67, 3400 (1991).
9. K. A. Crandall, C. Rosenblatt, and R. M. Hornreich, Liquid Crystal **18**, 251 (1995).
10. K. A. Crandall, M. R. Fisch, R. G. Petschek, and C. Rosenblatt, Appl. Phys. Lett. 65, 118 (1994).
11. G. Wulff, Z. Krist. 34, 449 (1901).
12. H. Liebman, Z. Krist. 53, 171 (1914).
13. M. von Laue, Z. Krist. 105, 124 (1943).
14. Dinghus, Z. Krist. 105, 304 (1944).
15. C. Herring, Phys. Rev. 82, 87 (1951).
16. R. Dobrushin, R. Kotecky and S. Shlosman, *The Wulff Construction: A Globe Shape from Local Interaction* (American Mathematical Society, Providence Rhode Island, 1992).
17. J. W. Gibbs, *The Scientific papers of J. Williard Gibbs, Vol. 1, Thermodynamics* (Longmans, Green & Co., 1906, pp. 315-326.
18. J. C. Heyraud and J. J. Metois, J. Crys. Growth 50, 571 (1980).
19. J. C. Heyraud and J. J. Metois, Surf. Sci. 128, 334 (1983).
20. P. Oswald, F. Melo and C. Germain, J. Phys. France 50, 3527 (1989).
21. P. Mach, S. Grantz, D. A. Debe, T. Stoebe and C. C. Huang, J. Phys. II France 5, 217 (1995).

# MODELING OF MACROSCOPIC/MICROSCOPIC TRANSPORT PHENOMENA IN ZEOLITE CRYSTAL SOLUTIONS UNDER MICROGRAVITY CONDITIONS

Dr. **Andreas Alexandrou**, Associate Professor and Director Aerospace Program, ME Dept., WPI, Phone: 508-831-5147, Fax: 508-831-5680, E-mail: andalexa@wpi.wpi.edu
Dr. **Nikos A. Gatsonis**, Assistant Professor, ME Dept., WPI Phone: 508-831-5576, Fax: 508-831-5680, E-mail: gatsonis@amyntas.wpi.edu
Dr. **William Durgin** Professor and Associate Provost for Academic Affairs, WPI Phone: 508-831-5065, Fax: 508-831-5774, E-mail: wwdurgin@wpi.wpi.edu
Dr. **Albert Sacco**, Head and Professor of Chemical Engineering Department, WPI Phone: 08-831-5333, Fax: 508-831-5853, E-mail: asacco@jake.wpi.edu

## Summary

Crystals grown from special liquid solutions find important industrial applications. Most often the physics and chemistry of the growth processes are not well understood due to complex microscopic chemical and thermo-fluid phenomena. Microgravity could help elucidate these phenomena and allow the control of defect concentration and crystal size. We are proposing to study zeolites grown in silica solutions as a typical crystal growth system. By using macroscopic fluid dynamics, coupled with first-principle microscopic fluid physics and advanced particle simulations, we will study: (a) the effect of transport phenomena and nutrient flow under microgravity conditions along with (b) the nucleation process and (b) the microscopic crystal growth dynamics. The macroscopic model will account for the bulk fluid-crystal motions. The microscopic model will include multiple nutrient species and growth sites, and microscopic interactions during the nucleation and crystallization processes. The numerical results will be compared with data we obtained from terrestrial and space experiments.

## Project Description

In general, crystals grown from solutions are relatively inexpensive and find extensive use in many industrial applications. Many of the phenomena associated with crystal growth processes are not well understood due to complex microscopic and macroscopic

interactions. Since many physical parameters are simultaneously involved in the process, experiments are difficult to interpret, and cannot be easily used to derive empirical or other laws. At the same time, there is increased urgency in the development of such an understanding in order to more accurately quantify the process.

In the past, extensive efforts have been made to characterize zeolite structures and to understand their nucleation and growth mechanisms so as to be able to custom-make crystals for a desired application. To date, for most solution systems both the nucleation mechanics and chemistry are as yet still unknown. Furthermore, the effects of the transport phenomena in the growth process are effectively unknown. The problem is compounded by a "gel" phase that forms upon mixing which controls the degree of supersaturation. The gel undegoes a continuous "polymerization" type reaction during nucleation and growth.

It was hypothesized that the microgravity levels achieved in an orbiting spacecraft could help isolate the effects of natural convection and minimize sedimentation so crystals would stay suspended in the nutrient pool under diffusion-limited growth conditions. Microgravity is expected to promote larger crystals by allowing growing crystals a longer residence time in a high-concentration nutrient field. It is hoped that larger, more defect-free zeolite crystals in high yield would result. Zeolite crystallizations performed in space resulted in mixed results. Earlier experiments (STS-50, STS-57) indicated an enhancement in size in the range of 10 to 50 percent compared to ground based controls with a corresponding reduction in lattice defects. However, the knowledge gained from the first space flight experiments has resulted in ground samples being grown to approximately the same size as those grown in these initial space flights. More recent space samples (STS-73) indicate an additional 10 to 50 increase in size. Again, when compared to the ground-based results, there appears to be a reduction in lattice defect concentration (although less than seen previusouly) , as well as a substantial difference in the OH concentration. Currently, the results from these space experiments are still being analyzed.

## Modeling Plan

There have been no substantive studies on the fluid physics and mass transport associated with crystallization of zeolites to help quantify the experimental observations. Our computational model will attempt to elucidate some of the parameters that influence the growth process and to provide the framework for future extensions. Despite the idealized nature of the model, it will include the essential features of the real process.

At the macroscopic level, upon mixing the solution undergoes instantaneous ``polymerization" resulting in the formation of a gel phase with liquid pockets. The crystals then grow suspended in the liquid phase while the gel continuously dissolves by releasing nutrients into the liquid. Gel dynamics and dissolution then, coupled with diffusion in the liquid, control the growth of the crystals. As nucleation and growth proceeds the gel phase finally disappears. In the early stages of the growth, the dynamics are dominated by diffusion-limited processes. However, as the crystals increase in size, gravity and particle migration become important. Along with the gel-liquid dynamics, there is coupling between crystal-crystal and liquid-crystal interactions which induce macroscopic fluid motions. The macroscopic motions, and the growth dynamics are then coupled to the concentration fields affecting the rates of growth. Bulk mass and flow transport, along with gravity, can force the crystals to the bottom of the reactor resulting in a sedimentation layer where the growth rate of the crystals slows down as the crystals compete for limited nutrients.

At the microscopic level there are normally two different but parallel stages during the crystal growth of zeolites, nucleation and growth The number of nuclei is proportional to the amount of gel that is formed. If this number decreases, the average crystal size in the final distribution increases. Therefore, among other factors, the crystal size distribution is a function of the nucleation rate and growth.

At the early stages of our study we are proposing a parallel modeling effort in order to develop separately the macroscopic and microscopic models. Eventually, the two models will be combined to yield a complete analysis.

Macroscopic Model: The macroscopic model will be built on our experience with the dynamics of suspension flows and phase change phenomena in complex flows [Ahmed and Alexandrou 1994, Alexandrou and Papanastasiou 1990]. As a prototype flow geometry, we will consider a 3-D cubic container, with randomly distributed nuclei sites and uniform concentration fields. At this level we will consider the solution as a continuun mixture of solid crystals in a matrix of gel and liquid phases. Mass conservation for each is given by

$$\frac{\partial \rho_s f_s}{\partial t} + \nabla \cdot (\rho_s f_s \mathbf{v}_s) = \dot{r}_s$$

$$\frac{\partial \rho_l f_l}{\partial t} + \nabla \cdot (\rho_l f_l \mathbf{v}_l) = \dot{r}_g - \dot{r}_s$$

$$\frac{\partial \rho_g f_g}{\partial t} + \nabla \cdot (\rho_g f_g \mathbf{v}_g) = -\dot{r}_g$$

where subscripts $l$, $s$ and $g$, refer to the liquid, solid and gel phases. Here $\rho$ is the density and $\mathbf{v}$ the velocity field. $f$ is the volume fraction. The term $\dot{r}_s$ is the rate of growth of the crystals and depends on the local concentration field in the liquid and the local microscopic growth dynamics. Similarly $\dot{r}_g$ represents the rate at which the gel dissolves into liquid. At first, these parameters will be estimated using empirical and experimental data. However, eventually, they will be provided by the microscopic model. Therefore, $\dot{r}_s$ and $\dot{r}_g$ represent the coupling between the macroscopic and microscopic models. To keep track of the nutrient species, for simplicity we will introduce the concentration field for a single component. At a later stage the number of species will be increased.

The momentum equation introduced for each phase provides the dynamic evolution of the three phases i.e.

$$\frac{\partial \rho_s f_s v_s}{\partial t} + \nabla \cdot (\rho_s f_s v_s \mathbf{v}_s) = F + \rho_s f_s g$$

$$\frac{\partial \rho_l f_l v_l}{\partial t} + \nabla \cdot (\rho_l f_l v_l \mathbf{v}_l) = -\nabla \cdot ((1 - f_g)\nabla P) - F + \nabla \cdot ((1 - f_g)\tau_l) + \rho_l f_l g$$

$$\frac{\partial \rho_g f_g v_g}{\partial t} + \nabla \cdot (\rho_g f_g v_g \mathbf{v}_g) = -\nabla \cdot (f_g \nabla P) + \nabla \cdot (f_g \tau_g) + \rho_g f_g g$$

where P is the pressure. The force per unit volume F, represents the interaction between the solid and liquid phases. At the dilute limit, the interaction is due to the drag force on the solid particles. However, as the concentration of the crystals increases the force will be modified accordingly. The liquid stress tensor will be described as a Newtonian fluid and the gel stress tensor as a non-Newtonian power-law type of fluid. The numerical solution to the macroscopic theory will be obtained using the Finite Element method. The solution procedure will be formulated and solved using an iterative solver.

Microscopic Model: The microscopic model will be based on our experience in hybrid Monte Carlo/particle-in-cell methods in the areas of dust particle interactions in space plasmas [*Gatsonis et al.*, 1994a] and hybrid fluid/particle-in-cell methods in plasma flows [*Gatsonis et al.*; 1994b; *Roy et al.*, 1994].

The model will include both the nutrients and the growing crystals in a liquid solution. At this stage we will not model the dissolution of the gel into liquid at the microscopic level. The theory and model will be developed for a domain with dimensions much larger than the typical crystal size. The cell structure will be non-uniform to allow for the macroscopic

variation of the flow parameters. Nutrients p with mass $m_p$ in the system will be treated as separate species, following a prescribed velocity distribution with mean velocity $\mathbf{U}(\mathbf{r},t)$ which will be obtained form the mean flow equations. The random motion will determine the diffusive fluxes of nutrients. At this level, the model will be able to reproduce previous DLA results. The macroscopic fluid parameters will be varied and the effects on crystal growth will be examined. The nutrients will be moved under the action of gravity force or liquid drag. A discussion of the treatment of forces within the concept of particle simulations can be found in *Gatsonis et al.* [1994a]. In addition to their motion, nutrients will undergo collisions which in a real system can be elastic, inelastic or chemically reacting. These types of collision processes can be modeled with the Direct Simulation Monte Carlo technique. The elastic collisions between the nutrients will be modeled using the No-Time-Counter model of *Bird* [1994]. In addition, those nutrients that are attached to the crystal will be removed from the domain, thus allowing the study of the nutrient depletion process [*Gatsonis et al.*, 1994a]. Since the DSMC is particularly suited for chemical reactions, such possible reactions could be introduced in the model as well [*Bird*, 1994].

The nucleation will be introduced with a Monte Carlo based model that resembles closely the actual process. In a zeolite solution nucleation and growth overlap and interact with each other. The nucleation sites will be created in random with a probability based on a model that describes the nucleation as a function of local thermodynamic and macroscopic variables. Another alternative is to introduce nucleation via a chemically reacting process based on a rate coefficient that depends on thermodynamic parameters. Ultimately, this issue must be resolved using experimental data. Once a nucleation site is established, the growing crystal will move under the influence of forces such as gravity and collisional drag. The inclusion of this effect is a significant departure from all previous crystal growth models which consider only stationary sites on a lattice. The nucleation sites will eventually grow to crystals of finite size. At this level we will introduce the dynamic interactions with the fluid. The motion of nucleation sites will also affect the crystallization process since subsequent crystal growth will depend on whether the sites are in rich or poor nutrient areas. The motion of the crystals is, therefore, expected to be very important in determining the crystal size distribution in the system.

The details of modeling of the growth however, is dictated by the computational requirements. Our approach is to describe the key physical processes with a model which will be refined through successive iterations with data comparisons. For this reason, we

will initially concentrate our efforts in the determination of the size distribution of the crystals under the influence of microgravity. As such, the crystals will be considered as spherical particles that grow after their attraction and attachment of nutrients. An attachment probability will be evaluated in those cells in which nucleation sites or crystals exist. This probability will be calculated on concentrations or surface kinetics based on impingement rates. At first, the model will not examine morphological characteristics of the crystals but we will instead develop appropriate crystallization models. At a later stage this additional complexity will be addressed with the introduction of a fine grid structure around each one of the growing sites.

As a first approximation, we will assume a stationary liquid in which the motion of the crystals will be determined by gravity and drag forces based on the local crystal velocity. This procedure will allow the parametrization of the sedimentation process under variable gravity conditions. At a later stage we will introduce the effect of the mean flow and copule the microscopic with the previously described macroscopic model.

## Experimental Verification

The computational results will be verified using our extensive database of experimental results. This long term ongoing experimental program on zeolite growth includes various solution systems under different growth conditions. Some of these experiments have been performed under microgravity conditions and are helpful in understanding the effects of crystal settling and nutrient flow/depletion. As part of our work we will use the theoretical/ computational model to evaluate and analyze existing data. The model will also be used in the design of future terrestrial or space based experiments.

## References


1. Ahmed, A. and A.N. Alexandrou, *Journal of Non-Newtonian Fluid Mechanics*, 55, 115 (1994)
2. Alexandrou, A.N. and A.C. Papanastasiou, *International Journal of Polymer Processing*, V , 1, 15 (1990).
3. Bird, G., Molecular gas dynamics and the direct simulation of flows, Oxford, 1994.
4. Gatsonis, N.A., Erlandson, R.E. and Meng, C.I, "Simulation of Dusty Plasmas Near surfaces in Space", *J.Geophys. Res. - Space Physics*, 99 (1994a).
5. Gatsonis, N.A., Samantha Roy, R., and Hastings, D.E., "Numerical Investigation of Ion Thruster Plume Backflow", *AIAA 94-3140*, (1994b).

# GRAVITATIONAL EFFECT ON THE DEVELOPMENT OF LASER WELD-POOL & SOLIDIFICATION MICROSTRUCTURE

Dr. Jogender Singh
Applied Research Laboratory
Pennsylvania State University
P.O. Box 30
University Park, PA 16804-0030

Voice: 814 863-9898
Fax: 814 863-1183
E-mail: jxs46@psu.edu

## Introduction

For welding of materials in space, it is essential to have a better understanding of laser welding. Laser welding is a simple process but it involves many interacting phenomena during melting and solidification. These phenomena includes convection, surface tension, heat and mass transfer, which have an influence on the microstructure and weld pool shape during solidification. These processes are all dependent directly or indirectly on gravitational forces. In order to have a better understanding of these interrelated phenomena, a thorough investigation is required that combines microstructural analysis with physical modeling and numerical simulation as well as modeling. Proposed efforts will be carried out in an integrated approach as described below.

## Phase I: Ground-Based Experimental and Mathematical Modeling

### *Laser Welding of Single Crystals of Pure Iron & Fe-15%Ni-15%Cr Alloy*

In this phase, laser welding experiments will be conducted on single crystals in order to obtain better understanding of the factors governing microstructural evolution and weld pool shape. For microstructural investigations, efforts will be focused on the early stages of nucleation and subsequent growth mechanisms of dendrites, the concentration gradients ahead of the solid-liquid interface, and fluid flow mechanisms. A single crystal alloy will be used to establish a relationship between the growing dendrites and partially melted crystal. Though the material to be used will be a single crystal, it will have multiple components. Due to rapid melting and quenching processes that occur during laser welding, there will be micro-segregation of alloying additions ahead of the dendrites which will result in concentration gradients.

Using a single crystal alloy will simplify the analysis of microstructural evolution that will occur from the melt pool by the moving laser heat source. The advantage of employing single crystal specimens is the ability to study initial (epitaxial) nucleation at the solid-liquid interface and subsequent growth of the solidification cells. This will provide detailed microstructural information which cannot be obtained from polycrystalline specimens. Mapping of the initial melt pool shape will be clearly established by microstructural development produced under different solidification rates.

### *Laser Welding of Ni-Al Alloys with Tracer Elements*

Similar welding investigations will be conducted on Ni-Al alloys. This alloy system has been selected because Ni and Al have significantly different densities (Ni=8.9 and Al=2.7 gm/cm$^3$).

This alloy system is an ideal candidate for investigating the effect of gravitational forces during solidification. The nucleation of dendrites will start with high concentrations of Ni, and there will be a high concentration of Al in the liquid ahead of the dendrite tip. This will also provide critical data concerning the effect of fluid flow mechanisms during solidification. The difference in component densities will emphasize effect of gravity-driven buoyancy flow, which will be revealed through variation in the solidification microstructure under different g-forces. Such information will be very useful for understanding the welding process applied to materials with different densities in space.

In the present investigation, analytical high resolution electron microscope (HRTEM) and atomic force microscopy (AFM) will be employed. The advantage of using these state-of-the-art techniques is to establish a better understanding of the concentration gradient of alloying elements under different gravitational solidification conditions (0 g, 1 g, and 2 g). Such efforts have not been carried out previously and represent a key link between operating mechanism and resulting weldment quality.

## Modeling and Simulation of Free Surface Shape, Cooling and Solidification Rates

To model the free surface profile, we have to solve the mass, momentum, and energy conservation equations simultaneously. The mass and momentum equations provide the velocity field in the weld pool, which are used to calculate the solute redistribution in the liquid phase. The solution of the energy conservation equations are used to determine the cooling and solidification rates. Please note that the key feature of this modeling effort will be to incorporate interactions between the vapor phase and the liquid phase. The vapor phase will be more seriously affected by the change of gravity than the liquid and solid phases. The basic governing equations that describe the processes within the weld region include the momentum (fluid flow) equations in the liquid phase, mass conservation in the flowing liquid, and the heat flow equation in both the liquid and solid phases. The flow equations include appropriate gravity dependent buoyancy terms. The momentum and mass flow equations allow us to determine the velocity field, which will be used to predict: (i) the redistribution of various constituents of the alloy that is being welded, and (ii) the change in chemistry in the fusion zone. The temperature field, which is obtained by solving the heat flow equations, will be used to predict: (i) the cooling rate; (ii) the solidification speed; (iii) the solute segregation due to rapid solidification; and, (iv) the microstructure in the solidified and heat-affected zones.

Considering the temperature at the solid/liquid interface is equal to the melting temperature, Tm, and far from the heat-affected zone the solid temperature become equal to the temperature, Tr, background, appropriate stefan conditions are used at the vapor-liquid and liquid-solid interfacial regions. At the solid-liquid interface, this leads to a balance equation that relates the conductive heat flows into both phases to the net rate of phase change through the latent heat of transformation. This yields an appropriate expression for the motion of the solid-liquid interface in terms of the various energy flows in the phases. At the liquid-vapor interface (vaporization front), the stefan condition relates the interface location to the various temperature fields and vaporization rate. In this study, heat conduction is neglected in the vapor phase. This leads to a zero temperature gradient in the liquid adjacent to the vapor. For determining the boundary conditions of the momentum equations, we consider that the laser beam is moving at a constant speed along a line. The problem is thus symmetrical in the plane perpendicular to this direction. This symmetry greatly simplifies a number of boundary conditions in this moving-source problem. An important aspect of laser welding is mass/energy interactions that occur at the vaporization front. This is described by the jump conditions for mass, energy and momentum transfers across the free surface. Considerable progress has already been made in solving these equations for 1 g condition under a separate program sponsored by ONR. Major emphasis for

this program will be to study the relative role of buoyancy and thermocapillary forces under different gravity conditions.

Phase II: NASA's KC-135 Aircraft Maneuvers Experiments (0 g, 1 g, and 2 g effect on laser welded microstructure and pool shape)

In this phase of the proposed research effort, the effects of microgravity on the shape of the weld pool and the resulting changes to the heat transfer conditions will be investigated. Temperature distribution within the weld pool and the circulation of the melt within the pool will affect the final weld microstructure and composition. Surface tension driven convection, which is the major fluid driving force in laser welding, will be investigated as a function of gravitational force during weld pool solidification. Since stainless steel has a strong negative surface tension temperature coefficient, heat from the laser weld will be transported to the edges of the pool across the surface. Natural convection due to buoyancy effects contributes to heat transfer when a gravity field is present. Buoyancy driven flow adds to the surface tension driven flow if the temperature coefficient of surface tension is negative. This flow mechanism is non-existent in a micro-gravity environment. Changes in the flows caused by microgravity need to be studied since the weld pool will be of significant size relative to the metal thickness. All metallurgical aspects of the weld will be investigated. The size and shape of the HAZ, the surface characteristics of the weld bead, and the solidification structures of the fusion zone will all be influenced by the heat transfer changes. Changes in convective flow will affect porosity, can lead to lack of fusion, and may lead to variable penetration along the weld bead.

The austenitic stainless steel single crystals and Ni-Al alloy will be used for the proposed study of convection-flow patterns in both stationary and transient melt pools. These investigations will be proceeded through the addition of a tracer element which will be introduced after the melt pool has been formed by the laser. After sectioning the specimen, the location of the tracer element can be determined and mapped by various techniques including back-scattered electron microscopy. Similarly, the concentration gradient or segregation of the tracer element in the dendrites will be determined by the analytical HRTEM. This technique will give better understanding of the physical phenomena associated with the mass transport and heat and fluid flow occurred during welding. Comparison of these analyses with flow-field simulations will allow refinement of the simulation model and more accurate determination of the appropriate thermophysical parameters.

The long term objective of this research effort is to carry out KC-135 low-g experiments in order to provide a basis for the development of a series of solidification experiments for future development on the Space Shuttle and ultimately on Space Station Freedom. In addressing this goal, the research effort is directed towards increasing our basic understanding of gravitational, surface tension, natural-convection, and other mass transport effects on solidification processes in general and on fusion-welding processes specifically.

The ground-based experiments will be conducted at The Pennsylvania State University, which has a world-class laser and materials characterization facility. Flight experiments will be conducted on NASA's KC-135 utilizing the "Enhanced Gravity Laser Materials Process" (EGLMP) system developed under the NASA grant (NAGW-1195) at The University of Tennessee Space Institute, Tullahoma, Tennessee. Professor M.H. McCay at the University of Tennessee Space Institute, will coordinate this effort.

# FLIGHT EXPERIMENT TO STUDY DOUBLE-DIFFUSIVE INSTABILITIES IN SILVER DOPED LEAD BROMIDE CRYSTALS

N. B. Singh, S. S. Mani, S. R. Coriell, M. E. Glicksman, and W.M.B. Duval
Northrop Grumman Corporation, Science & Technology Center
1310 Beulah Road
Pittsburgh, PA 15235-5098

## ABSTRACT

Single crystals of lead bromide doped with silver bromide were grown by the vertical Bridgman method. Direct observations were made in order to investigate the interfacial instabilities. Numerical studies were carried out to provide a framework for interpreting the observed convective and morphological instabilities. Observations on interfacial instabilities in lead bromide with 500 and 5000 ppm silver bromide impurities supported the numerical results predicted for 1-g conditions. X-ray rocking curves, X-ray contour scans, and etch-pit studies showed that increasing solutal convection deteriorated the quality of the crystals.

## 1. BACKGROUND

During the crystal growth of optical and electronic materials by the Bridgman method, the prevention of convection is important in order to minimize micro- and macrosegregation and to obtain homogeneous properties throughout the crystal. The convection in the liquid phase can be driven by several forces. On earth, the most important source of convective flow is ordinarily density differences due to temperature and composition differences within the sample. Additional flows can be due to volume changes and surface energy gradients. In the presence of gravitational forces , density-induced convection can be prevented if special conditions are met. In pure materials, it is sufficient that the temperature increases with height and that no gradient be present in the horizontal directions. However, in an actual furnace it is extremely difficult to eliminate the radial temperature gradient completely. Unavoidable radial gradients may give rise to flows which lead to lateral segregation in the solidified material. In a binary system, if the solute "piled up" ahead of the solidification front is lighter than the solvent, this alone would cause a positive density gradient [1-3]. The net density gradient can then have various profiles,

depending on the properties of the melt such as the thermal conductivity and diffusion coefficient or growth conditions such as the growth rate and thermal gradient. Even if the net resulting density gradient is stable, convection can occur due to the double-diffusive character of solute and temperature with different diffusivities.

Heavy-metal halides have very diverse applications in the optoelectronic industries. Lead bromide and lead iodide crystals in particular have great promise for acousto-optical devices and room-temperature X-ray and gamma-ray detectors. Their applications are, however, limited because of the unavailability of good-quality single crystals. We have used [4-6] the Bridgman method to grow single crystals of these materials, however, during the cool down period, pure lead bromide crystals crack due to a phase transformation. Also, in common with many halide crystals, cutting, polishing, and device fabrication can cause crystal damage. Hardening of the crystal by dilute silver doping has been evaluated but uniform bulk doping for which the resulting crystal is optically homogeneous is difficult to achieve in normal gravity. We hypothesize that the inhomogeneity arises from thermal-solutal convection. We propose to test this hypothesis in reduced gravity and to relate the results to the growth of device-grade crystals. The lead bromide system, because it is optically transparent in the visible (both as a solid and liquid), also serves as a model Bridgman system permitting real-time visualization of the growing solid-liquid interface.

## 2. EXPERIMENTAL METHOD

Purification of Source Material: As-supplied lead bromide (listed at a 99.999% purity) was further purified [4,5] by a directional-freezing method. Silver bromide was listed as 99.999% pure, and it was used without further purification.

Crystal Growth and Characterization: Lead bromide crystals doped with silver bromide were grown in a two-zone transparent Bridgman furnace. All of the crystals were grown in a <010> orientation [6] by using a preoriented 4 x 4 x 8 $mm^3$ seed.

Lead bromide crystals doped with silver bromide were characterized [4] by X-ray rocking curve and X-ray contour scan evaluations. Etch-pit studies were carried out by using a mixture of HCl, $HNO_3$, $NH_4Cl$, and water.

## 3. RESULTS AND DISCUSSION

### 3.1 Observations on Solid-Liquid Interface:

Direct observations were made in 1-g conditions for two lead bromide samples doped with 500 and 5000 ppm concentrations of silver bromide. The temperature gradient of the furnace at the solidifying interface was 20 K/cm. When the sample was held stationary (zero growth velocity), any convection present in the liquid was attributed to the effect of radial heat losses. Figure 1 shows an approximately flat interface in a sample with 5000 ppm silver bromide. When the growth was initiated by moving the ampoule, a velocity which was lower than critical velocity of interface breakdown was used. The interface became depressed, and the shape of the depressed "pit" varied with the ampoule velocity. The interface became sharply pointed and then slowly formed the instability pulling down the central part of the interface. The convective-flow pattern was present with a flow downward near the wall and upward in the center of the tube. As a function of time, the instability developed [Fig. 1(b-d)] with a much longer amplitude. When we increased the translation rate, the interface started breaking down. The instability curve determined by Coriell et al. [1] was used to compare the experimentally observed results. The preliminary data [7] showed that the theoretically predicted curve agrees very well with the experimental values. Similar observations were made using the lead bromide sample doped with 500 ppm silver bromide. We could increase the growth rate approximately one order of magnitude without observing interfacial breakdown.

The flow pattern observed in the $PbBr_2$-AgBr system can be described as a "toroidal roll" as shown in Fig. 2. We have observed that a slight asymmetry of the system resulted in the displacement of the node and axis of the torus from the central axis of the tube. When the toroidal flow persisted for many hours and the tube was moving, we observed a pinching of the interface at the node where the radial inward flow converges and a line defect is formed as shown in Fig 2. This observed toroidal flow can be explained as follows: When crystal growth starts, the radial gradients increase due to the effect of drawing the hotter material downward through the viewing block and due to latent heat emitted from the solid-liquid interface. The convective-flow pattern is correspondingly altered.

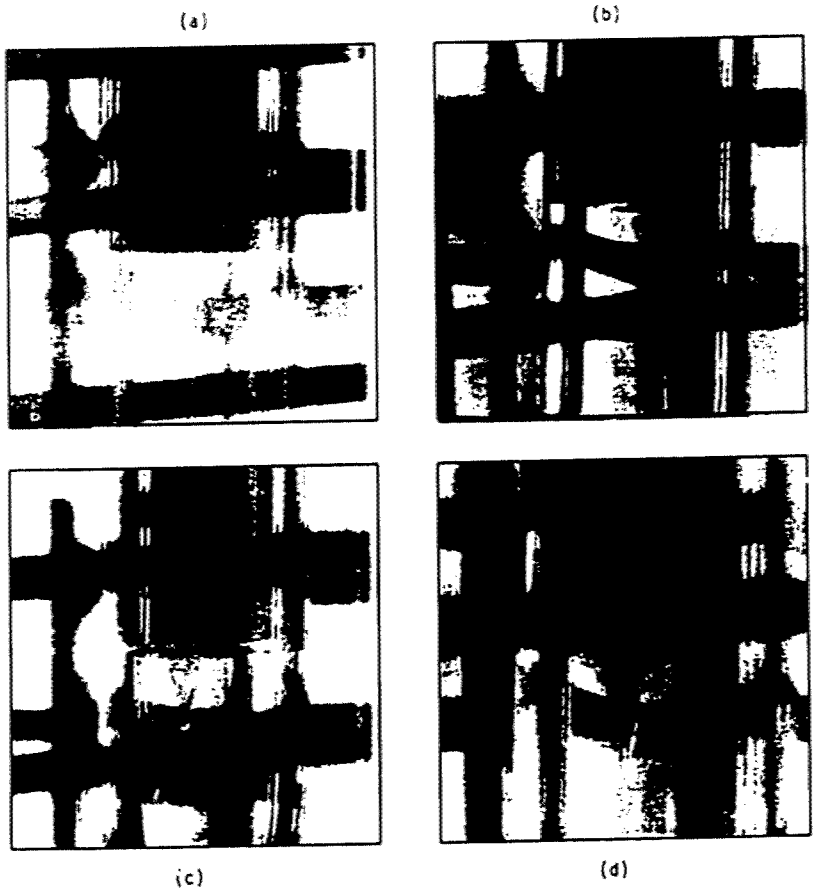


Fig. 1 Instability observed with a 5000 ppm AgBr doped lead bromide sample. (a) planar interface in stationary position, (b) depressed interface (c) well-developed convective instability and (d) morphological breakdown of the interface.

3.2 Effect of Solutal Convection on Crystal Quality:

Two lead bromide crystals doped with silver bromide (designated as LBAB-2 and LBAB-4) were grown in identical thermal conditions. The solutal Rayleigh numbers [4] were $5.83 \times 10^3$ and $2.70 \times 10^4$. The X-ray rocking curves and X-ray contour scans are shown in Fig. 3 for both crystals. The full width at half maxima (FWHM) are $0.2^\circ$ and $0.52^\circ$ for the LBAB-2 and LBAB-4 crystals respectively indicating that crystal grown at lower solutal Rayleigh results in better quality. X-ray contour scans provided information which was valuable in understanding the optical homogeneity. The vertical section showed a variation $2\,\theta/\omega$ from -1.0 to +1.0 for LBAB-2 and -1.5 to +1.5 for LBAB-4 i.e. showing a larger variation of the lattice

parameters for LBAB-4 due to a change in the solutal Rayleigh number. Figure 4 shows the results of etch-pit studies on crystals LBAB-2 and LBAB-4. We did not observe any gross defects such as precipitates and microcracks. Etch-pit density for crystals grown at a higher solutal Rayleigh number was approximately 4 times higher than for the crystal grown at lower solutal Rayleigh number. These results are consistent with the results of the X-ray studies.

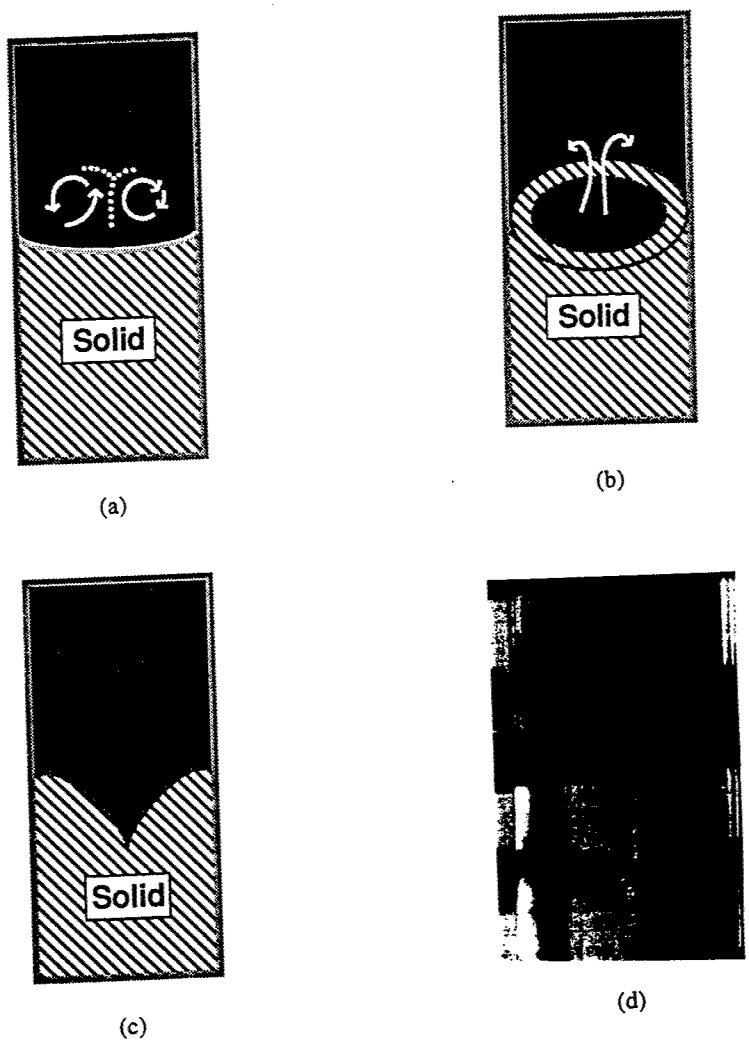


Fig. 2 Development of toroidal flow (a) initiation (b) less-developed flow (c) well-developed instability and (d) a defect formed in the solid due to toroidal instability.

## 4. SUMMARY

Direct observations were made in order to study the three dimensional characteristics of interfacial instabilities. The observations follow the numerically predicted results for lead bromide-silver bromide systems. X-ray rocking curves, X-ray contour scans, and etch-pit studies showed that crystals grown at a lower solutal Rayleigh number exhibited smaller variations in the lattice parameter and better crystal quality.

## 5. ACKNOWLEDGMENTS

We sincerely thank NASA Headquarters, Code UG for financial support.

## REFERENCES

[1] S. R. Coriell, M. R. Cordes, W. J. Boettinger, and R. F. Sekerka, J. Crystal Growth 49 (1980) 13.

[2] S. R. Coriell and G. B. McFadden, in Handbook of Crystal Growth, Vol. 1b, ed. D.T.J. Hurle (Elsevier, Amsterdam, 1993) p. 785.

[3] R. Z. Guerin, B. Billia, and P. Haldenwang, Phys. Fluids A3 (1991) 1873.

[4] N. B. Singh, A. M. Stewart, R. D. Hamacher, R. Mazelsky, W.M.B. Duval, G. J. Santoro, R. DeWitt, and S. L. Lehoczky, J. Crystal Growth, 139 (1994) 158.

[5] N. B. Singh, M. Gottlieb, T. Henningsen, R. H. Hopkins and R. Mazelsky, J. Crystal Growth, 123 (1992) 221.

[6] N. B. Singh, R. Mazelsky, S. R. Coriell, M. E. Glicksman, G. J. Santoro, W.M.B. Duval, and R. Sokolowski, Adv.Space Res. 13 (1993) 195.

[7] S. R. Coriell, ASM-TMS Fall Meeting, Oct. 30, 1995, Cleveland, OH.

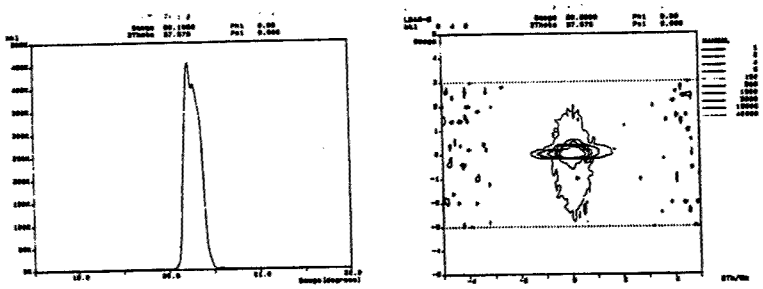

(a)

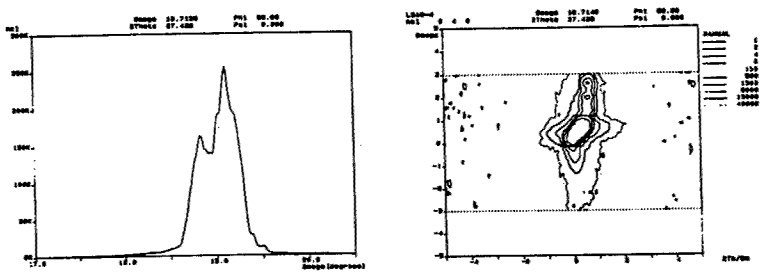

(b)

Fig. 3 X-ray rocking curves and contour scans showing mosaic spread (w axis) in the lattice constant (2θ/ω axis) for (a) LBAB-2 and (b) LBAB-4 crystals.

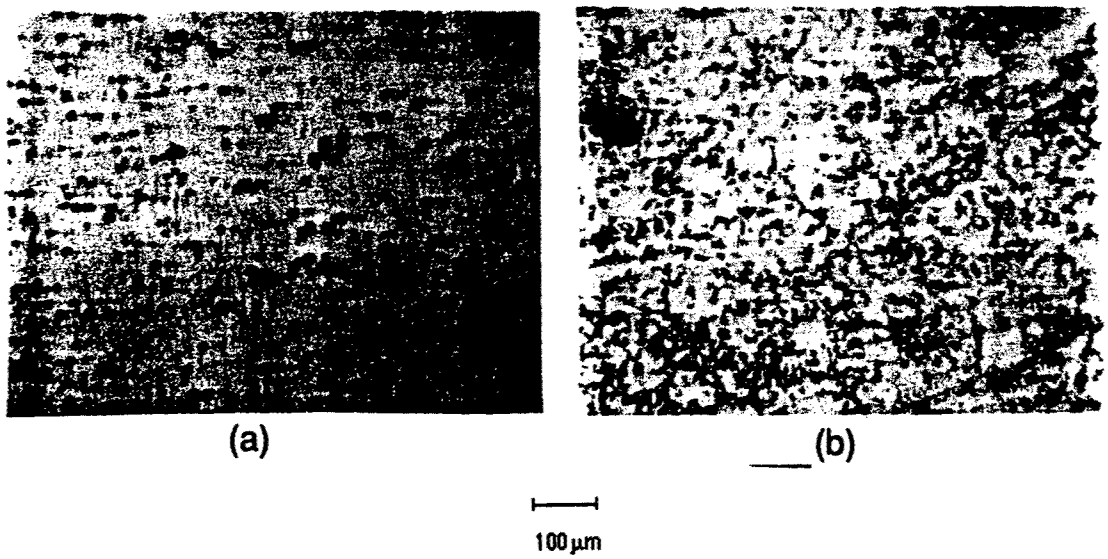


Fig. 4 Microphotographs showing chemical etch-pits for (a) LBAB-2 and (b) LBAB-4 crystal showing higher defect density for a crystal grown at a larger solutal Rayleigh number.

# FRACTAL AGGREGATES IN MICROGRAVITY.

R. J. Slobodrian, C. Rioux, L. Potvin & P. Deladurantaye
Département de physique
Université Laval
Ste. Foy, Québec, G1K 7P4
CANADA
FAX: 418 656 2040, Tel.: 418 656 3869, 5116.
EM: 36130008@VM1.ULAVAL.CA

## Introduction.

Fractal aggregates are believed to represent a new state of matter with properties at variance from those of ordinary bulk matter, and still to be studied and determined [1]. Mandelbrot has introduced the word **fractal** and the expressions **fractal geometry** and **fractal dimension** [2], to characterise a special class of topological systems. The rigorous theory of measures developed by mathematicians in the 19th and 20th centuries is essential to the generalisation of the concept of dimension leading to non-integer dimensions (fractal dimensions). Mandelbrot gave a tentative definition of a fractal in 1982: "A set for which the Hausdorff-Besicovitch dimension strictly exceeds the topological dimension". The latter is zero for a point, one for a line, two for a surface, etc. This definition is suitable for mathematical (also called deterministic) fractals, but it would exclude many physical fractals. Thus in 1986 Mandelbrot in troduced the concept of **self-similarity:** A fractal is a shape made by parts similar to the whole in some way [3]. This implies a scale invariance of parts of a whole. Material (natural) fractals exhibit mostly random features and a finite range of scale invariance. Mathematical fractals exhibit an infinite range of scale invariance and patterns are obtained with definite rules, hence they are sometimes called deterministic fractals [4].

Fractal aggregates constitute a class of material fractals which may be thought as stochastic polymers, and thus the smallest constituent elements are usually called **monomers** [5]. They are formed by large numbers of atoms and have approximate spherical shapes Particular interest is attributed to metals, due to their high electrical and thermal conductivity as well as high reflectivity of electromagnetic fields and light. Some finely divided metals are efficient catalisers, presaging the relevance of surface properties which are enhanced when surfaces become large with respect to mass. Such is precisely the case of fractal aggregates. The monomers have microscopic sizes and thus offer very large sufaces with respect to the matter enclosed, without substratus. The properties of matter in such form may differ markedly from those of bulk matter and bear promise of providing useful new varieties of atomic associations still largely unknown [5].

When our research was initiated there existed already abundant experimentation on physical fractals imbedded in two-dimensional

space. Thus, the main thrust of our work was on fractal aggregates imbedded in three-dimensional space and on aggregation dynamics, developing specialized apparatus as well as methods of data acquisition and analysis.

## Fractal dimension.

It is a generalisation of the concept of integer topological dimensions based on the measure of a set [6] and on the limit of a series, leading to non-integer values: **fractal dimensions**. There are abundant examples in nature of systems requiring a reformulation of the concept of dimension, like coastlines [3] or surfaces. An example of a self-similar set in mathematics allows to appreciate this generalisation: Cantor's triadic dust [7]. It is generated from a unit segment [0,1] (closed interval), eliminating the central third of it and of each subsequent segment. The resulting set can be expressed as an infinite intersection of terms $C_k$ (see Fig. 1)

$$C = \bigcap_k C_k \qquad (1)$$

The generic term of C consists of 2**k closed intervals of length (1/3)**k. Therefore, the total "length" of $C_k$ is $L_k$ = (2/3)**k and

$$\lim_{k \to \infty} L_k = 0 \qquad (2)$$

Consequently, although Cantor's dust contains an infinite subset of points of the segment [0,1], it is of topological dimension 0. Such dimension corresponds in fact to a point but logically it could be expected that an infinite set of points of [0,1] should be reflected by a more meaningful parameter than provided by discrete topological dimensions. A measure of a set can be obtained by covering its elements with n-dimensional "volumes" (n = 1,2,3,...) of variable linear sizes $\epsilon$, to any desired accuracy. The "capacity" CA of a covering "volume" can be expressed in general as

$$CA = K \epsilon^n \qquad (3)$$

For squares and disks K = 1 and K = $\pi$ respectively, with n = 2, for spheres K = (4/3) $\pi$, n = 3. If $N$ is the number of CA's necessary for covering a given volume V (dense set) in n-dimensional space

$$V = N K \epsilon^n \qquad (4)$$

If a set is not dense (like Cantor's dust), it is possible to write formally for the capacity of covering "volumes"

$$CA = K \epsilon^{D'} \qquad (5)$$

Understandably D' differs from the topological dimension of the imbedding space and it accounts either for the "non-dense" character or the "structure" of the self-similar system.

Therefore $$V = N(V,\epsilon)\, K \epsilon^{D'} \qquad (6)$$

and it follows $$D' = \frac{\ln N(V,\epsilon) - \ln K'}{\ln (1/\epsilon)} \qquad (7)$$

The term $\ln K'$ can be omitted upon taking the limit for $\epsilon \to 0$ leading to the fractal dimension D

$$D = \lim_{\epsilon \to 0} \frac{\ln N(V,\epsilon)}{\ln (1/\epsilon)} \qquad (8)$$

Applying expression (8) to the interval [0,1] (dense) $N(V,\epsilon) = 1/\epsilon$ and clearly D = 1, thus coinciding with the topological dimension. Instead, Cantor's "dust" distributed along the same interval [0,1] (not dense) yields $N(V,\epsilon) = 2^{k}$ and $1/\epsilon = 3^{k}$ as seen above. Hence, according to (8) $D = \ln 2/\ln 3 = 0.63$, differing from the topological dimension of the dense interval [0,1] imbedding Cantor's "dust" and also from the value of (2) based on the conventional evaluation of its length as a limit. Thus the infinite set of points has given a **fractal dimension** D, between the topological dimensions 0 and 1. The concept based on (8) is used to characterize fractals (aggregates and other), and allows to establish an interesting property of the physical density of a fractal because it reflects the occupancy of space. The mass of a fractal enclosed in a cube of side L is expressed by $M \approx L^{D}$, where $D < 3$. It follows that the average density of matter is given by

$$\delta \approx L^{(D-3)} \qquad (9)$$

and it goes to zero when $L \to \infty$. Fig. 2 shows the image of a three dimensional fractal aggregate with typical dendritic structure.Continued growth of the aggregate's dendrites would yield an ever more tenuous and delicate structure, reflected by (9). A proper study of large fractal aggregates can thus only be carried out in an environment of highly reduced gravity.

## Reduced gravity environments.

Fractal aggregates are limited in size by the pull of gravity on earth. If the maximum linear dimension of a fractal on earth is L under g the corresponding linear dimension under another value is $L' = (g/g')\,L$. This simple expression is based on the maximum static moments of forces bringing about the collapse of the aggregate. The sizes of aggregates obtained in our experiments under the earth's gravity were close to 1 mm (10 to 100 times larger than reported previously in the literature), therefore,as $L' = (10^{6})L$ going to microgravity, a growth to sizes of 1 km appears possible, i. e. to very large sizes, limited only by the aggregation volumes or times. Real reduced gravity experiments have been carried out worldwide on aircraft in parabolic flight, the KC-135 of NASA (used by our group) and a Caravelle of ESA (European Space Agency), providing up to 20 sec at a level of 0.01 to 0.001 g and sequences of 20 such periods in parabolic flight. Space shuttles and stations

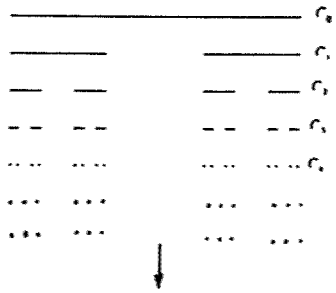

Fig. 1 Cantor's triadic dust.

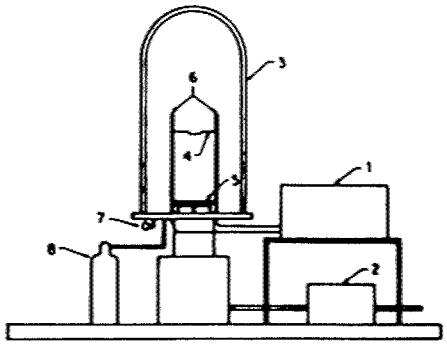


Fig. 3 Evaporation-Condensation apparatus: 1. Vacuum pumps. 2. Power supply. 3. Glass jar. 4. Evaporation "boat". 5. Collector. 6. Supporting conductors. 7. Air valve. 8. Gas bottle.

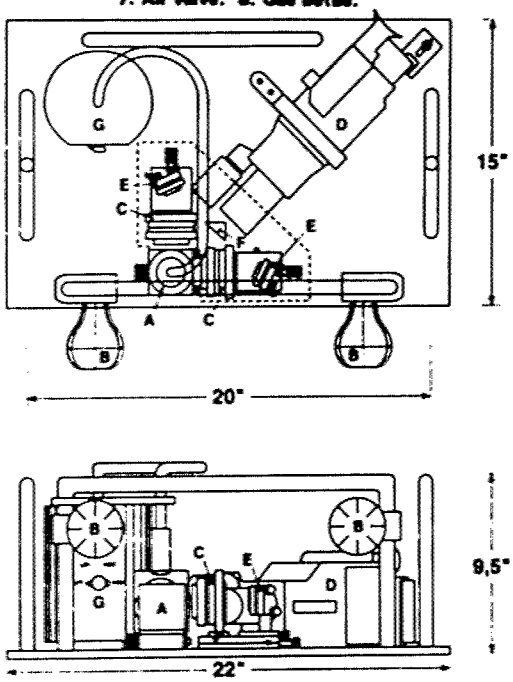


Fig. 5 Apparatus for experiments on the KC-135 NASA aircraft. A: aggregation cell. B: Bellows to activate the powder (calcium carbonate, sodium chloride). C: Magnifying lenses. D: Recording camera. E: Flat mirrors. F: Aluminized 90 degrees prism. G: Fiber optic light source with focussing lens. The field of view obtained using 28 mm lenses id 2.65x2 mm with 1.2 mm depth at maximum magnifying power.

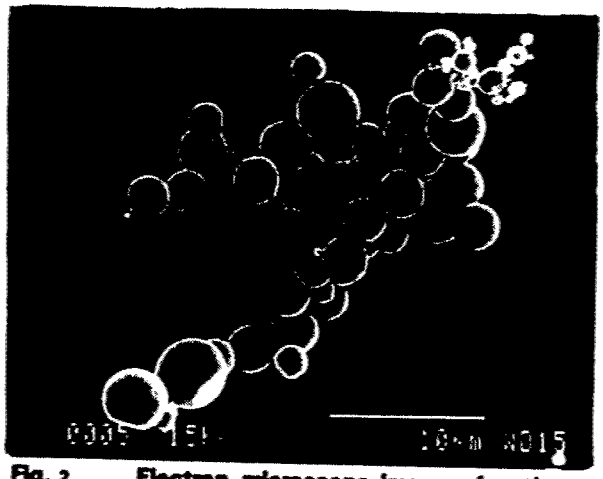

Fig. 2 Electron microscope image of a three dimensional Zn aggregate obtained by condensation of vapors, with typical dendritic structure.

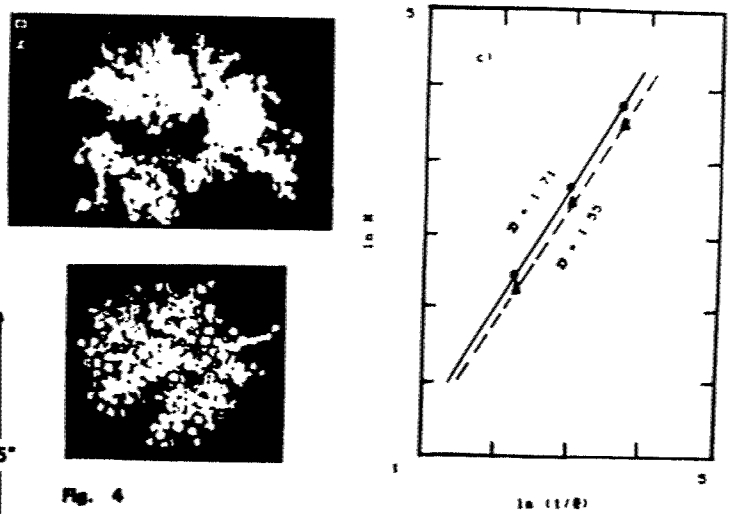

Fig. 4 Comparison of a real aggregate (top) with simulated aggregate (bottom). The graph at the right shows the fractal dimensions of the two dimensional images, the data correspond to the real aggregate and the triangles to the simulation.

Fig. 6 Images of three dimensional powder aggregates obtained in reduced gravity with the apparatus of Fig. 5. They show typical dendritic structures.

provide prolonged periods of reduced gravity, from weeks to years at mean levels of 0.01 to 0.0001 g (lower with an isolation mount). There is still the yet unexplored possibility of orbiting a laboratory in the interplanetary space for microgravity experimentation, at stable and vanishingly small values of g.

Except for fluid convection phenomena, a simulation of weightlessness can be obtained through flotation of particles in liquids or gases due to equilibrium of gravitation and buoyancy, allowing particle-particle interactions to manifest themselves.This is also the case for the fall of particles through fluids such that, due to equilibrium of gravitational and dissipative forces, it results in a motion with limiting uniform velocities and allows the formation of three dimensional aggregates of significant dimensions. Our group has produced such aggregates in simulated reduced gravity through flotation in inert, dense liquids and gases using fine powders and an evaporation-condensation technique [5,8],at a ground based laboratory. The evaporation-condensation apparatus is depicted on Fig.3 and aggregates were obtained from 12 elements, mostly metals reported in the literature [8-12]. Fig.4 exemplifies the determination of fractality of an aggregate as well as a simulation based on the diffusion limited aggregation model (DLA). Fine powder aggregation was also studied in the real reduced gravity environment offered by the KC-135 NASA aircraft, to determine the dynamics (forces) behind the process, inappropriately ignored by models describing it, like DLA or the ballistic models which rely only on random walk collisions and "sticking" of the particles in contact, without regard to atomic, molecular or other forces. In particular,for fine particles polluting the atmosphere, densities are rather low and aggregation should be induced or at least enhanced by long range forces.We have designed and constructed an apparatus for the observation and rerecording of the aggregation processes of particles ranging mostly between 1 and 10 μm in diameter. The schematic is shown in Fig. 5 and an image of a powder aggregate is reproduced in Fig. 6. The type of forces inducing two particle aggregations was ascertained [10] and results are shown in Fig.7, they should prove relevant to the understanding of aggregation of fine particles, atmospheric pollutants included. A technique for accelerating the precipitation of the latter is fairly obvious: large scale seeding of electric charges in the appropriate layers of the atmosphere. This could be particularly indicated for dust clouds from volcanic eruptions or meteoric collisions, to avoid induced "winters" (v.l. nuclear winter). Finally, Figs. 8 and 9 show results from the ground based laboratory and from the KC-135 environment respectively with multifaceted monomers reminiscent of carbon fullerenes [11] but at a different scale.The contention is that the space isotropy in reduced gravity enhances the production of matter in structures of polar (spherical) symmetry.In conclusion, our experiments can be pursued whithin standard containers on board of space shuttles or stations,allowing the enhanced production of such new structures, as well as truly macroscopic aggregates allowing the determination of physical properties like the conduction of electriciy, heat and acoustic vibrations, interactions with radiations and fields, catalysis, possible superconductiviy of long dendrites, etc.

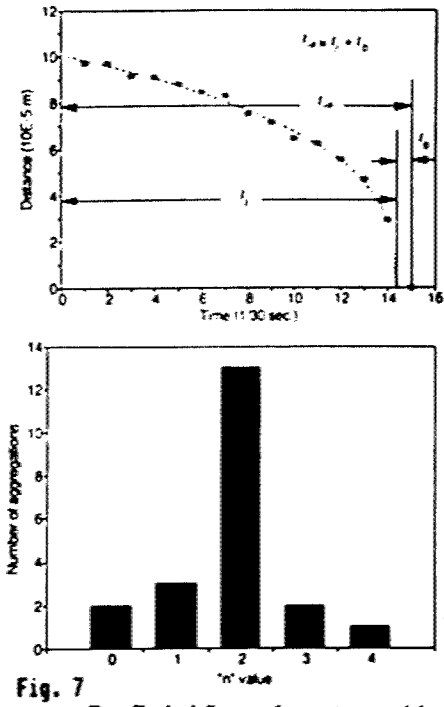


Fig. 7

Top: Typical diagram from a two particle aggregation. Bottom: Histogram of events showing that the most probable n = 2, for 1/r² forces.

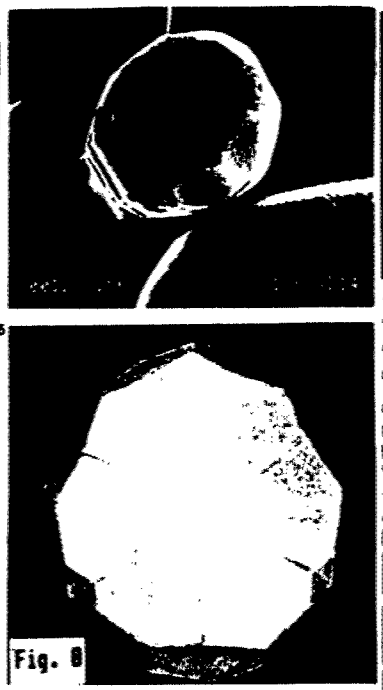

Fig. 8

Top: Copper monomer. Bottom: Its paper model. It is a triacontaoctahedron, implying a structure of 72 atoms at the lowest level. The symmetry is triaxial (cubic) and the envelope is manifestly spherical.

Fig. 9

Aggregates and multi-faceted crystals of Zn indicated by arrows and obtained in reduced gravity of KC-135 by the evaporation-condensation method.


## Acknowledgements.

The support of the Canadian Space Agency is gratefully thanked. The assistance of Mr. Lawrence Vezina of the Agency and of NASA personnel on the KC-135 operation was essential for this work. One of us (P. D.) benefitted from the Fond pour la formation de chercheurs et l'aide à la recherche - Québec. Many colleagues and technicians at the Physics Department and the Faculty of Science and Engineering have helped us, allowing rapid progress, we thank all very heartily.


## References.


[1] Space Science in the Twenty-first Century, Imperatives for the decades 1995 to 2015, National Academy Press, Washington, D.C. (1988). Collective work of a large number of specialists.
[2] B.Mandelbrot, Fractal Geometry of Nature,W.H.Freeman (1982) N.Y.
[3] J.Feder, Fractals, Plenum Press (1988) N.Y.
[4] R.Jullien, Contemp. Phys. **28** (1987) 477.
[5] R.J.Slobodrian, Phys. Can. **51** (1995) 245, and Refs therein.
[6] Classics on Fractals, Ed. G. A. Edgar, Addison-Wesley (1993)
[7] E.Lauwerier, Fractals, Princeton University Press (1991) N.J.
[8] R.J.Slobodrian, M.Cossette, B.Larouche, L.Potvin and C. Rioux, Chaos, Solitons and Fractals **1**(1991)529.
[9] M.Gauthier,M.Cossette,C.Rioux and R.J.Slobodrian,ibid.**3**(1993)687
[10]C.Rioux,L.Potvin and R.J.Slobodrian, Phys.Rev. **E52**(1995)2099.
[11]R.J.Slobodrian,P.Deladurantaye,M.Gauthier,C.Rioux and L.Potvin, Chaos, Solitons and Fractals, **7**(1996)25.
[12]P.Deladurantaye,C.Rioux and R.J.Slobodrian,ibid.in press.

# KINETICS OF NUCLEATION AND GROWTH FROM UNDERCOOLED MELTS

Michael J. Aziz and Frans Spaepen
Division of Applied Sciences, Harvard University, Cambridge, MA 02138
Phone: 617-495-9884, 617-495-3760; Email: aziz@das.harvard.edu, spaepen@das.harvard.edu

Our work falls in two general categories, based on the experimental techniques that are being employed. In the first category, fluxing, a drop tube or vacuum processing are used to achieve undercooling of fairly large melt quantities for the study of crystal nucleation and glass formation. In the second category, laser heating and thin film diagnostic techniques are used to study crystal growth and liquid diffusion.

## 1. Undercooling of bulk liquid silicon in an oxide flux.

We developed a new flux that is chemically compatible with silicon and is still sufficiently fluid at 1000°C. An extensive search led to the identification of the composition (in weight %): 47.5 $SiO_2 \cdot 13.5$ CaO $\cdot$ 39.0 BaO. Pieces of silicon, about 6 mm in diameter, were surrounded by this flux, melted and cooled at 4K/s in an Ar atmosphere with continuous monitoring of the temperature. Nucleation was observed through recalescence or changes in surface reflectivity. Undercoolings up to 350K were obtained, the largest ones to date in bulk Si [1]. These undercooling are 75K greater than those achieved in earlier experiments on bulk uncoated Si [2]. The result implies that homogeneous crystal nucleation did not occur in the earlier experiments; most likely, it did not occur in our present experiments either.

The nucleation rate was estimated from the volume of the sample, V, and the cooling rate, dT/dt, according to $I=dT/dt/(T'V)$, where T' is approximately 3K [1]; a value $I=4\times10^{9}m^{-3}s^{-1}$ was obtained. Application of the classical theory for homogeneous nucleation, $I(T)=I_0\exp(-C\sigma^3/\Delta G_v^2 kT)$, where $C=16\pi/3$ and $\Delta G_v=\Delta S_f(T_M-T)$ ($\Delta S_f$: entropy of fusion per unit volume of crystal, $T_M$: melting point), yields a lower limiting value for the crystal-melt interfacial tension: $\sigma=0.38Jm^{-2}$. The undercoolings and nucleation frequencies obtained by Stiffler et al. [3] in crystallization experiments on laser-irradiated thin films of silicon were larger than those in the bulk samples because the times and volumes were smaller: $\Delta T=500K$ and $I=10^{28}$ $m^{-3}s^{-1}$, respectively. The corresponding lower limiting value for the interfacial tension is 0.34 $Jm^{-2}$. This value is the same

as that obtained from the earlier bulk undercooling experiments [2]. These results are illustrated in Figure 1. The new bulk data can be reconciled with those from the laser-melting experiments using a homogeneous nucleation model only if the interfacial tension has a positive temperature coefficient.

It should be kept in mind that the temperature dependence of the interfacial tension invoked in the analysis of nucleation experiments is different from that for equilibrium interfaces. In the latter case, the interface is flat, and a change in the temperature is accompanied by a change in the pressure specified by the slope of the coexistence line. The temperature coefficient of the interfacial tension in that case is the excess interfacial entropy, determined with respect to a dividing surface that corresponds to zero excess volume [4]. In the case of the nucleation experiments, the interface is curved because the temperature change occurs under non-equilibrium conditions: the ambient pressure remains constant and the liquid is undercooled. In that case, the interfacial tension is simply another way to express the work, W*, to form the critical nucleus: $\sigma=[C^{-1} W^* \Delta G_v]^{1/3}$. Since $\Delta G_v(T)$ is a macroscopic quantity available from specific heat measurements on the undercooled liquid, $\sigma(T)$ can be determined from calculations of $W^*(T)$ for a specific interface model.

This has been worked out for a simple model, involving a uniform interface of constant thickness, $\delta$, and constant interfacial enthalpy and entropy, $H_i$ and $S_i$ [5]. The model has been applied to Turnbull's I(T) data for the crystal nucleation in liquid mercury [6]. Extraction of the interfacial tension from Turnbull's data, according to $\sigma(T)=\{C^{-1} \ln[I_0/I(T)] \Delta G_v(T)]^{1/3}$, shows a positive temperature dependence of $\sigma$. Since the model has three fitting parameters, and the data provide only two values to fit ($\sigma$ and $d\sigma/dT$), one of the fitting parameters must be chosen a priori. The interfacial thickness was therefore set at $\delta$=1.46 monolayers, based on physical modeling of simple hard sphere liquids [7]. The resulting fitting parameters showed that the interfacial entropy and enthalpy were, respectively, $0.68\Delta S_f$ and $0.10\Delta H_f$ lower than the values in the bulk liquid. These changes are similar to those predicted from the localization of the liquid near the crystal surface in the physical model [8,9].

Application of the model to the results on Si (i.e., a fit to the values of $\sigma$ found in the our bulk experiments and in the laser-melting experiments) was performed in a similar manner: $\delta$ was fixed at 1.46 monolayers, and the resulting values for the interfacial entropy and enthalpy were, respectively, $0.67\Delta S_f$ and $0.32\Delta H_f$ lower than the values in the bulk liquid. Since liquid silicon is structurally similar to liquid metals, one expects the degree of localization near a crystal surface to be similar as well. The similarity in the values for the entropy drop in Si and Hg is therefore

plausible. The enthalpy change in the silicon interface is difficult to predict *a priori*, since the bonding and the energetics in this metal-semiconductor interface can not be simply determined. Note also that the model predicts a value of 0.45 $Jm^{-2}$ for the interfacial tension at the melting temperature.

Undercooling of liquid germanium has been more successful than that of silicon, mainly because liquid $B_2O_3$ has proven to be a very effective and chemically compatible flux [10]. Undercoolings as large as 415K have been obtained. Application of an analysis similar to that for silicon gives a lower limiting value for the interfacial tension, $\sigma$=0.32 $Jm^{-2}$. To apply the model for the interfacial tension to this single data point, an additional assumption must be made. Since liquid germanium is metallic, and structurally similar to liquid silicon, it is reasonable to assume that the entropy drop in their interfaces is the same. The fit than provides the remaining fitting parameter: an enthalpy drop in the interface of $0.20\Delta H_f$ [11]. As in the case of silicon, this drop is greater than that in a purely metallic interface like in mercury.

## 2. Nucleation of polytetrahedral phases from the melt.

There are a number of experimental indications that nucleation of polytetrahedral structures, such as Frank-Kasper phases and quasicrystals, from the melt occurs at fairly low undercoolings [12]. Confirmation of these results is important, since it provides evidence for the proposed similarity between short range order in metallic liquids and in these structures [9]. Polytetrahedral alloy droplets, such as Ga-Mg-Zn, have been solidified in a newly renovated gas-filled drop tube. Copious, uniform nucleation of $MgZn_2$ dendrites (a Frank-Kasper phase) is observed, and initial indications are that the undercooling is indeed small. The extraction of the nucleation parameters, in particular the interfacial tension, requires the development of an analysis that combines heat transfer in a gas-filled drop tube, fluid flow in the droplet, and the kinetics of nucleation and growth, all at fairly low undercooling. Such an analysis is currently underway.

## 3. Glass formation.

Our group has a longstanding interest in the kinetics of glass formation, and developed one of the earliest bulk metallic glass formers: $Pd_{40}Ni_{40}P_{20}$ [13]. The techniques used in the earlier work (fluxing, the drop tube, vacuum treatments) will be applied to some of the recently discovered easy

glass formers, such as Al-Zr-Ni, as well as to an extended study of the Pd-Ni-P and related systems.

## 4. A quantitative test of dendrite growth in alloys.

A parameter-free test of the dendrite growth theories using Herlach's results from solidification experiments at DLR-Köln on levitated drops [14] requires knowledge of the diffusive speed of the interface. Coordinated experiments, on the same alloy, of the temperature dependence of the interface velocity at DLR, and of the solute trapping behavior, using laser heating and thin film diagnostic techniques, developed in our laboratory [15] are being planned. For practical reasons, Ni alloys appear to be best suited to this study.

## 5. A search for predicted oscillatory instabilities.

A number of theories of interface stability during the solidification of alloys have produced predictions for the conditions under which oscillatory instabilities, thought to be related to the so-called "banded" microstructures, occur [16]. Our laser and thin film techniques can be used to measure some of the parameters in these theories, such as the liquid diffusivity and the diffusive velocity of the interface [17]. These parameters will be used to make quantitative predictions of the conditions for an oscillatory instability, which will then be investigated directly in the experimental regime of pulsed laser heating rates and thin film length scales.

## 7. New method for measuring liquid diffusivities.

We have demonstrated that thin film techniques combined with pulsed laser melting can be used to eliminate convection and reactivity problems in the study of diffusion in liquid metals [17]. We propose to make an important improvement in this technique by incorporating in situ, time-resolved temperature measurements with a new thermistor technique recently developed in our laboratory [18].

References


1. Y. Shao and F. Spaepen, J. Appl. Phys. 79, 2981 (1996).
2. G. Devaud and D. Turnbull, Appl. Phys. Lett. 46, 844 (1985).
3. S.R. Stiffler, M.O. Thompson and P.S. Peercy, Phys. Rev. Lett. 60, 2519 (1988).
4. J.W. Gibbs, *The Scientific Papers of J. Willard Gibbs*, Vol. I, p.55, Longmans-Green, London (1906); J.W. Cahn, in *Interfacial Segregation*, edited by W.C. Johnson and J.M. Blakeley, ASM, Metals Park, OH (1979), p. 3.
5. F. Spaepen, Solid State Physics 47, 1 (1994).
6. D. Turnbull, J. Chem. Phys. 20, 411 (1952).
7. F. Spaepen, Acta metall. 23, 729 (1975).
8. F. Spaepen and R.B. Meyer, Scripta Met. 10, 257 (1976).
9. D.R. Nelson and F. Spaepen, Solid State Physics 42, 1 (1989).
10. G. Devaud and D. Turnbull, Proc. Mat. Res. Soc. Symp. Proc. 57, 89 (1986).
11. F. Spaepen and Y. Shao, Proc. Mat. Res. Soc. Symp. Proc. 398 (1996).
12. S. Ebalard, F. Spaepen, R.F. Cochrane and A.L. Greer, Mat. Sci. Eng. A133, 569 (1991); S. Ebalard, Ph.D. Thesis, Harvard University (1989).
13. A.J. Drehman, A.L. Greer and D. Turnbull, Appl. Phys. Lett. 41, 716 (1982); H.W. Kui, A.L. Greer and D. Turnbull, Appl. Phys. Lett. 45, 615 (1984).
14. R. Willnecker, D.M. Herlach and B. Feuerbacher, Phys. Rev. Lett. 23, 2707 (1989); K. Eckler and D.M. Herlach, Mater. Sci. Eng. A 178, 159 (1994).
15. D.E. Hoglund, M.J. Aziz, S.R. Stiffler, M.O. Thompson, J.Y. Tsao and P.S. Peercy, J. Crystal Growth 109, 107 (1991); J.A. Kittl, M.J. Aziz, D.P. Brunco and M.O. Thompson, J. Cryst. Growth 148, 172 (1995); P.M. Smith and M.J. Aziz, Acta Metall. Mater. 42, 3515 (1994); R. Reitano, P.M. Smith and M.J. Aziz, J. Appl. Phys. 76, 1518 (1994).
16. W.J. Boettinger, D. Shechtman, R.J. Schaefer and F.S. Biancaniello, Metall. Trans. 15A, 55 (1984); S.C. Gill and W. Kurz, Acta metall. mater. 41, 1563 (1993).
17. N. Isono, P.M. Smith and M.J. Aziz, Metall. & Mat. Trans. A 27A, 725 (1996).
18. D.P. Brunco, J.A. Kittl, C.E. Otis, P.M. Goodwin, M.O. Thompson and M.J. Aziz, Rev. Sci. Instruments 64, 2615 (1993).

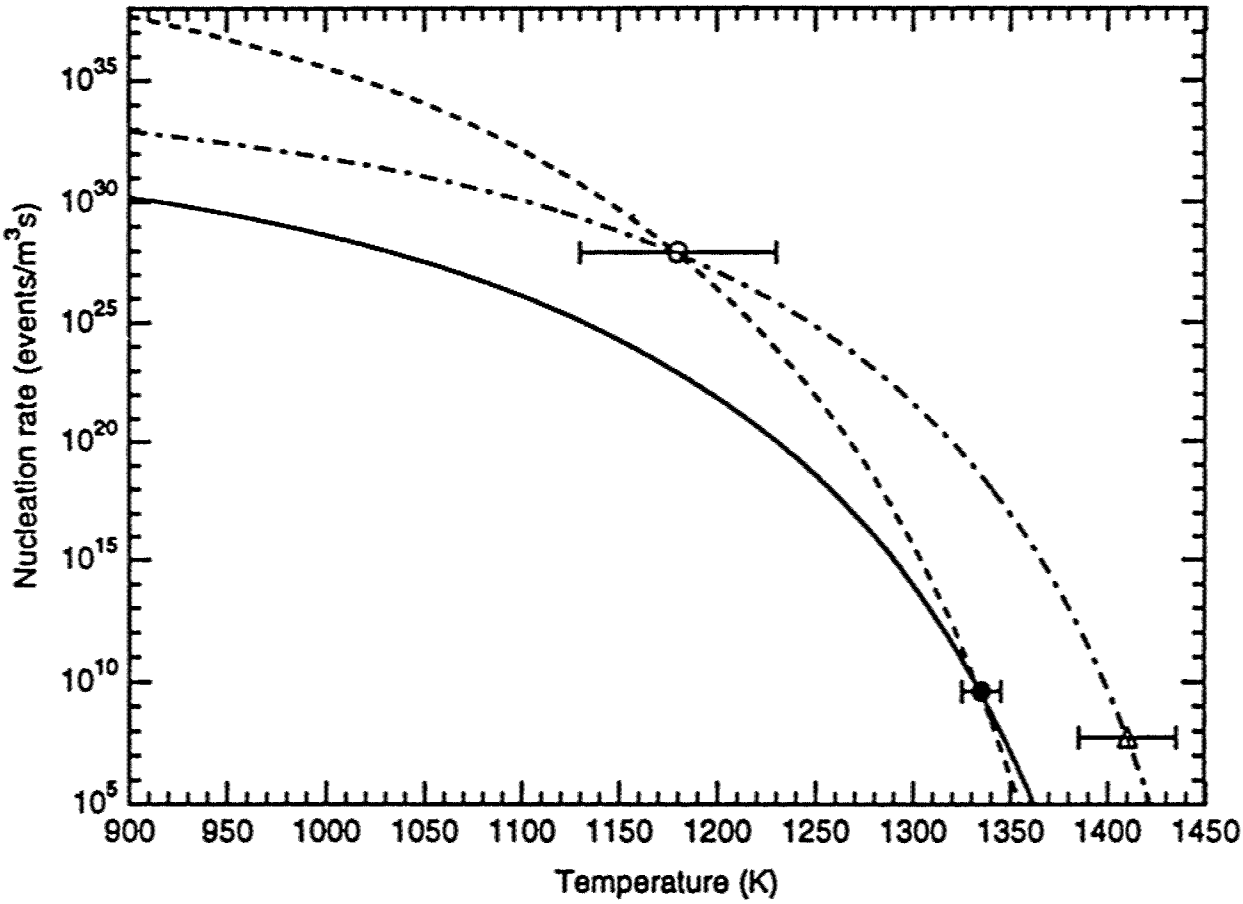


Figure 1: Nucleation rates of silicon crystals from the melt derived from undercooling experiments. Open circle: laser-irradiated thin film [ref. 3]; triangle: uncoated bulk sample [ref. 2]; filled circle: flux-coated bulk sample [ref. 1]. The lines are fits from classical nucleation theory. Solid curve: $\sigma$=0.38 Jm$^{-2}$; dot-dashed curve: $\sigma$=0.34 Jm$^{-2}$; dashed curve: $\sigma(T)$, according to the fit to the model of ref. 5, using the fitting parameters cited in the text.

# THE PUSHING / ENGULFMENT TRANSITION FOR ZIRCONIA PARTICLES IN ALUMINUM AND ZINC MATRICES

D. M. Stefanescu, F. R. Juretzko, B. K. Dhindaw
The University of Alabama Department of Metallurgical & Materials Eng., P.O.Box 870202, Tuscaloosa, Al 35487
Tel: (205) 348-1749
Doru@COE.ENG.UA.EDU

S. Sen
USRA
Assoc. 4950 Corporate Dr. Suite 100
Huntsville Al 35806
Tel: (205)544-8264

P. Curreri
NASA/MSFC
ES 74 MSFC
Huntsville, Al 35812
Tel: (205) 544-7758

The experimental evidence demonstrates that there exist a *critical velocity* of the planar solid/liquid (SL) interface below which particles are *pushed* ahead of the advancing interface, and above which particle *engulfment* occurs. Applications for this kind of fundamental research can be found in the area of superconductors[1], biological cell preservation[2], and geology[3]. However, the majority of research work involving particle pushing is aimed at metal matrix composites[4]. Only with a homogeneous distribution of the reinforcement phase the improved mechanical properties of these materials can be fully exploited. The term "engulfment" is used to describe incorporation of a particle by a planar interface, and the term "entrapment" is used for particle incorporation by a cellular or dendritic interface because the mechanisms are rather different. While numerous models have been proposed over the years in an attempt to explain particle behavior at the SL interface, a paucity of experimental data exist in particular for ceramic particles dispersed in metal matrices. An extensive literature review of experimental data yielded no reliable results which could be used to validate the proposed models, since the basic assumptions of the models - spherical and inert particles, pure matrix material, and a macroscopically planar SL interface - were not satisfied. The main goal of this work is to provide reliable experimental data that can be used for validation of models describing particle behavior at the solidifying interface in metal matrix composite materials.

**Theoretical Evaluation of the Critical Velocity.** Over the years several models have been proposed to describe the pushing-engulfment transition (PET). Most models [4,5,6,7,8,9] solve the balance between the drag force exercised by the liquid on the particle (which pushes the particle into the interface), and the repulsive force between the particle and the S/L interface (the interface interaction force). Some models assume mass transport by diffusion in the particle-interface region [10]. The critical velocity calculated by these models is an inverse function of particle radius at some power. The influence of melt convection on the particle-interface interaction is ignored. To unambiguously validate the different models against the experimental data obtained, it is necessary

to accurately evaluate the various thermophysical parameters that determine the values of the interacting forces. There is a clear lack of data and/or methodology for such an evaluation (see for example ref. 11). The drag force can be accurately calculated as parameters such as melt viscosity and particle radius are well quantified. Even contribution from localized distortions of the S/L interface due to differences in thermal conductivities between melt and particles have been theoretically analyzed in several models [7,8]. The repulsive force in most models originates from the difference in surface energies between the particle and the matrix material. Accurate calculations are lacking because of unavailability of relevant data such as interfacial energies.

From the analysis of experiments performed on transparent organic materials containing insoluble particles[12], it was concluded that three regimes of particle-interface interaction can be rationalized as follows:

- no or low melt convection, $V > V_{cr}$ ⇒ engulfment
- no or low melt convection, $V < V_{cr}$ ⇒ pushing
- significant melt convection ⇒ no particle - interface interaction

In the current work, only the first two regimes will be analyzed theoretically.

In the Shangguan, Ahuja and Stefanescu (SAS) [8] model the interaction force was attributed to the difference between the interfacial energies of the liquid, solid matrix, and particle, $\Delta\sigma_o$ . An equation for the critical velocity at which the PET occurs was derived as:

Eq. 1 $$V_{cq} = \frac{\Delta\sigma_o d}{3\mu K^* R}\left(\frac{a_o}{a_o + d}\right)^n$$

where $\mu$ is melt viscosity, $R$ is particle radius, $K^*$ is the particle /liquid thermal conductivity ratio, $a_o$ is the atomic distance, and $d$ is the minimum particle /interface distance. In this model it was assumed that $d = a_o$, and n has been determined as n=2.

Two modifications of the SAS model are suggested. The first one is related to the use of the thermal conductivity ratio. This quantity was introduced in the velocity equations from the shape of the interface. For trough formation it was shown that $K^* = R_I/(R_I-R)$, where $R_I$ is the radius of the interface. For bump formation it can be demonstrated that $K^* = R_I/(R_I+R)$ and then that Eq.1 is valid for both bump and trough formation. In this formulation it is assumed that the interface can take any shape as dictated by $K^*$. However, the interface curvature will be restricted by interface stability criteria. Calculation with the Mullins-Sekerka instability criterion for the case of the aluminum-zirconia system shows that the curvature of the interface is an order of magnitude smaller than that obtained from simple thermal considerations ($K^*$). In the

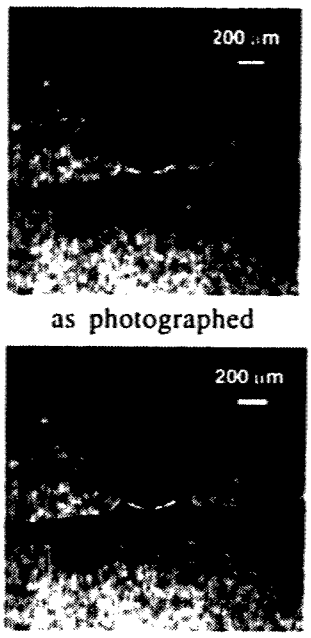


as photographed

computer enhanced

Fig. 1 XTM picture showing trough formation in the bump. Pure aluminum / zirconia (720 µm dia.) system. Interface velocity is 4 µm/s.

aluminum-zirconia system, a recent experiment[13] has demonstrated that a trough can form in the bump, Fig. 1. For all practical purposes this cancels the effect of $K^*$. Thus, in the absence of a more complete model for bump-forming systems, the SAS model should be used with $K^* = 1$. The second modification is that the minimum particle-interface distance has to be in the order of 50 $a_o$ for the liquid to maintain its properties, as discussed by Cottrell [14]. Thus, Eq.1 that was derived on the assumption of fluid flow in the particle-interface gap is not valid unless $d \geq 50\ a_o$.

**Calculation of surface energies.** In the SAS model the calculation of the critical velocity is based upon the surface energy difference, $\Delta\sigma_o$. Calculation of this parameter is not trivial. In this work, $\Delta\sigma_o$ defined as $\sigma_{PS}$ -$\sigma_{PL}$ will be used. Thus, $\sigma_{PS}$ and $\sigma_{PL}$ are needed. $\sigma_{PL}$ can be calculated from Young's equation: $\sigma_{PL} = \sigma_{PV} - \sigma_{LV}\cos\theta$ . Both $\sigma_{PV}$ and $\sigma_{LV}$ are typically available in the literature. The contact angle $\theta$ can be measured using sessile drop experiments. $\sigma_{PS}$ can be calculated by using the work of adhesion. The underlying assumption behind the work of adhesion approach is that, when two solids that are in contact are separated because of the creation of two new solid-vapor interfaces, the interface energy in the system is increased by the work of adhesion, $W_{ad}$, and the strain energy, $W_{str}$: $\sigma_{PS} = \sigma_{PV} + \sigma_{SV} - a(W_{ad} + W_{str})$. The coefficient $a$ accounts for the degree of particle/solid contact. In turn, the work of adhesion can be calculated from the Girifalco-Good relationship[15]: $W_{ad} = 2\Phi\sqrt{\sigma_{PV} \cdot \sigma_{SV}}$. The coefficient $\Phi$ can have values between 0.24 (calculated based on data from ref. 16) and 1.15 [15]. Then, if $\sigma_{PV}$ and $\sigma_{SV}$ are known, $\sigma_{PS}$ can be calculated. For non-wetting metal-ceramic systems it is reasonable to assume that $a = 0$. The relevant interface energies as well as the sources used for the Al - $ZrO_2$ system are summarized in Table 1.

Table 1 Interfacial energies in the Al - $ZrO_2$ and Zn - $ZrO_2$ systems.

| Energy mJ/m$^2$ | Al - $ZrO_2$ | Source | Zn - $ZrO_2$ | Source |
|---|---|---|---|---|
| $\sigma_{PV}$ | 697 | 17,18 | 697 | 17,18 |
| $\sigma_{LV}$ | 870 | 19 | 770 | 20 |
| $\sigma_{SV}$ | 896 | 20 | 1133 | estimated* |
| $\sigma_{PL}$ | 1450 | $\theta = 150$ 21 | | $\theta =$ |
| $\sigma_{PS}$ | 1593<br>1198 | $a = 0$<br>$a = 1, W_{str} = 0$ | 1830<br>1403 | $a = 0$<br>$a = 1, W_{str} = 0$ |
| $\Delta\sigma_o$ | 143<br>-252 | poor contact<br>ideal contact | | poor contact<br>ideal contact |

* from the ratio between solid surface energy and grain boundary energy

From the calculation of $\Delta\sigma_o$ given in Table 1, it is apparent that when choosing the two limiting values for $a$, $\Delta\sigma_o$ may vary from negative to positive values. The negative value will be conducive to spontaneous engulfment, since the critical velocity becomes zero according to the SAS model. This is in direct contradiction to the experimental observations, where a clear PET was observed. Accordingly, the positive value is more reasonable. Nevertheless, the case must be made for poor contact between the engulfed zirconia particle and the surrounding aluminum matrix. Indeed, as shown in Fig. 2, upon fracture, the zirconia particle is pulled out of the matrix leaving very limited particle-solid contact. Since the aluminum-zirconia contact angle measurements performed in our laboratory also showed poor contact, it is reasonable to conclude that $a$ should be nearer to zero than to one. Thus, in further calculations the values of $\Delta\sigma_o$ resulting from $a = 0$ were adopted.

**Selection of metal matrix-ceramic particle system** Based on the restrictions imposed by the model, the experimental system chosen consisted of spherical zirconia particles dispersed in a pure aluminum and a pure zinc matrix. Zirconia particle were selected because they do not react with aluminum up to temperatures of 900°C. Another issue pertaining to sample characterization is the ability to locate the particle position in the samples before and after directional solidification (DS). The non-destructive method used is X-ray Transmission Microscopy (XTM) [22] for the Al-$ZrO_2$ samples. Post-experimental characterization is done by XTM and metallograpy. The samples to be used for directional solidification were prepared by melt processing and casting. Melting of the metal was done in a resistance furnace under high purity argon. Aluminum was degassed by argon purging. 2 to 3 vol% zirconia particles were added to the liquid and mechanically mixed. The molten composite was then poured into a graphite mold to produce cylindrical specimens of 9 mm diameter and 100 mm length. An example of an XTM picture of an aluminum-zirconia sample is provided in Fig. 3. This technique could not be used for the zinc samples because of the high density of zinc. The samples were directional solidified in a Bridgman-type furnace. The gradients as measured with the main heater temperature set at 800 °C and the trim heater temperature set at 850 °C were 100 K/cm.The experimental variables were the matrix metal and a single translation velocity of the furnace. For evaluation of the critical velocity the *average solidification velocity* was used rather than the furnace translation.

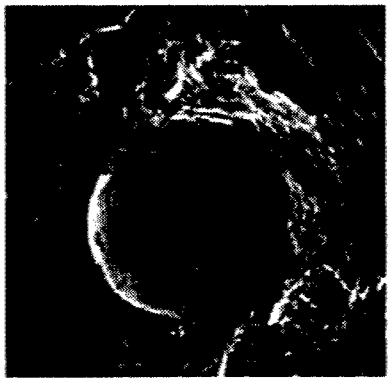

Fig. 2 Scanning electron micrograph of a fracture surface from a directionally solidified aluminum - zirconia sample

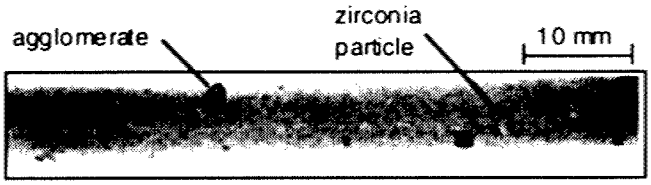


Fig. 3 XTM picture of aluminum - zirconia sample before DS processing.

**Post-Solidification characterization.** A number of selected samples were examined by XTM. All samples were examined metallographically. The samples were grinded layer by layer to map the volumetric particle location. As previously shown, particle distribution is affected by remelting [23]. It was not possible to correlate the position of the particles in the samples after sample preparation with that after melting. Consequently, some criteria for interpretation of experimental results were established. These rules resulted in "clean" data for the evaluation of the PET.

**Experimental results.** Out of 28 experiments, 13 were considered "clean", i.e., satisfying the rigid criteria, and were used for the evaluation of the PET. Some typical examples of particle distribution after DS are shown in Fig.4. Note that on sample Al-14 two particles present in the DS region were not considered as engulfed because they were engulfed during the initial transient when the solidification velocity is not steady.

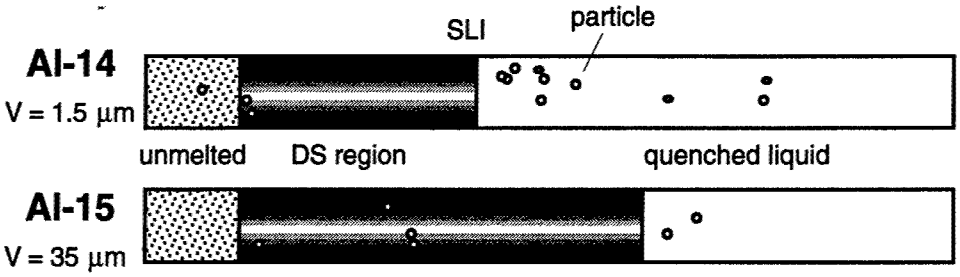


Fig. 4 Schematic representation of particle distribution in DS aluminum - zirconia samples: top - pushing; bottom - engulfment.

The results of the directional solidification experiments for the aluminum-zirconia system are summarized in Table 2. From these data it is obvious that a clear PET exists at a solidification velocity between 1.9 and 2.4 μm/s.

Table 2 Experimental results for aluminum - zirconia samples

| Sol.Vel.[μm/s] | 1.3 | 1.3 | 1.5 | 1.9 | 2.4 | 2.6 | 5.8 | 6.5 | 10.9 | 11.9 | 15 | 44.8 | 85 |
|---|---|---|---|---|---|---|---|---|---|---|---|---|---|
| Sample no. | Al-22 | Al-27 | Al-28 | Al-14 | Al-23 | Al-21 | Al-29 | Al-30 | Al-17 | Al-18 | Al-24 | Al-16 | Al-15 |
| Result | P | P | P | P | E | E | E | E | E | P | E | E | E |

* P: pushing, E: engulfment

Similar experiments were run on zinc-zirconia samples. The results of the directional solidification experiments for the zinc-zirconia system are summarized in Table 3. Again, a clear PET is seen at velocities between 1.9 and 2.9 μm/s.

Table 3 Experimental results for zinc-zirconia samples

| Sol.Vel. [μm/s] | 1.2 | 1.9 | 2.9 | 7.3 | 13.6 | 19.4 | 40 |
|---|---|---|---|---|---|---|---|
| Sample no. | Zn-2 | Zn-8 | Zn-9 | Zn-6 | Zn-5 | Zn-7 | Zn-3 |
| Result* | P | P | E | E | E | E | E |

* P: pushing, E: engulfment

**Model validation.** Since at the time this report was written, not al necessary data for calculation of the surface energy of the zinc-zirconia system were available, validation is limited to the aluminum-zirconia system. The data required for model validation are available in the literature except the ones for the interfacial energy difference. Using the models from Uhlman, Chalmers, Jackson[10] (UCJ), Bolling and Cissé[7] (BC), Chernov, Temkin, Mel'nikova[5,6] (CTM), and Shangguan, Ahuja, Stefanescu[8] (SAS), the calculated critical velocities are given in Table 4. Comparing the calculated values with the experimental results it is apparent that only the SAS model predicts a critical velocity which is in the right order of magnitude.

Table 4 Experimental and calculated critical velocities (μm/s).

| Particle radius, μm | Aluminum - $ZrO_2$ | | | | |
|---|---|---|---|---|---|
| | UCJ | BC | CTM | SAS | Experimental |
| 250 | $4.6 \cdot 10^{-5}$ | 0.03 | 0.04 | 0.89 | 1.9 - 2.4 |

## References


1 A. ENDO, H.S. CHAUHAN, T. EGI, Y.SHIOHARA: *J. MATER. RES.*, VOL. 11, NO. 4, 1995, PP. 1037
2 C. KÖRBER, G. RAU, M.D. COSMAN, E.G. CRAVALHO: *J. CRYST. GROWTH*, VOL. 72, 1985, PP. 649
3 K.A. JACKSON, B. CHALMERS: *J. APPL. PHYS.*, VOL. 29, NO.8, 1958, PP. 1178
4 D.M.STEFANESCU, B.K.DHINDAW, S.A.KACAR, A.MOITRA: *MET.TRANS. A*, 1988 , VOL. 19A, PP. 2847
5 A.A. CHERNOV, D.E. TEMKIN, AND A.M. MEL'NIKOVA: *SOV. PHYS. CRYSTALLOGR.*, 1977, VOL. 22 (6), PP. 656
6 A.A. CHERNOV, D.E. TEMKIN, AND A.M. MEL'NIKOVA: *SOV. PHYS. CRYSTALLOGR.*, 1976, VOL. 21 (4), PP. 369
7 G.F. BOLLING AND J.A. CISSÉ: *J. CRYST. GROWTH*, 1971, VOL. 11, PP.25
8 D.K. SHANGGUAN, S. AHUJA, AND D.M. STEFANESCU: *METALL. TRANS.* A, 23A, 1992, PP. 669
9 J. PÖTSCHKE AND V. ROGGE: *J. CRYST. GROWTH.*, 1989, VOL. 94, PP. 726
10 D.R. UHLMANN, B. CHALMERS AND K.A. JACKSON: *J. APPL. PHYS.*, 1964, VOL. 35 (10), PP. 2986
11 P.K. ROHATGI, S.RAY, R. ASTHANA AND C.S. NARENDRANATH: *MAT. SCI AND ENG.*, 1993, VOL. A162, PP. 163
12 S. SEN, B.K. DHINDAW, H. PANG AND D.M. STEFANESCU: SUBMITTED TO J. CRYSTAL GROWTH
13 S. SEN, PRIVATE COMMUNICATION
14 A. COTTRELL: *INTRODUCTION TO THE MODERN THEORY OF METALS*, THE INSTITUTE OF METALS, LONDON (1988)
15 A.W. ADAMSON: *PHYSICAL CHEMISTRY OF SURFACES*, JOHN WILEY & SONS, INC., NEW YORK, 1982
16 R.M. PILLIAR AND J. NUTTING: *PHIL. MAG.* 16 (1967) 181
17 D.T. LIVEY AND P. MURRAY: *J. AMER. CERAMIC SOC.*, 1956, VOL. 39 (11), PP. 363
18 W.D. KINGERY: *J. AMER. CERAMIC SOC.*, 1954, VOL. 37 (2) PP. 42
19 S.H. OVERBURY, P.A. BERTRAND AND G.A. SOMORJAI: *CHEMICAL REVIEWS*, 1975, VOL. 75 (5), PP. 547
20 L.R. MURR: *INTERFACIAL PHENOMENA IN METALS AND ALLOYS*, ADDISON WESLEY, MA, 1975
21 J.G. LI: *CERAMICS INTERNATIONAL*, 1994, VOL. 20, PP. 391
22 P.A. CURRERI AND W.F. KAUKLER: *MET.TRANS.*, 1996, VOL. 27A, PP. 801
23 B.K. DHINDAW, P. GANGULY, F.R. JURETZKO AND D.M. STEFANESCU, PROCEEDINGS TMS ANNUAL CONFERENCE SPRING 1996 ANAHEIM CALIFORNIA

# CRYSTAL GROWTH OF ZnSe AND RELATED TERNARY COMPOUND SEMICONDUCTORS BY VAPOR TRANSPORT

Ching-Hua Su
Space Sciences Laboratory
NASA/Marshall Space Flight Center(MSFC)
Huntsville, Alabama 35812
Tel: (205)544-7776
e-mail address: ching.hua.su%msfc28po@x400gw.msfc.nasa.gov

Co-Investigators:
Prof. Robert F. Brebrick, Marquette University
Dr. Arnold Burger, Fisk University, NASA Center for Photonic Materials and Devices
Prof. Michael Dudley, State University of New York at Stony Brook
Prof. Richard J. Matyi, University of Wisconsin, Madison
Drs. Narayanan Ramachandran and Yi-Gao Sha, USRA, NASA/MSFC
Dr. Martin Volz, Space Sciences Laboratory, NASA/MSFC
Industrial Co-Investigator:
Dr. Hung-Dah Shih, Central Research Laboratories, Texas Instruments

## I. Summary

Interest in optical devices which can operate in the visible spectrum has motivated recent research interest in II-VI wide band gap materials. The recent challenge of semiconductor opto-electronics is the development of a laser at short visible wavelengths. With an energy gap of 2.7 eV at room temperature, ZnSe has been studied extensively as the primary candidate for blue light emitting diode for the applications of optical displays, high density recording, and military communications because of its efficiency in band-to-band transition. Adding another element to ZnSe to form the ternary compounds such as $ZnSe_{1-x}S_x$, $ZnSe_{1-x}Te_x$, and $Zn_{1-x}Cd_xSe$ gives tunability to the energy

band gap so as to cover a wider range of the visible spectrum. In the past several years, major advances in the thin film technology such as molecular beam epitaxy (MBE) and metal organic chemical vapor deposition (MOCVD) have demonstrated the important applications of these materials. While issues related to the compositional inhomogeneity and defect incorporation are still to be fully resolved, ZnSe bulk crystals and ZnSe-based heterostructures such as ZnSe/ZnSeS, ZnSe/ZnCdSe and ZnCdSe/ZnSeS have showed photopumped lasing capability in the blue-green region at a low threshold power and high temperature. At the same time, the development in the crystal growth of bulk materials has not advanced far enough to provide low price, high quality substrates needed for the thin film growth technology.

Crystallization from vapor has various advantages over melt growth. These advantages result mostly from (1) the lower processing temperature involved — the high melting temperatures of the wide band gap materials make the melt growth process very difficult to handle, (2) physical vapor transport (PVT) acts as a purification process because of the differences in the vapor pressures of the native elements and the impurities, and (3) most solid-vapor interfaces exhibit higher interfacial morphological stability during growth because of their low atomic roughness and, consequently, the pronounced growth rate anisotropy. The technique of vapor transport in closed ampoules is especially attractive for space investigation due to its experimental simplicity and minimal needs for complex process control.

Two reasons have been put forward to account for the better structural and electrical properties observed previously for crystals grown by vapor transport in low gravity. The first is weight-related reductions in crystal strain and defects which are caused by the weight of the crystals during processing at elevated temperatures and retained on cooling, particularly for materials with low yield strength. The second, and more general, reason is related to the reductions in density-gradient driven convection. Reductions in such convection in low gravity is expected to yield nearly diffusion-limited growth condition which results in more uniform growth rates (in the microscopic scale) and hence greater crystalline perfection and compositional homogeneity.

Compositional non-uniformity, microstructural crystal defects (e.g. dislocations, low-angle grain boundaries, twins and second phase precipitates), and deviation from stoichiometry (native point defects) can seriously limit state-of-the-art device performance and future device applications. The reduction of gravity-driven convective fluid flows in a low-gravity environment is expected to be advantageous in minimizing these compositional variations and structural defects. Density gradient driven convection may result from either thermal gradients, axial and radial, or from solutal gradient which can develop from many sources, including non-stoichiometric rejection of vapor at the crystal interface and unequal molecular weights for transport and residual impurity vapor species. By a judicious ampoule orientation with respect to gravity, these thermal and solutal gradients can be arranged to oppose one another. In this Earth-bound, but convectively stable case, bulk convection occurs when the solutal gradient exceeds both the thermal gradient and viscous resistance. Viscous resistance, in turn, depends on both material properties and ampoule aspect ratio. Hence even in this brief, and simplified, picture of vapor growth conditions, a number of gravity-related issues deserve detailed and quantitative investigation.

## II. Objectives

The following are the objectives of the proposed investigation:

1. to determine the relative contributions of gravity-driven fluid flows to the incorporation of impurities and defects and the deviation from stoichiometry (native point defects) observed in the crystals grown by vapor transport as results of buoyancy-driven convection, irregular fluid-flows and growth interface fluctuations.
2. to evaluate the effects of gravity on vapor transport process and on growth kinetics of the solid-vapor interface by real time *in-situ* non-invasive monitoring technique and by examining the compositional distribution within the ternary compounds grown in the process.
3. to assess the relative amount of strain developed during processing at elevated

temperatures and retained on cooling caused by the weight of the crystals.

## III. Experimental and Theoretical Analyses

The crystal growth experiment will utilize a novel vapor transport three-thermal-zone heater translating method. The investigation consists of an extensive ground-based study followed by flight experimentation and involves both experimental and theoretical work. The objectives of the ground-based work are to establish the characteristics of the crystals grown on Earth as a basis for subsequent comparative evaluations of the crystals grown in a low gravity environment and to obtain the experimental data and perform the analyses required to define the optimum parameters for the flight experiments.
The deviation from stoichiometry of the starting materials, an important factor in determining the vapor transport rate, will be characterized by partial pressure measurements and the results will be used in the selection of the heat treatment methods of the starting materials. The thermodynamic properties of the ZnSe binary and the ternary systems, such as the chemical potentials of the elements, the Gibbs free energy of formation of the vapor phase and the characteristics of the ternary solid solutions will also be established by partial pressure measurements. Mass flux of the vapor transport process, a critical parameter in the optimization of the growth parameters, will be measured by an in-situ dynamic technique for these materials. The fundamentals of the current vapor transport theories will be evaluated by performing in-situ simultaneous measurements of the partial pressures of the individual vapor species and the transport rates in the transport ampoules. Unseeded and seeded growths of ZnSe and related ternary crystals will be performed by physical vapor transport in both horizontal and vertical (stabilized and destabilized) configurations to evaluate the effects of gravity-driven convection on the grown crystals. Crystal growth by chemical vapor transport will also be conducted as a complimentary study on the effects of total vapor pressure in the system on the fluid flows and, consequently, the grown crystals. For the first time, the in-situ partial pressure measurements will be performed during crystal growth process to establish the correlation between the vapor transport process and the properties of the crystals. A schematics of the thermal profile provided by the three heater zone furnace

and the initial ampoule positions for unseeded and seeded growth is given in Figure 1 where optical windows for the in-situ monitoring are also shown. The growth process starts by translating the furnace to the right.

In the proposed investigation, various technique will be applied to characterize, mainly, the crystalline structural properties as well as the electrical and optical properties of the grown crystals. The studies on the structural defects, including impurities, voids, precipitates, dislocations, slip bands, small angle grain boundaries, twins and compositional variation in ternary compounds will be accomplished by various technique such as Spectroscopy (atomic absorption (AA), spark source mass spectroscopy (SSMS) and secondary ion mass spectroscopy (SIMS)), X-ray diffraction (Laue reflection and rocking curve), synchrotron radiation images of white X-ray beam (reflection and transmission), Microscopy (optical, electron (SEM and TEM), and atomic force (AFM)), sample polishing and etching and optical transmission. The electrical and optical characterization will be performed by Hall measurements, optical transmission, photoluminescence, and transient charge technique (TCT) for mobility and lifetime measurements. Figure 2 shows the flow chart of material and samples preparation and characterization plan.

Mathematical modeling, including one-dimensional diffusion limited theory of mass transport, analytical study of three-dimensional axisymmetrical system and three-dimensional numerical simulation of both mass transport and heat transfer, will be developed to delineate the multi-species fluid flows in vapor transport systems.

Characterization and analysis of the samples will be done in MSFC, Fisk University, State University of New York and University of Wisconsin. Mathematical modeling will be developed to delineate the multi-species fluid flows in vapor transport systems by USRA/MSFC Co-Investigators and will give guidance in the selection of optimized growth parameters for the flight experiments and in the interpretation of the characterization results of the crystal properties.

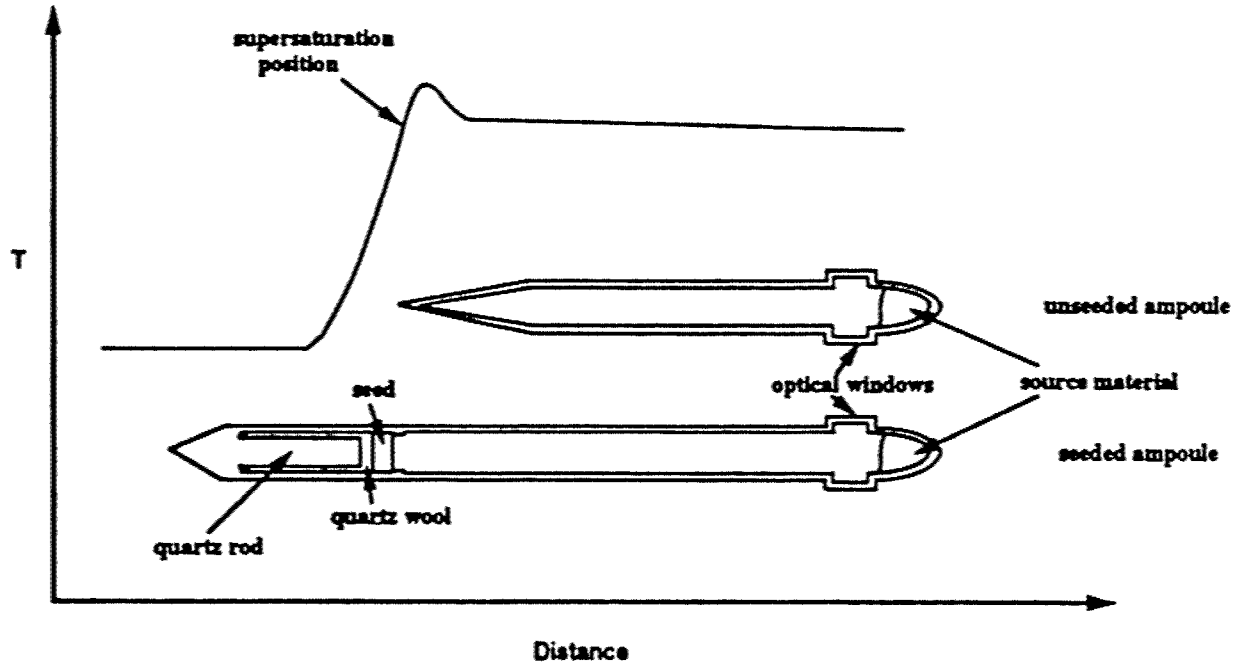


Figure 1. Schematics of thermal profile and initial ampoule positions for unseeded and seeded growth

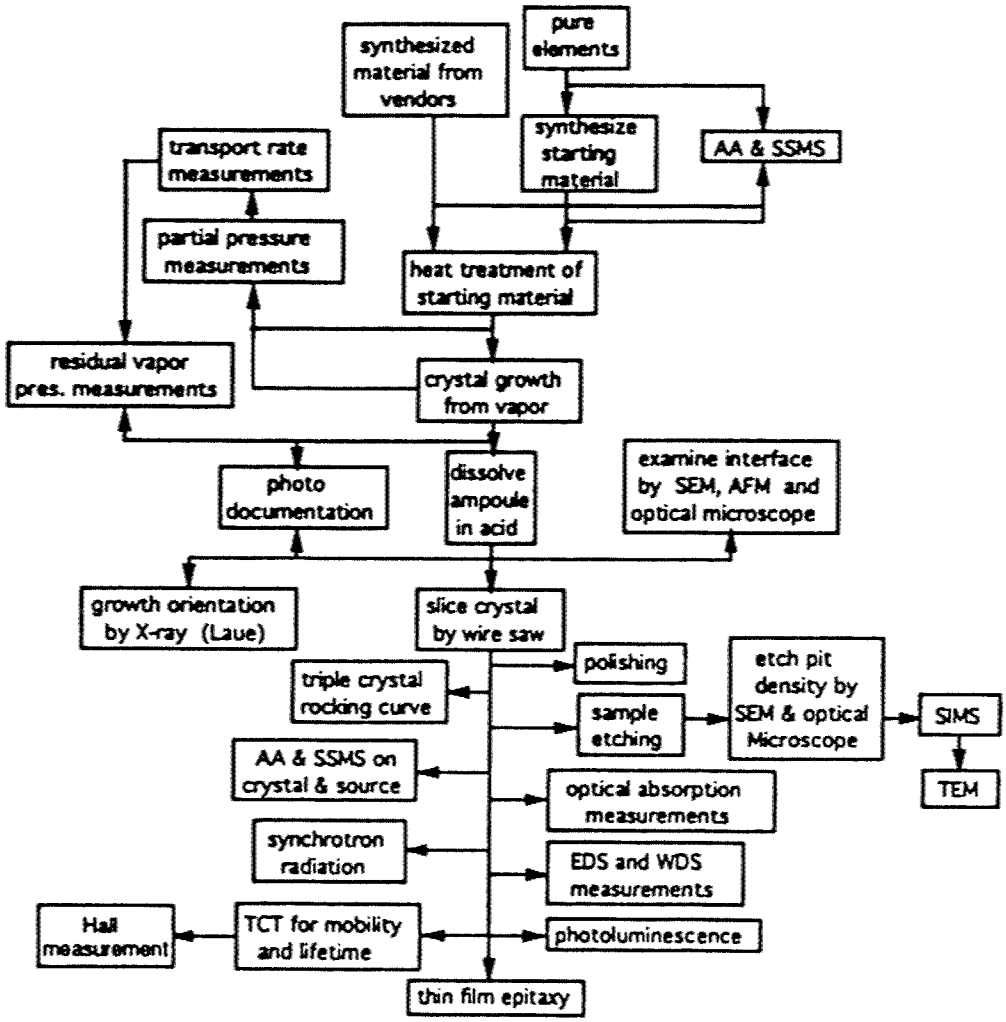


Figure 2. Flow chart of sample preparation and characterization plan

# MAGNETIC DAMPING OF SOLID SOLUTION SEMICONDUCTOR ALLOYS

Dr. Frank R. Szofran, Principal Investigator
ES75/Space Sciences Laboratory, NASA Marshall Space Flight Center, Huntsville, AL 35812
Phone: 205-544-7777, Fax: 205-544-8762, e-mail: frank.szofran@msfc.nasa.gov

Co-Investigators:

Prof. Dr. K.W. Benz, Dr. Arne Cröll, Dr. Peter Dold
Kristallographisches Institut der Universität, Freiburg, Germany

Ms. Sharon D. Cobb, Dr. Sandor L. Lehoczky, Dr. Martin P. Volz, Mr. Dale A. Watring
ES75, Marshall Space Flight Center, Huntsville, AL

Dr. Shariar Motakef
Cape Simulations, Inc., Wellesley, MA

## 1. Objectives of the Investigation

The objective of this study is to conduct the Earth-based research sufficient to successfully propose a flight experiment (1) to experimentally test the validity of the modeling predictions applicable to the magnetic damping of convective flows in conductive melts as this applies to the bulk growth of solid solution semiconducting materials in the reduced gravitational levels available in low Earth orbit and (2) to assess the effectiveness of steady magnetic fields in reducing the fluid flows occurring in these materials during space processing. To achieve the objectives of this investigation, we are carrying out a comprehensive program in the Bridgman and floating-zone configurations using the solid solution alloy system Ge-Si. This alloy system was chosen because it has been studied extensively in environments that have <u>not</u> simultaneously included both low gravity and an applied magnetic field. Also, all compositions have a high electrical conductivity, and the materials parameters permit high growth rates compared to many other commonly studied alloy semiconductors.

An important supporting investigation is determining the role, if any, that thermoelectromagnetic convection (TEMC) plays during growth of these materials in a magnetic field. Compositional anomalies observed by us in magnetic grown crystals may be caused by TEMC and, if so, would

have significant implications for the deployment of a Magnetic Damping Furnace in space. This effect may be especially important in solid solutions where the growth interface is, in general, neither isothermal nor isoconcentrational. It could be important in single melting point materials, also, if faceting takes place producing a non-isothermal interface.

## 2. Microgravity Relevance

During Bridgman or floating zone growth of semiconductors, generation of destabilizing temperature gradients in the melt is unavoidable, resulting in buoyancy-induced convective mixing of the liquid phase. On Earth this convective mixing is generally very intensive and interferes with segregation of melt constituents at the growth front. A floating zone is also subject to Marangoni or surface tension gradient driven convection which is gravity independent. Crystal growth in low Earth orbit provides the opportunity to reduce the buoyancy-induced convective intensity; and, in some cases, diffusion-controlled mass transfer during growth may be achieved if the residual acceleration direction and magnitude can be controlled. However, calculations[1] and recent flight experiment results[2] clearly indicate that simply reducing the steady-state acceleration to values achievable in low-Earth orbit will not provide diffusion controlled growth conditions for solid solution melts ~1cm in diameter if accelerations transverse to the growth axis are not controlled. Magnetic damping of convection in electrically conductive melts can be used to provide a higher degree of control on convection in the melt. Magnetic damping effects both buoyancy-induced and Marangoni convection and may enable diffusion controlled growth without the control of the growth direction relative to the residual steady-state acceleration. Thus our understanding of convective influences on melt-growth processes can be further advanced, and our ability to interpret space experimental results may be significantly improved.

## 3. Approach and Procedures

Si, Ge, and Si-rich alloys have been grown in a monoellipsoid mirror furnace[3] by the floating-zone technique and Ge and Ge-rich alloys have been grown by the vertically stabilized Bridgman technique in both a multi-zone tube furnace[4] and the mirror furnace with the lamp used as the

heat source moved toward the center of the ellipse from the focus to provide a more uniform thermal profile than is used for float zone growth. Thus far, the sample diameters have all been in the range of 8 to 10 mm. All float-zone samples were single crystalline rods contained in sealed fused silica ampoules. Among the types of samples were those coated with a 5μm thick oxide layer for which the ampoule contained pure oxygen as well as uncoated samples in argon. A variety of dopants, dopant schemes, and magnetic fields ranging up to 5 T have been used. Interface demarcation in Ga-doped Ge samples by means of mechanical disturbance and current pulses has been carried out successfully in the tube furnace. Sample analysis has included Nomarski microscopy, four-point probe and spreading resistance measurements, and infrared transmission spectroscopy.

## 4. Results and Discussion

### *4.1 Floating Zone*

Observations have generally been as expected but there have been some surprises, as well. The coring observed at lower fields[5] has been observed at higher fields with the thickness of the surface layer continuing to reduce as the field is increased. In the initial millimeters of growth, striations are reduced by the higher fields as expected. However, in Sb- and As-doped samples, after growing striation free for several millimeters in fields of 1-4T striations suddenly appear. An example is shown in Figure 1. We are currently working to understand this phenomenon with TEMC being considered as one of the possible causes.

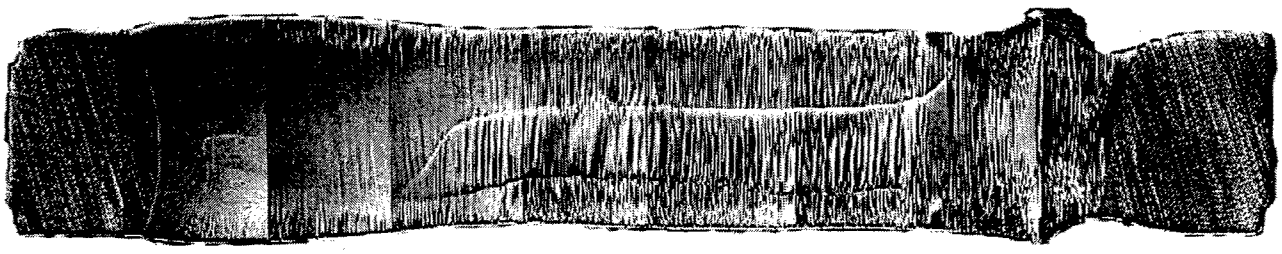

**Figure 1. Nomarski photograph of Sb-doped Si FZ sample 3Sb33 grown at 1 T. Growth is from left to right.**

## *4.2 Bridgman*

### 4.2.1 Mirror furnace

Eight Ge samples and six Ge-rich alloy samples have been grown recently and are being analyzed. One Ge:Ga sample grown at zero field grew for about 27mm such that the solid was not in contact with the ampoule wall. There was an initial length of about 6mm and a final length of about 8mm that grew in normal contact with the wall. In between, the surface looks like a free surface except for a few widely separated narrow (~10μm wide) ridges that are presumed to have been in contact with the wall. The radius of the non-contact region is uniformly smaller that the ampoule inside diameter by 30μm. Possible reasons for this unusual, if not unique, behavior are being investigated. Observation of the samples during growth showed rapid motion of particles on the top, free surface of the samples and, in some cases, wave-like motion that could not be attributed to vibrations. These phenomena, which cannot be observed in the opaque tube furnace, occurred at fields up to 3 T.

### 4.2.2 Tube furnace

We have grown numerous Ge:Ga samples of 8 mm diameter with lengths of 7 to 12 cm in fields up to 5 T. One series of crystals showed good agreement with the numerical simulations carried out for the specific thermal conditions used; that is, fields higher than ~3T reveal an initial compositional transient followed by a plateau that closely resembles diffusion-controlled growth. In most instances, however, the compositional profile begins to vary after several centimeters of constant composition growth; the cause of the convection producing these variations is believed to be related to the applied thermal profile. We have now achieved axial composition profiles consistent with diffusion controlled growth to within 3 cm of the last-to-freeze end when no attempt is made to avoid thermal end effects. When a sliding graphite plug is placed on top of the melt and an additional length of Ge above that, as shown in Figure 2, the axial profile remains diffusion controlled much nearer to the end. An example of the latter is shown in Figure 3 where the carrier concentration has not been corrected for the geometry of the sample. Both mechanical and current pulsing have been used successfully to demarcate the growth interfaces in these samples. In addition to applying a magnetic field, we have used crucibles with a range of

conductance and used two types of thermal field. The first type of thermal field was the usual profile defined by two isothermal zones and an intermediate gradient region. The second type was an approximately constant thermal gradient over the entire melt. For one specific set of experiments using a two-zone thermal profile in which only the magnetic field was varied, the approach to a diffusion-controlled initial axial composition profile occurred at a field which agreed very well with numerical simulations. Nonetheless, to maintain a diffusion-controlled profile beyond the first 30% of sample length, it was necessary to use a constant thermal gradient. Under these conditions, crucibles with lower thermal conductance yielded flatter growth interfaces and generally approached diffusion-controlled growth more closely. In summary, the application of a large magnetic field has a pronounced effect, but it does not by itself ensure diffusion controlled growth.

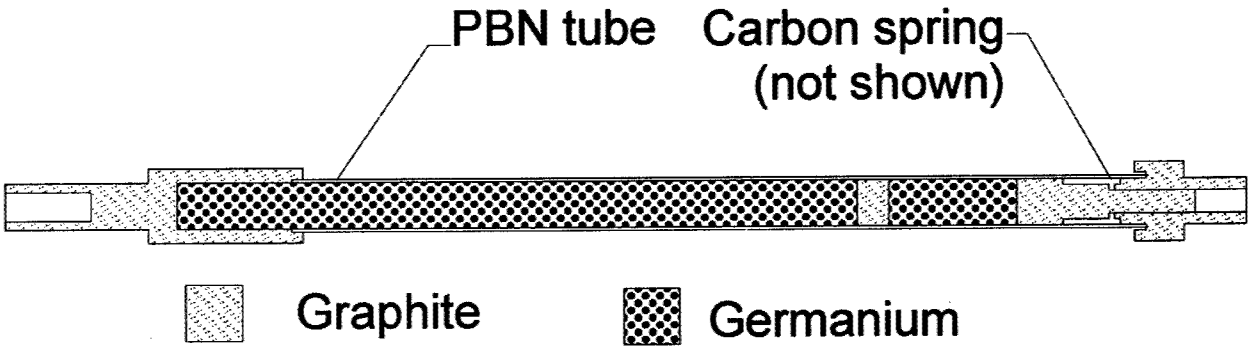


**Figure 2. Pyrolitic boron nitride (PBN) sample holder for current pulsing.**

One $Ge_{0.95}Si_{0.05}$ Bridgman sample has been grown in a 5T field. A sudden increase in Si concentration after the sample had grown normally through 60% of its length may be another manifestation of TEMC.

## 5. Conclusions and Plans

The three growth schemes employed, floating zone and Bridgman growth in two configurations, have been shown to be complementary. Each one provides a part of the information that will be needed to understand more thoroughly the role of gravity in the solidification of solid solution semiconductor alloys. Work on doped Ge will be completed soon and attention turned to the Ge-

Si alloy system. Continued attention will be given to the contribution, if any, of TEMC in the growth process of these materials. For this reason among others, considerable effort will be made to measure selected thermo-physical properties of the alloys with compositions in the range of interest.

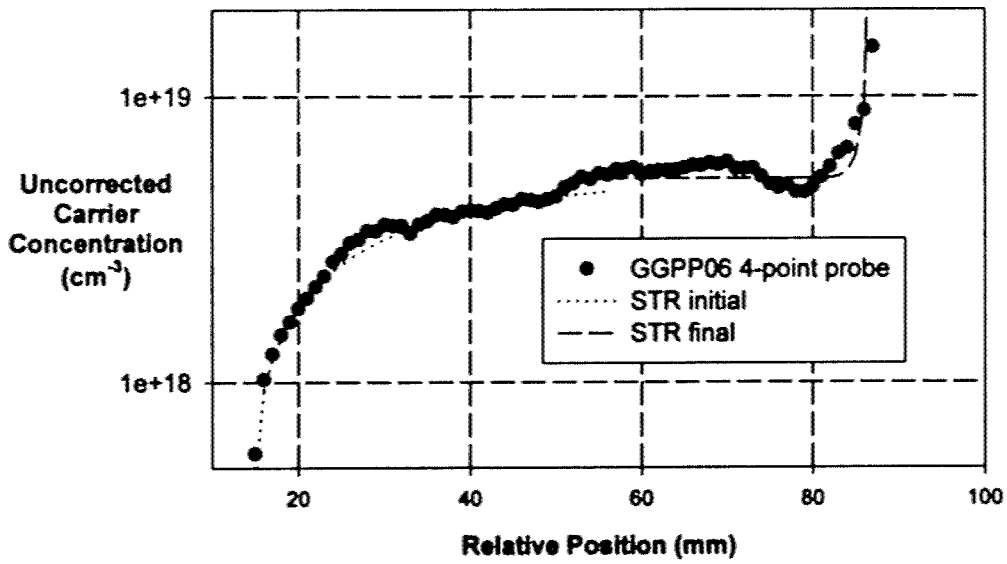


**Figure 3. Axial Ga distribution in a Ge:Ga sample grown at 8μm/s in a 5T field.**

---

[1] See, for example, S. Motakef, J. Crystal Growth **102** (1990) 197, and R.J. Naumann, J. Crystal Growth **142** (1994) 253.

[2] See papers in these proceedings by S.L. Lehoczky and co-workers and references therein.

[3] A laboratory version of the ELLI furnace. See K.W. Benz, Prog. Crystal Growth and Charact. **26** (1993) 267.

[4] The furnace is similar in size and thermal characteristics to the NASA Advanced Automated Directional Solidification Furnace (AADSF). See **Crystal Growth of HgCdTe in the AADSF on the USMP-2 Mission**, AIAA 95-0609, S.L. Lehoczky, D.C. Gillies, F.R. Szofran, F.A. Reeves, J.D. Sledd, J.M. Cole, T.K. Pendergrass, D.A. Watring, C.R. Coppens, J.E. LeCroy, and D. Popok, presented at the 33rd Aerospace Sciences Meeting and Exhibit, January 9-12, 1995, Reno, NV.

[5] A. Cröll, P. Dold, and K.W. Benz, J. Crystal Growth **137** (1994) 95.

# THE FEATURES OF SELF-ASSEMBLING ORGANIC BILAYERS IMPORTANT TO THE FORMATION OF ANISOTROPIC INORGANIC MATERIALS IN MICROGRAVITY CONDITIONS

Daniel R. Talham
Department of Chemistry
University of Florida
Gainesville, FL 32611-7200
(352) 392-9016
talham@pine.circa.ufl.edu

James H. Adair
Department of Materials Science and Engineering
University of Florida
Gainesville, FL 32611
(352) 392-6594
jadai@eng.ufl.edu

## Hypothesis and objective.

This report presents a research plan for a new MSAD investigation into particle formation at micellular structures, aimed at extending methodologies to the preparation of anisotropic inorganic particles. The major objective of the proposed program is to develop a fundamental understanding of the growth of anisotropic particles at organic templates, with emphasis on the chemical and structural aspects of layered organic assemblies that contribute to the formation of anisotropic inorganic particles. Target systems include both metal particles important to conductive pathways in microelectronics, such as Ag/Pd alloys and Pt, and II-IV semiconductors such as CdSe and CdS.

Materials with directional properties are opening new horizons in a variety of applications including chemistry, electronics, and optics. Structural, optical, and electrical properties can be greatly augmented by the fabrication of composite materials with anisotropic microstructures or with anisotropic particles uniformly dispersed in an isotropic matrix. Examples include structural composites, magnetic and optical recording media, photographic film, certain metal and ceramic alloys, and display technologies including flat panel displays. The new applications and the need for model particles in scientific investigations are rapidly outdistancing the ability to synthesize anisotropic particles with specific chemistries and narrowly distributed physical characteristics (e.g. size distribution, shape, and aspect ratio).

Anisotropic particles of many compositions have been produced but only a few (such as $\gamma$-$Fe_2O_3$ and AgI) are produced with any degree of chemical and physical control.[1-3] While we generally know what systems yield single crystal, anisotropic-shaped particles, we do not know how to

make powders of these crystals with the desired control of shape uniformity, aspect ratio and phase composition, and there is no systematic fundamental methodology for generating anisotropic particles that can be extended to other chemical compositions. Furthermore, using conventional synthetic routes, the reproducible synthesis of anisotropic particles with nanometer sizes in at least one dimension remains a profound challenge.

There are two ways that anisotropically shaped particles have been produced from solution.[4] The first is crystallographically controlled growth, producing particle shapes dictated by the relative growth rate among the various habit planes. Growth rates are often controlled by the inclusion of adsorbates or "poisons" that selectively restrict the growth of certain faces. A second approach is to control nucleation and growth by the synthesis of materials in the presence of molecular templates (Figure 1). While this method has been successfully used to restrict the size of particles,[5-8] there have been few attempts to control particle shape. The current profect applies principles from both of these approaches to achieve particle shape control by employing amphiphilic molecules assembled into specific lyotropic micellular structures as templates for the formation of anisotropic inorganic particles. An important aspect of our approach is to include careful analysis of the chemical nature of the particle/template interface, as this interaction can play an equally important role in determining the shape and orientation. Our hypothesis is that uniform dispersions of anisotropic inorganic particles can be produced with templating methods if the chemical interaction between the organic template and the particle is carefully controlled.

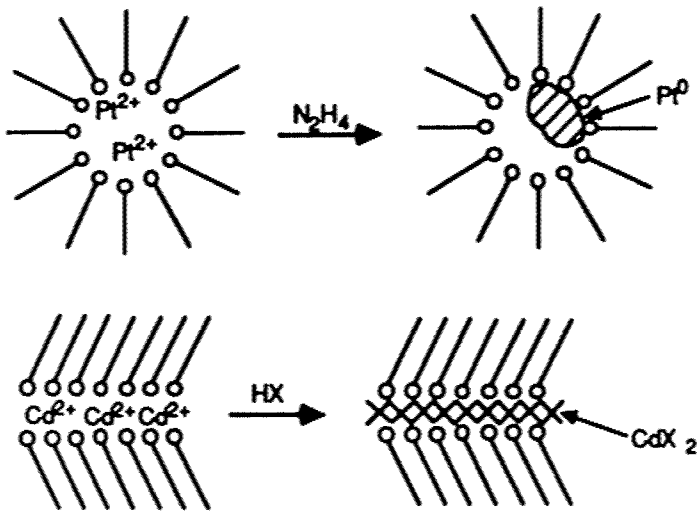


**Figure 1.** Formation of inorganic solids at organic micellular structures. Top, reduction of $Pt^{2+}$ ions to form $Pt^o$ within reversed micelles. Bottom, an inorganic salt prepared within a bilayer structure. The bilayer can be assembled on a solid support by Langmuir-Blodgett methods, or in solution as a lamellar oil-water-surfactant phase.

As part of our studies, we will make extensive use of model membrane systems prepared by Langmuir-Blodgett (LB)[9] methods in order to efficiently survey possible template systems and establish the important chemical and geometric features of the templates that influence particle growth. It is planned to use what is learned on the model systems to develop larger-scale preparations of the targeted inorganic materials at bilayer structures formed from "oil-in-water" segregated phase systems. It is these systems that will eventually lead to high yield, monodisperse preparations. When going from the model systems toward larger scale solution preparations, the fundamental chemical and templating interactions will be in competition with effects caused by convection and in some cases sedimentation, and the limits of templating will be masked by gravity effects. A further objective of this project is to develop template/particle systems that are suitable for potential microgravity investigations probing the mechanism of templated particle growth.

## Justification for Microgravity Experiments.

The advantages of a microgravity environment for studying crystallization, nucleation and growth processes are well-documented.[10,11] In the present project, minimizing convectional induced fluid shear and sedimentation in the microgravity environment should allow extended structure organic templates to form rather than fragments or "rafts" that result at normal Earth's gravity. Convection limits the size of uniform template domains and also creates a non-uniform size dispersion. These imperfections in the template structures make it difficult to assess the role that the chemical and geometric identities of the template play in controlling particle size and dispersion. Reducing convection will also minimize the agglomeration of particles that are produced.

Sedimentation is less of a problem than convection in the synthesis and processing of nanoscale particles or particles with nanometer scale in at least one dimension. Analysis[12] demonstrates that the displacement due to gravity becomes less dominant as the particle size becomes smaller than about 0.25 μm. In contrast, sedimentation will begin to mask template effects as particle sizes increase beyond several hundred nanometers. Convection is much more difficult to accommodate both theoretically and experimentally. Preliminary work indicates that bilayer domain sizes and, therefore, face dimensions of plate-like particles or rod length greater than about 0.1μm will be difficult to achieve. The masking imposed by convection on the degree of particle shape anisotropy that may be achieved has been confirmed in our preliminary experiments on Earth. Nonetheless, attempts to simulate near gravity-free conditions with an absence of convection will be attempted by performing the precipitation experiments in a cone and plate viscometer with high shear yet within the laminar flow regime. The head of such a viscometer is insulated thermally, but temperature gradients due to the heat of reaction for the precipitation reaction are expected to

generate conventional currents. The aim of the applied shear is to test whether the conventional currents can be counteracted by the applied shear.

**Description of Experimental or Analytical Method.**

The research plan addresses the basic chemical issues associated with forming inorganic particles within the restricted domains of anisotropic micelles including the roles that sedimentation and convection processes play in limiting the template and therefore the resulting particle size. The micellular templates are bilayer or cylindrical structures. The bilayer templates should limit particle growth in the interlayer dimension and promote growth in the direction within the plane resulting in plate-like particles, while cylindrical templates should permit rod-like particles. Given an ideal template where the geometric and chemical characteristics are optimized, particle growth is determined by diffusion within the confines of the template structure, and ultimately particle sizes in the growth dimension are limited by the template size.

The research approach combines investigation of single bilayer systems, prepared by LB methods, with the target higher-yield solution systems. Motivation for studying single-layer systems is two-fold. First, the chemical and structural properties of LB films are easily manipulated and characterized, allowing us to tailor the template system to the inorganic material being formed. Secondly, LB films on surfaces are less subject to the convectional shear, sedimentation, and agglomeration normally experienced by particles synthesized in the bulk solution, and therefore can be used to simulate the hydrodynamic conditions that systems experience in the microgravity environment of space. The surface confined bilayers can be used to establish how particle growth is limited by chemical and geometric considerations in the absence of convection and sedimentation effects. The research plan is laid out in the form of individual tasks. The tasks include:

Task 1. Development of surfaces with functional groups with affinities toward specific inorganic species. Model organic templates will be prepared by LB techniques. Template variables include the chemical affinity of the functional groups for the inorganic species under investigation, template periodicity, and template rigidity. Each of these variables can be investigated systematically using LB model templates.

Task 2. Forming inorganic particles within deposited LB templates. Reactions to produce the inorganic particles from the pre-assembled ions within LB films will be performed. By forming the particles within the deposited films we can determine how the templates interact with the inorganic particle and observe orientation and shape selectivity. These observations will be used to design further template systems.

Task 3. Determination of the bilayer and rod-shaped regimes in the Pseudoternary phase diagram for the amphiphilic molecule-oil-water system. Assessment of the affinity for the specific cation (or anion) at tailored sites on the template, as determined in Task 1, will indicate the general classes of amphiphilic molecules that may be used. In the event that the pseudoternary phase diagram is not established in the literature on lyotropic liquid crystals, experiments will be performed to determine the nature of the structures in the microemulsion system as a function of composition.

Task 4. Experiments evaluating the deposition of inorganic materials. Deposition of the inorganic materials depends on a number of factors in addition to the structure of the microemulsion and the affinity of the precipitating cation and anion toward the polar head groups. The complex ionic equilibria of the aqueous solution will be calculated using suitable computer methods and the relevant relationships for the chemical reactions.

Task 5. Modelling. A number of computer programs are available to model both the chemistry and the templating in the amphiphilic systems. These programs will be used to help guide the choice of systems and to help explain experimental results.

Task 6. Develop systems suitable for potential microgravity experiments. As template/particle systems are developed, they will each be evaluated to determine if the factors that influence size and shape selectivity are masked by convection or sedimentation. These are the cases where microgravity experiments will help elucidate the mechanism of anisotropic particle growth and control. As suitable systems are identified, they will be refined to make them compatible with the restrictions of microgravity experimentation.

## References


(1) Hartman, P. *J. Cryst. Growth.* **1980**, *49*, 166.

(2) James, J. A.; Kell, R. C. In *Crystal Growth*; B. R. Pamplin, Ed.; Pergamon Press: New York, 1975; pp 557-575.

(3) Matijevic, E. In *Chemical Processing of Advanced Materials*; L. L. Hench and J. K. West, Ed.; John Wiley and Sons: 1992; pp 513-527.

(4) Calvert, P.; Mann, S. *J. Mat. Sci.* **1988**, *23*, 3801-3815.

(5) Chandler, R. R.; Coffer, J. L. *J. Phys. Chem.* **1993**, *97*, 9767-9770.

(6) Petit, C.; Lixon, P.; Pileni, M.-P. *J. Phys. Chem.* **1993**, *97*, 12974-12983.

(7) Fendler, J. H. *Chem. Rev.* **1987**, *87*, 877-899.

(8) Dameron, C. T.; Reese, R. N.; Mehra, R. K.; Kortan, A. R.; Carroll, P. J.; Steigerwald, M. L.; Brus, L. E.; Winge, D. R. *Nature* **1989**, *338*, 596-597.

(9) *Langmuir-Blodgett Films*; Roberts, G. G., Ed.; Plenum Press: New York, 1990.

(10) *Materials Processing in the Reduced Gravity Environment of Space*; Doremus, R. H.; Nordine, P. C., Ed.; Materials Research Society: Pittsburgh, 1987; Vol. 87, pp 366.

(11) Vaderhoff, J. W.; Micale, F. J.; El-Aasser, M. S.; Sudol, E. D.; Tseng, C. M.; Sheu, H. R. *J. Disp. Sci. Tech.* **1984**, *5*, 231.

(12) Allen, T. *Particle Size Measurement;* 4th ed.; Chapman Hall: New York, 1990.

# DYNAMIC NUCLEATION OF DEEPLY UNDERCOOLED MELTS AND MEASUREMENT OF THE SURFACE TENSION AND VISCOSITY

E.H. Trinh and K. Ohsaka
Jet Propulsion Laboratory, MS 183 401
4800 Oak Grove Drive, Pasadena, CA 91109
(818) 354 7125; email: eugene.h.trinh@jpl.nasa.gov

## INTRODUCTION

The undercooling, or supercooling (cooling of a liquid below its nominal melting point) and superheating (heating of a liquid above its nominal boiling point) phenomena are not just esoteric natural anomalies, their occurrence is quite common in many practical industrial applications involving alloy solidification and liquid distillation. A recently suggested application of undercooled liquids has been in the area of biochemical products storage, where low temperature could be achieved without the drastic changes brought about by crystallization (Mathias, 1991)[1]. Undercooled and superheated liquids are metastable because they are not thermodynamically at equilibrium, remaining in the liquid state because of a kinetic barrier to phase transformation. Although, the extent of the metastable liquid range is often *greater* than that of the normally considered stable phase, it is much less accessible because the phase with lower free energy is thermodynamically favored (solid phase in the undercooled liquid phase). Classical nucleation theory is generally successful at explaining the ability to undercool and to superheat liquids, and it predicts the limits of the metastable liquid phase in ideal situations. These homogeneous nucleation limits have been verified only for very few specific cases under considerably constrained experimental conditions involving very small ultra-pure samples or at perhaps ultra-high temperature. In practice, however, excursions into the metastable liquid state is usually very restricted for most substances and for realistic manufacturing process parameter ranges. The problem of understanding *some* of the determining factors associated with the premature nucleation of the solid phase in the case of an undercooled liquid is the subject matter of this proposed research. In particular, we shall endeavor to rigorously demonstrate the viability of the concept of *dynamic nucleation* (Chalmers, 1982)[2] in undercooled liquids subjected to *isotropic pressure excursions*. In addition, we also propose to develop a novel experimental method to measure two physical parameters

very relevant to the nucleation process, the *viscosity and surface tension of deeply undercooled, highly viscous liquids*. Such a capability is not currently available.

We believe that experimental conditions in microgravity make it feasible to control both the supercooled droplet and the enclosed single microscopic bubble, and they allow accurate measurements by implementing a droplet rotation technique which was developed and validated during a previous microgravity investigation. Gravity significantly affects the three principal elements of the advocated experimental approaches: (1) The controlled bubble dynamics are perturbed by the large density mismatch between the gas bubble and the undercooled droplet and by the high intensity acoustic field; (2) The free rotating drop bifurcation transition and the shape relaxation dynamics of quiescent deformed drops are both strongly modified by large levitation fields required in 1 G; (3) "Dynamic" nucleating effects could reduce the undercooling potential of freely suspended melts; such evidence has been obtained in previous ground-based experiments.

## 1.0 DYNAMIC NUCLEATION OF DEEPLY UNDERCOOLED LIQUIDS

### 1.1 SCIENTIFIC BACKGROUND

Circumstantial evidence for "dynamically induced nucleation" exists in the form of numerous experimental observations of the sudden onset of solidification coinciding with the imposition of a mechanical disturbance of significant amplitude. Ultrasonic irradiation of undercooled and solidifying melts has been used for many years for the purpose of grain refining. Although these artificially-induced disturbances are generally associated with both fluid flows and pressure waves, it is generally viewed as improbable that the spatial or temporal scales of the liquid flow fields would extend down to the levels of molecular or atomic aggregates relevant to nucleation dynamics. Analytical studies have also concluded that the large pressure fluctuations accompanying acoustic cavitation can potentially induce phase transition in an undercooled liquid[3] . During a cavitation event, vapor or gas bubbles are generated in the acoustically irradiated liquid because the associated negative pressure excursions exceed its tensile strength. The large amplitude volume oscillations of the bubbles thus generated also drive large positive pressure excursions during the violent bubble collapse phase[4] .

We propose to investigate the phenomenon of acoustic pressure-induced nucleation by using a novel approach involving the large amplitude resonant radial oscillations and collapse of a

*single bubble intentionally injected in a droplet of undercooled liquid.* Using a combination of previously developed and proven techniques (Trinh and Apfel, 1980[5], Gaitan et al.,1992[6]), the fluid particles will be suspended in a fluid host by an ultrasonic field which will supply both the levitation capability as well as the forcing of the bubble radial oscillations. The highly nonlinear behavior of a gas bubble in a liquid and under acoustic forcing, has been investigated for many years, and leads to such phenomena as the fascinating single bubble sonoluminescence which involves periodic bubble growth and collapse (Crum, 1994[7], Putterman, 1995[8]). We plan to observe the effects of the increase in pressure (due to bubble colla*pse*) in a region no larger than 100 μm within the undercooled melt to rigorously prove the hypothesis of pressure-induced nucleation of the solid phase. For a *non-collapsing* bubble (i.e. for lower amplitude bubble radial oscillations), the effects of micro-streaming generated in the liquid by the steady-state bubble radial oscillations on the achievable level of undercooling will also be examined. *The use of single bubbles operating in narrow temporal and spatial scales will allow the direct and unambiguous correlation between the origin and location of the generation of the disturbance and the location and timing of the nucleation event.*

## 1.2 RESEARCH OBJECTIVES AND PLAN

Because we want to probe for the effects of these perturbations within a range of intensity, we also want to control the initial level of undercooling. The deepest undercooling would be achieved by using a single levitated undercooled millimeter-size droplet containing a bubble. For more modest undercooling, however, one can use specially designed small containers (Trinh and Apfel, 1978)[9] to hold the liquid and the bubble would be trapped within it by an ultrasonic standing wave. We shall therefore divide the experimental tasks into two parts: the first will deal with the study of dynamic nucleation of undercooled liquids contained in small acoustically resonant cells, and the second will involve the levitation and ultrasonic probing of undercooled droplets containing a bubble. The latter configuration is of course the best suited for the microgravity environment because it allows the centering of the bubble within the undercooled droplet and the pressure antinodes of the sound field.
The specific objectives are listed below.

*Dynamic nucleation in undercooled liquids contained in cells.*
A single bubble will be trapped by an ultrasonic standing wave in a cell filled with a transparent and outgassed high purity liquid (water, succinonitrile, O-Terphenyl,...) which

will be undercooled to predetermined level. A series of undercooling runs will be carried out to determine a distribution of experimentally observed nucleation temperature using the cell without the bubble but with the ultrasonic standing wave activated at power levels below any cavitation threshold. The same set of undercooling runs will be performed with a trapped bubble. The dynamic state of the bubble will be monitored using previously developed Mie scattering methods. Appropriate acoustic parameters will then be determined in order to drive the bubble into radial oscillations of increasing amplitude while monitoring its motion as well as the radiated sound field using shadowgraphic methods and Mach Zehnder interferometry. These experiments will be repeated for several pre-determined undercooling levels. *A correlation between the bubble oscillation amplitude and onset of nucleation with undercooling as a parameter will be sought.*

. *Dynamic nucleation in levitated undercooled droplets.*
In this case a single liquid drop will be levitated in an immiscible host, and a bubble will be injected into the drop. The same experiments as described above will be carried out for various levels of drop undercooling. The bubble dynamics monitoring optical diagnostics will be modified to accomodate a non-ideal geometry including the curvature of the droplet.

. *Parametric study of the nucleation process.*
Experimental parameters will be varied in order to document their impact of the nucleation onset. *Effects of the the purity and the viscosity of the undercooled liquid will be studied in order to delineate the parameter region where cavitation-induced nucleation remains effective.* Detailed analysis of the timing of the nucleation event with respect to the bubble radial oscillations will be examined in detail, and the recording of the location of the nucleation event will be attempted.

## 2.0 MEASUREMENT OF SURFACE TENSION AND VISCOSITY

### 2.1 BACKGROUND

There has been a renewal of interest in the viscosity of liquids, especially at temperatures below the melting point, and in connection with glass formability (Bettezzati and Greer, 1989[10]; Miani and Matteazzi, 1992[11]; Egry et al., 1993[12]; Wachter and Sommer, 1990[13]; Taborek et al., 1986[14]). A glass is formed from a liquid if nucleation of a crystal is avoided by rapid cooling. The glass is a metastable phase and its true identity (whether or

not it is thermodynamically independent from the liquid phase) is still a subject of debate. Since the identity is not directly related to the topic of present interest, we take the stand that the glass is the frozen liquid that has lost excess configurational entropy. Glass has been formed in most metallic liquids including pure elements (Kim et al., 1989[15]). The degree of glass formability is expressed by the critical cooling rate for glass formation or the temperature ratio, $T_g/T_m$, where $T_g$ is the calorimetrically measured glass transition temperature and $T_m$ is the melting point (or liquidus temperature or the congruent melting point for alloys). The glass formability widely varies depending on elements (fcc metals are the worst glass formers) and compositions (eutectic alloys are easy glass formers). Viscosity plays an important role in the classical nucleation theory used to construct the time-temperature-transformation (TTT) curves for determining the critical cooling rate. Apart from the specific application of viscosity to determine the glass formability, the way in which the viscosity of an undercooled liquid changes as the temperature falls toward $T_g$ provides useful information about the mechanism of atomic mobility in undercooled liquids.

## 2.2 EXPERIMENTAL APPROACH AND PLAN

Currently used non-invasive methods of surface tension measurement for the case of *undercooled liquids* generally rely of the quantitative determination of the resonance frequencies of drop shape oscillations, of the dynamics of surface capillary waves, or of the velocity of streaming flows [16-17]. These methods become quickly ineffective when the liquid viscosity rises to a significant value. An alternate and accurate method which would be applicable to liquids of significant viscosity is therefore needed. We plan to develop such a capability by measuring the equilibrium shape of levitated undercooled melt droplets as they undergo solid-body rotation. The experimental measurement of the characteristic point of transition (bifurcation point) between axisymmetric and two-lobed shapes will be used to calculate the surface tension of the liquid. Such an approach has already been validated through the experimental verification of numerical modeling results [18]. The experimental approach will involve levitation, melting, and solidification of undercooled droplets using a hybrid ultrasonic-electrostatic technique in both a gaseous as well as a vacuum environment.

A shape relaxation method will be investigated in order to derive a reliable method to measure the viscosity of undercooled melts. The analysis of the monotonic relaxation to equilibrium shape of a drastically deformed and super-critically damped free drop has been used to derive interfacial tension [19] of immiscible liquid combinations where one of the

component has high viscosity. A standard approach uses the initial elongation of a droplet through shear flows, but an equivalent method could involve the initial deformation of a drop levitated in a gas by ultrasonic radiation pressure, electric stresses, or even solid body rotation. The dynamic behavior of the free drop relaxing back to equilibrium shape has already been modeled, and its characteristic time dependence will provide a quantitative means to evaluate the liquid viscosity.

## REFERENCES


1. Mathias, S.F.,"Undercooling-low temperature without freezing", Tibtech, **9**, 70-372 (1991)
2. Chalmers, B., *Principles of Solidification*, Robert E. Krieger Publishing Co., page 86-89 (1982)
3. Hickling, R,"Transient, high pressure solidification associated with cavitation in water", Phys. Review Lett. **73**, 2853-2856 (1994)
4. Suslick,K.S., D.J. Cassadonte, M.L.H. Green, and M.E. Thompson,"Effects of high intensity ultrasound on inorganic solids" Ultrasonics, **25**, 56-59 (1987)
5. Trinh, E. and R.E. Apfel,"Sound velocity of supercooled water down to -33 C using acoustic levitation" J. Chem. Phys. **72**, 6731-6735 (1980)
6. Gaitan, D.F., Crum, L.A., Church, C.C., and Roy, R.A.,"Sonoluminescence and bubble dynamics for a single, stable, cavitation bubble", J. Acoust. Soc. Am. **91**, 3166-3183 (1992)
7. Crum, L.A., "Sonoluminescence", Physics Today, September 1994, 22-29 (1994)
8. Putterman, S.J,"Sonoluminescence: Sound into Light", Scientific American , Feb. 1995, 46-51 (1995)
9. Trinh, E. and R.E. Apfel,"Method for the measurement of the sound velocity in metastable liquids, with an application to water", J. Acoust. Soc. Am., **63**, 777-780 (1978)
10. Battezzati L. and A.L. Greer,"The viscosity of liquid metals and alloys" Acta Metall. **37**, 1791 (1989)
11. Miani, F, and Matteazzi, P.,"Estimation of the viscosity in undercooled liquid metal alloys", J. Non-Cryst. Sol. **143**, 140-146 (1992)
12. Egry, I., Lohöfer, G. and Sauerland, S.,"Surface tension and viscosity of liquid metals", J. Non-Crystall. Soli. **156**, 830-832 (1993)
13. Wachter, J. and Sommer, F.,"Glass transition temperature and viscosity of supercooled melts", J. Non-Crystall. Sol. **117/118**, 890-893 (1990)
14. Taborek, P., Kleinman, R.N. and Bishop, D.J.,"Power-law behavior in the viscosity of supercooled liquids", Phys. Rev. B, **34**, 1835-1840 (1986)
15. Kim, Y.W., Lin, H.M. and Kelly, T.F., Acta Met. **37**, 1791 (1989)
16. Trinh, E.H., Marston, P.L. and Robey, J.L.,"Acoustic measurement of the surface tension of levitated drops", J. Coll. Interf. Sci. **124**, 95-103 (1988)
17. Fraser, M.E., Lu, W-K, Hamielec, A.E., and Murarka, R.,"Surface tension measurements on pure liquid iron and nickel by an oscillating drop technique", Metall. Trans. **2**, 817-823 (1971)
18. Trinh, E.H. and Leung E.,"Ground-based studies of the vibrational and rotational dynamics of acoustically levitated drops and shells", AIAA Paper **90-0315**, Am. Institute of Aeronautics and Astronautics, Washington DC (1990)
19. Tjahjadi, M., Ottino, J. and Stone H.A., "Estimating interfacial tension via relaxation of drop shapes and filament break-up", AIChE J. **40**, 385-394 (1994)

# INTERFACE PATTERN SELECTION CRITERION FOR CELLULAR STRUCTURES IN DIRECTIONAL SOLIDIFICATION

R. Trivedi, Principal Investigator, Department of Materials Science and Engineering, Iowa State University, Ames, IA 50011. Phone: 5515-294-5869; FAX 515-294-4291; trivedi@ameslab.gov
S. N. Tewari, Co-Investigator, Chemical Engineering Department, Cleveland State University, Cleveland, OH, 44115,
D. Kurtze, Department of Physics, North Dakota State University, Fargo, ND, 58105.

## Introduction

This investigation focuses on to the key scientific concepts that govern the selection of cellular patterns in directional solidification of alloys. Critical scientific concepts in the selection of interface patterns will be addressed first, and then the ground-based experimental studies in metallic and organic systems will be presented. It will be shown that the experimental conditions under which stable cellular structure form are precisely the ones where convection effects are dominant, so that microgravity environments are required for the comparison of experimental results with the theoretical predictions based on diffusive growth.

Pattern formation is important in many disciplines of science. Since the growth conditions in directional solidification can be precisely controlled and measured, it provides a powerful technique to study the principles that govern the formation of ordered, disordered or chaotic patterns. Furthermore, the formation of a cellular or dendritic structure is accompanied by microsegregation of solute which can generate stresses or lead to the formation of a new stable or metastable phase in intercellular region that can significantly alter the properties of the alloy. Thus the reliability of products made by solidification techniques such as casting and welding largely depends upon our ability to control solute segregation patterns so as to minimize stresses or to avoid the formation of undesirable phases in the intercellular region.

Cellular structures form when the velocity is increased beyond the threshold of planar interface stability. In the cellular structure, different cells in an array are strongly coupled so that the cellular pattern evolution is controlled by complex interactions between thermal diffusion, solute diffusion and capillarity effects. These interactions give infinity of solutions, and the selection criterion then quantitatively narrows the actual range of solutions.

Scientific concepts

When a planar interface becomes unstable and forms a cellular structure, the linear stability analysis predicts a wide range of possible wavelengths at a given velocity. Experimental studies, on the other hand, show a very narrow band of spacing so that nonlinear effects play a crucial role in the selection of cellular spacings, Fig. 1. The precise interaction of the stabilizing effects of thermal gradient and capillarity, and the destabilizing effects of solute gradient is complex, and theoretical models show this balance to be given by a selection criterion that has the general form[1]: $mG_c - G = \Gamma/(\sigma^* R^2)$, where $G_c$ is the solute gradient in the liquid at the cell tip, G the temperature gradient, $\Gamma$ the capillarity constant, R the cell tip radius, and $\sigma^*$ is the stability parameter whose precise nature for cellular structure is not yet established.

For cellular structures, the above selection criterion is complex since the shape of the interface is strongly influenced by the interactions between the neighboring cells. Thus, both the thermal and the solute field interactions must be considered simultaneously, along with the capillarity effect, to obtain the stable steady-state shape of the interface which then controls the concentration gradient at the cell tip. Cellular structures in metallic systems grow mainly in the heat flow direction so that the precise role of anisotropy on the selection parameter, $\sigma^*$, needs to be evaluated. Numerical calculations on the evolution of cellular structures[3] show that anisotropy plays a crucial role in the selection of the shape of cells[4] and the spacing of cells[3].

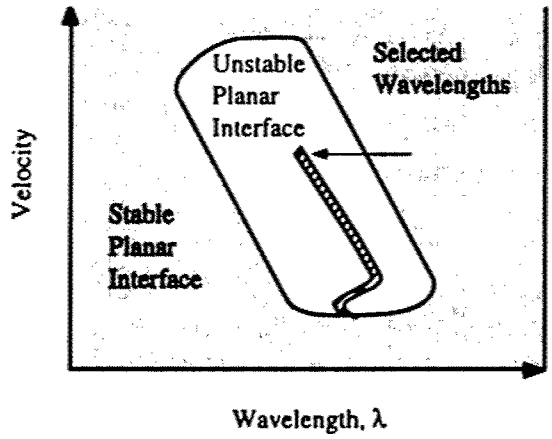


Fig. 1. The possible wavelengths of a planar unstable interface according to the linear stability analysis[2]. Only a narrow band of wavelengths are selected in the nonlinear regime, as observed by the experimental study.

Experimental studies, Fig. 2, and theoretical predictions for cellular spacing show that a finite range of spacing can exist under given experimental conditions[5]. Thus, the scaling law between the spacing and the velocity can only be quantitatively established for minimum (or maximum) stable spacing. This physics of selection criterion for different velocities should also be able to predict the range of spacing that occur under a given velocity condition. The scientific goal is to establish the general pattern selection criterion for cellular structures that can encompass all the crucial features of cellular microstructures, including all relevant length scales and a microsegregation pattern. By examining the cellular and dendritic growth near the cell-dendrite transition, we shall also establish the physics that leads to the cell to dendrite transition.

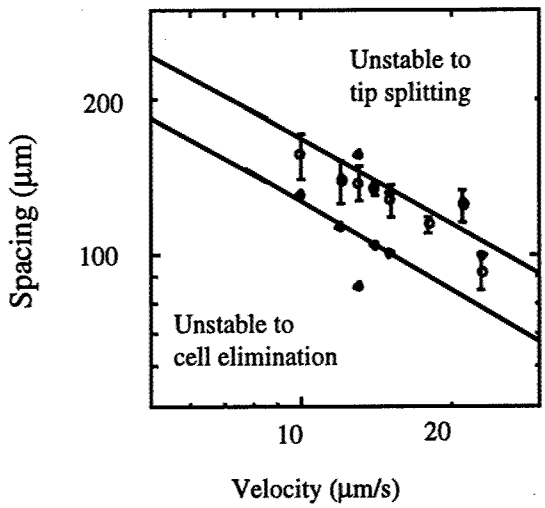


Fig. 2. The selection of a band of spacing, characterized in thin samples (150μm thick) of succinonitrile-acetone[5].

Ground-based studies/Need for Microgravity

Significant ground based experiments in the cellular regime have been carried out in several metallic systems, and it has been well-established that *the conditions under which cellular microstructure is stable are precisely the ones where convection effects are significant.* Consequently, significant departures of experimental results from the theoretical predictions have been observed in experiments carried out under 1g. The following convection effects have been found to be dominant in the cellular regime. (1) The solute is heavier than the solvent, so that the macroscopic interface becomes curved and exhibits a "steepling effect", which prevents the analysis of the cellular pattern formation [6]. (2) the three-dimensional arrangement of cells shows a

significant disorder[7]. (3) The cell tip radius in the cellular region deviates significantly from the results predicted by the theoretical model[8] for bulk metallic samples, as shown in Fig. 3. Thus, convection effects in bulk samples do not allow one to examine the cell shape and cell tip radius/spacing selection criterion precisely.

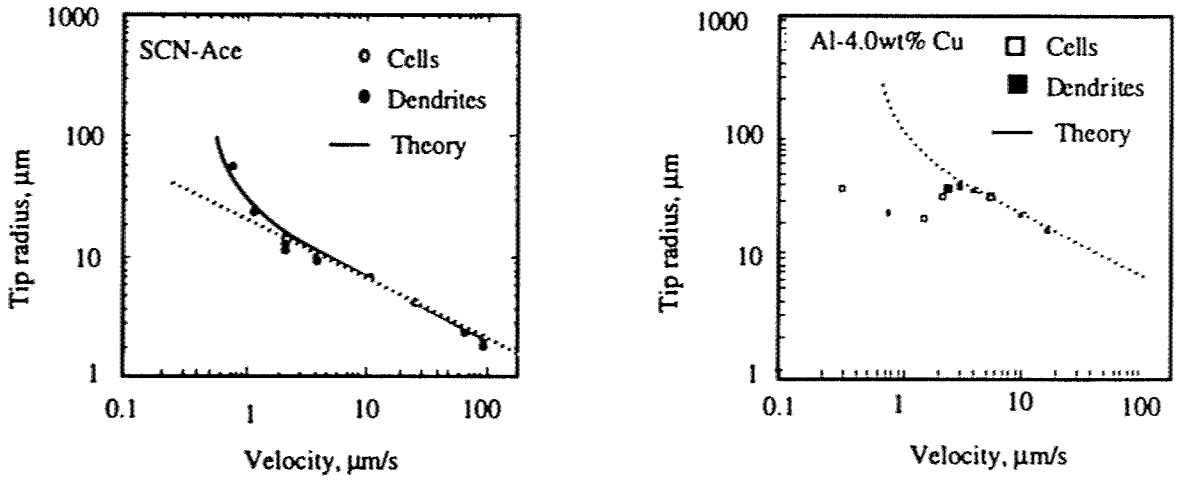


Fig. 3. (a) A comparison of theoretical predictions with the experimental data in (a) thin samples (150µm) of succinonitrile-acetone [9], and (b) bulk samples of Al-4.0 wt % Cu[10].

In experimental studies in thin samples, where convection effects are not significant, the presence of curvature along the thickness significantly influences the shape of the interface and thus the spacing and the amplitude of cells. Also, the steady-state cell far from the tip is truncated as the cells reach the wall surfaces. Since the cell shape away from the tip plays a crucial role for cellular structures, the precise steady-state conditions for a cellular structure can not be achieved in thin samples. Furthermore, two-dimensional growth does not give any information on the spatial distribution of cells which is very important in characterizing microsegregation patterns. Consequently, a three dimensional cellular growth needs to be examined quantitatively under the condition of diffusive growth to obtain benchmark data which can be accurately compared with the diffusive model to obtain the precise physics of the cellular shape selection criterion.

Figure 4 shows macrosegragation profiles in two samples in which a cellular structure is obtained at a lower velocity, i.e. 2 µm/s, and a dendritic structure is obtained at a higher velocity, i.e. 20 µm/s. No significant macrosegregation for dendritic growth is seen, whereas a large macro-segregation is observed for cellular structures[11]. Since the velocities differ by an order of magnitude, the characteristic length also differs by an order of magnitude so that the Rayleigh

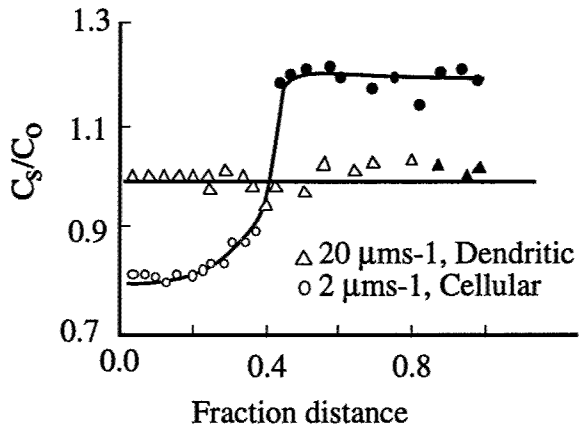


Fig. 4. Macrosegregation patterns in directionally solidified Pb-Sn alloys at V=2 μm/s which produces a cellular structure and at V = 20 μm/s which produces a dendritic structure[11].

number differs by three orders of magnitude. Consequently, to obtain no macrosegregation at a lower velocity, in the cellular regime, one would require the Rayleigh number to decrease by three orders of magnitude which can be achieved through microgravity experiments at g levels of $10^{-3}$. A detailed numerical calculations are now being carried out to characterize the effect of g on convection in the Al-Cu system.

Proposed Microgravity Experiments:

Microgravity experiments are planned in the HGFQ furnace that will be used in the Space Station Furnace Facility. Directional solidification will be carried out in Al-4 wt % Cu alloys under a temperature gradient of 100 K/cm. The alloys will be directionally solidified at different velocities that encompass the entire range of deep cells and the onset of dendrites. Aluminum nitride ampoules will be used to contain the sample, and the temperature profiles will be characterized by several thermocouples placed just outside the ampoule and inside the ampoule. The sample will be quenched when the solidification front just passes the inside thermocouple. From the knowledge of the thermal profile and the distance between the thermocouple tip and the cell tip, the temperature of the cell tip will be determined. For each sample, several key parameters will be measured: (i) Cell spacing and spacing distribution in three-dimensions, (ii) cell tip radius, (iii) cell amplitude, (iv) cell shape (v) microsegregation patterns, and (vi) cell tip temperature. The quantitative examination will be carried out by studying the three dimensional microstructure of each sample through successive polishing by using a microtome polishing unit that will give a series of sections at about 1-2 μm interval. Each section will be photographed and the pictures will then be digitized and a three-dimensional structure will be recreated by using an appropriate software program. Besides

the optical micrographs, each section of the sample will also be analyzed for microsegregation by using a microprobe equipment. The benchmark data obtained in this study will then be compared with rigorous theoretical models to establish the cellular pattern selection criterion.

## Further studies

Ground-based studies will be carried out in very thin samples to evaluate how the microstructure characteristic alter as the size of the sample, and the convection effect, is reduced. Several tube diameters, ranging from 0.2 to 5 mm will be used for this study. Experiments will also be carried out at the Marshall Space Flight Center in the duplicate of the HFGQ furnace using an appropriate ampoule material and ampoule design.

Theoretical studies are being initiated to quantitatively evaluate the following: (i) Finite element method to examine the effect of g on convection in the liquid. (ii) Finite element method to characterize steady-state shape, tip radius, amplitude, spacing and tip temperature of cells. Also, microsegregation patterns will be evaluated for steady-state cells, and the role of anisotropy on tip shape will be determined. A cellular selection criterion will then be established. (iii) A phase field method will be used to characterize the evolution of cellular pattern in the nonlinear regime, and to obtain an independent check on the cellular shape selection criterion.

## References


1. B. Billia and R. Trivedi, Handbook of Crystal Growth, ed. by D.T.J.Hurle, Pergamon Press, N.Y. 1993, vol. 1b, pp. 899-1073.
2. W. W. Mullins and R. F. Sekerka, J. Appl. Phys., 1964, vol. 35, pp. 444-453.
3. J. D. Hunt and S-Z. Lu, Metall. et Mater. Trans.A, 1996, vol. 27A, pp. 611-623.
4. A. Karma, Private Communications, Northeastern University, Boston, MA, 1996.
5. S. H. Han and R. Trivedi, Acta Metall et Mater., 1994, vol. 42, pp. 25-41.
6. J. D. Verhoeven, J. T. Mason and R. Trivedi, Metall. Trans., 1986, vol 17A, pp. 991- 1000.
7. S. N. Tewari and R. Trivedi, Unpublished work, Cleveland State University, 1995.
8. B. Billia, H. Jamgotchian and R.Trivedi, J. Cryst. Growth, 1992, vol. 12, pp. 399-410.
9. R. Trivedi and K. Somboonsuk, J. Mat. Sci. Engg, 1984, vol. 65, pp. 65-74.
10. Y. Miyata, T. Suzuki and J-I Uno, Metall. Trans. A, 11985, vol. 16A, pp. 1799-1804.
11. S. N. Tewari and R. Shah, Metall. Trans. A, 1992, vol. 23A, pp. 3383-92.

# INVESTIGATION OF THE EFFECTS OF MICROGRAVITY ON TRANSPORT PROPERTIES IN A VIRTUAL SPACE FLIGHT CHAMBER

**Principal Investigator:** James D. Trolinger, MetroLaser Inc., 18006 Skypark Circle, Ste. 108, Irvine, CA 92714-6428. (714) 553-0688, email: jamest@deltanet.com
**Co-Investigators:** Ravindra B. Lal, Alabama A&M University, Dept. of Physics, Rm. 145 Chambers Hall, Meridian St., Normal, AL 35762, (205) 851-5309, email; lal@caos.aamu.edu
Roger Rangel, University of California Irvine, Dept. of Mechanical & Aerospace Eng., Irvine, CA 29717, (714) 824-4033, email RHRangel@uci.edu and
William Witherow, Marshall Space Flight Center, M/S ES74 SSL Bldg. 4481, Huntsville, AL 35812,(205) 544-7811. email: witherow@ssl.msfc.nasa.gov

## Objectives:

1. Advance the understanding of microgravity effects on crystal growth.
2. Observe and measure transport parameters in microgravity that are important in materials processing in space.
3. Develop a space flight apparatus and experiment that exploits the "virtual space chamber concept".

## Virtual Space Flight Chamber Concept:

Certain space flight experiments can be recorded in holograms in such a manner that having the holograms on earth is optically equivalent to being back in space with unlimited time to view the experiment. Properly exploited, this concept can save a significant amount of experiment time in space by effectively bringing the experiment optically back to earth.

## Approach:

Exploit existing holograms recorded during the IML-1 space flight.

1. Use existing data extraction/reduction capability.
2. Extract additional data for g-jitter, transport properties, and particle interaction.
3. Use IML-1 experience to produce design data for new chamber.
4. Develop simplified, holographically-instrumented crystal growth chamber for potential GAS can or flight deck locker experiment with potential crystal candidates of proteins, LAP, KDP, and $LiIO_3$.

## Work Plan

### *Tasks*

1. Produce an inventory and prioritize the value of data relevant to materials processing in space that potentially exists in the IML-1 holograms.

2. Extract additional supporting data for measurements, conclusions, and unanswered questions that have already resulted from the IML-1 holograms.

   a. More complete data in z-axis.
   b. Regions not previously explored.
   c. Views not previously explored.
   d. Secondary holocamera views.

3. Examine additional data types from IML-1 holograms not already considered.

   a. Three-dimensional convection map as a function of time and event parameters.
   b. Individual particles with large separation distance from other particles that are out of the range of influence.
   c. Ensembles of particles close to one another, but isolated from other particles within a range of interactive influence.
   d. Particles in clusters containing all three sizes.
   e. Particle doublets that can be used for rotation and vorticity measurement.
   f. Particles near walls exhibiting wall influence.
   g. Particles exhibiting unusual motion.

4. Analyze and interpret IML-1 data.

   a. Support existing measurements and conclusions.
   b. Correlate convection to temperature gradients, concentration gradients, and shuttle attitude.
   c. Refine fluid models to incorporate observed phenomena.
   d. Explain unexpected, long-term persistence of convection.
   e. Resolve other previously unanswered questions.
   f. Provide new understanding of convection in the space shuttle environment in materials processing experiments.

5. Produce a preliminary experiment design which consists of:

   a. Acceleration measurements.
   b. Microgravity measurements (residual gravity / g-jitter).
   d. Crystal growth monitoring.
   e. Particle movement with force field.
   f. Preliminary selection of crystal, fluid, and particle type/size.

6. Produce a preliminary instrument design.

   a. Select chamber type and size.
   b. Holocamera.
   c. Crystal growth hardware.
   d. Incorporate existing particle tracking data reduction system into the proposed requirement.
   e. Select individual components.
   f. Optimize the cell for crystal-growth-in-space research.

g. Design the cell mounting and temperature control system.
h. Select the control computer.

7. Model the proposed instrument.

   a. Reduce the equations of motion to the applicable set.
   b. Conduct computer experiments to optimize component choice.
   c. Determine anticipated instrument requirements.
   d. Specify instrument design parameters.
   e. Perform and apply a full error analysis accounting for all relevant variables.
   f. Incorporate results of the error analysis into the design.

8. Breadboard and test the instrument.

   a. Assemble the optical breadboard to provide a test bed for instrumentation development.
   b. Test for spatial resolution.
   c. Confirm optimum component selection.
   d. Select and use high viscous liquid to simulate microgravity effects.
   e. Introduce chosen crystal and particles.
   f. Test data reduction procedures.
   g. Produce final design information.

9. Perform ground crystal growth demonstration.

   a. Record holograms of crystal growth incorporating particles with g-jitter simulation.
   b. Characterize and evaluate the system capability.
   c. Identify critical issues and problems in using the instrument concept's space shuttle experiments.

10. Design a flight package:

    a. Housings.
    b. Controls.
    c. Diagnostics.

11. Produce final report and recommendations.

***Theoretical analysis***

Much of the supporting, theoretical analysis was produced during past analysis of the IML-1 data, although not all of the analysis was applied to the data. Since our interests in this investigation are much broader, a much broader theoretical analysis is required. The theory will be expanded to cover the additional areas of interest and refined to cover the following phenomena:

a. G-jitter (partially completed in IML-1).
b. Residual g. (completed in IML-1).
c. Convection caused by maneuvers.
e. Convection at extremely low Reynolds numbers.

f. The persistence of convection in microgravity.
g. The interaction of particles in two phase flow at low Reynolds numbers.
h. Influence of walls on convection.
i. Temperature and concentration effects on convection in microgravity.
j. Residual g effects on convection.
k. Space shuttle attitude effects on particle motion and convection.

*Flight Experiment Design*

The proposed four year program would be a ground based effort. One of the primary objectives of this work, however, would be the design of a cost efficient flight experiment that would: 1) allow investigation of the microgravity environment and its effect on fluid convection and transport phenomena, and 2) allow for better monitoring of crystal growth experiments than that produced by existing flight systems. This section describes our approach to this design.

Since convection and the resulting gradients play such an important role in the crystal growth process, and since they cannot be removed entirely, even in space, they must be measured to understand their importance. Optical diagnostics to record experimental conditions play a critical role since the entire experiment in space must be conducted by astronauts with severely limited time and contact with scientists on earth. Measuring extremely low levels of convection and low values of acceleration requires a highly sensitive method. Holographic particle image displacement velocimetry is chosen as a principal tool for the experiment to maximize data collection, minimize recording time, and transfer the time consuming part of the experiment back to an earth laboratory.

A small, windowed chamber will contain a crystal growing from solution especially selected for spaceflight. The particles will include several sizes and weights, chosen in such a manner that different weights will be identifiable in the data. A holographic time history will be produced of the particle distribution and the crystal profile, allowing particles to be precisely tracked in three dimensions in time and allowing the crystal growth rate to be monitored as described below.

The following hardware and experimental design approach will be implemented:

1. The instrument will be fully automated. The only crew involvement will be in deploying the instruments, turning them on, and changing film. This approach will result in considerable cost savings and ease of inclusion in a spaceflight.
2. More measurement time will be available to take advantage of the microgravity environment. Particle motion is extremely slow so more experiment time will provide proportionally greater accuracy.
3. A wide range of particle sizes, shapes, and masses with size coding of the mass will provide significantly superior data to any data of this type collected before.
4. Higher resolution will be designed into the holocamera to improve system accuracy and to extend the capability to monitor crystal growth as well as to make the system usable in shorter time experiments such as in the KC135.

5. Orthogonal views will provide accurate, three-dimensional velocity vectors and crystal profile views.

**Figure 1** illustrates the instrument concept, which is based upon simplicity and reliability. A laser diode will produce diverging light that illuminates one or more chambers after collimation. As the light passes through the chamber, it will pick up particle and crystal profile information and in-line holograms will be recorded on 35 mm film. In our previous work, we have shown that the edge of a particle or object, such as a crystal, can be located with an accuracy of better than 2 micrometers. This will be over an order-of-magnitude improvement above our work in the IML-1 spaceflight. This ability will allow the particle position to be precisely tracked, thus permitting the detection of very small motions.

Fast growing crystals can be expected to grow as much as one micron per second (e.g. KDP) so that growth rate can be monitored in the holograms at a meaningful rate. The purpose of the measurement is not necessarily to produce a high quality crystal, but more to determine how the crystal grows in microgravity. Therefore, choice of a suitable material must be made accordingly. Whether the crystal is to be sting mounted or free floating has not yet been determined. Finally, whether the crystal is to be released into the solution after arriving in orbit or whether it can remain in the solution at all times will be answered during the second year.

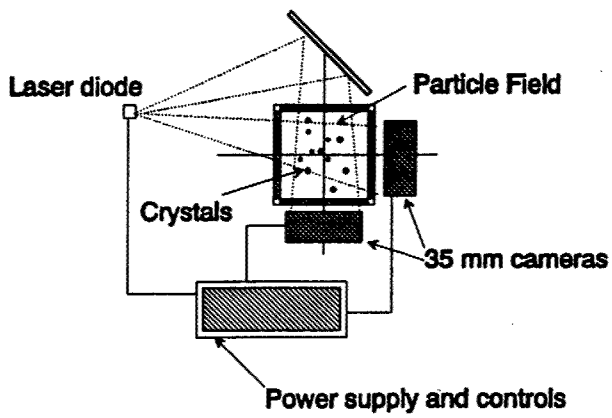


**Figure 1. In-line holographic camera test cell.**

Since particles of density greater than the fluid accelerate in the direction of g and particles of density lower than the fluid accelerate opposite to g they can be selected so that, under constant microgravity, they move at terminal velocities in opposite directions, thus enhancing the measurement of g and identifying the direction of the residual gravity. This will allow residual gravity to be measured with greater accuracy than is currently possible. Different types of fluid, particle sizes, and masses will be selected to improve dynamic range and accuracy.

Since the system is compact, two or more cells can be operated in a shoebox-sized container. **Figure 2** illustrates a flight system concept. By employing more than one cell, crystals can be released into the solutions at different times or, alternatively, different types of materials can be grown at the same time, comparing the influences of microgravity on two types of material.

In other configurations to be explored, multiple chambers can be used to separate particles and fluids. Since the holographic recording preserves the 3-D information, the same hologram can contain information from different chambers in a separable form. All of these optional configurations will be examined for advantages. The prime candidates will be tested in the laboratory breadboard before a final selection is made.

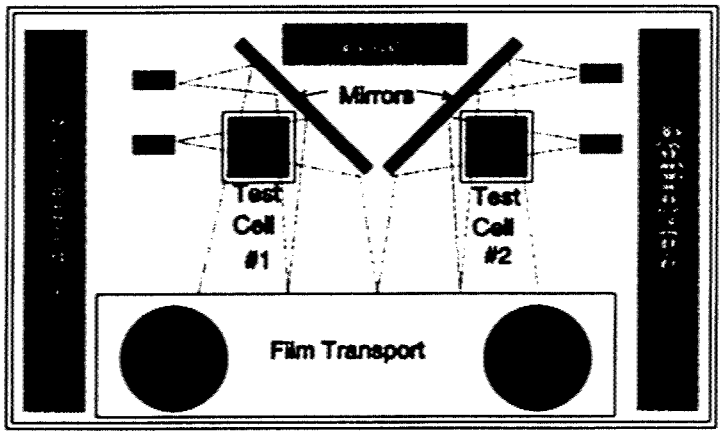


**Figure 2. Flight system.**

# FUNDAMENTALS OF MOLD FREE CASTING: EXPERIMENTAL AND COMPUTATIONAL STUDIES

Prof. Gretar Tryggvason (P.I.)
Prof. Steven Ceccio (co-P.I.)
Mechanical Engineering and Applied Mechanics
University of Michigan, Ann Arbor, MI 48109-2121
(313)-764-4254
(313)-764-4256 (FAX)
gretar@engin.umich.edu
ceccio@engin.umich.edu

## Objective

Researchers are developing the technology of "Ballistic Particle Manufacturing" (BPM) in which individual drops are precisely layered onto a substrate, and the drops are deposited so as to prevent splatting. These individual drops will ultimately be combined to form a net-shape, three-dimensional object. Our understanding of controlled drop deposition as applied to BPM is far from complete. Process parameters include the size and temperature of the liquid metal drop, its impact velocity and trajectory, and the condition and temperature of the substrate. Quantitative knowledge of the fluid mechanics and heat transfer of drop deposition and solidification are necessary to fully optimize the manufacturing process and to control the material microstructure of the final part. The object of this study is to examine the dynamics of liquid metal drops as they impinge upon a solid surface and solidify under conditions consistent with BPM (*i.e.* conditions which produce non-splatting drops). A program of both numerical simulations and experiments will be conducted. Questions this study will address include the following:

- How do the deformation and solidification of the drop depend on the properties of the fluid drop and the solid substrate?
- How does the presence of previously deposited drops affect the impingement and solidification process? How does the impingement of the new drop affect already deposited material?
- How does the cooling rate and solidification of the drops influence the material microstructure?

## Numerical Examination of Drop Deposition and Solidification

We use a unified approach to deal with fluid flow, heat transfer, and phase change during complex solidification processes. A single set of equations governing the conservation of mass, energy, and momentum are written for all phases involved and the phase boundary is treated as an imbedded interface by adding the appropriate source terms to the conservation laws. These source terms are in the form of delta functions localized at the interface and are selected in such a way to satisfy the correct matching conditions at the phase boundary. The resulting "one-field" Navier-Stokes equations are [1]:

$$\frac{\partial \rho \bar{u}}{\partial t} + \nabla \cdot \rho \bar{u}\bar{u} = -\nabla p + \bar{f} + \nabla \cdot \mu\left(\nabla \bar{u} + \nabla \bar{u}^T\right) + \int_F \bar{F}_s \delta\left(\bar{x} - \bar{x}_f\right) da$$

Here, $\bar{u}$ is the velocity vector, $p$ the pressure, and $\rho$ and $\mu$ are the discontinuous density and viscosity fields, respectively. $\bar{f}$ is a body force that can be used to initiate the motion. The surface forces, $\bar{F}_s$ act only on the interface between the different fluids and appears in the current formulation multiplied by a three-dimensional delta function, $\delta$. The integral is over the entire front. It is important to note that this equation contain no approximations beyond those in the usual Navier-Stokes equations. In particular, it contains implicitly the proper stress conditions for the

fluid interface. The momentum equation is supplemented by an equation of mass conservation. For incompressible flows this leads to an elliptic equation for the pressure. To advect the material properties, and to evaluate the surface tension term in the momentum equation, we track the interface between the different phases explicitly by using a moving grid of lower dimension than what we use for the conservation equations. This grid is usually referred to as a front. The one-field formulation used here is common to other techniques for multifluid flows such as the VOF (Volume of Fluid) and level set methods. In these methods, however, the phase boundary is not tracked explicitly, but reconstructed from a marker function. Explicitly tracking the interface avoids the difficulty of advecting such marker function and allows accurate evaluation of surface forces. This formulations has been used to examine the dynamics of fluid drops and bubbles in the following work: [2, 3, 4, 5].

The approach taken for the fluid flow, works also for heat flow and phase changes. In Juric and Tryggvason [6] we developed a method to simulate phase changes in a pure material in the absence of any fluid motion. With these assumptions we have only to solve one heat conduction equation:

$$\frac{\partial \rho c T}{\partial t} = \nabla \cdot k \nabla T + \int_F \dot{q} \delta(\bar{x} - \bar{x}_F) da$$

where $\dot{q}$ is adjusted in such a way that the temperature of the interface is given by the Gibbs-Tompson conditions

$$T_F = T_M \left(1 - \frac{\sigma \kappa}{L}\right)$$

Here, $T_M$ is the melt temperature, $T_F$ is the temperature at the front, $\kappa$ is the conductivity, and $L$ is the volumetric latent heat. Additional terms can be added to the right hand side to account for variability in surface tension as well as anisotropy. We have compared the method with exact solutions for stable solidification and found excellent agreement, even with relatively coarse resolution. The same approach can also be used for the solidification of binary alloys where the solidification temperature depends on the composition of the melt. In this case we also need to solve an equation for the solute concentration [7, 8]. For real multiphase flows, the fluid code and the phase change have to be combined. This introduces additional complications, such as a volume source at the phase boundary, that can be dealt with in several ways.

## Numerical Results

The method described above has been used to simulate the pure and binary solidification of non-flowing systems [9]. These simulations have captured interfacial instabilities during solidification and the growth of dendritic structures. Although predicting the microstructure formation during solidification is a problem of immense importance and complexity (and we have only addressed relatively simple aspect so far), it is one aspect of predicting the solidification of a realistic system. Often, the range of scales between the size of the microstructures and the dimensions of the system we need to predict are very large and resolving the formation of every microstructure is completely impractical. In those cases it is necessary to make some assumptions about what happens at the small scale level in order to be able to resolve the large scale features of the system. How the collective behavior of small scale features is manifested at larger scales is, of course, a central problem in the modeling of physical system and is far from a solved problem. In fluid/solidification simulations some success has been achieved by allowing for a "mushy zone" at the boundary between a fluid and a solid which represents a partially solidified region consisting of fluid and microstructurs such as dendrites. We have simulated drops colliding with cold walls with an even simpler model where we simply assume that a melt solidifies if its temperature falls below the solidification temperature. Although simple, this model captures at least some aspects of the interaction of fluid flow and solidification. Figure 1 shows the collision and solidification of two drops at three times. In the first frame the first drop has already collided with the wall and is

partially solidified. In the second frame the first drop is completely solid but the second drop is still fluid. In the third frame both drops have solidified. In this simulation the drop Weber number is high so the drops deform greatly and the drop thermal conductivity is low so the drops have time to deform before they solidify. In figure 2, however, where we show two drops after they have solidified the conductivity is high and Weber number low, thus resulting in much less deformations. In these simulations we solve for the motion of both the fluid in the drop as well as the ambient fluid. Figure 3 shows the temperature in both the drop and the fluid as well as the streamlines at a time when the first drop has solidified but the second has not. We see that the bottom drop has reached the temperature of the wall, but the second still has essentially its original temperature. Since the drop looses heat to the ambient fluid, a thermal wave is clearly visible.

## Experimental Examination of Drop Deposition and Solidification

The experimental examination of drop deposition and solidification required the construction of an apparatus which can controllably create a single drop of prescribed size which will then be propelled toward a sub-cooled substrate. A drop ejector has been devised to create and deliver a drop of liquid material. The drop must be uniformly melted and the velocity and trajectory of the drop must be repeatable. Once ejected, the drops will travel to the substrate. The substrate is mounted on a computer controlled X-Y traverse, and a substrate can be moved to provide a virgin surface for drop deposition or move a previously deposited drop into the impact zone of an incoming drop. The table has been constructed to accommodate a variety of different substrate materials. The experiments will be conducted in a vacuum chamber to eliminate the effect of an ambient atmosphere on the drop deposition process. A variety of instrumentation will be used to quantitatively monitor the deposition process such as still and motion image acquisition, dynamic temperature acquisition, and IR imaging. We have used Gallium, Wood's metal, and Rose's metal as materials in our preliminary experiments. Images of the deforming and solidifying drops acquired to date are qualitatively similar to the numerical predications.

## Need For Experiments in Microgravity

Experimental studies of drop deposition can be significantly enhanced if performed in microgravity. In terrestrial applications of BPM, small drops are used and gravity is important. However, it is quite difficult to quantitatively observe small, fast moving drops, and thus we would like to scale up the size of the drops. This leads to the well known difficulty that while gravity may be negligible for the small drop, it is likely to be the dominant effect for a drop that is sufficiently large to be easily observable. A microgravity environment would permit the proper scaling of the experiment. For high Reynolds numbers both experiments and numerical simulations show that the drop deformation is only weakly dependent on the Reynolds number. Thus, in the absence of gravity, the drops can be made larger for a given Weber number simply by reducing their velocity. Dimensionless parameters associated with the process of heat transfer and solidification of the drop are the Prandtl and Stefan numbers which would not be effected by a change of size scale. The time constants associated with these processes are proportional to the square of the drop diameter for given thermal conductivities of the liquid drop and substrate material and given temperature differences. By scaling up the drop size it also becomes easier to observe the slower process of drop heat exchange and solidification. Consequently, the micro-gravity environment offers unique opportunities to study the complete process of drop deposition and solidification in detail by examining large, slowly moving drops.

## Significant Results to Date

We have used a pilot grant from NASA to initiate our research effort. Significant Results are summarized below:

- We have developed the capability to simulate the deformation of multiple metal drops as they impinge on a substrate. These are fully resolved, three-dimensional calculations.
- These simulations have been extended to include the solidification of drops of pure material, and we expect that these simulations can be extended to binary solutions.
- We have developed a drop producing apparatus which is capable of producing individual drops of liquid metal. We are modifying this device to ensure its function in a microgravity environment.
- The traverse and cooling system for the substrate has been developed, and a design of the vacuum chamber has been completed.

We have conducted experiments in which relatively large metal drops are dropped into hot oil which will impinge and solidify on a cooled substrate. data from these is being compared with numerical simulations. The role of direct numerical simulations in material processing is currently in its infancy, but the prospect that it will ultimately have a significant impact are enormous. Several groups are currently active in various aspects of such simulations. We have presented a unified approach for heat transfer, phase changes and fluid flow that is applicable both for exploration of the formation of small scale structures as well as to more global aspects of the solidification process where the details of the microstructure are not resolved.

## Acknowledgments

Our work on direct numerical simulations of fluid flow and solidification has been supported by NASA grant NAG3-1317, NCC3-355, and NASA Graduate Student Fellowship NGT-51070, and NSF grants CTS-913214 and CTS-9503208. The computations have been done at the San Diego Supercomputer Center, NASA Lewis and the Center for Parallel Computing at the University of Michigan.

## References

[1] Unverdi, S. O. and G. Tryggvason, "A Front Tracking Method for Viscous Incompressible Flows." *J. Comput Phys*, 100, (1992), 25-37.
[2] Yu, P.-Y., S. L. Ceccio, and G. Tryggvason. "The Collapse of a Cavitation Bubble in Shear Flow-A Numerical Study." *Phys. of Fluids* 7, 2608-2616 (1995).
[3] Nobari, M. R., Y.-J. Jan and G. Tryggvason. "Head-on Collision of Drops--A Numerical Investigation." *Phys. of Fluids* 8, (1996), 29-42 .
[4] Nobari, M. R. and G. Tryggvason, "Numerical Simulations of Three-Dimensional Drop Collisions." *AIAA Journal* 34 (1996), 750-755.
[5] Esmaeeli, A. and G. Tryggvason, "An Inverse Energy Cascade in Two-Dimensional, Low Reynolds Number Bubbly Flows." *J. Fluid Mech.* 314 (1996), 315-330.
[6] Juric, D. and G. Tryggvason, "Full Simulations of Flows with Phase Change," AIAA 95-0700. Proc. *AIAA Aerospace Sciences Meeting*, (1995).
[7] Juric, D. and G. Tryggvason, "A Front Tracking Method for Dentritic Solidification." *J. of Comput. Phys.* 123, (1996), 127-148.
[8] Juric, D. and G. Tryggvason, "Direct Numerical Simulations of Flows with Phase Change," AIAA 96-0857 *Proc. AIAA Aerospace Sciences Meeting*, (1996).
[9] Juric, D., *Computations of Phase Change.*, Ph. D. Dissertation, The University of Michigan, (1996).

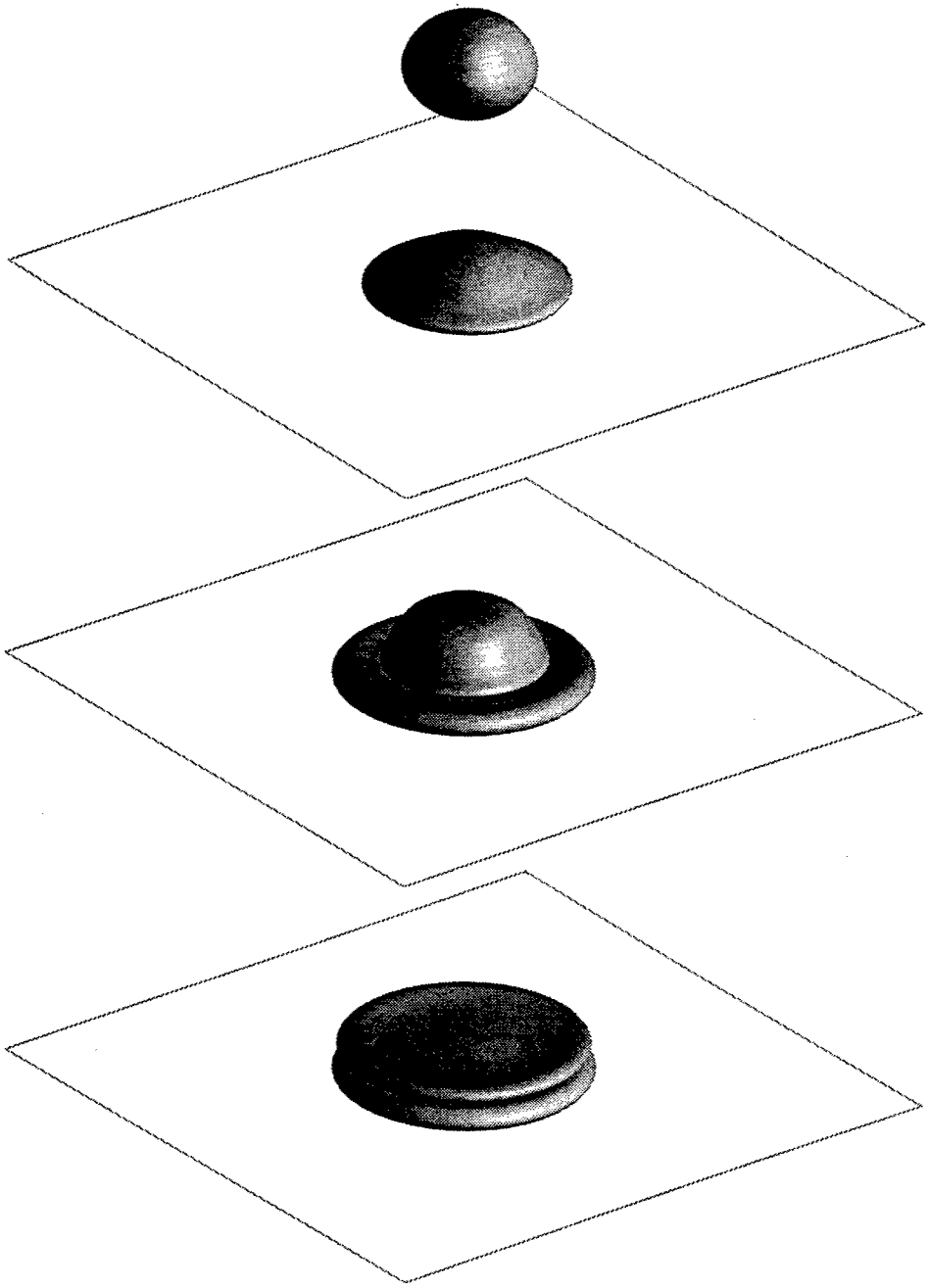

Figure 1. The solidification of a two drops colliding with a cold wall. In the top frame the first drop is splatting on the wall, but has not solidified yet. In the middle frame the first drop has completely solidified, but the second drop has not. Both drops have solidified in the bottom frame. In this case the drops are not allowed to coalesce. The thermal conductivity is relatively low and the Weber number high, thus resulting in highly deformed drops after solidification.

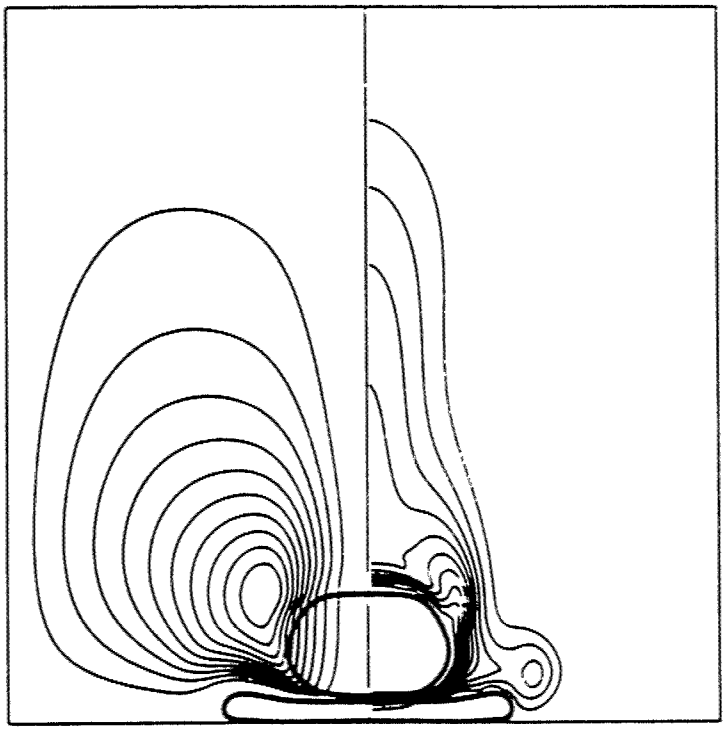

Figure 2. The temperature field and the streamlines for the drops in Figure 3 as the first drop has collided with the wall and solidified and the second drop is just about to collide with the first one. Since both the flow in the drops as well as the ambient fluid are simulated, we plot the contour values there also. Here, no streamlines cross the bottom drop, indicating that it is fully solidified. A large thermal wave is left behind the drops and hot wake fluid is entrained in a vortex formed by the wake fluid that is moving outward near the bottom.

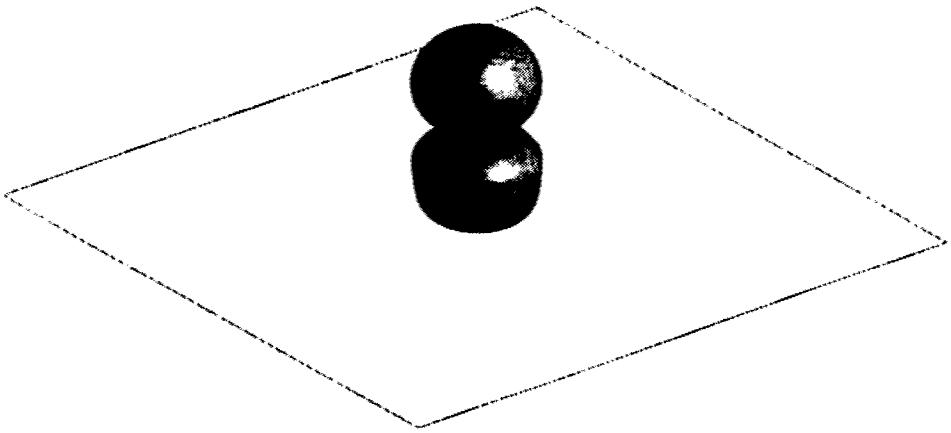

Figure 3. The final, solidified shape of two drops colliding with a cold wall. In this case the Weber number is low and thermal conductivity high, so the drops do not deform much and solidify rapidly as they hit the wall.

# COARSENING IN SOLID-LIQUID MIXTURES

P.W. Voorhees
Department of Materials Science and Engineering
Northwestern University
2225 N. Campus Rd.
Evanston, IL 60208
847-491-7815
p-voorhees@nwu.edu

## Introduction

The late-stages of a first-order phase transformation process are usually characterized and by the growth of second-phase domains with low interfacial curvature at the expense of domains with high interfacial curvature. This process, also known as Ostwald ripening or coarsening, occurs in a wide variety of two-phase mixtures ranging from multiphase solids to multiphase liquids, and has a significant impact on the high temperature stability of many technologically important materials. Unfortunately, an understanding of the dynamics of ripening processes is not in hand. Many of the recent theories for the effects of a finite volume fraction of coarsening phase on the kinetics of Ostwald ripening have proposed divergent expressions for the dependence of the coarsening rate of the system on the volume fraction of coarsening phase [1-8]. As there are virtually no experimental data of sufficient quality to differentiate between these theories, or even provide qualitative information on the coarsening dynamics of low volume fraction systems, the controversy over the dependence of the coarsening rate of the system on the volume fraction remains unresolved.

Previous NASA sponsored work showed clearly that solid-liquid mixtures consisting of Sn-rich solid particles in a Pb-Sn eutectic liquid are ideal, and perhaps unique, systems in which to explore the dynamics of the Ostwald ripening process [9]. The high coarsening rate in these systems permit accurate kinetic data to be obtained, and the thermophysical parameters necessary to make a comparison between theory and experiment are known [10-13]. However, in a terrestrial environment experiments can be performed only at the relatively high volume fractions of solid where the presence of a solid skeletal structure prevents large-scale particle sedimentation. Even in these high volume fraction solid solid-liquid mixtures, however, it is unclear that the particles are

truly motionless. As the theory assumes that the particles do not move during the coarsening process, an unambiguous comparison between theories of diffusion controlled Ostwald ripening and experiment is difficult, if not impossible, using terrestrial-based experiments.

This experiment will provide still more information on the coarsening process in solid-liquid systems. We will also be able to determine the effects of gravity on the morphology of solid-liquid mixtures during coarsening. Gravity may play a major role in determining the morphology of the particles as it leads to large numbers of particle-particle contacts and a small, but possibly non-negligible, body-force. We shall examine the effects of gravity on the morphological development of solid-liquid mixtures in a number of ways. For example, we shall compare the circularity of the sectioned particles and the three-dimensional morphology of a small collection of particles found in the ground-based and microgravity experiments. As absence of gravity can alter the number of particle contacts, it may also affect the number of grain boundaries that form between particles and the distribution of grain boundary misorientations. Thus the distribution of grain boundary misorientations, and the temporal evolution of this distribution, produced in the space-flight and ground-based experiments will be compared. Finally, we shall determine the effects of gravity on the formation of the solid skeleton. The information on the distribution of grain boundary misorientations and particle morphology are expected to provide important insights into the reasons for the formation of these surprisingly stable solid skeletal structures.

## Objectives

The primary objective of this project is to measure the temporal evolution of the average size-scale of a solid-liquid mixture during coarsening in microgravity. Specifically, we shall measure the average intercept length and the average section area of the solid particles at various times, and for various volume fractions of solid. Using this data, the amplitude of the temporal power law for the average section area and intercept length will be determined. Once the amplitude of the temporal power law is known, the results will be compared to the theoretical predictions on the dependence of the amplitude of the power law on the volume fraction of coarsening phase. We shall also determine the steady-state particle size distribution. The hallmarks of this experiment are the large range of volume fractions of solid over which this comparison can be made, the conclusive elimination of gravitationally induced matrix and particle motion, and that a comparison between theory and experiment can made for the first time without any adjustable parameters.

The microgravity experiment will also provide information on the effects of gravity on the morphology of solid-liquid mixtures during coarsening. Gravity may play a major role in determining the morphology of the particles as it leads to large numbers of particle-particle contacts and a small, but possibly non-negligible, body-force. We shall examine the effects of gravity on the morphological development of solid-liquid mixtures in a number of ways. For example, we shall compare the three-dimensional morphology of a small collection of particles found in the ground-based and microgravity experiments. As absence of gravity can alter the number of particle contacts, it may also affect the number of grain boundaries that form between particles and the distribution of grain boundary misorientations. Thus the distribution of grain boundary misorientations, and the temporal evolution of this distribution, produced in the space-flight and ground-based experiments will be compared.

## Progress

We have finalized the science requirements for the Coarsening in Solid-Liquid Mixtures spaceflight experiment. We have also interacted extensively with engineers in the design of a furnace for the spaceflight experiment. Our specimen preparation procedures have been refined and improved. We can now produce spatially uniform mixtures of Sn particles immersed in a Pb-Sn eutectic liquid at a variety of volume fractions of solid. The spatial uniformity of these mixtures was confirmed, even in low volume fraction mixtures, through short-time coarsening experiments.

We have developed an automated serial sectioning procedure. The spacing between each serial section can be as small as 2 μm. The entire process is quite efficient; we can acquire approximately 8 sections per hour. These digitized images are then used to reconstruct the three-dimensional morphology of the microstructure using a computer. This three-dimensional image can be viewed from various directions to analyze the morphology of the solid-liquid mixture.

An example of such a three-dimensional image is shown in Fig. 1. The sample volume that is reconstructed is approximately 1.2 mm X 1.6 mm X 1.6 mm. This volume is denoted by the outline of the box. The volume of the reconstruction is large compared with average particle diameter on a 2-D section of 0.35 mm. The volume fraction of solid in the solid-liquid region is 0.78. This figure shows that it is possible to construct a continuous chain of particles that spans the entire distance over the sampled region. Each of the eight particles in this figure is in direct "contact" with its nearest neighbor. All but three of these "contacts" are grain boundaries. In three

cases, the particles are joined by boundaries which are likely partially wetted grain boundaries or very thin, less than 1 μm thick, liquid films. In addition, this figure shows that many of the particles are not spherical. The solid-liquid interfacial energy in the Pb-Sn system is isotropic, thus, if interfacial energy dictated the particle morphology, the particles would be spherical. In this case, the symmetry of the particles is a function of the local arrangement of the neighboring particles.

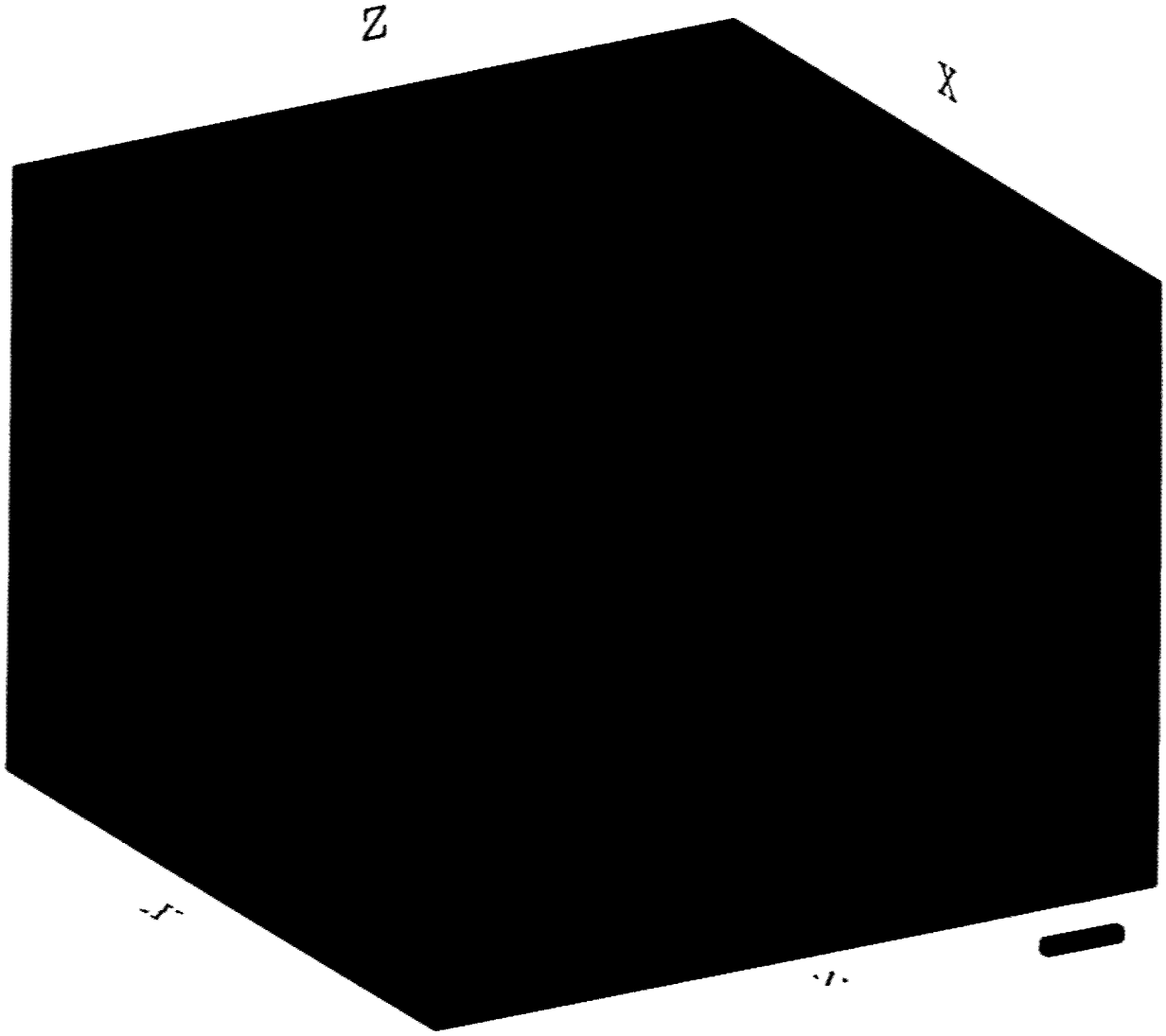


Fig.1. A particular chain of Sn-particles in a three-dimensional region. The marker in the lower right-hand side of the picture is 170 μm. Evident is the nonspherical shape of the particles as well as the presence of a chain of particles which stretches from one side of the sampled region to the other, a distance of approximately 1.6 mm.

Terrestrial-based experiments using Pb-Sn solid-liquid mixtures have shown that grain boundaries occasionally form between particles. In an effort to quantify the nature of these grain boundaries for comparison with the results of the spaceflight experiment, we have measured the misorientations of grain boundaries and the crystallographic texture of the solid particles using a scanning electron microscope. We have examined the temporal evolution of the misorientation distribution, as well as the dependence of the distribution on the volume fraction of solid.

## Future Plans

In the future we will:

1. Perform the coarsening in solid-liquid mixtures experiment aboard MSL-1. The launch date for the mission is March 1997.
2. Analyze the results of the spaceflight experiment.
3. Continue our investigation of the grain boundary misorientation distribution in these solid-liquid mixtures.
4. Further refine the three-dimensional reconstruction technique.

## Acknowledgments

We are most grateful for the financial support of the Microgravity Sciences and Applications Division of NASA, and the many helpful and insightful comments of the Coarsening in Solid-Liquid Mixtures review panel.

## References

[1] Y. Enomoto, K. Kawasaki, and M. Tokuyama, Acta metall. **35**, 915 (1987).

[2] M. Tokuyama and K. Kawasaki, Physica **123A**, 386 (1984).

[3] A. Brailsford and P.Wynblatt, Acta Metall. **27**, 489 (1979).

[4] S.P. Marsh and M.E. Glicksman, *in Modeling of Coarsening and Grain Growth*, edited by S.P. Marsh and C.S. Pande,TMS, Warrendale, 1992.

[5] M. Marder, Phys. Rev. A. **36**, 858 (1987).

[6] J.H. Yao, K.R. Elder, H. Guo, and M. Grant, Phys. Rev. B **47**, 14110 (1993).

[7] J.A. Marqusee and J. Ross, J. Chem. Phys. **80**, 536 (1984).

[8] N. Akaiwa and P.W. Voorhees, Phys. Rev. E **49**, 3860 (1994).

[9] S.C. Hardy and P.W. Voorhees, Met. Trans. A **19A**, 2713 (1988).

[10] K. Davis and L. Hogan, J. Australian Inst. Met. **15**, 29 (1970).

[11] R. Jordan and J. Hunt, Metall. Trans. **2**, 3401 (1971).

[12] M. Gunduz and J. Hunt , Acta Metall. **33**, 1651 (1985).

[13] S.C. Hardy, G.B. McFadden, S.R. Coriell, P.W. Voorhees, and R.F. Sekerka, J. Cryst. Growth **114**, 467 (1991).

# MODELS OF MAGNETIC DAMPING FOR SEMICONDUCTOR CRYSTAL GROWTH IN MICROGRAVITY

John S. Walker
Mechanical & Industrial Engineering, University of Illinois
140 Mechanical Engineering Bldg., 1206 West Green St.
Urbana, Illinois 61801
Phone: 217-333-7979
E-mail: jswalker@uxh.cso.uiuc.edu

## Summary

Models will be developed for the effects of magnetic damping on melt motions and dopant transport during semiconductor crystal growth in space. The models will be based on assumptions which are valid for typical Bridgman and floating-zone crystal-growth processes with a 0.2 Tesla axial magnetic field. The models will use asymptotic and numerical methods.

## Magnetic Damping of Thermally Driven Buoyant Convection in the Bridgman Process

Any experiment on a space vehicle is subjected to a steady residual acceleration and to g-jitters whose direction and magnitude are random functions of time. For a typical Bridgman process with a 0.2 Tesla magnetic field, Coriolis effects, magnetic fields produced by electric currents in the melt, non-linear inertial effects and convective heat transfer are all negligible. If dopants and composition gradients do not affect the buoyant convection, then the governing equations are linear, so that (1) solutions for g-jitters whose directions vary randomly with time are given by time-dependent superpositions of the solutions for two uni-directional g-jitters, namely axial g-jitters and transverse g-jitters, and (2) solutions for g-jitters whose magnitudes vary randomly with time are given either by Fourier-transform superpositions of solutions for sinusoidal g-jitters for all frequencies or by Laplace-convolution superpositions of solutions for delta-function g-jitters. The solutions for the sinusoidal axial and transverse g-jitters have been obtained [1]. The results show that the velocities driven by the transverse g-jitters are much larger than those driven by the axial g-jitters. As the frequency of the g-jitters increases, the velocities decrease and shift to a quarter-period phase lag relative to the g-jitters. Therefore the largest buoyant convections will be driven by the transverse steady residual acceleration and by the lowest-frequency components of the transverse g-jitters. The analyses for the delta-function g-jitters and for the steady residual acceleration with an arbitrary orientation to the axis of the ampoule are in progress. Models have also shown that tailoring a non-uniform magnetic field provides no

benefit, so that the optimal magnetic damping is provided by the strongest field in the center of the solenoid around the Bridgman furnace [2]. These solutions also showed that deviations from magnetic-field uniformity have a negligible effect on magnetic damping.

## Magnetic Damping Effects on Dopant Transport

The objectives of dopant-transport models are to predict the radial and axial macrosegregations and to predict the striations or microsegregation in the crystal. Many previous models assumed (1) that the dopant concentration in the melt is given by a steady-state solution at each moment during crystal growth and/or (2) that the dopant is well mixed at a given distance from the crystal-melt interface. These assumptions might be valid with turbulent mixing, but even a very weak magnetic field eliminates turbulence. With magnetic damping, the dopant distribution is always very different from the instantaneous steady state, and the dopant is not well mixed anywhere in the melt. We are developing a transient model to predict the dopant distribution at every moment throughout the growth of a crystal. Initially we are focusing on a two-dimensional model with only thermally driven buoyant convection in order to identify the appropriate asymptotic relationships between the important dimensionless parameters for various magnetic field strengths, ampoule sizes, temperature differences, etc. Our first results show that the dopant which is convected out of the mass-diffusion boundary layer adjacent to the crystal-melt interface returns to this layer at a later time. After a brief period at the start of crystal growth, the dopant concentration carried by the melt entering the crystal-face diffusion layer is far from uniform and is strongly time-dependent because the melt entering this layer at some time left this and other diffusion layers at very different previous times, i.e., the time to complete one circulation varies greatly within the melt. The entering non-uniform dopant distribution may compensate for the transverse convection of dopant within the layer, so that there is negligible radial macrosegregation in the crystal for a wide-range of magnetic field strengths. A model assuming an instantaneous steady-state dopant distribution or assuming thorough mixing anywhere in the melt would give a completely erroneous dopant distribution in the crystal. The models being developed are the first models which can accurately predict the transient, global mass transport of dopants for the length of time needed to grow an entire crystal. Many previous dopant-transport models used hundreds of hours of supercomputer time in order to simulate a few minutes of actual crystal growth. We will extend this model to the transient, three-dimensional melt motions for crystal growth in space.

## Magnetic Damping of Compositionally Driven Buoyant Convection in the Bridgman Process

Many compound semiconductors such as mercury-cadmium-telluride are alloys of two II-VI semiconductors, e.g., mercury-telluride (HgTe) and cadmium-telluride (CdTe). Rejected HgTe accumulates in the diffusion boundary layer in the melt adjacent to the crystal-melt interface, increasing the local density. If the interface is plane and if the gravitational vector is parallel to the ampoule's axis, then the melt is stably stratified and no convection would occur. However, differences between the thermal conductivities of the melt, crystal and ampoule lead to an interface which is always concave into the crystal. With a HgTe-rich diffusion boundary layer adjacent to a concave interface, there is a radial density gradient which drives a radially inward melt motion along the interface. This convection decreases and increases the mole fraction of HgTe at the ampoule wall and at the centerline, respectively. Since the solidification temperature of the alloy decreases with increasing local HgTe content, the solidification temperature decreases along the interface from the ampoule wall to the centerline, making the interface even more concave into the crystal, thus leading to more convection. The crystal has an unacceptable radial segregation with high CdTe content at the periphery and high HgTe content at the centerline. In space, the steady residual acceleration vector may not be parallel to the ampoule's axis, leading to a non-axisymmetric, three-dimensional convection with the HgTe carried laterally in the direction of the transverse component of the residual acceleration. A magnetic field can suppress the compositionally driven buoyant convection, leading to a more planar crystal-melt interface and to a more radially uniform alloy of HgTe and CdTe. Models will be developed to predict the compositionally driven buoyant convection and associated transport of both constituents for various magnetic field strengths and for both aligned and misaligned gravitational or residual acceleration vectors. These models will use the methods described in the previous two sections, but they will be much more complex. For compositionally driven buoyant convection, the melt motion and the mass transport are intrinsically coupled, and the problems are always non-linear. In addition, the melt's properties vary greatly as the relative fraction of the two constituents changes. This is particularly true for the density and electrical conductivity since HgTe is much denser and has a much higher electrical conductivity than CdTe.

## Magnetic Stabilization of Thermocapillary Convection in the Floating-Zone Process

The advantage of the floating-zone process over the Bridgman process is the lack of contact between the crystal and an ampoule wall, but its disadvantage is the thermocapillary convection driven by the gradient of the surface tension along the free surface. Without a magnetic field, the thermocapillary convection is almost always unsteady, leading to undesirable striations in both terrestrially grown and space-grown crystals. A sufficiently strong magnetic field stabilizes the flow, eliminates the unsteadiness and controls the residual steady convection. Our first study

focused on the control of the steady convection for floating-zone crystal growth in space and on the benefits of tailoring a non-uniform magnetic field in order to eliminate convective disruption of the mass-diffusion boundary layer adjacent to the crystal-melt interface [3]. One current study treats the convective heat transfer due to the strong thermocapillary convection which is confined to a thin boundary layer adjacent to the free surface. The heat flux into the free surface is redistributed axially inside the high-velocity free-surface layer so that the heat flux entering the bulk of the melt is concentrated near the crystal and feed rod. A second current study treats the dramatic effects on the thermocapillary convection of even a small deviation from axisymmetry in the heat flux to keep the floating zone above the melting temperature. An axial magnetic field strongly suppresses axisymmetric motions because there is very little electrical resistance to the azimuthal electric currents which produce the electromagnetic (EM) body force opposing such motions. However, an axial field provides much less suppression of azimuthal velocities near the free surface because the electrically insulating atmosphere blocks the radial electric currents which would produce the EM body force opposing these velocities. Therefore a small deviation from axisymmetry in the heat flux to the melt can lead to relatively large swirling motions around the floating zone adjacent to the free surface. Most of our future research on magnetic-field effects for the floating-zone process will focus on predicting the minimum magnetic field strength needed to stabilize the thermocapillary convection in order to eliminate striations in the crystal. We have shown that the key dimensionless parameter is

$$\alpha = \frac{\rho(-d\gamma / dT)\Delta T}{B^{3/2} L^{1/2} \sigma^{3/4} \mu^{5/4}} , \qquad (1)$$

where $d\gamma / dT$, $\rho$, $\sigma$, and $\mu$ are the melt's negative derivative of the surface tension with respect to temperature, density, electrical conductivity and viscosity, respectively, while $\Delta T$ is the temperature difference along the melt's free surface, $B$ is the magnetic field strength and $2L$ is the axial length of the floating zone. This parameter is essentially a magnetic Marangoni number. For a given semiconductor and zone aspect ratio, there is a critical value $\alpha_{cr}$ such that the thermocapillary convection is steady and periodic for $\alpha < \alpha_{cr}$ and $\alpha > \alpha_{cr}$, respectively. From Eq. (1), one might conclude that a larger zone is more stable than a smaller zone, but this is only true if the temperature difference along the free surface $\Delta T$ is the same for both sizes. If the average temperature gradient along the free surface $G$ is the same for both sizes, then $\Delta T = GL$ and a larger floating zone is less stable than a smaller one. Croll, Dold and Benz [4] grew silicon crystals on earth with a 0.5 Tesla axial magnetic field and found only faint residual striations near the periphery of the crystal. We estimate that $\alpha = 91$ for their experiments. We will numerically integrate the appropriate fully non-linear governing equations in time to either a steady state or to a periodic solution in order to determine the values of $\alpha_{cr}$ and in order to determine the characteristics and frequencies of the periodic melt motions for $\alpha > \alpha_{cr}$.

## Magnetic Damping of Free Surface Motions Driven by g-Jitters

For the floating-zone process in space, g-jitters drive an oscillatory motion of the entire melt which acts as a liquid bridge. Without a magnetic field, only surface tension limits the amplitude of these oscillations and only viscosity dissipates their energy. Such free-surface motions also occur in the Bridgman process if the ampoule is not entirely full. With a uniform axial magnetic field, most of the melt moves as a rigid body (the Hartmann effect), so that the much larger surface-tension forces at the edges of the crystal and feed rod lead to much smaller displacements of the melt. The joulean heating with a magnetic field dissipates the energy in the oscillatory motions far more effectively than viscosity, so that disturbances following spikes of g-jitters decay much faster, and large-amplitude resonant motions at natural frequencies are eliminated. Models will be developed for the magnetic field effects on g-jitter driven motions of the melt in the floating-zone process.

## References

[1] Nancy Ma and John S. Walker, "Magnetic damping of buoyant convection during semiconductor crystal growth in microgravity. Continuous random g-jitters," *Physics of Fluids*, **8**, 944-953, 1996.

[2] Nancy Ma and John S. Walker, "Tailored magnetic damping of g-jitter driven buoyant convection during Bridgman growth of semiconductor crystals in space," AIAA paper 96-0252, 34th Aerospace Sciences Meeting & Exhibit, Reno, Jan. 1996.

[3] Timothy E. Morthland and John S. Walker, "Thermocapillary convection during floating-zone silicon growth with a uniform or non-uniform magnetic field," *Journal of Crystal Growth,* **158**, 471-479, 1996.

[4] A. Croll, P. Dold and K. W. Benz, "Segregation in Si floating-zone crystals grown under microgravity and in a magnetic field," *Journal of Crystal Growth,* **137**, 95-101, 1994.

# PROCESS-PROPERTY-STRUCTURE RELATIONSHIPS IN COMPLEX OXIDE MELTS

Richard Weber and Paul Nordine
Containerless Research, Inc.
Evanston, IL 60201-3149
Phone: 847/467-2678
email: weber-r@nwu.edu

Background:

An understanding of process-property-structure relationships in high temperature liquids is essential to (i) a scientific understanding of the liquid state, and (ii) technological advances in liquid-phase processing. Due to the highly corrosive nature of these melts and the extreme conditions required to form them, practically all of the experimental results have been obtained by using containerless processing methods [1-10].

The present project builds on the results of research supported under a previous NASA grant to investigate containerless liquid-phase processing of molten ceramic materials. The research used an aero-acoustic levitator in combination with cw $CO_2$ laser beam heating [1,2] to achieve containerless melting, superheating, undercooling, and solidification of poorly-conducting solids and liquids. Experiments were performed on aluminum oxide, binary aluminum oxide-silicon dioxide materials, and oxide superconductors, the results and their interpretation are presented in detail in the referenced publications [1-9].

Accomplishments in the prior research were to:

1. Investigate liquid-phase processing, undercooling, and solidification of aluminum oxide, alumino-silicate, and YBaCuO melts *vs* the ambient ($pO_2$) and thermal history.

2. Conduct $CO_2$ laser melting experiments in reduced gravity aboard the KC-135 in collaboration with scientists from École Polytechnique Université de Montréal.

3. Develop a new method, laser hearth melting, for synthesis of bulk, high purity ceramic oxide materials from powders.

4. Characterize processed materials using SEM, X-ray diffraction analysis, and optical microscopy.

5. Perform collaborative research with other NRA-supported investigators at Jet Propulsion Laboratory, University of Missouri-Rolla, University of Wisconsin-Madison, and Vanderbilt University.

6. Publish and present results.

Experimental Methods:

Containerless melting experiments were performed with *ca.* 0.3 cm. diameter spherical specimens of oxides which were made by laser hearth melting [9]. Specimens were levitated in an aero-acoustic levitator [1,2]. The levitation force is primarily aerodynamic and is stabilized by the smaller acoustic forces to obtain precise control of the position of levitated solid and liquid samples. Laser beam heating and melting become possible to allow liquid phase processing and property measurement experiments under containerless conditions at very high temperatures.

A schematic plan view layout of the instruments used to observe the levitated specimen is presented in Figure 1. The levitator provides wide optical access to the specimen making it possible to integrate a variety of non-contact diagnostic instruments.

Results:

Selected results from our prior research are presented below. Full reports of the methods and results used in this research can be found in the literature [1-10].

The ambient oxygen fugacity (or pressure) was shown to have a large effect on the properties and solidification behavior of oxide melts. Figure 2 presents measurements of the degree of undercooling for molten aluminum oxide as a function of the ambient oxygen fugacity and cooling rate. Figure 3 presents the oxygen fugacity dependence of the absorption coefficient for molten aluminum oxide.

Aluminum oxide is a highly stoichiometric material for which any composition changes in response to changes in the ambient oxygen fugacity are exceedingly small. Nevertheless, it can be seen in these results that the small composition changes that do occur have a profound influence on the measured properties and phenomena. Other systems in which a large effect of the ambient oxygen fugacity have been found include the formation of amorphous (glass) materials upon cooling of melts for materials with (i) the yttrium-aluminum garnet (YAG) composition and (ii) the mullite ($Al_6Si_2O_{13}$) composition [10].

Pask [11] predicted that aluminum oxide-silicon dioxide melts should exhibit liquid-liquid phase separation under non-equilibrium undercooled conditions. However observation of this phenomena must contend with the fact that cooler regions of the liquid become transparent, and it is the development of transparent regions that is taken to indicate phase separation. Since rapid cooling or large temperature gradients are needed to access the undercooled state, ambiguities occur. We observed that regions of different optical brightness formed in the liquid for rapidly cooled melts. The distribution of these regions was not related to the known temperature gradients that also occurred. Upon further cooling, the samples crystallized to form solids of different composition, which could occur whether or not liquid phase separation was present. The results suggest that liquid-liquid phase separation occurred, but further work is required to prove that the observation has no other interpretation. It may be necessary to perform undercooling experiments under more

quiescent levitation conditions, e.g., in low gravity, to fully investigate this phenomenon.

The residual $Cr^{3+}$ content of aluminum oxide was investigated in collaboration with Dr. A. Biswas (Jet Propulsion Laboratory) by performing LIF studies after containerless melt purification. It was demonstrated that containerless processing decreased the $Cr^{3+}$ content by several orders of magnitude from the already small amount of a few ppm. Final $Cr^{3+}$ contents of the samples were as small as $10^{12}$ atoms/cm$^{-3}$. Figure 4 shows the $Cr^{3+}$ concentration in processed specimens as a function of the processing conditions.

Additional liquid-phase processing experiments were performed on (i) glass formation in the calcium oxide-gallium oxide system with Professor Delbert Day and Dr. Chandra Ray from the University of Missouri-Rolla; (ii) levitation melting of basalt materials with Professor Reid Cooper and Mr. John Fanselow from the University of Wisconsin-Madison; and (iii) levitation melting of YBaCuO superconductors with Professor William Hofmeister and Mr. James Olive from Vanderbilt University.

Objectives of the Planned Research:

The continuation of the research develops from recent work on molten oxides which shows that melt structure does change in response to ambient oxygen fugacity [3-10]. This recent work provides the basis for the experimental hypothesis:

> **"The ambient oxygen fugacity and ionic:covalent ratio in a melt can be used to modify the metal coordination number and bonding in oxide melts and significantly affect liquid viscosity, surface tension, solidification behavior, and product structural and electronic properties."**

Melts to be investigated are of low to medium viscosity (0.1 to 1000 poise) and formed from phase-pure aluminum oxide and mixtures of aluminum oxide with calcium, magnesium, silicon, yttrium and zirconium oxides. Specimens for levitation will be made by laser hearth melting [9]. Materials will be processed in containerless conditions using an aero-acoustic levitator with cw $CO_2$ laser beam heating [1,2]. Specimens will be processed under a range of ambient oxygen fugacities from 1 to about $10^{-7}$ bar by levitating them in gases with the appropriate composition.

We will make *in-situ* non-contact measurements of (i) viscosity, (ii) surface tension, (iii) undercooling, (iv) drop shape, and (v) growth front velocity during solidification. Viscosity and surface tension will be measured using surface fluctuation spectroscopy (SFS). An SFS instrument design for measurements on planar surfaces will be modified for operation with the curved surfaces of levitated liquids. Specimen temperature will be measured at a wavelength of 0.65 $\mu$m using an optical pyrometer with a 0.1 cm. spot size and at rates of up to 500 Hz. The levitated drop will be imaged using video cameras and image processing will be performed with a frame grabber and associated image analysis software. The video records will be used to identify conditions for liquid-liquid phase separation and for investigation of crystallization and solidifaction kinetics.

Melt properties will be measured as a function of the ambient oxygen fugacity, melt composition, temperature, and thermal history. Processed materials will be examined by SEM, XRD and optical microscopy. Chemical analysis will also be performed on selected specimens. Process-property relationships will be derived from the results. In separate work, we are performing liquid phase structural studies that will provide structural information for some of the molten systems of interest.

Need for Microgravity:

Containerless ground-based research capabilities will ultimately be insufficient to fully investigate the research hypothesis. Microgravity conditions will be required to achieve sufficient mechanical quiescence and thermal and chemical homogeneity while also obtaining the control of melt chemistry and purity provided in containerless experimental conditions. For example, in microgravity, chemical transport rates can be made sufficiently small, after isothermal equilibration with the ambient gas, that negligible composition changes during subsequent processing steps. Rapid stirring of the melts resulting in rapid composition changes is unavoidable on earth, due to natural convection, the forces required in levitation, and the Marangoni and the buoyant forces that result from intensive property gradients in the liquid specimens.

References:


1. J.K.R. Weber, D.S. Hampton, D.R. Merkley, C.A. Rey, M.M. Zatarski and P.C. Nordine, "Aero-acoustic Levitation - A Method for Containerless Liquid- phase Processing at High Temperatures," Rev. Sci. Instrum., **65**, 456-465 (1994).
2. J.K.R. Weber, J.J. Felten, B. Cho and P.C. Nordine, "Design and Performance of the Aero-Acoustic Levitator," J. Jpn. Soc. Microgravity Appl., **13**, 27-35 (1996).
3. J.K.R. Weber and P.C. Nordine, "Containerless Liquid-Phase Processing at High temperatures," Microgravity Science and Technology, VII, 279-282 (1995).
4. J.K.R. Weber, P.C. Nordine, K.C. Goretta, and R.B. Poeppel, "Effects of Oxygen Pressure on the Structure of Y-Ba-Cu-O Materials Formed by Containlerless Melting and Solidification," J. Mat. Res. **9**, 1657-60 (1994).
5. J.K.R. Weber, C.D. Anderson, S. Krishnan and P.C. Nordine, "Structure of Aluminum Oxide Formed from Undercooled Melts," J. Am. Ceram. Soc., **78**, 577-82 (1995).
6. A.B. Biswas, J.K.R. Weber and P.C. Nordine, "$Cr^{3+}$ Fluorescence in Containerless Melt-purified Aluminum Oxide," J. Mat. Res. **10**, 1823-27 (1995).
7. J.K.R. Weber, S. Krishnan, C.D. Anderson and P.C. Nordine, "Spectral Absorption Coefficient of Liquid Aluminum Oxide from 0.420-0.780 $\mu$m," J. Am. Ceram. Soc., **78**, 583-87 (1995).
8. J.K.R. Weber, S. Krishnan and P.C. Nordine, "Effects of Melt Chemistry on the Spectral Absorption Coefficient of Liquid Aluminum Oxide," J. Am. Ceram. Soc. **78**, 3067-3071 (1995).

9. J.K.R. Weber, J.J. Felten and P.C. Nordine, "New Method for High Purity Ceramic Synthesis," Rev. Sci. Instrum., **67**, 522-24 (1996).
10. J.K.R. Weber, "Containerless Property Measurements on Molten Aluminum Oxide and Alumino-Silicate Binary Mixtures," Proc. 4th Asian Thermophysical Properties Conference, Tokyo, 5-8 Sept., 1995, Ed. A. Nagashima, pp. 873-876.
11. S.H. Risbud and J.A. Pask, "Calculated Thermodynamic Data and Metastable Immisciblity in the System $SiO_2$-$Al_2O_3$," J. Am. Ceram. Soc. **60**, 418-24 (1977).

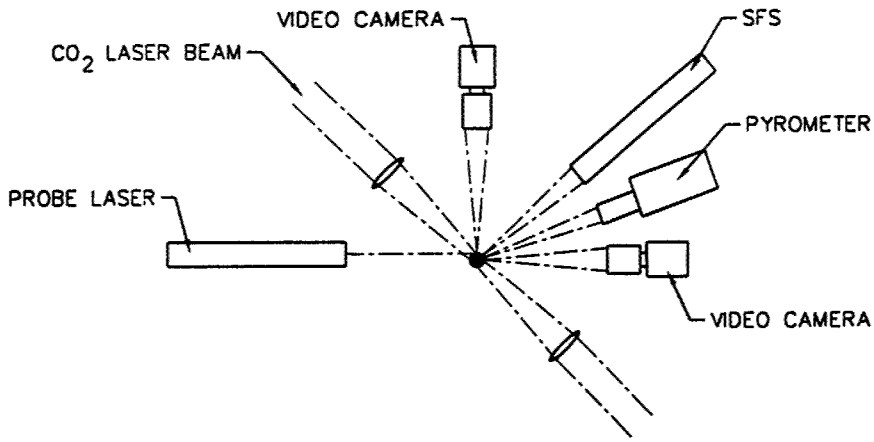


Figure 1. Schematic layout of the aero-acoustic levitator and associated instruments.

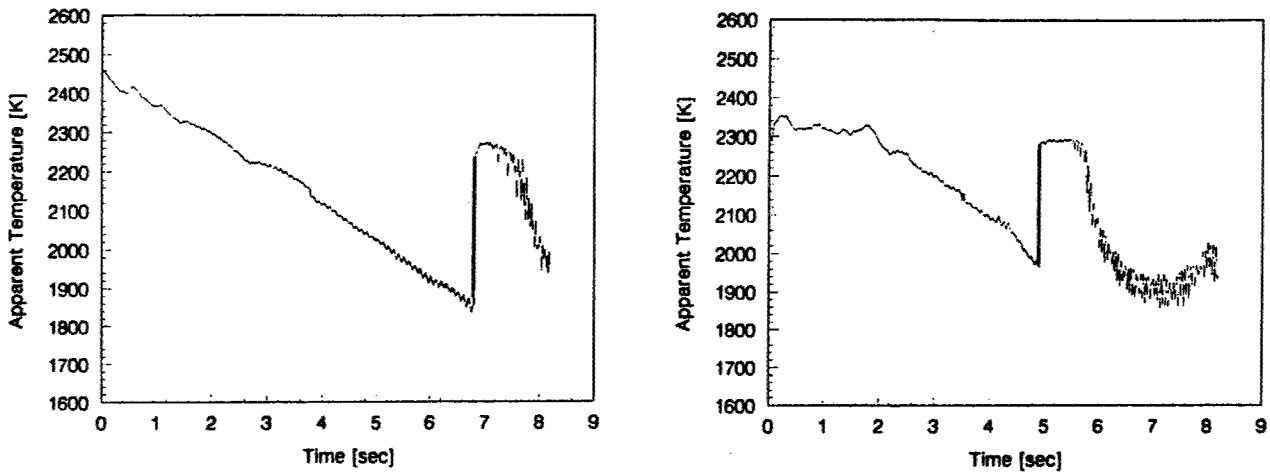


a b

Figure 2. Cooling curves showing undercooling and recalescence of liquid aluminum oxide formed from sapphire. (a) Slow cooling in argon, and (b) slow cooling in oxygen by programmed reduction of laser intensity. From ref. 5.

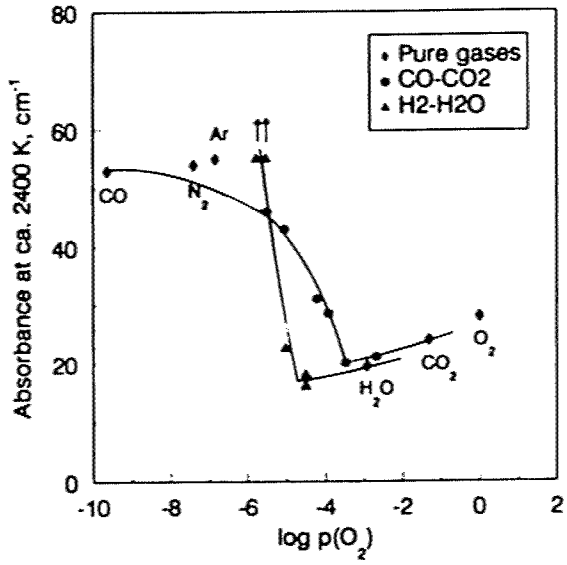


Figure 3. Spectral absorption coefficient at $\lambda = 0.633\ \mu m$ of molten aluminum oxide at approximately 2400 K *vs* ambient oxygen pressure. From ref. 8.

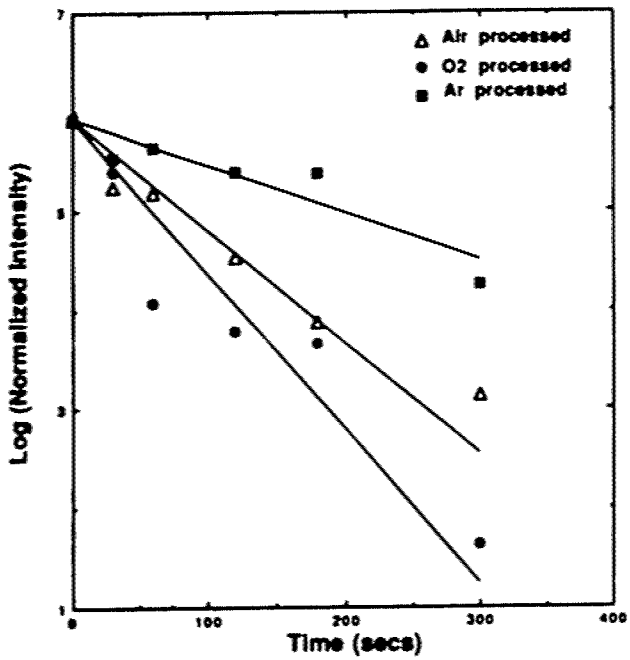


Figure 4. Logarithm of normalized LIF intensity *vs* time for molten sapphire specimens processed in argon, air and oxygen. The lines represent least squares fits to the data obtained by constraining the intercept. From ref. 6.

# THIN FILM MEDIATED PHASE CHANGE PHENOMENA: CRYSTALLIZATION, EVAPORATION AND WETTING

J.S. Wettlaufer
*Applied Physics Laboratory, Box 355640*
*and Department of Physics*
*University of Washington*
*Seattle, Washington 98105*
Phone: 206-543-7224
Fax: 206-543-3521
Internet: wett@apl.washington.edu

M. Elbaum
*Department of Materials and Interfaces*
*Weizmann Institute of Science*
*Rehovot 76100, Israel*

H. A. Stone
*Division of Applied Sciences*
*Harvard University*
*Cambridge, Massachusetts, 02138*

M. G. Worster
*Department of Applied Mathematics & Theoretical Physics*
*University of Cambridge, Cambridge, CB3 9EW, UK*

## Report of Proposed Research

This project will begin in June of 1996. Therefore, this description focuses on the proposed research. We are interested in the thermodynamics and dynamics of thin films, and the role they play in mediating a several phase change phenomena important in microgravity materials science. Our proposal is focused on experimental and theoretical studies of volatile thin liquid films that originate in two distinct physical settings, but which are linked by similar theoretical descriptions. The films are either (i) deposited on a substrate via direct adsorption from the vapor or (ii) formed at the interface between a solid and its vapor through the process of surface melting. The relevance to microgravity materials research lies in the fact that during wetting, drying, and spreading the configurations of fluid--solid interfaces control nucleation processes and directly affect heat and mass transfer rates. During Czochralski growth, laser welding, float-zone processing, nucleation on substrates, Ostwald ripening, physical vapor transport, and sintering, the shape of fluid--solid and fluid--vapor interfaces can control a materials structure and properties. Cohesion and adhesion of thin films in microgravity is dominated by intermolecular interactions and interfacial tensions, and inertial effects that are independent of gravity can control thin film dynamics in space. As the capillary length is extended, the thin film phenomenon we observe on earth may extend to much larger scales in space. Therefore, earth--based thin--film studies offer an ideal test bed for the phenomena that dominate space--based processes. The focus areas of our research plan are as follows.

## Liquid Films on Inert Substrates

Attractive interactions between a substrate and the liquid, can stabilize sufficiently thin films in a subsaturated atmosphere. Partly due to this effect during the evaporation of an initially uniform, thick (greater than 1000Å) water film from a mica substrate, Elbaum and Lipson[1] observed that the `uniformly dry' state evolves through a highly nonuniform sequence of transitions: circular dry patches are nucleated and, while spreading, undergo a series of hydrodynamic instabilities that leave the surface decorated with evaporating droplets. The droplets continually evaporate while resting on the thin film. The film is completely wetting (zero contact angle) at equilibrium, yet beads up during evaporation, effectively preempting complete wetting. The finding is akin to a substrate mediated boiling, qualitatively similar to the droplet configuration assumed by water splashed on a hot pan.[2] The dynamics controlling the pathway toward the minimum free energy state are rich and varied and remain elusive. We will study the dyamical mechanisms associated with this heterogeneous dewetting processes. Experiments will use the same two-cell system Elbaum and Lipson used. They will quantify the relation between the driving force and the spreading/dewetting rates. They will search for crossovers in which the breakup process is coupled to gravity. Theory seeks to determine the origin of the observed instabilities, so we can extend understanding to other vapor/liquid/substrate systems.

Addition of impurites to the film reveals another interesting phenomenon which Wettlaufer and Stone are investigating. The solute in the film is nonvolatile, and evaporation drives solidification of the solute. We have shown experimentally that a surface spreading phenomenon occurs; the original radius of the impure droplet is continually *extended* by the growing crystals. It represents novel growth process coupling evaporation with solidification and spreading. Using simple experiments, we will study the dynamics of the growth. Theoretically, we begin looking at the initial instability that drives the extension.

These processes are important because they have significant implications for fluid containment or transport. The dewetting/spreading behavior is a relatively unexplored area of the volatile wetting, and also displays the interaction between crystallization and thin film dynamics. Evaporation and condensation processes are continually encountered when handling liquids and, as they are driven or mediated by surface tension or surface interactions, we expect them to play a significant transport role in microgravity. Uniformity and composition of thin--film coating's will depend on the integrity of the wetting and dewetting processes. Interfacial phenomena also affect fuel handling, welding, brazing, soldering and other processing techniques. Finally, there are theoretical analogies between thin film stability and the interaction of biomembranes with substrates. We intend to explore these links experimentally.

## Films on Crystal Surfaces

There are a host of mechanisms that can cause the stable existence of liquid at temperatures and pressures outside of the normal equilibrium range, including static and dynamic, chemical, mechanical, interfacial, and structural processes. "Interfacial premelting" or "surface melting" is one such process wherein a qausi-liquid disjoins the solid from its vapor or an inert wall at temperatures below the bulk melting transition. The process occurs in metals, semiconductors, solid rare gases and molecular solids, typically beginning with a film thickness of one or two monolayers, which thickens gradually with increasing temperature, and diverges at bulk melting point.[3-5] The film thickness depends on the temperature and the types of interactions in the material.

Commonly one studies this surface phase transition within the context of either a Landau-Ginzburg or Solid-On-Solid model, depending on the nature of the interactions. The upper critical dimension $d^* = 3$ for short range forces and $d^* < 3$ for long-range forces. The relation between film thickness and temperature as the transition is approached is generally studied quasi-statically. However, novel nonequilibrium (nonisothermal) experiments on single crystal interfaces have teased out the fundamental flow behavior[6]. We have recently developed a (mean field) dynamical theory that reveals the nature of the interactions responsible for the experimental melting behavior, and hence have explained the essential physics of so-called premelting dynamics[7,8]. These dynamics may dominate sintering, annealing and whisker growth. Furthermore, in the case of complete interfacial melting, the film thickness diverges at the triple point, so that there is an important crossover where the premelted film couples with gravity. We will conduct theoretical studies of this coupling and the role it plays in the shape dynamics of growing crystals.

The controlled growth of single crystals has a long history in space--based materials processing. The role of surface melting in mediating growth from the vapor has not been investigated, and morphological instabilities originating in the diffusion field are major obstacles to the growth of uniform crystals in space. The presence of a liquid film between the solid and the parent vapor may act to suppress these instabilities, and control the redistribution of impurities. Modern ceramics are polycrystalline aggregates which densify through sintering processes that are driven by minimization of surface energy. Surface melting will enhance the sintering process due to the presence of a mobile surface--melted film. Finally, the role of gravity and surface tension in determining the shape of a surface melted layer must be investigated in order to assess the likelihood of whisker growth via this transport mechanism.

## REFERENCES


[1]M. Elbaum and S.G. Lipson, *Phys. Rev. Lett.* **72**, 3562 (1994); *Israel J. Chem.* **35**, 27 (1995).

[2]M. Elbaum, S.G. Lipson and J.S. Wettlaufer, *Europhys. Lett.* **29**, 457 (1995).

[3]A.A. Chernov, *Prog. Cryst. Growth Char. Mat.* **26**, 195 (1993).

[4]H. Löwen, *Phys. Rep.* **237**, 249(1994).

[5]J.G. Dash, H-Y. Fu and J.S. Wettlaufer, *Rep. Prog. Phys.* **58**, 115 (1995).

[6]L.A. Wilen and J.G. Dash, *Phys. Rev. Lett.* **74**, 5076 (1995)

[7]J.S. Wettlaufer and M.G. Worster, *Phys. Rev. E* **51**, 4679 (1995).

[8]J.S. Wettlaufer, M.G. Worster, L.A. Wilen, and J.G. Dash, *Phys. Rev. Lett.* **76**, 3602 (1996).

# DEFECT GENERATION IN CVT GROWN $Hg_{1-x}Cd_xTe$ EPITAXIAL LAYERS UNDER NORMAL AND REDUCED GRAVITY CONDITIONS

H. Wiedemeier and Y. R. Ge
Department of Chemistry
Rensselaer Polytechnic Institute
Troy, New York 12180-3590
USA
Telephone: 518-276-8444, e-mail: wiedeh@rpi.edu

## Material Properties

The technologically very useful infrared detector properties of the alloy-type semiconductor $Hg_{1-x}Cd_xTe$ are well known. The band gap and related properties of this mixed crystal system change with composition, and are affected by structural imperfections such as vacancies and other crystallographic defects. For the use of this material in electronic devices, a high degree of compositional and structural microhomogeneity of the $Hg_{1-x}Cd_xTe$ single crystals is necessary.

The complexity of this ternary semiconductor system is further increased owing to the thermodynamic properties of the material. These are reflected in the very high vapor pressures of mercury at practical growth temperatures, while those of the other components are several orders of magnitude lower. These properties have very important practical consequences for the growth of single crystals of this material.

## Crystal Growth of $Hg_{1-x}Cd_xTe$

The inherent advantages of vapor phase crystal growth in terms of lower temperatures are useful to reduce the excessive Hg partial pressure. However, in order to reduce the vapor pressure differences between the components, separate source reservoirs and/or flow methods are required. These are presently not feasible under space flight conditions. The chemical vapor transport (CVT) technique allows the use of one source material in a closed container for the growth of single crystals. This method also excludes a priori any forced flow.

## Scientific Basis of Proposed Experiments

Extensive ground-based studies of the unseeded bulk growth of $Hg_{1-x}Cd_xTe$ and of the epitaxial growth of $Hg_{1-x}Cd_xTe$ on CdTe substrates by CVT in closed containers demonstrated the effects of gravity-driven convection on the growth morphology and crystallinity of this material. In particular, these investigations showed the sensitivity of this system to even small convective disturbances, and led to the prediction that higher quality single crystals could be obtained under microgravity conditions.

The USML-1 experiments confirmed the above predictions and yielded $Hg_{1-x}Cd_xTe$ epitaxial layers on (100) CdTe substrates of significantly improved compositional and structural microhomogeneity and uniformity relative to ground-control test experiments. For the first time, it was observed that the $Hg_{1-x}Cd_xTe$/CdTe layer/substrate interface obtained in space had a considerably lower dislocation density than interfaces of ground test samples. The results to date of the USML-2 experiments for much shorter growth times (thinner layers) are consistent with those of the earlier experiments. In particular, the growth interfaces of the islands and of the thin layer have significantly fewer defects than those of ground samples. The combined observations strongly suggest that fluid flow interacts with processes at or near the growth interface and that these interactions are affected by gravity-driven convection. The comparative analysis also suggests that the interface morphology influences the subsequent growth morphology and properties of the single crystalline layers.

## Objectives of Proposed New Experiments

For the further elucidation of fluid flow interactions with chemically active surfaces under normal and reduced gravity conditions, new experiments are proposed. Considerable experience has been gained with the $Hg_{1-x}Cd_xTe$/CdTe epitaxial growth system on ground and in microgravity. Because of this and the technological interest in this material, the employment of this growth system for the new research maintains continuity with the above discussed previous results.

It is generally known that the compositional and structural uniformity of single crystalline layers are affected by the crystallographic orientation (off-orientation) of the seed, by the quality of the substrate surface, by the growth rate and temperature, and by annealing. Our ground-based and microgravity experiments of the $Hg_{1-x}Cd_xTe$ system and other investigations have demonstrated the effects of gravity-driven convection on the generation of defects. The combined influences of the above parameters on crystal growth and quality are most likely interrelated, yielding a rather complex mechanism of defect formation. The decoupling of the various origins of defect formation and their ultimate control represent major challenges in the field of crystal growth. These tasks require long range and comprehensive efforts.

The goals of this project are to perform new research towards the further elucidation of the interactions of the above parameters with the growth processes. In order to vary the effects of gravity-driven convection on fluid flow and crystal growth, the proposed experiments will be performed under different orientations of the density gradient relative to the gravity vector.

## Experimental and Analytical Approach

In order to achieve the above objectives, high quality and low dislocation density substrates will be used for the epitaxial growth of $Hg_{1-x}Cd_xTe$ layers by CVT on CdTe employing new experimental conditions, which have not been reported in the literature for this material. These include the investigation of the influence of

crystallographic orientation of the substrate on layer growth and quality for different orientations of the density gradient relative to the gravity vector. Similar experiments will be performed for the growth of epitaxial layers on vicinal surfaces to investigate the effects of substrate off-orientation on the morphology of grown layers. The influence of different growth rates on layer quality and properties can be studied by appropriate changes of the chemical vapor transport conditions. Employing different growth times and temperatures also reveals the effects of annealing on the growth properties of the layer.

To achieve the objectives, a detailed analysis of the compositional and structural microhomogeneity and of their spatial distributions within the epitaxial layer and interface are required. For the structural characterization of the substrate-layer interface and of the epitaxial layer, optical and electron microscopic techniques (SEM, TEM, WDS), X-ray diffraction (Laue, rocking curves) and topographic methods, chemical etching, spectroscopic techniques, and electrical measurements will be employed.

## Significance and Utility

The above investigations are expected to provide valuable information concerning the influence of the individual growth parameters on the properties of epitaxial layers relative to gravity-driven convection effects. This will contribute to the better understanding of the complex defect generation mechanism. In addition, these investigations provide the basis for an evaluation of different methods for the in situ characterization of deposition and growth processes of epitaxial layers for this system. The combined results expected represent important ground-based data for the development of future flight experiments.

# VAPOR TRANSPORT CRYSTAL GROWTH OF MERCURY CADMIUM TELLURIDE IN MICROGRAVITY - USML-2

H. Wiedemeier, Y. R. Ge, and M. A. Hutchins
Department of Chemistry
Rensselaer Polytechnic Institute
Troy, New York 12180-3590
USA
Telephone: 518-276-8444, e-mail: wiedeh@rpi.edu

## Material and Growth Technique

The alloy-type semiconductor $Hg_{1-x}Cd_xTe$ is one of the most important materials for variable energy gap intrinsic infrared detectors operating in the 3-5 and 8-14 μm regions. This material is a mixed crystal system with well-defined band structures, in which the energy gap and other band parameters vary with composition between their values for the constituent compounds. For the alloy composition with x=0.2, $Hg_{0.8}Cd_{0.2}Te$, the band gap is about 0.1 eV at 77K.

In order to optimize the infrared properties of this material for device applications, a high degree of compositional and structural microhomogeneity is required. The ternary nature and Hg-vacancy formation contribute to the structural complexity of $Hg_{1-x}Cd_xTe$ crystals. In addition, the thermodynamic properties of this material are such that the resulting vapor pressures of the elemental and binary components differ by several orders of magnitude.

Under these conditions, the vapor growth of single crystals requires the use of separate source reservoirs and/or flow techniques which are presently not feasible for space flight conditions. The only method allowing the growth of single crystals of $Hg_{1-x}Cd_xTe$ from one source material in a closed container is the chemical vapor transport (CVT) technique. This method combines the inherent advantages of vapor growth (lower temperatures, less contamination) with the a priori absence of forced flow. This enables the investigation to be focused on gravity-driven convection effects on crystal growth and properties of this important material.

## Experiment Development

Extensive ground-based studies of the unseeded bulk growth of $Hg_{1-x}Cd_xTe$ and of the epitaxial growth of $Hg_{1-x}Cd_xTe$ on CdTe substrates by CVT in closed containers demonstrated the effects of gravity-driven convection on the growth morphology and crystallinity of this material. In particular, these investigations showed the sensitivity of this system to small convective disturbances, and led to the prediction that even better single crystals could be obtained under microgravity conditions.

The results of our USML-1 experiments [1] confirmed the above predictions and demonstrated considerably improved compositional and structural uniformity of

epitaxial layers grown in microgravity on CdTe substrates relative to ground-control samples. Most importantly it was observed, for the first time, that the layer-substrate interface of the $Hg_{1-x}Cd_xTe/CdTe$ system obtained in microgravity had a significantly lower dislocation density than those of the ground test samples. These observations strongly suggested that convective flow may affect growth processes at or near the growth interface.

## Objectives of the USML-2 Experiments

The primary objectives of the USML-2 experiments were to observe microgravity effects on the early growth of the layer. This was not possible during the USML-1 mission because of the annealing of the layer during subsequent growth. Therefore, the epitaxial growth times of the USML-2 experiments were considerably shorter (2.5 and 1.5 hours) than those of the earlier mission (8 and 6 hours). The shorter growth times were selected to observe any annealing effects, and to possibly "bracket" the transition from island to layer growth.

The specific objectives include the observation and measurement of microgravity effects on

- the transient behavior and morphology of the growth islands and epitaxial layer,
- the compositional and structural microhomogeneity of the islands and layer,
- the growth interface morphology of islands and layers,
- the propagation of "birth" defects from the interface into the layer, and
- the properties of space-grown epitaxial layers.

The assessment and evaluation of the above effects is based on a direct comparison between microgravity and ground-based test experiments under otherwise identical conditions.

## Results to Date of the USML-2 Experiments

The results to date are based on the characterization of space and ground samples employing optical and scanning electron microscopy, Laue X-ray diffraction techniques, infrared absorption methods, and chemical etching of the (011) substrate-layer cross-sections.

The present characterization results are summarized below.

- Both the islands (short growth time) and layer (longer growth time) obtained in microgravity environment are high quality single crystals as expected.
- The as-grown surface of the thin layer (Fig. 1, top) and facets of the islands (Fig. 2) obtained in space are considerably flatter than those of the ground-based test samples. These observations for a thinner layer (and islands) show that the morphology is affected by convection throughout the entire growth process.
- The compositional microhomogeneity of the epitaxial layer grown during the USML-2 flight is considerably greater than those of the deposits obtained on ground (Fig. 3). In order to further elucidate the effects of

convection on the composition of ground-grown layers and islands (Fig. 3b), attempts will be made to analyze individual islands.

- The interface morphology of the space-grown epitaxial layer of $Hg_{1-x}Cd_xTe$ on (100) CdTe has a considerably lower dislocation density than those of the ground-based samples. A typical etched (011) cross-section of the layer/(100) substrate shows the growth interfaces observed on ground and under microgravity conditions. Similar differences are observed for space and ground-grown islands during the shortest growth times. The etched (011) cross-sections of the island/(100) substrate growth on ground and in microgravity in Fig. 2 show the different interface morphology. These observations are consistent with the above morphological and compositional improvements of the $Hg_{1-x}Cd_xTe$ layer grown in microgravity.

The continued characterization of the USML-2 flight and ground-based experiments in terms of compositional analysis, electrical measurements and defect concentration is in progress.

## Significance and Utility

The results to date of the USML-2 experiments significantly extend, confirm, and are consistent with those of the USML-1 flight.

In particular, the improved growth interface morphology of the layer and of the islands grown in space demonstrates the effects of gravity-driven convection on processes at or near the solid-vapor interfaces on ground. This experimental evidence strongly supports the conclusion that fluid flow interacts with solid surfaces on smaller dimensional scales than generally accepted.

The combined results are of basic scientific importance and of technological value for the better understanding of vapor deposition and growth processes of this and other vapor growth systems. The experimental observations provide basic data for future investigations and modeling of fluid flow interactions with solid-vapor interfaces.

## Acknowledgments

The authors are pleased to gratefully acknowledge the support of this work by the National Aeronautics and Space Administration through the Microgravity Science and Applications Division, Washington, D.C., and through the Experiments Development Office, George C. Marshall Space Flight Center, Huntsville, Alabama. We would also like to thank the Crew and Payload Specialists of the USML-2 mission for their valuable contributions to the success of these experiments.

## References

[1] Heribert Wiedemeier, Yu-Ru Ge, Mark A. Hutchins, Yi-Gao Sha, J. Crystal Growth, 146, 610 (1995).

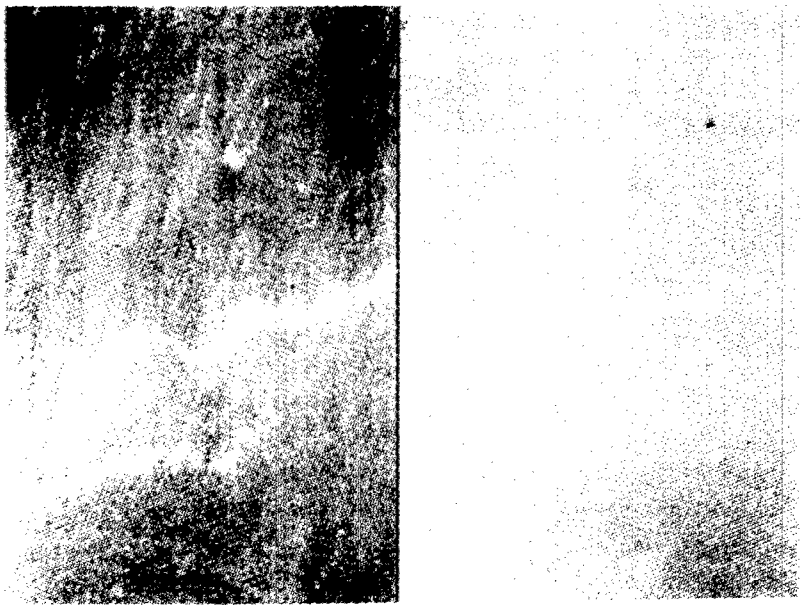

a b

Morphology of as-grown surfaces of ground (a) and space (b) grown epitaxial layers of $Hg_{1-x}Cd_xTe$. Magnification 200 X.

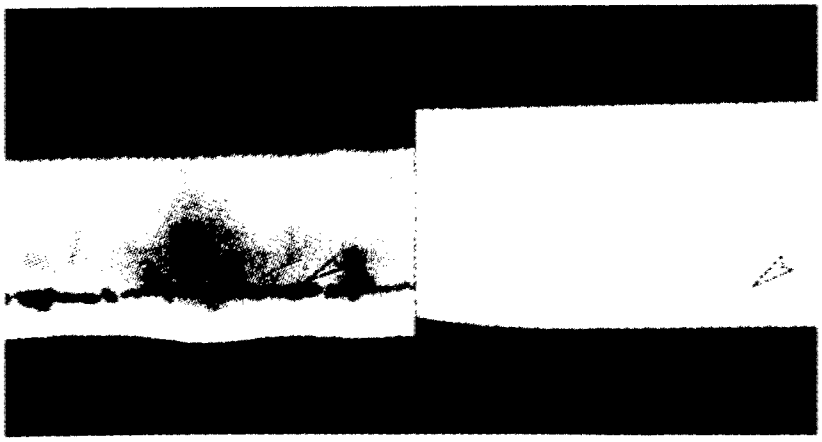

a b

Morphology of the growth interfaces of ground (a) and space (b) grown epitaxial layers of $Hg_{1-x}Cd_xTe/CdTe$. The interface is marked by an arrow. Magnification 1000 X.

Fig. 1

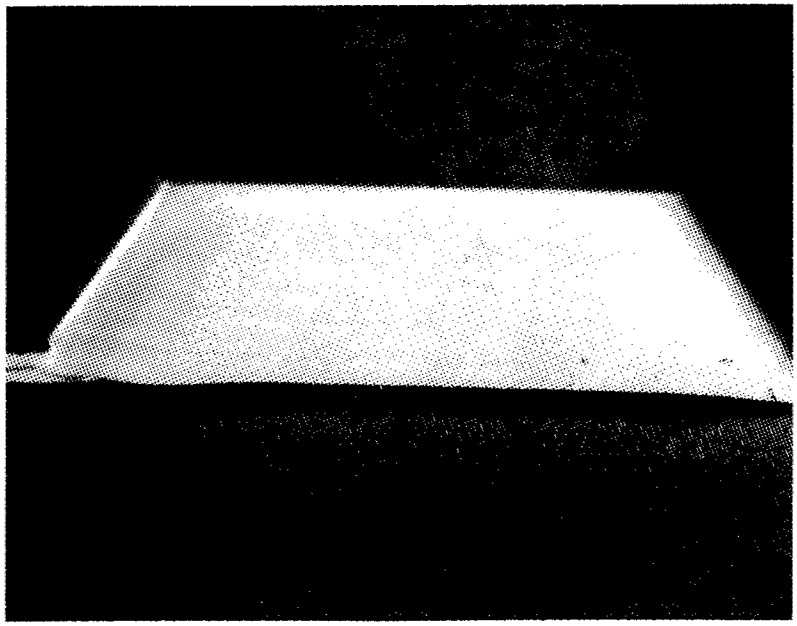

a

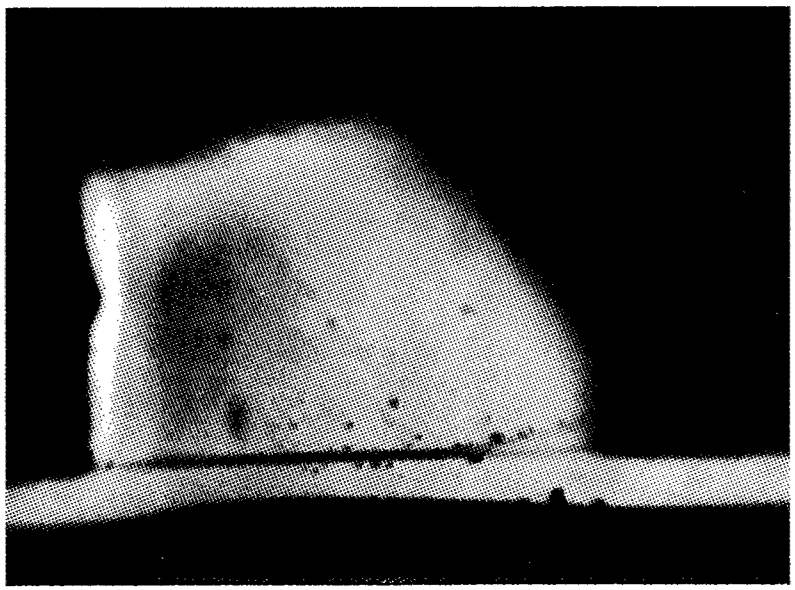

b

$Hg_{1-x}Cd_xTe$ islands (short growth time) grown under microgravity (a) and normal gravity (b) conditions. Magnification (a) 800 X and (b) 1000 X.

Fig. 2

## HgCdTe
## Spatial Composition Maps

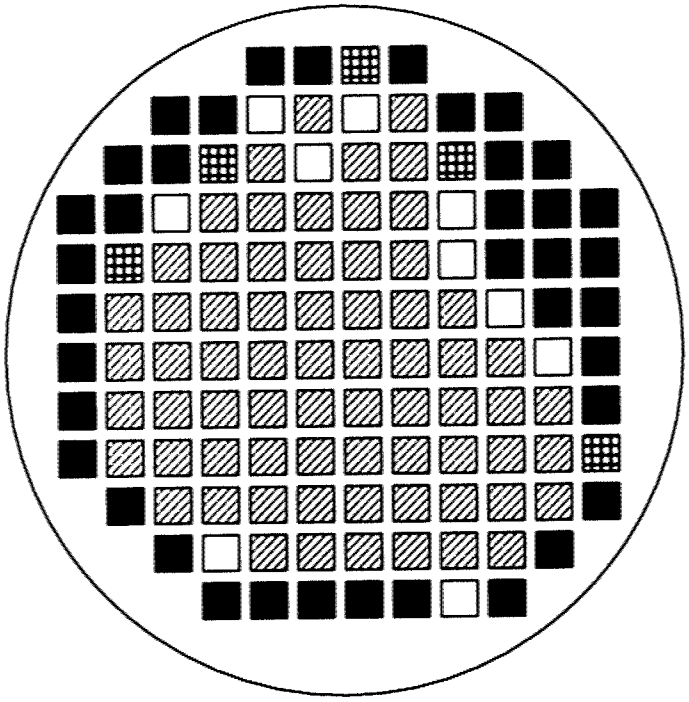

Flight
RPI2-21

- 0.250 - 0.263
- 0.263 - 0.267
- 0.267 - 0.303
- 0.303 - 0.330

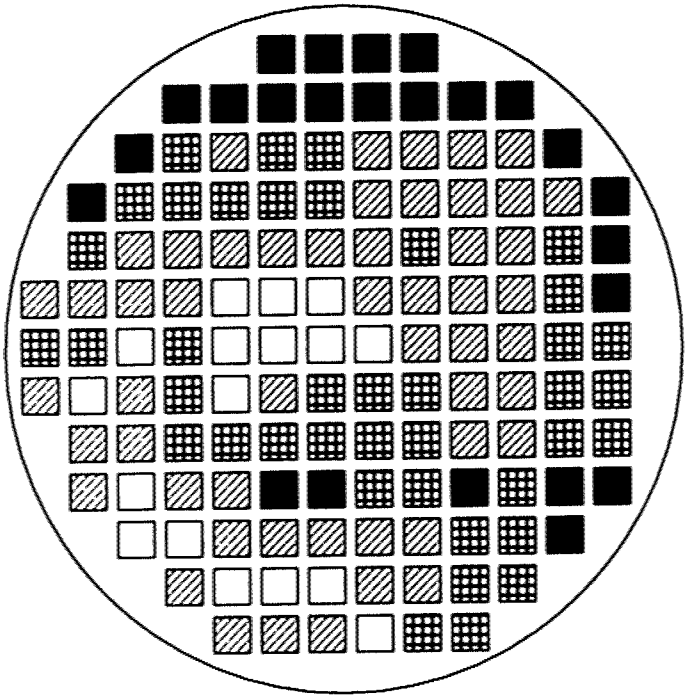

Ground Test
RPI2-16

- 0.320 - 0.340
- 0.340 - 0.350
- 0.350 - 0.360
- > 0.360

Fig. 3

# USE OF MICROGRAVITY TO CONTROL THE MICROSTRUCTURE OF EUTECTICS

William R. Wilcox and Liya L. Regel
International Center for Gravity Materials Science and Applications, Clarkson University Potsdam, NY 13699-5814, USA; 315-268-7672; wilcox@agent.clarkson.edu

Reginald W. Smith
Department of Materials and Metallurgical Engineering, Queen's University
Kingston, Ontario, Canada K7L 3N6; 613-545-2753

## Summary

Our long term goal is to be able to control the microstructure of directionally solidified eutectic alloys, through an improved understanding of the influence of convection. The primary objective of the project described here is to test hypotheses for the influence of convection on the microstructure of three fibrous eutectics (MnBi-Bi, InSb-NiSb, $Al_3Ni$-Al). A secondary objective is to determine the influence of convection on the microstructure of other eutectic alloys. Experimental and theoretical research will be carried out at Clarkson University and at Queen's University. The Queen's research is to be funded by the Canadian Space Agency, which has also been supporting the development of flight furnaces and experiments on the Priroda module of MIR. The present program will incorporate some experiments in this apparatus.

We reviewed the results of experimental research by ourselves and others on the influence of convection on rod eutectic microstructure, including solidification in space, mechanical stirring, use of a magnetic field, electric current pulses, and solidification at high gravity. We compared the experimental results with the predictions of mechanisms proposed for the influence of convection on eutectic microstructure. We concluded that vigorous mechanical stirring probably coarsens the microstructure by altering the concentration field in front of the freezing interface. On the other hand, our theoretical analyses showed that gentle buoyancy-driven convection does not alter the concentration field sufficiently to yield an observable change in the microstructure of either lamellar or fibrous eutectics. Thus, our hypothesis is that gentle convection alters the microstructure of a fibrous eutectic only when it causes a fluctuating freezing rate with a system for which the kinetics of fiber branching differs from that for fiber termination. These fluctuations may cause the

microstructure to coarsen or to become finer, depending on the relative kinetics of these processes. This is the primary hypothesis we plan to test.

## Background: directional solidification of fibrous eutectics

A wide variety of microstructures are produced when eutectic alloys are directionally solidified. The class of eutectic microstructures of interest to us here is an array of fibers, more-or-less parallel to one another and more-or-less regular. Experimentally, one often finds that $\lambda^2 V$ is constant, where $\lambda$ is the average distance between fibers and V is the macroscopic freezing rate. Hunt and Jackson developed the classical theory explaining this relationship, by estimating the influence of $\lambda$ on the compositional supercooling and the curvature supercooling at the freezing interface and then minimizing the total supercooling with respect to $\lambda$. Because the fibers and the matrix are of different composition, the composition in the melt varies out to a distance on the order of $\lambda$. Since $\lambda$ is small, on the order of a few μm, one would not expect gentle buoyancy-driven convection to influence $\lambda$. Thus it was surprising in 1976 when Larson reported from his Apollo-Soyuz Test Project experiment that directional solidification of MnBi-Bi in space caused a significant reduction in the MnBi fiber spacing $\lambda$.

Since Larson's ASTP experiment on Mn-Bi, a large number of experimental and theoretical studies have been performed to try to understand the influence of convection on fibrous eutectic microstructures. The relevant experimental results are summarized in the table on the following page. Note that conflicting results were obtained for the influence of microgravity. The challenge has been, and remains, to explain these surprising and conflicting results.

At Clarkson, over the last 20 years we have performed an extensive theoretical investigation of the influence of convection on eutectic microstructure. The bottom line is that gentle buoyancy-driven convection, by itself, should not produce a measurable change in $\lambda$. This led us to propose that convection influences the microstructure of a fibrous eutectic only when the following two conditions are met. First, that the convection is oscillatory or chaotic, leading to a fluctuating freezing rate. Second, that the kinetics of fiber formation differs from the kinetics for fiber termination. This hypothesis was tested by imposing electric current pulses during solidification

**Experimental results on influence of solidification conditions on microstructure of fibrous eutectics.**
Basis: Directional solidification upward on earth, with eutectic composition in the melt.
(Source: W.R. Wilcox and L.L. Regel, Microgravity Quarterly 4(1994)147-156.)
Here λ is the average fiber spacing for rod-like microstructures, V is freezing rate, N ampoule rotation rate.
Note that L&P denotes work by Larson & Pirich, S&K by Smith & Kaya, M&K by Müller & Kyr,
F&dG by Favier & de Goer, W&R by Wilcox & Regel *et al.*, B by Barczy *et al.*

| CONDITION | MnBi-Bi | InSb-NiSb | $Al_3Ni$-Al |
|---|---|---|---|
| Basic structure | Irregular MnBi fibers above 1 cm/hr freezing rate | Fibers | $Al_3Ni$ rods |
| Microgravity | λ~40% smaller & %MnBi smaller @ 3-49 cm/hr (L&P)<br>λ unchanged @ λ=5-8μm (S&K) | λ ~14% smaller @ 0.6-10.8 cm/hr (M&K) | λ ~15% larger @ 7.9-8.4 cm/hr (F&dG) |
| Magnetic field, | λ ~40% smaller with 3-30 kG @30-50 cm/hr (L&P) | | |
| Temperature gradient | No influence @ 3-30 cm/hr (L&P, W&R) | | |
| Horizontal solidification | No change in λ @ 30 cm/hr, slightly larger @ 3 cm/hr (L&P) | | |
| Solidification downward (thermally unstable) | λ ~67% larger @ 3 cm/hr (L&P)<br>T fluctuations & banding (S&K) | λ increased 9% @ all freezing rates (M&K) | λ decreased, independent of freezing rate (F&dG) |
| Solidification downward in centrifuge | | λ increased 38% @ 5-30g (M&K) | |
| Accelerated Crucible Rotation Technique (spin-up/spin-down) | % increase in λ larger with higher N and lower V (W&R) | | |
| Electric current pulses | λ increased propor. to current amplitude and time (W&R) | | |
| Deviation from eutectic comp'n | No discernible change (W&R) | | cellular, λ increase with % Ni (B) |

of MnBi-Bi eutectic[1]. In qualitative agreement with our hypothesis, $\lambda$ increased with increasing current density and increasing pulse length. However, one could argue that current pulses generate convection due to heating and buoyancy, and so the only increased the convection in the melt. Such experiments need to repeated in microgravity.

Two other hypotheses remain to be tested completely. One, by Favier and de Goer, is that the melt is not exactly at the eutectic composition, so that even gentle convection would alter the average melt composition at the freezing interface. While the available experimental evidence appears to contradict this model, a complete test has not been performed. Another possibility that recently occurred to us is that a habit-modifying impurity could be responsible. It is known that the morphology of eutectics can be very sensitive to trace amounts of an impurity. Gentle convection could alter the impurity concentration at the growth interface and thereby change $\lambda$.

Thus we have three hypotheses for the influence of gentle convection on the microstructure of fibrous eutectics. The objective of this project is to test these hypotheses, by a combination of theory, experiments on earth, and experiments in MIR.

## Research planned

We will select several fiber-forming eutectic systems for investigation, with a range of faceting tendencies (entropy of solution of minor component) and habit-modifying impurities. At Clarkson University, we will perform ground-based directional solidification experiments on one of these systems using a vertical Bridgman apparatus with a stabilizing temperature gradient. We will explore the influence of periodic current pulses on microstructure using a wider range of freezing rates and pulsing parameters (amplitude, frequency and duration) than we used with Mn-Bi. Experiments will also be performed with and without application of a magnetic field, with off-eutectic compositions, and with a habit-modifying impurity added.. At Queen's University, similar ground-based experiments will be performed on other systems.

Flight experiments will be performed using the Queen's University furnace, QUELD II. Two of

[1] W.R. Wilcox and L.L. Regel, "Influence of gravity on the microstructure of fibrous eutectics," Micrograv. Quart. 4(1994)147-156.


☆U.S. GOVERNMENT PRINTING OFFICE—1996—532-128/40062

these rack-mounted gradient furnaces are in Priroda/MIR. Each furnace has 3 zones, programmable and automated, suitable for both isothermal diffusion and gradient freeze experiments. It is planned to modify the apparatus to permit thermocouple measurements inside the ampoules, so as to yield temperature gradients, freezing rates, and interfacial temperatures. If additional funding becomes available from Canadian Space Agency, current pulsing capability will be added to the flight furnace. Clarkson and Queen's personnel will collaborate on preparation of the flight ampoules, testing the flight furnace, and characterizing the flight samples. Eutectic, hypo-eutectic and hyper-eutectic samples will be solidified over a range of freezing rates and pulsing conditions, as suggested by the results of the ground-based experiments. In order to determine the freezing rate, periodically a large current pulse will be applied in order to mark the interface. Some melts will be held in a temperature gradient and then quenched, in order to determine the Soret coefficient.

All results will be compared with theoretical predictions. We will develop a new theoretical model for a fibrous microstructure with an oscillatory freezing rate. The composition field in the melt will be calculated numerically, using the following assumptions:

1. Regular hexagonal array of fibers.
2. Faceted fibers, with known growth kinetics on the fiber's sides and tips.
3. Non-faceted matrix, with known isotropic properties and growth kinetics.
4. Fiber branching when the supercooling at the tip reaches a specified value.

Starting conditions will be assumed for fiber spacing, projection of the fibers in front of the matrix, and fiber width. The structure will be allowed to evolve to a quasi-steady oscillatory state without assuming minimum supercooling.

# REPORT DOCUMENTATION PAGE

Form Approved
OMB No. 0704-0188

Public reporting burden for this collection of information is estimated to average 1 hour per response, including the time for reviewing instructions, searching existing data sources, gathering and maintaining the data needed, and completing and reviewing the collection of information. Send comments regarding this burden estimate or any other aspect of this collection of information, including suggestions for reducing this burden, to Washington Headquarters Services, Directorate for Information Operations and Reports, 1215 Jefferson Davis Highway, Suite 1204, Arlington, Va 22202-4302, and to the Office of Management and Budget, Paperwork Reduction Project (0704-0188), Washington, DC 20503.

| 1. AGENCY USE ONLY (Leave Blank) | 2. REPORT DATE | 3. REPORT TYPE AND DATES COVERED |
|---|---|---|
| | October 1996 | Conference Publication |

**4. TITLE AND SUBTITLE**

NASA Microgravity Materials Science Conference

**5. FUNDING NUMBERS**

**6. AUTHOR(S)**

F. Szofran, D. McCauley*, and C. Walker**, Compilers

**7. PERFORMING ORGANIZATION NAME(S) AND ADDRESS(ES)**

George C. Marshall Space Flight Center
Marshall Space Flight Center, AL 35812

**8. PERFORMING ORGANIZATON REPORT NUMBERS**

M-819

**9. SPONSORING/MONITORING AGENCY NAME(S) AND ADDRESS(ES)**

National Aeronautics and Space Administration
Washington, DC 20546

**10. SPONSORING/MONITORING AGENCY REPORT NUMBER**

NASA CP-3342

**11. SUPPLEMENTARY NOTES** Proceedings of a conference held in Huntsville, AL on June 10-11, 1996. The conference was implemented by the Alliance for Microgravity Materials Science & Applications (AMMSA-NASA, MSFC, UAH, & USRA) under contract to NASA/MSFC.
*University of Alabama in Huntsville **Universities Space Research Association

**12a. DISTRIBUTION/AVAILABILITY STATEMENT**

Unclassified-Unlimited
Subject Category 88

**12b. DISTRIBUTION CODE**

**13. ABSTRACT** *(Maximum 200 words)*

The Microgravity Materials Science Conference was held June 10-11, 1996 at the Von Braun Civic Center in Huntsville, AL. It was organized by the Microgravity Materials Science Discipline Working Group, sponsored by the Microgravity Science and Applications Division at NASA Headquarters, and hosted by the NASA Marshall Space Flight Center and the Alliance for Microgravity Materials Science and Applications (AMMSA). It was the second NASA conference of this type in the microgravity materials science discipline. The microgravity science program sponsored approximately 80 investigations and 69 principal investigators in FY96, all of whom made oral or poster presentations at this conference. The conference's purpose was to inform the materials science community of research opportunities in reduced gravity in preparation for a NASA Research Announcement (NRA) scheduled for release in late 1996 by the Microgravity Science and Applications Division at NASA Headquarters. The conference was aimed at materials science researchers from academia, industry, and government. A tour of the MSFC microgravity research facilities was held on June 12, 1996. This volume is comprised of the research reports submitted by the principal investigators after the conference and presentations made by various NASA microgravity science managers.

**14. SUBJECT TERMS**

microgavity, materials science, crystal growth, metals and alloys, electronic materials, optical materials, polymers

**15. NUMBER OF PAGES**

582

**16. PRICE CODE**

A25

| 17. SECURITY CLASSIFICATION | 18. SECURITY CLASSIFICATION OF THIS PAGE | 19. SECURITY CLASSIFICATION OF ABSTRACT | 20. LIMITATION OF ABSTRACT |
|---|---|---|---|
| Unclassified | Unclassified | Unclassified | Unlimited |

National Aeronautics and
Space Administration
Code JTT
Washington, DC
20546–0001

*Official Business*
*Penalty for Private Use, $300*

*Postmaster: If Undeliverable (Section 158 Postal Manual), Do Not Return*